January 2014

Advanced Reactors And Novel Reactions For The Conversion Of Triglyceride Based Oils Into High Quality Renewable Transportation Fuels

Michael James Linnen

[How does access to this work benefit you? Let us know!](#)

Follow this and additional works at: https://commons.und.edu/theses

ADVANCED REACTORS AND NOVEL REACTIONS FOR THE CONVERSION
OF TRIGLYCERIDE BASED OILS INTO HIGH QUALITY RENEWABLE
TRANSPORTATION FUELS

by

Michael James Linnen
Bachelor of Science, Iowa State University, 2008

A Dissertation

Submitted to the Graduate Faculty

of the

University of North Dakota

in partial fulfillment of the requirements

for the degree of

Doctor of Philosophy

Grand Forks, North Dakota
December
2014
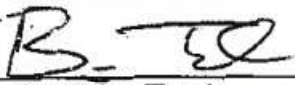
This dissertation, submitted by Michael James Linnen in partial fulfillment of the requirements for the Degree of Doctor of Philosophy from the University of North Dakota, has been read by the Faculty Advisory Committee under whom the work has been done and is hereby approved.

Dr. Wayne Seames, Chairman

Dr. Robert Wills

Dr. Brian Tande
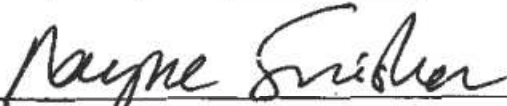
Dr. Evguenii Kozliak

Dr. Alena Kubatova

This dissertation is being submitted by the appointed advisory committee as having met all of the requirements of the School of Graduate Studies at the University of North Dakota and is hereby approved.

Wayne Swisher
Dean of the School of Graduate Studies

December 10, 2014
Date

iii

PERMISSION

Title   Advanced Reactors and Novel Reactions for the Conversion of Triglyceride
           Based Oils into High Quality Renewable Transportation Fuels

Department Chemical Engineering

Degree   Doctor of Philosophy

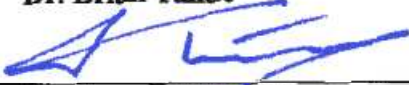   In presenting this dissertation in partial fulfillment of the requirements for a graduate
degree from the University of North Dakota, I agree that the library of this University shall make
it freely available for inspection. I further agree that the permission for extensive copying for
scholarly purposes may be granted by the professor who supervised my dissertation work, or in
his absence, by the Chairperson of the department or the dean of the School of Graduate Studies.
It is understood that any copying or publication or other use of this dissertation or part thereof for
financial gain shall not be allowed without my written permission. It is also understood that due
recognition shall be given to me and to the University of North Dakota in any scholarly use
which may be made of any material in my dissertation.

                                        Michael James Linnen
                                        December 4, 2014

TABLE OF CONTENTS

LIST OF FIGURES

xv

LIST OF TABLES

xxii

LIST OF ABBREVIATIONS

UND   (The) University of North Dakota

TAG   Triglyceride based oil

NCP   Noncatalytic cracking process

CT   Cracked TAG

CTL   Cracked TAG liquid

CTG   Cracked TAG gas

CTD   Cracked TAG distillates

CTR   Cracked TAG residue (from distillation)

DCB   Drop-in compatible biofuel

DCBP   Drop-in compatible biofuel product

DCBI   Drop-in compatible biofuel intermediate

HONO   High oleic acid novelty oil (a TAG feedstock)

VHONO   Very high oleic acid novelty oil (a TAG feedstock)

HENO   High erucic acid novelty oil (a TAG feedstock)

GC   Gas chromatograph

FID   Flame ionization detector

TCD   Thermal calorimetry detector

MS	Mass spectrometer (refers to EIMS unless otherwise specified)
EIMS	Electron ionization mass spectrometer
FI	Field ionization
FIMS	Field ionization mass spectrometer
PIMS	Photoionization mass spectrometer
GC-FID/MS	GC with simultaneous detectors in parallel: FID and MS
GC-FID/TCD	GC with simultaneous detectors in parallel: FID and TCD
GC-FID/FIMS	GC with simultaneous detectors in parallel: FID and FIMS
SimDist	Simulated distillation
FIMSDIST	High throughput compositional analysis by GC-FID/FIMS
COC	Cool-on-column (refers to a type of GC inlet)
UCM	Unresolved complex mixture
Pd/C 5	5 wt. % palladium on activated carbon catalyst
Ni/C 31.7	31.7 wt. % nickel on activated carbon catalyst
Ni/SiO2 55	55 wt. % nickel on activated carbon catalyst
Ni/SiAlZrOx 60	60 wt. % nickel on silica aluminum zirconium oxide catalyst
MABP	Mean average boiling point

ACKNOWLEDGEMENTS

xxxi

To my wife, my children, and especially to Jesus Christ, the I Am.

ABSTRACT

Sustainable energy continues to grow more important to all societies, leading to the research and development of a variety of alternative and renewable energy technologies. Of these, renewable liquid transportation fuels may be the most visible to consumers, and this visibility is further magnified by the long-term trend of increasingly expensive petroleum fuels that the public consumes. While first-generation biofuels such as biodiesel and fuel ethanol have been integrated into the existing fuel infrastructures of several countries, the chemical differences between them and their petroleum counterparts reduce their effectiveness. This gives rise to the development and commercialization of second generation biofuels, many of which are intended to have equivalent properties to those of their petroleum counterparts.

In this dissertation, the primary reactions for a second-generation biofuel process, known herein as the University of North Dakota noncatalytic cracking process (NCP), have been studied at the fundamental level and improved. The NCP is capable of producing renewable fuels and chemicals that are virtually the same as their petroleum counterparts in performance and quality (i.e., petroleum-equivalent). In addition, a novel analytical method, FIMSDIST was developed which, within certain limitations, can increase the elution capabilities of GC analysis and decrease sample processing times compared to other high resolution methods. These advances are particularly useful for studies of highly

heterogeneous fuel and/or organic chemical intermediates, such as those studied for the NCP. However the data from FIMSDIST must be supplemented with data from other methods such as for certain carboxylic acid, to provide accurate, comprehensive results,

From a series of TAG cracking experiments that were performed, it was found that coke formation during cracking is most likely the result of excessive temperature and/or residence time in a cracking reactor. Based on this, a tubular cracking reactor was developed that could operate continuously without coke formation. The design also was proven to be scalable. Yields from the reactor were determined under a variety of conditions in order to predict the outputs from the NCP and to establish relationships/correlations between operating parameters and the product distribution. These studies led to the conclusion that the most severe operating conditions which do not induce coking are optimal over the experimental domain.

In order to develop economical deoxygenation catalysts for use within the NCP, a series of experiments were performed using nickel catalysts, demonstrating that nickel catalysts could outperform their predecessor, a high cost palladium-based catalyst. A nickel catalyst was then tested in a packed bed reactor in order to determine suitable operating conditions for its commercial utilization in packed bed reactors.

CHAPTER I

INTRODUCTION AND BACKGROUND

This dissertation describes a thorough series of experiments and their results that helped to determine the capabilities of a process for producing drop-in compatible biofuel products (DCBPs) from triglyceride oils (TAG) by noncatalytic cracking and subsequent refinement, referred to as the noncatalytic cracking process (NCP). An important goal of this work was to overcome chemical process obstacles for commercialization of the NCP and to optimize the NCP for producing the best yields of renewable transportation fuels and chemicals. Research efforts focused on the reactive process operations whose process outcomes cannot be solely estimated by commercial process simulators, whereas the associated nonreactive process operations can be optimized through simulation.

The first chapter of this dissertation provides a thorough review of relevant biofuel production technologies in order to introduce the following three chapters. The second chapter describes the NCP and related research projects that have supported its development and optimization. The theory behind noncatalytic cracking from the petroleum industry is reviewed in the third chapter and applied in order to illustrate expectations about TAG cracking and to provide a basis for future reaction simulation studies. The fourth chapter of this dissertation reviews the analytical strategies for determining the composition of complex mixtures. This is done in order to conceive and introduce a new method for the high throughput compositional

analysis of cracked triglyceride liquid (CTL), known herein as FIMSDIST. FIMSDIST is utilized in this dissertation to determine the composition of CTL.

The fifth chapter of this dissertation explains the methodology used for experimental hypothesis testing herein. Equipment is described, including various reactors for TAG noncatalytic cracking and catalytic deoxygenation of cracked TAG distillates (CTD). Additionally, other processing equipment and analytical equipment is described, with the necessary reagents and procedures to complete the hypothesis testing.

The sixth chapter of this dissertation describes the data reduction and results of the FIMSDIST method for characterization of CTL. This was necessary due to the intensity of the data and the nonstandard method utilized for CTL characterization.

The seventh chapter of this dissertation describes the results of various experiments to produce data that is representative and/or important to the NCP. This included data that supported the development of new reactors and catalysts to improve the NCP's efficiency. Furthermore, experiments were performed to produce high quality jet fuel, which was tested in order to obtain insight into factors that may affect the distribution of fuels yielded by the NCP. Reactors were also operated in order to determine limits of their operation and factors which influence their efficiency. Additionally, yields were estimated from the noncatalytic cracking process based on the experimental data in Chapter VII.

The eighth chapter discusses the significance of the results in light of related literature and the NCP's intended purpose as a commercially viable process. Conclusions are summarized in Chapter IX of this dissertation.

I.A. Background

This chapter reviews the history and classifications of renewable fuels, technology for

converting lipids to renewable fuels, and analytical strategies for assisting in the development of

renewable fuel processes. Emphasis was placed on technologies that can be related to

noncatalytic cracking of triglyceride-based oils (TAG), a subset of lipids, although the results

will be generally applicable to most lipids. Relatable topics include those technologies which

utilize lipid feedstocks, those which produce drop-in compatible biofuels, those which are

pyrolytic processes (i.e., degradation, pyrolysis, cracking), and analytical strategies which

support the research and development of such processes.

First generation biofuels such as fuel ethanol and biodiesel were the first commercial

responses to the demand for renewable transportation fuels, and they have continued to make

significant contributions to the transportation industries of several developed nations. One of the

characteristics of these first-gen-biofuels is that they are physically and chemically different from

the petroleum counterparts which they are intended to replace/supplement. Although some of

the differences are advantageous (e.g. clean burning, reduced carbon emissions), the fuels also

have limitations compared to petroleum-based fuels such as reduced fuel economy or cold

weather usability. These limitations have left a lot of room for improvement on first-gen-

biofuels, motivating the development of processes for drop-in compatible biofuels (i.e. DCB)

which are petroleum-equivalent fuels, having essentially the same fuel properties as their

petroleum analogs.

Since the term *second-gen-biofuels* is used to describe a wide variety of biofuel processes

(e.g., cellulosic ethanol, higher alcohol technologies, lignin conversions, etc.), processes which

exclusively produce DCB are considered a special subset of second-gen-biofuels. This review especially emphasizes DCB processes which utilize lipids as feedstocks due to their relevance to the subject matter of later chapters.

I.B. First-Generation Renewables

Ethanol fermentation was first mastered over 6000 years ago[1], and due to its long history, it was easy to adopt fuel ethanol industrially. Although it is not a lipid biomass renewable, its importance to the renewable transportation fuel sector cannot be ignored. Fuel ethanol has been integrated into the infrastructure of many countries including the US, Brazil, Canada, Japan, India, China, and parts of Europe.[2] Formed from the fermentation of saccharide feedstocks, fuel ethanol has a high octane rating making it useful as a replacement to gasoline. Although sugars and starches were among the first feedstocks to be utilized, fuel ethanol technologies have expanded to include new feedstocks for commercialization such as cellulose, lignin, lignocellulose, and others.[3,4] Topics of fuel ethanol controversy include water contamination, pretreatments, food vs. fuel, etc.[1,5,6]

The most visible drawback of ethanol is the low energy density (66 % by volume) compared to gasoline.[1] By contrast, an acclaimed advantage of ethanol is its superior octane rating which is sufficient to boost the fuel economy from 66 % to approximately 80 % (relative to gasoline) on certain engines that are optimized for ethanol burning. However, most vehicles in service do not see such gains, so there is reason for consumers to consider the cost-to-benefit ratio of ethanol use at fuel economies near 70 % that of gasoline.[7] Furthermore, the energy density of fuel ethanol is far less than kerosene and diesel fuels, so it is unlikely that fuel ethanol will be able to adequately fulfill all the needs that liquid transportation fuels have been required

4

to satisfy.

The other first-gen-biofuel in the US is biodiesel, which is especially pertinent to this review because it utilizes lipid biomass as a feedstock. Biodiesel is industrially formed from the base-catalyzed transesterification of TAG oils. Other technologies for the production of biodiesel include esterification pretreatments, transesterification of oils via acid catalysis, and heterogeneous catalysis.[8,9]

Like fuel ethanol, biodiesel is sought after for numerous reasons, and it has both advantages and inferiorities compared to its petroleum counterpart, no. 2 diesel fuel. The primary advantages of biodiesel are similar to fuel ethanol and all renewable fuels, including clean burning as a fuel in existing diesel engines, increased market demand for agricultural production of crops, and the benefit to national security of potentially decreasing reliance upon imported diesel fuel stocks for military applications (see Vasudevan[9]).

Although the energy density of biodiesel is still markedly lower than petroleum diesel, the fuel economy of biodiesel is closer to its analog when compared to fuel ethanol.[1,10] But the drawbacks are substantial enough to limit biodiesel's universal applicability. When compared to conventional diesel, biodiesel has higher viscosity and density, poor oxidative stability, and a potentially unacceptable cold filter plugging point, as remarked by Shahidi.[11] These properties prevent biodiesel's cold weather use in conventional engines and makes it hazardous to use it in conventional aircraft.

I.C. Socioeconomic Implications

Before discussing second-gen-biofuels, important lessons can be learned about the economics of biofuels by examining Brazil, which was previously hailed as an example for other

5

countries to follow concerning renewables. After the country's record setting ethanol usage accounted for 55% of all transportation fuels in 2008, Brazil had two successive poor sugarcane crops, elevating the price of ethanol and dropping its usage to 35% in 2012.[12] A large percentage of Brazil's ethanol plants had to choose between either shutting down or importing feedstock at elevated costs to continue functioning. Angelo claims that overexpansion and over-litigation caused unnecessary risks in the biofuel sector which could have been avoided with a more insightful and/or conservative approach.[12] This is a good illustration that although biofuels are capable of providing national security by buffering the price elasticity of petroleum, biofuels are equally capable of creating economic turmoil when a country becomes overly dependent on short-term crop yields.

It is additionally important to consider the practical role of biofuels and the potential impact they can have on our society. It is common knowledge that biofuels originate from carbon sequestration via photosynthesis driven by solar radiation. Therefore, from a scientific perspective, it is possible to estimate the amount of energy which the earth can provide via agricultural processes, by thinking of the earth as a large bioreactor thriving on sunlight bioenergy. Our earth's sunlight bioenergy capacity can then be compared to our global energy needs, which is the sum total of all fuel consumption processes on the earth. Multiple comprehensive studies have been performed using this bioreactor-earth perspective, and in all cases, similar findings show that the incident sunlight energy reaching the earth's surface is more than three orders of magnitude greater than the global energy needs (even neglecting radiation over large bodies of water). The studies also demonstrate that although the limit of photosynthetic efficiency is approximately 3% in most plants, the actual observed energy that is

captured and utilizable in agriculture is typically on the order of 0.1%, although some plantations can approach 1% according to Pearman,[13] typically in arid or tropical regions according to Gowik[14] (e.g., sugarcane). This implies that the usable, available energy for biosynthesis is typically on the order of what we need for fuel, not even considering the amount of energy necessary to sustain life. When the efficiency of conversion of biomass to fuel is considered, this puts practical constraints on the capabilities of biorenewables to completely replace fossil energy consumption.[1,13] These studies convey a message that biofuels are outmatched concerning the availability of energy and the efficiency of conversion, and they tend to push the readers towards other alternatives such as renewable electricity or further technological advancements.

These conservative interpretations appear to stem from an unfair expectation that biofuels should entirely remove the carbon footprint of humanity on the earth, as gleaned from Chisti.[15] As technology continues to advance, such a lofty accomplishment may one day be achievable using a combination of sustainability technologies, but it is not likely that biofuels can achieve this all alone and certainly not without technologies breakthroughs to substantially improve the capabilities of carbon sequestration/utilization and energy utilization at large.

A fair interpretation of the global bioreactor assessment can be derived from a more practical viewpoint that biofuels will not entirely replace all fossil fuels or guarantee a carbon neutral society. Instead, biofuels should be expected to accomplish three things: (1) supplement fossil fuels by mitigating the inevitable decline in fossil fuel availability, (2) offer increased stability through diversification in the event of shortages of any single resource, and (3) decrease the rate of emission of fossil-derived carbon into the atmosphere. Considering the variety of energy sectors in the US, the transportation fuel sector accounts for only a fraction of the total

energy consumption, which biofuels are uniquely purposed to serve.[16] This leaves opportunity for other renewables such as wind and solar energy to contribute to electric power generation, since those are currently less suitable for the transportation fuel sector.

The most commonly acclaimed reasons for developing biofuels often include (1) the net reduction of greenhouse gas emissions, (2) improved trade economy for countries that produce little fossil fuels, and (3) increased security of the overall fuel supply for the transportation sector according to Shahidi.[11]

On the other hand, one of the most potent criticisms of biofuel production is that foodstocks are primarily utilized for these processes, and the food vs. fuel debate continues to be argued. The natural consequence is that food prices will tend to adjust with supply/ demand towards an equilibrium price that is a function of the fuel conversion efficiency, fuel economy, and the cost of petroleum, based on the interpretations of Du.[7] Despite the rise and fall of food and fuel prices, biofuel technology should be developed that is flexible to accommodate foodstocks, fuel-purposed stocks that positively integrate into foodstock crop rotations, and waste stocks in order to optimize the integration of biofuels into the existing economy. With proper planning, the biofuels sector will then be capable of consuming foodstocks in the event of a major surplus, and capable of operating on other stocks (rotation crops, waste stocks, etc.) in the event of a shortage to keep the biofuel process operating and mitigate economic turmoil. Either way, the potential for economic disturbances can only be mitigated, not eliminated.

It is important to consider waste feedstocks not only because of aforementioned reasons, but especially on the basis of cost. Vasudevan and Briggs describe, "the high cost of virgin vegetable oil feedstock as the source of TAGs plays a large role in process profitability. To

reduce production costs and be competitive with petroleum diesel, low cost feedstocks, such as nonedible oils, waste frying oils, and animal fats could be used as raw materials."[9] More importantly, there is substantial waste stock availability. Sharma et al. give insight into the magnitude of capable waste stocks, citing that waste grease and animal fat could account for 5.2 billion kg of lipid feedstock per year in the US alone, on the order of 1.5 billion gallons of fuel.[8] These capabilities make it practical to pursue the research and development of feedstock-flexible second-gen-biofuel processes. By this same reasoning, it is sensible to be wary of biofuel processes that are unable to or otherwise less effective at processing waste feedstocks.

I.D. Second-Generation Renewables

The term 'second-generation' when describing biofuel processes is used to describe so many types of renewable technology that it necessitates deeper classification for it to have any categorical use. Penultimate classifications are typically based on the type of feedstock being utilized for fuel production, such as cellulose-derived fuels[17], lignin-derived fuels[18,19], direct photosynthetic derivatives[20,21], lipid-derived fuels[22–24], and feedstock-flexible bioconversion processes utilizing multiple feedstock arenas. For each of these penultimate classifications, typically only a small subset has demonstrated capability to produce drop-in-compatible biofuels (DCB)[17,22,23]; whereas others produce ethanol or other homogeneous chemical substances (furfural, butanol, etc.), or combustible chemicals which are uniquely different from petroleum fuels and shall be only classified as second-gen-biofuels.

According to Eber of the National Renewable Energy Laboratory, processes capable of producing DCB have the advantage of being easily adopted into our existing fuel infrastructure, transferred in existing pipelines, and consistent fuel economy.[25] Many DCBs can also be directly

blended with petroleum-derived analogs. This makes them economically appealing, especially considering that the existing fuel infrastructure is very capital-intensive.

Even among drop-in compatible biofuels, there is additional confusion caused by identifying "not quite compatible" fuels as DCBs. Many processes identify as 'drop-in compatible' because they produce distillate/residue products that can be directly utilized at petroleum refineries and/or biorefineries but are not engine-ready in their current state. These processes provide drop-in compatible biofuel *intermediates* (DCBI), whereas those producing a fuel that is engine-ready would be classified as a drop-in compatible fuel *product* (DCBP) process. True DCBP processes produce fuels that comply with all of the key specifications for existing petroleum-based fuels set forth by ASTM International[26,27] and other global standardization authorities.

With so much biofuel technology available, it is nearly impossible to classify, describe, and compare all technologies on a practical basis. The focus of this dissertation is to introduce technologies that are capable of producing DCBPs, especially those which are derived from lipids. However, other significant DCB technologies are discussed herein due to their direct comparability and relevance to this dissertation.

I.D.1. Hydrotreatment of Triglycerides

Triglyceride hydrotreatment is a maturing technology for making DCBI with some potential to produce DCBP. Triglyceride hydrotreatment was sought after more than two decades ago by Stumborg et al. in colder climates like Canada to provide a diesel replacement without the cold-flow problems of biodiesel.[28] Since that time, it has seen development in other countries and organizations, providing a large volume of published literature on hydrotreatment.

During hydrotreatment, TAGs are deoxygenated into saturated hydrocarbons using a heterogeneous metal catalyst under high heat and high hydrogen gas partial pressure. The result of these reactions are the complete deoxygenation of the feedstock into a liquid hydrocarbon product composed primarily of saturated hydrocarbons plus water, carbon monoxide, and/or carbon dioxide.[29–31] Hydrocarbon yields on the order of 80 % have been reported in the diesel fuel range for reductive hydrotreatment.[28]

There is wide diversity of hydrotreatment processes, with differences influencing the composition of the final product DCBIs. The dominant reactions are typically (1) hydrocracking, (2) hydrodeoxygenation, (3) decarboxylation, and (4) hydrogenation, respectively characterized by (1) carbon chain scission followed by reduction, (2) reductive deoxygenation to produce water, (3) decarboxylative deoxygenation to produce CO_2 (or CO/CH_4), and (4) the reductive saturation of carbon-carbon double bonds. Mohammad et al. states that depending on the type of catalytic material, support, and reaction conditions; the reaction specificity can vary between any of these reactions.[32] Guzman et al. have shown that hydrotreatment may require high pressures of hydrogen gas to complete the reaction properly.[33] Raseev indicates that high pressures of hydrogen gas are also characteristic of hydrocracking.[34] To some extent, the hydrogen is consumed in the reaction or used to saturate all carbon-carbon bonds, but to a much greater extent it is used to prevent coke forming reactions that would otherwise foul the catalyst and deactivate it. Unspent hydrogen must be re-purified before it can be reused in the process.

Another important aspect of hydrotreatment is that catalysts are used at the front of the fuel conversion process. Some hydrotreatment catalysts are prone to catalyst deactivation.[28,33,35] Ryymin shows that deactivation can result from loss of sulfur from sulfided catalysts, which

consequentially requires the addition of H_2S to sustain catalyst activity.[36] Furthermore, sulfided catalysts often contaminates the effluent fuel stream in minor amounts of sulfur, coinciding with the deactivation.[36] On the other hand, Zuo et al. remark that noble metal catalysts have high activity and especially stability, but their high cost limits their utilization commercially.[37]

Concerning final products from hydrotreating processes, the abundance of unbranched aliphatics tends to result in cold-flow properties that are inferior to those of conventional fuels, so blending and/or additional reactions such as isomerization or aromatization are necessary to yield a quality fuel product. This is especially shown by Stumborg et a., who studied the hydrotreatment of rapeseed oil and then compared the properties of diesel, the hydrotreated fuel, and various blends. Stumborg reports that although most of the diesel fuel properties were improved by the addition of the hydrotreated fuel, the cold flow properties were made worse, even at small blending percentages (5 – 30 wt. %).[28] Nevertheless, the cold-flow properties were still notably superior to typical biodiesel (methyl ester) blends.

Despite some of these concerns, if sufficient hydrogen is available, hydrotreatment can be used to produce transportation fuel intermediates that are capable of being blended into jet fuel and cold-weather diesel.[23,28,38] For example, hydrotreated fuels have been successfully blended and/or modified in order to meet the current fuel specifications set by ASTM International.[27] Furthermore, Honeywell/UOP has developed a process to hydrotreat soybean oil, tallow, and jatropha oil into a product that can be blended with a petroleum cut to produce a drop-in compatible jet fuel product.[38] More recently, Honeywell/UOP demonstrated a process to convert TAGs into a jet fuel that is 100% renewable utilizing paraffin isomerization or blending with renewable aromatics formed in parallel.[23] Additionally, engine tests were conducted with either

pure hydrotreated renewable jet fuel or a 50% JP-8 blend, showing generally equivalent or better

performance in terms of fuel consumption, power output and emissions when compared to

petroleum JP-8.[23]

I.D.2. Catalytic Cracking of Triglyceride Oils

Triglyceride (TAG) hydrotreatment can be thought to have evolved from the catalytic

cracking of TAG oils, which is similar in concept. However high pressures of hydrogen are not

employed in catalytic cracking, permitting advanced cracking reactions to occur that otherwise

won't occur during hydrotreating. The TAG cracking reactions that take place during catalytic

cracking are sufficient to degrade the TAG molecule into cracked TAG liquid (CTL), which is an

intermediate product of substantial diversity, including branched paraffins, cyclics, olefins,

aromatics, and others, whereas hydrotreatment predominantly produces linear paraffins as

products. The absence of hydrogen in most cases leads to added technical challenges, including

the deactivation of catalysts via the formation of solid amorphous carbonaceous deposits (coke)

on catalysts surfaces which, in turn, leads to changes in activity, reduced activity, and/or

difficulties with reactor operation.

Various studies have been conducted to investigate the potential yields from TAG

catalytic cracking. Dandik et al. performed the catalytic pyrolysis of used sunflower oil in the

presence of a catalyst (HZSM-5 zeolites, silica-alumina, Na_2CO_3), ultimately converting 73.2 %

of TAG into products containing 33% liquids (predominantly carboxylic acids, hydrocarbons),

with the balance of the products consisting of synthesis gas, an unidentified aqueous phase, coke,

unreacted feedstock, and residual oil.[39,40] Junming et al. used basic catalysts (Al_2O_3, Na_2CO_3,

K_2CO_3, and others) to crack soybean oil, reporting as much as 81.3 % yield with reduced coke

yields as low as 6 %, although the chemical composition of the products was not reported.[41]

Dupain et al. studied the cracking of rapeseed oil using short residence times under fluid catalytic cracking conditions achieving short residence times nominally from 0.05 seconds to 8 seconds and in the temperature range of 480 to 585 C. They reported yields of up to 34 % in the gasoline range for rapeseed oil, but as high as 57 % for saturated stearic acid. Dupain reported rapid coke formation at about 4-5 wt. % in the first 50 ms of the reaction; remaining otherwise constant with temperature.[42] This is an illustration of how quickly catalysts can be fouled in triglyceride catalytic cracking under certain conditions. Specifically, the coke formation is very rapid initially due to the activity of the catalyst, which is quickly fouled and then no more coke results.

Katikaneni et al. used a fluidized bed to study the cracking of canola oil using various HZSM-5 catalysts, silica alumina, and others, reporting coke yields of 4-5% and high gas yields of 18 – 60 % over the temperature range of 400 – 500 C and depending on the type of catalyst to some extent.[43] Katikaneni et al. made some significant observations in another paper using various catalysts (silica-alumina, HZSM-5, and hybrid catalysts) to catalytically crack canola oil, ultimately yielding between 22 and 63 wt. % liquid products over 400 – 550 C temperatures at ambient pressure in the presence and absence of steam.[44] Katikaneni observed that higher temperatures yielded lower percentages of liquid product and also that the HZSM-5 catalyst was less coke-prone than silica-alumina catalyst in this study.

Katikaneni also reports that steam provided important benefits, including promoting dehydrogenation reactions, affecting the product specificity, and especially prolonging catalyst life through a reduction in coke deposition. The reduction in coke deposition was explained by

the competitive adsorption between coke precursors and water molecules on the acid site of the catalysts, and/or the partial gasification of coke deposits by steam. The magnitude of this observation is such that coke formation was reduced on HZSM-5 catalysts from 5 % to 0 % and on silica-alumina catalysts from 36 % to 20 % or better. This finding may be useful for future research into the catalytic cracking of TAG oils.

In general, two major obstacles to catalytic cracking of TAG oils include the deactivation of the catalyst and/or the excess formation of low value process gas. One thought is that the high activity of certain catalysts combined with the high reactivity of TAG is responsible for both obstacles. In general, catalyst deactivation by coke formation effectively reduces the yield of salable products, and the production of process gas has a similar economic effect. With the deactivation of catalyst, reactor performance problems soon result. The coupling of these problems make it difficult for catalytic cracking processes to function adequately.

I.D.3. Catalytic Hydrothermolysis

Applied Research Associates, Inc. is developing a competitive DCBP technology known as catalytic hydrothermolysis (CH), in which lipid biomass is processed under high pressure water (supercritical-range) and high temperatures with or without a dilute homogeneous catalyst. Although the CH process literature described the addition of a homogeneous catalyst to cracking, it is the interpretation of this author that the catalytic effect is negligible in comparison to the pyrolytic effect, based on examining the patent and published literature of Lixiong Li.[24,45] It appears that the high pressure/temperature reaction near the supercritical range of water is primarily responsible for the observed reactions in the CH process, with the dilute homogeneous catalyst being of minimal importance. This is further evidenced since the dilute catalyst doesn't

appear to be mentioned and/or highlighted in ARA's recently provided literature on their website. As a result, the CH process may be considered a pyrolytic renewable fuel process rather than a catalytic process.

One key difference between the CH process and aforementioned DCB processes is that a high percentage of aromatics can be directly formed with the CH process, which permits the production of fuel that very closely resembles the density and cold weather performance of petroleum derived fuels.[45] Aromatics have furthermore been shown to be superior fuel constituents for improving the cold-weather and density performance of fuels, even more so than cyclic hydrocarbons. This is a significant advantage of the CH process (which is similar to the Noncatalytic Cracking Process (NCP) developed at UND). By contrast, aromatization, isomerization, and/or blending are required for TAG hydrotreatment to achieve similar results.

Although the CH process utilizes lipid feedstock, it is noticeably different from hydrotreating due to the absence of a heterogeneous catalyst and, likewise, the absence of hydrogen gas in the primary reactor. It should be noted that the latter-stages of the CH process eliminate fuel acidity and oxygenation via catalytic deoxygenation,[24] so that DCBP meets international fuel requirements. This catalytic deoxygenation at the tail-end of the process more closely resembles hydrotreatment in that a catalyst and hydrogen are needed. The CH process has currently been commercialized to a demonstration scale using 24/7 operation and processing 100 barrels/day of TAG oil to produce drop-in compatible diesel and jet fuel.[46]

The strong effect of the high temperature water on TAG is furthermore evidenced by an earlier study performed under the USDA by Holliday et. al, where TAGs were reacted under supercritical and subcritical water to hydrolyze TAGs into free fatty acids.[47] Under subcritical

16

water and at lower temperatures (260 – 280 C), 18 – 20 min of reaction time were required for the complete hydrolysis of TAGs into fatty acids. At these lower temperatures, there appears to be less CH type reactions (e.g. cracking/aromatization). However, at higher temperatures approaching critical values (i.e., 374 C), Holliday reported a product consistent with pyrolysis oil and/or hydrothermolysis. Effectively, Holliday's study was an earlier occurrence of CH, although Holliday makes no mention of implications for renewable fuel production.

I.D.4. The Noncatalytic Cracking of Triglycerides

The catalytic hydrothermolysis of TAG described in the previous section is an evolution of TAG noncatalytic cracking (also commonly known as noncatalytic cracking, pyrolysis, mild pyrolysis, thermal degradation, etc.), one of the oldest methods of lipid conversion to DCB. Some of the first records of TAG pyrolysis are rooted in the early 1900s, producing a variety of petroleum-relevant compounds including paraffins, olefins, aromatics, and naphthalenes. It should be mentioned that literature also cited the utilization of heterogeneous and homogeneous catalysts for cracking in that era. Noncatalytic cracking proceeds through a characteristic radical mechanism in which predominantly larger molecules (e.g., TAG molecules) are broken apart into smaller (e.g., fuel appropriate) molecules under high temperatures in the absence of catalysts and in an oxygen depleted or anaerobic environment.

I.D.4.i. Triglyceride Cracking in Batch / Semi-Batch Reactors

One of the earliest appearances of TAG cracking was in the 1930s when Egloff and Morrell cracked and processed cottonseed oil to yield 71.1 wt. % distillates and 5.3 wt. % aqueous phase with the balance being coke, gas, or loss for the production of fuels; intentionally motor gasoline.[48] The cottonseed oil was cracked in a pressurized semi-batch reactor at

17

moderate pressures of 931 kPa and temperatures in the range of 445 – 485 C. During cracking,

the vapor phase was continuously removed to sustain pressure, condensing vapors in a water-

cooled condenser. Using basic fuel refinement methods, Eglaff and Morrell were ultimately able

to produce approximately 59 wt. % of fuel in the motor gasoline range consisting of 9.9 %

naphthalenes, 25.9 % aromatics, and 27.1 % unsaturates. It was also mentioned that cottonseed

oil was more costly than petroleum, preventing the profitability of such a cottonseed-oil-to-fuel

process in the US, a fact which is still noted for lipid biofuel processes in recent times.[9]

Higman et al. studied the thermal degradation of tripalmitin, tristearin, and soybean oil at

400 C in a batch, miniature distillation apparatus at ambient pressures, reporting relatively large

yields of long chain carboxylic acids when saturated feedstocks were used.[49] On the other hand,

when soybean oil was pyrolyzed, they reported greater percentages of hydrocarbons, but still

contained a substantial amount of acids.

Although Higman didn't report the overall yield of liquids, presumably due to small

volume capture limitations, Schwab et al. performed a similar study using an ASTM batch

distillation apparatus to study the cracking of soybean oil in comparison to safflower oil (high

oleic), yielding as much as 79 % distillates with slightly more than 5% residue and 10 % losses

from noncondensable gas.[50] Likewise, Schwab's results show high acidity of distillates (up to

16.1 %), with as much as 41 % alkanes and 13 % aromatics which are on par with what Higman

was reporting.

These semi-batch studies are useful for demonstrating the potential of TAG cracking, but

not for illustrating a complete process for producing DCBPs. One potential consequence of

using semi-batch reactors is the potential for coke formation as a result of accumulating (and

18

therefore concentrating) dense carbonaceous residue in the bottoms of distillation. The coke formation can be a significant challenge to refining processes, which is later demonstrated during this dissertation. Furthermore, when considering the greater efficiency of a continuous process vs. a batch process, it is attractive to consider the results of studies in which continuous TAG cracking reactors were successfully used. Furthermore, it is necessary to focus on continuous studies for yield data, primarily because the yields from semi-batch processes are not necessarily representative of the yields that can be obtained from a continuous process.

I.D.4.ii. Triglyceride Cracking in Continuous Reactors

The noncatalytic cracking of canola oil was studied by Idem et al. in a continuous, flow-style tubular reactor in the presence and absence of steam, at ambient pressure, over a variety of temperatures (400 – 500 C), and over a variety of inert supports (quartz, ceramics, and glass) in comparison to an empty reactor.[51] One key observation was that the percentage of residual oil was reduced from as much as 46 % at low temperatures with high rates of steam to as low as 0 % at high temperatures and low steam rates. Inversely, coke formation did not appear at lower temperatures and with steam, but as temperature was elevated and without steam, coke formation is present up to 4 %. Noncondensable gas formation was as low as 9.9 % and strongly dependent on steam at low temperatures, with virtually no dependence on steam at high temperatures, increasing to upwards of 75% yield of process gas.

These strong dependences of residual oil, process gas, and coke on reaction conditions are very important to process economics, implying that temperature control is extremely important. Being published in 1996, it should be mentioned that Idem's work was regarding the formation of short chain olefins (e.g. ethylene, propylene) as an economically attractive outcome,

so the elevated gas yields were favored. Interests of today tend to point towards the yield of middle distillate hydrocarbons for the refinement of drop-in compatible renewable jet fuel. Another significant observation is that they found negligible impact of the inert support in reference to an empty reactor, which is important for other studies including the work of Adebanjo et al. as follows.

Adebanjo used a similar flow style micro reactor packed with quartz chips to noncatalytically crack lard into a diesel-like fuel at atmospheric pressures and substantially elevated temperatures of 500 – 700 C.[52] Adebanjo reports a similar array of distillates and process gas, with yields of cracked TAG distillates (CTD) approaching 75% at the lowest temperature. In good agreement with Idem et al., Adebanjo reported substantially increased yield of process gas (approximately thirtyfold greater gas production by volume) as the temperatures were elevated, which can have a potentially undesirable economic effect by today's standards. Adebanjo also reported coke type products on the order of 5 – 10 wt. %.

The fraction of diesel range distillates in the CTD were approximately 30 %, remaining relatively constant with changing temperature over the range of 500 – 600 C. Nevertheless, the yield of CTD was declining over the temperature range of 500 – 600 C and furthermore from 600 – 700 C, due to the increased formation of process gas. Above 600 C, the fraction of diesel range components in the CTD dropped sharply, as did the yield of CTD as the reaction moved from cracking/pyrolysis into the temperature range of gasification.

In distilling and testing the diesel range fraction from the CTD, Adebanjo reported similar cetane index and density to that of petroleum-derived no. 2 diesel fuel. However, the viscosity and heat of combustion were above and below the diesel specification, respectively,

likely resulting from the inclusion of oxygenates in the fuel product. A potentially important inference from Adebanjo's study is that waste TAGs (e.g. lard) were used, indicating that they are potentially compatible with the noncatalyzed cracking processing pathway.

Additional studies have shown that waste TAG feedstocks can be utilized with the noncatalytic cracking process for the production of fuels, especially fuel blends according to the work of Doll et al.[53] In Doll et al.'s work, soybean oil and soapstock were cracked by a destructive distillation method and subsequently fractioned to produce a diesel range fraction of each separately. The diesel range fraction (i.e., cracked-diesel) was then blended with petroleum diesel and physical properties were assessed, including density, viscosity, and surface tension in compared to methyl ester biodiesel.

The cracked-diesel had a similar viscosity to biodiesel, both of which were higher than petroleum-derived diesel, presumably due to the inclusion of oxygenates as mentioned in the previous paragraph. Density and surface tension of the cracked-diesel more closely resembled petroleum diesel at similar purity. Blending was offered as an acceptable option for refining of fuels in this way, but based on intimate subject matter knowledge, it is the opinion of this author that deoxygenation or other refining methods will be necessary to produce fuel even via blending this way, due to the confirmed presence of carboxylic acids in the CTD from triglyceride cracking by Luo.[54]

One of the publications with TAG cracking experiments performed at larger scale in this review was a study published by Wiggers et al. [55], where soybean oil was converted at a rate of approximately 3 kg/h into CTL via fast pyrolysis at ambient pressures and approximately 10 – 37 s residence time in the temperature range of 450 – 600 C. Steam was also utilized at 0 – 10 % to

study its effect on the pyrolysis reactions. Yields of up to 92 % CTL were reported at low temperatures without steam, and the addition of steam reduced CTL yields by 4 %. At elevated temperatures, the yield of CTL was reduced to as low as 34 %, showing a dependency on steam addition.

Interestingly, carboxylic acids were cited by the study in its background section through reviewing related literature; however, Wiggers makes no other mention about oxygenates or carboxylic acids in the CTL produced from his experimentation. Based on other studies with similarly short residence times, it is presumed that carboxylic acids were present in the CTL. These may have been overlooked due to complications in the analysis of carboxylic acids. Additionally, the study makes no mention of coke formation or problems thereof.

I.D.4.iii. Summary

In examining and summarizing comparable literature for TAG noncatalytic cracking, studies have shown the dependence of yields on temperature, steam, and other factors, typically indicating that liquid yields increase as the temperature is decreased. Although residue formation has been described in a number of studies, it is not typically made clear to what extent the residue results from unreacted feedstock or from the formation of 'tar.' In general, it is observed that lower temperatures (e.g. 400 – 500 C) tend to promote the formation of distillates, whereas at higher temperatures (e.g., > 550 C), cracking reactions tend to yield excess formation of process gas, which has less value by today's standards. It also appears that TAG cracking processes are commonly being utilized for the production of DCBIs, e.g., for blending. However there are very few examples of refining the products into DCBPs that also utilize deoxygenation. (e.g., petroleum-equivalent jet fuel) through distillation, complete deoxygenation, and

fractionation to final fuel.

I.E. Triglyceride Cracking Research at the University of North Dakota

Prior to the present work, affiliated research had been conducted at the University of North Dakota (UND) under Luo et al. to study the noncatalytic cracking of soybean and canola TAG[54] and methyl esters in semi-batch reactors.[56] For methyl ester cracking in the range of 350 to 440 C, it was found that the optimal reaction temperatures were above 400 C. At those temperatures, shorter chain hydrocarbons and esters were produced through chain scission, improving the cold weather properties of biodiesel's cloud point and pour point.[56] Additionally, the cracking of TAGs vs. TAG methyl esters was compared using pressurized semi-batch reactors (i.e., pressurized destructive distillation).[54] Luo reported CTD yields from TAG cracking at up to 76 wt. %, remarking that this CTD would be suitable for fuel refinement.

I.E.1. Triglyceride Cracking Mechanistic Insights

The mechanisms and/or representative reaction sets for TAG cracking are summarized by Maher and Bressler.[57] Most scientists agree on the first step of TAG cracking to be either scission of the triglyceride ester bond to produce free fatty acids and/or scission of the ester bond to produce ketene equivalents of saturated fatty acids and acrolein. However, many of the reaction sets leave a lot to be desired in that they do not provide either (1) complete reaction sets and/or (2) the relative reaction rate data.

Kubatova et al. explained that some of the reasons for this ambiguity may stem from the variety of experimental methods, reactors, and conditions utilized to produce CTK; a lack of truly quantitative analytical methods of analyzing CTL; and the overall complexity of cracking reactions/products.[22,58] It is the opinion of the author of the present work that a variety of studies

are performed with the major emphasis being the production of fuels and/or target products (e.g., small olefins), such as the present work which emphasizes liquid fuel production. Such studies supplement the primary work with mechanistic insights, whereas truly mechanistic TAG cracking studies may take different approaches to experimentation, such as radiolabeling.

Nevertheless, cracking reactions, theory, and kinetics are discussed in Chapter III to provide a basis future continuation studies to this present work of a mechanistic nature. Recommendations are made for future coordinated experiments involving progressive simulation and experimental studies in triglyceride cracking. These could lead to better understanding of triglyceride cracking operating parameters than proposed herein. In any case, the current state of reaction mechanisms is that they lack organization, completeness, and/or kinetic data sufficient to determine optimal reaction conditions from a theoretical perspective.

Kubatova et al. have offered some mechanistic insights that differ from the TAG cracking mechanisms/reaction sets reviewed by Maher and Bressler.[57] The most commonly cited cyclic/aromatic ring formation mechanism during TAG cracking is a Diels–Alder reaction (the intermolecular cyclization of a diene and an dienophile) typically leading to the formation of six-membered rings.[57] This is potentially rooted in the anticipated presence of butadiene during cracking, which is expected in cracking of feedstocks rich in C=C bonds (e.g., TAGs) as indicated by Raseev[34] (albeit at higher temperatures). The anticipated butadiene formation is also discussed in Chapter III, Section III.F.3. However, Kubatova et al. states that up to 30 mol % of cyclic products were five membered rings, which is not consistent with the Diels–Alder reaction.[22] Kubatova suggests that an intramolecular cyclization of alkenyl radicals is the best explanation for the formation of many cyclics during TAG cracking.

24

Furthermore, Kubatova et al.[58] suggest that hydrogen is a rate-controlling step in cracking, especially based on observing differences between lower temperature TAG cracking (< 400 C) and high temperature TAG cracking (≥420 C) of data presented by Luo[54]. The hydrogen controlled reaction rate explanation indicates that at lower temperatures, the addition of hydrogen increases the production of shorter chain molecules, signifying cracking. At higher temperatures however, the cracking reaction generates hydrogen in situ, so that benefits of external hydrogen addition are not readily observed. This is also discussed herein in Chapter III, Section III.F.1.

I.E.2. The Noncatalytic Cracking Process

Based on Luo et al.'s work[54], the Noncatalytic Cracking Process (NCP) was developed at the University of North Dakota in order to convert triglyceride-based oils (TAG) into high quality renewable transportation fuels. The process is described in greater detail in Chapter II; however, for the sake of its introduction, it is briefly described here. First, the TAG is noncatalytically cracked in a reactor to produce cracked TAG (CT), which consists of CT gas (i.e., CTG) and CT liquid (i.e., CTL). The CTL is then processed by fractional distillation in order to produce (1) CT distillates (i.e., CTD) and (2) cracked TAG vacuum distillation residue (i.e., CTR). These are subsequently processed by (1) catalytic deoxygenation and (2) coking or pitching for carbon fiber production, respectively. After catalytic deoxygenation, the oxygen-free distillates are then processed by fractional distillation into their final fuel products, including naphtha (a gasoline blendstock), jet fuel, diesel fuel (no. 2), fuel oils (no. 2 and no. 4), and other products. A schematic of the process is shown in Figure 1 (see page 33).

This process has roots that are similar to the noncatalytic cracking literature described in

Section I.D.4, whereby TAG is noncatalytically cracked in the first refinement step. However, the NCP adds additional steps to fuel refinement so that DCBP can be produced (i.e., fuels that meet the specifications for petroleum-derived fuels). The catalytic deoxygenation of CTD is particularly important because it removes acidity and oxygenation, so that the final fuel products may comply with the specifications of conventional fuels (i.e., petroleum-derived fuels). The production of high quality fuels via the NCP is proven in literature published by the present author and associates (Linnen[59]), and further demonstrated through this dissertation in Section VII.D (see page 360). The majority of the literature that was reviewed lacked the catalytic deoxygenation step, so the fuel produced would be expected to have greater viscosity, elevated freeze point, and elevated acidity (among other potential fuel quality problems). Ultimately, the fuel would not be a drop-in compatible fuel product.

I.E.3. Deoxygenation of Cracked Triglyceride Distillates from Triglyceride Cracking

Deoxygenation has been studied by various authors especially as a facet of TAG hydrotreatment, which was previously described in Chapter I, Section I.D.1. One particular study by Snare et al. compared 20 different catalysts for deoxygenation in order to identify catalysts that were optimal for deoxygenation of stearic acid (as a model compound for triglyceride deoxygenation).[31] Snare compared active catalytic components such as palladium (Pd), platinum (Pt), ruthenium (Ru), iridium (Ir), osmium (Os), rhodium (Rh), nickel (Ni) and co-precipitated components such as nickel-molybdenum (NiMo) and palladium-platinum (PdPt). These catalysts were typically supported on materials such as alumina (Al_2O_3), silica (SiO_2) chromium oxide (Cr_2O_3), magnesium oxide (MgO), or activated carbon (C).

Snare et al. compared these catalysts in semi-batch reactors for deoxygenating stearic

acid, ultimately concluding that 5 wt. % palladium supported on activated carbon (Pd/C 5) was an ideal catalyst for deoxygenation. Based on this, Snare and associates continued their research using Pd/C 5 in latter publications for the hydrotreatment of TAG feedstocks and representative feedstocks.[30,60,61] For this reason, Pd/C 5 was used as a preliminary catalyst for deoxygenation of CTD in the NCP, demonstrated through the refinement of fuels by the author of the present work (Linnen[59]).

However, the high cost of palladium makes it economically unattractive and/or cost prohibitive to use palladium-based catalysts for the deoxygenation of CTD in the NCP. In examining Snare's comparison of catalysts,[31] it was evident that nickel catalysts were capable of deoxygenation, even though the extent of deoxygenation was much greater with the palladium catalyst. It was the belief of the present author that nickel should be pursued further as a deoxygenation catalyst, due to nickel's greatly reduced cost relative to palladium (about three orders of magnitude cheaper by weight). It was hypothesized in this dissertation that nickel is a suitable active component for catalyzed deoxygenation of CTD in the NCP in order to produce high quality renewable transportation fuels.

I.E.4. Coke Formation in Triglyceride Cracking Reactors

A longstanding goal of the research pertaining to the NCP was to design cracking reactors that are 'industry-ready.' Such reactors were intended to be capable of fully continuous operation without severe coke formation so that they may be readily scaled-up. However, coke formation has been found in triglyceride cracking reactors, which can result in untimely reactor shutdowns, laborious cleaning efforts, reduced liquid fuel product yield, and dangerous reactor line plugging.

In a master's thesis presented to UND, Sander designed a bench-scale cracking continuous-stirred-tank-reactor (CSTR) that was an improvement upon a predecessor reactor (i.e., a wide tubular cracking reactor), which was prone to coking and low CTL yields.[62] Nevertheless, Sander's reactor was still marked by severe coke formation, as described in the present work (see Chapter VI Section VIII.B), so improvements to the reactor were still needed.

In reviewing the literature of Idem et al., the continuous cracking of canola TAG at temperatures of 400 C did not show any signs of coke formation. However at temperatures of 500 C, coke formation was observed at up to 4 %. Adebanjo et al. showed comparable results through the continuous cracking of lard at temperatures of 500 – 700 C, which led to coke yield of 5 – 10 %.[52] (These were described previously in Chapter I, Section I.D.4.)

These studies indicated that coke formation in TAG noncatalytic cracking could be mitigated or eliminated by operating at lower temperatures. However, in the operation of the cracking CSTR at 400 C and even with design improvements that were attempted in the present work, severe coke formation still resulted (see Chapter VI, Section VIII.B). As a result, experimentation was needed to identify causes of coke formation in TAG cracking reactors in the present work. Furthermore, the second hypothesis of this dissertation was that coke formation in TAG noncatalytic cracking reactors was preventable so that reactors may be scaled up without coke formation. This involved a series of exploratory tests and the creation of a new type of tubular cracking reactor, as described in Chapter V (see Section V.B.1.ii).

I.E.5. Methodology for Compositional Analysis of Cracked Triglyceride Liquid

In order to effectively evaluate the CTL from TAG cracking, novel analytical methods were previously developed at UND by Stavova[63] for the detailed compositional analysis of CTL

using a GC–FID/MS[*] with fully comprehensive quantitation. Among other sources, the detailed

composition data provided by this method has been published in Sander[62], Luo et al.[54], and

Kubatova et al.[22,58] for cracking various TAGs and/or methyl esters under a variety of conditions.

In addition, the present work presents summary data from this method in Section VI.B and the

fully detailed composition data in Appendix A for TAG cracking in (1) batch reactors in the

present work and (2) CSTRs by Sander[62].

Some important observations were made about the detailed composition data provided by

Stavova et al.'s method when attempting to estimate the yields from the NCP based on the

detailed composition data. The compositional detail that is provided by the method is partially

dependent upon the lengthy chromatography column (100 m long) which resolves the analytes.

This lengthy column has the advantage of increased stages of separation for analytes (as

compared to shorter columns having otherwise identical method parameters). This is

advantageous because analyte quantitation in gas chromatography is typically dependent upon

the chromatographic resolution of analytes. Furthermore, the present author is unaware of any

other literature methods which can give this same level of quantitative detail on CTL.

Nevertheless, the consequence of the long chromatography column is that low volatility

analytes in the CTL are difficult to elute from the column and/or quantitatively distinguish above

the column's baseline signal (i.e., from the column's bleed). Furthermore, due to the high

compositional diversity of CTL samples, it is not possible for the chromatography column to

---

[*] GC-FID/MS signifies a gas chromatograph with two detectors connected in parallel: a flame
ionization detector and mass spectrometer.

resolve all components. Although Stavova et al.'s method quantitates an CTL sample's mass

fraction of 'non-elutables' and mass fraction of 'unresolved analytes,' more information is

desirable in order to make representative inferences about fuel refining with the NCP. This is

noted for the detailed composition data presented in this work (see Chapter VI, Section VI.B),

whereby approximately half of an CTL sample's mass is nondescript, ultimately complicating

the estimation of overall process fuel yields from such data.

As a result, methodology for CTL sample analysis was reviewed and is presented in

Chapter IV in the present work. This review led to the conception and development of a new

method for CTL characterization: high throughput compositional analysis by GC-FID/FIMS[*]

that is described in Chapter V (see Section V.B.4.ii). This method is known herein as

FIMSDIST because it is the simultaneous combination of the method of simulated distillation

(a.k.a. SimDist) by GC (e.g., ASTM D7500[64]) and field ionization mass spectrometry (FIMS).

The data provided by this method are described in Chapter VI (see Section VI.A), and some of

its analytical advantages and analytical shortcomings are discussed in Chapter VII (see Section

VIII.C).

I.E.6. Effects on and Estimations of Product Yields from the Noncatalyic Cracking Process

The development of new cracking reactors that could operate in the absence of coke

formation and new nickel-based catalysts for deoxygenation were necessary endeavors to

support the commercialization of the NCP. Nevertheless, these new developments required new

---

[*] GC-FID/FIMS signifies a gas chromatograph with two detectors connected in parallel: a flame ionization detector and field ionization mass spectrometer.

process data to estimate the yields from the process so that appropriate commercial predictions could be made. The result of this would enable future scientists to direct new research and development efforts appropriately.

Previous attempts to use data from crude analytical distillation methods and detailed compositional analysis were found to be difficult to estimate the yields from the NCP for reasons that are described in Section VIII.C (see page 412). Additionally, it was difficult to draw conclusions from data provided by more versatile analytical distillation methods (e.g., ASTM D1160[65]), which were resultantly omitted from this dissertation. It was however hypothesized that data from triglyceride cracking reactors could be used to estimate the yields from the noncatalytic cracking process and to determine the effects of various operating parameters. The FIMSDIST method was utilized in this endeavor.

CHAPTER II

THE NONCATALYTIC CRACKING PROCESS

The Noncatalytic Cracking Process (NCP) is capable of transforming triglyceride-based oils (TAG) into renewable fuels and chemicals that are virtually the same as their petroleum counterparts in performance and quality (i.e., petroleum-equivalent) through noncatalytic cracking and subsequent refinement. During noncatalytic cracking, the TAG is broken down under high temperatures and elevated pressures to yield an intermediate product that is a diverse organic mixture similar to petroleum crude (i.e., an oily black mixture suitable for fuel refinement). The cracked intermediate is refined into an array of fuels and organic products using reactive chemical transformations and nonreactive chemical separations that are likewise similar to petroleum refinement. Jet-A-1 fuel, no. 2 diesel fuel, and no. 2 fuel oil are some of the distillate fuels that can be produced by the NCP. Each of these fuel products is capable of meeting all the current fuel specifications defined by the American Society for Testing and Materials (ASTM) for petrochemical fuels. The NCP has been shown to accommodate virtually any predominantly triglyceride feedstock, such as soybean oil, palm oil, animal fat, algae oil, etc. The NCP is described in the following several sections in order to provide background knowledge and information necessary for the interpretation of data in this dissertation.

In Section II.A, the essential process subsystems are described. Then in Section II.B, the optional process subsystems are described, along with literature references that describe

32

expectations from them. After that, a process simulator is described (Section II.C) for the simulation of the NCP which can be used to determine useful process information. In the last section, II.D, economic considerations are examined for the NCP to establish prices of feedstocks, value of products, and to examine existing and trending markets in the renewable/fossil fuel industries.

II.A. Essential Process Subsystems

The NCP was devised as a multistep process comprised of five essential process subsystems: (1) TAG cracking, (2) CTL fractionation, (3) residue processing, (4) catalytic deoxygenation, and (5) fuel purification. A schematic of the NCP is shown in Figure 1, with process subsystems grouped in gray shaded regions. Each subsystem consists of multiple unit
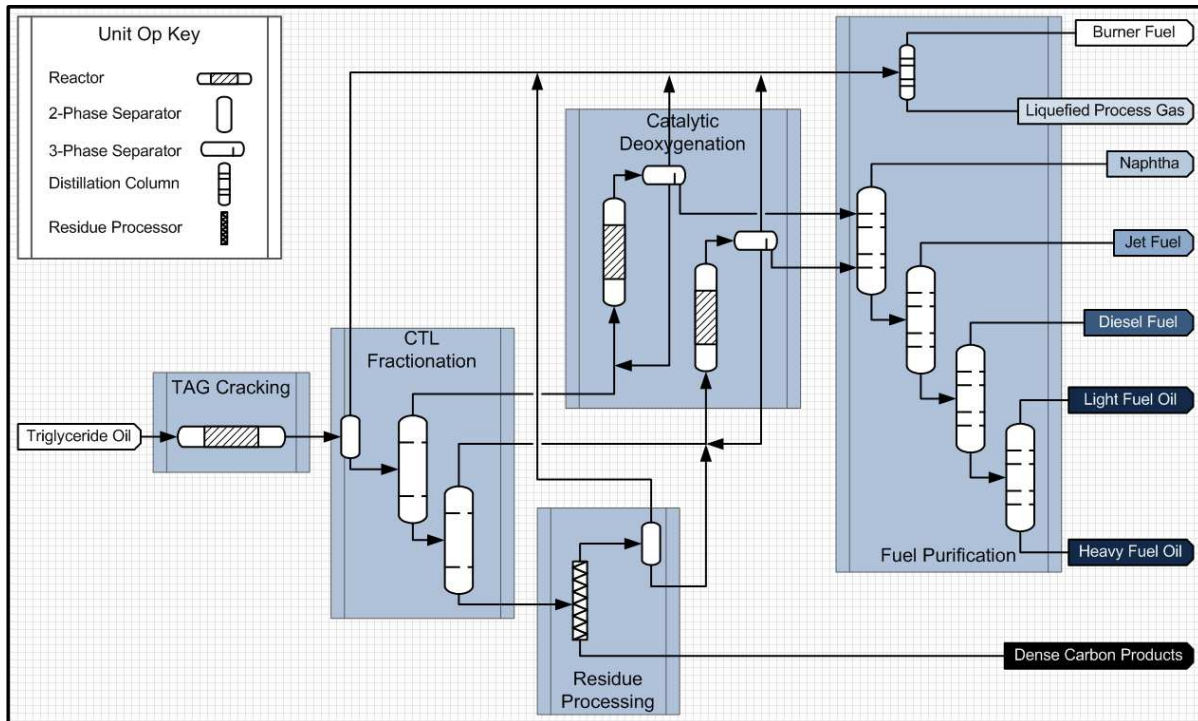
Figure 1. Noncatalytic Cracking Process (NCP) Schematic

operations (i.e., unit ops), but only the major ones are indicated in the schematic, depicted as white icons and described by the unit op key. These five subsystems are briefly described in the following subsections. In addition, there are optional process subsystems that are described in the next section of this chapter.

II.A.1. TAG Cracking

The significant unit operation in the TAG cracking subsystem is the TAG cracking reactor which converts TAG into a petroleum-like liquid called cracked TAG liquid (CTL) and to a lesser extent, cracked TAG gas (CTG). The CTL can be further refined into renewable products by the other subsystems in the NCP. TAG may be cracked under a variety of operating temperatures, pressures, and space times. Example operating ranges may be over temperature range of 380 – 550 C, pressure range of 0.1 – 5.5 MPa, and/or space time range of 0.4 – 1.3 hours. Other cracking conditions may also exist, depending on the type of equipment utilized and the desired products.

The TAG cracking subsystem is the most chemically influential subsystem in the entire process, whereby TAG is entirely transformed from the highly ordered triglyceride molecule into the relatively chaotic product which is similar to petroleum. Once brought to near ambient conditions, the cracked TAG (CT) is comprised of at least a liquid portion (CTL) and a gaseous portion (CTG). The potential for solids (coke) to form during cracking has also been observed as previously described in Section I.E.4. The TAG cracking reaction is illustrated in Figure 2, with a TAG molecule (top) being converted into CTL (below). This is intended to represent TAG cracking,
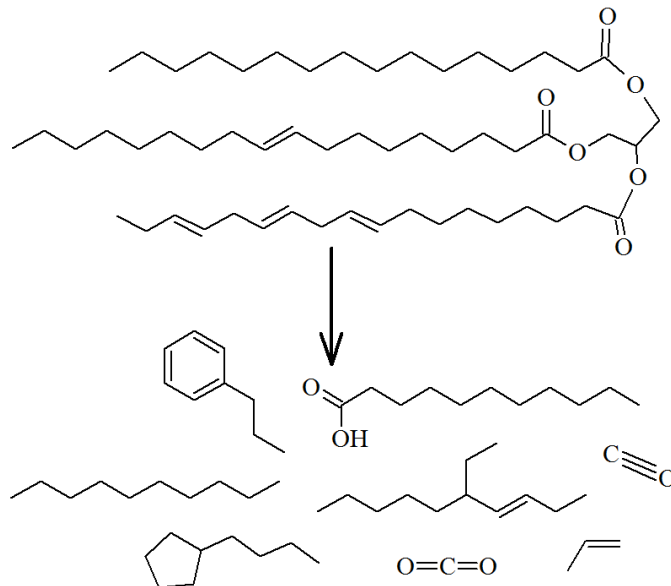
Figure 2. Representative cracking reaction(s) for triglyceride molecule

whereby, a TAG molecule is completely transformed into diverse products that are suitable for fuel production. Only some of the expected products are shown in Figure 2, whereas a virtually limitless number of product molecules are possible from cracking. As shown, the CTL is compositionally diverse, potentially having functionality such as cyclics, olefins, aromaticity, carboxyl groups, and formula isomerization, with some products exhibiting combinations of these functionalities.

II.A.2. CTL Fractionation

The CTL fractionation subsystem is a non-reactive subsystem characterized entirely by phase separations. The significant unit operations in the CTL fractionation subsystem are a flash separation vessel and two distillation towers. The flash separation vessel first separates CTG and CTL from CT. After that, CTL is fractioned to separate distillates (CTD) from distillation residue (CTR).

The final, commercial engineering design of this subsystem is subject to special ongoing considerations that are dependent upon ongoing research in the residue processing subsystem. If residue processing is capable of producing a mesophase pitch that successfully leads to high quality (continuous strand) carbon fibers, then the second distillation column should be designed to operate under a high vacuum in order to remove as much volatile material as possible before the bottoms of this distillation step are sent to residue processing. The size of the second distillation column is inversely dependent on the operating pressure, i.e., and as the operating pressure is decreased, the size increases. Therefore, a distillation column operated at 1 kPa might be assumed to have on the order of $100\times$ greater volume than a distillation column operated near ambient conditions. As a result, the performance specifications for this subsystem must be examined carefully to determine how severe a vacuum is necessary in order to form a high quality carbon fiber end product.

If on the other hand a high quality carbon fiber product cannot be successfully derived from the distillation bottoms, it may be worthwhile to consider operating the distillation columns at elevated pressure instead. The elevated pressure in the distillation column would decrease the size of the equipment and therefore decrease the upfront capital costs. In addition, re-cracking of the bottoms and/or destructive distillation should then be examined in order to improve process yields of middle distillates for fuel products. Another technology that could be considered is catalytic cracking / hydrocracking of the residue.

In either case, the heavier products generated in the fractionation subsystem have the potential to form solids when condensed using near ambient cooling water due to their elevated melting temperature, especially from long chain carboxylic acids in the CTL. As a result, the

36

condenser in the second distillation column must be operated at elevated temperatures on the order of 100 C, and cold points must be minimized.

II.A.3. Residue Processing

The major unit operation in the residue processing subsystem is the residue processing reactor, which separates dense carbon products from material that can be volatilized. Dense carbon products may be either coke or pitch. The current unit operation of the residue processing is anticipated to be a delayed coker, with coke being the dense carbon end product. However, research is ongoing that attempts to convert distillation residue into high quality (continuous strand) carbon fibers, which is a much more lucrative end product.

Previous research from the petroleum industry demonstrates that the residue from distillation can be converted into coke, which may be burned for thermal energy or utilized for electrochemistry applications as an anode support.[34] The formation of high purity coke has been investigated by Bosquez at UND and published in a master's thesis.[66] Distillation residue samples were processed in a crude residue processing furnace in order to accomplish two objectives, (1) estimate yields from commercial coking processes and (2) investigate the feasibility of heat/vacuum treatments for converting distillation residue into a pitch that can be successfully spun into long, high quality carbon fibers. A schematic of Bosquez's system is shown in Figure 40.

One of Bosquez findings was that the overall coke yield from the process tended to be on the order of 4-6 wt. %. This was found despite the conditions with which he operated the crude residue processing furnace. This makes it sensible to use Bosquez's data to estimate the coke that will be produced by TAG cracking at about 5 wt. %. The experimental methods leading to

this estimation are described in Section V.C.4.i with experimental results described in Section VII.C.

In addition to coke experimentation, Bosquez attempted to use heat/vacuum treatments to produce a pitch that could be spun into high quality (continuous strand) carbon fibers. Although he successfully converted distillation residue into a pitch that could be spun into carbon fibers, the carbon fibers that were produced were short and brittle. This potentially indicated that high quality carbon fiber production is a possibility, but obstacles to the formation of a viable carbon fiber pitch still need to be identified and overcome.

The author of the present work hypothesized that more advanced equipment may be necessary and conceived a new prototype reactor for reactive film evaporation of CTR in order to produce a viable carbon fiber pitch. The prototype reactor was designed and constructed as shown in Figure 3. This design is a substantial improvement on the crude residue processing furnace that was previously utilized.

Attempts to refine a high quality carbon fiber pitch from distillation residue are currently in progress at UND through the work of a master's thesis under the direction of Foerster. Foerster is utilizing the prototype reactor for the production of mesophase pitch from CTR. It is hoped that the research being performed by Foerster will lead to the production of an excellent quality pitch capable of being manufactured into high quality carbon fibers. A detailed description of the reactor components is described over the next few pages.

The purpose of the reactor was to sustain a very thin film of vacuum residue under high vacuum (~ 0.04 kPa) and high temperature (350 – 450 C). This was intended to concentrate the asphaltenes in the pitch by removing as much semi-volatile matter as possible, while promoting

condensation reactions in the liquid film due to the high temperature and increased concentration of asphaltenes. The film of vacuum residue fell down the sides of the reactor, and was kept as a thin film due to the high-speed rotating helical brush that wiped the reactor walls approximately 1000 RPM. The concept of the thin film being the result of high-speed rotational wiping has already been demonstrated for spinning band distillation columns, albeit for a different purpose.[67]

Vapors evolved from the falling film as it proceeded down the reaction volume, with the vapors moving upwards in counter-current fashion to the falling film. Thermal reactions also occurred, causing the film to generate light gases that also flow countercurrent to the film flow, creating additional phase separation similar to a stripping column.

At sufficiently high brush speeds, centrifugal action prevents feedstock material from occupying any volume except the thin film volume, ensuring the smallest possible film. The thin film progresses down the reaction volume (R-1), collecting at a drip cone at the base of R-1. From the pointed tip of the drip cone, a single stream of asphaltene-enriched pitch is guided to fall through a wide bore ball valve (V-2), without touching the side walls, into the base of a collection receiver (TK-2).

The reactive film evaporator was operated semi-continuously by first stabilizing the temperature/pressure at operating conditions and then initiating the feed to start a reaction.

Intended operating conditions were pressures of about 0.04 kPa, temperatures in the range of 350 – 450 C, a feed rate of 1 g/min, and brush speeds of 950 RPM. Product formation rates were determined at the end of experimentation, assuming pseudo-steady-state operation.
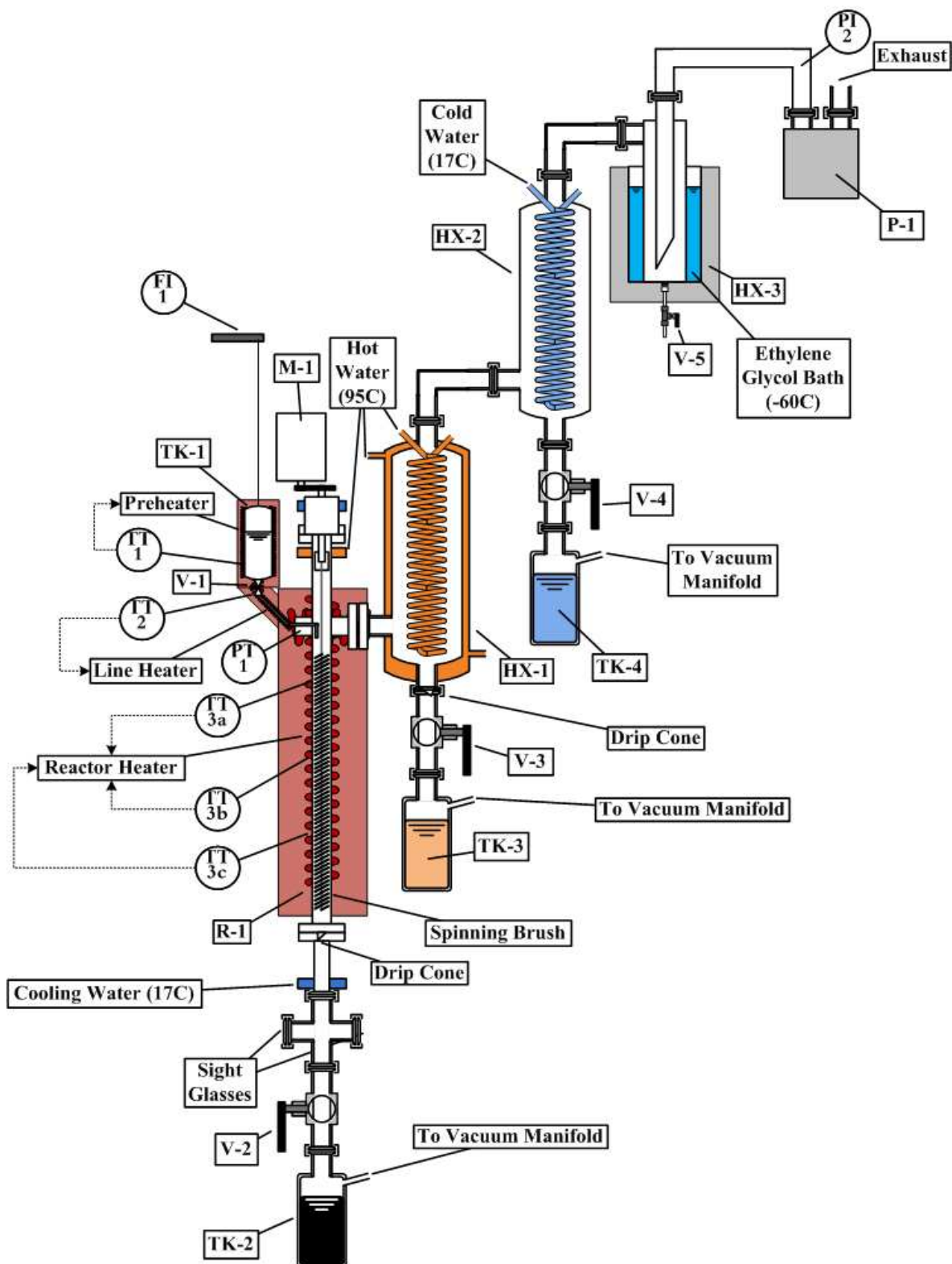
Figure 3. Reactive film evaporator for processing residue into high quality pitch

Molten distillation residue was drawn into the reaction volume (R-1) by the reactor's internal vacuum from the feedstock tank (TK-1). A load cell (FI 1) was installed above TK-1 in order to monitor the feed rate during operation. A flow control valve (V-1) was used to manually control the feed rate. It was necessary to heat all lines in contact with the feed stream to prevent freezing of the molten distillation residue. TK-1 was continually purged with nitrogen to prevent oxidation of the feed.

Temperature control was utilized for the feedstock tank (TK-1), the feed line, and R-1. Feedback temperature control utilizes TT 1, TT 2, and TT 3a-b, respectively. Pressure was maintained by an Edwards RV-8 vacuum pump (P-1). Pressure was uncontrolled, but monitored by a pressure transducer (PT 1) and a pressure indicator (PI 2).

Two sight glasses were positioned at the lower outlet of R-1 to permit visible confirmation that the pitch product stream was flowing into the pitch receiver (TK-2), being guided by a drip cone. This sight glass / drip cone configuration was important because pitch is a solid at room temperature—if the falling product stream of pitch touched the cool walls, it would solidify and form a progressive reactor plug.

The spinning brush was single-spiral, double-stem construction and made out of 304 stainless steel with 30 AWG bristles. The dimensions of the brush were 3.175 cm diameter (equal to the inner diameter of the reaction volume) and 0.76 m length. The brush was rated to a speed of approximately 2000 RPM at room temperature, but only on the order of 1000 RPM at reaction temperature. A 1000 RPM rated rotary feedthrough was coupled to the brush in order to facilitate high rotation speed without compromising vacuum integrity. A 560W motor (M-1) rated to 1750 RPM was coupled to the feedthrough using a non-slip, high torque timing belt,

with a 20:36 speed reduction ratio facilitated by timing belt pulleys. A daisy wheel was attached

to the motor's shaft with a digital tachometer (not depicted) in order to monitor the speed of the

brush.

Condensation was configured to be operated in three stages to collect distillate products

across a full range of volatility without freezing the distillates, thereby ensuring strong vacuum

and minimizing pump maintenance. Additionally, care was taken to design heat exchangers that

minimized holdup and pressure drop. The first stage heat exchanger (HX-1) was jacketed, and it

utilized 95 C water as a heat transfer fluid in order to prevent cold spots. Otherwise, cold spots

would freeze the distillate product and form a progressive reactor plug. As indicated, HX-1 also

utilized a drip cone to prevent the distillates from touching cold reactor walls before first falling

to the base of the HX-1's receiver (TK-3). The second stage heat exchanger (HX-2) used 17 C

water coils to condense much of the remaining distillates. The third stage heat exchanger (HX-3)

was a mesh-packed trap in a cryogenic bath maintained at -80 to -60 C in order to condense as

much distillate material as possible and prevent it from entering the vacuum pump (P-1).

Most reactor components were made of 304 stainless steel or better, although copper

gaskets were used at high temperature flanged connections. Additionally, two sight glasses were

installed as indicated. Otherwise the reactor was free of glass and readily breakable parts

because the contents of R-1 were processed above their autoignition temperature. As a result,

the contents of the reactor were at risk for explosion if they accidentally came in contact with

oxygen molecules. At temperatures below 100 C this was not a problem.

A LabVIEW system was used to maintain operating conditions of the system and to

record the value of various process sensors every 15 seconds during operating. The temperature

was measured at several points in the reactor to estimate the temperature profile, and the temperature and pressure of the phase-separation zone was carefully measured as well.

Preliminary testing of the unit by Foerster has shown that the system behaves as intended, pulling a strong vacuum of about 0.04 kPa during operation at 350 C temperature and 4 g/min feed rate.

II.A.4. Catalytic Deoxygenation

The cracking of TAG has been shown to produce carboxylic acids,[54] which must be removed in order for the fuel products to comply with the total acidity requirements of international fuel specifications.[26,27] This can be accomplished by a variety of means, including extraction and various reactions. Deoxygenation is used to describe a suite of reactions that are characteristic of the removal of oxygen from organic molecules (e.g., ketonization, reduction, decarboxylation/decarbonylation, etc.). The most commonly sought after reaction is decarboxylation, which may be catalyzed by a variety of metals.[31]

The major unit operations of the catalytic deoxygenation subsystem are packed bed reactors, which utilize a catalyst to transform CTD into deoxygenated CTD, which are virtually oxygen free (i.e., hydrocarbons). High quality fuel may be purified from deoxygenated CTD.

The catalytic deoxygenation subsystem had previously been based on the master's thesis work of Khambete,[68] who utilized an activated carbon supported palladium catalyst to deoxygenate CTD sufficiently to comply with the national fuel specifications for diesel fuel.[26]

Research in this dissertation aimed to utilize nickel-based catalysts to replace palladium catalysts due for catalytic deoxygenation of CTD, as described in Section VII.A. These catalysts are substantially less expensive than the palladium catalyst that was elucidated through

Khambete's work.[68]

II.A.5. Fuel Purification

Separation equipment dominates the fuel purification subsystem. As indicated in Figure 1, the subsystem consists of no less than five distillation columns, used to separate the products into several different types of fuels. These subsystems are nonreactive and are not benefitted by further explanation herein.

II.B. Optional Process Subsystems

In addition, the NCP has optional process subsystems (known as process options) that withdraw specialty products from the process which can be sold for elevated profits. Much of the optional process subsystems rely on the diverse composition of CTL, including significant concentrations of carboxylic acids and aromatics. The most important process options include carboxylic acids extraction, aromatics reformation, and aromatics extraction. The specialty chemicals that are produced from these optional systems can be used as building blocks for additional products, such as the production of ketones, esters, polymers, and other products. The optional process subsystems are briefly described in the following sections.

II.B.1. Carboxylic Acid Extraction

The cracking of TAG produces a diverse organic mixture comprised of predominantly hydrocarbons and carboxylic acids, known as cracked TAG (CT). The carboxylic acids in CT cover a wide range, including acids as small as C2 and, for some TAGs, as large as C24 or larger. Whereas the deoxygenation products of longer chain acids (C9-C24) are useful for diesel production, the short chain acids (C2-C5) are deoxygenated to gaseous molecules which have low value as fuel. Further, carboxylic acids in the range of C3-C8 have a higher commercial

value when purified into commodity chemicals than when they are deoxygenated into their fuel-equivalent hydrocarbons.

Extraction of carboxylic acids from CTD by liquid-liquid extraction (LLE) has been previously investigated at UND and presented in the literature by Braegelman et al.[69] Amines were demonstrated to be effective for bringing virtually all carboxylic acids from their nonpolar CTD phase into the polar phase of the amines. In particular, trimethylamine and dimethyl ethanolamine were very effective, having single-stage extraction efficiencies of 93 % and 100 %, respectively.

Braegelman's study forms the basis for the development of a scalable, continuous process to produce commodity fatty acid chemicals from TAGs by the NCP. Furthermore, the extraction of the carboxylic acids may be useful for future research and development into improving deoxygenation reactor performance and/or specificity or for the production of ketones (described below).

II.B.2. Catalytic Reformation

The naphtha produced by the core NCP described in this dissertation could be referred to as a "gasoline intermediate" because its octane number, like petroleum light straight run naphtha, is too low to be considered a complete fuel for internal combustion engines. One way to generate an acceptable renewable gasoline product is to feed some or all of the naphtha into a catalytic reforming unit where a series of catalytic reactors are used to convert naphtha into BTX aromatics (i.e., benzene, toluene, and xylene(s) which boost the fuel's octane rating.

Catalytic reformation involves a series of catalytic reactors that are fed a stream of low octane (paraffinic) naphtha and produce a stream right in BTX aromatics (i.e., benzene, toluene,

and xylene(s)) for use as gasoline or in manufacturing applications. Semi-regenerative catalytic reformation processes are the most common, employing multiple fixed bed reactors in series (typically three online in series and a rotating offline reactor). The use of multiple reactors is to combat the high endothermicity of the reforming reactions and to permit continuous operation even when a reactor is taken offline for catalyst regeneration, typically occurring every several months. Additionally, some catalytic reformation processes utilize continuously regenerative technology via moving bed reactors, which are more effective but have higher capital costs. Both of these processes are described in greater detail in Raseev.[34] These processes may be applied to naphtha directly without substantial research and development experimentation.

Another approach is to feed a partially purified CTL to a reforming reactor using Si-Al zeolite catalysts for the production of BTX aromatics. This concept was studied at the University of North Dakota using batch reactors by Fegade.[70] The results of this work suggest that middle chain olefins contained in the CTL are not efficiently reformed into BTX aromatics, but instead form higher order aromatics.

This work also explored the reforming of cracking reaction light ends, since these gases contain a high concentration of propylene, ethylene, and butylene. Fegade concluded that BTX aromatics were more efficiently produced from this intermediate stream than from the liquid CTL.

II.B.3. Aromatics Extraction

Whether the aromatics are formed during the cracking reaction or in a subsequent reformer, they must be separated from other compounds in order to be commercially useful. These aromatics may be extracted from their streams and purified as high octane blendstocks

and/or commodity chemicals, as described below.

According to Ahmad,[71] the purification of aromatics by distillation in petrochemical refining applications has been demonstrated to be problematic due to the formation of several azeotropes between the aromatics and aliphatics constituents which with they reside. As a result, aromatics are typically separated from aliphatics by LLE using sulfolane as the extraction agent. Aromatics form a complex with sulfolane and these complexes have a much lower volatility than the other components in the mixture. As a result, the aromatic-sulfolane mixture is readily separated out by distillation. Usually the two steps are combined in a process known as reactive distillation. Once isolated from the aliphatics, the sulfolane and aromatics are dissociated by heat and distilled, producing a nearly pure aromatics stream plus a sulfolane stream that can be recycled to the reactive distillation unit.

Aromatics extraction has been previously investigated at UND, being published by Khatibi as a master's thesis.[72] This led to the synthesis of benzene and toluene from TAG using the NCP, with purities on the order of 99.5 wt. %.

Some considerations for aromatics extraction from CTL involve carboxylic acids. If LLE is defined as a ternary system, comprised of (1) the aromatics, (2) the nonaromatic hydrocarbons, and (3) the sulfolane; then CTD could be considered a quaternary system due to the presence of carboxylic acids. It is currently not well understood how the presence of carboxylic acids will alter the phase equilibrium of the quaternary LLE system. It should be considered that carboxylic acids should be extracted first, as described above. This aspect of aromatics extraction still needs further laboratory investigation.

Additionally, the use of aromatics extraction may be important for the production of

higher quality fuels. The research emphasis of deoxygenation in this dissertation was to provide

a low cost deoxygenation catalyst substitute for palladium. Whether aromatics would be

hydrogenated by the catalyst or not was not considered during this dissertation. Future

experiments may be valuable to investigate this aspect, whereby some percentage of aromatics in

the final fuel are helpful to improve the density, freeze point, and heating value. However, it

should be mentioned that carboxylic acid extraction would potentially have additional benefits

for catalytic deoxygenation that aromatics extraction alone is unable to provide.

II.B.4. Ketonization Upgrading

The ketonization reaction occurs by joining two carboxylic acids by their carboxyl

groups, forming a ketone group through the concurrent elimination of CO_2 and H_2O.[73]

Ketonization has a lot of potential because it is an upgrading reaction, whereby small molecules

such as C1–C4 acids can be recombined to make larger molecules.

Ketonization typically takes one of two forms. The first involves reaction of carboxylic

acids with a divalent metal oxide such as magnesium oxide, forming a dicarboxylic acid salt such

as $(RCOO^-)_2Mg^+$. Afterwards, the salt is cracked using destructive distillation, in which ketones

are released as a product. The second involves the production of ketones in the bulk phase

(typically vapor phase) over a metal oxide catalyst such as SiO_2, TiO_2, or Al_2O_3 as investigated

by Glinski.[74] In order to improve the desirability of ketonization reactions for commercial

applications, condensed phase ketonization is currently a topic for ongoing research.[75]

Ketonization has been thoroughly reviewed by Pham,[73] including a variety of catalysts,

yields, mechanism, selectivities, etc., with the most potent catalysts involving cesium oxide

and/or zirconium oxide and converting ketones with up to 97 % yield. Little experimental work

has been performed in the formation of ketones using carboxylic acids from the NCP, so this is a topic for continued research and development. If successful, ketones may be readily reduced to alcohols, dehydrated to olefins, and reacted in any number of reactions to produce fuels or chemicals. Ketonization has excellent potential to improve the efficiency of the process, although laboratory experiments are needed to validate that potential for commercial systems.

II.C. Process Simulation

ChemCAD, a chemical process simulation software suite by Chemstations, Inc. (Houston, TX, USA), was used to simulate aspects of the NCP for gaining insight into the process. This was accomplished using the experimentally determined composition data from triglyceride cracking. The product composition is 'compressed' into a representative chemical composition (RCC).

It was neither possible nor practical to incorporate all possible chemical constituents of CT into the chemical composition of the SIM because of the large number of components that can occur during TAG cracking. As a result, a list of 182 components was selected to represent the expected chemical constituents in CT. This set of components is hereafter referred to as the representative chemical composition, RCC, and is shown in Appendix Q.

The RCC included a fully comprehensive range of functionally grouped organic constituents: paraffins, isoparaffins, olefins, cycloparaffins (i.e., cyclics), aromatics, and carboxylic acids. A small number of necessary additional compounds were included: water, carbon monoxide/dioxide, asphaltenes, coke, and triolein. All n-paraffins within the range C1-C36 were included, and even numbered paraffins were included from C38-C74. The remaining four functional groups included all possible constituents up to C24 and even numbered

constituents up to C30, except for a few neglected components: formic acid, cyclopropane, and cyclobutane. These were neglected because their formation was considered to be disfavored in the process. Naphthalenes and higher order aromatics were not incorporated into the RCC for the sake of simplicity.

The intention was to represent all isoparaffins in the SIM with a singly-branched formula isomer with a methyl group on the 2nd position of the main carbon chain (e.g., C10 isomer is 2-methylnonane). When a closely similar isomer was available in the component library of ChemCAD (e.g., 3-methylnonane for C10) but the desired isomer was not available, then the similar isomer was incorporated as a substitute. Cyclics followed a similar trend, with n-alkylcyclopentanes being the intended representation in the RCC, although n-alkylcyclohexanes were used as substitutes. All aromatics were represented by n-alkylbenzenes. Carboxylic acids were represented only by saturated linear carboxylic acids.

ChemCAD's library did not contain all desired components or suitable substitutes, so it was necessary to create new components to fill those database gaps. These components were created by estimating their properties using group UNIFAC contribution methods built in to ChemCAD's simulation suite. Out of the 182 components in the simulator, 72 of the components were created using UNIFAC group contribution methods (most of these were higher molecular weight components, e.g., > C20).

This required supplying at least two inherent properties, the molecular weight and the UNIFAC groups, and two physical properties, the normal boiling point and the specific gravity (at 15.6 C). Additionally, the molecular formula (inherent) and normal melt point (physical) were also supplied to the simulator for created components.

The physical properties for creating new components were obtained from the NIST online database,[76,77] the CRC Handbook by Lide,[78] and a thermophysical properties handbook by Yaws[79]. Despite these comprehensive sources, some component physical property data (specific gravity, boiling point, melting point) were still unavailable, so these were either interpolated (a total of 10 properties) or correlated to existing data based on the carbon number of the molecule (a total of 5 properties) in reference to n-paraffin data.

Other components that were created included triolein, asphaltenes, and coke. A pure stream of 'triolein' is used as a representative feedstock to replace triglycerides of varying composition. Additionally, the normal boiling point of triolein was set to 850 C so that it would be considered practically non-distillable. The properties of asphaltenes and coke were obtained from Raseev,[34] as indicated in Appendix Q.

The thermodynamic package included using the UNIFAC model for the global K values model. The global enthalpy model was the latent heat model. Other parameters utilized were set to ChemCAD defaults.

II.D. Process Economic Considerations

II.D.1. Price of TAG Feedstocks

The price of various TAGs for their presumed suitability as feedstocks for the NCP were obtained from the USDA Economic Research Service.[80] A variety of TAGs were considered, but expensive and/or low production volume TAGs were neglected from the figures so as not to obscure the more relevant TAGs that have reasonable cost and availability. Some of the TAGs that have available data but were not tabulated include castor oil, peanut oil, tung oil, and sunflower oil. Coconut oil data was included due to its application for island economies that

51

lack a liquid fossil fuel source. Data were not readily available for volume/price of camelina oil,

brassica oil, or novelty oils.
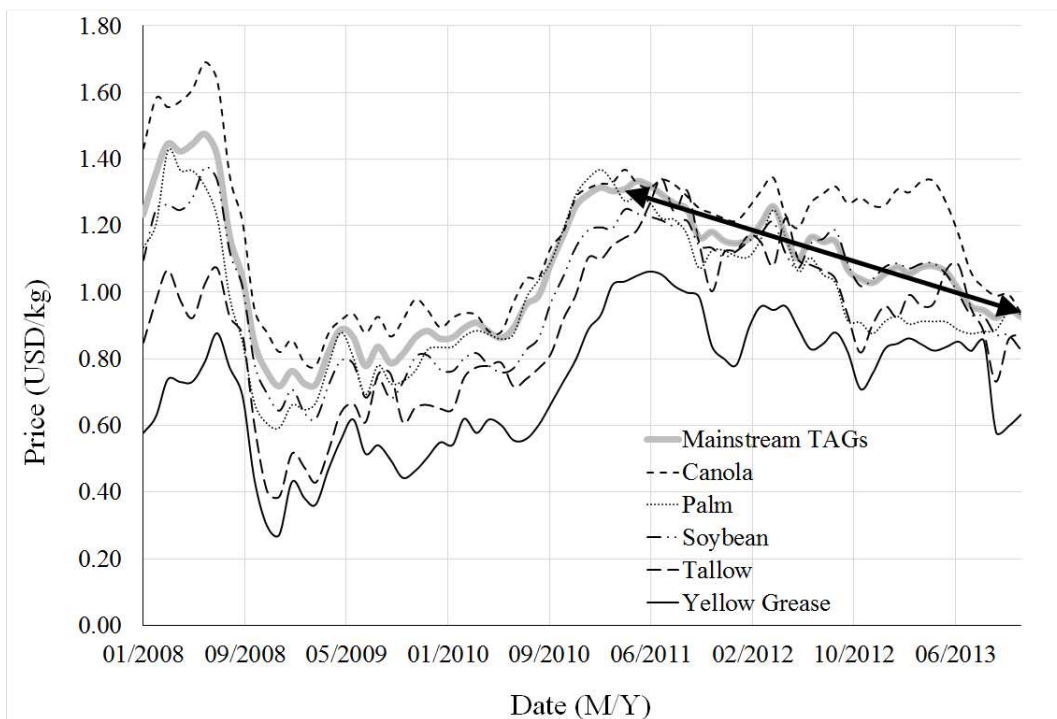
Figure 4. Price of triglycerides vs. time

The price of TAGs has been plotted over the past five years in Figure 4 for five TAG

feedstocks. This includes three dominant TAGs which make up for over ¾ of the world's total

commercial TAG production: palm oil, soybean oil, and canola oil. The weighted average price

of those three dominant TAGs represents the mainstream price of TAG mass, and it has been

plotted by a thick gray line in the figure. The price of various other TAGs can be evaluated with

respect to the mainstream price of TAG mass.

A linear regression was performed on the mainstream price of TAG mass from July 2011

to present, shown by the thick black line terminated by arrows. This reveals that the mainstream TAG price has been decreasing annually by approximately 14 USC/kg, and evaluated at July 2014, the current mainstream price is 0.93 USD/kg. This will inevitably level out or change dramatically in the coming years, since it cannot continue to decrease in price by 14 USC/kg annually, indefinitely.

Over time, the price of TAGs tends to rise and fall with the economy and/or supply in respect to demand trends. For example, canola oil was as costly as 1.70 USD per kg in early 2008, dropping to half that a year later. Despite these market fluctuations, TAG prices relative to each other tend to be somewhat consistent. This is easily noticeable from the figure and the mainstream price of TAGs, where most of the oils tend to follow a co-correlated trend.

It follows then, that although the price of TAGs may vary substantially with time, their relation to the mainstream TAG mass price will be relatively uniform. Relative price percentages (RPPs) have thus been computed for all of the TAGs and averaged over 5 years. Then the anticipated price of the TAGs was computed using RPPs to adjust from the linear trend of the mainstream TAG mass price, evaluated for July 2014. These prices and RPPs are plotted below in Figure 5, which are used for converting between fuel cuts and economic value in this study. This method of estimation gives an approximation of the price with smaller standard errors than a simple 2 year average or similar price estimation method.

The RPPs are more reliable and informative than the prices themselves. For example, sunflower seed oil can be expected to cost 51% more cost than soybean oil. Yellow grease and inedible corn oil can be expected to cost 23% less. These RPPs may be expected to extrapolate relatively well, whereas the price/time of the oil will extrapolate more poorly. Most of the TAG

feedstocks that were considered are within +/- 10% cost.
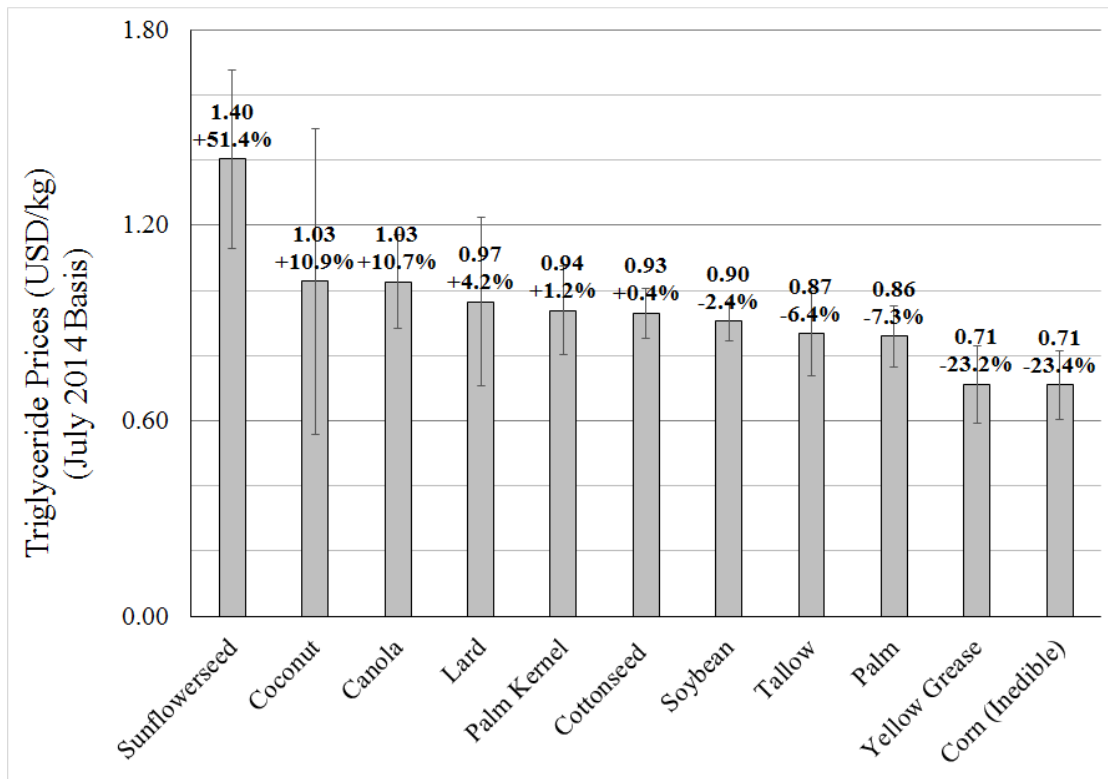
Figure 5. Anticipated prices and relative price percentages for triglyceride feedstocks

Yellow grease and inedible corn oil from ethanol milling are substantially low cost oils which are most suitable for fuel production. Yellow grease can refer to a number of different kinds of waste oils/fats. Often it refers to waste, used, or recycled TAG from businesses and industries that utilize TAG for cooking. It can also be a low quality animal fat (tallow, lard, chicken fat, etc.) or a blend of these. The primary utilization of these is in industries involving soap, cosmetics, clothes, rubber, and detergents.

II.D.2. Price of Fuel Products

US spot prices for significant fossil fuels have been obtained from the US Energy Information Agency (EIA)[81] and plotted vs. time in Figure 6. A composite average of liquid fuel prices, hereafter referred to as the mainstream price of liquid fossil fuel mass, was plotted from the weighted average price of each fossil fuel over the past five years[*] obtained from the US EIA.[82] Natural gas futures prices were also obtained from the US EIA and plotted on the secondary (gaseous) ordinate axis. All fuel prices were adjusted from a volume-basis to mass-based pricing using the density of the fuels at standard conditions and an assumed 54 MJ/kg heating value of natural gas. The densities of fuels were based upon the ASTM standard specifications previously cited for the fuel products. In Figure 6, propane is considered a liquid fuel since it is readily liquefiable under mild pressures. As a result, it is plotted on the primary (liquid) ordinate axis with the other liquid fuels. The dual-axis configuration is supplied in order to obviate the trend between the gaseous and liquid fuels.

In examining the prices of the fuels over the past several years, it is evident that most liquid fossil fuels have similar wholesale prices in proximity to the mainstream liquid fossil fuel price, being on the order of 1.00 USD/kg for the past 3 years, trending slightly downward. The trend of the mainstream price is shown by a thick, black linear trend line marked by arrows on its termini, with a yearly price decline rate of approximately 2 USC/kg. The price of natural gas has also remained relatively steady in the range of 0.020 USD/kg over the past few years, declining

[*] Weighting of each fuel: propane (4%), gasoline (55%), jet fuel (10%), diesel (26%) and fuel oils (5%), described by Figure 8 elsewhere.

slightly. A trend line is similarly shown for natural gas with a yearly price decline of
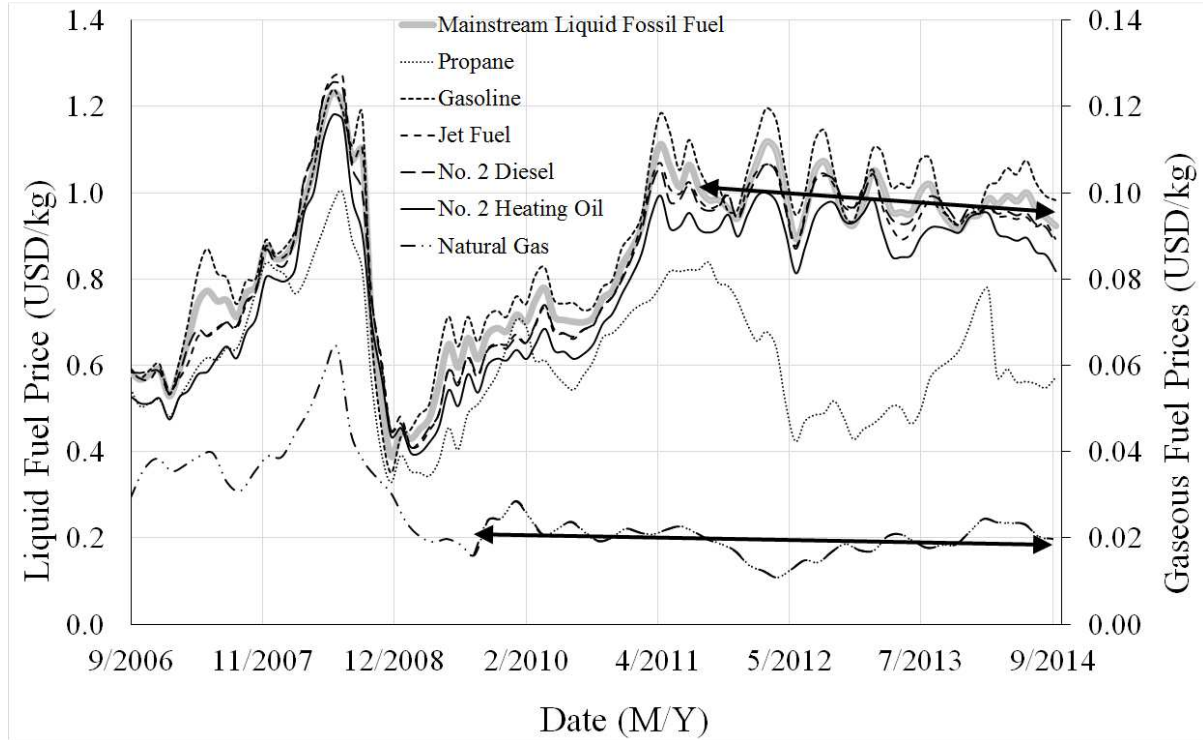
Figure 6. Price of fossil fuels over several years

approximately 0.05 USC/kg. Natural gas (methane) has dramatically lower value on a mass

basis than the other fuels, by more than an order of magnitude, probably the result of a very

different supply/demand ratio. This is especially reflected by natural gas having a separate

ordinate axis on the graph from the liquid fuels.

From late 2006 to late 2008, it can be seen that the liquid and gaseous fuel prices

increased steadily by a factor of two until reaching prices of almost 1.30 USD/kg for liquids,

until the fuel prices dropped sharply (to under 0.30 USD/kg liquids) in late 2008 due to

economic recession. Over the next 2.5 years following, the prices for non-propane liquid fuels

increased steadily to approximately 1.00 USD/kg, where they tended to remain for the following

56

3 years. On the other hand, the price of natural gas stayed in the range of 0.020 USD/kg since

that time. At the same time, the price of liquid propane has diverged from the other liquid fuels,

but it remains still approximately twentyfold higher than the price of methane by mass.

In like manner to TAG prices, the prices of liquid fuels were interpreted using relative

price percentages (RPPs), evaluated over 3 years with respect to the trending mainstream fossil

fuel mass price. The prices were evaluated for the date of July 2014 and provided in Figure 7

with error bars and RPPs. Since the price of propane is diverging from the trend of the other

fuels, there is less confidence in the price and/or RPP of propane than for other liquid fuels,

reflected by large error bars. The RPP is especially informative about the nature of the fuels

being produced, whereas the fuel price may vary with time, the RPP will presumably vary less.
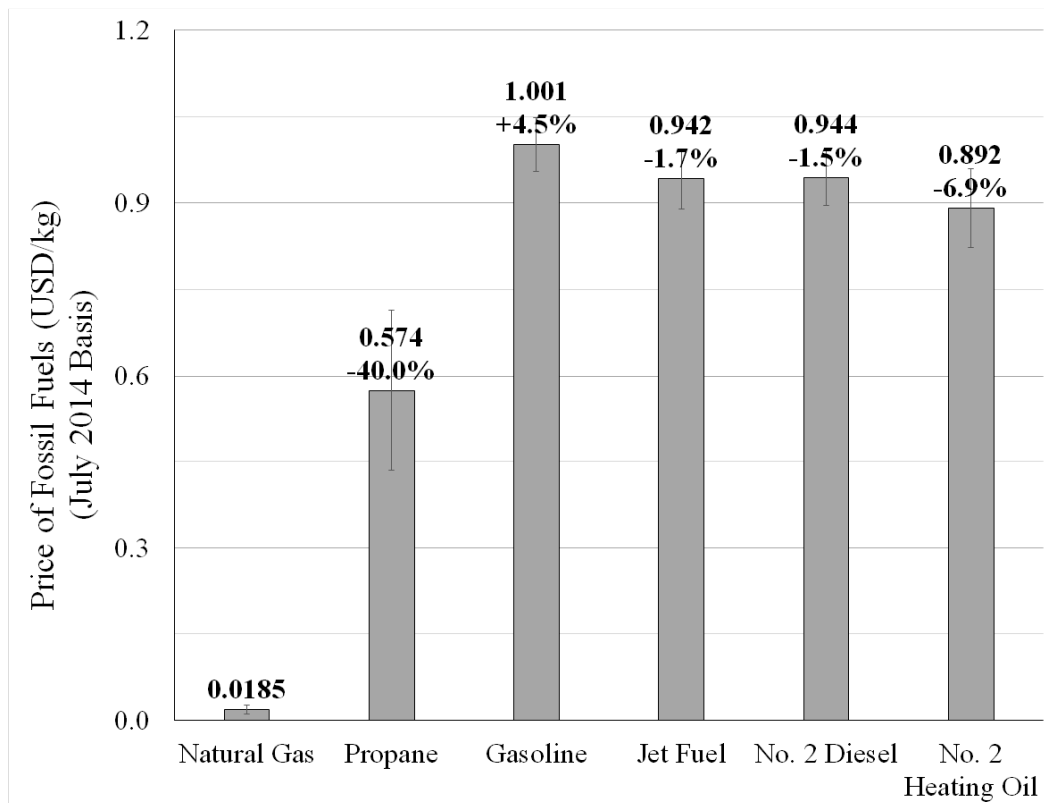
Figure 7. Anticipated prices and relative price percentages for fossil fuels

The supply of natural gas and supply of petroleum are not necessarily codependent, so that the natural gas has no RPP, nor should it be evaluated with respect to the mainstream fossil fuel mass price, but rather is calculated on its own. An important calculation is also the 3.68 USD/GJ heating price of natural gas, which can be used for determining the value of a variety of burner fuels having various compositions. As previously mentioned, the price of natural gas has been declining gradually from its indicated price by approximately 0.05 USC/kg.

Other than methane being obviously low value, and propane being relatively low value with considerable price variation, the remainder of the fossil fuel prices are fairly uniform. This is also true when comparing fossil fuels to TAG. There is a slight correlation between price and lightness of liquid fuel, whereby gasoline is the most expensive, followed by jet fuel, then diesel, and ending with fuel oil at least 10% less valuable than gasoline by mass. As a result, the lighter transportation fuels (excluding propane and LPG) should be considered target fuels for biofuel processes such as the NCP.

II.D.3. Demand of Fossil Fuels and Availability of TAG Feedstocks

The total U.S. sales of fossil fuels by type were obtained from the U.S. Energy Information Administration.[82] They were averaged over the past five years (beginning August 1st, 2009) and presented in Figure 8. In order to simplify the figure, some data consolidations were performed. First, the bar representing jet fuel was summed to include all sales of Jet-A-1, Jet-B, no. 1 diesel/distillate, and kerosene (non-jet) fuels. Second, the residual fuel oil was summed to incorporate no. 4 distillate fuel oil as well. Finally, data was transformed from a volume basis to a mass basis using the densities of the fuels from the ASTM standard specifications of the fuels.

These consolidations provide a most-clear representation of the volume of liquid fossil fuels being utilized in the US. Although data from other countries were not included, the US petroleum consumption relative to the rest of the world has been in minor decline from approximately 23% to 21% over the past five years.[83] As such, the world utilization of these fuels could be estimated at 4 to 5 times greater, neglecting deviations caused by petrochemical use for non-fuel production.

Motor gasoline makes up for more than half the petrochemical sales in the US. As such, it is sensible to assume that reformation and alkylation processes will be important for lipid-
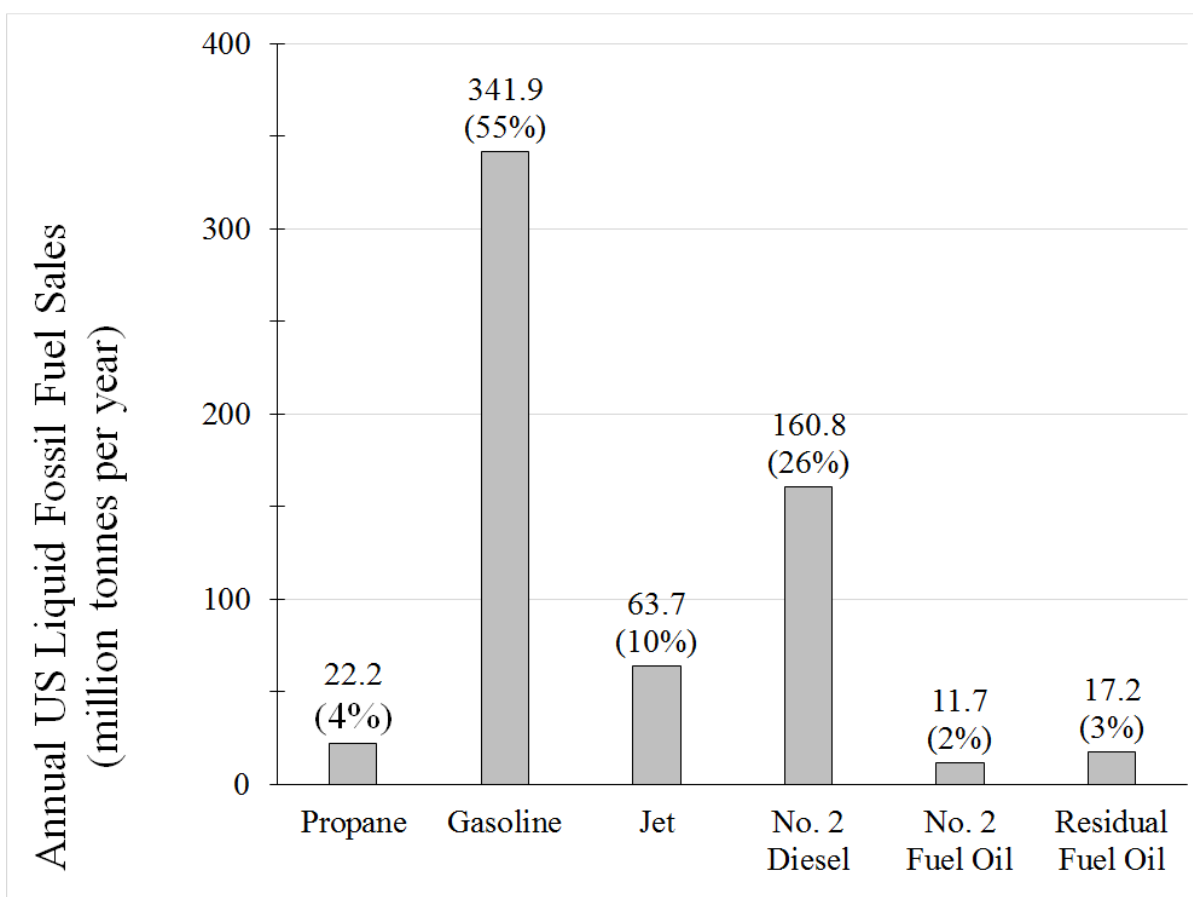
Figure 8. Average annual US sales of liquid fossil fuels over the past five years

based biofuel processes to compete in the fossil fuel environment for which they are intended to supplement. Distillate fuel oil (no. 2) and residual fuel oil only account for approximately 5% of the total fuel sales, so the volume of low volatility fuel that is produced by the NCP must also be considered.

The commercial availability of various TAGs that could be utilized as feedstocks in the NCP are shown in Figure 9, having been obtained from the USDA Economic Research Service.[80] Out of these 150 million tonnes per year, over ¾ of the production can be accounted for in palm oil, soybean oil, and rapeseed (i.e., canola) oil.
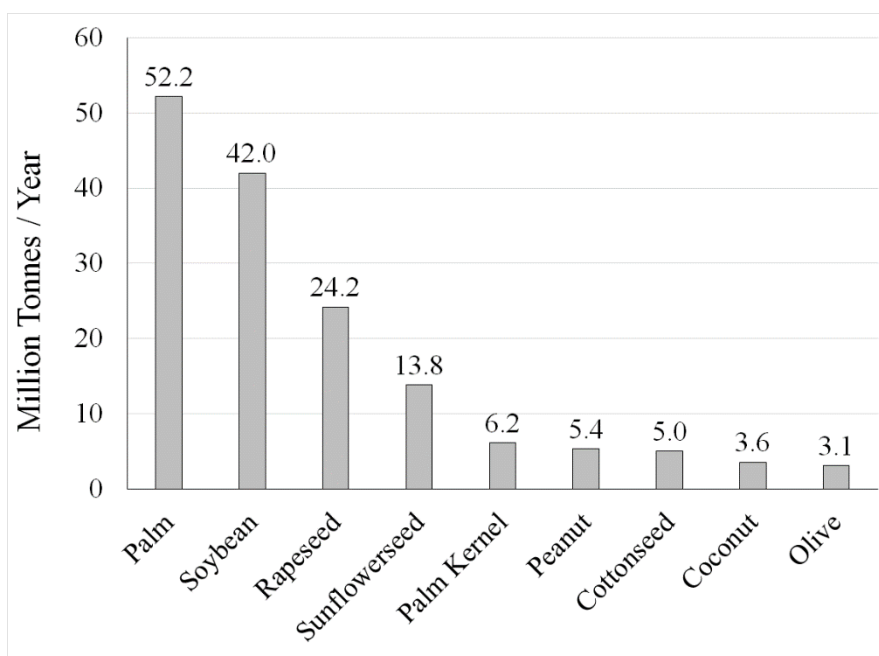
Figure 9. Commercial availability of various triglyceride feedstocks

Some important observations must be mentioned from observing the supplies of fossil fuels and TAGs. The total global availability of TAG is on the order of slightly over 150 million

tonnes per year, and it has increased steadily by 20% over the last five years.[80] Although the total world petroleum consumption has only increased by 7% over the same time frame, it can be estimated at approximately 3 billion tonnes per year.[83] The order of magnitude difference explains the role of biofuel production processes to supplement and stabilize the consumption of petroleum, not to supplant it. The current supply/demand makes it improbable that TAG to fuel processes will be able to eliminate the demand on fossil fuels, only mitigate it.

Considering the large volume of soybean oil, palm oil, and canola oil, it might be suggested that biofuel processes such as the NCP will be restricted to the oil compositions provided by these dominant oils. As a result, biofuels processes might be expected to tailor the operating conditions to best accommodate the composition of these oils. However, there is ongoing development of new mutant strains of these seed crops and other seed crops, yielding product oils that are sometimes referred to as novelty oils. The composition of the novelty oils can differ greatly from the native strain of the seed crop. As a result, it is most sensible to correlate the products of the NCP process to the oil composition instead of concentrating on a few compositions, so that the process is flexible enough to accommodate a variety of oils rather than just a few. The continuing development of novelty oils may make it possible to have the seed crops accommodate the NCP, rather than the reverse.

CHAPTER III

NONCATALYTIC CRACKING REACTION THEORY AND MECHANISMS

Noncatalytic cracking is the spontaneous high-temperature tendency for bonds in a molecule to disassociate homolytically, breaking apart the molecule into two radicals that start a chain reaction. Once initiated, the radicals propagate through the reaction system, facilitating radical reactions until each of the radicals are eventually combined with a secondary radical, terminating the chain reaction. During cracking, the larger feedstock molecules are predominantly broken down into smaller molecules that are more suitable for fuels, oils, lubricants, etc., as represented by triglyceride cracking in Figure 2.

In an earlier era, noncatalytic cracking was utilized by the petroleum industry in the refinement of fuels and chemical products. Nowadays, it is rarely if ever used, being displaced by catalytic cracking technologies.[34] This stems from the adoption of more specialized technologies, especially fluid catalytic cracking. For the production of petroleum middle distillates (e.g., naphtha, jet fuel), fluid catalytic cracking has more favorable reaction speeds, yields, and specificity.

In contrast, the application of catalytic cracking to triglycerides has been relatively problematic due to the rapid formation of coke on catalyst surfaces, an issue that was described previously in Section I.D.2. In general, triglycerides have a high degree of order, thermal reactivity, and frequency of functional groups when compared to raw petroleum.[11] As a result,

noncatalytic cracking and triglycerides may tend to complement each other, offering good reaction predictability, selectivity, and speed; despite the absence of a catalyst.

Some of the remaining noncatalytic cracking technologies in the petroleum industry involve low carbon number olefin production from ethane/propane cracking (e.g., ethylene and propylene) and visbreaking.[34] In this chapter, the discussion focuses on cracking for small olefin production, in which the feedstocks are often completely characterized, with the identity and percentage of all chemical constituents. On the other hand, feedstocks for visbreaking are often highly complex and their composition is relatively nondescript. Visbreaking is consequently less benefitted by theory and less translatable to triglyceride cracking, so this chapter avoids the discussion of visbreaking almost entirely. Quite advantageously, the composition of triglyceride feedstocks is well known, enabling the efficient use of noncatalytic cracking theory for making inferences about specificity.

 The following sections describe the theory of noncatalytic cracking reactions in order to illustrate expectations of triglyceride cracking. Most of the theory has evolved from noncatalytic cracking in the petroleum industry, though it can still be applied in a similar manner. These sections are heavily based upon the text *Thermal and Catalytic Processes in Petroleum Refinement* by Serge Raseev,[34] which offers additional technical information and resources for defining the nature of cracking reactions. The methods and resources presented by Raseev have been adapted herein for characterizing the cracking of triglyceride feedstocks.

The cracking reaction set is classified into three major types of radical reactions: *initiation, propagation,* and *termination*. Radical initiation is the spontaneous homolytic bond disassociation under high temperature to form two radicals. Radical propagation is a reaction in

which a radical changes state molecularly. Radical termination is where two radicals meet and form a stable non-radical, typically of lower energy. In addition to radical reactions, some 'non-radical' reactions occur in tandem during cracking that can have an effect on the product yields, but these are not emphasized in this chapter.

III.A. Reaction Kinetics and Bond Energy in Noncatalytic Cracking

According to McMurry,[84] one of the primary obstacles to theoretically predicting the behavior of a molecule is understanding the nature of its chemical bonds. If that is true, then a bond's energy (i.e., dissociation energy) is one of the most important factors for determining its reactivity. This is especially true for noncatalytic cracking, where low energy bonds are potent sites for chain scission by cracking.[34] The following discussion examines cracking reactions with respect to bond energy in order to establish fundamental information that may elucidate the nature of triglyceride cracking-relevant phenomena in later sections.

The dissociation of bonds at the chemical level is indicated by Equation 1, in which a molecule R_1R_2 spontaneously undergoes homolytic bond scission into radical intermediates under high temperatures. The quantity of energy required to separate the molecule between R_1 and R_2 is the bond dissociation energy, E_D. The energy is typically quantified by terms of energy per quantity of bonds (kJ/mol).

$$R_1 : R_2 \quad \xleftrightarrow{E_D} \quad R_1 \cdot \; + \; \cdot R_2 \qquad\qquad (1)$$

Accurate bond energies are typically determined in stringently controlled experiments, while varying the temperature and correlating bond energy from the product formation rates, or other methods such as those described in greater detail by Blanksby.[85] The calculation of the

bond energy by experiment is based upon the dissociation energy being equal to the enthalpy of reaction (ΔH_R), which is equal to the difference between the activation energy of the forward and reverse reactions. It should also be noted that for irreversible reactions, such as bond scissioning, the activation energy of the reverse reaction is equal to zero.[34] The mathematical relation between these energies is described by Equation 2. Following the same logic, radical termination reactions have activation energy equal to zero and, therefore, are only dependent on the radical concentration(s) and the pre-exponential rate constant associated with each termination reaction.

$$E_D \;=\; \Delta H_{rxn} \;=\; E_{forward} - E_{reverse} \;=\; E_{forward} - 0 \;=\; E_{forward} \qquad (2)$$

It should be mentioned that the bond dissociation energy is equal to the bond enthalpy solved at 0 K. In some instances, bond enthalpy refers to the bond energy at 298 K. These two are related by a heat capacity correction, not described herein. Furthermore, they are usually within 12 kJ/mol of each other and consequentially they are sometimes assumed to be numerically equivalent. In this case where reaction kinetics are examined, it is recommended to know the exact bond energy.[85]

In order to illustrate cracking, the molecule $R_1R_2R_3$ in Equation 3 is considered. In this case, all but two initiation reactions are neglected, representing a molecule with only 2 low-energy bonds that are being cracked at relatively low temperatures. $R_1R_2R_3$ will then predictably split between either R_1–R_2 or between R_2–R_3, shown by the two reactions below.

$$R_1\!:\!R_2\!:\!R_3 \quad \xleftrightarrow{\;E_D\;} \quad R_1\cdot \;+\; \cdot R_2\!:\!R_3 \qquad\qquad (3.a)$$

$$R_1\!:\!R_2\!:\!R_3 \quad \xleftrightarrow{\;E_D\;} \quad R_1\!:\!R_2\cdot \;+\; \cdot R_3 \qquad\qquad (3.b)$$
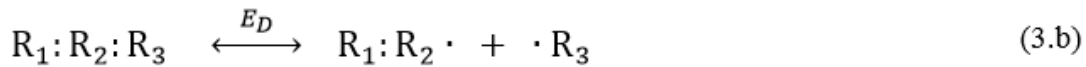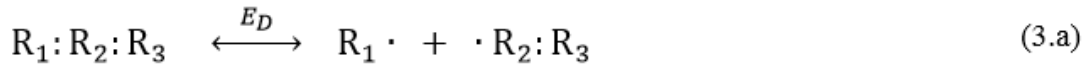
In reference to Equation 3, an energy diagram is shown in Figure 10. This energy diagram is consistent with the dissociation energy of bond R_1–R_2 being smaller than that of R_2–R_3. Therefore, dissociation of bond R_1–R_2 (denoted by Equation 3.a) will be relatively dominant with respect to scission of the other bond (Equation 3.b). These qualitative inferences help predict the preference/location of bond scission during the initiation of cracking.
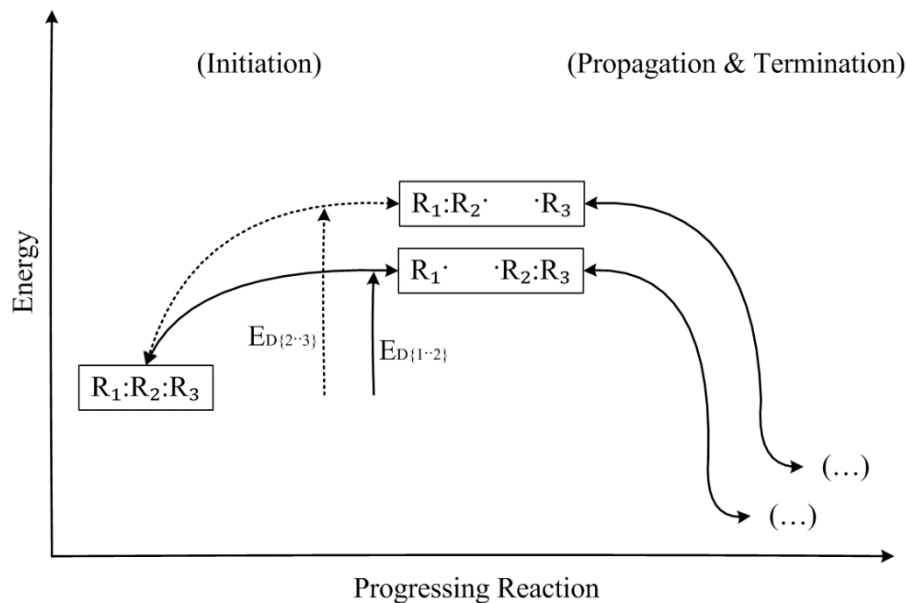
Figure 10. Energy diagram of competing initiation reactors for noncatalytic cracking

Relative rates of reaction are estimated to make quantitative inferences about preferential bond scissioning during initiation. The rate of initiation reaction follows the Arrhenius equation,

shown in Equation 4. The Arrhenius equation utilizes the temperature, T, in Kelvin; the pre-exponential constant, A, in units of s^{-1}; the gas constant, R, which is equal to 8.31×10^{-3} kJ·mol^{-1}·K^{-1}; and the activation energy, E_D, in kJ·mol^{-1} as follows.

$$r_{init} \;=\; A \cdot e^{\frac{-E_D}{R \cdot T}} \cdot C_{R_1 R_2 R_3} \tag{3}$$

Therefore the relative rate of Equation 3.a to Equation 3.b from above is equal to the quotient of the two reaction rates, shown below in Equation 5. In many cases, pre-exponential constants $A_{2.a}$ and $A_{2.b}$ are not readily available, but often they are of the same reaction order. So each constant may be approximated by 10^{16} (s^{-1}) according to Raseev[34], and they drop out of the relative rate expression. With experimental observation, A is typically on the order of 10^{15} to 10^{17}, with the majority of values towards the median 10^{16} (s^{-1}).[34] For smaller molecules (e.g., < C_5) the pre-exponential constants are typically more available, than for larger molecules.

$$\frac{r_{2.a}}{r_{2.b}} \;=\; \frac{A_{2.a}}{A_{2.b}} \cdot e^{-\left(\frac{E_{D,2.a} - E_{D,2.b}}{R \cdot T}\right)} \;\approx\; e^{-\left(\frac{E_{D,2.a} - E_{D,2.b}}{R \cdot T}\right)} \tag{4}$$

Expanding on these theories presented above, a summation of all reactions in a cracking system can be used in order to estimate the probability that a certain bond scission reaction will occur.

$$\sum_{r=1}^{n} r \;=\; r_1 + r_2 + \cdots + r_n = A \cdot \sum_{D=1}^{n} e^{-\left(\frac{E_D}{R \cdot T}\right)} \cdot C_{R_1 R_2 R_3} \tag{5}$$

The summation of all reactions for a single feedstock molecule system is shown in

Equation 6 above. By taking the quotient of a particular reaction, x, and the summation of all

reactions (1 through n), the probability of reaction x occurring can be estimated, shown in

Equation 7. It should be mentioned that methods have been developed for the estimation of bond

energies[86] which are becoming increasingly accurate with the availability of reliable

thermodynamic data.[85] This is helpful when comparing the relative rates of initiation reactions.

$$P_x = \frac{e^{-\left(\frac{E_x}{R \cdot T}\right)}}{\sum_{D=1}^{n} e^{-\left(\frac{E_D}{R \cdot T}\right)}} \tag{6}$$

It should be reiterated that this simplification suffices only when the pre-exponential

constants are of the same order of magnitude, as previously described. This assumption is useful

for making inferences when experimental data are unavailable and/or difficult to obtain

experimentally. Having complete kinetic data (with pre-exponential constants) is important to

improve the accuracy of these calculations.

III.B. Cracking Initiation Reactions – Bond Dissociation Energies

From a theoretical perspective, knowing the bond dissociation energies of a molecule is

potentially important to predicting noncatalytic cracking behavior. Therefore, triglyceride

molecule bond energies could be studied in an attempt to predict the products of triglyceride

cracking. Unfortunately, it is challenging to measure the bond energies of a TAG molecule due

to the molecule's significantly high number of bonds per molecule. A more feasible estimation

for the bond dissociation energy of a triglyceride can be readily obtained through determining the

bond energies of model compounds, which are generally smaller and more simply studied.

The bond dissociation energies for various representative molecules have been previously

studied by a number of scientists and compiled in a thorough text by Raseev.[34] All energies

reproduced herein may be assumed to originate from Raseev, and they are tabulated herein to

aide in the discussion and elucidation of bond energy trends. Trends from these small,

representative molecules are utilized to describe the bond energy of larger and/or more

complicated molecules such as TAG molecules in later sections.

III.B.1. Bond Dissociation Energies for Non-Functionalized Bonds

The bond dissociation energies for C–C and C–H bonds that are not in proximity to

functional groups (oxygenates and double bonds) are shown in Figure 11. These C-C and C-H

bonds are classified as *non-functionalized bonds* since they lack nearby functional groups on the

parent molecule. Non-functionalized bond energies are portrayed first because they establish the

baseline bond energies by which to compare the bond energies that are not isolated. In observing

these bond energies, they are typically all fairly high with energies greater than 300 kJ/mol.

Three trends are apparent in non-functionalized bond dissociation energies. First, the

bond energy of C–H bonds is on the order of at least 60 kJ/mol greater than C–C bonds. This

implies that the initiation step of chain scission (i.e., cracking) in molecules without

functionalization is more likely to be the separation of C–C producing two carbon containing

radicals rather than the separation of C–H to produce (in part) an atomic hydrogen radical.

Secondly, increasing chain length decreases the bond dissociation energy. Thirdly, chain

scission preferentially forms longer fragments, fragmenting towards the center of a hydrocarbon

chain rather than at a terminus.
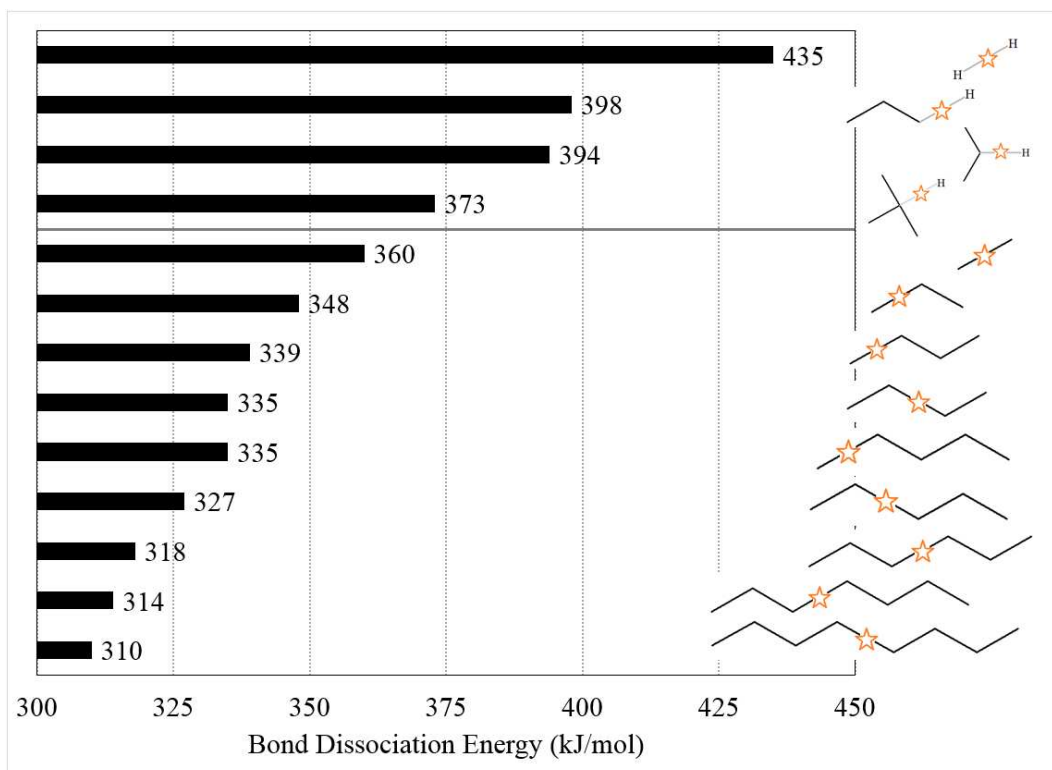
Figure 11. Bond dissociation energies for model paraffin compounds

Through observing the very high bond dissociation energy for H_2, it can be concluded that hydrogen molecule dissociation is unfavorable compared to C-C and C-H bond dissociation. Nevertheless, the addition of hydrogen to ethylene cracking reactors has been shown to increase reaction speed as the hydrogen is assumed to facilitate propagation reactions.

Based on the high dissociation energy of molecular hydrogen, it might also be considered that any two hydrogen radicals which do form and come into contact with each other will terminate to form H_2. This is not the case.[34] For two atomic hydrogen radicals to successfully form H_2, there must be a third participating molecule or surface to absorb the excess energy from the union of the two radicals. This ternary contact is rarely observed, such that radical

70

termination is typical a result of (1) a hydrogen radical colliding with another radical that is

capable of absorbing the hydrogen radical's excess energy, or (2) the hydrogen radical colliding

with a non-radical and propagating the reaction via a radical substitution reaction.

III.B.2. Bond Dissociation Energies in Proximity to C=C Bonds

In comparing the bond energies of C–C and C–H for small paraffins vs. small olefins, the

bond energies are potentially much lower in proximity to C=C bonds rather than in isolation.

This can be seen by comparing Figure 11 (above) to Figure 12 (below), in which bond

dissociation energies appear as low as 176 kJ/mol in proximity to C=C bonds. This implies that

a large molecule containing C=C bonds will preferentially initiate cracking in the vicinity of the
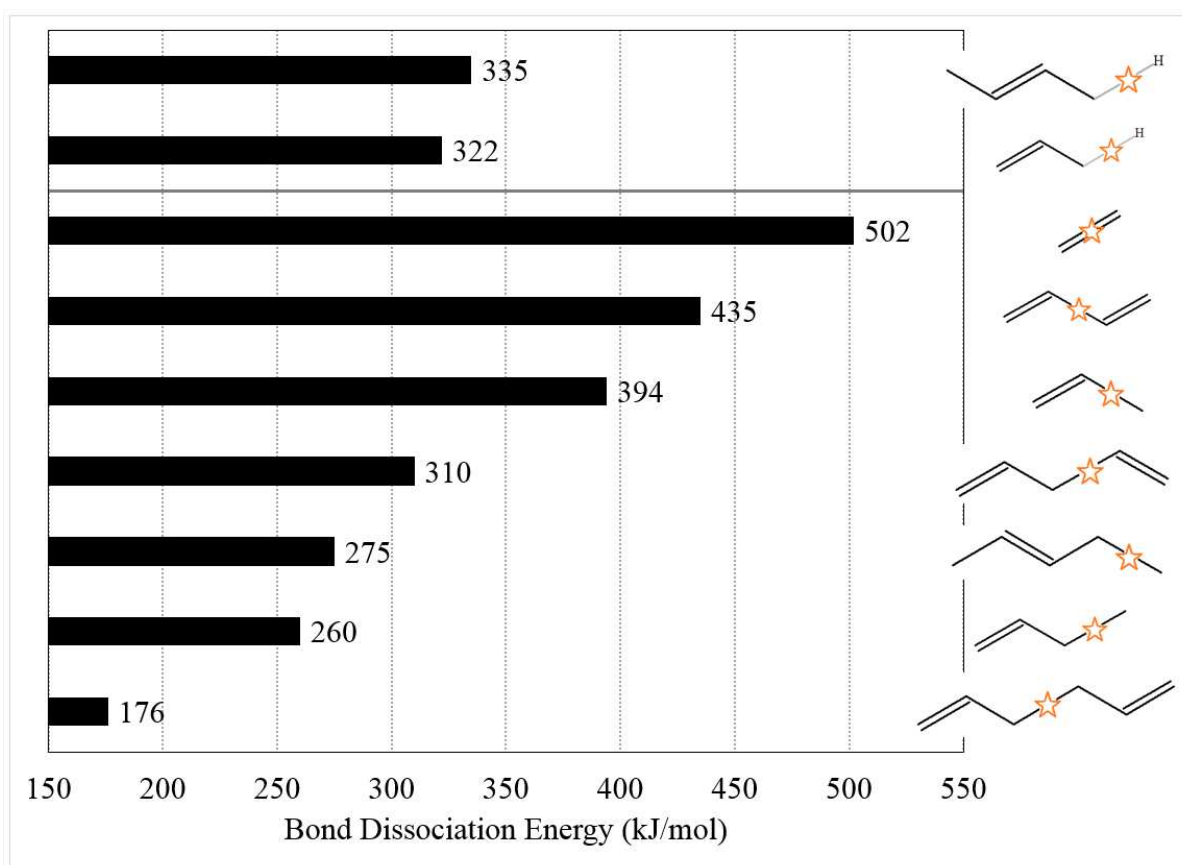
Figure 12. Bond dissociation energies for model olefin compounds

71

C=C bonds rather than for bonds that are isolated.

It can be deduced from the observation of ethylene fragmentation that the olefin bond energy itself is very high. Although the C=C bond potentially has a dramatic influence on cracking reactions, it is unlikely that the C=C bond can be fragmented by radical reactions.

As such, fragmentation of C=C bonds might be neglected from relative bond dissociation calculations in many cases. Fragmentation of C–C bonds adjacent to a C=C bond appears to be similarly disfavored. This can be seen by the fragmentation of the C–C bond in propylene, having a high energy of 394 kJ/mol, which on the order of 80 kJ/mol greater than most isolated C–C bond energies.

The lowest energy bonds are those that fragment to produce a radical at the allylic carbon to a C=C bond. Such bonds will be considered homoallylic bonds for simplicities sake, whether they are C–H or C–C bonds. The phenomenon of homoallylic bond dissociation energies being substantially lower energy can be explained by resonance stabilization of the radical intermediate. As shown in Figure 13, if a radical is formed at the allylic position, the intermediate state is a resonance stabilized radical. Rather than multiple distinct states in rapidly changing transition, the resonance stabilized state should be considered a single unified state. The state may be considered equal to the physical average of states denoted by brackets. Other resonance stabilized radicals in this document will be drawn using partial bonds (appearing as a bond and a half, ⤢) and a black radical for easy recognition. Also, gray radicals will be depicted showing other resonance-stable radical positions, not denoting more than one radical.

The resonance stabilizes the radical state and therefore reduces the energy level of that state. As a result, the bond dissociation energy leading to the formation of that state is lowered.

72

The resonance may also help explain increased variety in the products of noncatalytic cracking due to molecular rearrangement as a result of resonance stabilization.

For the case of C–C bond scission of 1,3-butadiene, the adjacent olefin bonds are conjugated so that the C–C bond energy should be substantially higher from the contributions of olefin bonds on either adjacent side. Thus it is not surprising that its energy (435 kJ/mol) is 41 kJ/mol larger than a C–C bond adjacent to a single olefin bond (394 kJ/mol). Such a conjugated bond system is anticipated to be very resilient to bond scission by noncatalytic cracking.
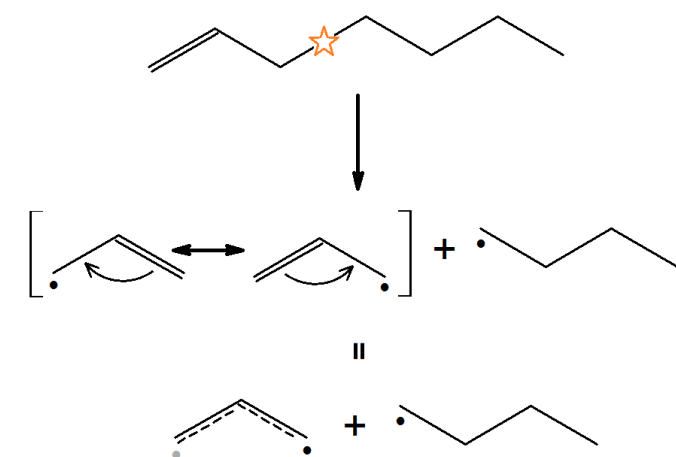
Figure 13. Resonance stabilization of allylic radicals.

For the case of C–C bond scission of 1,4-pentadiene, the C=C bonds would be considered to be nonconjugated. Either of the two C-C bonds within would be considered *both* homoallylic *and* C=C adjacent. For this reason, the bond energy has a positive contribution from the adjacent C=C bond and a negative contribution from its homoallylic nature, which makes it difficult to anticipate the true bond energy. By experiment, these bond energies were found to be 310 kJ/mol, slightly lower than isolated C–C bond energies, but not dramatically lower. In general,

this could indicate that chain scission may preferentially occur outside the two nonconjugated C=C bonds and at the allylic position, where the dissociation energy is lowest, rather than in between them.

Finally with the case of 1,5-hexadiene, the favored fragmentation site would be considered a bisallylic C–C bond. The anticipated result would be a dramatically reduced C-C bond energy due to the negative effect of the allylic position twice, which is indeed observed in Figure 12 with one of the lowest reported bond energies in this case study at 176 kJ/mol. Such C–C bonds would be highly susceptible to scission by noncatalytic cracking reactions.

III.B.3. Bisallylic Hydrogen Abstraction

Even at its lowest reported energy, the scission of C–H bonds still requires a fairly large amount of energy. For this reason, the spontaneous formation of hydrogen radicals as an initiation reaction might be considered disfavored in cracking, even when considering the relatively large quantity of C–H bonds on feedstock molecules (relative to carbon/carbon bonds). However, hydrogen abstraction from 2-butene and propylene is reported at 322 kJ/mol, which is in the range of non-functionalized C–C bond fragmentation. This is due to resonance stabilization by the allylic radical.

From this observation, the abstraction of a hydrogen radical from in between nonconjugated bonds should have substantially lower energy due to the radical being twice-stabilized by resonance, as indicated in Figure 14. This bisallylic C–H bond energy would be predictably less than 322 kJ/mol, but it was not found in the literature. When considering that the allylic C-H bond energy of 2-butene (335 kJ/mol) is 59 kJ/mol less than that of C-H bonds in propane (394 kJ/mol), it is reasonable to estimate that the bond energy of bisallylic hydrogen is

on the order of 276 kJ/mol by adjusting from 335 kJ/mol. A similar method of approximation from bisallylic C-C cleavage estimates the bond energy at 235 kJ/mol, and the average of these two estimations is 256 kJ/mol, which will be used in the present work. This estimation of bond energy is similarly performed by Blanksby.[85]

In considering that the C–C bond energies are estimated at 310 kJ/mol, the abstraction of bisallylic hydrogen at approximately 256 kJ/mol is a low energy, favorable initiation reaction. Therefore the radicalization of the nonconjugated double bonds by C–H homolytic scission might be more favored. This type of C–H scission reaction is regarded as bisallylic hydrogen abstraction, and it has been briefly considered to explain TAG oxidation.
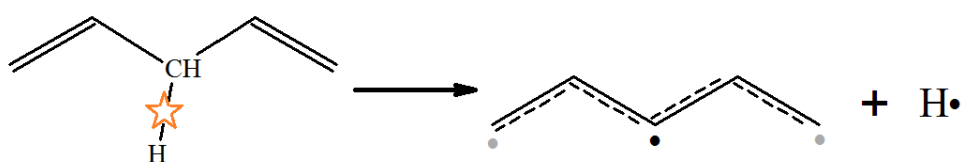
Figure 14. Resonance stabilized hydrogen abstraction from nonconjugated C=C bonds

III.B.4. Bond Dissociation Energies for Oxygenated Molecules

Concerning oxygenated molecules which are relevant to triglyceride (TAG) cracking, model ester compounds methyl butanoate and ethyl propanoate were studied to determine their bond energies.[35] It was found that they make reasonable approximations for the ester-bond dissociation energies of a TAG molecule. The bond energies of the carboxylic acid group's hydrogen has been estimated elsewhere for hexanoic acid.[85] These bond dissociation energies are shown in Figure 15 relative to other bond energies for comparison and discussion.

By comparing non-functionalized C–C bond energies to the C–O and C–C bond energies in surrounding ester groups, two low energy bonds are observed around the ester bond. For long chain ester cracking, two dominant initiation reactions might occur. The first would be strongly favored at 210 kJ/mol, leading to the formation of a carboxyl radical and an alkyl radical. The second would be less dominant, leading to the formation of an alkyl acetate. It is also plausible that the formation of an acetic acid radical could be the result of advanced cracking of long chain esters, as a stepwise transformation of the first reaction to produce a carboxylic acid radical, eventually leading to the fragmentation at the acetic-acid position due to its low energy.
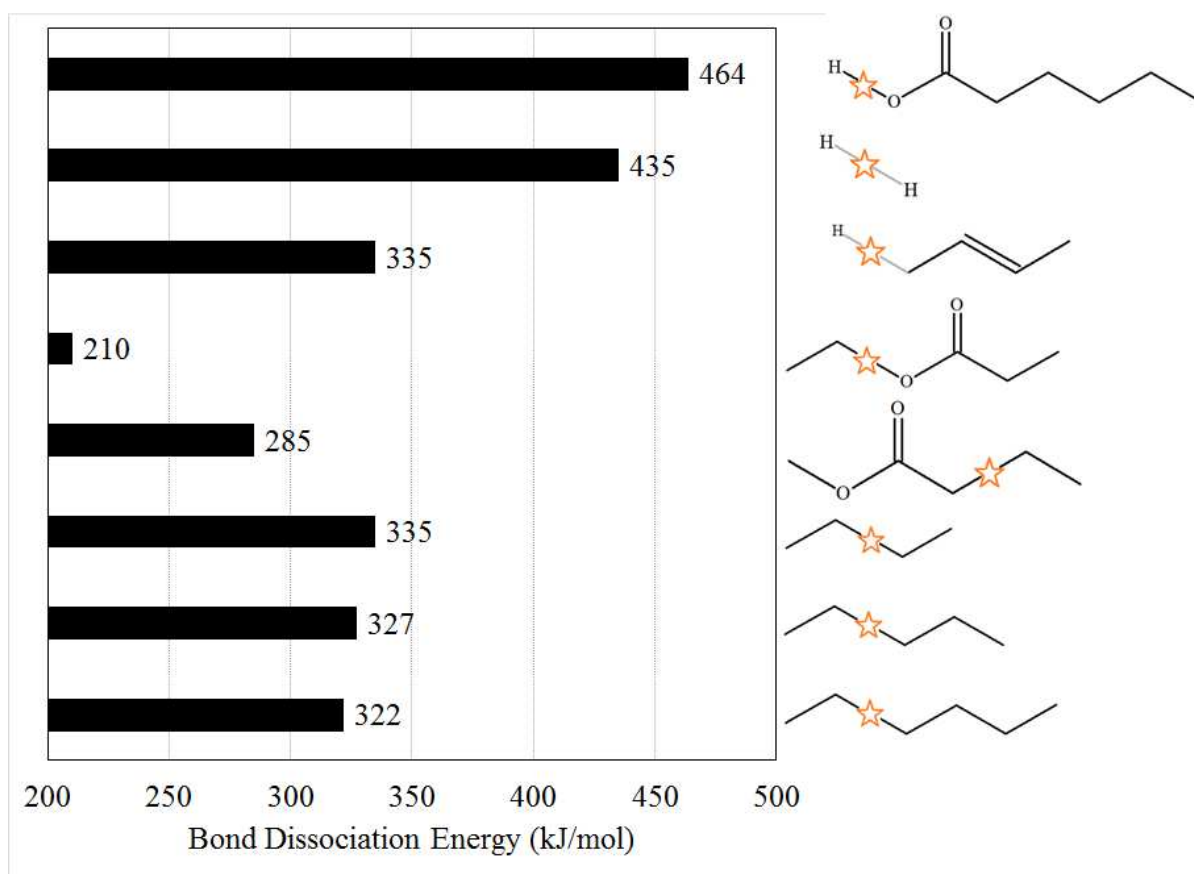
Figure 15. Bond dissociation energies for oxygenates[35,85] with respect to hydrocarbons[34]

In either case, the low bond energy is the result of the radical intermediates being stabilized by resonance as previously described. The dramatically low energy may be very important because it may be the primary initiation reaction for triglyceride cracking, producing radicals for various propagation reactions that carry out subsequent reactions. Bond energies in triglycerides are discussed in Section III.F.4.

Another important bond is the C-H bond at the allylic position to the C=O bond on carboxyl groups (ester/carboxylic acids). Due to its allylic proximity to a double bond, it may be an important bond energy. Its bond energy may be estimated using analogies between the dissociation energy of the C-C in butane (335 kJ/mol) and C-C at the allylic position in methyl butyrate (285). Their difference in 50 kJ/mol, so the C-H bond energy at the allylic position to the C=O bond in methyl butyrate could be estimated at 344 kJ/mol, based on adjusting the bond energy of the C-H bond in propane (394 kJ/mol). This hydrogen bond is probably higher energy than other allylic bonds, but it is still useful to illustrate its energy. This estimated bond energy is shown below in Figure 16.

Additional bond dissociation energies (E_D) have been compiled by Raseev[34] with pre-exponential constants (A) and other valuable insights into the mechanisms of triglyceride cracking. The bond energies that were presented herein were listed due to their importance for mechanistic insights to triglyceride cracking. Similarly estimated bond energies, which are of particular importance to triglyceride cracking, are shown in Figure 16 for later utilization as well. It should be reiterated that these bond energies were not published in literature, but other authors corroborate the methods used to estimate them.
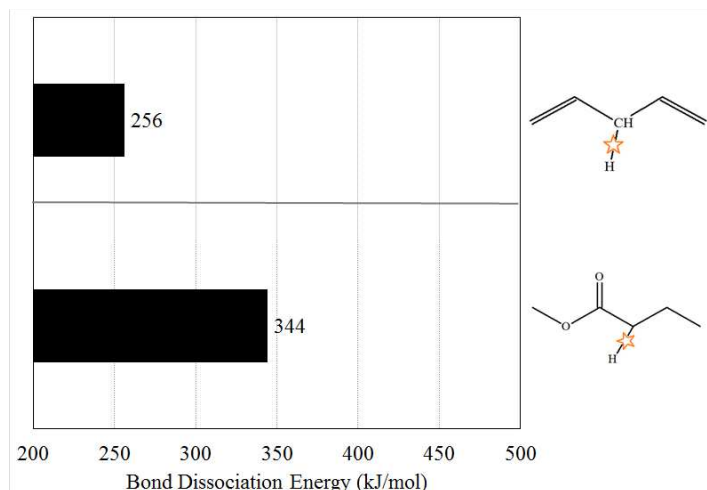
Figure 16. Estimated bond dissociation energies for important representative molecules

III.C. Cracking Propagation Reactions

Cracking propagation reactions involve the change of a radical's state, either on the same molecule or being exchanged among molecules. The forms of radical reactions involve isomerization, degradation, or substitution. These are briefly described in the following sections.

III.C.1. Propagation by Radical Isomerization

Radical isomerization is characterized by a rearrangement of the position of the radical on a molecule. It should be mentioned that radical isomerization is different from radical resonance. Isomerization relocates the position of the radical on a molecule. Therefore, the radical has changed state. Resonance is a single state, characterized by the union of multiple states.

Figure 17 shows the activation energies and kinetic constants for five isomerization reactions that was taken from Raseev.[34] What can be seen from the figure is that the radical isomerizations are not trivially calculated. Whereas some are characterized by higher activation

energy (e.g. 171.7 vs. 49.0 kJ/mol), they also are characterized by increased rate constants

$(5.2 \times 10^{14}$ vs. 3.2×10^{10} s^{-1}) In order to make sense of this data requires the use of numerical

computation as outlined by Raseev, which is beyond the scope of the current literature

investigation.[34]

There is minimal data for radical isomerization on olefin molecules. This is potentially

because the presence of the double bond localizes the radical in its proximity by

Reaction	A (s^{-1})	E (kJ/mole)
$1 - \overset{\bullet}{C}_4H_9 \rightarrow 2 - \overset{\bullet}{C}_4H_9$	5.2×10^{14}	171.7
$1 - \overset{\bullet}{C}_6H_{13} \rightarrow 2 - \overset{\bullet}{C}_6H_{13}$	3.2×10^{10}	49.0
$1 - \overset{\bullet}{C}_6H_{13} \rightarrow 3 - \overset{\bullet}{C}_6H_{13}$	2.0×10^{11}	78.3
$2 - \overset{\bullet}{C}_6H_{13} \rightarrow 1 - \overset{\bullet}{C}_6H_{13}$	5.0×10^{10}	67.0
$3 - \overset{\bullet}{C}_6H_{13} \rightarrow 1 - \overset{\bullet}{C}_6H_{13}$	3.2×10^{11}	96.3

Figure 17. Activation energy and kinetic constants for isomerization reactions
of selected radicals (reproduced from Raseev[34])

resonance, which in turn stabilizes the radical and reduces its likelihood of isomerization.

Nevertheless, more reaction data may be desired to apply radical isomerization reaction sets to

triglyceride cracking phenomena.

III.C.2. Propagation by Radical Degradation

Radicals can degrade to form two products, a radical and a nonradical. Examples of

radical degradation are grouped by olefins and paraffins in Figure 18 that was taken from

Raseev.[34] Rate constants and activation energies are reported for each reaction. When duplicate

data are indicated for the same reaction, it is due to multiple literature values.

In examining Figure 18, it is apparent that the lower energy radical degradation reactions (e.g. 120 – 130 kJ/mol) are those which involve an olefin degrading to produce a small olefin such as ethylene or propylene and an alkyl radical.

Radical degradations to produce a hydrogen radical are higher energy, typically on the order of 20-30 kJ/mol higher. This is expected due to the higher energy of the hydrogen radical that is produced.

Reaction	A (s^{-1})	E (kJ/mole)
$\dot{C}_2H_5 \rightarrow C_2H_4 + \dot{H}$	3.2×10^{13}	167.5
$1 - \dot{C}_3H_7 \rightarrow C_2H_4 + \dot{C}H_3$	4.0×10^{13}	136.5
$1 - \dot{C}_3H_7 \rightarrow C_3H_6 + \dot{H}$	2.0×10^{13}	160.8
$2 - \dot{C}_3H_7 \rightarrow C_3H_6 + \dot{H}$	2.0×10^{13}	162.0
	2.5×10^{13}	170.8
$1 - \dot{C}_4H_9 \rightarrow C_2H_4 + \dot{C}_2H_5$	4.0×10^{13}	121.4
$1 - \dot{C}_4H_9 \rightarrow 1 - C_4H_8 + \dot{H}$	1.3×10^{14}	163.3
$2 - \dot{C}_4H_9 \rightarrow C_3H_6 + \dot{C}H_3$	1.0×10^{14}	138.1
$2 - \dot{C}_4H_9 \rightarrow C_4H_8 + \dot{H}$	1.6×10^{14}	171.6
$i - \dot{C}_4H_9 \rightarrow i - C_4H_8 + \dot{H}$	3.3×10^{14}	150.7
$i - \dot{C}_4H_9 \rightarrow C_3H_6 + \dot{C}H_3$	2.0×10^{14}	142.3
$i - \dot{C}_4H_9 \rightarrow 2 - C_4H_8 + \dot{H}$	4.0×10^{13}	153.2
$\dot{C}_5H_{11} \rightarrow C_5H_{10} + \dot{H}$	5.0×10^{13}	153.2
$\dot{C}_5H_{11} \rightarrow 1 - C_4H_8 + \dot{C}H_3$	3.2×10^{13}	131.9
$\dot{C}_5H_{11} \rightarrow C_2H_4 + 1 - \dot{C}_3H_7$	4.0×10^{12}	120.2
$1 - \dot{C}_6H_{13} \rightarrow C_2H_4 + 1 - \dot{C}_4H_9$	1.0×10^{14}	125.6
$2 - \dot{C}_6H_{13} \rightarrow C_3H_6 + 1 - \dot{C}_3H_7$	1.0×10^{14}	129.8
$3 - \dot{C}_6H_{13} \rightarrow 1 - C_4H_8 + \dot{C}_2H_5$	1.0×10^{14}	129.8
$3 - \dot{C}_6H_{13} \rightarrow 1 - C_5H_{10} + \dot{C}H_5$	1.0×10^{14}	136.1
$\dot{C}_2H_3 \rightarrow C_2H_2 + \dot{H}$	2.0×10^{9}	131.9
$\dot{C}_3H_5 \rightarrow C_2H_2 + \dot{C}H_3$	3.0×10^{10}	151.6
$\dot{C}_4H_7 \rightarrow C_4H_6 + \dot{H}$	1.2×10^{14}	206.4
$\dot{C}_4H_7 \rightarrow C_2H_4 + \dot{C}_2H_3$	1.0×10^{11}	154.9
Methyl – allyl $\rightarrow C_3H_4 + \dot{C}H_3$	1.0×10^{13}	136.5
Methyl – allyl $\rightarrow C_2H_4 + \dot{C}_2H_3$	1.0×10^{12}	117.2

Figure 18 Activation energy and kinetic constants for decomposition reactions of selected radicals (reproduced from Raseev[34])

III.C.3. Propagation by Radical Substitution

Radical substitution reactions involve a radical 'attacking' a nonradical molecule. Effectively, the radical's state is transferred, leaving a new radical molecule and a new nonradical molecule. Examples of radical substitution reactions are shown in Figure 19 (taken from Raseev[34]).

Reaction	A $(L \cdot mol^{-1}s^{-1})$	E (kJ/mole)
$\dot{H} + H_2 \rightarrow H_2 + \dot{H}$	4.6×10^{10}	28.8
$\dot{H} + CH_4 \rightarrow H_2 + \dot{C}H_3$	7.24×10^{11}	63.1
$\dot{H} + C_2H_6 \rightarrow H_2 + \dot{C}_2H_5$	1.0×10^{11}	40.6
$\dot{H} + C_3H_8 \rightarrow H_2 + 1 - \dot{C}_3H_7$	1.0×10^{11}	40.6
$\dot{H} + C_3H_8 \rightarrow H_2 + 2 - \dot{C}_3H_7$	9.0×10^{10}	34.8
	4.0×10^{10}	34.3
$\dot{H} + n - C_4H_{10} \rightarrow H_2 + 1 - \dot{C}_4H_9$	1.5×10^{11}	40.6
$\dot{H} + n - C_4H_{10} \rightarrow H_2 + 2 - \dot{C}_4H_9$	9.0×10^{10}	35.2
$\dot{H} + i - C_4H_{10} \rightarrow H_2 + i - \dot{C}_4H_9$	1.0×10^{11}	35.2
$\dot{C}H_3 + H_2 \rightarrow CH_4 + \dot{H}$	1.55×10^{10}	64.9
$\dot{C}H_3 + C_2H_6 \rightarrow CH_4 + \dot{C}_2H_5$	3.8×10^{11}	69.1
$\dot{C}H_3 + C_3H_8 \rightarrow CH_4 + 1 - \dot{C}_3H_7$	3.4×10^{10}	48.1
$\dot{C}H_3 + C_3H_8 \rightarrow CH_4 + 2 - \dot{C}_3H_7$	4.0×10^{9}	42.3
$\dot{C}H_3 + n - C_4H_{10} \rightarrow CH_4 + 1 - \dot{C}_4H_9$	3.5×10^{10}	48.6
$\dot{C}H_3 + n - C_4H_{10} \rightarrow CH_4 + 2 - \dot{C}_4H_9$	3.5×10^{9}	39.8
$\dot{C}H_3 + i - C_4H_{10} \rightarrow CH_4 + i - \dot{C}_4H_9$	9.5×10^{9}	37.7
$\dot{C}H_3 + C_6H_{14} \rightarrow CH_4 + \dot{C}_6H_{13}$	1.0×10^{8}	33.9
$\dot{C}_2H_5 + H_2 \rightarrow C_2H_6 + \dot{H}$	3.0×10^{8}	45.2
$\dot{C}_2H_5 + CH_4 \rightarrow C_2H_6 + \dot{C}H_3$	2.3×10^{8}	47.7
$\dot{C}_2H_5 + C_3H_8 \rightarrow C_2H_6 + 1 - \dot{C}_3H_7$	1.2×10^{9}	52.8
$\dot{C}_2H_5 + C_3H_8 \rightarrow C_2H_6 + 2 - \dot{C}_3H_7$	8.0×10^{8}	43.5
$\dot{C}_2H_5 + n - C_4H_{10} \rightarrow C_2H_6 + 1 - \dot{C}_4H_9$	2.0×10^{9}	52.8
$\dot{C}_2H_5 + n - C_4H_{10} \rightarrow C_2H_6 + 2 - \dot{C}_4H_9$	4.5×10^{8}	43.5
$\dot{C}_2H_5 + i - C_4H_{10} \rightarrow C_2H_6 + i - \dot{C}_4H_9$	1.5×10^{9}	43.5
$\dot{C}_2H_5 + n - C_7H_{16} \rightarrow C_2H_6 + n - \dot{C}_7H_{15}$	9.8×10^{9}	44.4
$1 - \dot{C}_3H_7 + n - C_4H_{10} \rightarrow C_3H_8 + 2 - \dot{C}_4H_9$	2.0×10^{8}	43.5
$2 - \dot{C}_3H_7 + n - C_4H_{10} \rightarrow C_3H_8 + 2 - \dot{C}_4H_9$	2.0×10^{8}	52.8
$2 - \dot{C}_3H_7 + i - C_4H_{10} \rightarrow C_3H_8 + i - \dot{C}_4H_9$	1.0×10^{8}	56.1
$\dot{H} + C_2H_4 \rightarrow H_2 + \dot{C}_2H_3$	8.0×10^{8}	16.7
$\dot{H} + C_3H_6 \rightarrow H_2 + \dot{C}_3H_5$	2.5×10^{9}	17.2
$\dot{H} + 1 - C_4H_8 \rightarrow H_2 + \dot{C}_4H_7$	5.0×10^{10}	16.3
$\dot{H} + 2 - C_4H_8 \rightarrow H_2 + \dot{C}_4H_7$	5.0×10^{10}	15.9
$\dot{H} + i - C_4H_8 \rightarrow H_2 + Methyl - allyl''$	3.0×10^{10}	15.9
$\dot{C}H_3 + C_2H_4 \rightarrow CH_4 + \dot{C}_2H_3$	1.0×10^{10}	54.4
$\dot{C}H_3 + C_3H_6 \rightarrow CH_4 + \dot{C}_3H_5$	2.0×10^{9}	51.1
$\dot{C}H_3 + 1 - C_4H_8 \rightarrow CH_4 + \dot{C}_4H_7$	1.0×10^{8}	30.6
$\dot{C}H_3 + 2 - C_4H_8 \rightarrow CH_4 + \dot{C}_4H_7$	1.0×10^{8}	34.3
$\dot{C}H_3 + i - C_4H_8 \rightarrow CH_4 + Methyl - allyl''$	3.0×10^{8}	30.6
$\dot{C}_2H_5 + C_3H_6 \rightarrow C_2H_6 + \dot{C}_3H_5$	1.0×10^{8}	38.5

Figure 19. Activation energy and kinetic constants for substitution reactions for selected radicals (reproduced from Raseev[34])

In comparison of radical substitution reactions to radical degradation reactions, the trends appears to be that the activation energy is less for radical substitution reactions. However, many of the rate constants are between 2 and 4 orders of magnitude less, so it is difficult to obviate the comparison between radical substitution and radical degradation.

What can be noticed is that radical reactions carried out by hydrogen have consistently higher rate constants (e.g., 1×10^{11} L·mol^{-1}·s^{-1}) than ethane radicals (e.g., 1×10^8 L·mol^{-1}·s^{-1}) for similar reactions. The trend for methylene radicals is also there, but it is less obvious.

III.C.4. Summary

Trends in radical propagation reactions include that degradation to produce short olefins and alkyl radicals is favorable, whereas degradation to produce higher energy radicals (e.g., hydrogen radicals) is energetically less favored. Radical substitution reactions have substantially smaller activation energy. Therefore, degradation reactions may be more dominant at higher temperatures, whereas substitution reactions may tend to dominate lower temperatures. Substitution reactions carried out by higher energy radicals progress more rapidly than those carried out by lower energy radicals.

Due to the large quantity of reactions in the system, large computation models may be necessary to extract the most possible meaning from cracking kinetic data.

III.D. Cracking Termination Reactions

The initiation of cracking is the formation of two radicals, which depends on the bond dissociation energy. This is true when the energy for the reverse reaction is essentially zero in all cases. In other words, the radical termination step (i.e., union of two radicals to form a nonradical) has a negligible activation energy. Therefore, it follows that the radical termination

step is independent of temperature, and based only on the concentration of radicals and the pre-exponential constant, as follows in Equation 8.

$$r_{term.} \quad = \quad A \times e^{\frac{0}{R \cdot T}} \times C_{R_1.} \times C_{R_2.} \quad = \quad A \times C_{R_1.} \times C_{R_2.} \tag{7}$$

Pre-exponential constants are found on the order of 10^8 to 10^{11} (L·mol^{-1}·s^{-1}) according to Raseev. When pre-exponential constants are examined for various radical termination reactions, they tend to be higher for shorter and more aggressive radicals (e.g., atomic hydrogen, methyl radicals, etc.) and lower for larger molecules, on which the radicals have lower energy and are more stable. Nonetheless, radical lifetimes are typically extremely short either way.

As previously mentioned, two atomic hydrogen radicals are unable to terminate to form molecular hydrogen without a third participating molecule to absorb the energy. Such a ternary collision is rarely observed, so hydrogen radicals typically must be terminated by other means, i.e. terminating with a methyl radical.

III.E. Important Characteristics of Cracking Reactions

It is important to describe some of the general characteristics of radicals which govern the behavior of cracking reactions. First of all, the lifetime of an initiated radical tends to be extremely short, in most cases being on the order of 1 ms.[34] In addition, radicals are very dilute, being reported on the order of 0.01% to as low as three orders of magnitude less than that.[87] Undoubtedly, the concentration of radicals depends on the specific reaction conditions, but their dilute concentration is readily accepted.[34]

Radicals have different energies, with higher energy radicals such as atomic hydrogen being described as active radicals and lower energy molecules such as allylic radicals being

described as inactive radicals. When a radical is formed, it is often through the production of an

active radical and an inactive radical. Active radicals are much more suitable for propagation

reactions than inactive radicals, which can be demonstrated by comparing the activation energy

and rate constants for propagation reactions (previously tabulated). Hydrogen radicals and

allylic radicals represent two extremes of the radical spectrum, with many radicals of varying

activity lying in between them. Due to the full spectrum of radicals present during cracking, the

definition of an active radical vs. an inactive radical has relative meaning rather than absolute

meaning.

To illustrate the relative activity of radicals, Raseev estimates that propagation reactions

by atomic hydrogen radicals are between 10 and 100 times greater than for equivalent reactions

propagated by methylene radicals. These were computed at approximately 800 C, whereas at

reduced temperatures in the range of 400-450 C, the relative rate of hydrogen-radical-propagated

reactions are even 50 % greater than at 800 C, owing to the reduced temperature vs. activation

energy. Inactive radicals are lower energy, and do not have the ability to propagate through a

reaction system.

III.E.1. Retardation and Increasing Speed

The discussion in the last subsection leads to a couple of important features of

noncatalytic cracking, namely the utilization of hydrogen to increase cracking speed and the

observation of cracking retardation. In order to improve the reactivity of cracking, high

pressures of hydrogen gas are sometimes added to a stream, increasing the concentration of

hydrogen and therefore the likelihood of producing high energy hydrogen radicals.

In contrast, cracking retardation is an observed condition in which the addition of

propylene to a cracking reactor dramatically slows the reactivity of a stream. The high

concentration of propylene retards the reaction by absorbing active radicals on propylene in the

form of an allylic radical, which has too low energy to propagate further reaction. Once a

propylene radical is formed, the reaction chain effectively stops, awaiting a termination reaction.

The retardation effect is observed for adding propylene to a reaction only up until a certain point,

above which the propylene increases the reaction rate by supplying atomic hydrogen radicals

from the initiation reaction of propane decomposition to an allylic radical.[34]

III.E.2. Prediction of Cracking Reaction Yields

Simulations with extensive reaction sets have been utilized to predict the yield of

noncatalytic cracking with some reasonable accuracy. This can be said of reactors for cracking

butane, propane, and other light feed streams into products such as ethylene, propylene, and

other molecules, where the participating intermediates are very short chain. This keeps reaction

sets small so that most and/or virtually all of the potential reactions are known. When feedstocks

have molecules that are larger in size however, the reaction sets become impossibly complex to

simulate, especially due to a lack of reliable experimental data. As a result, it is doubtful that

simulation will be able to predict the outcome of triglyceride cracking with accuracy.

Nevertheless, qualitative trends in cracking can be anticipated based on the susceptibility of

bonds to attack.

III.E.3. Chain of Reaction

High energy radicals such as atomic hydrogen or methylene radicals are capable of

propagating a chain of reaction between 100 and 200 reactions before a radical terminates. For

this reason, the products of many cracking processes are typically determined by comparing the

relative rates of propagation reactions rather than the initiation or termination reactions. For example, to utilize the bond dissociation energies to predict the products of cracking would be unfair if the average length of reaction chain was 100 reactions, 98 of which are propagation reactions. This is especially true of cracking at high temperatures (600 – 850 C), where radical chain reaction fits the experimental data. However at lower temperatures (300 – 450 C), a different radical mechanism is observed in which the initiation reactions describe the products of noncatalytic cracking, described in the next section.

III.F. Application of Reaction Sets to Triglyceride Cracking

Theory and bond energy were discussed in the previous sections in order to enable the estimation of bond energies on triglyceride molecules and to provide sufficient background information to infer thoughtful expectations of triglyceride cracking reactions. Bond energies are hereafter presented for common forms of triglyceride molecules. Reaction rates are estimated at various temperatures for triglyceride reactions that are expected to occur during noncatalytic cracking. The compositions of various triglyceride feedstocks such as soybean oil, canola oil, etc., are also provided and their reactivity vs. composition is discussed. The differences between petrochemical cracking and triglyceride cracking are also described in order to establish a different expectation for triglyceride cracking. Proposed reaction mechanisms for triglyceride cracking are also reviewed.

III.F.1. Influence of Hydrogen

Hydrogen gas may be externally added to noncatalytic cracking reactors in order to observe increased cracking speeds as mentioned previously in Section III.E.1. The increased cracking speed is typically observed in ethylene cracking reactors (vapor phase cracking). The

effect of the H_2 addition is to provide excess hydrogen to facilitate radical propagation (not radical initiation). The molecular H_2 itself does not directly supply hydrogen radicals to a significant extent because it cannot readily disassociate into atomic hydrogen radicals due to its high bond energy. Instead, H_2 amplifies the reaction by providing an abundant source of high-energy propagation intermediates. This necessitates having a reasonably high molar concentration of H_2 in the phase in which radicals are being generated (i.e., vapor phase for ethylene cracking, liquid phase for TAG cracking).

The addition of hydrogen to TAG noncatalytic cracking was previously studied by Luo et al.[54] who noncatalytically cracked soybean and canola TAG in batch reactors in the presence of hydrogen gas at 2200 kPa in comparison to a vacuum. Luo et al. report that the effect of the hydrogen gas appeared to be negligible on the cracking reaction rates during the range in which cracking was exhibited. It should be mentioned that Kubatova et al. hypothesize that hydrogen had an effect at lower cracking temperatures, which is discussed in Section I.E.1.[58] However, the author of the present work offers an explanation for why Luo did not observe a significant effect from the addition of hydrogen: vapor liquid equilibrium.

Hydrogen addition is sensible in ethylene cracking reactors, where molar concentrations of H_2 are directly related to the flow of H_2 through the reactor. In TAG noncatalytic cracking however, the effect of H_2 will only be observed under very high pressures and/or special conditions, in which the H_2 is sufficiently concentrated in the reacting phase to permit propagation. The vapor liquid equilibrium (VLE) of Luo's reactor system was examined in detail using the process simulation software ChemCAD by Chemstations, Inc. (Houston, TX, USA) according to the simulation specifications described in Section II.C. At initial conditions

(20 C / 2200 kPa H_2), the liquid phase molar percentage of H_2 is only about 0.03 %, with the remainder being TAG oil (as triolein). If the reactor could be imaginatively elevated to reaction temperatures without thermal lag, the conditions would 430 C and 7300 kPa, for a molar percentage of H_2 at only 0.07 % in the liquid phase. Without the imaginative heating, the true molar percentage of H_2 could be assumed on a similar order of magnitude, or potentially less due to dilution of the molar hydrogen concentration as a result of cracking.

To illustrate the negligible contribution of hydrogen, the liquid phase molar percentage of H_2 was estimated by ChemCAD at extreme conditions of 430 C and 30,000 kPa. For this simulation, the liquid phase molar amount of H_2 only increased to 0.32 % with the balance being triglyceride oil. This explains Luo's observations, however, this explanation should be considered in light of Kubatova et al.'s mechanistic considerations about hydrogen rate control (see Section I.E.1).[58]

III.F.2. Molecular Mechanism, Speed of Cracking, and Cracking of Alkenes

Cracking in petroleum refining is typically performed at temperatures that are relatively high (600 – 850 C), utilizing small molecules as feedstocks for olefin production. At these higher temperatures, the expected reaction products are correlated to the propagation reactions in the system rather than the initiation reaction. This indicates a long reaction chain, which was previously remarked as being on the order of 100 to 200 reactions. Triglyceride cracking differs in a multitude of ways, which may result in triglyceride cracking proceeding through a different mechanism, considered herein. Major differences include: (1) the presence of C=C bonds in TAG oils, (2) the presence of oxygenated functional groups in TAG oils, (3) very different temperatures and residence times, and (4) reaction in the liquid phase and/or multiple phases.

A series of studies by Blouri et al. involved mild noncatalytic cracking of paraffins at lower temperatures (300 to 440 C) and elevated pressures.[88] Blouri found that the products of n-hexadecane cracking under these temperatures were predominantly linear paraffins and alpha olefins. The molar yield of each of the products was very well correlated to the bond dissociation energy. This implied that the radical initiation reaction was dominating the reaction set, rather than propagation reactions which dominate typical cracking reactors (e.g., ethylene cracking reactors).

Blouri explained the phenomenon as a *molecular* radical mechanism rather than by a *free* radical mechanism, demonstrated by Figure 20. In a molecular mechanism, radicals are constrained to the molecule(s) participating in the initiation reaction. By contrast, in a free radical mechanism the radicals are released with enough energy to propagate a chain reaction. The molecular cracking mechanism is essentially equivalent to the radical initiation reaction of cracking, concerted with the formation of a double bond adjacent to the cracking site through hydrogen rearrangement.
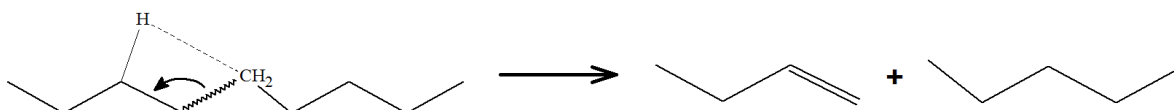
Figure 20. Example molecular cracking mechanism for C-C bond scission of paraffin chains

Blouri's experimental conditions were performed at mild temperatures (400-440 C) and elevated pressures that are similar to triglyceride cracking in the present work. For this reason, the molecular cracking mechanism might be expected for the type of triglyceride cracking utilized in this dissertation. This is significant because in a free radical mechanism, reaction

89

yields are typically computed from thorough reaction sets that are too advanced for triglyceride cracking at its present understanding. However, in the molecular cracking mechanism, reaction products can be predicted by initiation reactions alone rather than propagation reactions. Since cracking initiation reactions are easily characterized without experimental data, meaningful conclusions about triglyceride cracking might be obtainable from calculations alone. In any case, the molecular mechanism requires a different approach to determining the products and yields of triglyceride cracking than for a free radical mechanism, so it is valuable to consider this in future computations.

The rate of long chain paraffin cracking in Blouri's experiments was reported to be very slow, relative to the fragmentation of triglycerides. After four hours, conversion was observed on the order of 5 % at 400 C, 12 % conversion at 420 C, and 30-40 % conversion at 440 C. By contrast, Luo et al. reported at least 76 % conversion after only 30 minutes of reaction time at 440 C, based on the distillable material at a vapor cutoff temperature of 300 C.[54] True conversion may be substantially higher. It is useful to note that Blouri found negligible effect of adding high pressures of H_2 to increase reaction rates by hydrocracking. This aligns with Luo's observations for adding H_2 to triglyceride cracking.

In comparing the conversion/time for triglycerides and long chain paraffins, it is apparent that triglycerides crack at least an order of magnitude faster than long chain paraffins. Rather than discrediting the molecular mechanism's application to triglyceride cracking, the difference in reaction speed may be due to the high quantity of low energy bonds on triglyceride molecules in the vicinity of carboxyl groups and C=C bonds. It is also possible that triglyceride cracking is characterized by multiple reactions, some proceeding via molecular radical mechanism and some

via free radical mechanism.

III.F.3. Cracking in the Presence of C=C Bonds

There is a dramatic lack of literature pertaining to the cracking of olefin feedstocks relative to a wealth of literature on paraffin cracking in order to *produce* olefins. What little research has investigated olefin cracking has tended to do so from the perspective of paraffin cracking (i.e., very high temperatures, short residence times, low pressure). Although this research can be applied to triglyceride cracking, it must be reconsidered for the very different reaction conditions targeted in the NCP (i.e., lower temperatures, longer residence times, elevated pressures).

During paraffin cracking, the temperatures are so high that radicals form readily and have abundant energy with which to propagate chain reactions. As a result, the presence of olefins in the feedstock is commonly associated with a retarding effect by producing C_3 or C_4 allylic radicals that stunt the chain reaction. Olefins of C_5 and greater tend to result in the formation butadiene and isoprene having a similar retarding effect, although other dienes may also be produced, typically in much lower amounts. According to Surge Raseev, "It must be mentioned that the inactive allylic radicals may be formed not only by the extraction of a hydrogen atom from a molecule of propene or of isobutene, but also by the decomposition of […] some higher alkenes. Since alkenes are generally not present in the feed stocks submitted to pyrolysis of cracking process, the inhibition phenomenon becomes apparent only at advanced conversion, when the decomposition of other hydrocarbons leads to the formation of significant amounts of olefins."[34] This explanation speaks for itself, about the influence of cracking in the presence of olefins from the perspective of paraffin cracking.

It should be considered that when propylene is added to a cracking reactor, it induces a retarding effect *up until a certain* point, above which the propylene improves the reaction rate by providing an abundant source for radical initiation. It then follows that radicals that are produced by the propylene undergo fewer reactions before termination due to the high olefin concentration, which stunts the radical propagation. So under the right context, olefins can produce radicals that speed up a reaction, and they cause those radicals to be short-lived, limiting the number of successive reactions that a radical can cause to occur.

Triglycerides typically contain a very high molar quantity of C=C and C=O bonds. Under the low temperatures where triglycerides are typically cracked, there is a lack of abundant energy to propagate chain reactions, leading to fewer propagation reactions per radical, perhaps on the order of only a few reactions or less. This is demonstrated through the molecular mechanism described by Blouri et al., where there are negligible propagation reactions .[88] For this reason, the observance of a retarding effect caused by olefins in the feedstock may not be expected. On the contrary, C=C and C=O bonds will tend to reduce the bond energy of C-C and C-H bonds in their vicinity, leading to greater rates of cracking initiation reactions. This decrease in activation energy will tend to increase the overall rate of reaction dramatically, perhaps explaining the order of magnitude greater reaction speed for triglyceride cracking[54] relative to paraffin cracking under similar conditions.[88]

III.F.4. Triglyceride Structure and Representative Bond Energies

In this section, triglyceride (TAG) structure and bond energies are presented and discussed to identify potential sites for cracking and mechanisms for radical initiation that govern the triglyceride cracking reactions. Being comprised of three fatty acid moieties (FAs)

and a glycerol backbone, TAG molecules only vary by the chain length of the FAs and the number/location of double bond on the FAs. An example TAG molecule is shown in Figure 21 with bonds energies that are labeled when they are either significant and/or low energy. The depicted TAG contains three important fatty acid moieties for common, commercially viable triglyceride oils: oleic acid (C18:1), linoleic acid (C18:2), and linolenic acid (C18:3).
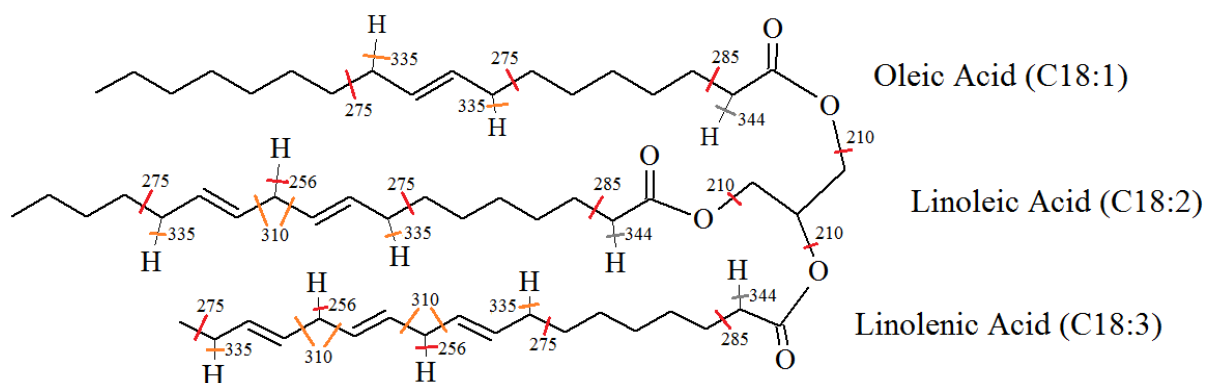
Figure 21. Triglyceride bond energies for glycerol -oleate, -linoleate, -linolenate

It should be mentioned that for each C-H bond shown, there is an additional C-H bond on the same carbon atom which is not shown. These are not drawn so as not to clutter the figure, but their existence improves the probability of C-H dissociation by a factor of two for every apparent C-H bond.

As shown, the three C-O bond energies adjacent to the triglyceride backbone are the lowest energy bonds in the molecule (210 kJ/mol). These bond energies are essentially universal to all triglyceride molecules, so it is anticipated to have negligible dependence on the fatty acid feedstock. Furthermore, the fragmentation of these C-O bonds is anticipated to result in the formation of carboxylic acids in the cracked product. It should also be mentioned that the

remaining bond energies in Figure 21 (i.e., those on the fatty acid chain) may be assumed to be accurate, whether the fatty acid moiety remains part of the intact triglyceride molecule or whether it has fragmented and stabilized as a carboxylic acid.

The second lowest bond energy in the triglyceride is the abstraction of a bisallylic hydrogen radical from the fatty acid moiety's chain, having an estimated dissociation energy of 256 kJ/mol. This produces an atomic hydrogen radical that has substantially high energy and can readily propagate through the system.

This hydrogen would be expected to release as a free radical, not confined to a molecular mechanism. As a result, at least one propagation reaction should be expected for this hydrogen radical before termination. The low temperature of the reaction, combined with the retarding effect of C=C bonds in the cracking fluid will tend to prevent this radical from propagating long chain reactions.

The production of hydrogen radicals in this fashion requires linoleic acid or linolenic acid moieties or some other fatty acid with at least two nonconjugated C=C bonds. By contrast, triglycerides rich in oleic acid or erucic acid are unlikely to abstract a hydrogen radical, so their cracking reaction rates may be less than oils rich in linoleic or linoleic acids.

The third lowest bond dissociation energy shown in the molecule is the fragmentation of C-C bonds at the allylic position to C=C bonds (275 kJ/mol). Depending on the type of fatty acid moiety, these will promote fragmentation at various sites on the fatty acid chain, as shown by Figure 21. For any of the unsaturated fatty acid moieties, fragmentation may tend to produce heptanoic acid due to a regularly positioned C=C bond at the ω-9 position. Fragmentation at the opposite end of the C=C bond(s) varies depending on the moiety. For example, 9-undecenoic

94

acid might be expected to result from the cracking of oleic acid,

The fourth lowest bond energy is the C-C bond at the α-2 position of the fatty acid moiety (285 kJ/mol), which is stabilized by resonance with the C=O bond. Fragmentation of this bond would presumably result in an acetic acid molecule. This bond energy is 75 kJ/mol higher than the lowest bond energy of 210 kJ/mol. As a result, acetic acid production could be anticipated to be much lower than the overall production of carboxylic acids. The bond energy is not feedstock specific because it is present on essentially all triglyceride molecules in this study.

The remaining bonds have moderate energies and/or high energies, such as the fragmentation of C-C bonds between nonconjugated C=C bonds (310 kJ/mol) or the abstraction of an allylic hydrogen in proximity to a C=C bond (335 kJ/mol). These sites might be less favored for the initiation of radicals in triglyceride cracking.

A triglyceride composed of another three important fatty acid moieties is shown with their bond energies in Figure 22. As previously described, bond dissociation on the triglyceride backbone tends to yield a carboxylic acid and on the fatty acid moiety's chain for the production of acetic acid are independent of the type of triglyceride / fatty acid. For saturated fatty acid moieties such as palmitic acid and stearic acid, fragmentation on the fatty acid chain is expected to not be favored, and considered to produce undercracked carboxylic acids or paraffins plus acetic acid due to the influence of the carboxylic acid group as product molecules. The erucic acid moiety has similar likeness to the oleic acid moiety that was described above in Figure 21, with the only significant caveat being the greater carbon chain length.
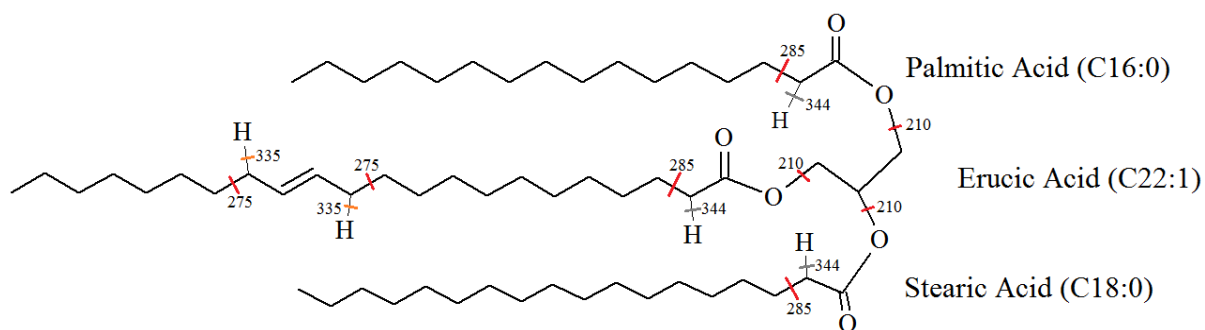
Figure 22. Triglyceride bond energies for glycerol -palmitate, -eruciate, -stearate

As already implied, the bond energies of the fatty acid moieties are assumed to be independent of the bond energies of their triglyceride backbone. This is a sensible simplification that permits the study of triglyceride cracking with respect to the fatty acid composition of a triglyceride oil. This reduces the complexity of triglyceride oils to a composition in several fatty acids for most of the non-tropical oils considered here. This is valid so long as the formation of a radical on the central region of one fatty acid chain does not (1) react with, (2) stabilize with, or (3) induce fragmentation in the central region of another chain, affecting the reactivity. Such interactions of the fatty acid moieties may be assumed to be small in comparison to un-interacted fragmentation. Otherwise, the distribution of fatty acid moieties on intact triglyceride molecules would have to be considered, thereby complicating the mechanistic interpretations of triglyceride cracking to a futile extent.

III.F.5. *Application of Cracking Kinetics to Triglyceride Cracking*

In this subsection, simplistic batch reaction calculations have been performed for a binary mixture of the two triglyceride molecules with their bond energies as shown in Figure 21 and Figure 22 above. The rate constant(s) (i.e., k) were determined using those bond dissociation

energies and the generalizations presented at the beginning of this section (e.g., A = 10^{16}).

Kinetic rate data are not presently available on such triglyceride cracking reactions, so this data

should be used for obtaining insight into triglyceride cracking rather than estimating yield. To

appropriately consider the situation, calculations herein incorporate not only the bond energy, but

also the quantity of bonds on the molecule. As a result, the conversions/times presented for this

example triglyceride oil mixture would need to be adjusted by scalar quantities in order to be

relevant for actual oil samples (e.g., camelina oil).

An example reaction rate equation is derived from the conservation of mass for a batch

reaction in Equation 9. For a well-mixed batch reactor having a single phase and a single first

order decomposition reaction, Equation 9 is solved to the form of Equation 10 for the time to

$$
\frac{dN_j}{dt} = \int^V -r_j \cdot dV \xrightarrow{well\ mixed} \frac{dN_j}{dt} = -r_j \cdot V \tag{8}
$$

$$
\frac{dN_j}{-r_j V} = \frac{dC_j}{r_j} = dt
$$

$$
\int_{C_{j,0}}^{C_{j,end}} \frac{-1}{Ae^{\frac{-E}{RT}} \cdot C_j} \cdot dC_j = \int_{C_{j,0}}^{C_{j,end}} \frac{-1}{k \cdot C_j} \cdot dC_j = \int_{t_0}^{t_{end}} \cdot dt = t_{end}
$$

$$
C = \frac{1-X}{1+X} \ ; \ dC = \frac{-1(1+X) - 1(1-X)}{(1+X)^2} dX = \frac{-2}{(1+X)^2} dX
$$

$$
t_{end} = \frac{2}{k} \cdot \int_0^1 \frac{(1+X)}{(1-X)(1+X)^2} \cdot dX
$$

$$
t_{end} = \frac{(X+1)}{2k} \left(\frac{-2}{X+1} - \ln(1-X) + \ln(1+X) \right) \Big|_{X=0}^{X=.99} \tag{9}
$$

97

reach a specified conversion (e.g., 0.99). The real system involves multiple simultaneous

reactions, multiple phases, chain reactions, transient temperature/pressure, and a more

complicated model of the feedstock. Nevertheless, this simplistic view gives an idea of the

speed of reactions that might be observed under noncatalytic cracking conditions. Furthermore,

these calculations are useful preliminary guides which can be used to determine which reactions

are relevant, irrelevant, and/or occurring simultaneously vs. stepwise.

Equation 10 has been used to determine the conversion of triglycerides into carboxylic

acids vs. time. The data have been plotted in Figure 23 for various temperatures. A clear

dependence of the conversion/time on temperature is evident from the figure. The temperatures

plotted are typically in the sub-cracking range, indicating that the majority of degradation to
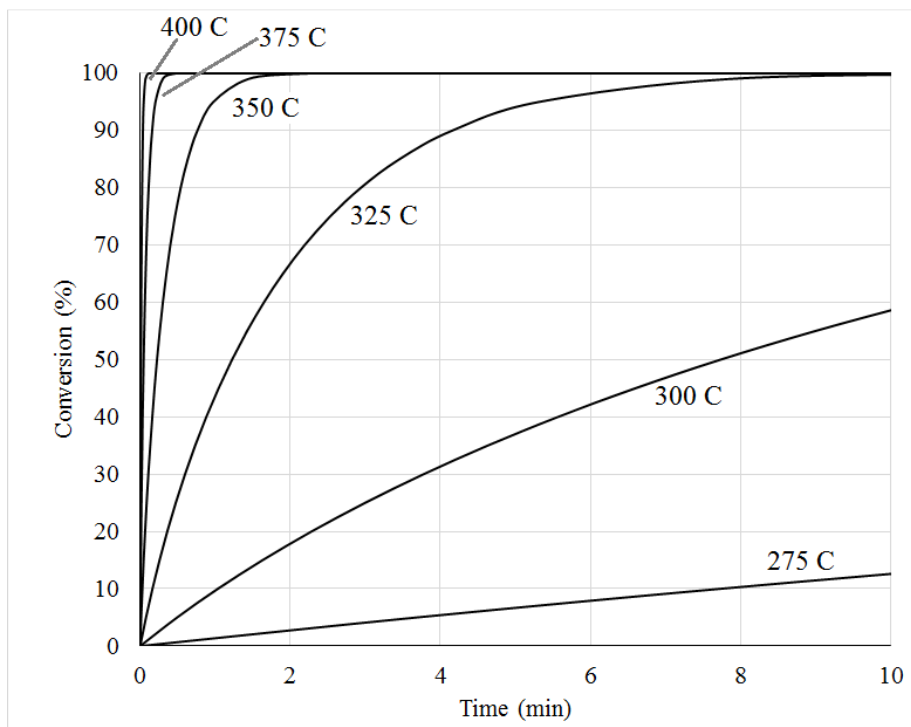
Figure 23. The theoretical conversion of triglyceride oil to
carboxylic acids vs. time at various temperatures

98

carboxylic acids can be expected to occur at low temperatures before substantial triglyceride

cracking begins. Hotter temperatures (e.g., 400 C) can be expected to approach essentially

complete conversion on the order of seconds, whereas at colder temperatures (e.g., 300 C),

minutes and/or hours are necessary to reach similar conversion.

Similar calculations were performed to observe the rate of bisallylic hydrogen abstraction

from between nonconjugated C=C bonds. This has been expressed as conversion vs. time, and

plotted for various temperatures in Figure 24. Bisallylic hydrogen abstraction has an activation

energy that is on the order of 46 kJ/mol higher than for degradation of a triglyceride molecule to

carboxylic acids. Whereas degradation to carboxylic acids may occur at temperatures below

triglyceride cracking conditions, bisallylic hydrogen abstraction is predicted to occur directly in

the range of the cracking temperatures/times utilized by Luo et al. for triglyceride cracking.[54]
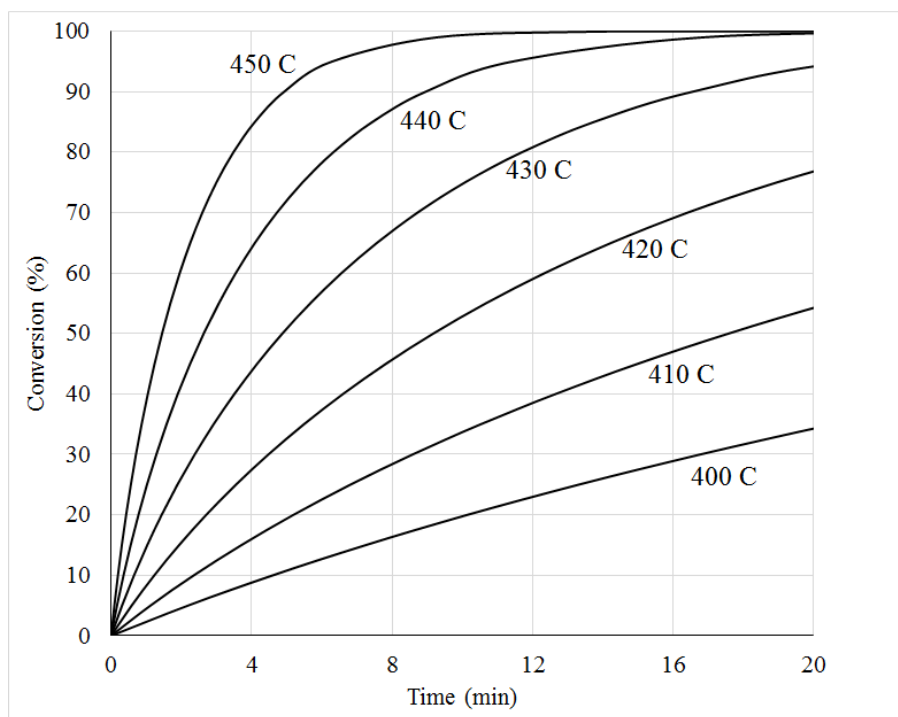
Figure 24. The theoretical abstraction of bisallylic hydrogen vs. time at various temperatures

As previously mentioned, this bisallylic hydrogen abstraction produces a free radical, which propagates at least one additional reaction. The substantially higher energy hydrogen radical could be expected to propagate any one of a vast set of reactions, despite the relatively low temperature of the cracking reaction fluid. Due to the complexity of the triglyceride cracking reaction set, it is difficult to anticipate the outcome of the atomic hydrogen produced under these circumstances.

The fragmentation of C-C bonds at the allylic position to C=C bonds is plotted in Figure 25 similar to Figure 24, with the only difference being that the plots reaction times have been extended from 20 to 90 min. This was performed on account of the slower speed of this C-C scission reaction, resulting from 19 kJ/mol higher activation energy than bisallylic hydrogen abstraction. Clearly the C-C scission reaction occurs at slower speeds than bisallylic hydrogen
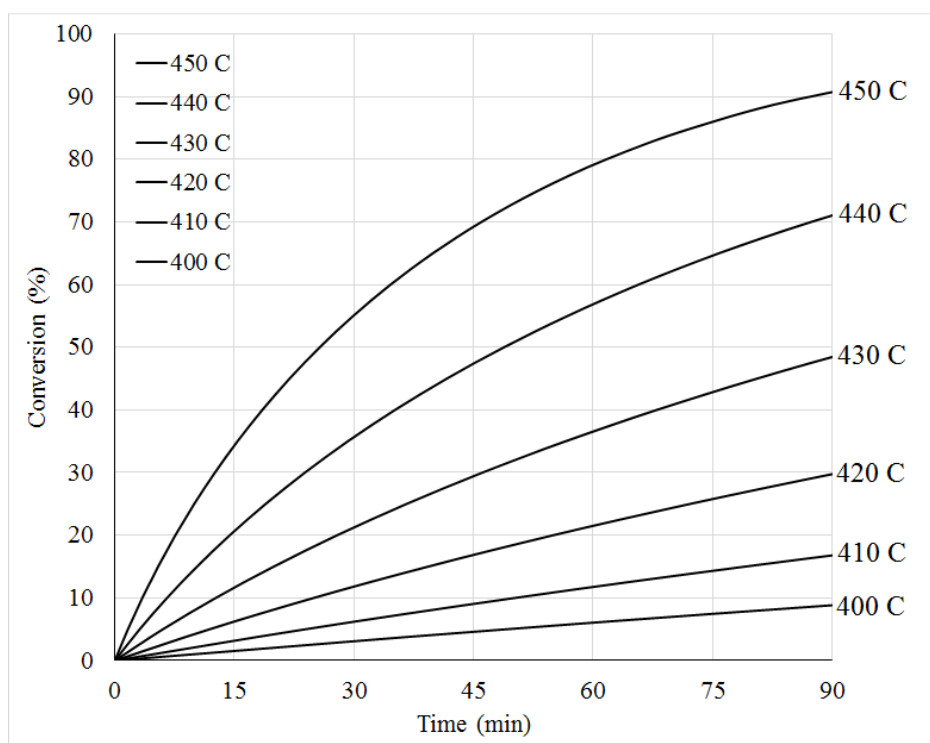
Figure 25. C-C scission at allylic position to C=C bonds vs. time and temperature

abstraction, but it is still on the same order of magnitude for triglyceride cracking reactions. In order to promote this C-C fragmentation, longer residence times might be desired, and complete conversion should not be anticipated. This reaction occurs for any unsaturated moieties (e.g., oleic, linoleic, linolenic, erucic), but does not occur for saturated moieties (e.g., palmitic, stearic).

The last reaction that is considered in this subsection is C-C scission at the α-2 position shown in Figure 26. This reaction leads to the formation of acetic acid as a cracked product, and its activation energy is 10 kJ/mol greater than the allylic C-C scission described previously. As expected, the reaction is substantially slower, so the plot's ordinate axis has been adjusted to provide better resolution for this reaction.
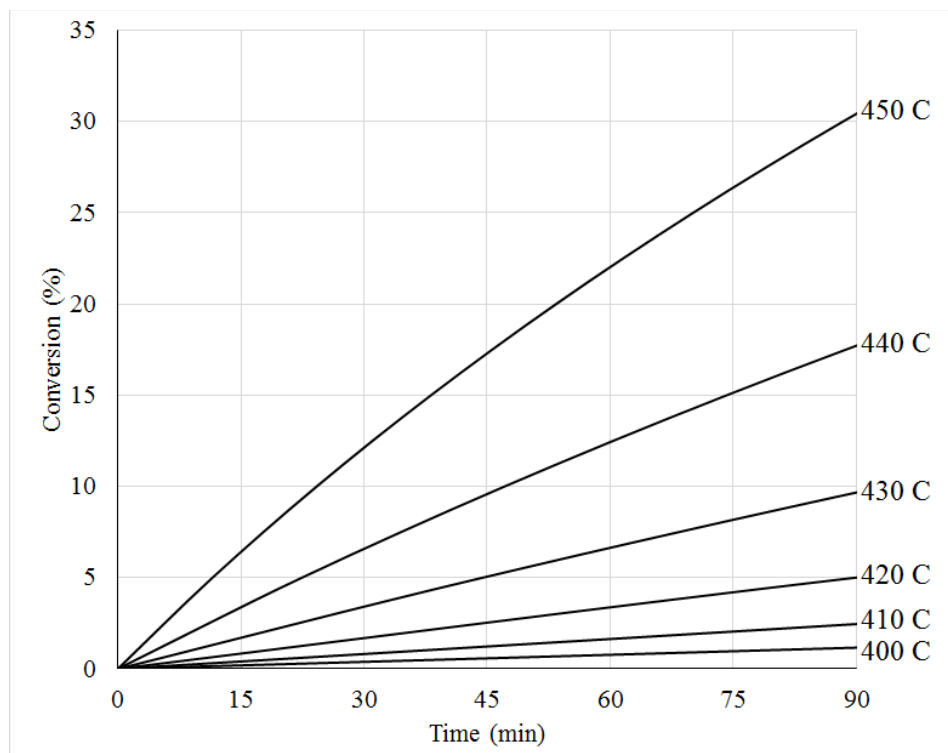
Figure 26. C-C scission at the fatty acid α-2 position vs. time and temperature

Based on this diagram, conversion to acetic acid should be anticipated in triglyceride cracking under typical conditions, but not to a great extent unless higher temperatures could be utilized. This production of acetic acid should be expected to be universal, despite the composition of the triglyceride feedstock, since this bond is present on all fatty acid moieties considered herein.

The next highest bond energy in the triglyceride molecule has an estimated activation energy that is 25 kJ/mol greater than C-C scission at the α-2 position. As a result, the remaining scission reactions in a triglyceride molecule are more likely to result from free radical mechanisms (propagation) rather than from initiation reactions. Such reactions are beyond the theory described in this section, and they will be examined by experiment in the present work.

III.F.6. Triglyceride Oil Sources and their Carboxylic Acids

The composition of the fatty acid moieties in feedstock TAGs depends on the source from which the TAG is derived. There is some deviation in the composition of TAGs depending on where they are produced and what strain is being harvested. However, different plant and animal species provide relatively predictable fatty acid compositions, as presented in this section. Additionally, there are standardized methods for determining the composition of TAG fatty acids (assuming the TAG is pure), which may prove useful for optimizing triglyceride cracking conditions for different feedstocks in future experimentation (e.g., ISO 5509[89]).

Table 1 through Table 3 show various species from which TAGs may be derived, and their literature reported compositions of fatty acid moieties. When necessary, data were averaged and/or normalized in order to provide values to the table rather than ranges. When

geographical data was referenced, oil compositions were averaged across North America rather than globally.

The majority of the fatty acid compositions were directly obtained from Bailey's Industrial Oil and Fat Products,[11] although other sources were utilized, and noted in the tables. Specialty oils were utilized in this study, and their compositions were provided by the vendors and included in the table for comparision purposes, however the vendors are not noted to preserve their anonymity. The fatty acid composition of crambe oil was taken from Singh.[90] Pennycress oil composition was obtained from Moser.[91] The oil composition for three species of microalgae were obtained from Abou-Shanab.[92] The composition of saturated oils was adapted from unsaturated oil compositions.

It should be mentioned that the sizable oil composition that is missing from these tables for n. pusilla algae oil is predominantly palmitoleic acid (COOH 16:1) and likewise for camelina oil is predominantly gondoic acid (COOH 20:1). The missing percentage of butter fat's composition is about one-third myristic acid (COOH 14:0), and the remaining two-thirds is mostly a varied blend of saturated moieties. These acids were not included in the tables since they are uncommon and less relevant to the present work. Other example oils were not included because their compositions sparingly contain common fatty acid moieties listed herein. Such oils include coconut oil (predominantly COOH 12 and COOH 14 saturates) and cuphea oil (predominantly COOH 8 – COOH 14 saturates).

In examining the mechanistically important fats/oils in Table 1, they are progressively sorted from oils rich in oleic (COOH 18:1) to erucic (COOH 22:1). Of the common commercial varieties shown here, the canola oil (column 4) is the richest in oleic acid (COOH 18:1).

Soybean oil, corn oil, and cottonseed oil are rich in linoleic acid (COOH 18:2), with varying

Table 1. Anticipated compositions of mechanistically important oils/fats (mol %)

Fatty Acid Moiety	VHONO	HONO	Canola	Soybean	Corn	Cotton Seed	Camelina	Linseed	HENO
Palmitic (16:0)	3.2	3.7	3.6	11.4	11.4	23.9	6.0	6.0	3.5
Stearic (18:0)	2.3	2.0	1.5	4.2	1.7	2.4	2.0	0.0	1.2
Oleic (18:1)	84.1	73.3	61.6	26.1	26.6	17.4	13.0	17.0	18.5
Linoleic (18:2)	4.0	14.8	21.7	50.3	57.6	53.4	16.0	14.0	13.2
Linolenic (18:3)	2.6	2.6	9.6	7.9	1.0	0.0	39.0	60.0	7.7
Erucic (22:1)	0.0	0.0	0.2	0.0	0.0	0.0	4.0	0.0	41.2
Other	3.8	3.7	1.8	0.1	1.7	3.0	20.0	3.0	13.6
Source:	Vendor	Vendor	Shahidi[11]	Shahidi[11]	Shahidi[11]	Shahidi[11]	Shahidi[11]	Shahidi[11]	Vendor

quantities of saturates in them as well (COOH 16:0 and COOH 18:0). Camelina oil and linseed

oil are rich in linolenic acid (COOH 18:3) while high erucic brassica and crambe oil are rich in

erucic acid (COOH 22:1).   These are especially important to the present work because they

were used in experiments designed to elucidate trends in triglyceride processing.

Table 2. Typical compositions of additional common oils/fats (mol %)

Fatty Acid Moiety	Palm Fruit	Butter	High Oleic Sunflower	Oleic Safflower	Olive	Peanut	Sunflower	Safflower	Crambe
Palmitic (16-0)	44.0	30.2	4.0	4.5	13.8	9.6	6.1	5.3	1.9
Stearic (18-0)	4.5	10.5	3.0	1.5	2.8	3.3	4.5	1.5	1.0
Oleic (18-1)	39.2	18.7	85.0	77.0	69.0	58.0	16.0	15.0	16.5
Linoleic (18-2)	10.1	2.1	8.0	15.0	12.3	22.4	71.0	77.0	10.1
Linolenic (18-3)	0.4	0.0	0.0	0.0	0.0	0.0	0.0	0.0	6.9
Erucic (22-1)	0.0	0.0	0.0	0.0	0.0	0.0	0.0	0.0	57.5
Other	1.8	38.5	0.0	2.0	2.3	6.8	0.0	1.3	6.0
Source:	Shahidi[11]	Shahidi[11]	Shahidi[11]	Shahidi[11]	Shahidi[11]	Shahidi[11]	Shahidi[11]	Shahidi[11]	Singh[90]

The compositions of additional fats/oils are listed in Table 2, sorted in a similar manner

to Table 1. These oils include oils such as palm fruit and butter that are rich in saturates (e.g.,

COOH 16:0) and a variety of oils rich in oleic acid and linoleic acid. One main difference

between these oils and the oils shown above in Table 1 is the lack of erucic acid, which has been

shown to be inedible. These oils illustrate that the majority of commercially available oils are comprised of fatty acids COOH 16 through COOH 18 in length. For this reason, mechanistic emphasis is placed on COOH 16 through COOH 18 range fatty acids.

Some oils provide shorter saturates as well (e.g., cuphea oil, butter fat, coconut oil). Such oils are typically higher cost and/or less available in bulk for commercial fuel production. Furthermore triglyceride feedstocks containing long chain fatty acid moieties have a low percentage of oxygen, whereas those with shorter-chain fatty acids have a greater percentage of oxygenation in the feedstock by mass. This leads to a reduced fuel yield per mass of oil.

Table 3. Typical compositions of inedible, hydrogenated,
waste, and renewable oils/fats (mol %)

Fatty Acid Moiety	HDO* Palm Fruit	HDO* Soybean	Field Pennycress	Tallow	Lard	Yellow Grease^	S. Obliquus Algae	N. Pusilla Algae	C. Ellipsoidea Algae
Palmitic (16:0)	44.0	11.4	3.1	24.9	25.7	11.4	21.5	31.0	26.0
Stearic (18:0)	54.2	88.5	0.5	19.0	14.0	4.2	0.0	0.0	0.0
Oleic (18:1)	0.0	0.0	11.1	43.0	44.0	26.1	21.0	0.0	4.0
Linoleic (18:2)	0.0	0.0	22.4	1.2	10.4	50.3	15.5	0.0	40.0
Linolenic (18:3)	0.0	0.0	11.8	0.5	1.0	7.9	38.0	6.0	23.0
Erucic (22:1)	0.0	0.0	32.8	1.0	1.1	0.0	0.0	0.0	0.0
Other	1.8	0.1	18.3	0.0	0.0	0.1	4.0	63.0	7.0
Source:	Shahidi[11]	Shahidi[11]	Moser[91]	Shahidi[11]	Shahidi[11]	Shahidi[11]	Abou-Shanab[92]	Abou-Shanab[92]	Abou-Shanab[92]

* Note: HDO indicates fully hydrogenated. Data have been adapted from their source for full hydrogenation.
^ Note: Yellow grease composition was approximated as soybean TAG composition because it often refers to used fryer TAG.

The fatty acid compositions of various inedible oils, hydrogenated oils, waste oils, and renewable oils are shown in Table 3. This disorganized group of oils is presented in order to establish trends in oil feedstocks. Used cooking oil and waste animal fats are relatively low value waste products that can be used for the production of renewables. Algae oil has been previously described as being an excellent renewable feedstock.

Concerning the compositions, used cooking soybean oil is shown here with assumedly

identical composition to that of ordinary soybean oil above. This is to be expected. The only difference is that some of the fatty acid moieties will have been severed from their triglyceride backbones as free fatty acids. This severance is oxidative, caused by high temperature reaction of the cooking oil with oxygen. It can be expected that only a small percentage of free fatty acids will be released into the oil before the oil is considered to be rancid and disposed. This minor percentage of fatty acids is expected to have negligible influence on the products of triglyceride cracking.

Hydrogenated oils are more expensive, and they would not be utilized for the production of renewables. However, beef tallow and pig lard are inexpensive oils, typically only usable for low cost applications such as fillers for animal feed. Hydrogenated palm oil and hydrogenated soybean oil are comprised of completely saturated fats, but it is clearly shown that animal fats such as beef tallow and pig lard still have approximately half of their fatty acids with unsaturated bonds. This is potentially important because the unsaturation creates nearby low energy bonds that enable cracking reactions in their vicinity, as previously discussed.

Finally, three strains of micro algal oil with different composition are shown in order to show some of the expected variety in algae oil. All of the algae strains herein show similarly elevated levels of palmitic acid (COOH 16:0). Otherwise, they vary substantially. The *S. obliquus* algae strain has an oil composition that is similar to camelina oil. *C. ellipsoidea* algae has a composition that can be likened to soybean oil. *N. pusilla* algae is largely comprised of palmitoleic acid (COOH 16:1) which is rarely seen in such a large percentage. These algae strains are helpful examples due to algae's potency as a renewable feedstock.

III.G. Summary

The theory and chemistry of noncatalytic cracking and triglyceride oils have been thoroughly examined with respect to literature relevant from the petroleum industry. The mechanisms discussed in the literature tend to support a mechanistic theory with limited chain of reaction steps, due to the relatively low temperature (compared to the bond energies) and high abundance of C=C bonds and C=O bonds in the feedstock.

Important triglyceride bonds energies (i.e., low energy bonds) were estimated for common fatty acid moieties. These data were then used to identify which reactions might be expected and which are unlikely based on bond cleavage reaction kinetics at various temperatures/conversions with time. Potential products of triglyceride cracking were determined, including acetic acid, heptanoic acid, undecenoic acid, and corresponding hydrocarbons of various lengths, such as tetradecane, hexadecane, undecene, nonane and others.

CHAPTER IV

STRATEGIES FOR COMPOSITIONAL ANALYSIS OF COMPLEX MIXTURES

In response to the growing motivation for renewable fuel sources, a number of catalytic and/or pyrolytic conversion technologies are being developed. Some of these technologies include the pyrolysis/cracking of lipids, cellulose, lignin, and/or combinations of these in the presence or absence of a catalyst. Pyrolysis products are often diverse liquid mixtures, comprised of highly and lowly volatile analytes. These are referred to as cracked triglyceride liquid (CTL), and for the purposes of this chapter, CTL will be used to describe any complex liquid mixture, whether it is petroleum-derived or biomass-derived. Depending on from where the CTL is derived, it may contain heteroatoms such as oxygen (e.g., from TAG cracking) and sometimes lesser amounts of nitrogen, phosphorous, and sulfur depending on the CTL source.

Sample characterization is a critical step in the evaluation and development of emerging technologies, since it is necessary to optimize and/or evaluate technologies and to demonstrate results in a meaningful way. CTLs are notoriously difficult to adequately characterize, and this creates a 'bottle-neck' in process development, which limits the progress of biomass pyrolysis technologies and establishes the critical importance of CTL characterization method development.

In order to discuss the features of various methods for CTL characterization, it is important to define three important metrics that describe the adequateness of such a method:

(1) the level of detail in the results, (2) the degree of sample representation, and (3) the ease of sample turnaround. The level of detail provided by a characterization method essentially indicates the type of data being provided by the method about a CTL sample. For example, analytical distillations provide a poor level of detail in the form of a distillation curve, whereas gas chromatography—mass spectrometry (GC-MS[*]) provides a high level of detail with potentially the exact identification and quantification of target analytes. A high level of detail is very desirable so that the differences between similar samples can be clearly seen in order to assist in process optimization and evaluation. In a similar way, the degree of sample representation must be high, with comprehensive representation being almost a necessity (i.e., near 100% mass balance closure by the characterization method).

Obviously, the ease of sample turnaround is also very important. Ideally, a method for CTL characterization provides the total chemical composition, representing the entirely of a sample, with minimal turnaround time and effort. Other important considerations for an ideal method involve the margin of error in the results and the universality of the method. Although there are certainly methods that exhibit many of these features, it is rare to find a suitable method that can provide all features even to a sufficient level. Some of the most powerful methods provide great detail and even comprehensive representation, but require extensive preparation, technical involvement, and data processing. They may also have limitations on what sample types they can properly analyze.

---

* Note: In this section and whenever not specified by content, MS refers to electron ionization mass spectrometry (EIMS).

IV.A. Basic Methods

Perhaps the most basic CTL sample characterization method is analytical distillation, which has long been a required specification for various fossil fuels,[93] providing a crude measure of sample volume vs. volatility in the form of a distillation curve. In its earliest form, the single-stage method is easy to perform and provides comprehensive results, at the cost of very poor resultant data, which makes it difficult to resolve the differences between two similar samples. Analytical distillation technologies have since evolved to provide reduced cracking error (e.g., vacuum distillation[65,94]), better resolution (e.g. multistage distillation[95]), reduced sample volume (e.g., miniature distillations[96]), and combinations of these features (e.g. spinning band distillations[67,97–99]).

From a basic perspective and under the best circumstances, analytical distillation has reasonable turnaround, can be automated, and provides comprehensive information about a CTL sample's volatility, thereby offering some insight into its value for fuel refinement (while saying little about specialty chemical refinement, which require higher compositional resolution). However, from a deeper perspective, analytical distillations provide mediocre information as a result of distillation losses, especially with very volatile components, and error induced by smaller sample volumes[96]. Furthermore, it is rare to find a distillation system capable of providing the best features with full automation/data collection (e.g., small sample size, vacuum compatibility, high resolution, low losses, small errors, and easy to use).

Finally, with the potentially high presence of oxygenates and specialty compounds in many CTL samples, comparable results may be obtained from the analytical distillation of CTL

110

samples that have substantially different compositions. It is necessary for a CTL characterization method to provide more compositional detail about the constituents of a CTL sample, such as alcohols, carboxylic acids, esters, ketones, aromatics, etc., so that meaningful information can be derived. This is especially true concerning the refinement of specialty chemicals from CTL samples, but also of fuel refinement in general.

ASTM International (West Conshohocken, PA) has devised a number of standard methods for semi-quantitative sample analysis, which provide accurate results but lack detail and/or comprehensiveness. For example, conventional fuels are tested with fluorescent indicator adsorption for aromatic and olefin content,[100] with ultraviolet (UV) spectrophotometry for naphthalene content,[101] and with low resolution MS for the determination of hydrocarbon types in middle distillates.[102] Other popular semi-quantitative methods include nuclear magnetic resonance (NMR) spectroscopy and Fourier Transform Infrared spectroscopy (FTIR). As stand-alone methods, or even when combined, these methods typically fail to provide information that is sufficiently detailed and/or comprehensive for proper CTL sample evaluation and process development, especially due to the convoluted nature of many of the compounds in CTL samples.

An evolution of the two previously described methods is referred to as the 'advanced distillation curve' method, which is a combination of semi-quantitative methods and analytical distillations to provide combined information about the volatility and chemical nature of a CTL sample. In this method, distillate fractions are subject to additional testing, typically of a semi-quantitative nature, although any number of tests may be applied to a fraction.[103–105] The advantage of combining these methods is that advanced distillation curves can provide some

111

compositional detail to supplement an existing distillation curve. Therefore, the results of advanced distillation are essentially comprehensive. Furthermore, appropriate tests can be applied to distillate cuts as desired by the user. A consequence of this is that the level of compositional detail is inversely proportional to the ease of sample turnaround. So then, the best results are only obtained with great effort and/or consolidation. Furthermore the results are always subject to some error and/or questionability due to problems mentioned above with analytical distillations.

IV.B. Gas Chromatography Methods

A potentially better choice for analyzing CTL is gas chromatography (GC). GC has many orders of magnitude more resolving power than distillation, while still maintaining the same underlying separation mechanism, in which CTL sample constituents are separated primarily based on their volatility (and also their functionality). Most GC methods have the following advantages over distillation: reduced potential for error, inherent automation of analytical operation, low required sample volume, and relatively short analysis times with respect to the highly detailed results that can be provided. Furthermore, with the hyphenation of GC to MS and/or other powerful detectors, GC is readily capable of identifying unknowns and distinguishing between chemicals in a single step. By contrast, distillation primarily distinguishes at the physical level.

Standardized chromatography methods have predominantly been developed for characterization of petroleum-based complex mixtures. One major limitation of standardized methods is their results are often selective, only providing information on a particular class of constituents (e.g., aromatics,[106] olefins,[107] etc.). The other major limitation is the non-universality

of the standardized methods, whereby a method is restricted to a certain subset of samples (e.g., spark ignition fuels[108–110]). Additionally, the standardized methods are only valid using the assumption that 100% of the species are eluted and resolved, normalizing the results to 100% and potentially invalidating the data with certain samples. In summary, standardized methods are only effective for their intended target samples, and are not well-suited for universal application or for novel renewable biofuel process development.

Stavova et al. discuss the significance of CTL characterization by GC in light of conventional methods and analytical strategies/challenges.[63] They recommend the use of high resolution GC and a simultaneous dual-detector flame ionization detector (FID) / electron ionization mass spectrometry (EIMS) arrangement (i.e., GC-FID/EIMS) as a practical method for characterizing CTL samples.[63] Stavova et al. establish the importance of the dual detector arrangement in a single instrument for both identifying and quantifying unknowns, based on the excellent linearity of the FID response in conjunction with the twice confirmed identification of target analytes by retention index and mass spectra. By contrast, Stavova demonstrates that employing a single detector alone is inadequate for this task.

Stavova et al. also cite a number of publications documenting CTL characterizations that do not address some important analytical considerations that may result in substantial systematic errors. These include inlet analyte discrimination, results normalization, and not accounting for the unresolved complex mixture (UCM) that forms a large nondescript 'hump' beneath identifiable analytes. Furthermore, Stavova offers solutions to account for these considerations, through proper inlet selection/operation, internal standardization, and the use of UCM quantification and reporting. In order to account for the notoriously poor elution behavior of

some analytes (e.g. carboxylic acids), Stavova et al. suggest derivatization as a compromising technique, although it requires auxiliary analyses.

Ultimately, the value of a detailed/comprehensive CTL sample characterization method for major and minor constituents that mitigates common systematic errors cannot be overstated. Such a method directly aids the development of new and complex biomass processes through elucidating potential fuel and/or specialty chemical yields and accurately differentiating between similar CTL samples.

Nonetheless, Stavova et al.'s CTL characterization still exhibits problems with (1) the lengthy sample turnaround times that result from (a) the inability to reliably automate the data processing and (b) the necessity for derivatization and (2) the nondescript nature of the reported UCM.

Accepting the fact that biomass pyrolysis commonly results in CTL with highly variable volatility, polarity and functional groups, there are recognizable limitations for any GC method such as high resolution GC or GC×GC to resolve all constituents. This is especially true as the molecular weight increases because of the exponentially greater quantity of formula isomers for larger molecules. While many chromatographers could confidently consider the notion of deconvoluting C_{10} isomers in high resolution GC, the same could not be said about higher chain lengths (e.g., C_{20} and greater). This challenge is further complicated by the variety of polarities present in CTL samples resulting in nonuniform elution behavior (e.g. carboxylic acids in mixture with hydrocarbons).

Ultimately their nature prevents analytes in CTL samples from being fully resolved, resulting in an UCM from which very limited data can be obtained by electron ionization (EI)

MS or FID. In the presence of the UCM, the identification and quantitation of analytes by EIMS cannot be entirely trusted to an automated data reduction method, ultimately requiring a well-trained lab technician to laboriously supervise the data processing, while likewise introducing the potential for human error.

IV.C. Simulated Distillation Methods

To sidestep the inability to resolve samples that is inherent in target analyte GC methods, simulated distillation (SimDist) methods have been developed and widely implemented in petrochemical analyses. SimDist methods use characteristically short/wide GC columns to approximate the distillation curve of a hydrocarbon sample by GC-FID.[111–113] SimDist methods do not focus on baseline resolution or separation of analytes. Instead, they use short/wide columns with thin stationary phase coatings in order to promote greater elution of analytes (up to C_{100}) and to provide a stable baseline between runs.[64] SimDist methods preferentially use on-column inlets (or programmed temperature vaporization inlets) to mitigate inlet analyte discrimination. Additionally they utilize universal (i.e., nonselective) detectors with high linearity (e.g. FID) in order to confidently integrate area respective of mass. Analytes are lumped into retention windows with respective normal boiling point ranges, effectively providing a distillation curve, although the chromatographic resolution is much greater than even the best distillation systems as long as analyte polarity is consistent.

SimDist methods are attractive as their equipment is relatively inexpensive and their results are easy to interpret, leading to quick sample turnaround times. When they are properly utilized, SimDist methods are able to provide volatility information on analytes ranging from low molecular weights up to C_{100} with full automation.[64] However, SimDist results lack any

compositional detail since they only provide volatility information.

The purpose of the present work was to hybridize the methods of dual-detector GC-FID/MS and SimDist in a new way to characterize CTL samples with fully comprehensive, chemically detailed results, over a full range of analytes and with easy sample turnaround. In order to accomplish this goal, a unique dual-detection system was implemented to combine field ionization mass spectrometry (FIMS) in a simultaneous configuration with a GC-FID (for SimDist). In comparison to target analyte methods (e.g., detailed GC-FID/EIMS), this method sacrifices GC resolution but compensates with reliable soft MS data that permits formula speciation even for heavily convoluted chromatograms. There is some precedent for the union of these two methods through published work by Chen et al.[114] and Ha et al.,[115] who collected SimDist data (e.g., GC-FID) and GC-FIMS data separately, among other data, eventually combining them to deduce the distributive composition of petroleum derived samples. The features of this method are described in Section V.B.4.ii.

IV.D. Field Ionization Mass Spectrometry Methods

Invented in 1953 by E. W. Mueller[116] and hyphenated to mass spectrometry soon after,[117] field ionization (FI) is a soft ionization technique that is capable of circumventing the limitations for GC to resolve complex samples by producing FI mass spectra. FI occurs in close proximity to a field emitter (electrode), where high electric field strengths remove an electron from analyte molecules through a quantum mechanical tunneling mechanism, producing molecular ions. Sharp-ended FI emitters (e.g., the microneedle coated wire shown in Figure 43 (see Section V.B.4.ii), conditioned razor blade, or platinum film, etc.) create the necessary field strengths on the order of 1×10^7 to 5×10^8 V/cm. When analytes are co-ionized and/or unresolved, the FI mass

spectra are readily interpretable, allowing the distribution of molecular formulas of a sample to be determined.

The FI mass spectra can contain ions of virtually pure molecular masses, and so the need for spectral deconvolution is negated. This permits reliable automation of data processing and likewise high throughput sample analysis and data processing, which is very attractive for CTL characterization. This is true to such an extent that FIMS is often used to characterize complex samples (such as diesel fuel) as a standalone detector, without chromatographic separation.[118,119] Other researchers cite similar motivations for using soft ionization to circumvent GC resolving limitations, demonstrating that even the resolving power of GC×GC can benefit from soft ionization methods.[120,121]

FIMS induces little vibrational energy, thereby producing a high purity molecular ion, i.e., with a very low abundance of ion fragments.[122] Although it is possible to get fragmentation of various molecules in field ionization under sufficiently high field strengths, metastable/fragment ions are often on the order of 1% or less under commonly utilized FIMS conditions (low/moderate field strengths), according to Hans-D. Beckey.[123] This tendency for pure molecular ions is true for a variety of organic functional groups (e.g., paraffins, olefins, alkynes, cyclics, ketones, and amines).[123]

The obvious effect of non-fragmenting ionization is the inability of FIMS to differentiate between analytes that are formula isomers such as cyclohexane and 1-hexene under commonly observed FI conditions. Although fragmentation of olefin molecules can occur in field ionization, the relative abundance of fragments are likewise minor in comparison to the molecular ion under such low/moderate field strengths.[124,125]

117

Although FIMS is considered to be fairly universal for ionization and production of a molecular ion, some authors have occasionally reported absent molecular ions from FI spectra, typically with halogenated organics (e.g., bromodecane) or alcohols.[126] Furthermore, analytes with quaternary carbons (e.g., isooctane) commonly fragment substantially, thus not producing molecular ions in high purity.

Another implication for FIMS is that high resolution mass analyzers help distinguish between analytes with very similar molecular weights (e.g., $C_{10}H_{21}OH$ vs. $C_{11}H_{24}$), for which unit resolution mass spectrometers are unable to differentiate.[127] Although field ionization reduces the resolution of MS instruments due to locally variable and/or fluxuating field strengths, FIMS has been utilized with mass resolutions of 30,000 or better.[123] For unit resolution FIMS, results are typically presented in what is referred to as a z-series table[128] or a double bond equivalence table,[119] organized two-dimensionally by (1) carbon number and (2) a classifier respective of functional group(s). Data from high resolution FIMS is structured in a similar manner. An example data table is included in Appendix K.

Concerning hyphenation of GC to soft ionization, GC-FIMS and GC-PIMS (photoionization MS) have been studied by multiple analytical research groups for analysis of complex samples. Prominent examples include the analysis of petrochemical samples by Chen et al.[114] and Qian et al.[129] using GC-FIMS and Zimmerman et al.[120,121,130,131] using GC-PIMS. Comparing GC-FIMS to FIMS, the gas chromatograph has the advantages of (1) convenient and reliable sample introduction mechanisms and (2) the confident separation of metastable/fragment ions from pure spectra based on retention indices. The dual detector configuration of GC-FID/FIMS has the added advantage of definitive mass-volatility data (i.e., the simulated

distillation curve) stemming from the high linearity of the FID in simultaneous union with the FIMS data which provides formula speciation.

FIMS has seen a general decline in use and publications due to the emergence and popularity of other soft ionization methods since its interest peaked around 1978.[116] For this reason, it is important to discuss other GC-MS appropriate soft ionization methods (chemical ionization—CI and photoionization—PI) similarly suited for complex sample analysis, in comparison to EI. Noteworthy advantages of EI over FI is that field ionization produces ions of lesser intensity, less repeatability (5-8 % variability, increasing as the peak intensity decreases[118]), and reduced mass resolution (not uncommonly reduced to ½ to ⅓ resolution). The advantage of FI over EI is the ability to generate predominantly molecular masses in the FI mass spectra, providing formula distributions for poorly and/or unresolved analytes.[123]

FI is commonly preferred over CI because chemical ionization is very selective (i.e., non-universal). The relative ionization efficiencies (RIEs) for chemical ionization vary substantially more than FI.[126] Furthermore, CI can produce spectra that are complicated by protonation, adduct formation, and the formation of other ions.[126]

From a purely theoretical perspective, PIMS appears to be superior to FIMS in concept due to PIMS' modal selectivity. PIMS is able to ionize either universally and/or selectively for specific functional groups, allowing it to differentiate between molecular formula isomers (e.g. cyclics / olefins). The differentiation is based on the energy of the vacuum ultraviolet (VUV) emissions vs. analyte ionization potential (in eV).

In the application of PIMS to poorly resolved analytes (e.g., UCM), however, PIMS has been shown to induce formation of substantial fragmentation ions typically due to the

119

transmission of excess energy to the target molecules during photoionization, which detract from its usefulness in comparison to FIMS. In fairness, these fragment ions are typically smaller fragments, so it is often possible to isolate the molecular ion based on GC retention indices.

There are other problems with PIMS such as low emissions of conventional (glow discharge) lamps, the rarity of tunable/selectable PIMS light sources (i.e., synchrotron radiation from major/national laboratories[132,133]), and large deviations in relative ionization efficiencies (RIEs) due to cross section differences. New developments into tabletop tunable PIMS light sources[134] and fragment-free PIMS from super-cooled molecular beams[135] may eventually make PIMS the soft ionization method of choice for this type of analysis, but as of current availability, high performing PIMS instruments are typically special purposed and/or customized.

In summary, FIMS is an advantageous and readily available soft ionization method for complex sample analysis. Despite its declining use, it continues to find utilization, especially in the analysis of petrochemical samples.

Considering the general application of FIMS, there are important observations that motivate the selection of equipment and method parameters for the purest, most predictable, and most repeatable spectral results which can also be compared to other available literature. Beckey notes that heating the ion source above 100 C (or well above 200 C depending on the analytes being investigated) helps to prevent and/or remove an adsorbed layer of analytes on the emitter surface.[123] The buildup of adsorbed analytes can be responsible for spectral fluxuations, including dramatically affected intensities and/or latent ionization, by a phenomenon sometimes referred to as *emitter memory*.

Similar heating of wire type emitters for removal of adsorbed analytes can also be

accomplished by applying a current through the emitter in order to elevate its temperature, via any of the following methods: (1) a brief/intense current pulse between periods of MS spectral acquisition, (2) a sustained current at all times, typically at a lower level, and/or (3) baking current in between analyses; all of which are common features for wire emitters due to their low thermal mass.[119] Surface adsorption of sample analytes in evacuated reservoirs attached to FIMS units can cause contamination of subsequent analyses inducing systematic errors and/or poor repeatability.[119]

There are three types of emitters for FI: wire emitters, razor emitters, and point emitters. The micro-needle wire emitter is considered to be best suited for obtaining intense and pure molecular ions, from both a theoretical and observational standpoint.[123] By contrast, single point emitters are capable of the highest practical field strengths on the order of 5×10^8 V/cm. At such field strengths, greater fluxuations in the intensity of ions and reduced total ion current may be expected. An advantage of high field strength is that it improves the mass resolution, reducing the resolution gap between EIMS and FIMS for an otherwise identical instrument. Additionally, high field strengths elicit the production of ion fragments and/or metastable ions,[123] which can be desirable but is typically not required for analysis. Less conventional FI emitters also exist, such as the volcano type emitter, which involves a 10 μm orifice with dendritic points and markedly low extraction voltages.[136]

FIMS has some important considerations that are noteworthy. Perfluorokerosene (PFK) and perfluorotributylamine (PFTBA), very popular EIMS mass calibrants, have been shown to destroy the microneedle protrusions of some FI emitters, reducing field strengths, although common tungsten wire emitters (activated in benzoic acid nitrile) resist their chemical attack.[137]

More importantly, PFK has been demonstrated to be incompatible with FIMS due to its negative mass effect, whereby the ions that are produced are of little use for calibration.[128] As such, mass calibrants should be chosen carefully since PFK cannot be utilized.

In light of these observations and notations, many general recommendations for FIMS method development can be suggested that will assist with reproducibility and quality of results. Concerning mass calibration, Yoshida found that the atomic isotopic ratios were overestimated by field ionization, increasingly so with decreasing ion intensity.[118] This warrants further consideration and/or close examination. Isotopic ratios should be monitored experimentally with standards so that any significant deviations from natural ratios can be identified.

Regardless of the optimal method parameters found by experiment, some degree of ion source heating and/or emitter current heating should be utilized in order to counteract emitter memory. This can be accomplished by ion source heaters and/or emitter *flashing* for compatible emitters (wire type). In any case, the existence of emitter memory should be monitored through the use of standards, and parameters should be adjusted as needed to eliminate this problem.

Although the field strength is very difficult to predict and/or measure due to the variable and/or dynamic surface morphology of field emitters, Speier et al. published a sufficient correlational method for determining the field strength using an n-heptane standard and comparing the intensities of the molecular ion and the $C_2H_5^+$ fragment ion using sharpened platinum point emitters and scanning electron microscopy to determine the point's radius of curvature.[138] The details of Speier's work are utilized in the present work as described in Section V.B.4.ii for monitoring the field strength of wire type emitters.

The field strength is clearly an important metric for FIMS, and it should be considered

whenever FIMS is utilized. At best, field strengths should be determined, monitored, and

documented for any important conditions studied so that results may be compared between

publications, and at worst, a produced FI spectrum of pure n-heptane should be provided in order

to qualify the data. Emitters at various ages should be considered (e.g. new emitters vs.

weathered emitters) in order to determine the effect of age on method performance.

The hyphenation of FIMS to GC should be utilized to take advantage of multiple

benefits. The maturity and repeatability of GC provides an ideal sample introduction method

that is also suitable when employing multiple detectors in parallel. Additionally,

chromatographic separation offers the potential ability to reject fragment/metastable ions from

otherwise clean spectra based on retention index mapping.

Most importantly, a full array of analytes should have their RIEs determined and

presented for FIMS data in order: (1) to establish trends for estimating the RIEs of 'non-target'

analytes, (2) to estimate the potential quantitation error from FIMS spectral data, which is the

relative standard error of all RIEs at a single exact mass, and (3) to identify any trends in the

relative standard error.

These considerations are also very important when considering published FIMS

literature. Ideally, publications disclose information such as the ion source temperature, type of

emitter, extraction voltage (potential between the emitter (anode) and cathode), and emitter

activation/conditioning (when applicable). Some publications even go so far as to provide

spatial information, such as the distance between the emitter/cathode and the clearance of the

cathode slit/rods.

Unfortunately, the trend in FI literature seems to be a lack of consistency in FI method

reporting whatsoever, with far too many publications only disclosing the make/model of the ion source used, only qualitatively reporting RIEs, and/or citing previous studies to generalize RIEs rather than measuring and reporting them. Although there may be justifications, the inconsistency in FIMS reporting does not seem to be well explained.

Field strength measurements/calibrations appear to be the least documented and/or controlled metric of FIMS publications, although its measure and monitoring is seemingly very important for the efficacy of results, especially when emitters are replaced, reconditioned, or otherwise changed due to emitter aging.

IV.E. Relatable Studies Using FIMS for Analyzing Complex Mixtures

Scheppele et al. have published RIEs for a variety of organic compounds including aromatics, thiophenes, and aromatics containing N/O heteroatoms[139] and linear and cyclic paraffins,[140] obtained at the substantially elevated ion source temperatures of 260 C and 270 – 300 C, respectively. They used stainless steel razor blades conditioned with acetone as emitters with extraction potentials of 7.1 – 7.3 kV and 5.0 – 6.6 kV, respectively. Concerning aromatic compounds, Scheppele reports RIEs with respect to ethylbenzene for various aromatics/derivatives being on the order of 1.0 ± 0.5, noting greater variation with increasing functional group variety. Concerning saturates, Scheppele et al. found RIEs with respect to n-decane for $C_6 - C_{19}$ linear alkanes were within 1.0 ± 0.3, being relatively constant in nature, whereas for $C_6 - C_{25}$ branched- or poly-cyclic paraffins the relative ionization efficiencies ranged from 2.2 to 5.2 and correlated functionally with ring structures to some extent.

Kuras et al. also studied saturated hydrocarbons using conditioned razor blades although at a milder ion source temperature of 120 C in order to study mixtures of n-paraffins,

isoparaffins, and monocyclic-, dicyclic- and tricyclic paraffins. Although Kuras et al. did not report the RIEs of individual compounds, they did report group-averaged RIEs close to 1.0 for all groups (0.706, 0.532, 0.616, 0.798, and 1.210, respectively), including cyclic paraffins which is a very different observation from Scheppele et al.

Kuras et al. also tested the relative ionization efficiencies of the same mixtures diluted 2:1 in ethylbenzene. These results showed even greater equalization to 1.0 for the mentioned groups (0.960, 0.704, 0.768, 0.756, and 0.731, respectively). They claim that the inclusion of aromatic hydrocarbons (specifically ethylbenzene) in the analyzed mixture (33% by vol.) helped to equalize the relative ionization efficiencies of all groups by suppressing the adsorption of higher MW analytes on the surface that would otherwise lead to preferentially greater ionization.

Comparing the results of Kuras and Scheppele, it is unfair to then conclude that Scheppele et al.'s results are due to higher adsorption of cyclic RIEs on the emitter surface, because Scheppele's ion source was maintained at substantially higher temperatures than Kuras. It is therefore difficult to draw a definitive conclusion from the RIE reports of these two papers concerning cyclic paraffins. On the other hand, these studies do indicate relatively invariant RIEs for linear paraffins, which is attractive for deducing the composition of complex samples. Neither study made mention of emitter memory.

Briker et. al. had success characterizing diesel fuel by GC-FIMS using volcano type (i.e., orifice) emitters with very good sample turnaround in comparison to multiple more laborious LC and GC methods.[127,141] Unfortunately, operating parameters were not reported, although these emitters have been reported in other sources as operating at dramatically reduced extraction voltages (e.g., 1.5 kV)[136] while still maintaining performance.

Briker et al.'s research appears to stem from earlier work of Malhotra that discloses group-averaged RIEs relative to *n-heptylbenzene* as follows: 0.34 (branched paraffins), 0.54 – 0.63 (paraffin cyclics), aromatics (0.91 – 1.03), and 1.03 – 1.44 (higher order aromatics). Malhotra stated that the RIEs did not vary more than ± 15 % over the range of carbon numbers C_5-C_{20}.[128,142] The multitude of papers stemming from this work do not appear to report RIEs, instead they originate back to the work of Malhotra.

IV.F. The Use of Wire Type Field Emitters

Whereas the prior several FIMS studies involved the use of conditioned razor blade emitters and/or volcano type ion sources, microneedle coated tungsten wire emitters are important for a number of reasons in addition to previously described benefits. A study by Lattimer and Schulten surveyed mass spectrometers throughout the country in 1989 and reported that 86 % of FIMS scientists were using such wire emitters, with 11 % using silicon microneedle wire emitters and 3 % using other means (razors, singular points, metallic microneedles, volcano, etc.).[116] With the high percentage of FIMS scientists utilizing wire type emitters, it is important to characterize their capabilities.

Wire type emitters are substantially advantageous because they may be transiently *flashed* during acquisition by energizing the wire with electric current for several milliseconds. This briefly creates extremely high emitter temperatures sufficient to desorb even very low volatility analytes from the emitter surface, negating emitter memory. Afterwards, the temperature quickly equilibrates with the surroundings to conditions more amicable for FIMS before continuing acquisition. The *flash* capability of a wire emitter is made possible by the miniscule thermal mass of a wire-type emitter. Similar thermal transient capabilities are difficult

to mimic with other types of emitters, and simply elevating the ion source temperature has its limits (thermal fragmentation temperatures) and drawbacks (reduced ion intensity).

The equilibrium temperature at the axial center of a microneedle coated tungsten emitter in like-new condition of dimensions 5 mm long x 10 μm diameter with 30 μm carbon fiber microneedle dendrites has been investigated, summarized, and modeled in the work of Fraley. The results are summarized in Table 4 below so that emitter temperatures could be estimated in reviewed literature where current was used to heat the emitter wire.[143] What is not obvious is that at low emitter currents ($\leq$ 10 mA), the temperature barely increases above its minimum, whereas at higher currents the temperature rises sharply. It should also be accepted that as the emitter ages, anticipated temperatures should be systematically higher due to dendrite blunting, shedding, fouling, etc. based on the recorded temperatures in the absence of microneedles, which coincides with theory.[143] The reported temperatures in Table 4 are in reference to an un-elevated ion source temperature (i.e. assumes 20 C), so that if an ion source is heated above ambient, the emitter temperatures should be likewise adjusted.

Table 4. Estimated temperature of microneedle coated tungsten wire emitter vs. current[143]

Current	(mA)	0	10	20	30	40	50	60
Temperature	(C)	<55	62	112	352	527	802	977

Qian et al. characterized petroleum middle distillate samples by high resolution GC-FIMS using microneedle coated tungsten emitters of 10 μm diameter positioned approximately 1.5 mm away from cathode extraction rods maintained at an extraction voltage of 12 kV. In their

original work,[144] Qian et al. demonstrated their methods and the benefits of high resolution GC-FIMS for identifying sulfur containing compounds in addition to hydrocarbons. They reported the relative ion abundances grouped into a comprehensive z-series table including both hydrocarbon and sulfur-containing classes. Unfortunately, they did not investigate the RIEs for various compounds. However, Qian et al. did report atomic isotopic ratios (e.g. C^{13}/C^{12}) that were very consistent with nominal values, as would be expected.[144] This leads one to question whether the unusual atomic isotope ratios reported in Yoshida's work[118] can be explained as a consequence of unit resolution mass analyzers rather than a consequence of FIMS.

In Qian et al.'s continuing work,[129] they utilized a flash current of 12 mA for 0.2 s between 1 s spectral acquisitions, so that anticipated nominal emitter temperature might be on the order of <55 C and flash temperature of the emitter might be approximately 72 C at the axial center, depending on the details and age of the emitter. There was no other reported indication of heating the ion source volume, so it must be assumed to be at low temperature near ambient. Qian et al. illustrated that the high resolution GC-FIMS setup is capable of providing three dimensions of separation: boiling point, polarity, and exact mass. However, they did not present RIEs for compounds that were identified, perhaps leaving the identification up to other detectors as necessary, or perhaps deducing qualitative information from the FIMS relative abundances for which to compare samples.

In further progression of this group's research, Androulakis et al. remark that the "variation in ionization efficiency of molecules with varying structures and sizes makes quantitative analysis of petroleum by FI-MS challenging." This is an interesting remark in light of a variety of research groups that were previously cited reporting ionization efficiencies

128

described as being relatively invariant, especially with carbon number, having some differences due to functional groups.[145] It is wondered what differences in equipment or conditions control the variation of RIEs. Androulakis et al. refer to a triple detector system published by Qian et al. for RIEs (described in the following paragraph) rather than reporting their own.

Qian developed a triple detector system (FID, FIMS, UV) utilizing supercritical fluid chromatography for separations in order to resolve classes of petrochemical compounds such as paraffins, monoaromatics, diaromatics, etc.[146] Qian utilized the FID in order to quantify non-aromatics and utilized FIMS to quantify aromatics. Furthermore, Qian reported RIEs for aromatics increasing linearly with carbon number, which Qian then validated with respect to prior literature by Schulz in 1993.[147]

In reviewing these studies, the majority of FIMS utilization has been for petroleum CTL sample analysis. However, the interpretation of these studies is that very few have properly justified their FIMS operating conditions through reported optimization studies, and fewer still have reported RIEs for various analytes sufficient to replicate and/or apply their work to similar and/or different FIMS equipment. This is perhaps an unfair observation, since the papers which have been reviewed were primarily English papers, perhaps accounting for only 10 % of all FIMS papers, with the largest majority of papers being German due to the origin of invention in Bonn, Germany. Nonetheless, there appears to be sufficient need for a thorough investigation into FIMS optima and RIEs using wire type emitters.

As previously mentioned, the present work investigates a dual-detection GC-FID/FIMS characterization method. In reviewing the similarly purposed work of Qian et al., who used a triple detector SFC instrument (SFC–FID/UV/FIMS), the multi detector concept is shown to not

be unique, and neither are the motivations for using it or the application of it to CTL. What is unique to the method of the present work are: (1) the illustration of the optimal conditions by which to operate a wire type FI emitter for the greatest invariance of RIE for various analytes and (2) the application of the multi detector method to pyrolyzed biomass CTL samples.

The advantage of using the FID detector in parallel to FIMS may not be straightforward, but it is advantageous for multiple reasons. The first reason is that the FID has excellent linearity, so that the quantitative data from the GC-FID/FIMS method is most reliable in terms of volatility (straight from GC-FID), and less reliable in terms of speciation (from FIMS). Secondly, having a well characterized detector split ratio permits a GC operator to easily monitor any changes in FIMS performance based on the FIMS/FID relative detector response measured by analyzing calibration mixtures frequently in between CTL samples.

This work considers a particular classification of advanced biofuels derived from thermal (or catalytic) degradation of TAG based oils, producing a biofuel intermediate CTL with the likeness of petroleum crude, containing various hydrocarbons and oxygenates (predominantly carboxylic acids) with varying amounts of heavy residue and/or partially intact TAG feedstock molecules. Extra special attention will therefore be exhibited for this type of carboxylic acid rich organic CTL.

CHAPTER V

EXPERIMENTAL

The development of renewable fuels have been discussed in Chapter I, beginning with first generation renewable transportation fuels, leading into more advanced fuels with drop-in compatibility. Special attention was paid to triglyceride (TAG) cracking which is relevant to this dissertation and publications that involve triglyceride cracking were scrutinized.

This set the stage for the introduction of the University of North Dakota's (UND's) noncatalytic cracking process (NCP), which was described in Chapter II, through which TAGs are cracked and then refined into drop-in compatible fuels and petroleum equivalent renewable chemicals.

Noncatalytic cracking theory was then described and applied to TAG cracking in Chapter III, which has some distinct differences from petroleum cracking. Interpretations of cracking literature from the petroleum industry were used to determine what to expect from TAG cracking. Bond energies were calculated for various triglyceride moieties and used to estimate reaction kinetics for various fundamental TAG cracking reactions. These preliminary calculations may lead to the development of numerical models for noncatalytic cracking once more experimental data on TAG becomes available.

Analytical methods were also investigated for characterizing cracked TAG liquid (i.e., CTL). A recommended analytical method was presented, utilizing gas chromatography with

simultaneous dual detection (flame ionization detector, FID / field ionization mass spectrometer, FIMS) that would potentially permit high throughput compositional analysis of CTL. This method was developed as part of the research described herein (see Section V.B.4.ii) and then utilized to determine the composition of CTL samples generated in the present work as well as samples from previous research in order to cross check the method. In this dissertation, the method is referred to as FIMSDIST because it is the simultaneous combination of a simulated distillation (SimDist) and field ionization (FI) mass spectrometry.

The underlying objectives of this dissertation were to identify technological and/or commercialization obstacles for the NCP and to hypothesize and test solutions for overcoming those obstacles and to estimate the yields of the NCP experimentally. The aforementioned reviews enabled a thorough experimental plan to accomplish those goals, which is described in this chapter and summarized below.

As previously described in Chapter II, the noncatalytic cracking process (NCP) consists of five core subsystems and a few optional subsystems that are used to convert triglyceride oils (TAGs) into petroleum-equivalent renewable fuels and chemical products. Major technical obstacles involve the process' three reactive subsystems: *Oil Cracking*, *Catalytic Deoxygenation*, and *Residue Processing*. Through the efforts of this dissertation, the commercialization obstacles in the first two subsystems have been solved, while the latter one is still subject to ongoing research and development at UND, described in Section II.A.3. The first two obstacles are summarized in the following paragraphs.

The first obstacle involved TAG cracking in continuous-stirred-tank-reactors (CSTRs), which were characterized by severe coke formation on the reactor walls. This made it difficult

132

and/or hazardous to scale up the process. Literature reviewed in Section I.E.4 implied that

cracking reactors could operate without the formation of coke under appropriate circumstances.

As a result, it was hypothesized that the reasons for coke formation could be identified and

demonstrated experimentally. It was furthermore hypothesized that this would lead to the

discovery of better operating conditions and/or reactor designs that could operate with negligible

coke formation. A series of experiments were conducted to identify potential reasons for coke

formation in NCP reactors and to design reactors potentially capable of operating in the absence

of coke formation. The experimental methodology for this hypothesis testing is described

Section V.C.2.

The second obstacle was evident when performing catalytic deoxygenation of cracked

TAG distillates (CTD). The cost of the catalyst (palladium-based) was so high that made the

entire process commercially challenging. Literature review in Section I.E.3 indicated that nickel

catalysts were capable of deoxygenation of carboxylic acids. As a result, it was hypothesized

that nickel catalysts could be suitable for replacing palladium-based catalysts in the NCP. This

incorporated two hypotheses: (1) that the nickel catalyst(s) would reach sufficient conversion to

enable the refinement of jet fuel complying with the total acidity specifications for Jet-A-1 fuel[27]

and (2) that operating conditions could be identified for the continuous deoxygenation of CTD in

packed bed reactors without catalyst deactivation. Additionally, it was hypothesized that nickel-

based catalysts could outperform the palladium-based catalyst under the appropriate operating

conditions. A series of experiments were performed to test these hypotheses as described in

Section V.C.1.

The final experimental hypothesis was that laboratory experiments could produce data

sufficient to estimate the yields of the NCP and to determine factors which affect those yields or the process economics that stem from them. Laboratory samples were generated under varying operating conditions (i.e., temperature, pressure, space time, feed composition, reactor type, etc.). Select samples were analyzed to determine their chemical composition, and products from the process were estimated from their composition. Then statistical regression was used in order to determine statistical factors that influence the process' fuel yields and/or economics. The experimental methodology used to test this hypothesis is described in Section V.C.3.

Additionally, miscellaneous supportive experiments were performed, as described in Section V.C.4. A sample of jet fuel was produced using laboratory equipment to model the refining of the NCP in four major experimental steps. This was produced in order to investigate important parameters for fuel production that could affect the product yields from the NCP. Furthermore, physical and chemical properties of the fuel were examined in comparison to a sample of petroleum-derived kerosene to obtain additional insights. Finally, experimental estimations were made for the yield of coke produced by the NCP, through the likewise utilization of laboratory equipment to model NCP refining in three major experimental steps.

Methodology is summarized below, sequentially ordered: reagents, equipment, and experimental methods.

V.A. Materials

V.A.1. Triglyceride Oil Feedstocks

The TAG feedstocks cracked in the TCR were predominantly food grade, except for specialty TAG crops which were obtained from other universities (in which case they were pressed), crude corn oil, which was obtained from an ethanol plant, microbial oil, which was

134

obtained from an industrial partner, or waste fatty acid oil sources such as waste cooking oil or animal fats.. Soybean oil was obtained from Ag Processing Inc (AGP®), a cooperative located in the state of Minnesota, USA. Canola oil was purchased from Archer Daniels Midland® (Chicago, IL, USA). In addition, oils of unusual and/or novel composition were also cracked, designated as very high oleic novelty oil (VHONO), HONO, Oleic 75), and high erucic novelty oil (HENO).

Virgin crambe oil and virgin cuphea oil were obtained by pressing the seeds from crambe and cuphea at North Dakota State University (NDSU) in 2009 and then filtering out debris from the oil. Others such as linseed oil, cottonseed oil, corn oil, and camelina oil were purchased from various agricultural co-ops, meeting the specifications for fully-refined oil (a.k.a. food grade). Typical literature reported compositions are shown in Table 1.

V.A.2. Catalytic Deoxygenation Test Feedstocks

Preliminary catalyst testing was performed using 5 wt. % palladium on carbon (designated as Pd/C 5 powder) from Sigma Aldrich, a.k.a. Sigma (St. Louis, MO, USA) and performed using 64 wt. % nickel on silica (designated as Ni/SiO2 64 powder) from Strem Chemicals (Newburyport, MA, USA).

Model compound feedstocks were prepared for screening deoxygenation experiments in batch and continuous reactors. For the screening of deoxygenation catalysts in batch reactors, a 10.1 wt. % octanoic acid feedstock solution was prepared in heavy mineral oil. For demonstration of deoxygenation catalytic potential in packed bed reactors, a 20.9 wt. % octanoic acid feedstock solution was prepared in cyclohexane. Octanoic acid (> 98 %) was purchased from Sigma. Heavy mineral oil was purchased from Fisher Scientific, a.k.a. Fisher (Waltham,

MA, USA). Cyclohexane (> 98 %) was purchased from sigma.

A CTD feedstock solution was prepared for miscellaneous deoxygenation experiments using processing equipment that is described in Section V.B.   This involved TAG cracking followed by sequential ambient and vacuum distillation. Fully-refined soybean oil was thermally cracked in the 100 mL lab-scale tubular cracking reaction (TCR) at 430 C temperature, 2.9 MPa pressure, and a space time of 0.7 hours. The CTL from cracking was sequentially distilled by the CTL fractionation system in two steps, with each step reaching a final boiling flask temperature of 350 C. The first distillation was under ambient pressure and the second was under vacuum, reaching a final pressure of less than 2.0 kPa. Ambient and vacuum distillates were recombined into a single organic distillate feedstock comprised of approximately 1.9 mol/L carboxylic acids, which was used as an CTD feedstock for deoxygenation testing.

V.A.3. Deoxygenation Catalyst Preparation and Testing

Crystalline nickel (II) nitrate hexahydrate was purchased from Sigma. NCB 20-50 mesh granular activated carbon was purchased from Nichem (Chicago, IL, USA). Nitric acid 70 vol. % was purchased from Fisher Scientific. Test reagents for the American Society for Testing and Materials (ASTM) test method D4607 to approximate catalyst surface area[148] were purchased from Sigma. Commercial entities providing Pd/C catalyst, Ni/SiO$_2$ catalyst, and Ni/SiO$_2$Al$_2$O$_3$ZrO$_2$ catalyst are not mentioned for the sake of their anonymity.

V.A.4. Reaction and Analytical Gases

Unless otherwise specified, all gases were obtained from Praxair, Inc. (Danbury, CT, USA), at a purity of 99.9 %. For non-analytical experimentation, gases included nitrogen for purging air from equipment before use, hydrogen for reduction of catalysts and operation of

catalytic reactors, and air for decoking process equipment as needed. For characterization of gaseous product samples by GC, gases were used (1) as analytical standards, including hydrogen, carbon monoxide, carbon dioxide, and ethylene and (2) for operation of the GC, including argon and hydrogen. For the compositional work by GC-FID/(FI)MS, gases were 99.999 % pure, and purification traps were installed on the gas lines to trap trace hydrocarbons, oxygen, and moisture. GC-FID/MS gases included nitrogen, helium, hydrogen, and air.

V.A.5. Standards for Analysis of Liquids by Fourier Transform Infrared (FTIR) Spectroscopy

Octanoic acid, n-decane, n-dodecane, and 1-tetradecene were obtained from Sigma at >98 % purity each, and fully refined soybean oil (as a TAG standard) was purchased from AGP®. Nine octanoic acid standards were prepared in n-decane solvent from 0 to 40 vol. % in increments of 5 vol. %, also with a 60 vol. % solution to help verify the end of the linear range. Seven TAG standards were prepared in n-decane solvent from 0 to 40 vol. % in increments of 10 vol. % and then up to 100 % in increments of 20 vol. %. Five 1-tetradecene standards were prepared in n-dodecane solvent at 0, 5, 10, 50, and 100 wt. %.

V.A.6. Standards for Detailed Compositional Analysis by Gas Chromatography

A number of standards were used for detailed quantitative compositional analysis of CTL samples by gas chromatography. For identification, the following standard mixtures were purchased from Supelco (Bellefonte, PA, USA): isoparaffin-, aromatic-, naphthene-, and olefin- Alphagaz PIANO[149]; naphtha, reformate, and alkylate qualitative reference standards; petroleum crude qualitative and quantitative standards[113]. For quantification of the cracking products, individual chromatographic standards of analytical grade were used representing the complete series of unbranched alkanes (C_5–C_{18}), selected alkenes (C_6, C_9, C_{14}, C_{18}), and aromatics

(benzene, toluene, o-xylene, m-xylene, p-xylene 1,2,4-trimethylbenzene, indane, naphthalene). Various solvents were purchased from Fischer (Waltham, MA, USA): acetonitrile (HPLC grade), methylene chloride (GC grade). N-methyl-N-trimethylsilyltrifluoracetamide (MSTFA) was used as a derivatization agent for GC analysis of carboxylic acids and alcohols (Supelco, Bellefonte, PA, USA).

Internal standard calibrations were performed in the range of 0.025–29.9 mg·mL^{-1}. A mixture of three internal standards was employed to control for sample volume changes and aging. These consisted of benzene-d$_6$ (102.1 mg·mL^{-1}), 2-chlorotoluene (100.1 mg·mL^{-1}), and o-terphenyl (49.8 mg·mL^{-1}) in methylene chloride. All were purchased from Sigma–Aldrich Corp.

For the quantification of acids and alcohols in derivatized samples, a calibration mixture (0.10–75.0 mg·mL^{-1}) was used consisting of several representative carboxylic acids (acetic, propionic, butyric, hexanoic, octanoic, decanoic, and palmitic), n-butanol, n-hexanol, 1,3-propanediol, glycerol, and n-decanol. For identification, a standard mixture consisting of C$_1$–C$_{16}$ carboxylic acids and C$_1$–C$_{10}$ alcohols was employed. Geraniol (Aldrich, St. Louis, MO, USA) and o-terphenyl were used as recovery (10 mg·mL^{-1} in acetonitrile) and internal standards (50.0 mg·mL^{-1} in methylene chloride), respectively.

V.A.7. Standard for High Throughput Compositional Analysis of Cracked Triglyceride Liquid Samples (FIMSDIST)

Solvents used for the preparation of standards were either carbon disulfide (99.9 %) from Sigma or dichloromethane 99.99 % from Fisher. Acetone (99.99 %) was also purchased from Fisher and used as a solvent. MS tuning and emitter field strengths determinations used 99 % *n*-heptane from Sigma. 99.9 % 2-bromobutane from Fisher was used as an internal standard in all samples/standards.

A GC-FIMS ionization calibration standard (identified as STDx56, for a 56 component standard) was prepared from n-paraffins (C_5-C_{20} and C_{23}), alpha olefins (C_6, C_8, C_9, and C_{11}-C_{20}), n-alkyl branched mono aromatics (C_6-C_{14}), unbranched higher order aromatics (C_{10}, C_{14}, and C_{16}), and carboxylic acids (C_2-C_{12}, C_{14}, C_{16}, C_{18}, C_{20}, C_{22}, C_{24}) at approximately 0.26 wt. % each in dichloromethane. This standard was diluted to 80 %, 60 %, 40 %, and 20 % by volume in carbon disulfide, creating a set of linear calibration standards for determining the response factors of the MS. A complete list of chemicals, associated purities and vendors that were used for standardization is included in Appendix E, along with the exact mass of each component and the weight percent of that component in the concentrated stock solution.

The hydrocarbon window defining standard (C_8-C_{40} at approximately 500 µg/mL in chloroform) was purchased from AccuStandard® (125 Market Street, New Haven, CT 06513 USA). A standard solution of Polywax 655 (i.e., narrow molecular weight distribution of even-numbered n-paraffins) was prepared from neat Polywax 655 (purchased from AccuStandard®) at 2.9 wt. % in a volumetric 1:1:1 solvent of n-heptane, n-decane, and n-dodecane for high range hydrocarbon window defining.

Exact mass calibration standards were a mixture of acetone (>99.99 %), hexafluorobenzene (>98.0 %), octamethylcyclotetrasiloxane (>99.0 %), and decamethylcyclopentasiloxane (>99.0 %) from Fisher and perfluorotributylamine (99.0 %) from Scientific Instruments Services, Inc. (1027 Old York Road, Ringoes, NJ 08551-1054, USA). These compounds were mixed in a volume ratio of 1:10:8:10:20, respectively, in order to provide the following ions {58.04186} : {185.99042} : {281.05169} : {355.07048} : {68.99520, 463.97433, 501.97114, 594.96635}, respectively (units: *m/z*).

V.B. Equipment

In this section, the equipment that was constructed, purchased, modified, and/or utilized for lab experiments and chemical analysis is described. The description of each equipment unit includes a schematic (where appropriate) and a short description of the operating instructions.

Conventions for equipment drawings depend on the type of equipment, with batch equipment being most closely drawn in resemblance to the equipment's physical appearance. Due to the congested, close-quarters configuration of batch equipment, their diagrams are drawn in color. In batch equipment, red/orange colored parts of the diagram serve to indicate elevated temperature and/or heating function. Blue colored parts of the diagram indicate cooling. Purple indicates either heating or cooling as deemed necessary by the experiment (i.e., a heat transfer fluid/surface).

In contrast to batch drawings, continuous equipment at the lab-scale is drawn in a different style similar to chemical process diagrams (e.g., process flow diagrams, piping & instrumentation diagrams) utilizing conceptual icons instead of icons that resemble the units physical appearance. Continuous equipment at the batch scale is drawn using icons and piping that more closely resemble their physical resemblance. Valves, tanks, reactors, pumps, and heat exchangers are intended to look like the equipment that is currently installed. However, control aspects of these diagrams are still drawn in the P&ID style in order to not complicate the diagram unnecessarily.

In any of these cases, it should be mentioned that dark/black valves are intended to indicate a valve that is normally closed and white valves are intended to indicate a valve that is normally opened. Light gray valves are nondescript intentionally because their use varies during

140

the course of experimentation. Equipment keys are not included because they were deemed unnecessary on account of the diagrams being thoroughly described in the text.

Temperature control was typically achieved using proportional-integral-derivative (PID) algorithms and thermocouples to supply process variables. When valve control was utilized, PD algorithms were used (neglecting an integral (I) term).

V.B.1. Triglyceride Cracking Reactors

For TAG cracking, several reactors were used of various types and sizes. Each of these reactors was capable of reaching temperatures in excess of 500 C in order to permit noncatalytic cracking of the TAG. Descriptions and schematics of these reactors are offered in the following several subsections.

V.B.1.i. Batch Cracking Reactor

This reactor can be summarized as a small reaction chamber, in which TAG was placed for exposure to high temperatures in the absence of air sufficient to exhibit noncatalytic cracking. Cracking was studied by collecting products at the end of the experiment for compositional analysis. A variety of operating conditions and different types of TAGs were used in experiments conducted using this reactor configuration.

The batch reactor was a modified 4575A bench-top stirred autoclave reactor with 500 mL internal volume from Parr Instruments (Moline, IL USA) as depicted in Figure 27. The reactor flanges were sealed by a grafoil gasket, which was replaced occasionally (as needed). A stirring impeller was installed as shown and typically operated at 400 RPM. A valve (V-2) was connected to the inlet side of the reactor to permit the delivery of gases to the reactor. A pressure transducer (PT 1) was installed as shown to measure the pressure of the reaction. The surfaces in

contact with liquids and gases in this reactor system were predominantly 304 or 316 stainless steel, Inconel, and glass.
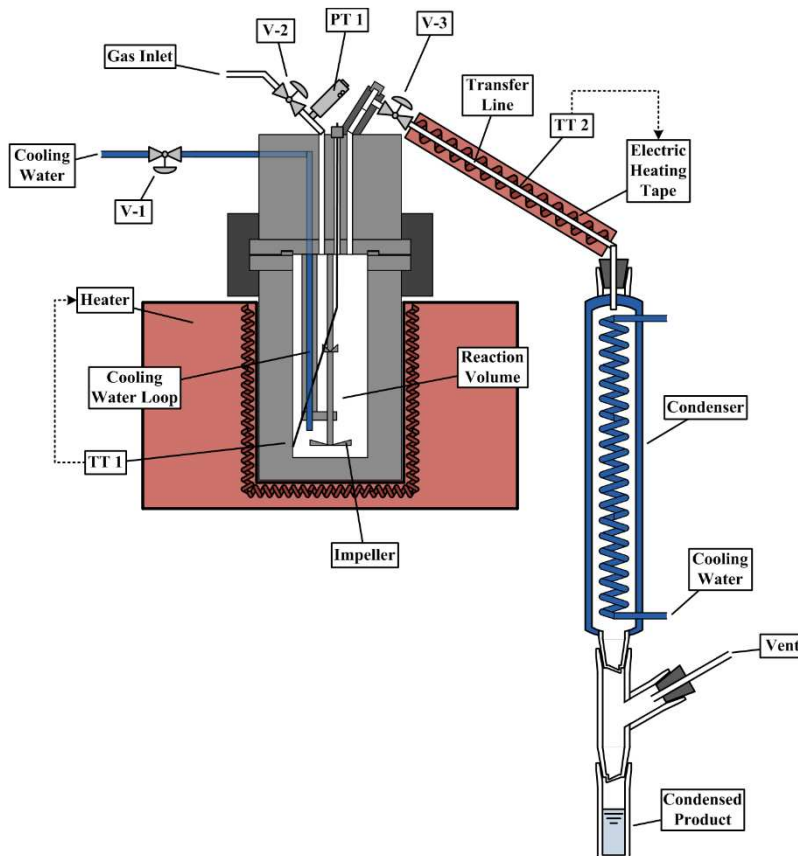
Figure 27. Batch reactor for triglyceride (TAG) noncatalytic cracking experiments

The reactor was heated by conduction via an electric coiled heater that was cupping the lower ~80% of the reaction volume, as shown. The heater could be lowered quickly when shutting down for fast cool down times. A 1.6 mm K type thermocouple probe (TT 1) was used for feedback temperature control of the reactor heater. TT 1 was inserted into the reactor and permitted to touch the inside of the reactor's wall, as shown, in order to restrict the wall

142

temperature of the reaction (i.e., the hottest temperature). Side experiments revealed that the temperature measured at the wall vs. in the free stream were within a few degrees C.

A valve (V-1) was installed to modulate the flow of cooling water through the stainless steel cooling water loop in the reaction chamber. When shutting down, lag times were minimized by simultaneously opening V-1 when the heater was turned off and lowered away from the reaction chamber.

A valve (V-3) was installed at the outlet port so that when it was desired, the reactor could be operated isobarically as a semi-batch reactor with removal of vapor phase products. A short transfer line wrapped in electric heating tape was installed to transfer vapor phase products to the condenser with minimal condensation as shown. A K type thermocouple (TT 2) was installed where shown and used for feedback control of the transfer line temperature. The condenser was a jacketed, high-efficiency condenser made of glass supplied with a copious flow of cooling water as shown. Condensed products were collected in glass vials with noncondensable gaseous products being vented to a fume hood, as shown. The procedure for operation of the batch reactor is as follows.

In its fully disassembled condition, the heater is lowered/set aside and the reactor is separated at its flange to reveal the reaction volume. An experimentally specified sample size of TAG (either 100, 200 or 300 mL) was weighed and placed in the reaction volume, which was then reinstalled to the reactor and sealed by its flange. Then the reactor was purged with N_2 gas three times to at least 500 kPa to remove residual oxygen. Afterwards, the reactor was pressurized with 7000 kPa of N_2 gas and tested to seal any leaks.

When leaks were shown to be properly sealed, the pressure was vented to the

143

experimentally specified starting operating pressure (either 100 or 1400 kPa) and the impeller was set to specified rotational speed (typically 400 RPM). Cooling water to the reactor was shut off until the end of the run, whereas cooling water to the condenser was always supplied during phase separation experiments. The set point temperature was supplied and the reactor was allowed to heat up to reaction temperature.

When the temperature reached 385 C, a reaction timer was started, and the reaction was allowed to progress until the experimentally specified reaction time had passed. For phase separation experiments, the pressure of the reactor was manually controlled at its desired pressure using the effluent valve. This produced condensed distillates in the condensed product graduated cylinder. Temperatures and pressures of the reaction were recorded as necessary, at least every five minutes and typically more regularly.

When the reaction was over, the heater was turned off and promptly lowered away from the reactor and cooling water was allowed to flow through the reactor's cooling loop. At temperatures < 30 C, gaseous and liquid reactor products were collected for subsequent analysis and the mass of the liquid products was determined.

V.B.1.ii. Prototype Tubular Cracking Reactor (TCR)

In summary, the prototype TCR was a briefly utilized reactor for testing the hypothesis that a long tubular reactor would be able to thermally crack TAG continuously with negligible formation of coke. The reactor is described as a long tubular coil that was kept at a high temperature, through which TAG was pumped under pressure, facilitated by a pressure regulating valve. Continuous samples were obtained from the reactor and examined qualitatively, however, the major experimental utilization of the reactor was to test if the reactor

was able to successfully operate without plugging due to coke formation. A schematic of the prototype TCR is shown below in Figure 28.

The reactor volume was formed by coiling a 6.1 m long × 0.46 cm stainless steel (304 grade) tube into a 9 cm diameter coil, for a total heated reactor volume of approximately 0.1 L. The reactor coil was placed inside a Eurotherm 301 tube furnace from Carbolite (Derbyshire, United Kingdom).

A compressed nitrogen gas tank (TK-2) was connected to the reactor system for purging the reactor of air before use. TAG feedstock was pumped from a glass Erlenmeyer flask (TK-1) through the reactor coil by an ISO-100 piston pump (P-1) from ChromTech (Apple Valley, MN USA).
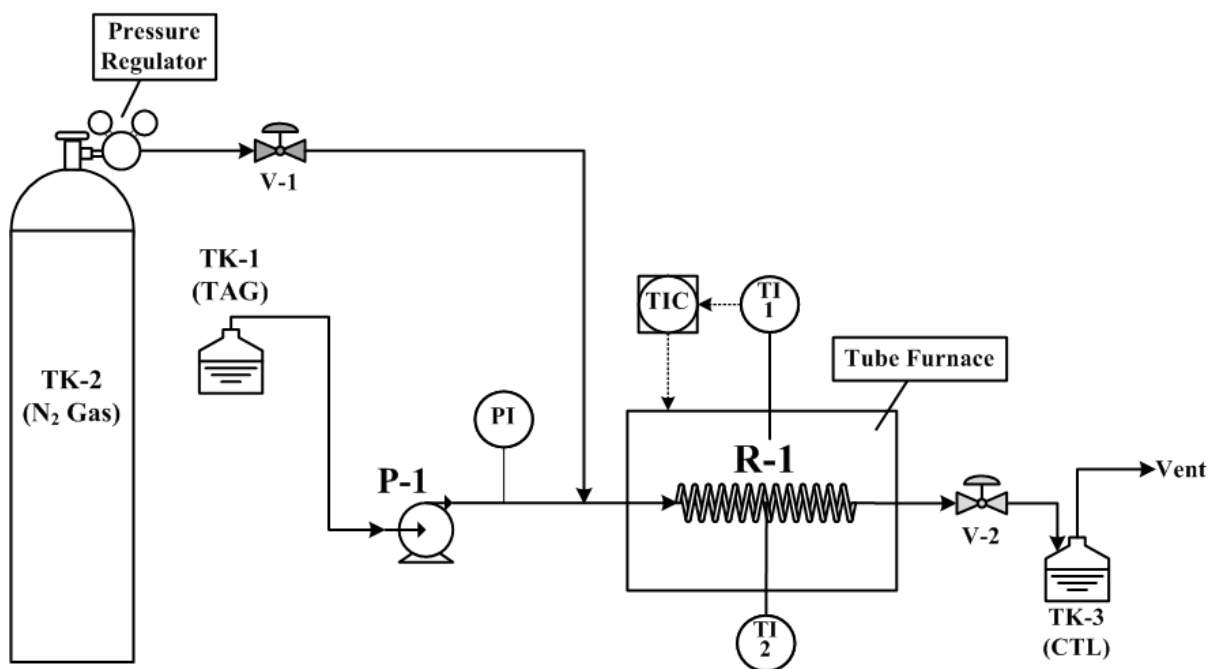
Figure 28. Prototype tubular cracking reactor (TCR) for hypothesis testing

Reaction temperature was maintained with feedback PID control, built in to the tube furnace, facilitated by a thermocouple probe (TI 1) that was imbedded into the heating coil refractory. A second K-type thermocouple probe was installed into the free air at the center of the coiled tube for estimating the fluid temperature in the coils, as shown.

A single dial-type pressure gauge (PI) was installed to monitor the reactor's inlet pressure. A needle valve (V-2) was installed on the effluent side of the reactor for manual pressure control, as indicated. The cracked triglyceride liquid (CTL) stream from the V-2 was drained to a glass Erlenmeyer flask (TK-3) to collect CTL. Noncondensible process gas was vented to a fume hood. No cooler/condenser was installed, and the reaction products relied on free convection and the Joule-Thomson effect to reduce the temperature sufficiently to condense volatile products.

As previously mentioned, this reactor was short lived and used to test the hypothesis that a tubular cracking reactor could operate without the formation of coke. The procedure for testing operable reaction conditions is described below.

The system was assembled and P-1 was primed with an experimentally specified TAG feedstock. Residual air was purged from the R-1 by closing V-2 and opening V-1 to pressurize the reaction chamber with N_2. Then the N_2 was vented by closing V-1 and opening V-2. This was repeated 3 times to a pressure of 500 kPa each time, analogous to purging batch reactors.

To startup the system from its original (ambient) conditions, P-1 was turned on and set to max flow rate and V-2 was adjusted manually to permit the flow of oil through R-1 and through V-2, filling R-1 with oil. After R-1 was filled, the flow of P-1 was set to the experimentally specified flow rate and flow was verified by observing the volumetric feed rate of TAG over

time regularly during experimentation. Then TIC was turned on and set to the experimentally specified reaction temperature to enable the R-1 to heat up. Throughout experimentation, V-2 was manually adjusted to maintain PI (i.e., the reactor pressure) at the desired experimentally specified reaction pressure.

Reaction products were collected continuously. Once the reactor reached its specified temperature/pressure and remained stable to within ±5C and ±300 kPa over several minutes, a timer was started and the reactor was manually monitored. After 3 hours had elapsed with no occurrence of reactor plugging/coking, the reactor was considered to be under 'operable conditions.'

The next operating conditions were then tested by adjusting the temperature of TIC, flow of P-1, and manually monitoring V-2 to adjust the reactor's pressure (PI) to their new experimentally specified conditions. Once the reactor reached its newly specified temperature/pressure and remained stable over several minutes, a timer was started again to test the new operating conditions. This procedure for testing conditions was repeated as necessary until all experimentally specified conditions were tested.

System shut-down consisted of shutting off the power to TIC to cool down the temperature of R-1. After temperature TI 2 was below 370 C, pump P-1 was turned off. V-2 was slowly opened to vent the contents of R-1 until PI was below 200 kPa. Then V-2 was sealed and the reactor was allows to cool to room temperature. At room temperature, the reactor was disassembled and cleaned.

V.B.1.iii. Lab-Scale Tubular Cracking Reactor (TCR)

Based on the prototype TCR described above, a more robust lab-scale TCR was

constructed to provide more experimental control than could be achieved in the prototype TCR, enabling the ability to obtain valuable process development information. Three different versions of the reactor were developed: 1) a 100mL sideways reactor with a 50 mL preheater, 2) a 500 mL upright reactor, and a) a 200 mL upright reactor. Main system components were a pump, a heated reactor coil (and sometimes a TAG preheater), a double-pipe condenser, filtration, and a pressure control valve. Continuous samples were obtained from the reactor under a variety of conditions in order to study the effect of operating parameters and TAG composition on product composition.

The 200 mL upright reactor was found to be the optimal design. It is depicted in Figure 29 and described below. The operation of the reactors is similar, so it is not necessary to describe them redundantly. The reaction chambers for the three different reactor versions are depicted in Figure 30 at the end of this subsection, with brief descriptions about the differences between the reactor versions.
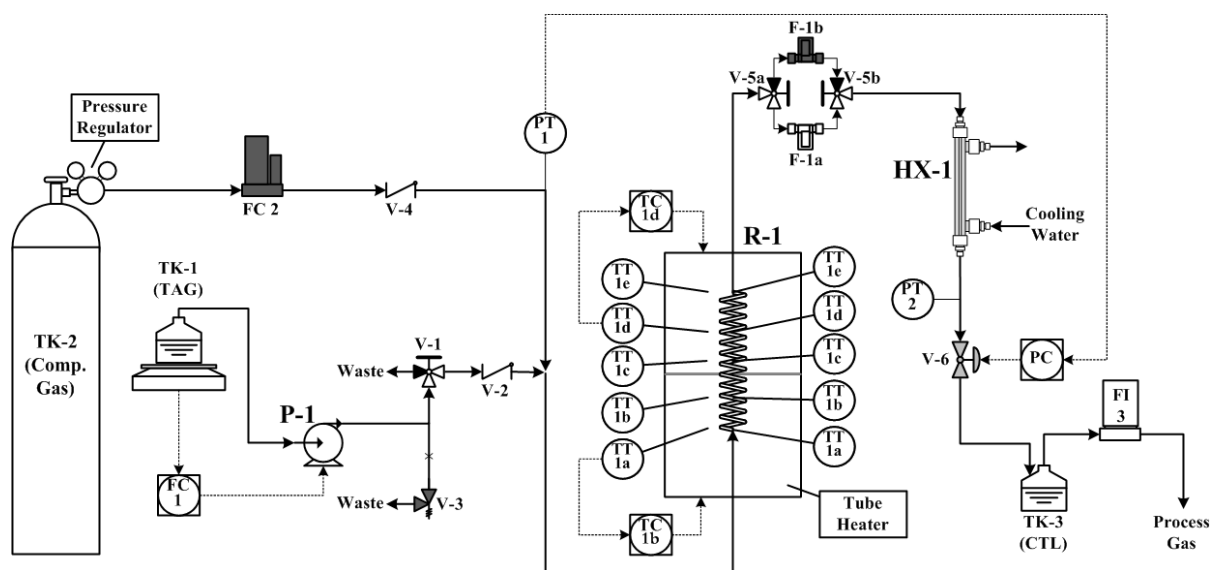
Figure 29. Lab-scale TCR for processing TAG

Except for negligible sealing components in valves/pumps, all reactor surfaces in contact with TAG/CTL were either stainless steel (304 or 316 grade), Inconel, or glass. All thermocouples were K type 1.6 mm diameter probes of various lengths.

Process monitoring and control were facilitated by a model cDAQ 9178 Compact DAQ (i.e., cDAQ) system from National Instruments (a.k.a., NI) out of Austin, TX, USA. The cDAQ utilized three modules to obtain sensor data and to control devices, including a voltage input module (NI 9206), thermocouple input module (NI 9213), and voltage output module (NI 9264). A computer application was programmed in NI's LabVIEW for interacting with the cDAQ and monitoring/controlling the process. Unless otherwise specified, all sensors were recorded by the supervising computer at frequencies of at least 1/min.

A compressed gas tank (TK‑2) was installed to the reactor system for delivering gases as needed (either nitrogen for purging the reactor before/after service or air for cleaning/decoking as necessary), with a corresponding mass flow controller (FC 2) and a check valve (V‑4) to protect FC 2 from hazardous/undesired backward flow, as depicted.

Feedstock was pumped from a glass Erlenmeyer flask (TK‑1) by an ISO-100 piston pump (P‑1) from ChromTech. Typically the feedstock was TAG, however, water or solvents were occasionally pumped when necessary (during decoking and/or cleaning). TK‑1 was set atop a Highland™ model HCB-3001 digital scale from Adam Equipment (Danbury, CT, USA) with a 3 kg capacity and 0.1 g readability. RS-232 communications between the scale, pump, and the supervising computer enabled feedback flow control (FC 1) of the TAG feed rate. A 3-way ball valve (V‑1) was installed downstream of P‑1 for assistance with pump maintenance and

149

priming when the reactor was not in service. A check valve V‑2 was installed to prevent

hazardous/undesired backward flow, as shown. As a safety precaution, a relief valve (V‑3) was

installed as shown and set for 6000 kPa.

The reactor (R-1) was formed by coiling a 21.2 m long × 0.46 cm diameter stainless steel

tube to form the cracking tube. Five thermocouples were installed inside the cracking tube to

measure the temperature of the cracking fluid as shown, effectively partitioning the cracking

tubes volume into four zones (25 % of the volume each) with temperature measurements in

between each zone. The cracking tube was installed inside an upright cylindrical furnace with

dimensions of 61 cm high × 31 cm inside diameter. The furnace consisted of an upper half and a

lower half, with independent heating coils in each segment, indicated by a gray partitioning line

in Figure 29. Thermocouple probes (TT 1a-e) were placed at five levels within the free air of

the furnace to measure the spatial distribution of temperature, as shown. Temperature of the

furnace was maintained by feedback control (TC 1b and TC 1d) as shown, utilizing TT 1b and

TT 1d for the process control variables.

The effluent from R-1 was filtered by a redundant parallel filter array, comprised of two

3-way ball valves (V‑5a/b) and two filters (F‑1a/b), as shown. The dual-filter arrangement was

utilized to enable changing the filter without interrupting operation. Filters were stainless steel

tee-type filters, capable of filtering all particles larger than 90 µm.

After the filter array, the product stream was condensed by flowing it through a short,

double-tube style condenser, (HX‑1), as shown. The process stream flowed through the inner

tube, having heat transfer dimensions 30.48 cm length × 0.46 cm inside diameter × 0.09 cm wall

thickness. Excess flow of cold water (17 C) was supplied to the outer tube of HX‑1 to ensure

sufficient cooling.

Pressure was continually monitored by two pressure transducers (PT 1 and PT 2) installed as indicated. After HX-1, the reaction products passed through a pressure control valve (V-6) that utilized PT 1 for feedback pressure control via a proportional-derivative (PD) control algorithm. V-6 was motorized by interconnecting an integrated stepper motor, driver, and controller (model 4118S) from Lin Engineering (Morgan Hill, CA USA); a 30:1 worm gear box (WDG30P) from RobotZone, LLC (Winfield, KS USA); and a needle valve (SS-SS4-EP) from Swagelok (Solon, OH USA).

Finally, the cracked TAG (CT) from the reaction was collected in a glass Erlenmeyer flask (TK-3), which was used for phase separation of the CTL and cracked TAG gas (CTG). Process gas products were vented to a fume hood through a 10 L/min N_2 flow meter (FI 3) from Aalborg Instruments and Controls, Inc. (Orangeburg, NY USA). A septum port (not depicted) was installed in-line before venting to permit sampling of the gas phase effluent for analysis. The procedure for testing TAG cracking and producing reaction samples at various operating conditions is described below.

The system was assembled and P-1 was primed with an experimentally specified TAG feedstock by turning V-1 (the 3-way valve) so that P-1 would lead to 'Waste' instead of leading to R-1 volume. Although not depicted, 'Waste' is a vacuum flask adapted to a vacuum pump, which exhausts to a fume hood. FC 1 was set to max flow rate. The negative pressure of the vacuum pump assisted with the priming of P-1. Once primed, V-1 was switched back towards R-1 and FC 1 was set to zero.

Then residual air was purged from the system by setting PC to 0.0 MPa (i.e., opening V-

6) and setting FC 2 to max. After a few minutes of purging, the system was pressure tested by

setting PC to 7.0 MPa (i.e., closing V-6), and allowing the reaction chamber to pressurize with

N_2. Once the pressure of the system (i.e., the average of PT 1 and PT 2) reached TK-2's pressure

regulator (about 6500 MPa), the flow indication of FC 2 was used to verify that leaks were

negligible. Then PC (system pressure) was set to the experimentally specified operating pressure

and FC 2 was set to 0 unless otherwise specified.

FC 1 was then set to the experimentally specified operating feed rate and temperature

controllers TC 1b and TC 1d were set to their experimentally specified operating temperature.

R-1 was allowed to heat up with TAG being pumped through it. Throughout experimentation,

products were collected continuously in TK-3 and process gas was vented continuously.

However, only samples and data collected at steady state were reported. In other words, a timer

was started once the reactor reached its specified temperature/pressure and remained stable to

within ±5C and ±300 kPa over several minutes. Time was allowed to continue until 3 equivalent

system volumes of product were pumped through the system and collected in TK-3 before

sample collection would begin.

To start sample collection, two actions were simultaneously performed: (1) an empty

replicate of TK-3 (product tank) was simultaneous inserted in place of the existing TK-3 and (2)

a timer was started. The steady-state CT sample was permitted to fill TK-3. Meanwhile, the

contents of the old TK-3 were disposed and the old TK-3 was thoroughly cleaned for reuse in

future sampling. At least 3 system-equivalent volumes of product CTL were collected at steady

state in the new TK-3 to form a steady-state CT sample. Near the end of sample collection

(within the last 10 minutes), a gas tight syringe was inserted into a septum in-line with the

process gas exhaust of the system (not depicted). A 100 µL sample of gas was withdrawn into the syringe and the contents of the syringe was injected into a GC within 20 seconds. This permitted the determination of the gas phase composition. At the end of sample collection, the timer was stopped and the replicate TK-3's was simultaneously swapped. The mass of the steady-state CTL sample was quickly recorded and the sample was sealed in a glass bottle for analysis. TK-3 was cleaned for reuse.

The next operating conditions were then tested by adjusting the experimental set points to their new experimentally specified conditions, including the temperatures (TC 1b and TC 1d) and pressure (PC). If a different TAG feedstock was tested, P-1 was briefly turned off (for less than 10 seconds) while TK-1 was swapped out for a replicate version of TK-1 containing the desired TAG feedstock. Then P-1 was quickly turned back on, and a new experimentally specified flow was set (FC 1). Once the reactor reached its newly specified conditions and remained stable, three reaction volumes were permitted to flow into TK-3 before a new steady-state CT sample was collected. This procedure for producing samples of CT at various operating conditions was repeated as necessary until all experimentally specified conditions were tested.

As needed, filters F-1a/b was cleaned by turning the valves V-5a/b from one filter to the other, and afterwards performing necessary maintenance on the filter that was taken off line. When this was necessary, it was considered to be a disruption of steady-state conditions, requiring re-stabilizing of steady-state as previously specified.

System shut down consisted of shutting off the power to TC 1b and TC 1d in order to cool down the temperature of R-1. After temperature TI 2 was below 370 C, pump P-1 was turned off. At room temperature, PC was set to ambient pressure and V-6 vented the pressurized

contents of the system. Then the reactor was cleaned using solvents as necessary.

Three different versions of the reactor were developed. These are described by their reaction volumes throughout the text (e.g., the '100 mL lab-scale TCR'), which is a distinctive feature of each version. Whereas the final version of the reactor is depicted in Figure 29 and described above (i.e., 200 mL lab-scale TCR), the three versions of the lab-scale TCR have their reaction chambers depicted in Figure 30.

Figure 30.a depicts the reaction volume of the 100mL version, which was a sideways tubular cracking coil with a 50 mL tubular preheater in a back/forth configuration. Figure 30.b depicts the reaction volume for the 500 mL version, which was an upright tubular cracking coil of fivefold increased length from the 100 mL version. Figure 30.c depicts the reaction volume for the 200 mL version, which was an upright tubular cracking coil of twice the length of the 100 mL version. Furthermore, the 200 mL version had significantly more thermocouples than predecessor versions, and heating control over an upper and a lower chamber. The operation of the 100 mL and 500 mL versions is negligibly different from the operation of the 200 mL TCR that was described earlier in this section, but there are differences in their configurations which are described as follows.

The first version of the lab-scale TCR was the 100 mL version, which utilized a 50 mL preheater that was wrapped with resistively-heated electric heat tape. The preheater incorporated two in-line thermocouples as depicted in Figure 30.a. One thermocouple was used for temperature observation at the half-way point (TT 1a), and the other was used for temperature control at the exit (TT 1b).

The preheater was used to preheat the TAG before it entered the reaction volume. The

original intent was to operate the preheater at the reaction temperature that was being studied. As a result, the TAG entering the reactor would have a clear residence time. This was found to be a major problem for coke formation, especially when pump rates (FC-1) were decreased to study cracking at longer residence times.

The coke formation was assumed to result from hot spots in the preheater, because the temperature from TT 1a (at the preheater's mid-way point) was often recorded at higher temperatures than TT 1b (at the preheater's exit). This was especially evident at low pump rates (FC-1). Neglecting heats of reaction in the preheater, this is observation is nonsensical unless heat generation and/or heat loss are uneven through the preheater. As a result, preheating was reduced to a temperature of 340 C for the bulk of the work in this dissertation (unless otherwise specified). This is well below the expected minimum temperature of TAG cracking (~400 C) described by Luo et al.[54] and other researchers in TAG cracking,[150] so that coking in the preheater would be minimal but the effect of the preheater was observed.
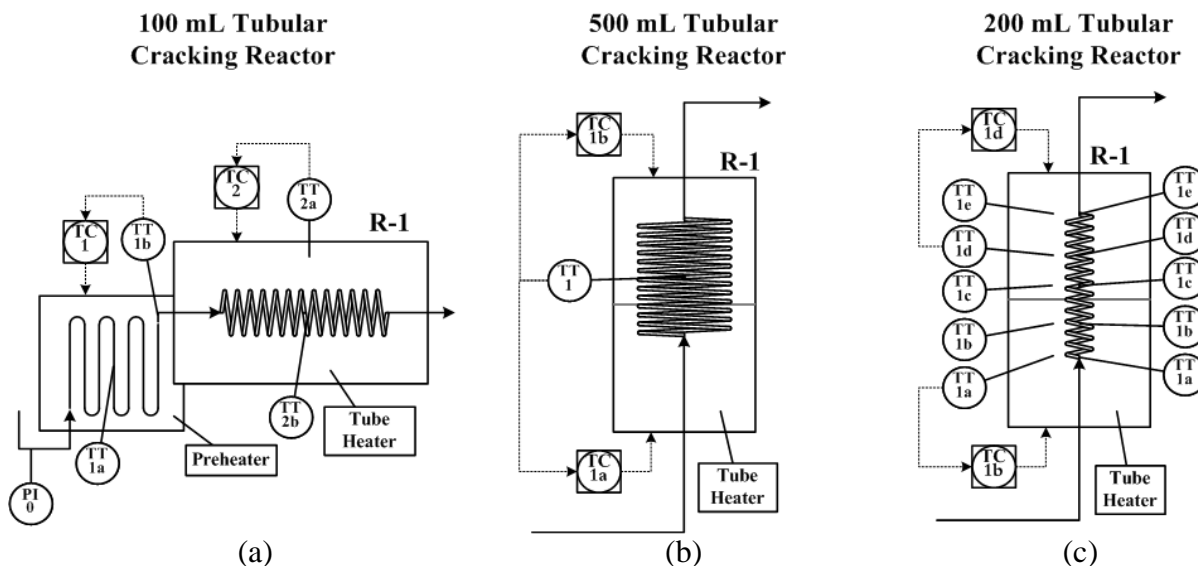
Figure 30. Three configurations of the lab-scale tubular cracking reactor

Due to the risk of coke formation, the preheater was not incorporated into newer versions of the lab-scale TCR. The second version was a 500 mL TCR, depicted in Figure 30.b. The reactor had extra volume by increasing the length fivefold, whereas otherwise, the dimensions remained the same. The 500 mL reactor was only used for a short time due to operating restrictions that essentially required the pump to operate near its maximum flow rate.

V.B.1.iv. Bench-Scale Tubular Cracking Reactor (TCR)

A larger TCR, designated herein as a bench-scale reactor, was designed based on design information from the successful operation of the lab-scale TCR. As a result, it is similar to its predecessor in that it consists of a long, narrow tube through which TAG is pumped under high temperatures and elevated flow rates in order to induce noncatalytic cracking. In addition, a large percentage of the bench-scale TCR was salvaged from the decommissioning of the previous bench-scale CSTR described in Sander[62] and in Section V.B.1.v. Salvaged equipment included the feedstock tanks, diaphragm pump, condenser, preheaters, and product tank. The experimental operation of the bench-scale TCR is similar to the lab-scale TCR in that samples are obtained under steady state conditions at various operating conditions.

Except for negligible sealing components in valves/pumps, all reactor surfaces in contact with TAG/CT were either stainless steel (304 or 316 grade), Inconel, or glass. All thermocouples were K type 1.6 mm diameter probes of various lengths sheathed in Inconel. All parts of R-1 exposed to the temperatures in the tube furnace were made of Inconel 625, Grade 2.

Data acquisition was facilitated by a model cDAQ 9178 Compact DAQ (i.e., cDAQ) from NI (i.e., National Instruments out of Austin, TX, USA). The cDAQ utilized two modules to obtain sensor data, including a voltage input (NI 9206) module and a thermocouple input (NI

9213) module. A computer application was programmed in LabVIEW for data acquisition and

monitoring of the system. Unless otherwise specified, all sensors were recorded by the

supervising computer at frequencies of at least 1/min.
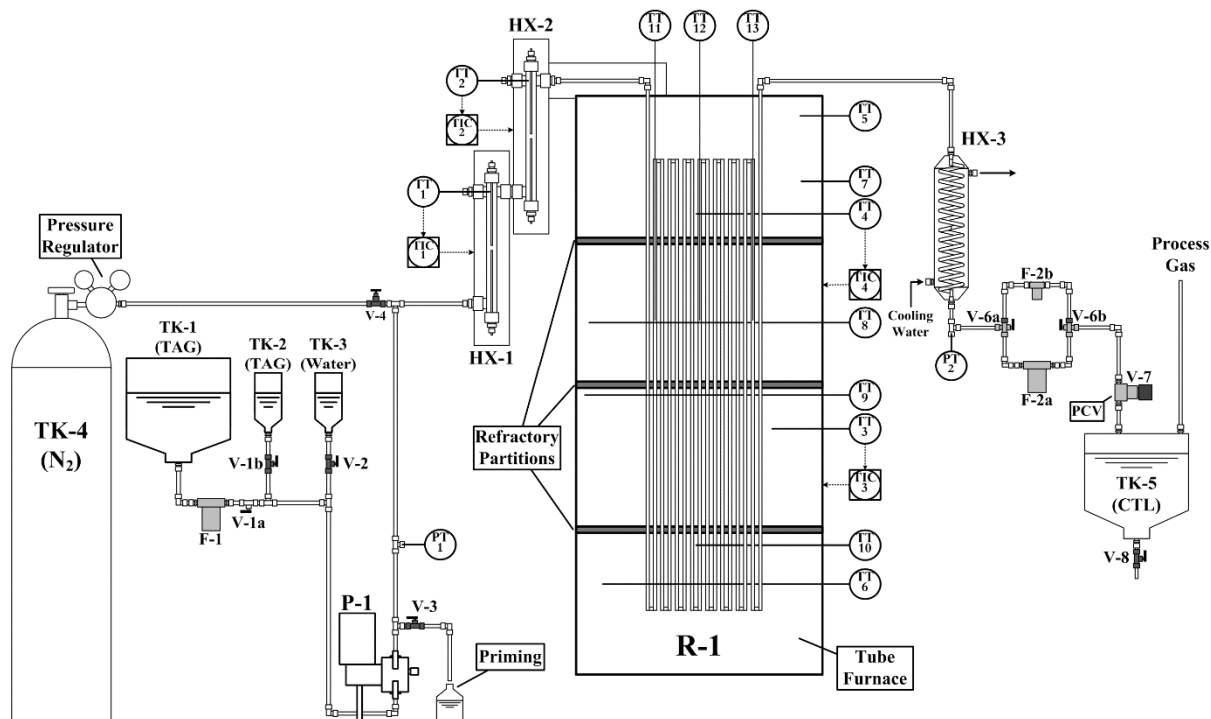
Figure 31. Bench-scale TCR for processing TAG

A compressed gas tank (TK‑4) was installed to the reactor system for delivering gases as

needed (either nitrogen for purging the reactor before/after service or air for cleaning/decoking

as necessary) and a valve (V‑4) was installed to shut off the gas line, as depicted.

TAG was pumped from either of a 68 L tank (TK‑1) through an oil filter (F‑1) and a ball

valve (V‑1a) or from a 1 L tank (TK‑2) and a ball valve (V‑1b). During normal operation, TAG

was pumped from TK‑1, however, the feed rate was occasionally monitored by pumping from TK‑2 and using the liquid level of TK‑2 for volumetric measurements with time. During operation, only one of V‑1a or V‑1b was opened, with the other shut. The exception to this was when TK‑2 was being filled by gravity-draining from TK‑1, in which both V‑1a and V‑1b were open.

In addition, a 1 L water tank (TK‑3) was installed with a ball valve (V‑2) in parallel to TK‑1/2 so that water could be pumped when desired (either for cleaning or for decoking). When water was pumped, V‑2 was opened and both V‑1a and V‑1b were shut. Otherwise, V‑2 remained closed during regular operation.

TAG was pumped by a proportioning diaphragm pump (P‑1) model 515-A-N3 from Neptune Chemical Pump Company (Lansdale, PA, USA) at variable feed rates up to 10 L/h. TK‑1, TK‑2 and TK‑3 supplied approximately 2.1 meters of liquid head atop P‑1 so that it could operate reliably. 10.8 mm inside diameter tubing was used to interconnect between all equipment before the pump, to minimize a friction head against the pump.

A ball valve (V‑3) was installed immediately downstream of P‑1 as a drain valve leading to a canister so that P‑1 could be easily primed or warmed up before operation of the reactor system. However, V‑3 remained closed during normal operation and TAG was pumped through two preheaters in series (HX‑1 and HX‑2) before entering the reaction volume. Two thermocouple probes (TT 1 and TT 2) were installed in their respective preheaters for feedback PID control (TIC 1 and TIC 2), as shown. The total combined heat capability of the preheaters was 4000 W, facilitated by 4 total heating rods of dimensions 34.5 cm long × 6.35 mm diameter

each.

After the preheaters, TAG flowed into the cracking TCR (i.e., R‑1) which was comprised of 16 seamless tubes made of Inconel 625, Grade 2. The tubes had dimensions of 1.53 m × 1.07 cm diameter × mm wall thickness each (i.e., 3/8 inch pipe size, schedule 80). The tubes were welded in series for an up/down/(…) flow path as shown in Figure 31. The total reactor volume was approximately 2.2 liters.

In addition to the 16 cracking tubes, 30 smaller diameter tubes were welded to the primary tubes (one on each exposed end) extending outside the furnace to serve as capillaries. The capillaries were thick-walled tubes, with dimensions of 45 cm long × 3.05 mm diameter × 1.7 mm each. Capillaries permitted the installation of various process sensors from outside the tube furnace (described below) utilizing standard tube fittings, Inconel fittings were cost prohibitive. The capillaries are shown in Figure 32, but they are left out of Figure 31 so as not to convolute the diagram.

The cracking tubes were placed within a tube furnace constructed out of four flat 1500 W ceramic heaters. The heaters were configured for heating in two zones (top/bottom) as shown in Figure 31. Two thermocouples probes (TT 3 and TT 4) were installed in the free air of the furnace and used for feedback PID control (TIC 3 and TIC 4) of the lower and upper heating zones, respectively. In addition, six other thermocouples probes (TT 5 through TT 10) were installed in the free air of the furnace for investigation the spatial distribution of temperature in the reactor. Three thermocouple probes (TT 11, TT 12, and TT 13) were installed through the sensor capillaries (described in previous paragraph) into the cracking fluid at the 2nd, 8th, and 15th tube, respectively, in order to monitor the temperature. The position of the thermocouples is

visible in Figure 31 and Figure 32.

Three refractory partitions were installed to partition the furnace vertically into four zones, as shown in Figure 32. These mitigated natural convection in the tube furnace, which helped keep the temperature relatively uniform throughout the height of the furnace.

Figure 32. Bench-scale TCR photograph of cracking tubes

The product stream from R‑1 was cooled by flowing it through a coiled-style shell and tube heat exchanger (HX‑3), as shown in Figure 31. The process stream flowed through the tube side of HX‑3, having heat transfer dimensions of 6.1 m length × 7.7 mm inside diameter × 0.9

mm wall thickness. An excess flow of cold water (17 C) was supplied to the shell side tube of HX‑3 to ensure sufficient cooling.

The effluent from HX-3 was filtered by a redundant parallel filter array, comprised of two 3-way ball valves (V‑6a/b) and two filters (F‑2a/b), as shown. The dual-filter arrangement was utilized to enable changing the filter without interrupting operation. Filters were stainless steel tee-type filters, capable of filtering all particles larger than 90 µm. F‑2a was the primary filter with approximately 350 cm^2 filtration area. F‑2b was a small backup filter with only a few cm^2 of area, utilized only when swapping out the filter of F‑2a while operating. During normal operation, V‑6a and V‑6a directed flow to F‑2a.

Pressure was continually monitored by two pressure transducers (PT 1 and PT 2) installed as indicated, encompassing HX‑1, HX‑2, R‑1, and HX‑3. Pressure control was facilitated manually by adjusting a spring-loaded back pressure regulator (V‑7) as needed.

The product stream exiting V‑7 entered a 68 L product tank (TK-5) where it was phase separated from the process gas, which was vented to a fume hood. A septum port (not depicted) was installed in-line before venting the process gas to permit sampling of the gas phase product for analysis. A ball valve (V‑8) was installed at the base of TK‑5 for draining product as necessary, however, it was normally closed during regular operation. The procedure for testing the bench-scale TCR and producing reaction samples at various operating conditions is described below.

TK-1 was filled with an experimentally specified TAG feedstock. P-1 was primed with TAG feedstock by closing V-7 and opening V-3 so that P-1 would lead to the 'priming' tank

instead of leading to R-1. P-1 was then set to max flow rate. Priming of P-1 was permitted to continue for at least 15 minutes before the system heat was turned on. Then V-3 was closed and P-1 was set to zero. Residual air was purged from the R-1 by opening V-4 to pressurize R-1 with N_2. Then the N_2 was vented by closing V-4 and opening V-7. This was repeated 3 times to a pressure of 500 kPa each time, analogous to purging batch reactors.

To startup the system from its original (ambient) conditions, P-1 was turned on and set to max flow rate and V-2 was adjusted manually to permit the flow of oil through R-1 and through V-2, filling R-1 with oil. After R-1 was filled, the flow of P-1 was set to the experimentally specified flow rate. Then TIC 1, TIC 2, TIC 3, and TIC 4 were turned on and set to the experimentally specified reaction temperatures to enable HX-1, HX-2, and R-1 to heat up and V-7 was set to the experimentally specified reaction pressure (although it was adjusted during experimentation as necessary). Flow was verified by observing the volumetric feed rate of TAG over time regularly during experimentation through TK-2 as previously described. TK-3 was only used for decoking procedures, which were later shown to be unnecessary.

Throughout experimentation, products were collected continuously in TK-5 and process gas was vented continuously. However, only samples and data collected at steady state were reported. In other words, once the reactor reached its specified temperature/pressure and remained stable to within ±5C and ±300 kPa over several minutes, a timer was started. Time was allowed to continue until 3 equivalent system volumes of product were pumped through the system and collected in TK-3 before steady-state sample collection would begin.

To start steady-state sample collection TK-5 was emptied by opening a drain valve V-8 at the base of TK-5 to drain the CTL into a separate container. Once drained, V-8 was shut and a

reaction timer was started. The steady-state CTL sample was permitted to fill TK-5. At least 3 system-equivalent volumes of product CTL were collected at steady state for any reaction sample. Near the end of sample collection (within the last 10 minutes), a gas tight syringe was inserted into a septum in-line with the process gas exhaust of the system (not depicted). A 100 µL sample of gas was withdrawn into the syringe and the contents of the syringe was injected into a GC within 20 seconds. This permitted the determination of the gas phase composition. At the end of sample collection, V-8 was opened to drain the contents of TK-5 into a storage container until TK-5 was empty. Then V-8 was shut, the reaction timer was stopped, and the reaction time was recorded.

The next operating conditions were then tested by adjusting the experimental set points to their new experimentally specified conditions, including the temperatures (TC 1b and TC 1d) and pressure (PC). If a different TAG feedstock was tested, P-1 was briefly turned off (for less than 10 seconds) while TK-1 was swapped out for a replicate version of TK-1 containing the desired TAG feedstock. Then P-1 was quickly turned back on, and a new experimentally specified flow was set (FC 1). Once the reactor reached its newly specified conditions and remained stable, three reaction volumes were permitted to flow into TK-3 before a new steady-state CT sample was collected. This procedure for producing sampled of CT at various operating conditions was repeated as necessary until all experimentally specified conditions were tested.

As needed, filters F-2a/b were cleaned by turning the valves V-6a/b from one filter to the other, and removing the filter for cleaning in solvents or replacing as necessary. When this was necessary, it was considered to be a disruption of steady-state conditions, requiring re-stabilizing of steady-state as previously specified. F-2a was the larger, main filter used during normal

operation, and F-2b was only used while cleaning F-2a.

System shut-down consisted of shutting off the power to TIC 1, TIC 2, TIC 3, and TIC 4 in order to cool down the temperature of HX-1, HX-2, and R-1. After all temperature readings were below 370 C, pump P-1 was turned off. At room temperature, V-7 was opened fully to vent the pressurized contents of the system. Then the reactor was cleaned using solvents as necessary.

V.B.1.v. Bench-Scale Cracking Continuous-Stirred-Tank-Reactor (CSTR)

Prior to the construction of the bench-scale TCR described in Section V.B.1.iv, an existing CSTR was used to crack TAG. The development of this reactor is described in detail in a thesis entitled 'A Study of Bench Scale, Pressurized, Continuous Flow Thermal Cracking of Crop Oil' produced by Blake Sander and published under the University of North Dakota in 2014.[62] Although there were potentially minor reconfigurations in the design of the reactor between the work of Sander and the present work, for the most part, the essential function and design of the original CSTR system remained unaltered between operation by Sander and the work described herein. The exception is modifications to the system described below.

A schematic of the cracking CSTR is shown in Figure 33 as it was configured and operated during this present work. The main system components includes a 68 L TAG feedstock tank, diaphragm pump, oil feed line preheater, 9.7 L reactor with three independently controlled external ceramic band heaters, water cooled condensing unit, and a 68 L CTL collection tank.

Except for negligible sealing components in valves/pumps, all reactor surfaces in contact with TAG/CT were either stainless steel (304 or 316 grade), Inconel, HDPE, or Teflon. All thermocouples were K type 6.4 mm diameter probes of various lengths sheathed in Inconel.
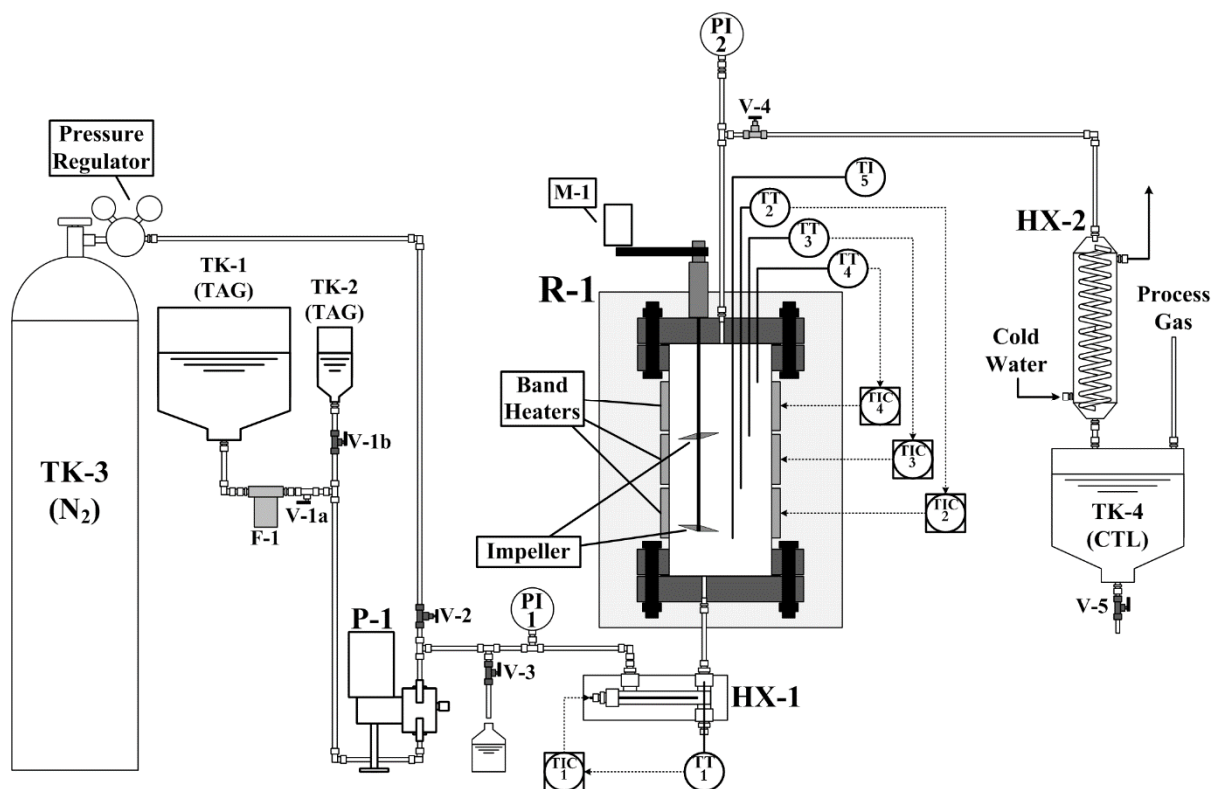
Figure 33. Bench-scale continuous stirred tank reactor (CSTR) for TAG cracking

A compressed gas tank (TK‑3) was installed to the reactor system for delivering gases as needed (either nitrogen for purging the reactor before/after service or air for cleaning/decoking as necessary) and a valve (V‑2) was installed to shut off the gas line, as depicted.

TAG was pumped from either of a 68 L tank (TK‑1) through an oil filter (F‑1) and a ball valve (V‑1a) or from a 1 L tank (TK‑2) and a ball valve (V‑1b). During normal operation, TAG was pumped from TK‑1. However, the feed rate was occasionally monitored by pumping from TK‑2 and using the liquid level of TK‑2 for volumetric measurements with time. During operation, only one of V‑1a or V‑1b was opened, with the other shut. The exception to this was

when TK‑2 was being filled by gravity-draining from TK‑1, in which both V‑1a and V‑1b were open.

TAG was pumped by a proportioning diaphragm pump (P‑1) model 515-A-N3 from Neptune Chemical Pump Company (Lansdale, PA, USA) at variable feed rates up to 10 L/h. TK‑1 and TK‑2 supplied approximately 2.1 meters of liquid head atop P‑1 so that it could operate reliably. 10.8 mm inside diameter tubing was used to interconnect between all equipment before the pump, to minimize a friction head against the pump.

A ball valve (V‑3) was installed immediately downstream of P‑1 as a drain valve leading to a canister, so that P‑1 could be easily primed or warmed up before operation of the reactor system. However V‑3 remained closed during normal operation and TAG was pumped through a preheater (HX‑1) before entering the reaction volume. A single thermocouple probe (TT 1) was installed in the TAG preheater for feedback PID control (TIC 1), as shown.

After the preheater, feedstock flowed into the cracking CSTR (i.e., R‑1) with a reaction volume of 9.7 L. R‑1 was constructed using a stainless steel pipe (SS 316 grade) of dimensions 57.7 cm long × 14.6 cm diameter, with flanges on either end. As shown, a rotary feedthrough was installed to enable the rotation of a mechanical agitator shaft, which was installed off-center from R-1's radial origin to minimize vortexing. The agitator was operated at rotation speeds of approximately 400 RPM by a motor (M‑1) outside the reactor. The two impellers were directionally reversed (i.e., one 'up-mixing' and the other 'down-mixing') in order to promote desirable mixing. R‑1's entrance was at the base and its exit was at the top, giving the illusion of an up flow reactor, however, its function was intended to be as a CSTR with ideal mixing.

Three ceramic band heaters were wrapped around R‑1 for heating the reaction volume. Four thermocouples probes (i.e., TT 2, TT 3, TT 4, and TT 5) were installed in R‑1 at height levels consistent with the top and/or bottom of the heaters, as shown. The former three thermocouples were used as process variables for feedback temperature control (i.e., TIC 2, TIC 3, TIC 4), connected as shown. TI 5 was used for measurements only, and it served no control purpose.

Pressure control was facilitated manually by adjusting a needle valve (V‑4) at the exit of R‑1. The pressure of R‑1 was monitored by two dial-type pressure gauges that were installed on either side of the pressurized zone (i.e., PI 1 and PI 2) as indicated by in Figure 33. Due to using manual pressure control in conjunction with two-phase flow (i.e., gas/liquid), the pressure typically oscillated on the order of ±0.3 MPa, and had to be carefully monitored during operation.

After V‑4, the product stream from R‑1 was cooled by flowing it through a coiled-style shell and tube heat exchanger (HX‑2), as shown. The process stream flowed through the tube side of HX‑2, having heat transfer dimensions of 6.1 m length $\times$ 7.7 mm inside diameter $\times$ 0.9 mm wall thickness. An excess flow of cold water (17 C) was supplied to the shell side tube of HX‑2 to ensure sufficient cooling.

The cooled product stream exiting HX‑2 was sent to a 68 L product tank (TK‑4) where it was phase separated from the process gas, which was vented to a fume hood. A septum port (not depicted) was installed in-line before venting the process gas to permit sampling of the gas phase product for analysis. A ball valve (V‑5) was installed at the base of TK‑4 for draining product as

necessary, however, it was normally closed during regular operation.

V.B.1.vi. Modified Cracking Continuous-Stirred-Tank-Reactor

In an attempt to alleviate and/or study coke formation, modifications were made to the cracking CSTR, as shown in Figure 34. Redundant features of the cracking CSTR are not depicted or noted, only features that are modified. Annotations in the diagram highlight the three modifications that were done to the system. These include a strategically placed thermocouple, a more substantial preheating system, and a 'bottoms draw' to permit the withdrawal of product from the base of the reactor. These modifications are described in detail below.

The first modification was the reorientation of a thermocouple probe (TT 5), which had previously measured the temperature at the base of R-1. Afterwards, it was reoriented to touch the inside wall of R-1 at the central height of the central band heater. This was the most coke-prone region of R-1. The reorientation was done in an attempt to gain an understanding of the wall temperature as coke begins to form. Since TT 5 was not previously being utilized for feedback control, this modification did not otherwise affect the temperature control of the reactor—control thermocouple probes were intentionally left unadjusted.

The second modification was the installation of 300 % additional preheating capability (HX-1a/b) before R-1. Originally the preheater (HX-1) consisted of a single 34.5 cm long $\times$ 6.35 mm diameter 1000 W preheating element with a stainless steel sheath. The TAG oil was made to pass around the element for conductive heat transfer. Unfortunately, previous experience had demonstrated that HX-1 was only capable of preheating the TAG to 150 C reliably, which is substantially lower than cracking temperatures. To improve the reactor system, the preheater was quadrupled from 1000W to 4000W so that the feedstock oil could be preheated to cracking
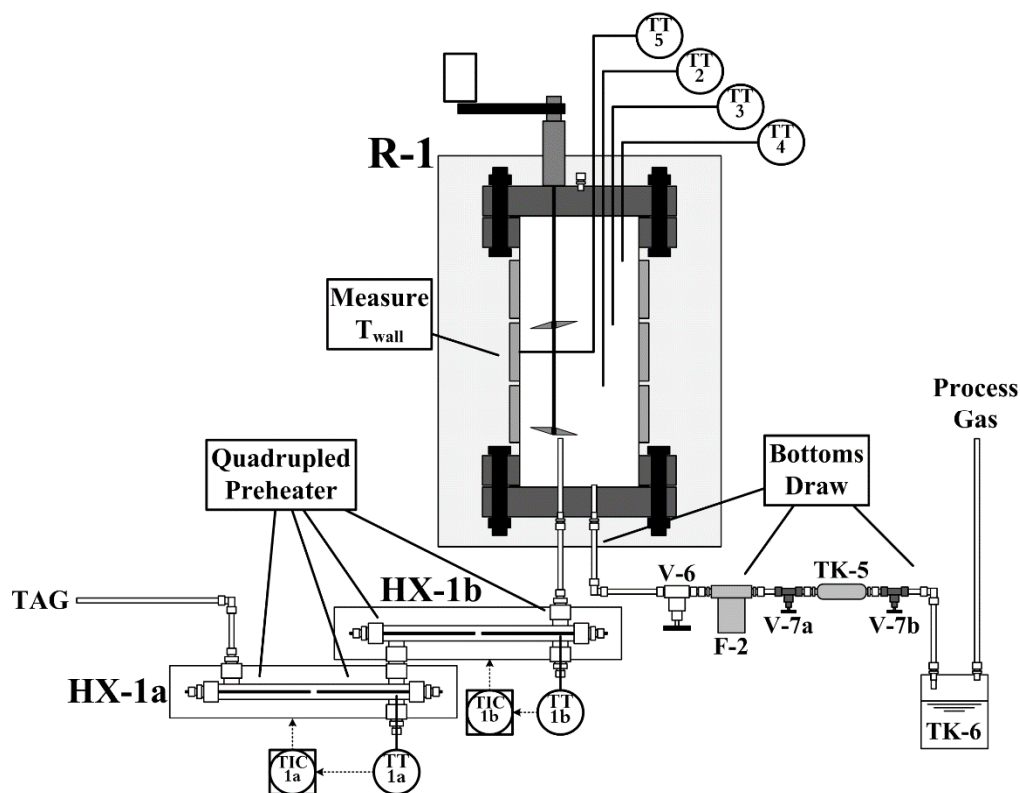
Figure 34. CSTR modifications in attempt to study coke formation

temperatures without causing coke in the preheater. A second control loop (TIC 1b / TT 1b) was also installed to permit modulation of the flux from HX‑1a and HX‑1b separately. The improved preheating system decreased the flux through the walls of R‑1, and, therefore, reduced the wall temperatures, potentially mitigating coke formation.

The final modification was adapting an outlet to the bottom of R‑1 to withdraw from the liquid phase at a semi-continuous rate (a.k.a., the 'bottoms draw'). A fitting was installed to the very base of the reactor for the withdrawal of product from there. Additionally, a feedthrough tube was installed up through the bottom of the reactor sufficient to introduce TAG feedstock

directly to the R‒1's agitator's lower impeller, within a clearance of 6 mm—this prevented TAG

feedstock from being immediately diverted through the bottoms draw without mixing/reactor.

The bottoms draw fitting led through a normally-opened, wide clearance needle valve (V‒6) and

through a filter (F‒2) into to a 200 mL stainless steel cylinder (TK‒5) which was isolated on both

ends by high temperature valves (V‒7a/b). Neither V‒7a nor V‒7b were opened at the same time,

however, they were sequentially opened/closed so as to fill/dump TK‒5 at regular intervals.

V‒7b dumped the contents of TK‒5 into a tank (TK‒6) for the withdrawn bottoms liquid. A

process line was installed from TK‒6 to a fume hood in order to permit ventilation of process

gas. Sequencing of V‒7a/b was timed in order to achieve a 10 % bottoms draw rate by volume

(respective of the feed rate).

V.B.2. Catalytic Deoxygenation Reactors

Catalyst deoxygenation equipment included a batch reactor and two packed bed reactors

(PBRs), one at lab-scale (approx. 100 g catalyst) and one at bench-scale (approx. 1000 g catalyst)

in nearly identical configuration. For this reason, the PBRs are described together. These

reactors permitted the study of various catalysts for CTD deoxygenation, and they were capable

of operating up to at least 3600 kPa and 400 C in order to ensure sufficiently severe conditions

for deoxygenation to occur. Descriptions and schematics of these reactors are offered in the

following subsections.

V.B.2.i. Batch Deoxygenation Reactor

The batch deoxygenation reactor was a small reaction chamber, in which catalyst was

placed for reduction, followed by rapid introduction of preheated reactants to start the reaction.

The reaction was studied with time sampling by obtaining negligibly-small sized samples from the liquid phase for analysis through a sampling capillary. The on-line sampling of the batch reactor made it possible to investigate potential catalysts for deoxygenation with only a few experiments per catalyst. This elucidated potential catalysts for use with the noncatalytic cracking process (NCP). A schematic of the reactor is shown in Figure 35.
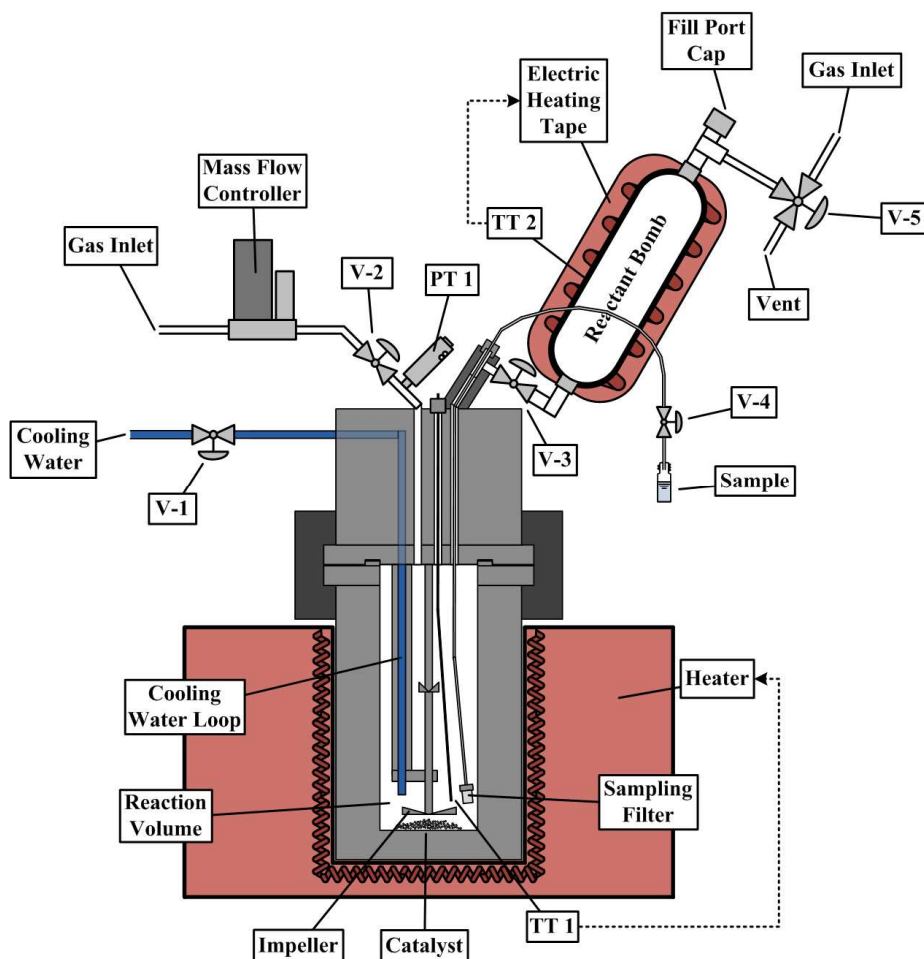
Figure 35. Batch reactor for deoxygenation catalyst screening

The batch reactor was a modified 4575A bench-top stirred autoclave reactor with 500 mL

internal volume from Parr Instruments (Moline, IL USA). The reactor flanges were sealed by a

grafoil gasket, which was replaced as needed. A stirring impeller was installed as shown and

typically operated at 400 RPM. A pressure transducer (P‑1) was installed as shown to measure

the pressure of the reaction. A valve (V‑1) was installed to modulate the flow of cooling water

through the stainless steel cooling water loop in the reaction chamber. When shutting down, lag

times were minimized by simultaneously opening V‑1 while turning off the heater and lowering

it away from the reaction chamber. The surfaces in contact with liquids and gases in this reactor

system were predominantly 304 or 316 stainless steel, Inconel, and glass.

A reactor was heated by conduction via an electric coiled heater that was cupping the

lower ~80% of the reaction volume, as shown. A 1.6 mm K type thermocouple probe (T‑1) was

used for feedback temperature control of the reactor heater. T‑1 was inserted into the reactor and

positioned within 5 mm of the impeller, as shown.

A mass flow controller for H_2 gas was adapted to a valve (V‑2), which together were

installed to the inlet side of the reactor to permit the delivery of gases at specified flow rates or to

seal the reactor when desired.

A 300 mL stainless steel reactant bomb was wrapped with electric heat tape and added to

valve (V‑3) above the reactor. A thermocouple (T‑2), and insulation were adapted to the bomb,

as shown. T‑2 was used for feedback temperature control of the reactant bomb. This permitted

preheating reactants before reaction, and rapid pressurized delivery to the reaction chamber when

the reaction was ready to begin. A fill port was installed with a removable stainless steel cap to

allow the bomb to be filled with reactants easily. A 3-way valve (V‑5) was installed to allow

pressurization and venting of the bomb, as shown.

A short 1.6 mm stainless steel liquid sampling line was inserted through the top of the reactor into the liquid phase with an exposed 0.5 µm sampling filter made of stainless steel. This permitted sampling of the liquid phase without catalyst plugging the sampling line, as shown. A valve (V-4) was added to the sampling line to modulate the flow of sampled liquid. Glass vials were cupped under the sampling line to catch liquid droplets, as shown. The total sampling line volume was 250 µL. The procedure for operation of the batch reactor is as follows.

In its fully disassembled condition, the heater is lowered/set aside and the reactor is separated at its flange to reveal the reaction volume. All valves are initially closed. An experimentally-specified sample amount of catalyst was weighed and placed in the reaction volume, which was then reinstalled to the reactor and sealed by its flange. Then the reactor was purged with H_2 gas three times to at least 500 kPa to remove residual oxygen by supplying gas through the inlet valve (V-2) and venting it through the outlet valve (V-4). Afterwards, the reactor was pressurized with 7000 kPa of H_2 gas and tested to identify any leaks.

When the reactor system was shown to be properly sealed, the pressure was vented to ambient pressure by opening V-4. Then the mass flow controller was set to a deliver an experimentally-specified flow rate of H_2 through the reaction volume for a specified number of hours as needed to fully reduce the catalyst. The impeller was set to a specified rotational speed (typically 400 RPM). The experimentally-specified temperature was applied to the reaction volume controller and the reaction volume was allowed to heat up to reduction temperature (typically 325 C). Reduction was allowed to take place for the experimentally-specified reduction time before introducing reactants to the catalyst.

Meanwhile, the reactant bomb was filled with an experimentally-specified volume of liquid reactant feedstock by removing the fill port cap. Afterwards, the reactant bomb was re-sealed by re-attaching the fill port cap. Then the bomb was purged of residual air and pressure tested in like manner to purging the reaction volume. Afterwards, the bomb was pressurized to the experimentally-specified reaction pressure of H_2. At 1 h before reduction was completed (i.e., before the reaction start time), the temperature control of the reactant bomb was turned on to 200 C and the contents were allowed to heat up in order to introduce pre-heated reactants to the reaction bomb.

After reduction was completed, V-2 and V-4 were closed to seal the inlet and outlet of the reactor. Then a timer was started while simultaneously opening valve V-3 to introduce the pressurized, preheated contents of the reactant bomb to the reaction volume. It took at least 5 – 20 s for the reactants to flow into the reaction chamber and for the pressure to reach 3.6 MPa. Afterwards V-3 was promptly shut. It should be noted that the introduction of 200 C reactants to the 325 C reaction chamber depressed the reactor chamber temperature measurement to as low as 270 C, which quickly recovered to above 300 C in under 3 min, stabilizing at approximately 325 C in under 6 min. For this reason, the first two reactant samples (comprising the first 7 minutes of reaction time) were neglected.

After exactly 1 min of reaction time had passed, the V-4 was opened slightly to extract approximately 0.8 ± 0.4 g/min of liquid phase reaction products into 4 mL screw-top sample vials for subsequent characterization by FTIR for activity measurements. 10 samples were collected at exactly 3 min intervals each for a final reaction time of exactly 31 minutes, removing no more than 6 wt. % of reactant mass in total.

After 31 minutes, the reaction was promptly stopped by turning off / removing the reactor heating mantle, supplying an excess flow of cooling water to the cooling water loop, and applying 1.5 Nm^3 of forced air convection to the outside of the reactor chamber. Reactor temperature dropped below 250 C in less than 5 min of cooling time, irrespective of the speed with which the reaction was stopped. Liquid phase sampling continued for one additional 6 min long sample for subsequent characterization by GC for product speciation. Afterwards, the liquid sampling valve was shut and the reactor was cooled.

Once cooled beneath 25 C, the reactor pressure head was slowly vented to ambient pressure over several minutes. When the reactor pressure was beneath 110 kPa, a 250 µL gas tight syringe was used to capture gas phase reaction products for qualitative analysis, promptly injecting 100 µL into the GC. The reactor was opened and product liquid/catalyst was collected for subsequent analysis.

V.B.2.ii. Continuous Packed Bed Reactors (PBRs) for Deoxygenation

Successful deoxygenation catalysts from screening experiments were tested in a continuous PBR system, incorporating one of two bed volumes that were capable of holding either approximately 0.1 kg or 1.0 kg of catalyst. The beds could be interchanged, having otherwise virtually identical configurations, so only a single description is provided. Main system components included two pumps and a compressed gas tank to feed the ternary reactant system to the reactor, two preheating coils for pre-vaporization and/or pre-equilibration, a packed bed reactor, a double-pipe condenser, and a pressure control valve. The reactor schematic is shown in Figure 36. Continuous samples were obtained from the PBR under a variety of conditions in order to prove the reactivity, stability, and/or scalability of various catalysts for use

with the NCP.

Except for negligible sealing components in valves/pumps, all reactor surfaces in contact with the process stream were either stainless steel (304 or 316 grade), Inconel, or glass. All thermocouples were K type 1.6 mm diameter probes of various lengths.
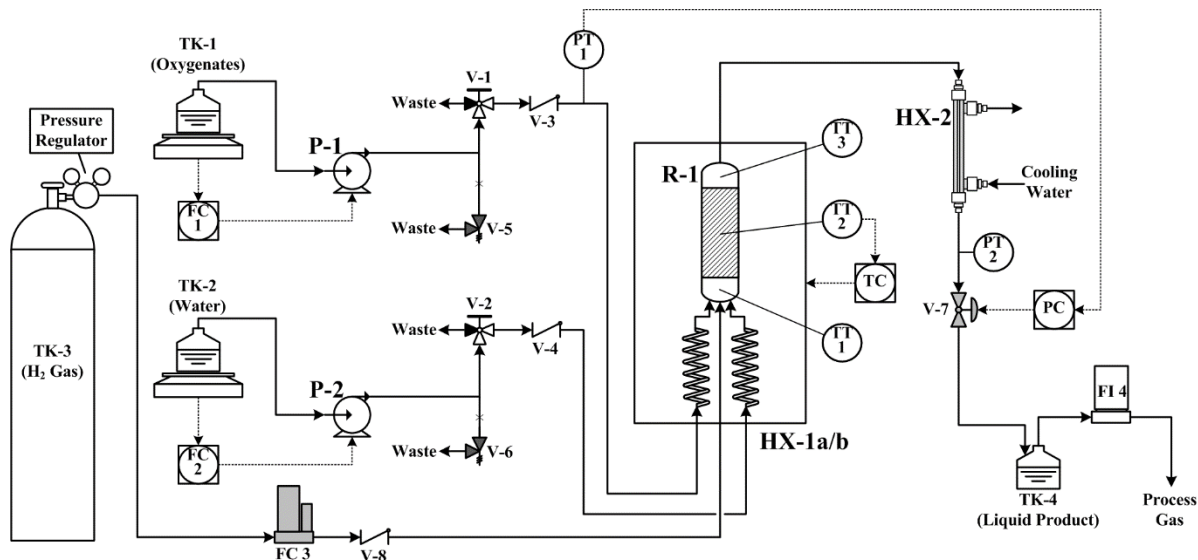
Figure 36. Packed bed reactor system for catalytic deoxygenation experiments

Process monitoring and control were facilitated by a cDAQ model 9178 Compact DAQ (i.e., cDAQ) from National Instruments (a.k.a., NI, Austin, TX). The cDAQ utilized three modules to obtain sensor data and to control devices: a voltage input module (NI 9206), a thermocouple input module (NI 9213), and a voltage output module (NI 9264). A computer application was programmed in NI's LabVIEW for interacting with the cDAQ and monitoring/controlling the process. Unless otherwise specified, all sensors were recorded by the supervising computer at sample frequencies of at least 1/min.

A H$_2$ gas tank (TK‑3) was connected to the reactor system with a corresponding mass flow controller (FC 3) and a check valve (V‑4) to protect FC 3 from hazardous/undesired backward flow, as depicted.

Oxygenates (CTD) were pumped from a glass Erlenmeyer flask (TK‑1) by an ISO-100 piston pump (P‑1) from ChromTech. Typically the oxygenate feedstocks were CTD mixtures from TAG processing in the laboratory, but model compounds were used in a few circumstances. TK‑1 was set atop a Highland™ model HCB-3001 digital scale from Adam Equipment (Danbury, CT) with a 3 kg capacity and 0.1 g readability. RS-232 communications between the scale, pump, and the supervising computer enabled feedback flow control (FC 1) of the feed rate. A 3-way ball valve (V‑1) was installed downstream of P‑1 for assistance with pump maintenance and priming when the reactor was not in service. A check valve (V‑5) was installed to prevent hazardous/undesired backward flow, as shown. As a safety precaution, a relief valve (V‑3) was installed as shown and set for 6000 kPa. An identical, redundant feedstock delivery system was installed for pumping water to the reactor, as indicated in Figure 36.

The reactor (R‑1) was a packed bed style reactor constructed out of a stainless steel tube that utilized 100 µm frits and glass wool to position the catalyst within the reactor. Three thermocouples were installed inside the reactor as shown in figure 21 to measure the temperature at the entrance to the bed (TT 1), the middle of the bed (TT 2), and the exit from the bed (TT 3). The volume of R‑1 depended on the size of the catalyst bed, either 100 g or 1000g, depending on the experiment.

H$_2$ gas was fed directly to R‑1 from V‑4, whereas water and oxygenates were first

177

preheated in separate coiled tubes (HX‑1a/b) within the reaction furnace. The dimensions of each preheating coil were 305 cm long × 4.6 mm inside diameter. Heated equipment such as R‑1, HX‑1a and HX‑1b, were installed inside an upright cylindrical furnace with dimensions of 61 cm high × 31 cm inside diameter. The temperature of the furnace was maintained by feedback control (TC) as shown, utilizing TT 2 and for the process control variable.

The product stream from the reactor was condensed by flowing it through a short, double-tube style condenser (HX‑2) as shown. The process stream flowed through the inner tube, having heat transfer dimensions of 30.48 cm length × 0.46 cm inside diameter × 0.09 cm wall thickness. An excess flow of cold water (17 C) was supplied to the outer tube of HX‑2 to ensure sufficient cooling.

Pressure was continually monitored by two pressure transducers (PT 1 and PT 2), installed as indicated in Figure 36. After cooling, the reaction products passed through a pressure control valve (V‑7) that utilized PT 1 for feedback pressure control. V‑6 was motorized by interconnecting an integrated stepper motor, driver, and controller (Part 4118S) from Lin Engineering (Morgan Hill, CA USA); a 30:1 worm gear box (WDG30P) from RobotZone, LLC (Winfield, KS USA); and a needle valve (SS-SS4-EP) from Swagelok (Solon, OH USA).

Finally, the liquid reaction products were collected in a glass Erlenmeyer flask (TK-3), which was used for separation of the gaseous and liquid products. Process gas was vented to a fume hood through a 10 L/min N_2 flow meter (FI 3) from Aalborg Instruments and Controls (Orangeburg, NY). A septum port (not depicted) was installed in-line before venting to permit sampling of the gas phase effluent for analysis.

The system was assembled and P-1 was primed with an experimentally specified CTD feedstock by turning V-1 (the 3-way valve) so that P-1 would lead to 'Waste' instead of leading to R-1. Although not depicted, 'Waste' is a vacuum flask connected to a vacuum pump, which in turn exhausts to a fume hood. FC 1 was set to max flow rate. The negative pressure of the vacuum pump assisted with the priming of P-1. Once primed, V-1 was switched back towards R-1 and FC 1 was set to zero. Likewise, P-2 was primed with water from TK-2 by turning V-2 to 'Waste' and performing similar actions.

Then residual air was purged from the system by setting PC to 0.0 MPa (i.e., opening V-6) and setting FC 3 to max. After a few minutes of purging, the system was pressure tested by setting PC to 7.0 MPa (i.e., closing V-7), and allowing the reaction chamber to pressurize with N_2. Once the pressure of the system (i.e., the average of PT 1 and PT 2) reached TK-3's pressure regulator (about 6500 MPa), the flow indication of FC 3 was used to verify that leaks were negligible. Then PC (system pressure) was set to zero, and FC 3 was set to the experimentally specified operating pressure for reduction of catalyst. Catalyst reduction was allowed to take place for an experimentally specified amount of time. Then the temperature (TC), pressure (PC), and flow rate of H_2 (FC 3) were adjusted to their experimentally specified operating conditions, and steady-state was achieved for at least one hour before introducing liquid phase reactants.

Liquid phase reactants were introduced by setting FC 1 and FC 2 to their specified operating feed rates. Throughout experimentation, products were collected continuously in TK-4, and process gas was vented continuously. A gas tight syringe was inserted into a septum in-line with the process gas exhaust of the system (not depicted). A 100 µL sample of gas was withdrawn into the syringe and the contents of the syringe were injected into a GC within 20

179

seconds. Samples of liquid product were obtained and analyzed by FTIR as described in a following subsection. Liquid samples were continuously monitored, and once sufficient liquid samples were obtained at a set specified experimental operating condition, then the conditions were adjusted to their new experimental operating conditions.

Daily shut down of the reactor system involving putting the catalyst into a reductive state simply by leaving the reaction temperature at operating temperature (TC), while increasing the H_2 flow to max (FC 3) and setting the pressure (PC) to 0. This helped to keep the catalyst fully reduced before experimentation the following day(s).

Long-term system shut-down consisted of shutting off the power to TC in order to cool down R-1. The feed rate of CTD from TK-1 was shut off by setting FC 1 to 0. Also, the feed rate of water was set to max by setting FC 2 to maximum. This flooded R-1 with water to protect the catalyst and ensure safety, because the catalysts used can become pyrophoric if exposed to oxygen. Once the reactor was cooled to room temperature, PC was set to 0 and V-6 vented the pressurized contents of the system. Then R-1 was disassembled and the catalyst bed was emptied.

V.B.3. Other Process Equipment

Other process equipment included (1) a dual-purpose batch reactor for cracking and deoxygenation, (2) a CTL fractionation system for separating CTL into process residue (CTR) and CTD, (3) a fuel fractionation system for fractionating deoxygenated CTD into fuel products, and (4) a crude residue processing furnace for converting CTR into coke, residue distillates, and process gas.

V.B.3.i. Batch Cracking/Deoxygenation Reactor

The dually-purposed batch reactor for refining fuel from TAG is summarized as a small reaction chamber that enabled the cracking of TAG or the deoxygenation of CTD in a batch configuration, performed separately (not simultaneously). This configuration utilized the most necessary features of the two batch reactors previously discussed in order to enable cracking of TAG and deoxygenation of CTD. A schematic of the reactor is shown in Figure 37.

The batch reactor was a modified 4575A bench-top stirred autoclave reactor with 500 mL internal volume from Parr Instruments (Moline, IL USA) that was configured as depicted in
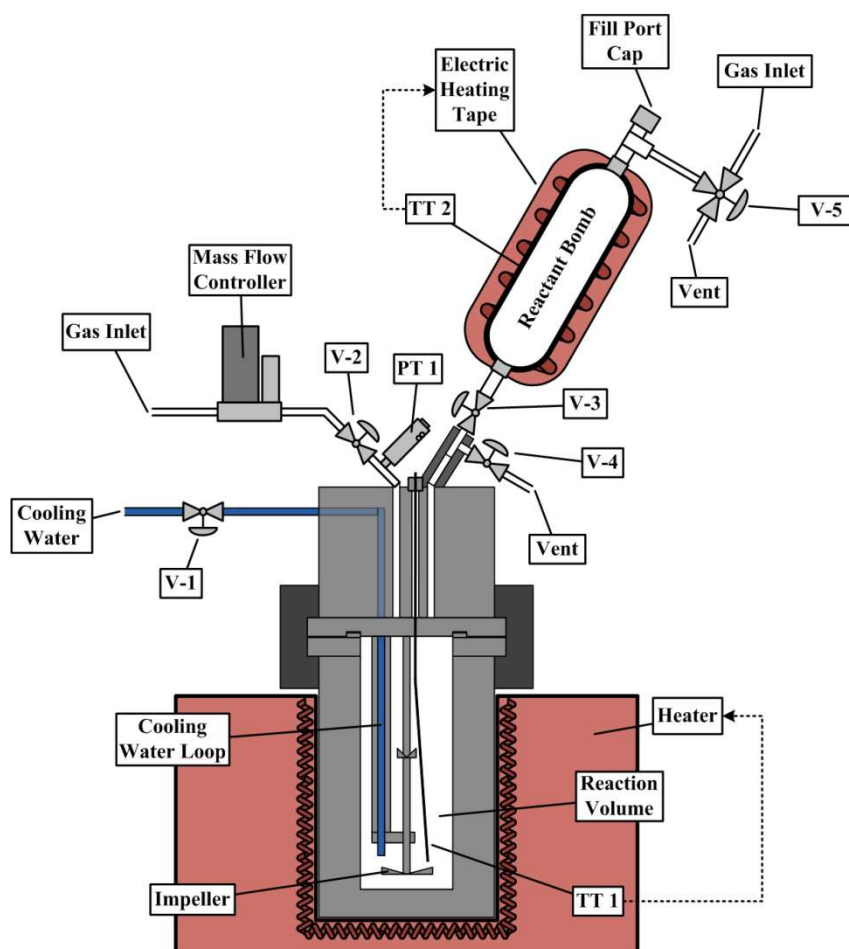
Figure 37. Dually-purposed batch reactor for fuel refinement by the NCP

Figure 37. This configuration was similar to batch reactor configurations that were previously

described in Section V.B.1.i and Section V.B.2.i for the TAG cracking and catalytic

deoxygenation, respectively.   Redundant features of the reactor are not described.

In its fully disassembled condition, the heater is lowered/set aside, and the reactor is

separated at its flange to reveal the reaction volume. All valves are initially closed. Either an

experimentally specified sample of TAG (for cracking) or an experimentally specified sample

amount of catalyst (for deoxygenation) was weighed and placed in the reaction volume, which

was then reinstalled to the reactor and sealed by its flange. Then the reactor was purged with N_2

gas three times to at least 500 kPa to remove residual oxygen by supplying gas through the inlet

valve (V-2) and venting it through the outlet valve (V-4).   Afterwards, the reactor was

pressurized with 7000 kPa of either N_2 gas (for cracking) or H_2 gas (for deoxygenation) and

tested to seal any leaks.

When leaks were shown to be properly sealed, the pressure was vented to reach ambient

pressure by opening V-4 (the vent valve). For cracking experiments, V-4 was then shut. For

reduction experiments, V-4 was left open and the mass flow controller was set to deliver an

experimentally specified flow rate of H_2 through the reaction volume. In either case, the

impeller was set to a specified rotational speed (typically 400 RPM).

When deoxygenating, reduction took place before reaction at 325 C for at least 6 hours

with approximately 200 mL/min flow of H_2. Meanwhile, the reactant bomb was filled with an

experimentally specified volume of liquid reactant feedstock by removing the fill port cap.

Afterwards, the reactant bomb was re-sealed by re-attaching the fill port cap. Then the bomb

was purged of residual air and pressure tested in like manner to purging the reaction volume.

Afterwards, the bomb was pressurized to the experimentally specified reaction pressure of H_2. At 1 h before reduction was completed (i.e., before the reaction start time), the temperature control of the reactant bomb was turned on to 200 C and the contents were allowed to heat up in order to introduce pre-heated reactants to the reaction bomb. After reduction was completed, V-2 and V-4 were closed to seal the inlet and outlet of the reactor. Then a timer was started while simultaneously opening valve V-3 to introduce the pressurized, preheated contents of the reactant bomb to the reaction volume. Afterwards, V-3 was promptly shut and a timer was started to signify the start of reaction.

TAG cracking experiments were performed instead by applying the experimentally specified temperature to the reactor volume's heating controller and the reaction volume was allowed to heat up to temperature. At 385 C, a reaction timer was started to signify the start of reaction.

Reactions were allowed to progress until an experimentally specified time had elapsed. Then the reaction was promptly stopped by turning off / removing the reactor heating mantle and supplying an excess flow of cooling water to the cooling water loop by opening V1. In addition, approximately 1.5 sm^3/min of forced air convection was applied to the outside of the reactor chamber to aide in cooling. Reactor temperature typically dropped below 250 C in less than 5 min of cooling time, whether cracking or deoxygenating.

Once cooled beneath 25 C, the reactor pressure head was slowly vented to ambient pressure over several minutes, being collected in a gas sample bag when desired. At ambient pressure, the reactor was opened and product liquid and/or catalyst were collected for subsequent analysis.

V.B.3.ii. CTL Fractionation System

      The CTL fractionation system was used to separate CTL into distillates (CTD) and residue (CTR) by stepwise distillation and vacuum distillation. The distillation path was intentionally kept short (about 3.8 cm) to aid in volatilization of material from the residue. All collected distillates were recombined after distillation for subsequent testing.

      A schematic of the CTL fractionation system is shown below in Figure 38. The system consists of a boiling flask, a short path spinning brush head, a hot water condenser (HX‑1), a cold water condenser (HX‑2), a cryo trap condenser (HX‑3), and a vacuum pump (P‑1). The boiling flask was glass, however the remainder of the structural components were comprised primarily of stainless steel. Rubber o-rings were utilized at connections in order to permit high vacuum seals. A copper gasket was also installed between the spinning brush column and HX‑1 to form a high temperature vacuum seal.

      Temperature control was utilized to ramp the temperature of the boiling flask with a simple ramp rate and soak time. The typical temperature program that was utilized was to ramp the temperature of the boiling flask from ambient to 350 C at a rate of 1.5 C/min, and hold at 350 C for 45 min before turning off the heat. Distillation was typically performed in two stages, with the first having disconnected P‑1 and the second having operated with P‑1 installed and operating at high vacuum.

      The boiling flask was enclosed by an all-around flask heater and set atop a magnetic stirring plate. A single Teflon coated magnetic stir bar was added to the boiling flask along with the sample to be processed. A single thermocouple probe (TT 1) was inserted into the thermowell of the boiling flask to monitor the boiling temperature. Since this system is not
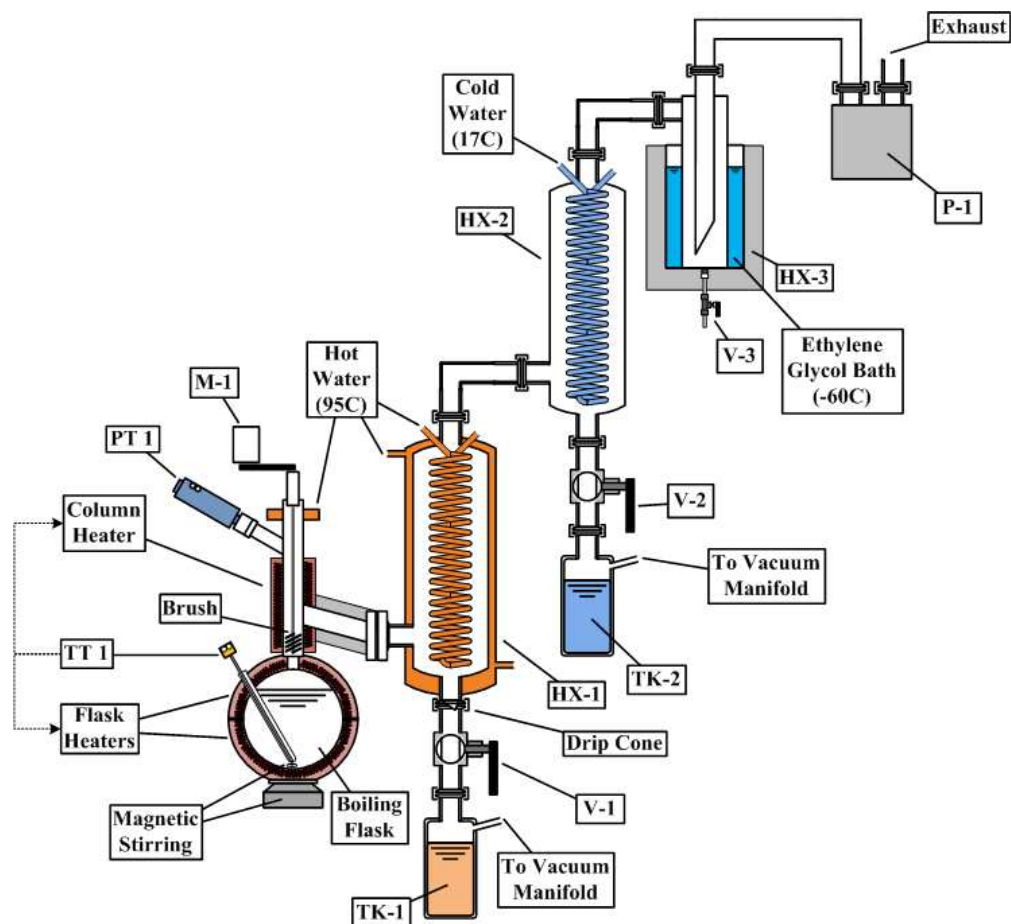
Figure 38. CTL fractionation system for distillation and vacuum distillation

intended for analytical distillation, a vapor temperature thermocouple probe was not necessary.

The boiling flask was connected to the short path spinning brush head (i.e., head) using a Viton o-ring to facilitate the glass/metal connection. A small 3.8 cm length x 3.8 cm diameter brush was installed at the base of the spinning brush distillation column in order to mitigate splash up from the boiling flask. The spinning brush was made of 304 stainless steel and was typically operated at rotation speeds of approximately 3 s^{-1}. A rotational feed through was installed through a flange at the top of the head in order to permit rotation of the brush which

was carried out by a motor (M‑1) via a belt drive. A pressure transducer (PT 1) was installed as shown to monitor the pressure of the still. Hot water was routed through a cooling water ring near the top of the head in order to prevent excess heat from reaching the feedthrough, which was only rated to approximately 40 C.

Distillates from the head progressed through HX‑1, HX‑2 and HX‑3 in series in order for volatiles to condenser in stages. The temperatures of the three condensers are indicated in Figure 38. The combination of the elevated temperature of HX‑1 and the use of a drip cone at the base of HX‑1 was required to condense heavy waxes and prevent them from solidifying on the walls of the condenser, which can lead to problematic and/or hazardous operating conditions. However, it was necessary to add additional, low temperature condensers in order to ensure condensation of as much volatile matter as possible to improve the life of the pump & pump oil.

The operation of the CTL fractionation system was characterized by filling the boiling flask with a specified volume of sample to be distilled of known weight. Initially, ambient distillation was performed by disconnecting P-1. M-1 was operated at 180 RPM, and coolants were supplied as specified in Figure 38. Then the flask was heated up at a rate of 1.5 C/min from ambient temperature until the temperature reached 350 C, at which it was maintained for 45 minutes. Then the heater was shut off, and the flask was allowed to cool to below 40 C, completing ambient distillation. TK-2 and TK-3 were disconnected and the distillate samples were collected in separate containers, also draining HX-3 to obtain its distillate sample. Then TK-2 and TK-3 were reconnected.

Vacuum distillation was then performed by reconnecting P-1 and then energizing P-1 to pull a vacuum on the distillation system. The procedure for ambient distillation was repeated,

and the vacuum pressure was not relieved until the system had cooled to < 100 C. Pressure was

ultimately relieved by disconnecting P-1. All distillate samples were again collected and drained

from their sources and combined. The mass of the residue remaining in the boiling flask was

obtained and compared to the mass of the original sample and the masses of distillates obtained.

All were recorded.

V.B.3.iii. Fuel Purification System

Liquid products were fractioned in a B/R 36-100 High Efficiency Distillation System

(B/R Instrument Corp., Easton, MD) as depicted in Figure 39. This was referred to as the *fuel*

purification system in this dissertation. The system consists of a boiling flask, an adiabatic

column with a Monel spinning band, a condenser (HX‑1), a reflux valve, and an automated

receiver carousel. The purpose of the system was to fractionate a sample of catalytically

deoxygenated CTD into various fractions for testing/blending into final fuel products.

The majority of the surfaces in contact with the sample were glass, Monel, or Teflon.

Two platinum RTD temperature sensors (TT 1 and TT 2) were installed as shown in Figure 39

in order to monitor the temperature of the boiling flask and the head of the distillation column,

respectively. The spinning band was installed in the adiabatic distillation column as shown, and

spun by a motor (HX‑1) at approximately 2000 RPM. Coolant was supplied to the condenser at

the top of the column at 10 C in order to condenser distillates and enable reflux. A reflux valve

was installed and utilized at a reflux ratio of 10.

The equipment was controlled by an associated supervisory control computer, which

monitored the temperatures of distillate and changed the fractions accordingly. During typical

operation, various boiling points were designated for 8 fractions, corresponding to 8 receivers on

the rotating receiver carousel. The supervisory control computer operated the distillation column

and adjusted the rotating carousel to collect each fraction separately as desired.
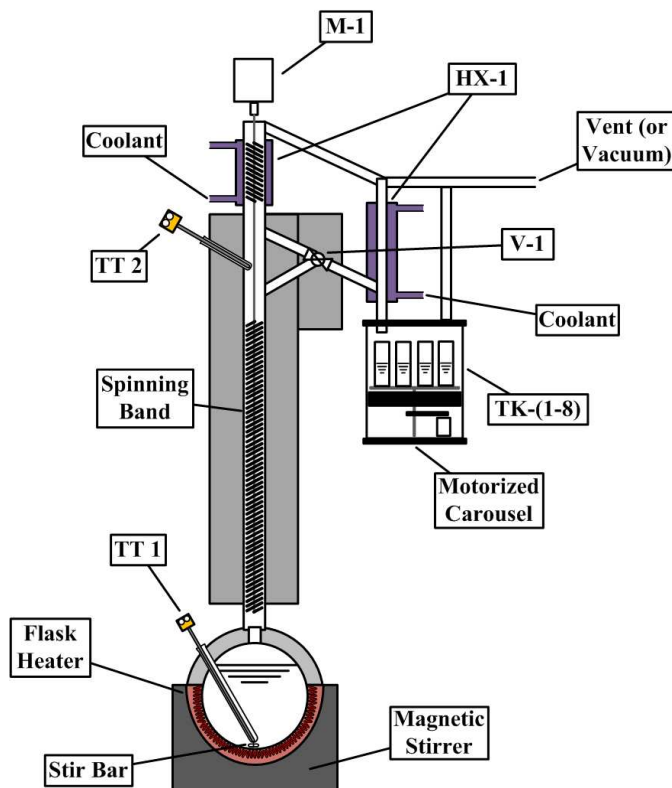
Figure 39. Fuel purification system

A vacuum pump and pressure transducer were also available, but they weren't typically

utilized due to the lightness of deoxygenated CTD. As a result, the exit of the distillation was

typically vented to a fume hood.

The operation of the system was fairly straightforward. The flask heater was lowered and

the boiling flask was disconnected from the spinning band column for loading. A sample to be

distilled was loaded into the boiling flask gravimetrically and a stir bar was added

gravimetrically. The boiling flask was then reconnected to the base of column and the flask heater was reapplied.

The system was configured to preheat the column under total reflux until 10 minutes as a vapor temperature > 40C was observed. Then the Monel spinning band was turned on and operated at 2000 RPM. The computer was setup to automatically create a reflux ratio of 10 by opening and closing V-1, accordingly. Coolant was supplied to the HX-1 system as indicate in Figure 39 from a cyclic coolant bath (not depicted), typically at a temperature of 10 C or otherwise specified. The carousel was set up to automatically collect up to 8 fractions as experimentally specified (e.g., 150 to 160 C is a single fraction) by adjusting V-1 and rotating the motorized carousel as necessary. The heating rate of the boiling flask (0 to 100 %) was manually adjusted as necessary to permit distillation at approximately 2-3 drops per second, visibly verified by observing a drip-rate near V-1. Collected fractions were stored in separate containers for fuel testing/blending.

V.B.3.iv. Crude Residue Processing Furnace

The crude residue processing furnace consisted of a semi-batch reaction chamber used for reactive separation of distillation residue into a coke product (or pitch product), distillates, and process gas, as shown in Figure 40 consisting of a small chamber, in which catalyst was placed for reduction, followed by rapid introduction of preheated reactants to start the reaction. The reaction was studied with time sampling by obtaining negligibly small-sized samples from the liquid phase for analysis through a sampling capillary. The on-line sampling of the batch reactor made it possible to investigate potential catalysts for deoxygenation with only a few experiments per catalyst. This elucidated potential catalysts for use with the noncatalytic cracking process

(NCP). A schematic of the reactor is shown in Figure 35.
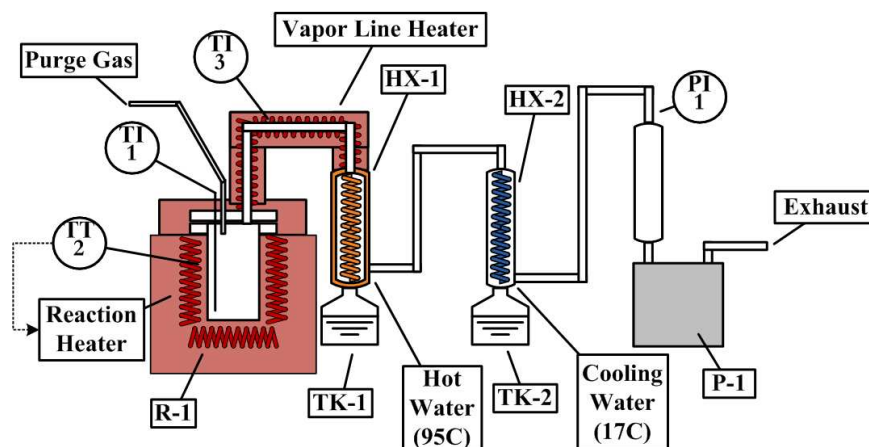
Figure 40. Crude residue processing furnace for producing coke/pitch

The operation of Bosquez's crude pitching furnace began with loading a sample of cracked TAG distillation residue (CTR) from CTL fractionation into the reaction volume (R-1). Then R-1 was heated until a final temperature in the range of 450 – 490 C to remove distillable material from the residue sample and to convert it to a coke product (or a pitch product).

The vapor line heater was used to maintain a vapor line temperature that was at least the temperature of R-1 in order to prevent premature condensation of distillates. Hot water and cooling water were supplied to the two heat exchangers (HX-1 and HX-2, respectively) for stepwise condensation of distillable material. The hot water condenser was necessary due to distillates that are solid at room temperature.

When the crude residue processing furnace was used to produce coke, the vacuum pump (P-1) was disconnected and a flow of N_2 was supplied as purge gas through the system to help remove oxygen and to provide a sweep gas to aid in volatilization of distillable material. On the

other hand, when the furnace was used to produce pitch, the purge gas line was closed off and the vacuum pump was connected and permitted to pull a vacuum on the system throughout operation.

V.B.4. Analytical Equipment

Various analytical instruments are described herein for their use in analysis of catalysts, reaction samples, etc. during experimentation.

V.B.4.i. Detailed Analysis of Liquid Products by Gas Chromatography

GC characterization was performed following the method developed by Kubatova and co-workers.[56,63,151] Details of the analytical equipment are described in various published works Kubatova and colleagues[56,63,151] and in a dissertation by Jana Stavova at the University of North Dakota.[152] This method used a GC-FID/MS (Agilent 7890N GC, 5975C MS) equipped with an autosampler (7386B series) and a split/splitless injector. Separations were accomplished using a 100 m long capillary column with a 0.25 mm internal diameter and 0.25 µm film thickness of a DB-1MS stationary phase. A constant helium flow rate was utilized. The MS and FID data was simultaneously acquired by employing a two-way splitter with a helium makeup gas, and the split flow ratio was 1:2 (MS:FID). The MS data was acquired in the full scan mode using electron ionization.

V.B.4.ii. High Throughput Analysis of Liquid Products by Gas Chromatography (FIMSDIST)

High throughput analysis of CTL samples was performed using a simultaneous dual-detector gas chromatograph (GC) as shown in Figure 41, with major components of the instrument shown in bold. The instrument was configured to simultaneously utilize a flame ionization detector (FID) and a field ionization mass spectrometer (FIMS) in parallel, referred to

as GC-FID/FIMS. This type of analysis is hereby referred to as a FIMSDIST analysis,

combining the aspects of FIMS and SimDist (simulated distillation).

The GC used in the FIMSDIST analyses was a model 6890N from Agilent Technologies,

Inc. (Santa Clara, CA USA) with all components/add-ons originating from Agilent unless

otherwise specified. Two inlets were installed on the GC, a cool-on-column inlet (COC inlet)

and a split-splitless inlet (S/S inlet). A 7683 series injector and autosampler were used for

sample injection, and a kit was used to permit automated on-column injection with 250/320/530

µm diameter columns. A liquid nitrogen cryo cooling adapter was installed to cool the GC oven

and COC inlet as low as −30C. The pressure and/or flow of all gases were modulated by

electronic pressure control. Helium was used as the carrier gas, and the FID was operated with

300 mL/min of air, 30 mL/min, of hydrogen, and 10 mL/min of makeup gas. A 1 mL methyl-

deactivated gooseneck glass liner with methyl-deactivated glass wool was utilized for inlet

vaporization with the S/S inlet.

An MXT-1HT SimDist chromatography column was purchased from Restek Corporation

(110 Benner Circle, Bellefonte, PA 16823 USA) and installed to the on-column inlet of the GC.

The column dimensions were 10.0 m length × 530 µm internal diameter with 0.21 µm film

thickness.

A SilTite µunion was used to connect a 0.20 m × 250 µm internal diameter fused silica

capillary (retention gap) to the exit of the analytical capillary, which was then connected to a 'Y

connector' to split the flow to the two detectors as shown in Figure 41. The Y connector was a

SeCure® Y-Union from Restek (Bellefonte, PA, USA). The two transfer capillaries leading to

the FID and MS were both 250 µm internal diameter with lengths of 0.53 m and 0.49 m

192
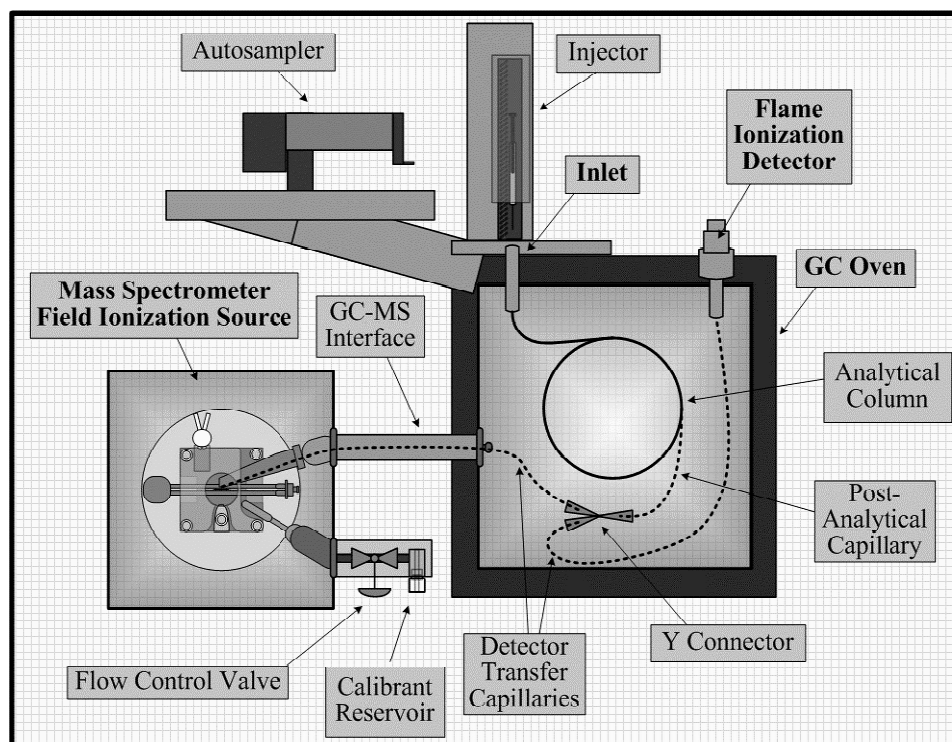
Figure 41. GC-FID/FIMS configuration for FIMSDIST

respectively. Head pressure was modulated as a function of temperature in order to facilitate 9

$mL \cdot min^{-1}$ flow of carrier gas through the analytical capillary. Due to the Y connector splitting

the flow, 2 $mL \cdot min^{-1}$ flow was diverted to the MS and 7 $mL \cdot min^{-1}$ flow was diverted to the FID.

The MS was a high resolution, time of flight JMS-T100GCe 'AccuTOF' from JEOL

USA, Inc. (Peabody, MA USA). The ion source was configured for FIMS, with the ion source

arranged as depicted in Figure 42. An isolation valve was used to segregate the ion source and

the mass analyzer as indicated, when necessary. The MS utilized an orthogonal acceleration

TOF mass analyzer (not depicted) with a single reflectron. A dual micro channel plate ion

detector was utilized with a continuous digital averager for MS data acquisition.

The detector voltage was operated near its maximum at 2500 V in order to increase the

193

ion intensity, which is notoriously lower for FIMS. The pusher/puller, reflectron, and flight tube voltages were operated at factory specified defaults for the instrument (778/-778, 990, and -7000 V respectively). Mass spectral data was acquired over the range of 3 to 990 *m/z* with the pusher/puller operating at frequencies of 1 ns. The vacuum of the mass analyzer was typically 2×10^{-5} Pa during analysis.

Schematics of the ion source for FIMS are shown in Figure 42. The side view shows the FI probe being inserted into the ion source block from its origin outside the MS through a vacuum feedthrough port with valve. The FI probe places the wire type field emitter approximately 1.0 to 1.5 mm from the centroid of the two extraction rods which are spaced 1.0 mm apart. Ions produced by FI are guided by lenses 1–3 through a slit into the mass analyzer, assisted by a deflector. The front view (Figure 42.b) shows the nozzles guiding the GC capillary to the emitter and directing analytes from the reservoir to the emitter. A source block surrounds the field emitter, and its temperature is maintained using a heating element as shown. A K-type thermocouple (not depicted) is also inserted into the source block for temperature control.

(a.)   (b.)
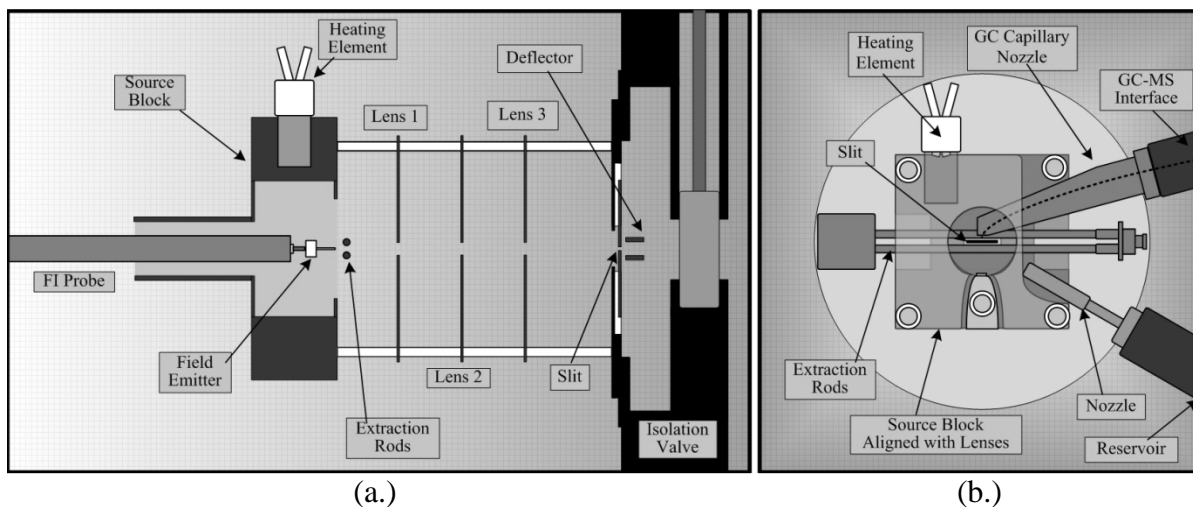
Figure 42. (a) Side view and (b) front view of FIMS ion source components

Typical ion source pressures were approximately 1.5×10^{-4} Pa. The GC-MS interface temperature was maintained at a maximum (350 C) to mitigate condensation of analytes in the transfer capillary. The calibrant reservoir's temperature was maintained at 120 C. In order to facilitate FIMS, the extraction rods (cathode) were maintained at -10 kV relative to the field emitter, which was maintained at ground potential. The source block was maintained at +36 V. The default voltages for the lenses (1–3) and the deflector were -1000, -700, -100, and -100 V, respectively. However once an emitter was installed, these four voltage settings were adjusted regularly to maintain optimal transfer of ions to the analyzer.

The field emitters were carbon fiber microneedle coated tungsten wire emitters with dimensions of 10 μm diameter by 4.0 mm length long needles coated with 20 – 35 μm carbon fiber (JEOL) which were inserted into the ion source using a JEOL direct exposure probe. An example wire emitter is shown in Figure 43 below, with micrographs taken by a JEOL JSM-7100F scanning electron microscope. The emitter points produce very high electric field
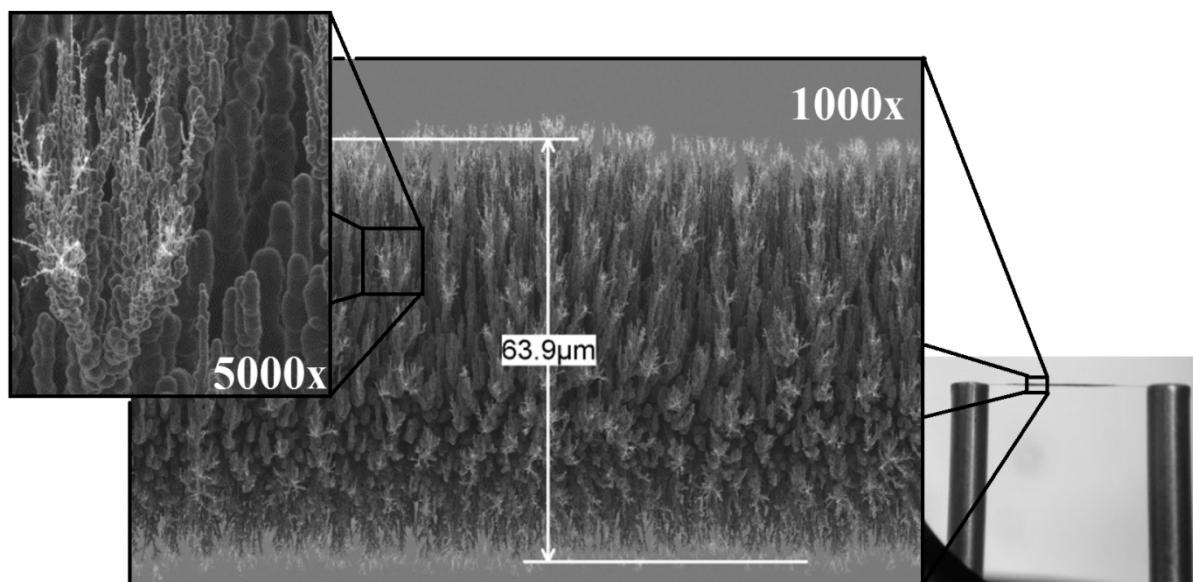
Figure 43. Micrographs and photo provided by JEOL of field ionization emitter

strengths as described in the introduction section.

The instrument was set up to 'flash' the field emitter with current during MS acquisition in order to achieve sufficiently high emitter temperatures to desorb and/or mitigate the adsorption of analytes on the emitter surface. This emitter flash feature has several variable parameters which are clarified by the discrete timing plot shown in Figure 44. Discrete timing involves three variable parameters: the ion accumulation time, the wait time, and the flash time. These were set to 1000 ms, 40 ms, and 35 ms, respectively, as shown in Figure 44.

In this configuration, ions are accumulated by the detector for 960 ms forming a single *scan*. This scan is immediately followed by 40 ms of *wait time* before another scan begins, repeating the cycle throughout data acquisition. During the wait time, the emitter is flashed for a specified *flash time* (e.g., 35 ms) with a corresponding *flash current* through the
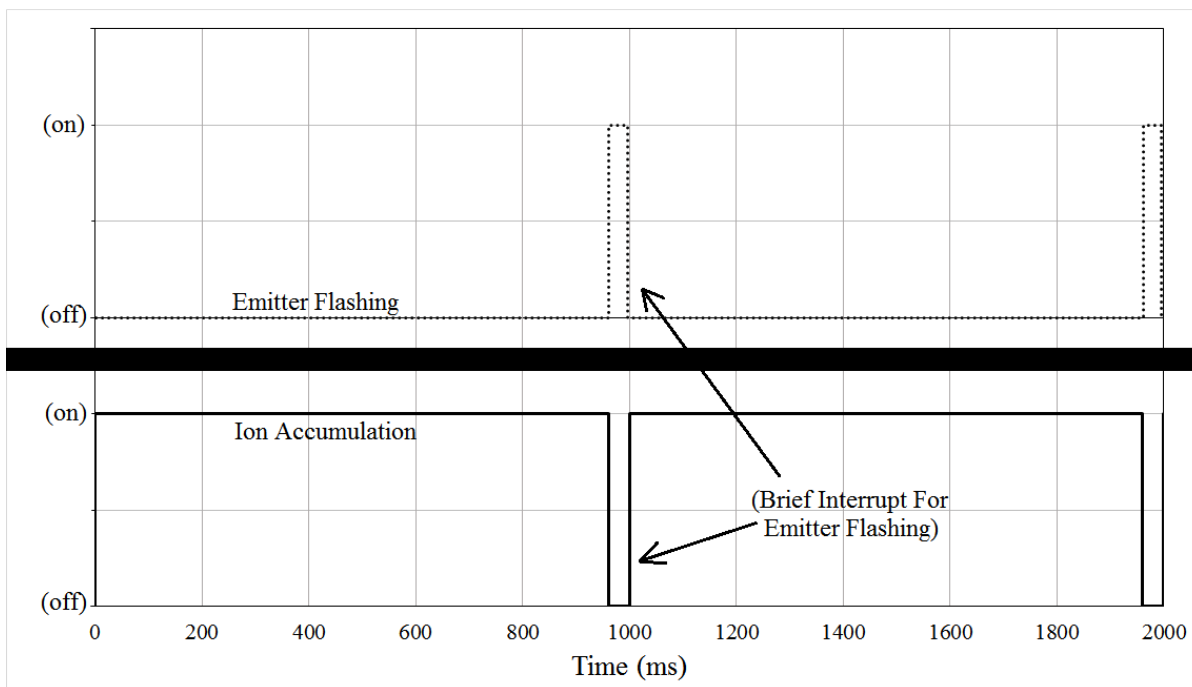
Figure 44. Field ionization spectral accumulation timing

emitter to elevate the emitter's temperature and desorb analytes form the emitter surface so that sensitivity is maintained throughout analysis. Flash current was set near maximum at 42 mA. There is also potential for a *sustained current* through the emitter at all times, but this was not utilized.

A summary of parameters for the operation of the FIMSDIST during analysis of CTL samples is described below in the following tables and text descriptions.

Table 5 described the gas chromatograph operating conditions during FIMSDIST analysis. During the FIMSDIST analysis, the FID was operated at the conditions specified in Table 6. The mass spectrometer operating conditions are briefly described below in Table 7.

Table 5. Parameters and operating conditions for the GC-FID/FIMS

Parameter / Equipment	Type/Value	Supplier/Unit of Measure
Gas Chromatograph	HP 6890	Agilent
Chromatography Column	MXT-1HT (SimDist)	Restek
Column Dimensions	10 × 530 × 0.21	m × µm × µm
Column Temperature Program	-30 | 10 | 380 | 34.0	C | C/min | C | min
Column Pressure Program	21.6 kPa | 1.60 | 87.0 | 34.0	kPa | kPa/min | kPa | min
Column Flow	~9.0	mL·min^{-1}
Column Gas Type	Clean He (> 99.999%)	Praxair
Post-Analytical Transfer Column	0.20 × 250 × 0	m × µm × µm
Inlet	On Column	Agilent
Inlet Temperature Program	Track Oven	-

Table 6. Parameters and operating conditions for the flame ionization detector

Parameter / Equipment	Type/Value	Supplier/Unit of Measure
Detector 1	FID	Agilent
Air Flow Rate	300	mL·min^{-1}
Hydrogen Flow Rate	30	mL·min^{-1}
Makeup Gas Flow Rate	15	mL·min^{-1}
Temperature	385	C
Data Rate	10	Hz
Pre-Detector Transfer Column	0.53 × 250 × 0	m × µm × µm
Analytical Flow (Approx.)	7 mL·min^{-1} (76.7 %)	-

Table 7. Features for the field ionization mass spectrometer (FIMS)

Parameter / Equipment	Type/Value	Supplier/Unit of Measure
Detector 2	FIMS	JEOL
GC/MS Interface Temperature	350	C
Pre-Detector Transfer Column	$0.53 \times 250 \times 0$	m $\times$ µm $\times$ µm
Analytical Flow (Approx.)	2 mL·min^{-1} (23.3 %)	-

A more thorough description of mass spectrometer operating conditions is summarized in Table 8. It should be reiterated that the voltages in the ion source were adjusted and tuned regularly during analysis in order to provide the most intense signal as possible. As such, default values for these are recorded above in the text, but the actual voltages utilized vary substantially and were not reported in the table so as not to confuse the reader.

Table 8. Detailed parameters for the operation of the FIMS

Parameter / Equipment	Type/Value	Supplier/Unit of Measure
Emitter Type; Dimensions	Wire Type; 4×10	JEOL; mm $\times$ µm
Length of Emitter Needles	20 – 35	µm
Emitter Voltage	10,000	V
Ion Accumulation Time	1000	ms
Acquisition Wait Time	40	ms
Emitter Flash Time	35	ms
Emitter Flash Current	42	mA
Ion Source Temperature	150	C
Ion Detector Voltage	2,500	V
Pusher / Puller Voltage	778 / -778	V
Flight Tube Voltage	-7000	V
Accumulated Mass Range	3 – 990	*m/z*
Pusher/Puller Frequency	1	ns
Mass Analyzer Pressure (Typical)	2×10^{-5}	Pa
Ion Source Pressure	1.5×10^{-4}	Pa
Calibrant Reservoir Temperature	125	C

CTL samples were injected by an autosampler equipped with a 5.0 µL syringe set to a slow needle speed, consistent with on-column injection. Internal standard (2-bromobutane) was

added to all standards/samples at 3 µL per 1003 µL (total) in order to monitor the FIMSDIST's behavior and provide a reference compound for data processing.

In preparation for using the FIMSDIST system, the calibrant reservoir was deeply evacuated. First, the system was inspected to ensure that the reservoir flow control valve was shut, ion source voltages were off, and isolation valve was closed. Then the reservoir selector valve was set to administer calibrant, and the reservoir flow control valve was slowly opened 7 turns to expose the reservoir to high vacuum, to which it was exposed for at least 10 min. After evacuation, the reservoir flow selector valve was either shut or set to administer to the ion source as required, and the reservoir flow control valve was either closed or set to a minimal level as appropriate.

When a new emitter was attached to the FIMS ion source, the emitter was first equilibrated and exposed to ion source vacuum pressure for 10 min while applying a sustained current of 30 mA to heat the emitter wire and assist in the desorption. Then the sustained current was removed. Afterwards, the field emitter was tuned in order to produce maximum ion current at good resolution as follows.

The calibrant reservoir (being previously deeply evacuated) was injected with 1 µL of n-heptane calibrant. n-Heptane was introduced into the ion source at ¾ of a full turn of the reservoir flow control valve to provide a strong molecular ion peak. The instrument autotuned the ion source voltages away from the factory default specifications to voltages that maximized the resolution and intensity of the acetone ion, with a resolution of not less than 3000, but typically on the order of 3500 using full width at half height.

After tuning, the field strength of the emitter was measured according to the method

developed by Speier et al.[138] For the sake of the subject matter, Speier's equation has been

reproduced here to compute the field strength (F) in units of 1.0×10^8 V/cm according the ratio of

ions I_{29} and I_{100} for pure n-heptane.[138] Speier's equation has been rearranged to solve for F as a

function of I_{29}/I_{100}, with the experimental domain (i.e., for the ratio I_{29}/I_{100}) being 0.006 to 0.92,

and having a mathematical limit of 0.0001, below which results in a negative correlated field

strength.

$$\frac{I_{29}}{I_{100}} = 1.6 \times 10^{-4} \times 10^{9.4 \times F} \qquad \therefore \qquad F$$

$$= \frac{\log\left(\frac{I_{29}}{I_{100}} \div 1.6\right) + 4}{9.4}$$

(10)

where I_x is the measured ion intensity at $m/z = x$ and F is the field strength in 10^8 V/cm

Quadruplicate field strength measurements were taken according to the FIMS instrument

operating parameters described in the tables above, with slight modifications as defined in Table

9. These modifications were made for no reason other than because field strength measurements

were originally performed at the conditions described by Table 9, whereas later on the conditions

in Table 8 were shown to be most favorable for FIMSDIST. In any case, field strength

measurements were taken while injecting n-heptane calibrant to the ion source from the calibrant

reservoir as described previously.

It was necessary to retune ion source parameters frequently during analyses. This was

discovered during preliminary analyses, in which the average intensity of ions in STDx56 would

drop steadily by more than an order of magnitude over the course of 1-2 days. As a result, ion

source parameter retuning was frequently performed during the middle of analyses. This is not characteristic of most modes of ionization (e.g., EIMS), however it was necessary in the FIMS analysis studied herein.

Table 9. Operating parameters for determining field strengths

Parameter / Equipment	Type/Value	Supplier/Unit of Measure
Ion Accumulation Time	600	ms
Acquisition Wait Time	60	ms
Emitter Flash Time	3	ms
Emitter Flash Current	40	mA
Sample Data Collection Time	1	min

This phenomenon is hypothesized by the author of the present work to be a result of (1) changing field strengths of the field emitter, creating different ion trajectories or (2) unexplained spatial shifting of the emitter's position in reference to the extraction rods during analyses. This observation was not documented in the reviewed literature, so it is yet unknown whether this retuning is a necessity for all FIMS instruments or only certain types, such as the one employed.

The sequence for analyzing samples consisted of analyzing all desired samples with blanks and standards in tandem as frequently as practical. Typically, an analytical sequence involved a repeated series of (1) a blank, (2) a 100 % concentrated STDx56 standard, (3) up to five samples, and (4) another blank. Afterwards, the ionization parameters were retuned using n-heptane as described in this section (see above). In between these repeated series, standardization series were performed utilizing STDx56 at 100 %, 80 %, 60 %, 40 % and 20 % concentrations. In addition, other standards were also injected regularly, such as the HWD standards. Standards used for FIMSDIST are described in Section V.A.7.

Samples were injected at 1.0 µL volume in order to provide sufficient quantity of sample for the FIMS unit, which has a notoriously lower sensitivity than EIMS units due to a 2x order of magnitude lower ionization efficiency. For standards however, the large presence of solvent was a concernas it might lead to arcing in the ion source. As such, only 0.5 µL volume of standards were injected.

Response factors were determined using a six-point calibration curve for each of the components in the STDx56 standard, and these were monitored throughout the run. Due to changing field strengths, relative response factors were determined, with respect to the internal standard (2-bromobutane). Data reduction is described in Section VI.A.

V.B.4.iii. Compositional Analysis of Gaseous Products by Gas Chromatography

Gas phase analysis was performed using a model 8610C gas chromatograph (GC) equipped with a standard Thermal Calorimetry Detector, TCD, (#8690-0007) and an FID (#8690-0010) utilizing an in-jet methanizer (#8690-0082) from SRI Instruments (Torrance, CA USA), The GC was capable of determining levels of hydrogen, carbon monoxide, carbon dioxide, and light hydrocarbons in the range of C1-C7.

The TCD was connected in series with the FID. The TCD was maintained at 105 C and the FID/methanizer were maintained at 375 C. H_2 and air were supplied to the methanizer at 21 and 217 mL·min^{-1} respectively. High purity Ar and H_2 (99.999%) gases were obtained from PraxAir, whereas air was supplied via an internal air compressor. The methanizer was supplemented with a nickel catalyst on silica/alumina (65% by wt.) from Aldrich Chemical (batch no. MKBD8654).

Injections were performed manually using a gas-tight syringe; injecting approximately

100 µL of sample to a simple gas inlet port on the instrument. Separations were performed using a 2.4 m HayaSep D packed column with Ar as a carrier gas. The column oven was initially held at 40 C for 3 min, and then the temperature was ramped at 20 C/min until reaching 280 C, where it was held for an additional 10 min. Carrier gas flow was maintained with constant pressure control at 183 kPa, having a flow rate of 12mL/min at initial GC program conditions. A summary of parameters and operating conditions for the instrument is shown in Table 10.

Table 10. Parameters and operating conditions for the GC-FID/TCD

Parameter / Equipment	Type/Value	Supplier/Unit of Measure
GC	8610C	SRI Instruments
Data Rate	5	Hz
Stationary Phase	HayaSep D	SRI Instruments
Column Dimensions	2.4 x 1.9mm	m x mm
Temperature Program	40 | 20 | 280 | 10	C | C/min | C | min
Carrier Gas	Argon (99.999%)	mL/min
Carrier Flow	12	mL/min
H_2	21	mL/min
Air	217	mL/min
Detector 1	FID+methanizer	SRI Instruments
FID Temperature	375	C
Detector 2	TCD	SRI Instruments
TCD Temperature	125	C

Response factors for each compound were determined using manually prepared calibration gas standards consisting of either pure H_2 or a mixture of CO, CO_2, and C_3H_8 diluted in Ar. Hydrogen was detected via TCD, whereas carbonaceous species were detected using the FID/methanizer. Response factors for all carbonaceous species (excluding CO and CO_2) were based on C_3H_8.

Six-point detector calibration was performed via manual injection of calibration standards

at various injection volumes with a 1 mL gas tight syringe. Calibration standards were prepared

volumetrically within 1 liter SKC gas sample bags via a 50 mL gas-tight syringe. Single-point

methanizer calibration was performed daily using a prepared standard of CO, CO_2, and C_3H_8

diluted in Ar. C_3H_8 gas was obtained from Worthington Cylinders and its purity was determined

to be 97.25% by mole, based on GC-FID. All other gases were obtained from PraxAir. The

purity of commercial CO and CO_2 was verified by the above-described GC-FID/TCD system by

FID chromatogram purify.

V.B.4.iv. Analysis for Oxygenation by FTIR

FTIR analysis was conducted on a Thermo Scientific® Nicolet IR200 equipped with a

multi-bounce horizontal attenuated total reflectance (HATR) trough having a ZnSe crystal at

45° angle of incidence (part no. 0072-603) . The source utilized was an IR source from

Thermo Scientific and the detector was a DTGS KBr detector.

Various standards described in Section V.A.5 were utilized to determine the spectral

absorbance pattern, molar absorptivity coefficient, and linear range (i.e., where the Beer-

Lambert law applies) of the FTIR spectrometer. Samples were loaded onto the ZnSe trough,

and the FTIR absorbance spectrum was acquired over a wavenumber range of 400 cm^{-1} to 4000

cm^{-1} with a resolution of 2, for data points being acquired at least every 1 cm^{-1}.

Samples were analyzed in tandem to standards each day of FTIR use. Linear

calibrations were developed for TAG ester bonds, carboxylic acids, and olefins using the linear

calibration standards described under reagents. Calibration spectra and linear plots are

included in Appendix E. For analysis of TAG ester bonds and carboxylic acids (i.e., carbonyl

groups), the FTIR instrument was blanked with a clean ZnSe trough. For analysis of olefins,

the FTIR was blanked with n-dodecane. Due to overlapping absorbance of carbonyl groups and olefin absorbance near wavenumber 910 – 930 cm^{-1}, quantification of olefins was limited to samples that were thoroughly deoxygenated.

The wavenumber for quantifying TAG (ester) bonds in samples was 1750 cm^{-1}, and the molar absorptivity coefficient was determined to be 0.98 A_{1750} / (mol·L^{-1}). The wavenumber for quantifying carboxylic acid bonds in samples was 1710 cm^{-1}, and the molar absorptivity coefficient was determined to be 1.35 A_{1710} / (mol·L^{-1}). The wavenumber for quantifying olefins in samples was 908 cm^{-1}, and the molar absorptivity coefficient was determined to be 0.21 A_{908} / (mol·L^{-1}).

V.B.4.v. Analysis of Nickel Content in Catalysts by UV-VIS Spectrophotometer

Accurate catalyst compositions (as nickel wt. %, dry basis) were determined in quadruplicate using a nitric acid digestion and UV-Vis spectrophotometric method in accordance with standardized methods[153]. Solutions of nickel nitrate for UV-Vis analyses were prepared from stock chemicals. Digestions were carried out in vented, closed-cap vials at 60 C for 24 h in a sonic bath. 35 wt. % nitric acid was used for the digestion at a ratio of 0.25 g catalyst to 2.0 mL of nitric acid solution. After reaction, digestion vials were centrifuged to pellet any undissolved material. Supernatant was transferred to 1 cm disposable cuvettes and the absorbance of nickel (II) nitrate was measured at a wavelength of 720 nm in a double beam Cary 50 UV-Vis Spectrophotometer from Agilent Technologies (Santa Clara, CA 95051, USA). Catalyst blanks were also tested using plain activated carbon, and found to have absorbance within 0.0010 of deionized water, simplifying subsequent testing. The molar absorptivity coefficient was measured to be 2.150 M^{-1}·cm^{-1} and the Beer-Lambert law was valid to 1.0 N or

greater of nickel nitrate.

V.C. Experimental Methods

This section describes the series of experiments that were performed under each topic (e.g., catalytic deoxygenation, cracking reactor design, cracking, fuel refinement) in order to assist in the dissertation's hypothesis testing.

V.C.1. Catalytic Deoxygenation Experiments

V.C.1.i. Preliminary Deoxygenation Testing

CTD were prepared from the cracking of soybean TAG into cracked CT which is then fractionation into CTG, CTD, and CTR as described by Section V.A.2. The CTD distillates were deoxygenated in the dually-purposed batch reactor described in Section V.B.3.i, according to the operating conditions described in Table 11.

Table 11. Operating parameters for preliminary deoxygenation testing in batch reactors

Deoxygenation System	-	Dual-Purpose Batch Reactor	Dual-Purpose Batch Reactor
Feedstock	-	CTD	CTD
Temperature	(C)	325	325
Pressure	(MPa)	1.8	1.8
Time	(h)	4	4
Catalyst	(ratio, type)	1:50, Pd/C 5 powder	1:50, Ni/SiO2 64 powder
Reaction Cycles	-	4	4

The deoxygenation reaction was performed in four reaction cycles. After the first reaction was completed and cooled to below 30 C, the gaseous products were vented from the reaction chamber, but the liquid and catalyst were not disturbed. The reactor was then thoroughly purged with hydrogen gas, pressurized with hydrogen gas, and heated to operating

temperate once again for an additional reaction cycle. This was repeated a total of 4 times as indicated in Table 11. This cyclic operating procedure was conceived by Khambete who recommended multi-step decarboxylation for batch processing in his thesis by stating, "It may be concluded that a multi-step process will required to be able to reduce the acid number […] to meet ASTM [fuel] specifications."[68]

Yield of deoxygenated CTD was determined gravimetrically. Deoxygenated distillates were collected and centrifuged to remove suspended catalyst in a simple swing-bucket centrifuge at approximately 1000 gravity. The extent of deoxygenation was determined by ASTM method D974 for total acidity by colorimetric titration[154] and FTIR (see Section V.B.4.iv). Additionally, samples were analyzed by FTIR to estimate the content of olefins in the final products.

V.C.1.ii. Preparation of Granular Catalysts

Six batches of Ni/C catalyst were prepared via the method of incipient wet impregnation. Solutions of nickel (II) nitrate were prepared in deionized water and added to volumes of activated carbon that had been previously dried for more than 10 h at 120 C. Then the catalyst was thoroughly mixed in a glass cup which was sealed within a vented stainless steel canister. Using a muffle-furnace with temperature ramp rates of 10 C·min^{-1}, the catalyst was subjected to a two-step calcining procedure, first held at 120 C for 2 h to remove moisture and then at 550 C for 10 h to convert precipitated $Ni(NO_3)_2$ to NiO. The catalyst was then safely cooled to room temperature and stored in desiccated jars.

The properties of the candidate catalysts were experimentally evaluated and are recorded in Table 42 (see Section VII.A.2.ii), with comparable information from commercial catalysts is tabulated where applicable. The performance of all catalysts was determined based on results

from experiments conducted in batch reactors under identical conditions in order to determine

trends and to determine which catalyst(s) would be suitable for testing in continuous reactors.

The catalysts are listed in Table 12, along with information regarding their compositions.

Table 12. Deoxygenation catalysts screened in batch reactors

Label	Active Metal	Metal Content	Support
-	-	wt. %	-
Ni/C 2.3	Ni	2.3	C
Ni/C 4.6	Ni	4.6	C
Ni/C 9.6	Ni	9.6	C
Ni/C 15.3	Ni	15.3	C
Ni/C 20.3	Ni	20.3	C
Ni/C 31.7	Ni	34.1	C
Pd/C 5	Pd	5	C
Ni/SiO2 55	Ni	55	SiO_2
Ni/SiAlZrOx 60	Ni	60	$SiO_2/Al_2O_3/ZrO_2$

V.C.1.iii. Characterization of Catalysts

Accurate catalyst compositions (as reduced nickel wt. %, dry basis) were determined in

quadruplicate using a nitric acid digestion and UV-Vis spectrophotometric method in accordance

with the standardized method[153] described in Section V.B.4.v.

Approximate surface areas of the catalysts were determined by adapting the standardized

method for iodine number of activated carbon ASTM D4607-94.[148] This method is intended for

determining the surface area of activated carbon, not carbon supported catalyst. As a result, test

results are considered to be qualitative and/or suggestive for the true surface area. The iodine

number test was suitable because it is easy to adapt to most laboratories, whereas the true BET

surface area test is a very involved and specialized test.

The presence of nickel oxide on the catalyst was expected to reduce the surface area of the catalyst by occupying pore volume that would otherwise be available for iodine absorption. Originally, the iodine number test was applied to the Ni/C catalyst using the standard method (i.e., without any alterations), however, it was unexpectedly observed that all batches of Ni/C appeared to have the same surface area. This didn't seem plausible, due to the loss of internal porosity by impregnated nickel. Further investigation concluded that the hydrochloric acid wash step in the standardized method was responsible for dissolving the majority of the nickel from the catalyst before measurement of the surface area, thereby reverting the surface area to that of blank activated carbon.

To compensate for this problem, the standardized iodine number test method was modified by simply eliminating the hydrochloric acid wash step so that the method would be useful for estimating the surface area of the Ni/C catalyst. In order to account for the systematic error caused by the procedural change, all surface area measurements were adjusted according to the test results from a blank activated carbon sample, on which the standard test and modified test were both applied. These procedural adjustments created systematic error on the order of only a few percent, based on blank measurements.

Dry bulk densities were estimated in triplicate using a 25.0 mL graduated cylinder and analytical balance.

The quantity of catalyst that was broken apart into fine particles (< 60 mesh) during the catalyst manufacturing process was determined in bulk using a column of standardized sieve trays and a vibrating table with an exposure time of 5 min.

V.C.1.iv. Batch Reactions to Screen Catalyst Activity and Specificity

In order to ensure that reactivity comparisons between commercial catalysts and the Ni/C catalysts weren't invalidated by particle size induced mass transfer error, the commercial catalysts were milled into the target particle size range of the Ni/C catalyst (i.e., 20 - 50 standardized mesh). This milling was accomplished by gently crushing the catalyst using a mortar and pestle followed by the use of sieve trays. All catalysts were subjected to the same sieve procedure so that their particle sizes were that of 20 – 50 standardized mesh (0.30 – 0.84 mm). All catalyst samples were maintained in a vacuum oven above 140 C and under 1 kPa pressure for at least 12 h prior to weighing and use.

Catalyst screening experiments were carried out in the bench-top deoxygenation reactor shown in Figure 35. Catalysts were loaded to the reactor and a 10.1 wt. % solution of octanoic acid in mineral oil was loaded into the reactant bomb and used as a reactant. All catalysts were tested in duplicate according to the procedure described in Section V.B.2.i. Experiments were carried out using the operating parameters provided in Table 13.

Table 13. Operating parameters for deoxygenation catalyst screening in batch reactors

Reaction Temperature	325	C
Reaction Pressure	2.9	MPa
Reaction Time	31	min
Impeller speed	400	RPM
Catalyst Mass	4.500	g
Reactant Mass	155 ± 5	g
Gas Reactant	H_2	-
Reduction Temperature	325	C
Reduction Time	6	h
Reduction Gas	H_2	-
Reduction Gas Flow	$200 + 50$	mL/min

Liquid reaction samples and gaseous product samples were collected during and after the reaction as described by the procedure in Section V.B.2.i. Gas samples were analyzed by GC according to Section V.B.4.iii in order to determine their composition. Liquid reaction products samples were analyzed by FTIR according to Section V.B.4.iv in order to determine the concentration of carboxylic acid groups in solution.

V.C.1.v. Deoxygenation in Continuous Packed Bed Reactors (PBRs)

Catalysts were evaluated for their ability to deoxygenate in continuous reactors using the PBR for deoxygenation described in Section V.B.2.ii. Either of two catalyst bed sizes were utilized, having approximately 0.1 kg and 1.0 kg beds, respectively. One bed was in use with the other in storage at any given time.

The catalyst used for these deoxygenation experiments in Table 14 was commercially procured Ni/SiO2 55. For this series of experiments, the catalyst was <u>not</u> milled to the size range of 0.30 – 0.84 mm, but instead it was utilized as intact cylindrical tablets (as received from the vendor), with dimensions of 6 mm diameter $\times$ 5 mm height.

A list of experiments is described in Table 14 including the bed mass, temperature, pressure, CTD feed rate (i.e., reactant rate), water feed rate, and H_2 feed rate.

Table 14. Deoxygenation experiments in packed bed reactors

Label	Bed Mass	Feed	Temperature	Pressure	Reactant Rate	H_2O Rate	H_2 Rate
-	(kg)	-	(C)	(MPa)	(g/min)	(g/min)	(mL/min)
Deoxy-19	0.1	Model	300	1.5	1	0	100
Deoxy-20	0.1	CTD	320	2.9	1	0	100
Deoxy-21	0.1	CTD	350	2.9	1	0	500
Deoxy-22	0.1	CTD	250	2.9	1	0	500
Deoxy-23	0.98	CTD	300	2.2	1	0.05	50
Deoxy-24	0.98	CTD	300	2.2	1	0.05	0
Deoxy-25	0.98	CTD	300	2.2	1	0.03	0
Deoxy-26	0.98	CTD*	300	2.2	1	.03	100

The reactant feedstock utilized for experiment 'Deoxy-19' was a model compound

feedstock of 20.9 wt. % octanoic in cyclohexane (see Section V.A.2). The other experiments in

Table 14 utilized a CTD feedstock prepared from soybean TAG cracking followed by CTL

fractionation according to the description in Section V.A.2. Liquid product samples were

collected from the reactor and analyzed by FTIR according to the procedure described in Section

V.B.4.iv to determine the carboxylic acid content. The catalyst bed was examined before and

after experiments in order to determine potential causes of failure to operate the reactor, when

appropriate.

Additionally, a sample of Deoxy-25 was recycled twice through the reactor in order to

observe a reactor effluent product that was virtually free of carboxylic acids. A recycle was

performed by cumulatively collecting over 1.5 liters of PBR effluent, and then using it as

feedstock for the PBR in another cycle.

The effluent was tested by standardized titrations (ASTM 974) in order to assess the

acidity of the reactor effluent. Acidity was compared with Jet-A-1 specifications as described by

ASTM international.[27] Olefin content of the reactor effluent was determined by FTIR as

described in Section V.B.4.iv.

V.C.2. Cracking Reactor Design

Cracking reactor design experiments were characterized by efforts to identify the reasons

for coke formation and to conceive, develop, improve, and characterize a reactor to

noncatalytically crack TAG into CT continuously without producing significant quantities of

coke. A short series of experiments were performed on the bench-scale cracking continuous-

stirred-tank-reactor (CSTR) which was characterized by severe coke formation. This motivated

the use of batch cracking reactors to determine the reasons for coke formation during TAG cracking. The results of those experiments elucidated the design of a prototype tubular cracking reactor (TCR) which was tested and found to be able to operate without coke formation. Steps were then taken to improve the TCR into a more robust lab-scale version, which was used to determine a suitable operating range which would not exhibit coke formation. Then a bench-scale TCR was developed based on the lab-scale TCR and tested in order to investigate and/or prove scalability of the TCR design.

V.C.2.i. Bench-Scale Cracking CSTR Experiments

A select number of experiments were performed with the bench-scale continuous stirred-tank cracking reactor (CSTR) that is depicted in Figure 33. The system was designed and operated during a master's thesis presented to UND by Sander.[62] An operating procedure and schematic of the bench-scale CSTR is included in Section V.B.1.v. A more detailed operating description can be obtained from Sander.

In attempting to utilize the CSTR to optimize the NCP, it was ultimately observed that coke formation was a significant problem. More specifically, reactor operation was limited to approximately 16 hours before coke formation became so significant that it had the potential to cause reactor problems, such as oscillating temperatures. If the reactor continued to operate, coke formation eventually built up to hazardous levels, sometimes leading to hazardous reactor plugging, which was a series concern due to the potential for catastrophic bursting of the reactor as a result of a pressure spike.

Samples were collected from the reactor, however, none of the samples were analytically pursued to determine their composition due to substantial coke formation making the samples

213

less desirable in light of the present work. Nevertheless, it should be mentioned that some CSTR samples were collected and analyzed to determine their detailed chemical composition by Sander in his master's thesis.[62] This series of experiments is described in Section V.C.3.i.

All bench-scale cracking CSTR experiments pertaining to this dissertation were performed using canola TAG as a feedstock. Operating factors that were studied for coke formation CSTR are included in Table 15.

Table 15. Factors and operating conditions studied using the CSTR cracking reactor

Temperature (C)	Pressure (MPa)	Space Time (h)
400	1.5	1.0
420	3.0	1.4
		2.4

Due to the difficulty in operating and handling the coke formation, less information could be deduced time effectively compared to the other reactor configurations utilized. As a result, only a limited number of experiments were conducted using this equipment, and coke experimentation was quickly switched to the utilization of batch cracking reactors.

A select number of modifications were also made to the CSTR in attempt to alleviate coke formation. These are described in Section V.B.1.vi and shown by Figure 34. Each modification reflected a single experiment to determine the effect of that operating condition on coke formation. For experiments to test these CSTR modifications, the operating conditions were consistently kept at 400 C temperature, 1.0 h space time, and 3.0 MPa pressure, which was

assumed to be the least severe cracking conditions.

V.C.2.ii. Batch Cracking Reactor Experiments

In order to improve the understanding of coke formation mechanisms at a more

reasonable turnaround rate, the batch cracking reactor (see Figure 27) was utilized to crack

soybean TAG under a variety of conditions. A list of conditions studied is described in Table 16.

The operating procedure and description of the batch cracking reactor is described in Section

V.C.2.ii.

Table 16. Factors and operating conditions studied using the batch cracking reactor

Temperature (C)	Pressure (MPa)	Oil Volume (mL)	Time (h)
430	0.1	100	0.5
445	1.5	200	1.0
		300	1.5
			2.0
			3.0

Two temperatures were studied to determine the influence of temperature on coke

formation. The effect of pressure on coke formation was studied in two ways: (1) by varying the

reactor head pressure at reaction start and (2) by varying the oil volume loaded to the 500 mL

reactor volume, as indicated (Table 16). Two different reaction times were studied at all

temperatures. At lower temperatures however, additional reaction times were added to observe

any onset of coke formation. In all cases, the stirring impeller was rotated at 400 rpm to improve

heat transfer and fluid mixing.

A complete list of experiments is described in Table 17 . To clarify, the sample labeled

'Coke-1' was performed to replicate some of Luo's work[54], in which the pressure was initially 0.1 MPa of N_2. However, during cracking the pressure rose to 2.9 MPa and then phase separation began.

Table 17. Batch TAG cracking experiments for coke formation investigation

Label	TAG Type	TAG Vol.	Temperature	Reaction Time	Head Pressure/Type	Phase Separation?
-	-	(mL)	(C)	(h)	(MPa) / Gas	Yes/no
Coke-1	Soy	200	430	0.3	0.1 to 2.9*	YES
Coke-2	Soy	100	430	1.5	1.5 / N2	NO
Coke-3	Soy	100	430	2.0	1.5 / N2	NO
Coke-4	Soy	100	430	3.0	1.5 / N2	NO
Coke-5	Soy	100	430	3.0	1.5 / N2	NO
Coke-6	Soy	200	430	0.5	1.5 / N2	YES
Coke-7	Soy	200	430	0.5	1.5 / N2	YES
Coke-8	Soy	200	445	1.0	1.5 / N2	NO
Coke-9	Soy	200	445	1.0	1.5 / N2	NO
Coke-10	Soy	200	430	1.0	1.5 / N2	NO
Coke-11	Soy	200	430	1.0	1.5 / N2	NO
Coke-12	Soy	100	445	1.0	1.5 / N2	NO
Coke-13	Soy	200	445	0.5	1.5 / N2	NO
Coke-14	Soy	200	445	0.5	1.5 / N2	NO
Coke-15	Soy	200	445	0.5	1.5 / N2	NO
Coke-16	Soy	100	445	0.5	1.5 / N2	NO
Coke-17	Soy	300	430	0.5	1.5 / N2	NO
Coke-18	Soy	200	430	0.5	1.5 / N2	NO
Coke-19	Soy	100	430	0.5	0.1 / N2	NO
Coke-20	Soy	200	430	0.5	0.1 / N2	NO
Coke-21	Soy	300	430	0.5	0.1 / N2	NO
Coke-22	Soy	100	430	0.5	0.1 / N2	NO
Coke-23	Soy	300	430	0.5	0.1 / N2	NO
Coke-24	Soy	300	430	0.5	0.1 / N2	NO
Coke-25	Soy	300	430	0.5	0.1 / N2	NO

After each experiment, gas samples were collected in a large gas bag (~25 liters) and analyzed by GC as described in Section V.B.4.iii. The reactor was examined for any signs of coke on the reactor walls and/or in the bulk fluid, and coke formation was classified as (1) none, (2) flocculating, (3) mature, or (4) severe. The experimental results from these batch cracking

experiments were used to develop a tubular cracking reactor (TCR) that was capable of operating in the absence of coke formation.

V.C.2.iii. Prototype Tubular Cracking Reactor Experiments

Based on the observations from TAG cracking with the CSTR, it was concluded that a new continuous reactor design was necessary. Based on observations from the batch cracking reactors described above, it was hypothesized that a long/narrow tubular cracking reactor (TCR) may be able to function with reduced coke formation. As a consequence, a lab-scale prototype TCR was constructed as shown in Figure 28. Its operation is described in Figure 29.

Five experiments were performed using the prototype TCR, with the operating parameters shown sequentially in Table 18. Soybean TAG was used as a feedstock for all operating conditions. All of these experiments had the same pressure and feed rate as indicated. Only the temperature was varied from 400 to 440 C.

Table 18. Factors and operating conditions studied using the prototype TCR

Temperature (C)	Pressure (Mpa)	Feed Rate (g/min)	Time (h)
400	3.6	5	3
410	3.6	5	3
420	3.6	5	3
430	3.6	5	3
440	3.6	5	3

Although continuous samples from the reactor were collected and observed, they were not used as experimental outputs. The experimental output was the qualitative observation of whether or not the reactor would coke at various operating conditions.   After the successful testing of the prototype TCR, it was rapidly decommissioned and a replacement reactor known

as the lab-scale TCR was constructed. The operation of the lab-scale TCR is described in the

next section so as not to be redundant. Together, these were used to enable the design and

construction of a bench-scale tubular cracking reactor (TCR) described as follows.

V.C.2.iv. Lab-Scale Tubular Cracking Reactor Experiments

As described in Section V.B.1.iii (see Figure 30), three different configurations of the

lab-scale TCR were used for cracking TAG: a 100 mL reactor, a 500 mL reactor, and a 200 mL

reactor. Whereas the 200 mL version of the TCR was primarily used to investigate the effect of

operating pressure on TAG cracking, the 100 mL and 500 mL versions of the TCR utilized under

a variety of operating conditions in order to elucidate the range of reactor operability without

coke formation and to determine the onset of coke formation. These operating conditions are

described in Table 19. In each case, soybean TAG was utilized as the feedstock. The reactor

Table 19. Lab-scale tubular cracking reactor experiments
for the exploration and investigation of coke formation conditions

Label	Temperature	Pressure	Reactor Volume	Space Time
-	(C)	(MPa)	(mL)	(h)
A-Soy	420	2.9	100	0.27
B-Soy	430	2.9	100	0.27
C-Soy	440	2.9	100	0.27
X1	450	2.9	100	0.27
X2	460	2.9	100	0.27
X3	470	2.9	100	0.27
X4	420	1.5	100	0.27
X5	430	1.5	100	0.27
X6	440	1.5	100	0.27
X7	450	1.5	100	0.27
X8	470	1.5	100	0.27
D-Soy	420	2.9	100	0.69
E-Soy	430	2.9	100	0.70
F-Soy	440	2.9	100	0.69
G-Soy	420	2.9	100	1.22
H-Soy	430	2.9	100	1.17
I-Soy	440	2.9	100	1.11
X9	450	2.9	100	1.16
X10	435	2.9	500	1.28

V.C.2.v. Bench-Scale Tubular Cracking Reactor Experiments

A bench-scale TCR was constructed as shown in Figure 31, and its operation is described in Section V.B.1.iv. Previous experiments with the prototype TCR and lab-scale TCR (described in the following section) had indicated that the bench-scale TCR would be capable of operating in the absence of coke formation under appropriate operating conditions.

In order to test this hypothesis, conditions were selected for operation of the bench-scale TCR as indicated in Table 20. As shown, both soybean TAG and yellow grease were used as feedstocks for the TCR in order to determine if there was a negative effect of using yellow grease. The preheaters were operated at the temperatures indicated to bring the oil up towards reaction temperature.

Table 20. Conditions for testing the bench-scale tubular cracking reactor

TAG Type	Space Time	Cracking Pressure	Cracking Temperature	Preheater 1	Preheater 2
-	(h)	(MPa)	(C)	(C)	(C)
Soy	0.69	1.9	420	340	410

Reactor operation was carried out for approximately 100 hours of operation in order to see if coke formation would result. Pressure transducers PT 1 and PT 2 were carefully monitored during experimentation in order to observe any coke formation. The bench-scale TCR was primarily used for validation of lab-scale TCR performance data at the larger scale and for the production of feedstock for side experiments not described herein.

When continuous reactors of this complexity are utilized, they are not described by a

residence time, but rather by a space time. The determination of the true residence time in a

continuous cracking reactor is difficult because of the complex vapor-liquid equilibrium

behavior under the extreme conditions in conjunction with the ongoing complex reaction. In

fact, most would describe residence time determination as futile. Instead, the space time is

utilized in place of residence time, computed based on a flow rate of feedstock at standard

conditions.

The space time (τ) is simply computed as the product of the reactor volume (V) and fluid

density (ρ) divided by the mass flow rate ($\dot{m}$), as shown in Equation 12.

$$\tau \;=\; \frac{V_{reactor} \cdot \rho}{\dot{m}} \tag{11}$$

The results of the bench-scale TCR operation are presented in Section VII.B.4.v.

V.C.3. Experiments to Determine the Effect of Various Parameters of Reactor Products

Multiple cracking reactors were operated under a variety of conditions to determine the

yields of cracking with various feedstocks. These experiments are described in the following

two subsections.

V.C.3.i. Detailed Products from TAG Cracking in Continuous Stirred Tank Reactors (CSTRs)

Soybean TAG was processed in the TAG cracking CSTR by Sander during his master's

thesis work under the University of North Dakota (UND).[62] Experiments were performed in a

full factorial design of experiments according to the methods of Lawson and Erjavec.[155] The

cracking CSTR is described in Section V.B.1.v with an associated operating procedure. These

experiments were performed by Sander,[62] and included herein for the utilization of the detailed

composition data.

Samples of CTL were collected at what was assumed to be steady state according to Sander's methodology and their composition was determined by detailed compositional analysis method of Stavova[152] described in Section V.B.4.i. Samples of CTG were collected in gas bags and analyzed by GC as described in Section V.B.4.iii.

Table 21. Operating parameters for TAG cracking experiments in the bench-scale cracking CSTR to determine the detailed product composition

Sample Designation	-	A	B	C	D	E	F	G	H
Feedstock	-	Soybean TAG							
Temperature	(C)	400	420	400	420	400	420	400	420
Pressure	(MPa)	2.9	2.9	2.9	2.9	1.5	1.5	1.5	1.5
Space Time	(h)	2.4	2.4	1.4	1.4	2.4	2.4	1.4	1.4

V.C.3.ii. Detailed Products from TAG Cracking in Batch Reactors

Several TAGs were cracked in the batch reactor depicted in Figure 27 with operating instructions described in Section V.B.1.i. In this section, the reactor was operated under identical operating parameters (e.g., temperature, time, head pressure) except for varying the type of TAG feedstock for cracking.

Samples of CTL were prepared and collected according to the batch reactor operating procedure previously described in SectionV.B.1.i. The composition of reaction products were determined by Stavova's detailed compositional analysis method using GC-FID/MS described in Section V.B.4.i.[152] The data from these experiments are included due to the utility of their detailed CTL composition. A list of operating conditions is described in Table 22.

Table 22. Batch TAG cracking experiments to determine the detailed product composition

Label	TAG Type	TAG Vol. (mL)	Temperature (C)	Reaction Time (h)	Pressure/Type (MPa) / Gas
-	-				
Batch-1a	Soybean	300	435	0.5	0.1 / N2
Batch-1b	Soybean	300	435	0.5	0.1 / N2
Batch-1c	Soybean	300	435	0.5	0.1 / N2
Batch-2	HONO	300	435	0.5	0.1 / N2
Batch-3	VHONO	300	435	0.5	0.1 / N2
Batch-4	HENO	300	435	0.5	0.1 / N2
Batch-5	Cottonseed	300	435	0.5	0.1 / N2
Batch-6	Linseed	300	435	0.5	0.1 / N2

V.C.3.iii. Effect of Various Parameters on the Distribution of Cracked Products from TAG Cracking in Tubular Cracking Reactors

Soon after the successful trial operation of the prototype TCR, it was decommissioned and used as the basis for the lab-scale TCR depicted in Figure 29. This reactor was also modified over the course of experimentation, involving three reactor configurations as described in Section V.B.1.iii. However, only two of the configurations were utilized for parametric study: the 100 mL version and the 200 mL version. This was due to operating restrictions inherent to the 500 mL version (see Section V.B.1.iii).

Figure 30.a depicts the reaction volume of the 100mL version, which was a sideways tubular cracking coil with a 50 mL tubular preheater in a back/forth configuration. Figure 30.c depicts the reaction volume for the 200 mL version, which was an upright tubular cracking coil of twice the length of the 100 mL version. These were used to determine the effect of various operating parameters on the distribution of products from TAG cracking. The wide range of operating conditions studied is shown in Table 23.

Operation of the lab-scale TCR and descriptions of the equipment are provided in Section V.B.1.iii. In each case, the reactor was operated at steady state in order to produce CTL and

CTG at conditions that were assumed to be representative of commercial yields. The yield of

CTL was determined gravimetrically, and the composition of the process gas was determined by

GC as described in Section V.B.4.iii. CTL samples were analyzed for their detailed composition

by FIMSDIST as described in Section V.B.4.ii.

Table 23. Factors and levels studied for the parametric study of TAG cracking

Temperature (C)	Space Time (h)	Pressure (MPa)
420	0.27	0.79
430	0.70	1.83
440	1.15	2.86
		3.90
		4.94

Whereas pressure was independently studied on the 200 mL TCR, temperature and space

time were investigated on the 100 mL TCR. The study of temperature and space time consisted

of a 2-factor, 3-level full factorial design using soybean TAG as the feedstock. The levels for

temperature and space time are shown in Table 23. Throughout that experimental series,

pressure was maintained at 2.9 MPa and replication was not utilized.

In addition to varying temperature, pressure, and space time, 9 different TAG feedstocks

were cracked under identical operating conditions (435 C temperature, 0.44 h space time, and 2.9

MPa pressure) on the 100 mL reactor to investigate the effect of TAG feedstock composition on

the CT composition. These samples were produced in triplicate to determine the yield of CTL

and CTG, and to determine the composition of process gas. However, the composition of the

CTL samples was determined without replication.

Pressure was studied on the 200 mL reactor which had no preheating system, but it had increased length and employed a greater number of thermocouples to monitor the temperature of the reactor. For the study of pressure, canola TAG was used as the feedstock. Pressure was studied at five different levels with temperature maintained at 435 C and space time maintained at 1.23 h. The levels of pressure are shown in Table 23.

A summary of all experiments used for investigating the mechanisms of TAG cracking is shown in Table 24. The table includes TAG type, temperature, pressure, reactor, and space time. As indicated, pressure was tested on a larger (i.e., longer) reactor having better pressure control, separate from the other tests.

Table 24. TCR experiments for cracking mechanism investigations

Label	TAG Type	Temperature	Pressure	Reactor Volume	Space Time
-	-	(C)	(MPa)	(mL)	(h)
AA-Soy	Soy	435	2.9	100	0.44
BB-VHONO	VHONO	435	2.9	100	0.44
CC-HENO	HENO	435	2.9	100	0.44
DD-Linseed	Linseed	435	2.9	100	0.44
EE-Camelina	Camelina	435	2.9	100	0.44
FF-Corn	Corn	435	2.9	100	0.44
GG-Cottonseed	Cottonseed	435	2.9	100	0.44
HH-Canola	Canola	435	2.9	100	0.44
II-HONO	HONO	435	2.9	100	0.44
A-Soy	Soy	420	2.9	100	0.27
B-Soy	Soy	430	2.9	100	0.27
C-Soy	Soy	440	2.9	100	0.27
D-Soy	Soy	420	2.9	100	0.69
E-Soy	Soy	430	2.9	100	0.70
F-Soy	Soy	440	2.9	100	0.69
G-Soy	Soy	420	2.9	100	1.22
H-Soy	Soy	430	2.9	100	1.17
I-Soy	Soy	440	2.9	100	1.10
J-Canola	Canola	435	0.79	200	1.23
K-Canola	Canola	435	1.83	200	1.23
L-Canola	Canola	435	2.86	200	1.23
M-Canola	Canola	435	3.90	200	1.23
N-Canola	Canola	435	4.94	200	1.23

In addition, for samples AA-Soy through II-HONO, the CTL that was produced from the reaction was quantified by GC-MS according to the procedure documented by Geetla at UND to determine the carboxylic acid composition of the samples in triplicate.[156] Finally, select CTL samples were analyzed by FTIR to determine the nature of their oxygenation according to the method described in Section V.B.4.iv. The results of these experiments are presented in Section VII.E.

V.C.4. Miscellaneous Processing

Miscellaneous processing was carried out using a variety of equipment in order to predict quality and/or yields with the NCP.

V.C.4.i. Residue Processing to Estimate Coke Formation in the NCP

Two samples of renewable coke were separately prepared in conjunction with Bosquez[66] using the equipment systems and operating parameters listed in Table 25. These equipment systems have their features and operating procedures described in Section V.B.3.

TAG was cracked in the 100 mL lab-scale TCR described in Section V.B.1.iii according to the operating parameters listed in Table 25. CTL was collected at steady state and its yield was gravimetrically determined.

Then CTL was fractioned using the fuel purification system described in Section V.B.3.iii to a final temperature of 350 C and a final pressure of 0.8 kPa, equivalent to an estimated atmospheric equivalent vapor temperature of 540 C, as estimated by the fuel fractionation system from B/R Instruments (see Section V.B.3.iii). The yield of distillation residue and combined yield of distillates were determined gravimetrically.

Distillation residue from CTL fractionation was collected and coked in the crude residue

processing furnace described in Section V.B.3.iv according to the operating parameters in Table

25. The yield of distillates, gas, and coke from the residue processing experiment were

determined gravimetrically.

Table 25. Equipment and operating parameters for determining the quantity of coke product that may be expected from the noncatalytic cracking process (NCP)

TAG Cracking			
System	-	100 mL lab-scale TCR	100 mL lab-scale TCR
Feedstock	-	Soybean TAG	Soybean TAG
Temperature	(C)	440	440
Space Time	(h)	0.77	0.43
Pressure	(MPa)	1.5	1.5
CTL Fractionation			
System	-	Fuel Purification System	Fuel Purification System
Feedstock	-	CTL	CTL
Final Temperature	(C)	350	350
Final Pressure	(kPa)	0.8	0.8
Residue Processing			
System	-	Crude Residue Processing Furnace	Crude Residue Processing Furnace
Feedstock	-	Distillation Residue	Distillation Residue
Final Temperature	(C)	490	490

V.C.4.ii. Fuel Refinement from Soybean TAG

Fuel was refined from soybean TAG in order to demonstrate that fuel could be

successfully refined with the NCP. The operating parameters for the various experiments are

listed in Table 26.

Fuel refinement was completed in four major steps, analogous to the four of the five

essential subsystems[*] in the NCP described in Section II.A. First, soybean TAG was cracked

according to the conditions described in Table 26 using the dual-purposed fuel refinement

version of the batch reactor (see Figure 37). Liquid products were collected for distillation. An

operation procedure for the reactor is described in Section V.B.3.i.

Table 26. Equipment and operating parameters for refinement of jet fuel from soybean TAG
using batch equipment to represent the noncatalytic cracking process (NCP)

TAG Cracking		
System	-	Dual-Purpose Batch Reactor
Feedstock	-	Soybean TAG
Temperature	(C)	435
Time	(h)	0.50
Pressure	MPa (X)	0.1 (N2)
CTL Fractionation		
System	-	CTL Fractionation System
Feedstock	-	Soybean CTL
Final Temperature	(C)	350
Final Pressure	(kPa)	0.8
Deoxygenation		
System	-	Dual-Purpose Batch Reactor
Feedstock	-	CTD
Temperature	(C)	325
Pressure	(MPa)	1.8
Time	(h)	4
Catalyst	ratio (type)	1:50 (Pd/C 5 powder)
Reaction Cycles	-	4
Fuel Fractionation		
System	-	Fuel Purification System
Feedstock	-	Deoxygenated CTD
Pressure	(kPa)	Ambient
Fractions	-	160 - 210 C surrounded by 5C increments

[*] Note: The residue processing subsystem was neglected because it was unnecessary for the
production of jet fuel. As a result, the distillation residue was simply discarded.

CTL was then distilled in the CTL fractionation system (see Figure 38) in order to volatilize as much CTL as possible from the CT, leaving a heavier CTR. An operation procedure for the CTL fractionation system is described in Section V.B.3.ii.

CTD were then deoxygenated in the dually-purposed batch reactor according to its operating description in Section V.B.3.i. Pd/C 5 catalyst was added at a weight ratio of 1:50 (catalyst:distillates) in order to catalyze the deoxygenation. The deoxygenation reaction was performed in four reaction cycles as previously described in Section V.C.1.i and furthermore indicated in Table 26. Deoxygenated distillates were collected and centrifuged to remove the catalyst in a simple swing-bucket centrifuge at approximately 1000 gravity. Deoxygenated distillates were decanted and collected for fuel fractionation.

Finally, the fuel purification system (see Figure 39) was used to fraction the deoxygenated CTD into cuts for final fuel blending. The operation of this system is described in Section V.B.3.iii.

The major distillate fuel fraction for kerosene jet fuel was collected over the boiling range of 160 – 210 C. Numerous additional (minor) distillate fractions were collected spanning 5 C boiling point intervals surrounding the major fraction (i.e., from 120 – 190 C and 483 – 250 C) to blend into the major fraction. The major fraction was preliminarily tested for freeze point[157], flash point[158], and density[159] using standardized test methods. Various minor fractions were blended into the major fraction and the blend was then retested. This blend-and-test sequence was repeated in order to achieve minimum quality giveaway and maximum yield of Jet-A-1 fuel, while ensuring compliance with international fuel physical property specifications.[27]

Once prepared, the quality of the final fuel was verified by performing all of the

standardized tests for: total acidity[154], density[159], freeze point [157], flash point [158], and energy density[160]. The Jet-A-1 product was analyzed by FTIR (Section V.B.4.iv) in order to quantify the concentration of olefins. A sample of the final Jet-A-1 fuel and a sample of petroleum-derived kerosene fuel were analyzed by FIMSDIST as described in Section V.B.4.ii.

In addition, the fuel purification system (see Figure 39) was used to prepare various distillate fractions spanning approximately 20 C increments from 100 to 300 C from the deoxygenated CTD (who preparation is described above) and from petroleum-derived kerosene fuel. Each fraction was characterized in order to determine its flash point[158], freeze point[157], pour point, and density using standardized methods. These are compared to assess the carbon number range of jet fuel produced by the NCP in comparison to this sample of kerosene fuel and to draw conclusions about product quality.

CHAPTER VI

ANALYTICAL METHOD FINDINGS, DATA PROCESSING, AND RESULTS

In order to estimate the fuels that could be derived from the noncatalytic cracking process (NCP), the composition of cracked TAG liquid (CTL) was estimated by a unique method that uses gas chromatography (GC) with simultaneous field ionization mass spectrometry (FIMS) / flame ionization detection (FID). This method is known herein as a FIMSDIST, incorporating aspects of FIMS and simulated distillation (i.e., SimDist). The limitations of this method were determined by interpreting ions and comparing the results to published literature and data from detailed composition methods. FIMSDIST was then used to determine the mass based composition of many CTL samples to determine trends and yields of triglyceride (TAG) cracking vs. cracking reaction parameters.

VI.A. Processing of FIMSDIST Composition Data of Various Samples

This section presents the data reduction and calibrations for the high throughput compositional analysis of CTL via the FIMSDIST method. Due to the complexity and uniqueness of data reduction, explanation is necessary in order to elucidate how the results were obtained.

VI.A.1. FID Data Processing

Figure 45 shows an example FID chromatogram that was obtained from the FIMSDIST analysis of CTL from sample 'AA-Soy' in the experimental list shown in Table 24 on page 224.

Without mass spectrometry data, the FID chromatogram alone is essentially the format of the data that might be expected from a SimDist analysis, such as those utilized by ASTM D7500[64] upon which this method was based.
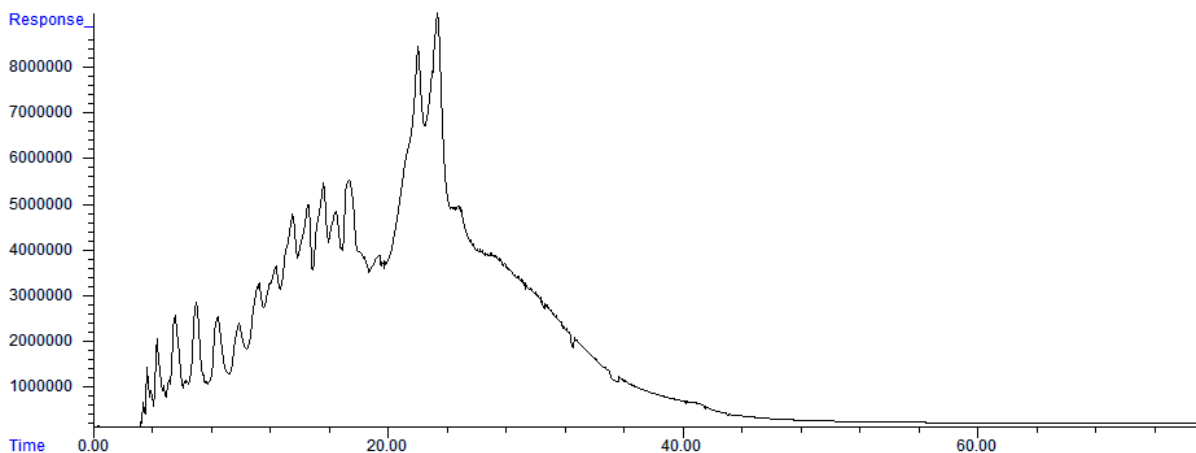
Figure 45. Example FID chromatogram of a CTL sample

In order to reduce the FID data, the relationship between retention time and boiling point was first determined in order to establish boiling point fractions (BPFs). Using a few standard solutions of either linear paraffins or polywax (as described in 'Materials' on page 134), the retention times were determined for linear paraffins spanning from C_5 to C_{74} as shown in Figure 131 and described by Appendix F. Although the plot is relatively linear, a fourth order polynomial most closely fit the experimental data (Figure 131). The fourth order polynomial was used to determine the retention times that correspond to boiling points in increments of 50 C spanning from 100 C to 650 C, shown in Table 27.

The retention times in Table 27 were used to form retention time boundaries around boiling point fractions (BPFs) in the FID chromatogram. Each BPF has a width of

Table 27. FIMDIST boiling point cuts / retention time cuts

Temperature (C)	Retention Time (min)
100.0	3.7
150.0	6.7
200.0	9.8
250.0	13.0
300.0	16.3
350.0	19.7
400.0	23.0
450.0	26.3
500.0	29.8
550.0	33.3
600.0	37.2
650.0	41.8

approximately 50 C, spanning from ambient to 650 C in increments of 50 C. The boundaries around the BPFs are shown by dotted lines in Figure 46, with each dotted line corresponding to a row in Table 27. The mass fraction of each BPF was determined using SimDist methodology (e.g., ASTM D7500[64]), compensating for (1) the baseline signal and (2) a minor deviation in the FID/MS detector split (approx. less than 2 %).

In SimDist analyses, the relative mass fraction of a BPF is estimated from the integrated FID area of a BPF relative to the total integrated FID signal area. SimDist is only valid for hydrocarbons,[64] whereas samples containing significant amounts of heteroatoms will deviate. Since CTL is rich in carboxylic acids, the relative mass fraction of that BPF must be adjusted for the quantity of carboxylic acids in that BPF. This is accounted for later in Section VI.A.2, and for this discussion it is assumed to be negligible.

As a result, it was possible to compile pseudo distillation curves (PDC) based on this information. Example PDCs are shown below. It should be mentioned that these data have not yet been adjusted to compensate for carboxylic acids in the sample (which has been
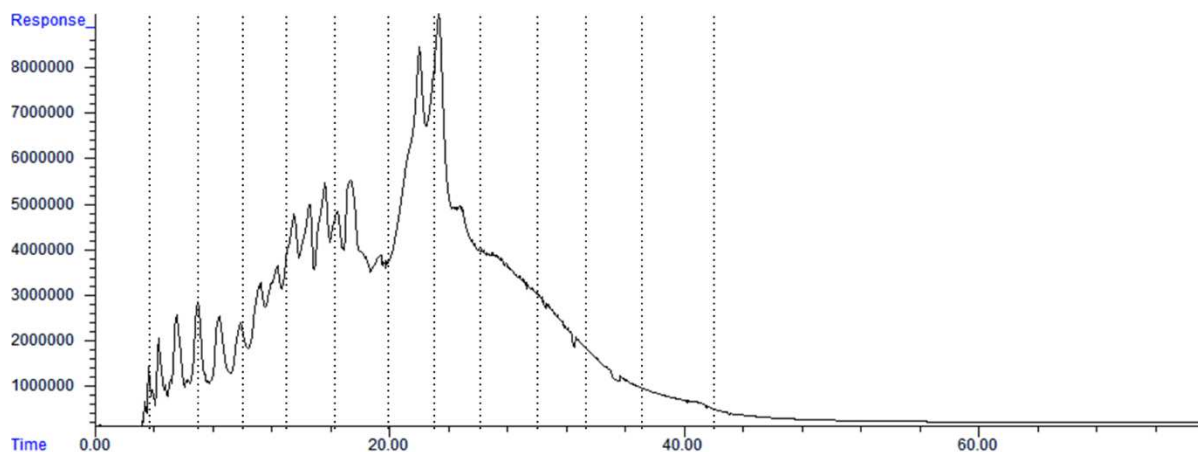
Figure 46. Boiling point fractions shown by dotted lines on example FID chromatogram

corrected later in this chapter), which is why the data are referred to as *pseudo* distillation curves. Nevertheless, it is informative to examine the data.

The PDCs are shown in Figure 47 for CTL samples that have been derived from a variety of TAGs. What can be first observed from the distillation curves is that all the CTLs from the various TAGs trend similarly. The TAGs have absolute vertical deviations in their PDCs mass fraction of approximately 10 wt. %, with some of the TAGS trending lower and some higher. In particular, HENO appears to trend lower than the majority of TAGs, potentially indicating a higher volume of residual material than other oils.

Secondly, it appears that a significant fraction of the CTL distills at relatively high boiling points for the conditions which these TAGs were processed. Above 250 C, approximately 78 to 86 % of a samples mass is expected to residue according to this PDC. In other words, distillation up to a boiling point of 250 C will only distill one-sixth to one-quarter of a samples mass as presented above. Above a boiling point of 400 C, as much as 40 to 50 % of a sample's mass is expected to residue. However, at a boiling point of 650 C, very little of a

233

samples mass remains.
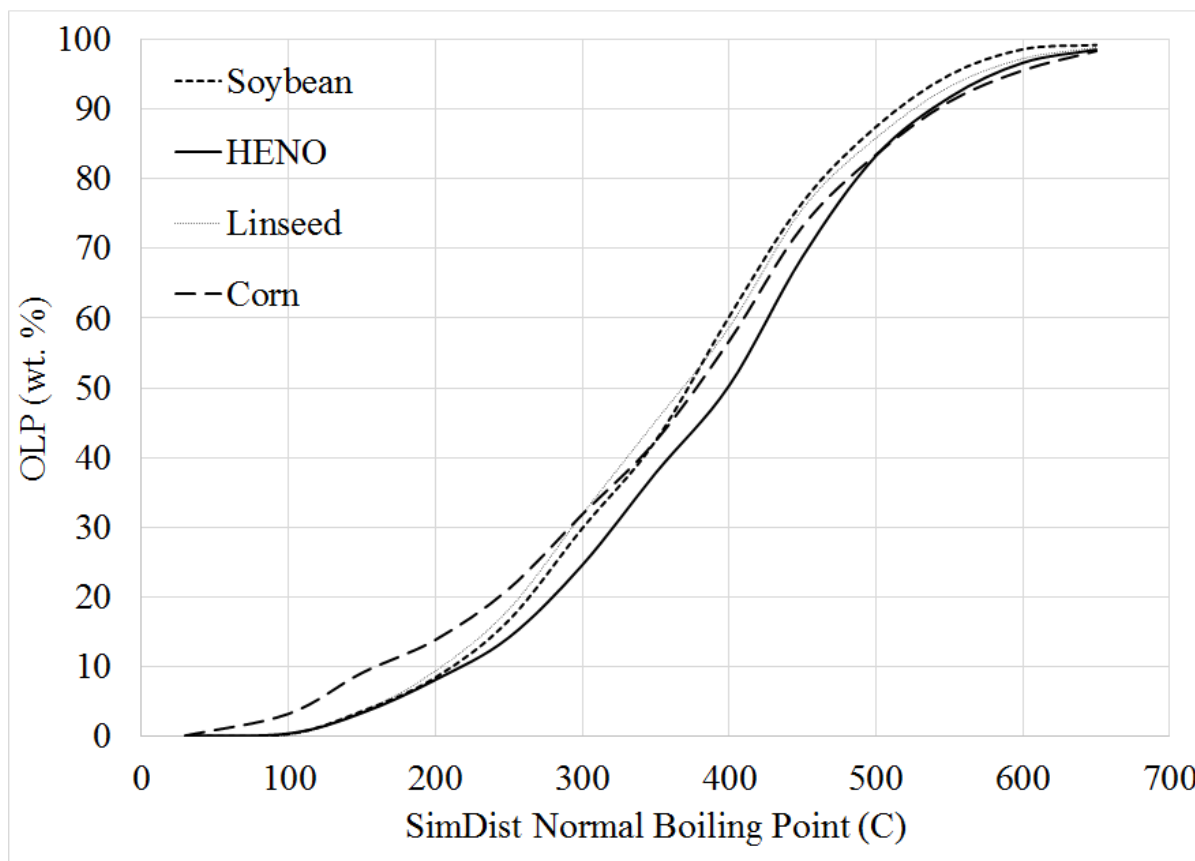
Figure 47. Pseudo distillation curves for CTLs derived from various TAGs at 435 C temperature, 0.44 h space time, and 2.9 MPa pressure in the 100 mL lab-scale TCR

Despite the fact that the data vary by as much as 10 wt. % between the TAGs, the data are fairly similar—so much so that it is difficult to derive meaningful trends from PDCs of these oils. Based on that observation, other means of examining the data may be more effective than examining it by analytical distillation.

More useful information might be gleaned from plots of fraction mass distributions (FMDs). An example FMD is shown in Figure 48 for this same variety of TAGs. This plot shows the 13 fractions of the CTL in 50 C increments spanning from ambient to 650 C and

beyond.
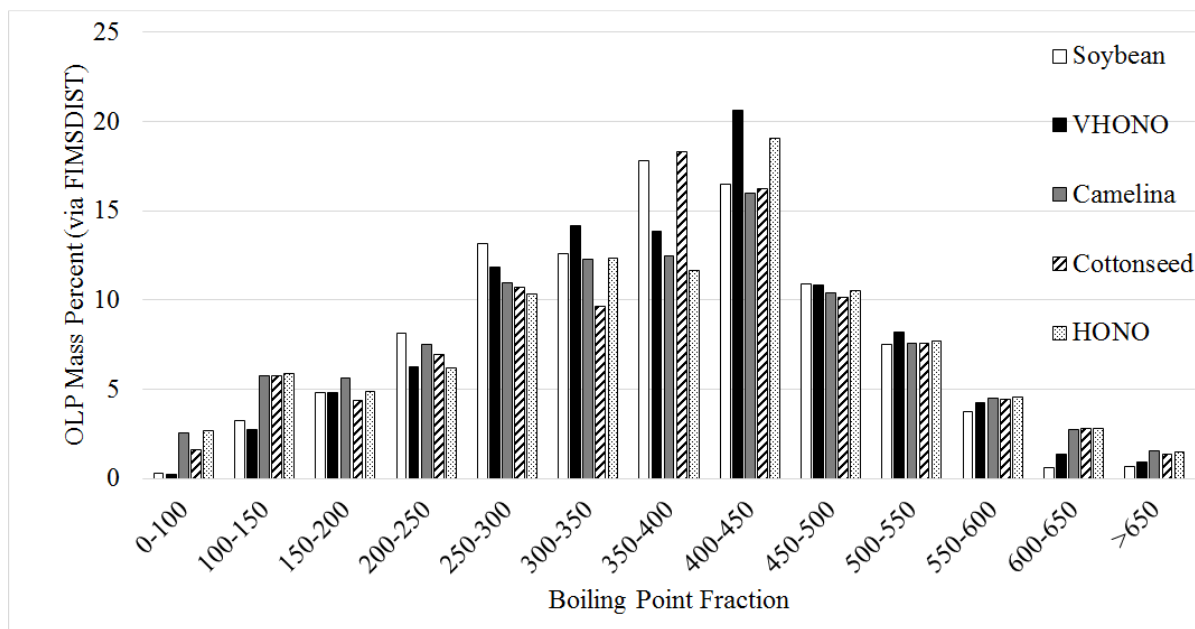
Figure 48. Fraction mass distribution of CTL samples from various TAGs at 435 C temperature, 0.44 h space time, and 2.9 MPa pressure in the 100 mL lab-scale TCR

The portion of the CTL in the fraction of 150 to 200 C is fairly consistent and only on the order of 5 % of a samples mass. This is a potential consideration for jet fuel production described in the discussion section. The combined fractions spanning 0 to 150 C vary somewhat for the different types of oils, and they account for approximately 7 to 10 % of a sample's mass. The highest mass fraction of the CTLs is consistently the 400 to 450 C range containing approximately 16 to 21 wt. % of an CTL sample's mass. Above 450 C, the mass appears to be dramatically reduced towards residual amounts on the order of a few percent.

Although FMDs aren't as clear for discerning different TAG feedstocks, FMDs can show some important observations for varying operating parameters. For example, Figure 49 shows the FMDs for soybean TAG processed at three different reaction temperatures (more sample

information is available in Table 24). In examining the FMDs, it is apparent that increasing the

temperature from 420 to 440 C is beneficial for raising the masses of lighter fractions by 20 - 30

% for fractions below 350 C, whereas heavier fractions above 500 C are decreased

correspondingly. As a result, increasing temperatures might be essential for improving the yields

of fuels such as gasoline and jet fuel.
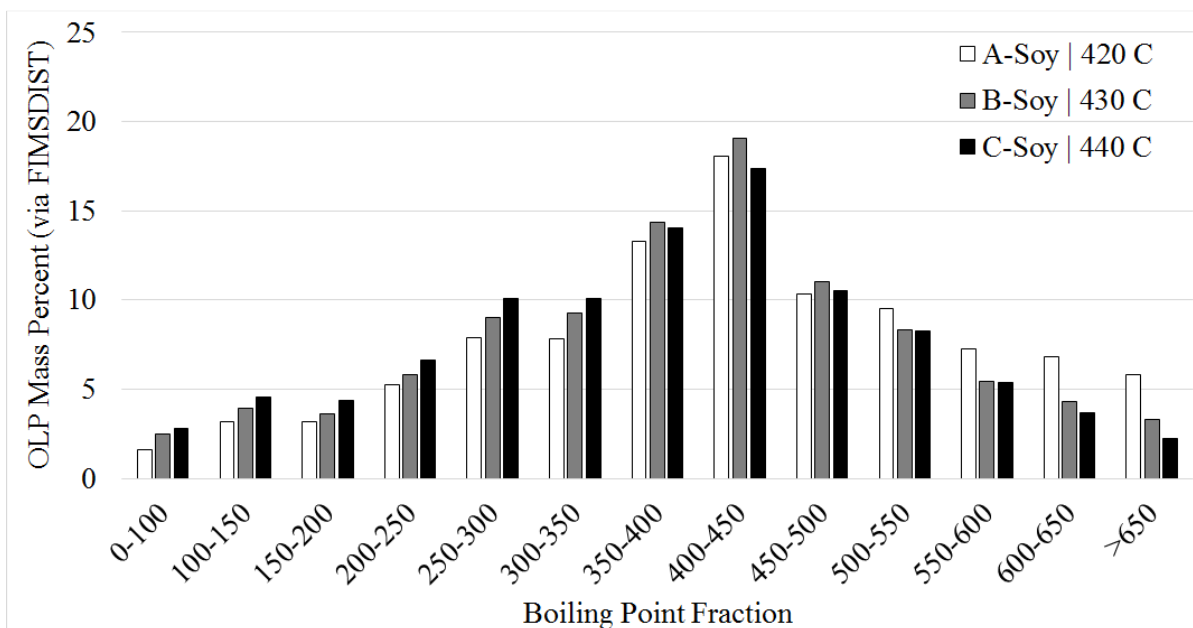
Figure 49. Fraction mass distribution for soybean CTLs at varying temperatures and at 0.27 h
space time and 2.9 MPa pressure in the 100 mL lab-scale TCR

To further examine the effect of operating conditions, the MFDs are shown in Figure 50

for cracking soybean TAG in the 100 mL lab-scale TCR at three different space times and a

temperature of 440 C. The effect of space time is even substantially more dramatic than that of

temperature over the range of conditions studied. In tripling the residence time, the lighter

fractions (up to 350 C) are increased by 50 to 100 %. Concurrently, the heavier fractions (above

400 C) are decreased by similar amounts.
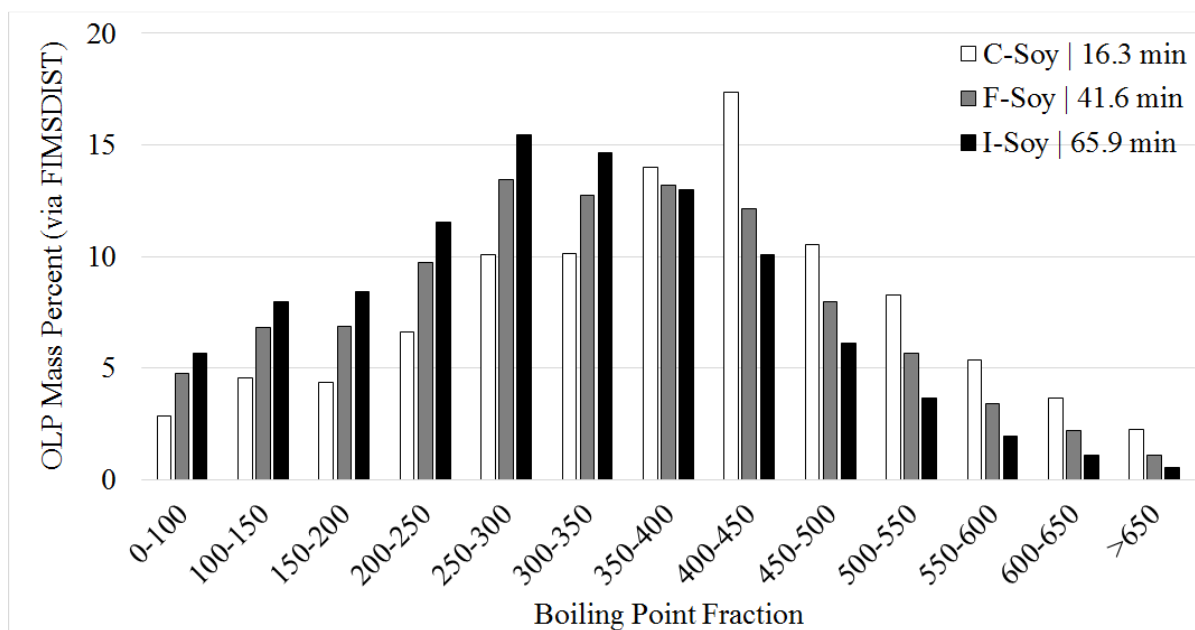
Figure 50. Fraction mass distributions for soybean CTLs cracked at various space times and at 440 C temperature and 2.9 MPa pressure in the 100 mL lab-scale TCR

The MFDs are shown in Figure 51 from canola TAG cracking at a variety of pressures on the 200 mL lab-scale TCR. Table 24 shows the other operating parameters for these samples. What is evident from the figure is that the increase of pressure has a positive effect on increasing lighter fractions and decreasing heavier fractions. In particular, the lowest pressure (0.79 MPa) is particularly detrimental to the production of light fractions on the order of 20 wt. %, with a similarly opposite effect on heavier fractions. Unlike the previous trends for temperature and space time, the increased pressure appears to only benefit fractions below 250 C (compare at 350 C) and the reduction of heavier fractions begins as early as fractions 300 C (compare at 400 C).
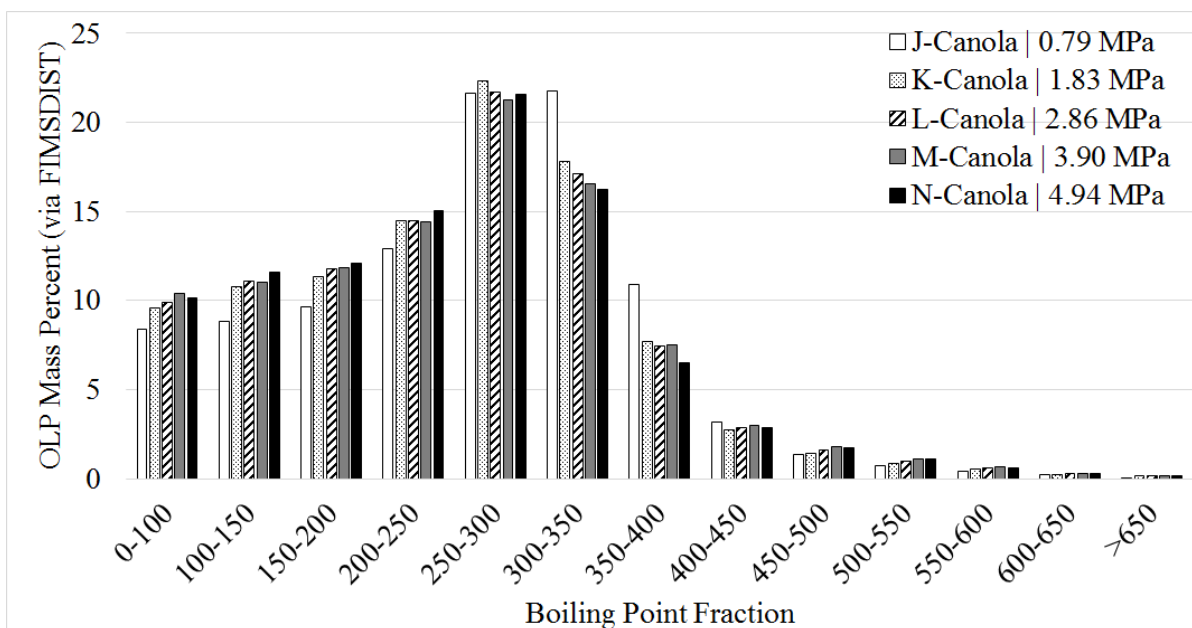
Figure 51. Fraction mass distributions for canola CTLs at various pressures and at 435 C temperature and 1.23 h space time in the 200 mL lab-scale TCR

Although these conclusions are for Canola TAG, the trends from canola could be applied to other TAGs.

From these data , it may be concluded that optimization of the operating conditions of TAG cracking can substantially increase the yield of lighter middle distillate fuel fractions compared to non-optimal conditions. The portion of CTL in the fraction of 150 to 200 C is improved from approximately 5% in Figure 48 to over 12 % of a sample's mass in Figure 51. Likewise, the combined fractions spanning 0 to 150 C can be increased from 7-10 % up to 22 %. Finally, the most prominent fraction in the optimal data set is 250 to 300 C, whereas previously the most prominent fraction was 400 to 450 C.

In summary, it is clear that higher temperatures, higher space times, and higher pressures are beneficial for producing lighter fuels. What is not clear is the influence of TAG composition

on the products of TAG cracking. In order to elucidate the difference, it is desirable to use the

mass spectrometry data from FIMSDIST to speciate the CTL. The mass spectrometry speciation

data is presented in the following section. Concerning the reduced FID data, a series of tables

for complete BPF data is included in Appendix H.

VI.A.2. FIMS Data Processing

Since it is difficult to draw definitive conclusions about the effect of TAG composition

from FID data in SimDist form, the field ionization (FI) mass spectrometry was considered to be

a vitally important tool for illustrating the differences between types of TAGs in noncatalytic

cracking reactors. FI mass spectrometry was utilized to speciate the unresolved complex mixture

as described in Section IV.C (see page 115).

The speciation provided by FIMS is demonstrated by observing Figure 52. The figure
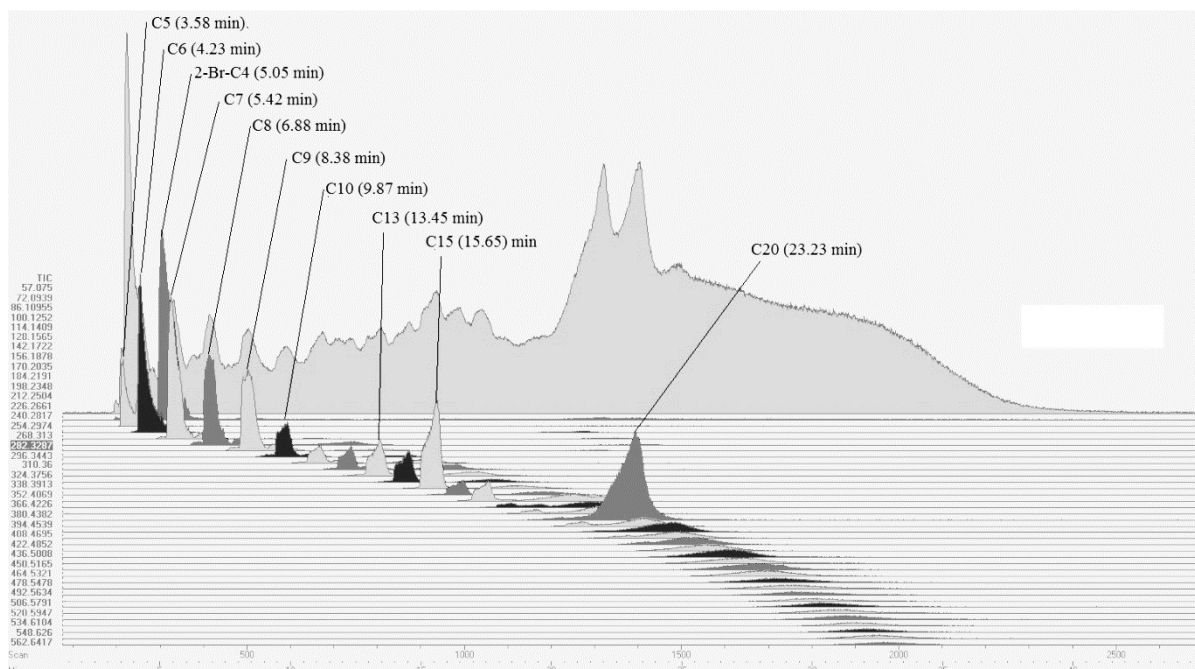
Figure 52. Example FIMSDIST data with extracted ion chromatograms for paraffins from soybean CTL for sample 'AA-Soy'

239

shows field ionization mass spectrometer (FIMS) data for soybean CTL with a series of extracted

ion chromatograms (EICs) for paraffins ranging from C5 to C40. The total ion chromatogram

(TIC) is also shown in the background of the figure, as indicated. The EIC for the internal

standard (2-bromobutane) is also included. The ions for these paraffins are clearly visible under

the unresolved chromatogram produced by the FIMSDIST analysis.

In like manner, Figure 53 shows a FIMS example chromatogram for soybean TAG with a

series of EICs for carboxylic acids ranging from C2 to C24 and the TIC is shown in the

background of the figure. Some of the more prominent carboxylic acids are identified in Figure

52, including acetic acid, propionic acid, decanoic acid, palmitic acid, and stearic acid.
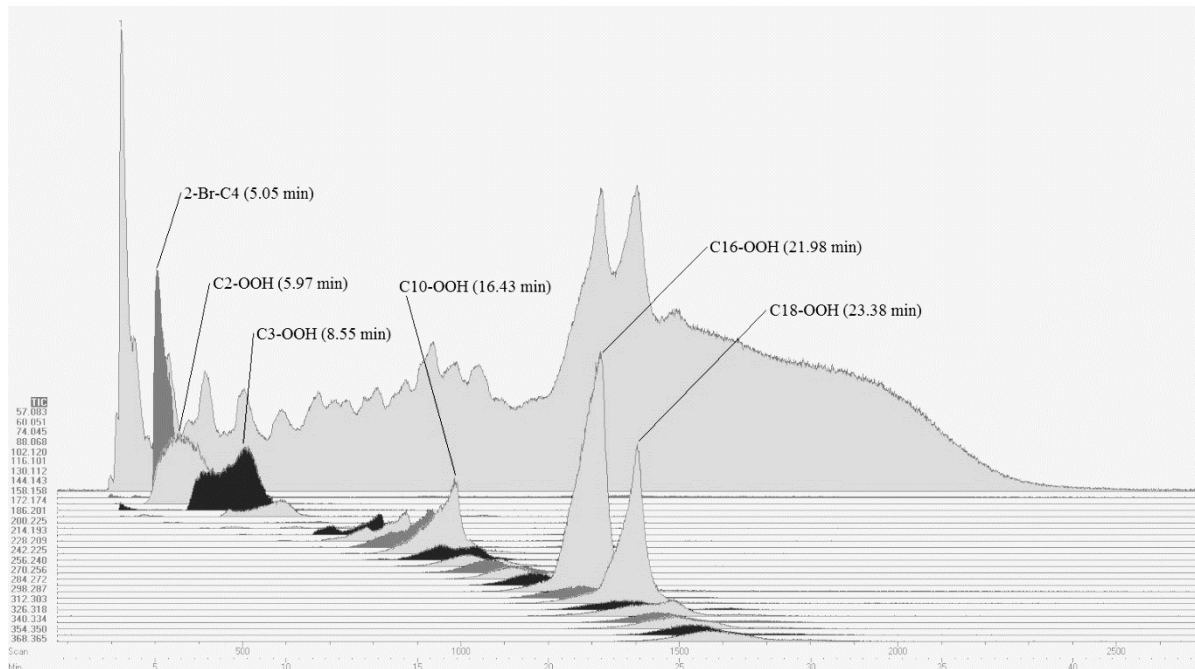
Figure 53. Example FIMSDIST data with extracted ion chromatograms for carboxylic acids from soybean CTL for sample 'AA-Soy'

Similar extracted ion chromatograms may be derived for olefins/cyclics, aromatics, and organic molecules of increased complexity. Although a multitude of components are contained within an unresolved complex mixture, as exampled by the detailed composition data of Table 57, the components are clearly visible by their EICs from FIMS. In order to put the EIC data into useable form, a series of data reductions were performed.

First, the mass spectra were averaged separately over each BPF range shown in Figure 46. Integrated mass spectra are shown in Figure 54 through Figure 56 for the 13 BPFs described previously for sample 'AA-Soy.'

As expected, the averaged mass spectra over the lightest BPF only contains very small molecular weight components, which agrees with their low boiling point and with the utilization of a SimDist like analysis for FIMSDIST.

Furthermore as expected, the molecular weight increases as the BPF increases in relevant temperature. Additionally, greater dispersion is observed in the molecular weight as the BPFs temperature ranges increase from ambient to 300 C.

The dispersion in the BPFs continues to increase as the temperatures increase from 300 to 550 C. This great dispersion reflects two things: (1) the great diversity, complexity, and convoluted nature of CTL constituents and (2) the futility of typical chromatographic methods (i.e., target analyte methods) for eluting, resolving, and quantitating such a complex mixture. Such conventional methods are described previously in Section IV.B on page 112.

The final highest temperature BPFs show the greatest dispersion, with the 650 C - Residual BPF having very low response. Part of the reason for the low response of the residual range BPF is due to the very minor percentage of sample being eluted from the column,

estimated on the order of 2% by the FID data presented in Appendix H. In order to provide a

better representation of the data, the fraction of 600 – 650 C and 650 C – Residual were

combined into a single range (600 C – Residual).
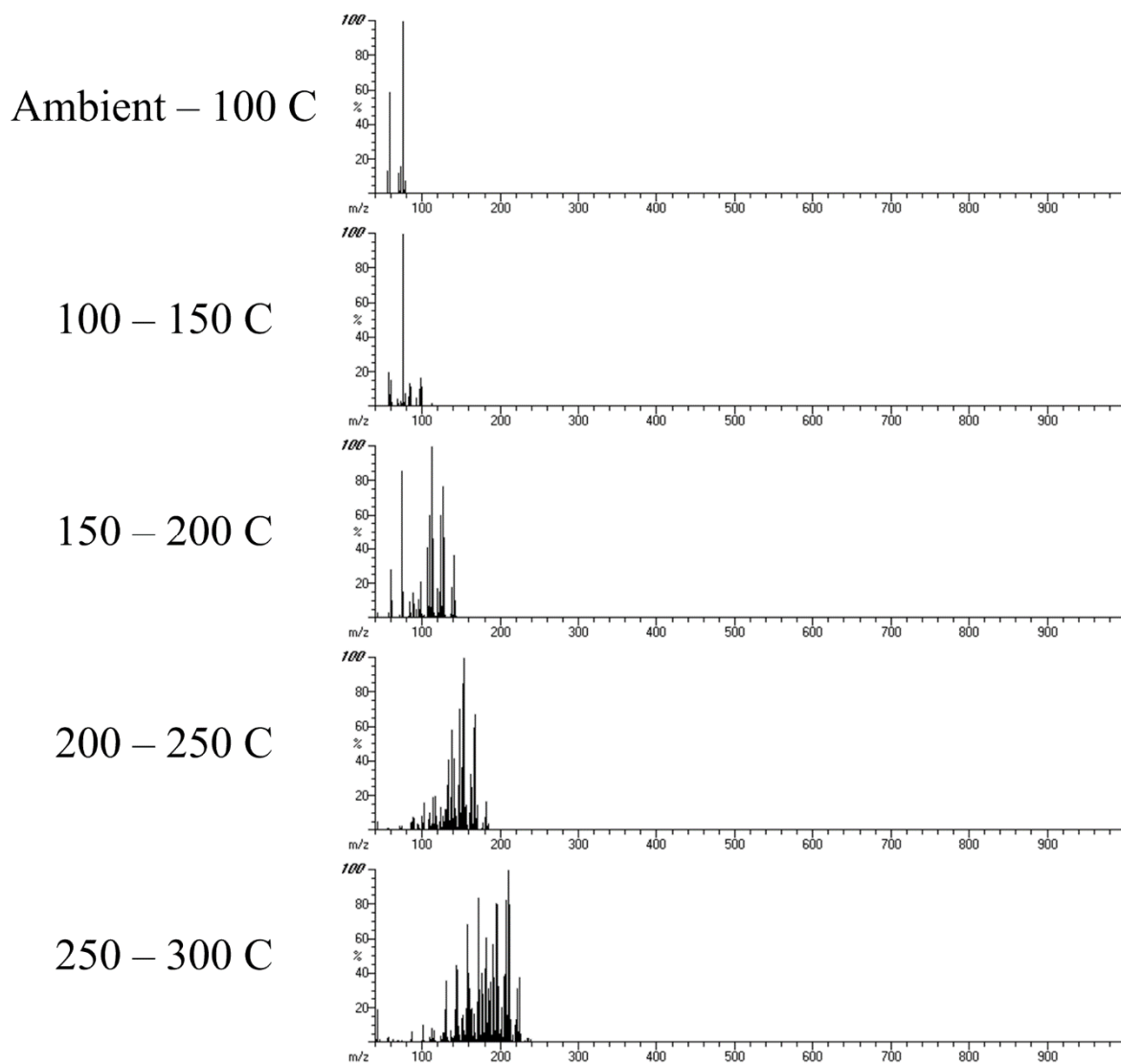
Figure 54. FI-TOF mass spectra of light-range boiling point fractions for soybean CTL sample
'AA-Soy'

300 – 350 C
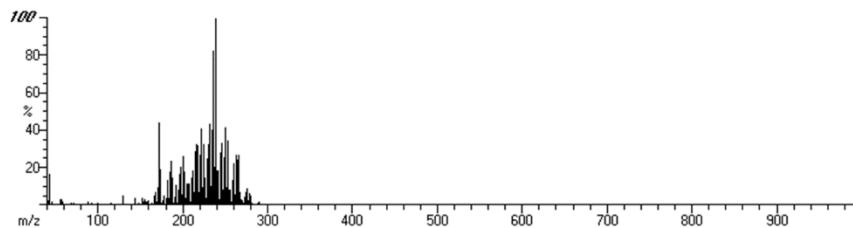
350 – 400 C
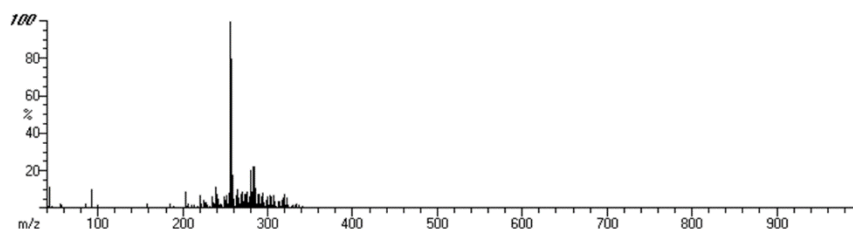
400 – 450 C
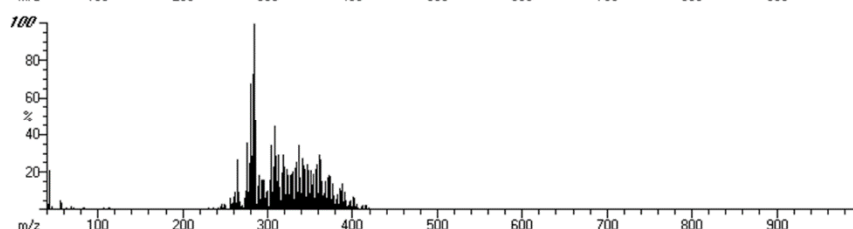
450 – 500 C
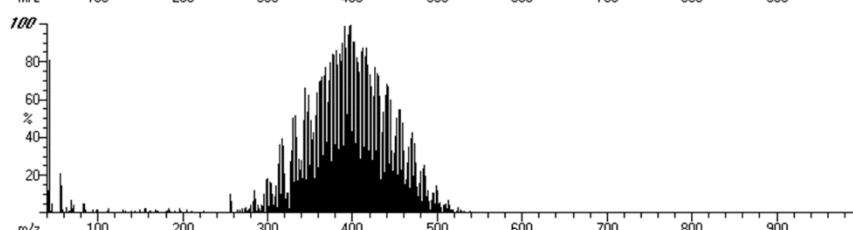
500 – 550 C
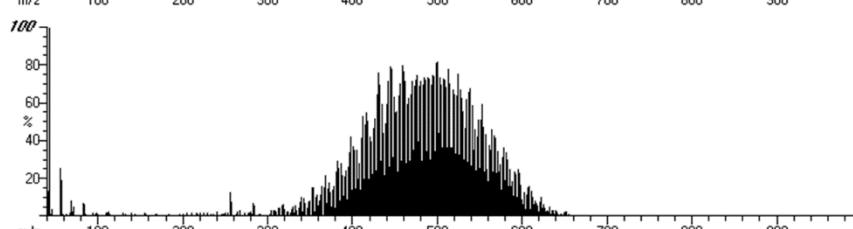
Figure 55. FI-TOF mass spectra of heavy-range boiling point fractions for soybean CTL sample 'AA-Soy'
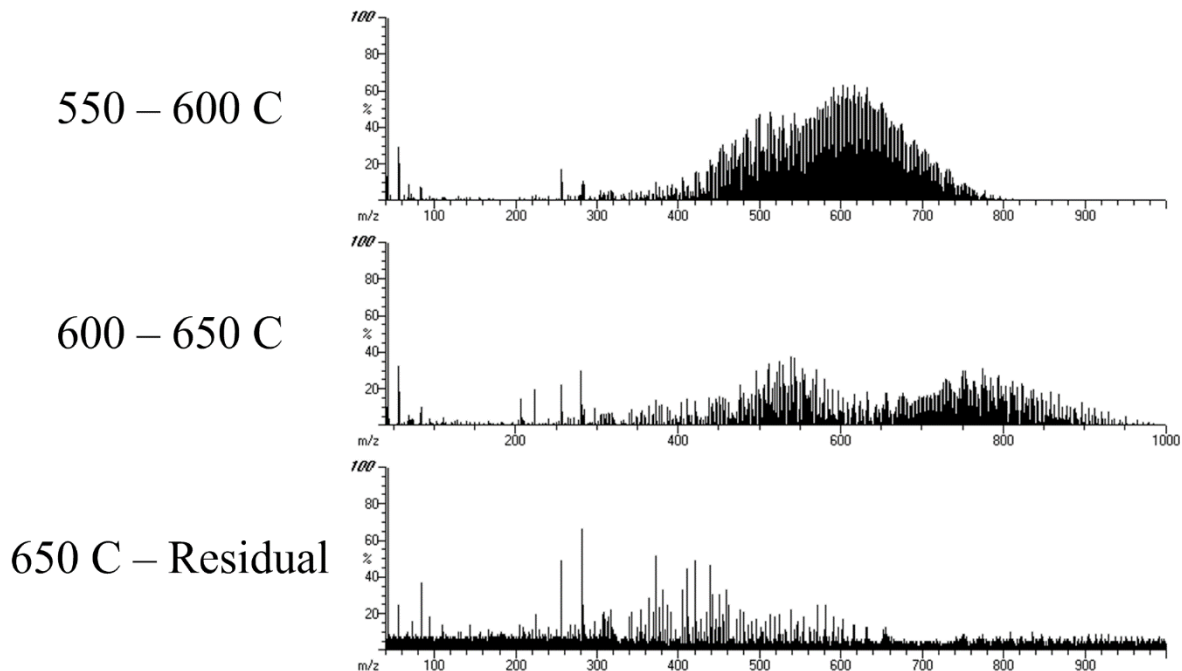
Figure 56. FI-TOF mass spectra of resin-range boiling point fractions for soybean CTL sample 'AA-Soy'

In the previous three figures, the mass spectra were presented as a faraway view in order to illustrate the trends and differences of the BPFs. In the following two figures, the mass spectra of the first two BPFs are observed more closely, because they have few enough ions that they may be readily interpreted. As previously mentioned, the mass spectra were computed by integrating over each BPF.

A close up view of the Ambient-100 C BPF's integrated mass spectrum for sample 'AA-Soy' is shown in Figure 57. Based on the FID data tabulated in Appendix H, this BPF only accounts for approximately 0.5% of the CTL's mass. Small amounts of C_4H_{10} and C_4H_8 (e.g., butane and butene) are observed at m/z 58 and 56, respectively. In addition, C_5H_{12} and C_5H_{10} (e.g., pentane and pentene) are observed at m/z 72 and 70, respectively while, carbon disulfide is observed at m/z 76 and 77, which was used as a solvent for syringe cleaning.

244

Figure 57. FI mass spectra of Ambient - 100 C boiling point fraction for soybean CTL

Although the carbon disulfide ion was the highest peak in the mass spectrum, it was neglected from the analysis since the FID is incapable of detecting the carbon disulfide. As a result, the influence of residual solvent in the analysis is negated.

The utilization of FIMS in this fashion makes it virtually impossible to differentiate reliably between formula isomers since they have the same exact masses. As a result, data are reported by their formulas rather than by exact components.

A close up view of the 100-150 C BPF's integrated mass spectrum for sample 'AA-Soy' is shown in Figure 58. This BPF accounts for approximately 3% of the CTL's mass. Some groups overlap from previous BPF (ambient-100 C), including C_4H_{10}, C_4H_8, C_5H_{12}, and C_5H_{10}.

Additionally, C6 and C7 groups were also found in this BPF, having increased formula variety. For example, C6 included the saturated paraffin form (m/z 86), the unsaturated/cyclic form (m/z 84), the twice unsaturated form (m/z 82, e.g. methylcyclopentene, C_6H_{10}), and the aromatic form (m/z 78, i.e., benzene). In addition, the internal standard (2-bromobutane) is visible in this spectrum at m/z 57, and carbon disulfide solvent is also visible.
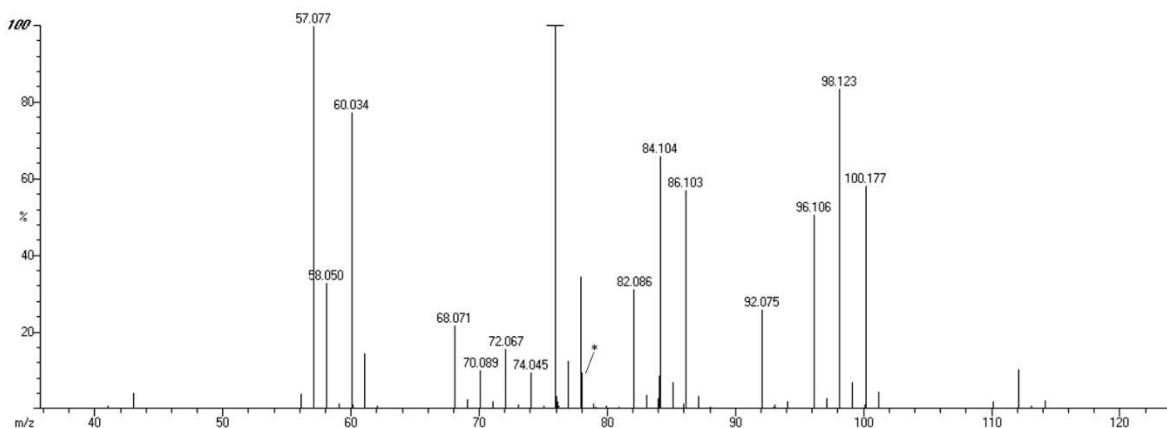
Figure 58. FI mass spectra of 100-150 C boiling point fraction for soybean CTL

Throughout the remaining 11 BPF's, ions were identified by the exact molecular weight of the ions formula. The exact molecular weights used for identification of components in CTL are included in Table 28 for various compounds spanning C1 to C30. Classes of compounds are named with codes at the top of the table. C# refers to Carbon Number; C- refers to a paraffin; C= refers to an mono-olefin or mono-cyclic; =C= refers to a di-olefin or di-cyclic or combination thereof; COOH refers to carboxylic acids; COOMe refers to methyl esters; (1x)Ar refers to alkyl branched monoaromatics; (1x)Ar= Refers to alkenyl branched or cyclic branched monoaromatics; (2x)Ar refers to alkyl branched di- aromatics of a naphthalene type; (2x)Ar= refers to alkenyl branched or cyclic branched di-aromatics of a naphthalene type; (3x)Ar refers to alkyl branched triaromatics of an anthracene type; (3x)Ar= refers to alkenyl branched or cyclic branched triaromatics of an anthracene type.

For ions with weights above C30, ions were identified according to a z-table similar to a low resolution FI mass spectrometer up to a carbon number of C74. This was done because there is too much exact mass variety above ~ C30 so that using exact mass determination is difficult

without specialized MS instruments. A z-table is a typical representation of FIMS data (see

Appendix K)

Table 28. Exact mass values (daltons) for main isotope of various organics

C#	C-	C=	=C=	COOH & COOMe	(1x)Ar	(1x)Ar=	(2x)Ar	(2x)Ar=	(3x)Ar	(3x)Ar=
1	16.031			46.005						
2	30.047	28.031		60.021						
3	44.063	42.047	40.031	74.037						
4	58.078	56.063	54.047	88.052						
5	72.094	70.078	68.063	102.068						
6	86.110	84.094	82.078	116.084	78.047					
7	100.125	98.110	96.094	130.099	92.063					
8	114.141	112.125	110.110	144.115	106.078	104.063				
9	128.157	126.141	124.125	158.131	120.094	118.078				
10	142.172	140.157	138.141	172.146	134.110	132.094	128.063			
11	156.188	154.172	152.157	186.162	148.125	146.110	142.078			
12	170.203	168.188	166.172	200.178	162.141	160.125	156.094	154.078		
13	184.219	182.203	180.188	214.193	176.157	174.141	170.110	168.094		
14	198.235	196.219	194.203	228.209	190.172	188.157	184.125	182.110	178.078	
15	212.250	210.235	208.219	242.225	204.188	202.172	198.141	196.125	192.094	
16	226.266	224.250	222.235	256.240	218.203	216.188	212.157	210.141	206.110	204.094
17	240.282	238.266	236.250	270.256	232.219	230.203	226.172	224.157	220.125	218.110
18	254.297	252.282	250.266	284.272	246.235	244.219	240.188	238.172	234.141	232.125
19	268.313	266.297	264.282	298.287	260.250	258.235	254.203	252.188	248.157	246.141
20	282.329	280.313	278.297	312.303	274.266	272.250	268.219	266.203	262.172	260.157
21	296.344	294.329	292.313	326.318	288.282	286.266	282.235	280.219	276.188	274.172
22	310.360	308.344	306.329	340.334	302.297	300.282	296.250	294.235	290.203	288.188
23	324.376	322.360	320.344	354.350	316.313	314.297	310.266	308.250	304.219	302.203
24	338.391	336.376	334.360	368.365	330.329	328.313	324.282	322.266	318.235	316.219
25	352.407	350.391	348.376	382.381	344.344	342.329	338.297	336.282	332.250	330.235
26	366.423	364.407	362.391	396.397	358.360	356.344	352.313	350.297	346.266	344.250
27	380.438	378.423	376.407	410.412	372.376	370.360	366.329	364.313	360.282	358.266
28	394.454	392.438	390.423	424.428	386.391	384.376	380.344	378.329	374.297	372.282
29	408.470	406.454	404.438	438.444	400.407	398.391	394.360	392.344	388.313	386.297
30	422.485	420.470	418.454	452.459	414.423	412.407	408.376	406.360	402.329	400.313

It should be noted that although the component table listed above encompasses the

majority of components presumed to form during triglyceride cracking with molecular weights

below C30, there is potential for some ions to not be tabulated. For each BPF, the recognized

ions were compared to the total ions and found to account for at least 85% of the ions in all cases

(including odd mass ions from C^{13} isotopes). Typically more than 95% of the ions were

accounted for.

Considering the natural abundance of C^{13}, there was increased potential for M+2 ion formation leading to incorrect integration of ions. For analytes with the formula $C_{10}H_{20}$, the ratio of M+2 ion formation is approximately 0.5% (i.e., relatively insignificant). On the other hand, M+2 formation increases to approximately 5% and over 30% at $C_{30}H_{60}$ and $C_{74}H_{148}$ respectively. This is due to the binomial distribution of the abundance of C^{13} isotopes. As a result, the integrated FIMS data was adjusted to remove the influence of C^{13} isotopes using isotopic ratios and assuming a natural C^{13} abundance of 1.082%. Other isotopes were considered minor and neglected from data processing.

In order to present the data, the integrated FIMS response of each target ion was normalized according to the mass fraction of each BPF (as determined by the FID integration). In other words, the integrated ions in Figure 54 through Figure 56 were normalized to the relative mass fraction of each BPF in Appendix H (page 492). This was done for all samples, producing a mass-adjusted representation of the components in each sample. It was also necessary to adjust the relative mass fraction of each BPF by for the quantity of carboxylic acids in each BPF. This is described later when carboxylic acids are quantified.

At first, the data from the BPFs were recombined into a single resultant data set by assuming that all of the analytes had the same FIMS relative ionization efficiency (RIE). As a result, the data are presented as 'mass-adjusted FIMS response.' An example of the mass-adjusted FIMS response is presented in the form of a carbon number distribution (CND) in Figure 59 for sample 'AA-Soy.'

The data were also processed using the relative ionization efficiency of various

representative components (described later) in order to provide data that is representative of the true mass fraction in each sample.

Figure 59 shows the relative intensities of the ions adjusted to the mass of each BPF across the entirety of the sample. Ar and Ar= functional groups have been shown using the same pattern for the sake of simplicity of representation. Above ~C30, ions are described by their z-group because it is difficult to identify the group of a particular ion with certainty among a multitude of potential component exact molecular weights. Major ions of interest are pointed out and discussed in the next section for insights into the cracking mechanism.
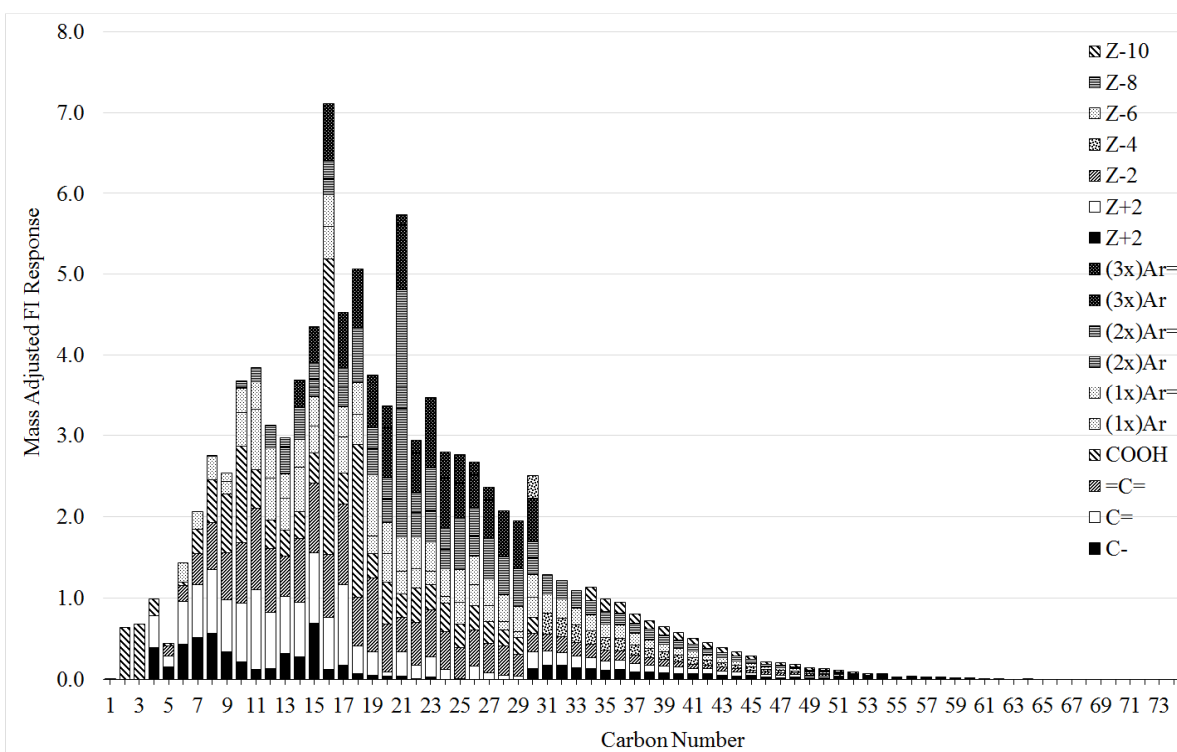
Figure 59. Carbon number distribution of the mass adjusted FI response for AA-Soy CTL

The data provided by FIMSDIST allows the sizes of various carbon number groups to be

examined and compared against a variety of operating conditions and TAG types in cracking reactors. This CND representation is advantageous because it helps provide a compositionally encompassing view of CTL that can be used with process simulation in order to discern what fuels and/or products might be obtained from the NCP.

In order to convert the mass adjusted FI data into a CND that was respective of mass, it was necessary to determine the relative ionization efficiencies for each component and recompute the CND. RIEs were determined for a representative set of compounds in an attempt to encompass the range of desired components in CTL.

The RIEs are computed relative to 2-bromobutane, which was used as an internal standard in all samples as described in Section V.B.4.ii. The RIEs are computed on a mass basis as shown by the following equation, where A refers to the integrated area of the target ion, X refers to the mass fraction in the sample, and subscripts Z and IS refer to the calibration standard and internal standard respectively.

$$\text{RIE} = \frac{A_z \div A_{IS}}{X_z \div X_{IS}} \tag{12}$$

A calibration mixture was created using 56 compounds containing n-paraffins, α-olefins, n-alkyl branched aromatics, polycyclic aromatics, and carboxylic acids, spanning the range of C1-C24 (a.k.a. STDx56, described in Table 66 on page 479 in Appendix F). This standard was serially diluted and used to produce linear plots for the RIEs for each of the compounds. Linear calibrations are shown in the next several plots for various components, although not all

components are shown in linear plots. The slope of the calibration plots is equal to the RIE of

each component. This is an important aspect of the RIE determination, whereas most FIMS

scientists do not report RIEs and a linear calibration plot has not been observed in any of the

literature for any reported RIEs.
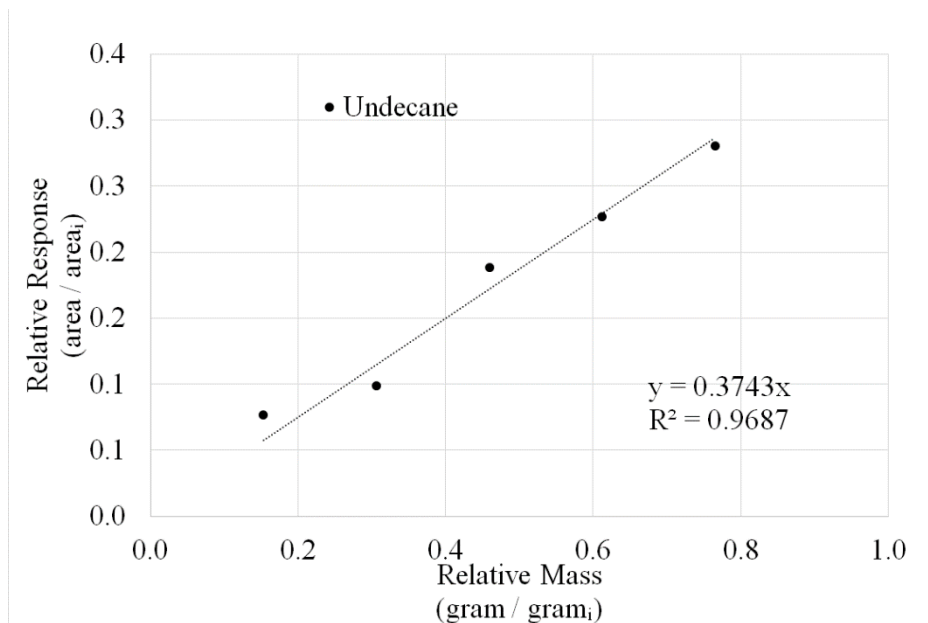
Figure 60. FIMS response vs. mass of n-undecane relative to internal standard
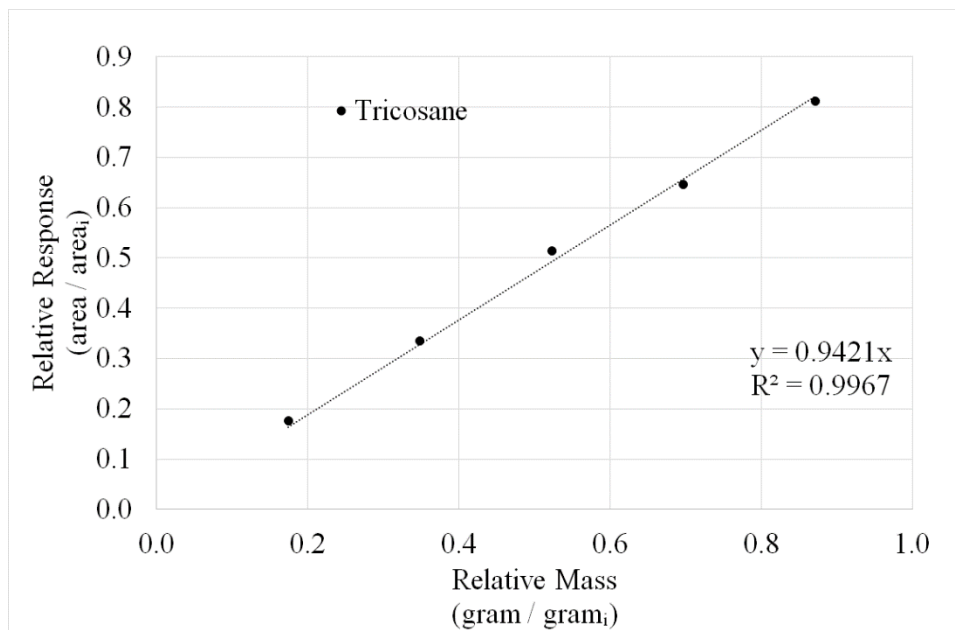
Figure 61. FIMS response vs. mass of n-tricosane relative to internal standard
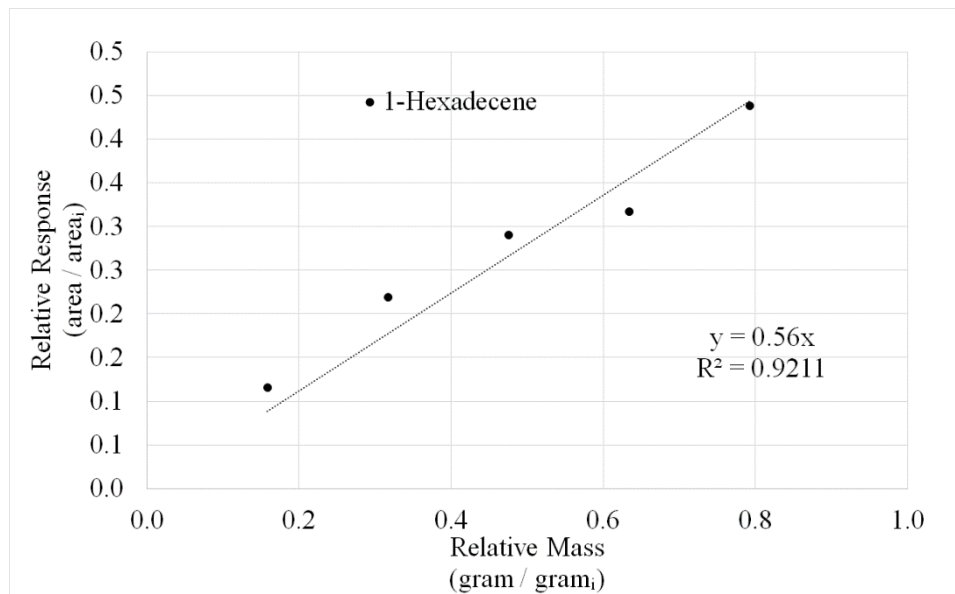
Figure 62. FIMS response vs. mass of 1-hexadecene relative to internal standard
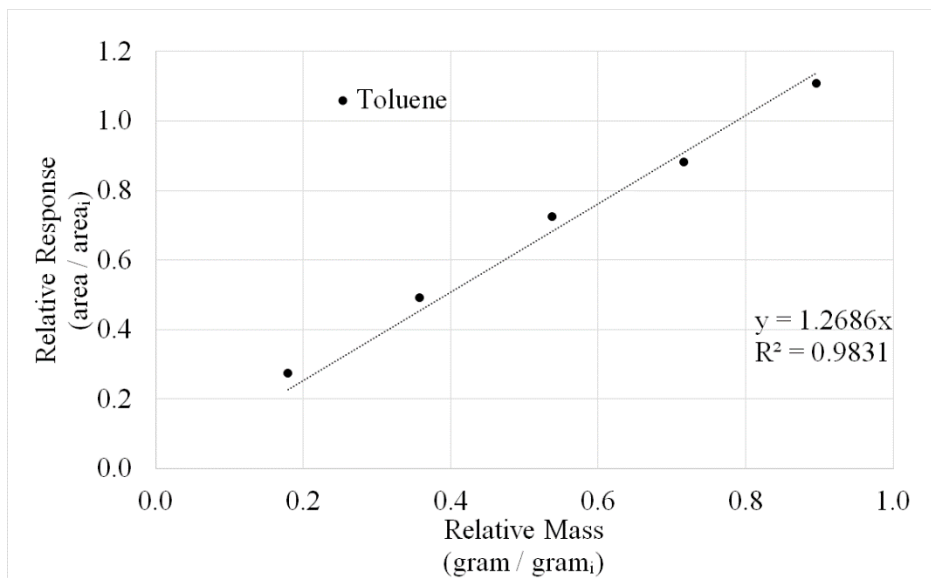
Figure 63. FIMS response vs. mass of toluene relative to internal standard
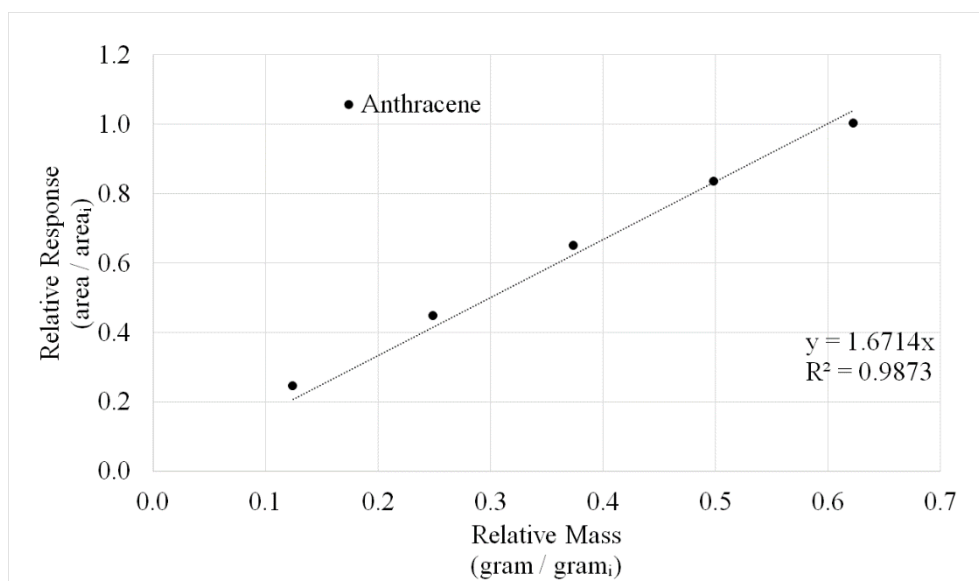
Figure 64. FIMS response vs. mass of anthracene relative to internal standard
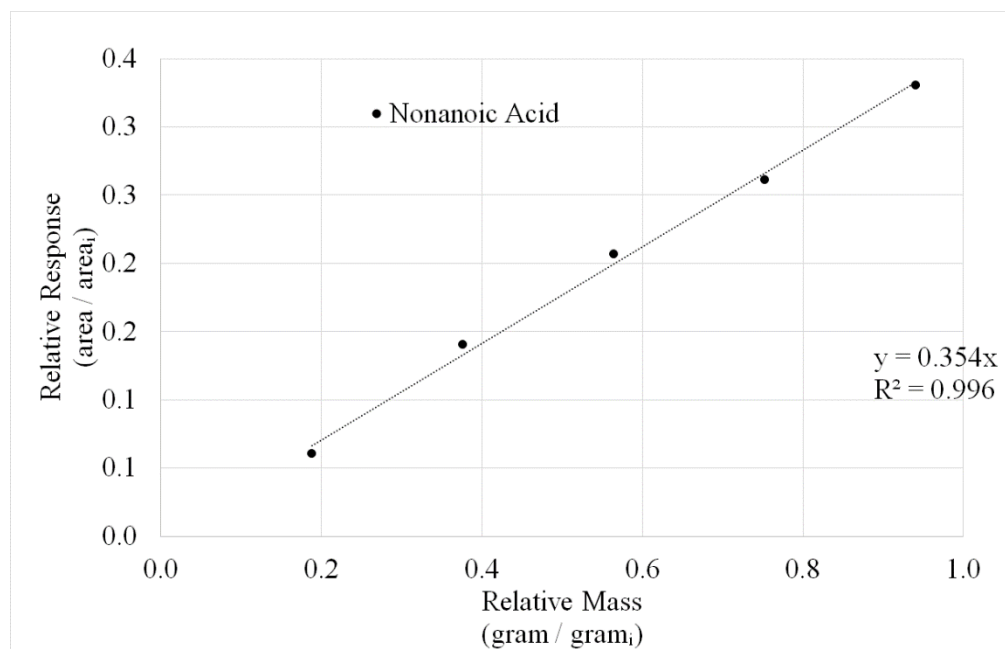
Figure 65. FIMS response vs. mass of nonanoic acid relative to internal standard

In addition, the relative responses of n-paraffins were obtained from a HWD standard (see Figure 130), consisting of n-paraffins in the range of C8-C40 at 500 mg/mL each. By linearizing data from the STDx56 standard and the HWD standard, it was possible to extend the range of FIMS calibration to C30. A complete plot of RIEs is shown in Figure 66 for various functional groups across a full range of carbon numbers.

Based on the author's supplementary experience with FIMS and a thorough review of FIMS literature, these RIEs reported herein would not be anticipated for direct-FIMS. Due to its nature, the RIEs are more uniform and more repeatable with GC-FIMS than for direct-FIMS. The analytes entering the MS from a GC column tend to have similar volatility that leads to similar response. However for direct-FIMS, there is no separation based on volatility and the responses are greatly affected by surface adsorption and/or condensation on the emitter surface.
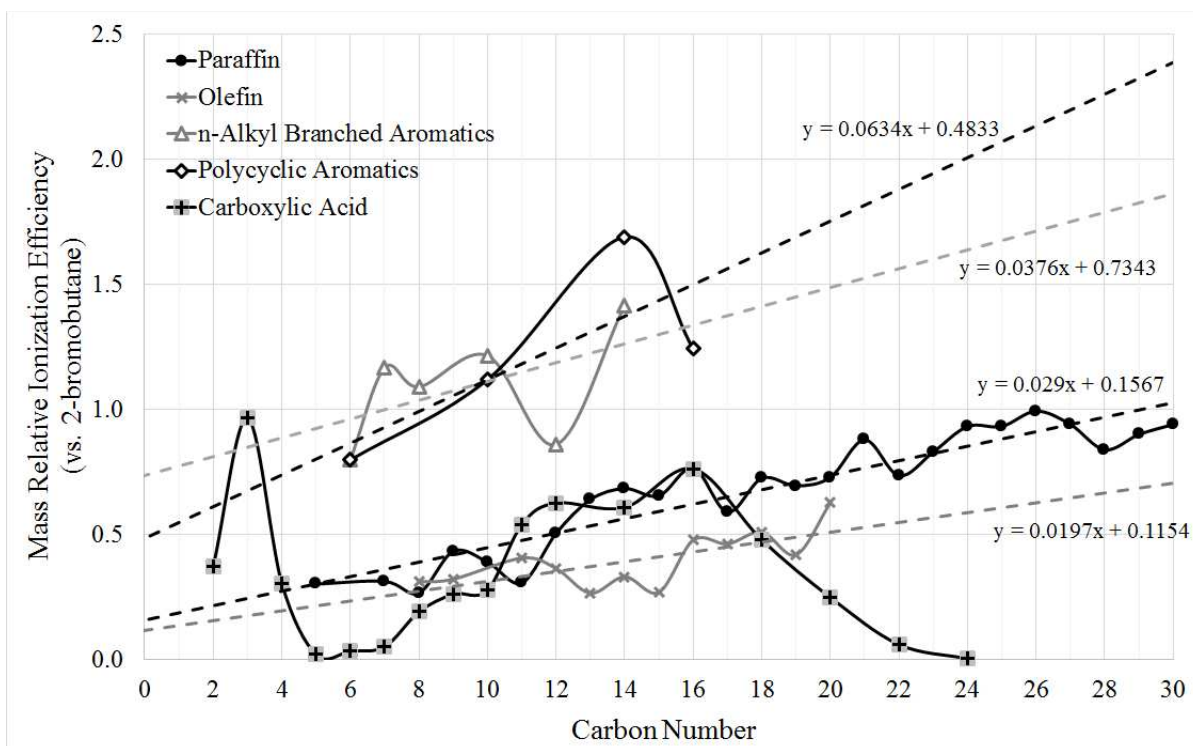
Figure 66. Plot of relative ionization efficiencies for analytes in FIMS

It appears as though most of the RIEs follow a relatively linear trend, except for the carboxylic acids. As indicated, the plots were linearized for n-paraffins, a-olefins, n-alkyl branched aromatics, and polycyclic aromatics.

For carboxylic acids however, it was not possible to linearize due to a dramatic reduction in the RIE in proximity to C5-C6 and above C20. The reason for this drop in RIE is unclear and it hasn't been examined by any of the literature reviewed herein. This drop may also occur in a similar carbon number range for methyl esters based on undocumented side experiments, but this has not been repeated or validated.

The carboxylic acids which have RIEs that were less than 0.25 times the RIE of their corresponding n-paraffin (e.g., C5-C7 and ≥C22) were considered to be too low for quantitation.

Unfortunately there is the potential to mislabel other components with similar exact mass to carboxylic acids if they were included. Since the mass response of a target component is computed (in part) by dividing the integrated response area by the RIE, the result of RIEs being substantially lower than other RIEs is a dramatic false positive of carboxylic acids. In other words, the smaller the RIE, the greater the potential magnitude of a false positive. Since the RIEs tended to remain within half an order of magnitude with one another, this was not a problem for the most of the components considered here. However, it was not possible to use FIMSDIST to quantify C5-C7 carboxylic acids and carboxylic acids above C22 (inclusive).

In order to make up for the inability of FIMSDIST to quantify C5-C7 acids, it was necessary to consider other analytical means. In this dissertation, data have been completed by incorporating data from detailed compositional analysis described in Section V.B.4.i. This analysis was carried out by Geetla in a master's student thesis at UND,[156] and the utilization of Geetla's data is described in Section VI.C (see page 279).

It should be mentioned that it was intended to utilize PIANO standards (see Section V.A.6) to further standardize the FIMS and determine responses for each of the diverse compounds in the PIANO standards, particularly cyclics and isoparaffins, but also aromatics and naphthalenes. Unfortunately the PIANO standards were too dilute, which prevented their utilization with FIMS. As a result, it was not possible to obtain desirable information on the response of isoparaffins and cyclics, and their responses are assumed to be represented by α-olefins and n-paraffins respectively. Future utilization of the FIMSDIST method should consider renewed attempts to use PIANO standards in higher concentration in order to determine the RIEs for a greater variety of components than those of the present work.

Using the RIEs from Figure 66 the CND was recomputed for sample 'AA-Soy' as above, by combining the relative fraction of components in each BPF from FIMS, normalized to the mass fraction of each BPF determined by FID, depicted in Figure 67.

Before doing this, the mass fraction of each BPF was adjusted (enlarged) according to the relative mass fraction of carboxylic acids that were quantified in the BPF. This is based on the assumption that the FID integrated area is linear for quantifying the mass of C_xH_x (according to SimDist methods), and nonlinearity is assumed to only result from the carboxylic acids oxygenation, which is not quantified by the FID. This was previously mentioned in Section VI.A.1. The relative mass fraction of each BPF was then resultantly enlarged to account for the mass of oxygen. Then the relative mass fraction of components quantified by FIMS in each BPF
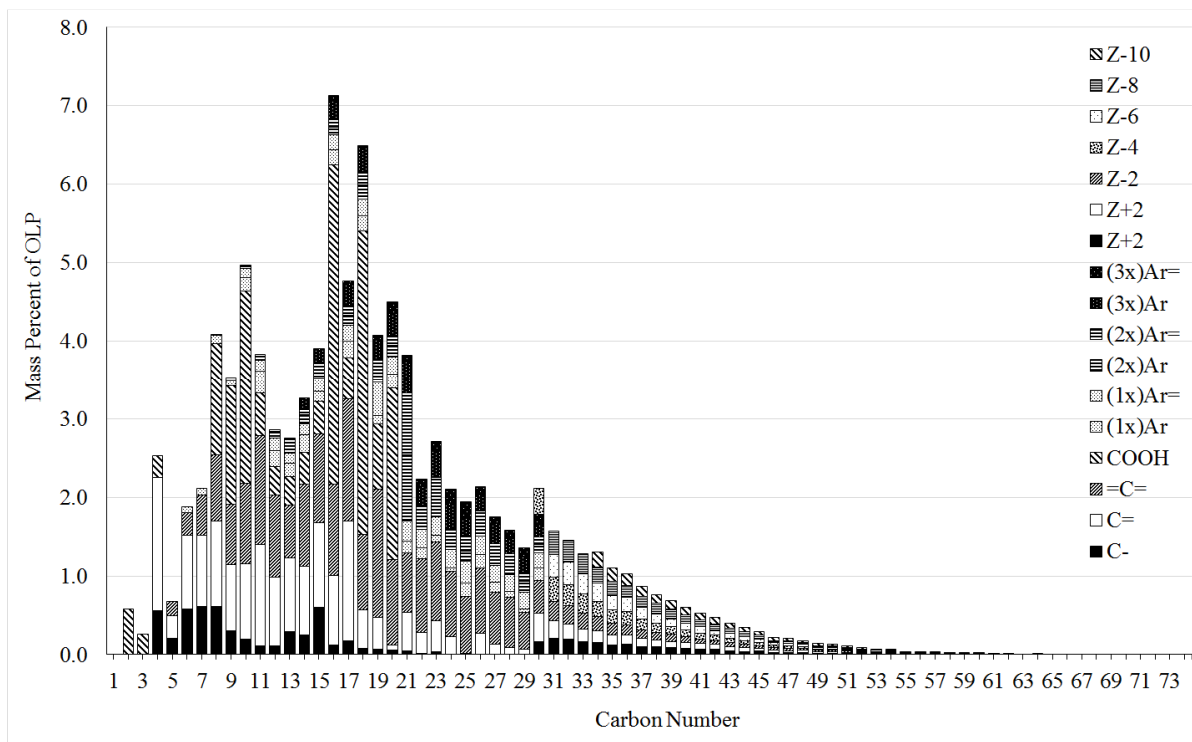
Figure 67. Mass fraction carbon number distribution for sample 'AA-Soy' CTL

were normalized to the adjusted relative mass fraction of each BPF by FID. The combined data was normalized to 100 %, in order to provide a representative composition of CTL.

It should be mentioned that without reliable quantitation for carboxylic acids, C5-C7 and $\geq$C22, there is some expected systematic error in this adjustment. To offer perspective, most of the relative mass fractions of the BPFs were either unaffected or enlarged slightly by between 2-5 %, although some were enlarged by up to 10 % when they were rich in shorter chain carboxylic acids.

For the range of components C31-C74 that are analyzed by the FIMSDIST method, components are reported by their z-group and utilizing an RIE of 1. The mass percentage of each BPF is the major effector of the response of those groups. This is a beneficial aspect of utilizing the dual detector FIMSDIST instead of simply GC-FIMS.

In comparing Figure 67 to Figure 59, the mass fraction CND is shifted towards the smaller carbon numbers. This is partially due to the RIEs becoming smaller as carbon numbers become smaller. In addition, this is due to the higher RIE of aromatics and the smaller RIE of paraffins/olefins. This leads to (1) an increase in the computed mass fraction of paraffins/olefins, which are more heavily concentrated in the lower carbon numbers and (2) a decrease in the computed mass of aromatics, which are more heavily concentrated in the higher carbon numbers.

VI.A.3. Summary of FIMSDIST Data Processing

The first step in FIMSDIST data processing was partitioning the detector data from FID and FIMS into various boiling point fractions (BPFs) spanning the full boiling point range of the analysis. The relative mass fraction of each BPF was determined by integrating the FID signal over each BPF vs. the total integrated FID signal, correcting for the baseline. The mass spectrum

of each BPF was determined by integrating the mass spectra over the entire BPF. Ultimately, the data from each BPF was recombined into a single resultant data set, however before that, the BPFs were processed separately.

The mass spectra of the BPFs were compared to an exact mass ion table (Table 28) in order to identify various ions up to C30. Likewise, the ions for components >C30 were identified by their z-groups, consistent with low resolution FI mass spectrometry (see IV.D and example tables in Appendix K). Typically the integrated quantity of identified ions accounted for over 95 % of the mass spectrum's total intensity and it was over 85 % in all cases, indicating good representation of the data. The mass spectrum of each BPF was adjusted to remove the influence of C^{13} isotopes. Then the relative mass response of each component in the BPF was computed via its relative ionization efficiency (RIEs) from calibration.

The relative mass fraction of each BPF was then enlarged by up to ~10 % to account for the assumed deviation in FID detector linearity on account of carboxylic acids. This assumed that the FID detector was able to detect the mass of C_xH_x linearly, and oxygenation was solely responsible for deviation in the FID detector's response. Then the relative mass fraction of components in each BPF were normalized to the relative mass fraction of each BPF resulting in a representative composition for the CTL.

Carboxylic acids were a source of systematic error, due to the inability to reliably quantify C5-C7 ranged carboxylic acids and ≥C22 acids. This was unexpected and not mentioned in the literature reviewed in Chapter IV.

Additional calibration was desired to further provide RIEs to encompass the range of expected analytes in CTL. The PIANO standards that were attempted to utilize with

259

standardization herein were found to be too dilute to obtain suitable RIEs from. Furthermore, the literature reviewed in Chapter IV did not offer any RIEs that could be utilized herein without severe speculation. As a result, the best possible calibration was utilized for quantitation, based on the data that are available at the present time.

Undoubtedly there is potential for overlapping exact masses of ions leading to misidentification and improper tabulation. However, due to the nature of FIMS being only able to differentiate by molecular weight, it is only possible to speculate about misrepresented ions if they are substantial enough in concentration to warrant further consideration. Such ions are discussed in the next section (VI.B) in order to point out some of the more prevalent ions that appear to be misidentified and/or mechanistically important. Furthermore, the FIMSDIST results are compared to the results from a detailed compositional analysis method in Section VI.C and Section VI.D.

VI.B. Massed-Adjusted FIMS Response

The mass-adjusted FIMS response is presented in the next several figures.

VI.B.1. Massed-Adjusted FIMS Response for Various TAGs

The carbon number distributions (CNDs) are plotted in the following several subsections for the cracking of various TAGs at 435 C temperature, 0.44 h space time, and 2.9 MPa pressure in the 100 mL lab-scale tubular cracking reactor (TCR). The cracking of these TAGs is described in greater detail in Section 0 (see Table 24). The CND's are plotted to represent data that is the mass-adjusted FIMS response. To reiterate, these are not mass fraction CNDs because they have not yet been adjusted to their relative ionization efficiencies (RIEs) for various components, as described previously in Section VI.A.2 (see Figure 59). Mass fraction CNDs

260

will be presented as needed, however all are included in Appendix J.

The CNDs comprised of mass-adjusted FIMS data are useful to discuss because there are some unexpected outlier ions that may be improperly identified and/or important to the mechanism.   In addition, this mass-adjusted FIMS response view is helpful for observing generalities about the CND of CTL from various types of TAG processed at various operating conditions.

In addition, the plots have been limited to carbon numbers C1-C30, in which the carbon numbers are described by functional groups. Higher carbon numbers are represented by z-groups in the form of a z-table. These can be combined in a single CND as depicted in Figure 59 (see Section VI.A.2), but the mechanistically interesting region of the CND is in the range of C1-C30. All tabulated data, including z-tables and CND tables are provided in Appendix I through Appendix K.

VI.B.1.i. Soybean TAG

A carbon number distribution is shown in Figure 68 for the CTL from the cracking of soybean TAG at 435 C temperature, 2.9 MPa pressure, and 0.4 h space time in the 100 mL lab-scale TCR (i.e., sample 'AA-Soy' from Table 24). A diverse composition of organic molecules is observed. The mass adjusted FIMS response for the total carbon numbers below C13 is relatively low in comparison to the carbon number range C13 and greater. This is an undesired outcome for producing lighter, more valuable fuels. However, previous observation from FID data indicates that better operating conditions should be utilized in order to increase the percentage in this range (as previously mentioned in Section VI.A.1).

Several large ions are noticeable in the CND, including palmitic acid (COOH 16), stearic

acid (COOH 18), *m/z* 280.2, and *m/z* 282.2 as indicated in the figure. Palmitic acid and stearic

acid are most likely the result of fatty acids that have cracked off the TAG molecule's backbone

and not undergone any subsequent cracking reactions during the reaction time that was allowed.

This is a sensible conclusion due to the mechanistic insights pointed out on page 86, combined

with the relatively brief space time of the reaction in comparison to other cracked TAGs.

Furthermore, the presence of these acids is significant in soybean TAG, as described by the TAG

composition data presented in Table 1.

Concerning ions 280.2 *m/z* and 282.2 *m/z*, these ions have very nearly equivalent exact

masses to the molecular ions of oleic acid (COOH 18:1) and linoleic acid (COOH 18:2)

respectively. The mass error between the (2x)Ar 21 and oleic acid (COOH 18:1) is only about
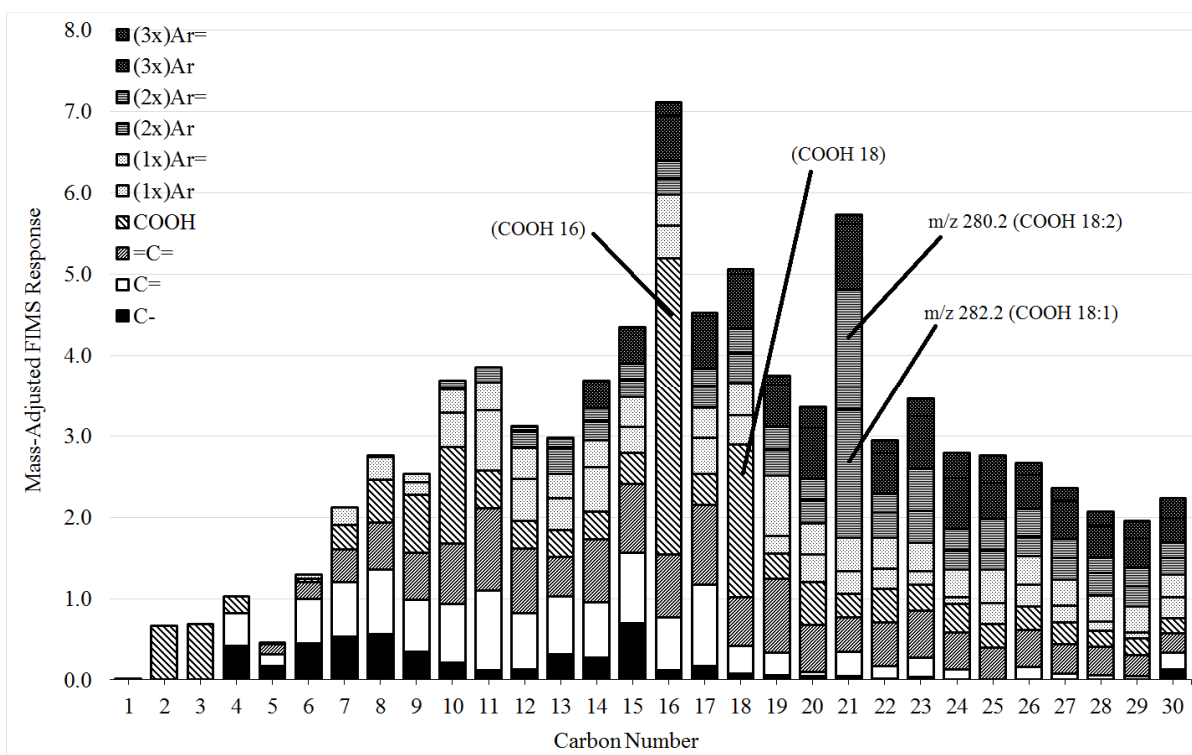
Figure 68. CND (1-30) of AA-Soy CTL, mass adjusted FIMS response

0.021 *m/z*. The same mass error is observed for (2x)Ar= 21 and linoleic acid. Due to their close mass proximity, it is very difficult to resolve the masses of their ions with FIMS in confidence, especially on account of (1) FIMS being subject to reduced resolution compared to EIMS and (2) FIMS cannot rely on PFK for exact mass referencing. As a result, the identity of the ions is determined intuitively and tentatively but not confirmed. Based on the high quantity of oleic acid and especially linoleic acid moieties in the soybean TAG feedstock, the ions are most likely unsaturated acids that have only cracked off the TAG backbone and cracked no further. So they will be stated as such herein.

It is curious why in previous literature referenced, such as Luo,[54] that unsaturated carboxylic acids did not present in significant quantities. However in the CTL produced from this study, the ions corresponding to unsaturated carboxylic acids are presenting in greater quantity (which will continue to be observed in the following several subsections). Without a greater resolution mass spectrometer, the FIMSDIST method used to analyze these CTL samples is poorly suited and otherwise incapable of resolving the mass differences between the (2x)Ar 21 and oleic acid and so forth.

VI.B.1.ii. Very High Oleic Novelty TAG

A carbon number distribution is shown below in Figure 69 for the CTL from the cracking of VHONO TAG at 435 C temperature, 2.9 MPa pressure, and 0.4 h space time in the 100 mL lab-scale TCR (i.e., sample 'BB-VHONO' from Table 24). A similar array of molecules are observed as with the previous sample AA-Soy CTL, including a low percentage of compounds ranged < C13.

Noticeable differences between Soybean CTL and VHONO CTL include a substantially

increased quantity of decanoic acid (COOH 10), a substantially decreased amount of palmitic

acid (COOH 16), and a slightly decreased amount of stearic acid (COOH 18). This may indicate

that decanoic acid is produced as a result of oleic acid decomposition.
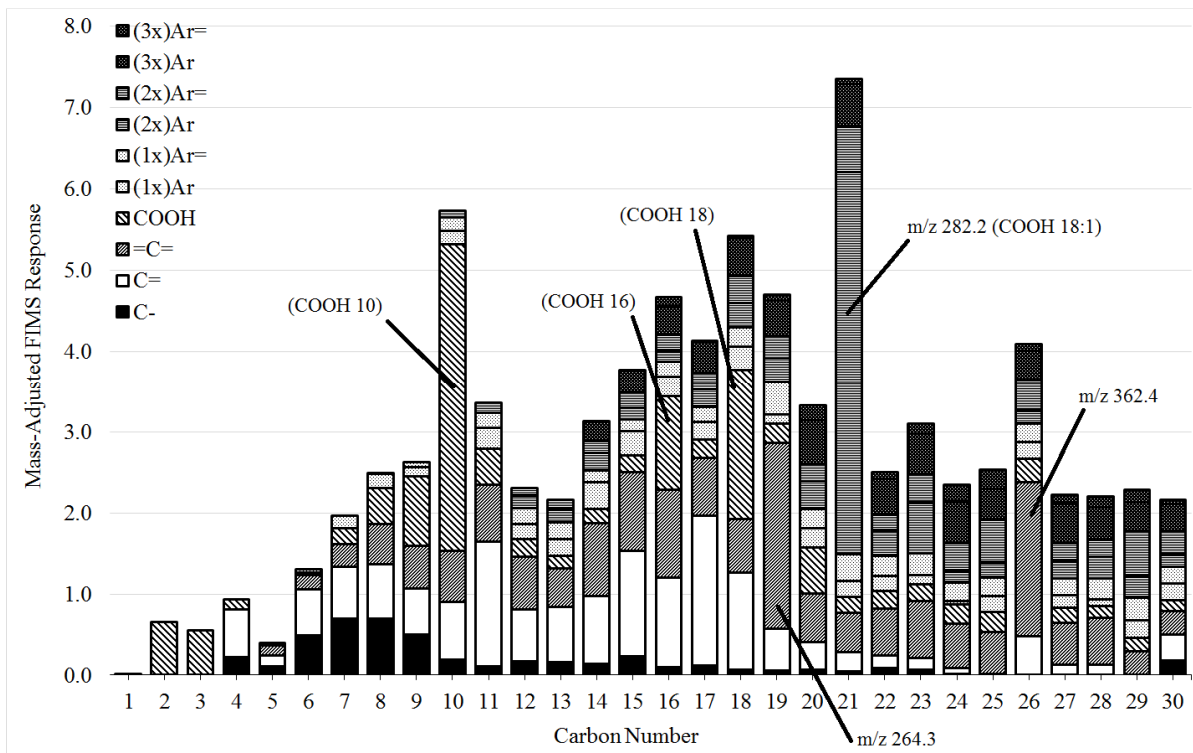
Figure 69. CND (1-30) of BB-VHONO CTL, mass adjusted FIMS response

In addition, the peak previously identified as being oleic acid (*m/z* 282.2) is on the order of three

times larger than for AA-Soy, and the peak that was previously identified as being linoleic acid

(*m/z* 280.2) is no longer reasonably significant in size. This coincides directly to the composition

of VHONO TAG described in Table 1, in which VHONO TAG has substantially more oleic acid

and substantially less linoleic acid moieties than soybean TAG. This increases the confidence

that ion *m/z* 282.2 is oleic acid.

Similar mass-adjusted FIMS response CND's for the CTL from Canola and HONO are also observed and included in Appendix I. The difference tended to be that oleic acid was slightly less in HONO and even less in Canola TAG respectively. Palmitic acid was also substantially greater in Canola TAG than for either HONO of VHONO. Although the decanoic acid response was extremely strong in VHONO, the response in HONO and Canola was only on the order of 50 % greater than for Soybean TAG. In examining the composition of VHONO, HONO, and Canola TAG in Table 1, the reduced response of decanoic acid may be due to a decrease in the concentration of oleate moieties in the HONO and Canola TAG compared to VHONO TAG.

Two ions are in high concentration in VHONO and potentially important from a mechanistic standpoint, *m/z* 362.4 and *m/z* 264.3. These may be linked to the composition of the TAG feedstock, which is predominantly oleic acid. Furthermore, they are 98 Da apart, potentially indicating that they are separated by 7x –(CH$_2$)– groups differing in mass. This will be re-examined and discussed in the following subsection for high erucic novelty TAG.

VI.B.1.iii. High Erucic Novelty TAG

A carbon number distribution is shown in Figure 70 for the CTL from the cracking of HENO TAG at 435 C temperature, 2.9 MPa pressure, and 0.4 h space time in the 100 mL lab-scale TCR (i.e., sample 'CC-HENO' from Table 24). In like manner to the previously cracked TAGs, the CTL here shows a relatively low response in the < C13 range molecules, indicating non-optimal formation of components that are relevant for lighter fuels. Out of the lesser acids, decanoic acid is fairly dominant, similar to VHONO. This is an interesting result, potentially

indicating that decanoic acid is a decomposition product from erucic acid (COOH 22:1) as well as oleic acid (COOH 18:1).

It is interesting that the HENO TAG produced a large variety of ions in the range of undercracked fatty acid moieties (C21-C25). Concerning longer chain saturated carboxylic
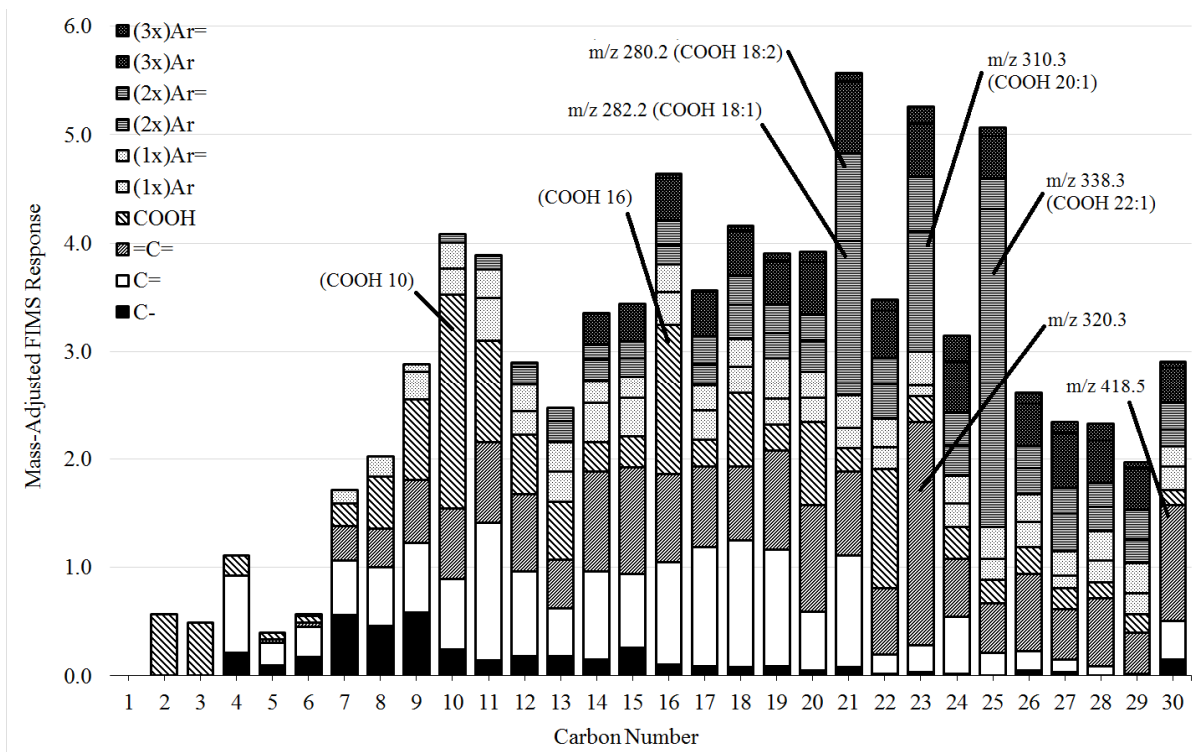
Figure 70. CND (1-30) of CC-HENO CTL, mass adjusted FIMS response

acids, HENO CTL appears to contain a fair amount of palmitic acid and docosanoic acid (COOH 22:0). Concerning unsaturates, HENO contains dominant ions that were previously identified as oleic acid and linoleic acid (not designated below).

HENO CTL also has a very prevalent ion at m/z 338.3, which is very nearly exactly the

mass of erucic acid (COOH 22:1), from which HENO derives its name. As a result, it is likely

that *m/z* 338.3 is actually free erucic acid in the CTL.

One disadvantage to having undercracked erucic acid in the CTL is that these very long

chain fatty acids (approximately > C20) have dramatically reduced FIMS response, as previously

mentioned in Section VI.A.2. At the present state of the research, there is no explanation for

why the FIMS response of these very long chain fatty acids is so low. However, the unfortunate

result is that the conversion of carboxylic acids which have a chain length C22 and greater to

mass basis using FIMS is not recommended. Furthermore, no calibration was made for

unsaturated carboxylic acids.

Other ions were present in significant quantities, including *m/z* 310.3, *m/z* 320.3, and *m/z*

418.5. Undercracked carboxylic acids in the CTL, specifically eicosenoic acid (COOH 20:1),

may be responsible for *m/z* 310.3, due to eicosenoic acid's minor presence in the HENO TAG,

however it was not one of the fatty acid moieties that were strongly considered in Table 1.

The identity of *m/z* 320.3 and *m/z* 418.5 are as of yet unknown. However, it is interesting

to observe that the masses are 98 Da apart, potentially indicating that they are separated by 7x –

(CH$_2$)– groups differing in mass. A similar occurrence was observed with two dominant,

unidentified contributors in VHONO (*m/z* 362.4 and *m/z* 264.3) that were also separated by 98

Da. The following table indicates these ions.

Table 29. Unidentified ions of mechanistic significance in VHONO and HENO CTL

TAG Type	VHONO	HENO
Dominant Fatty Acid Moiety	COOH 18:1	COOH 22:1
Unidentified Species 1 (*m/z*)	264.3	320.3
Unidentified Species 2 (*m/z*)	362.4	418.5

Whereas the rows are separated by 98 Da, it is interesting to note that the columns are separated by 56 Da, which is consistent with 4x –(CH$_2$)– groups. Furthermore, the dominant fatty acid moiety of VHONO and HENO are also separated by 56 Da. Due to the similar composition of the HENO TAG and the VHONO TAG, the identification of these ions may help clarify the mechanism of triglyceride degradation. This is examined in Section VIII.D.

VI.B.1.iv. Linseed TAG

A carbon number distribution is shown in Figure 71 for the CTL from the cracking of Linseed TAG at 435 C temperature, 2.9 MPa pressure, and 0.4 h space time on the 100 mL lab-scale TCR (i.e., sample 'DD-Linseed' from Table 24). Linseed TAG has one of the highest concentrations of linolenic acid (COOH 18:3) in any natural TAG source, so it was a proper choice for examining the effect of linolenic acid in the TAG feedstock.
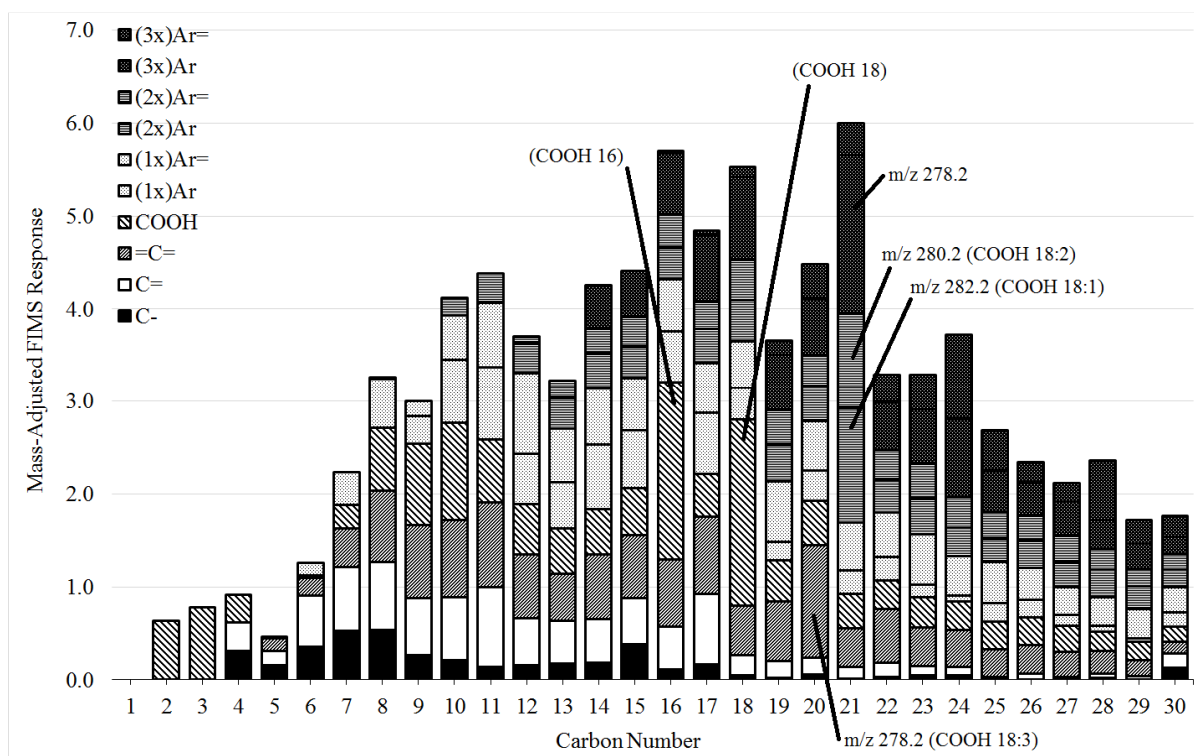
Figure 71. CND (1-30) of DD-Linseed CTL, mass adjusted FIMS response

As in previous findings of unsaturated carboxylic acids in the CTL, the mass error between linolenic acid (COOH 18:3) is closely observed with (=C= 20) of about *m/z* 278.2. Due to the high response of (=C= 20) in the linseed CTL, it is natural to assume that the (=C= 20) is indeed linolenic acid (COOH 18:3). This has been marked in the figure.

Additionally, oleic acid (COOH 18:1) and linoleic acid (COOH 18:2) are noticeable in the figure as noted according to the previous identifications of the ions. These presumably result from undercracked fatty acid moieties of the original TAG feedstock as previously alluded with other TAGs. Significant amounts of palmitic acid (COOH 16) and stearic acid (COOH 18) are also observed.

What is interesting to note is the presence of *m/z* 278.2 at an even higher response than for linolenic acid (COOH 18:3). This may be a result of a 4x unsaturated fatty acid (COOH 18:4), a.k.a. octadecatetraenoic acid. Additionally, this 4x unsaturated fatty acid may be a precursor for aromatic formation, which will be discussed in Section VIII.D.

VI.B.1.v. Camelina TAG

A carbon number distribution is in Figure 72 for the CTL from the cracking of Camelina TAG at 435 C temperature, 2.9 MPa pressure, and 0.4h h space time in the 100 mL lab-scale TCR (i.e., sample 'EE-Camelina' from Table 24). Camelina TAG was selected for this experiment due to its relatively balanced composition of fatty acid moieties. As such, it seems sensible that there aren't any noticeable outliers in the CND of its CTL.

In examining the ions, there appears to be relatively little that can be commented other than what-you-see-is-what-you-get. The significant carboxylic acids appear to be palmitic acid and eicosanoic acid. Groups such as C-, C=, =C=, and various aromatics do not appear to have

any dominant components throughout the CND.
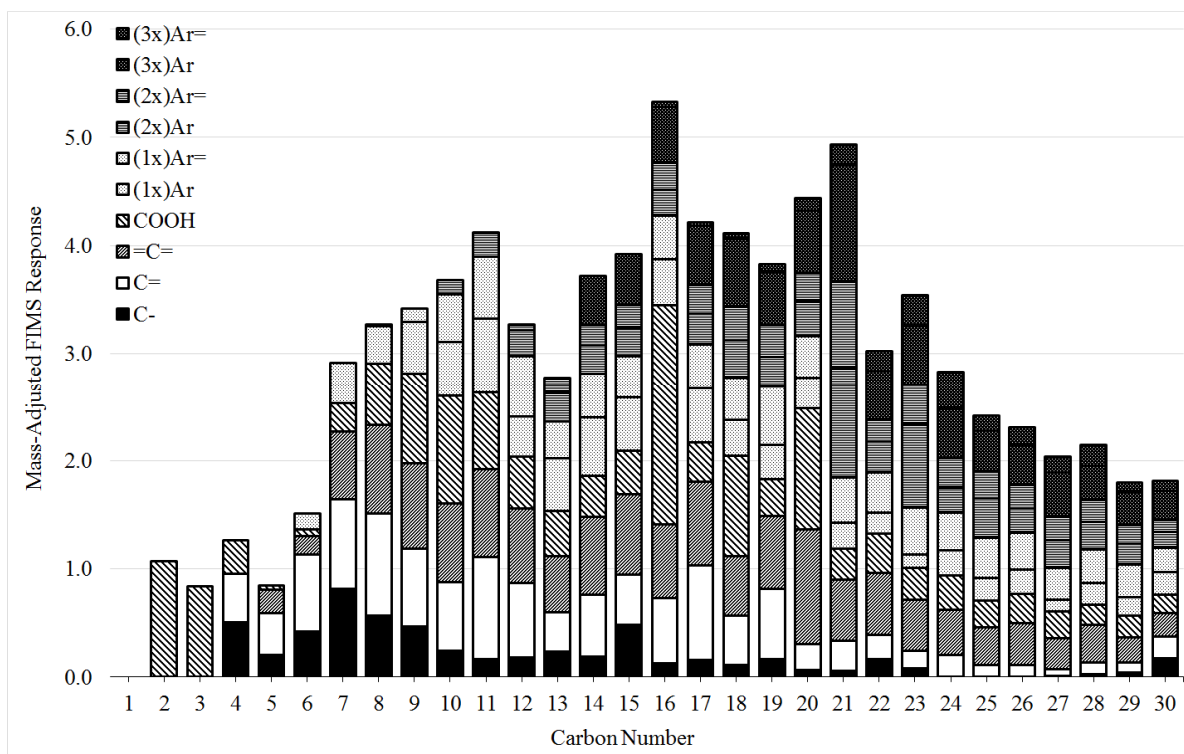
Figure 72. CND (1-30) of EE-Camelina CTL, mass adjusted FIMS response

VI.B.1.vi. Corn TAG

A carbon number distribution is shown in Figure 73 for the CTL from the cracking of Corn TAG at 435 C temperature, 2.9 MPa pressure, and 0.4 h space time in the 100 mL lab-scale TCR (i.e., sample 'FF-Corn' from Table 24). Some of the major acids include palmitic acid, linoleic acid, and oleic acid. These are present in relatively high amounts in both the CTL and in the feedstock TAG, which is indicative that they are undercracked fatty acid moieties. This agrees with the CTLs from other TAGs previously described.
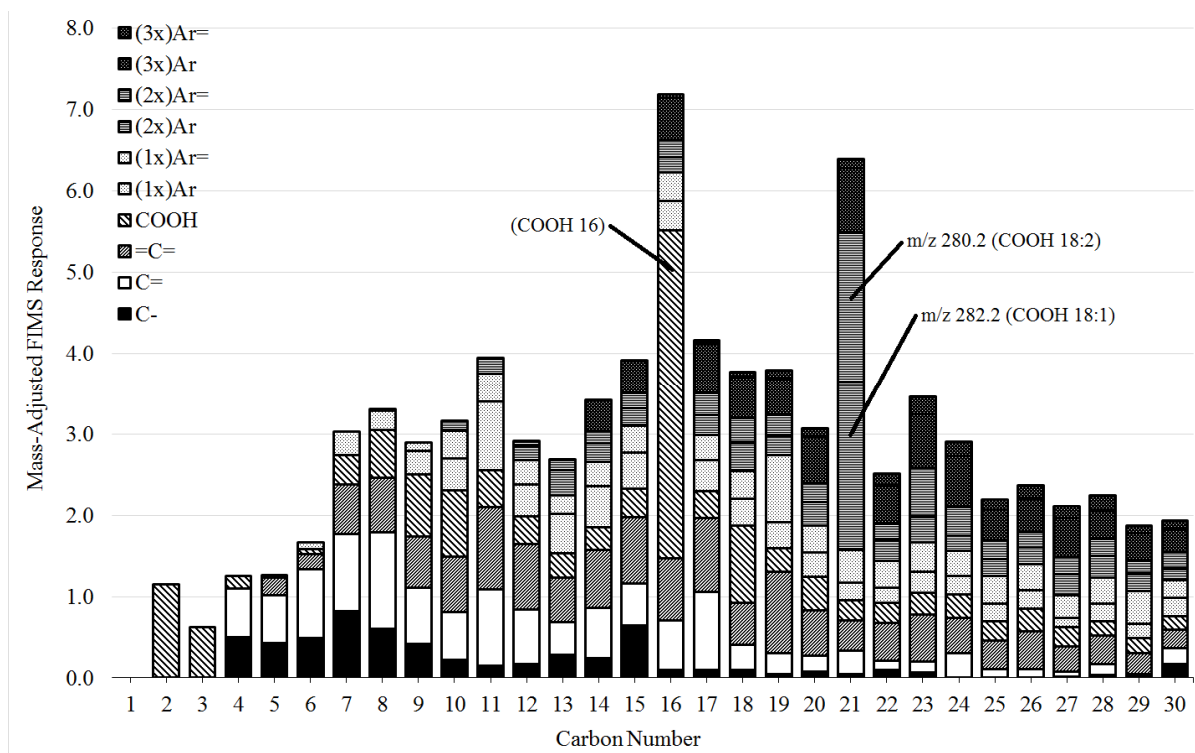
Figure 73. CND (1-30) of FF-Corn CTL, mass adjusted FIMS response

VI.B.1.vii. Cottonseed TAG

A carbon number distribution is shown in Figure 74 for the CTL from the cracking of Cottonseed TAG at 435 C temperature, 2.9 MPa pressure, and 0.4 h space time in the 100 mL lab-scale TCR (i.e., sample 'GG-Cottonseed' from Table 24). Consistent with previous CTLs, the largest outliers tend to be carboxylic acids. Palmitic acid greatly dominates the CTL, which is directly relatable to its high concentration as a moiety of the feedstock cottonseed TAG (Table 1). Other significant acids observed include oleic acid (COOH 18:1) and linoleic acid (COOH 18:2), corresponding to previous descriptions.
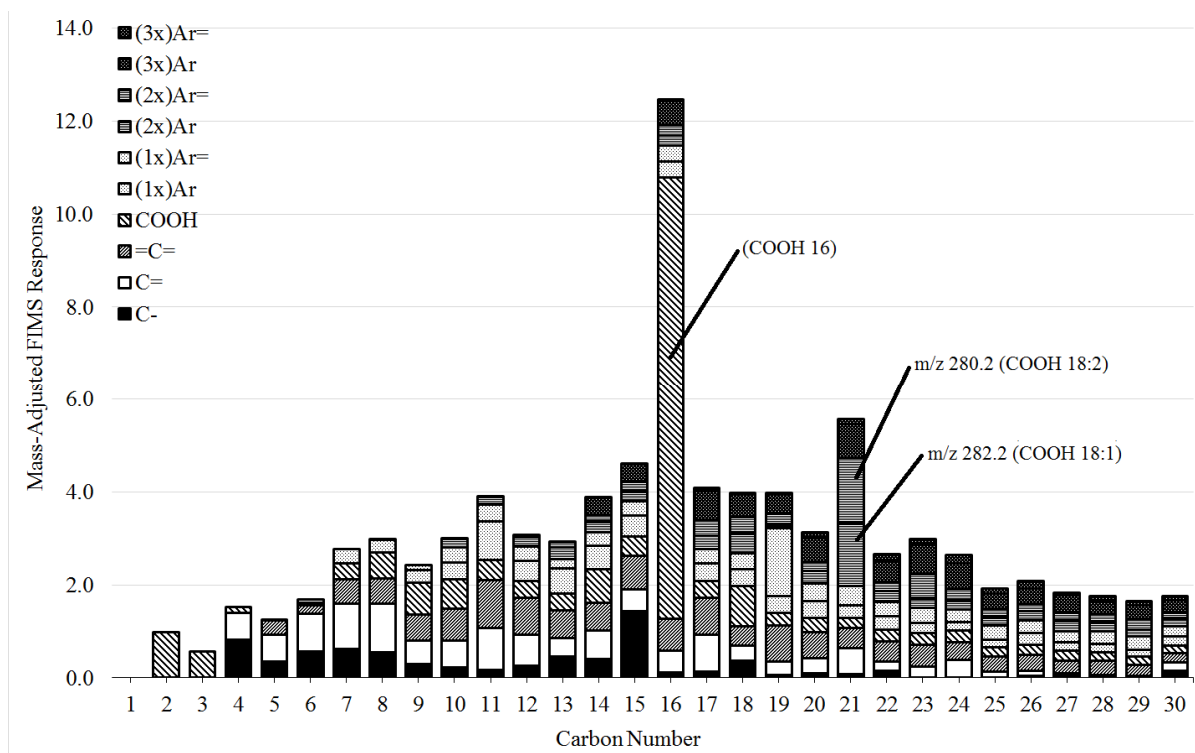
Figure 74. CND (1-30) of GG-Cottonseed CTL, mass adjusted FIMS response

VI.B.2. Mass-Adjusted FIMS Response for Various Operating Conditions

Various carbon number distributions are shown in the following subsections in order to visibly indicate the trends in the CTL distribution that result from cracking reaction temperature and residence time. This is done in order to help assess the validity of FIMSDIST in a latter section. Some carbon number distributions were not necessary to show herein, however all have been included in Appendix I.

VI.B.2.i. Low Temperature, Short Residence Time Soybean TAG Cracking

A carbon number distribution is shown in Figure 75 for the CTL from the cracking of soybean TAG at 420 C temperature, 2.9 MPa pressure, and 0.27 h space time in the 100 mL lab-scale TCR (i.e., sample 'A-Soy' from Table 24). In terms of operating conditions, these are the mildest reaction conditions that were utilized in this set of experiments, having a relatively low

temperature and a relatively short reaction time.

The dominant ions in Figure 75 are similar to those of Figure 68 above for sample 'AA-Soy,' indicating that they are undercracked fatty acid moieties from the original TAG feedstock. In the case shown in Figure 75 however, their magnitude is even stronger than for sample 'AA-Soy.' The ions are not redundantly marked because they are already marked in Figure 68.
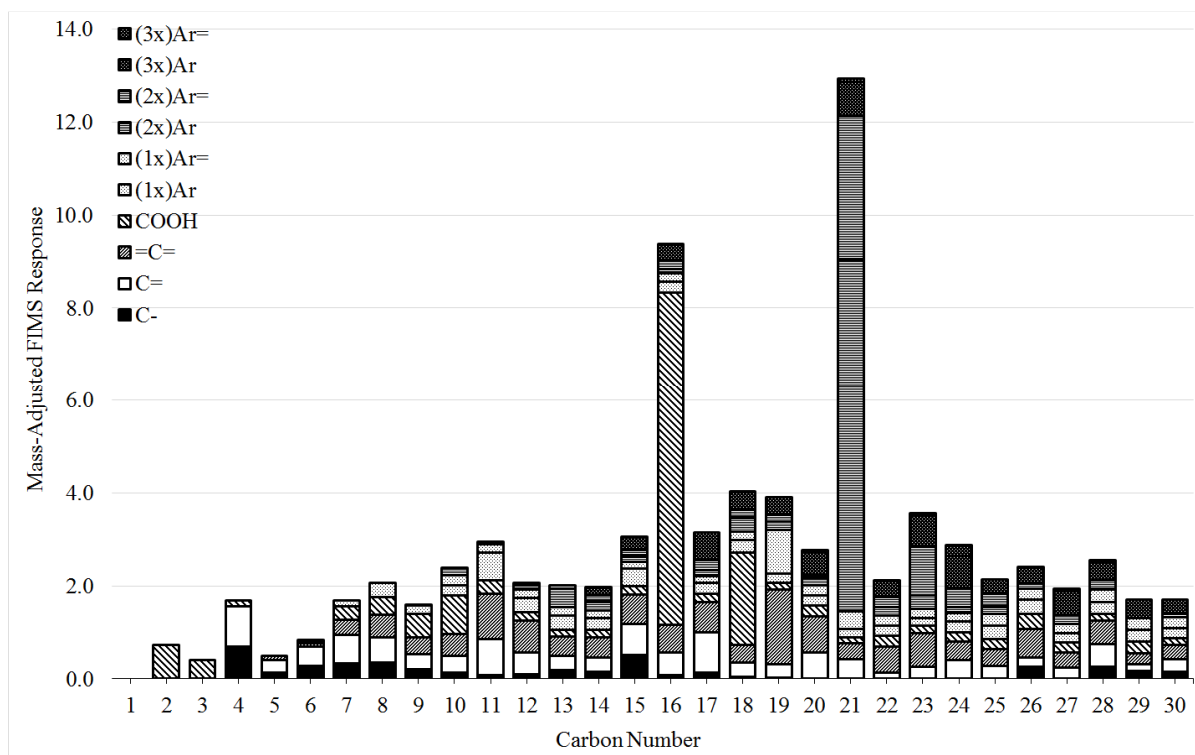
Figure 75. CND (1-30) of A-Soy CTL, mass-adjusted FIMS response

The increased response of the moieties compared to sample 'AA-Soy' may be explained by the 15 C cooler reactor temperature and/or the ~38% less residence time in the reactor when 'A-Soy' was produced (see Table 24). The cooler temperatures and shorter times were

273

characteristic of less-complete reaction. As a result, the fatty acid moieties tended to crack off the TAG backbone, but were not be given enough time/energy to further degrade into smaller fragments.

VI.B.2.ii. Middle Temperature, Short Residence Time Soybean TAG Cracking

A carbon number distribution is shown in Figure 76 for the CTL from the cracking of soybean TAG at 430 C temperature, 2.9 MPa pressure, and 0.27 h space in the 100 mL lab-scale TCR (i.e., sample 'B-Soy' from Table 24), with a 10 C increase in reaction temperature from the previous case. In like manner to sample 'A-Soy', the major undercracked fatty acid moieties are visible in the CTL from the TAG feedstock. However, due to the 10 C increase in reaction temperature, they are less prominent when compared to the rest of the groups than for 'A-Soy.'
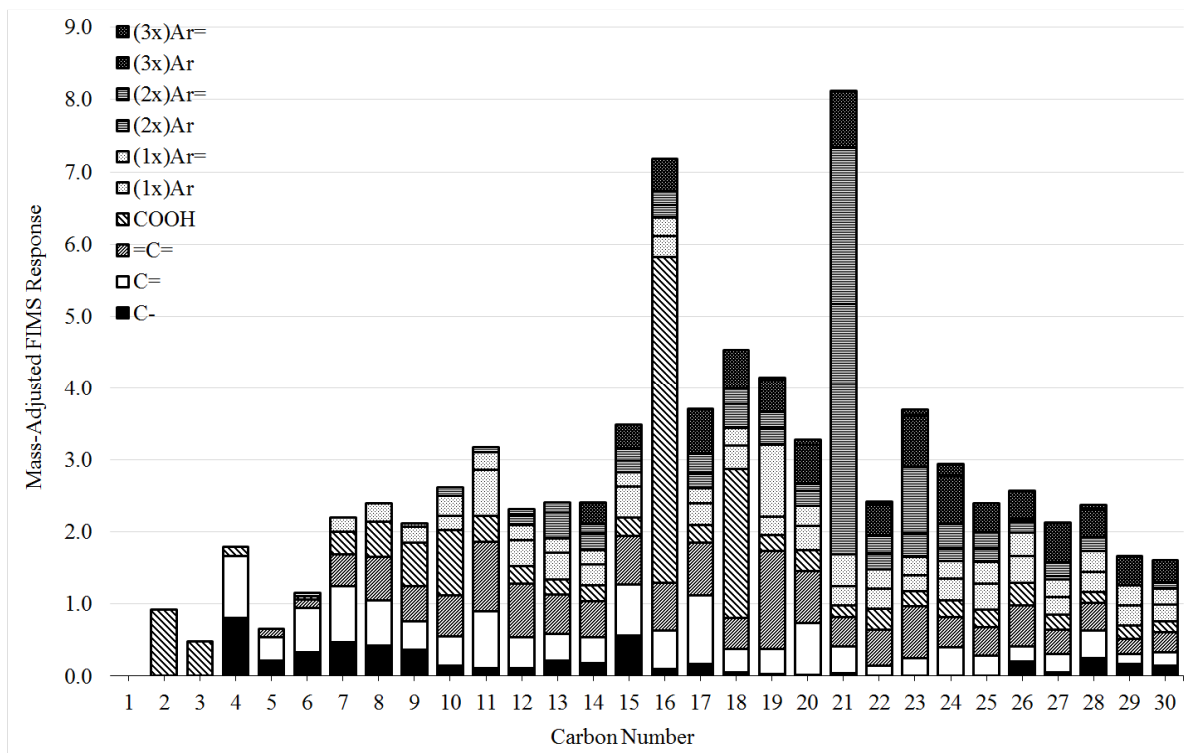
Figure 76. CND (1-30) of B-Soy CTL, mass-adjusted FIMS response

The increased temperature is therefore allowing increased cracking, which is apparent from the greater breakdown of fatty acid moieties and/or greater formation of various products.

VI.B.2.iii. High Temperature, Short Residence Time Soybean TAG Cracking

A carbon number distribution is shown in Figure 77 for the CTL from the cracking of soybean TAG at 440 C temperature, 2.9 MPa pressure, and 0.27 h space time in the 100 mL lab-scale TCR (i.e., sample 'C-Soy' from Table 24). Considering the range of operating conditions, this sample was produced at the highest temperature and the briefest residence time.

In likewise trend with samples 'A-Soy' and 'B-Soy,' fatty acid moieties are clearly visible in the CTL, standing out from the other components. However, the moieties become even less significant with further increasing reaction temperature. It therefore follows that as temperature increases, the fatty acid moieties which are released from their TAG backbone are
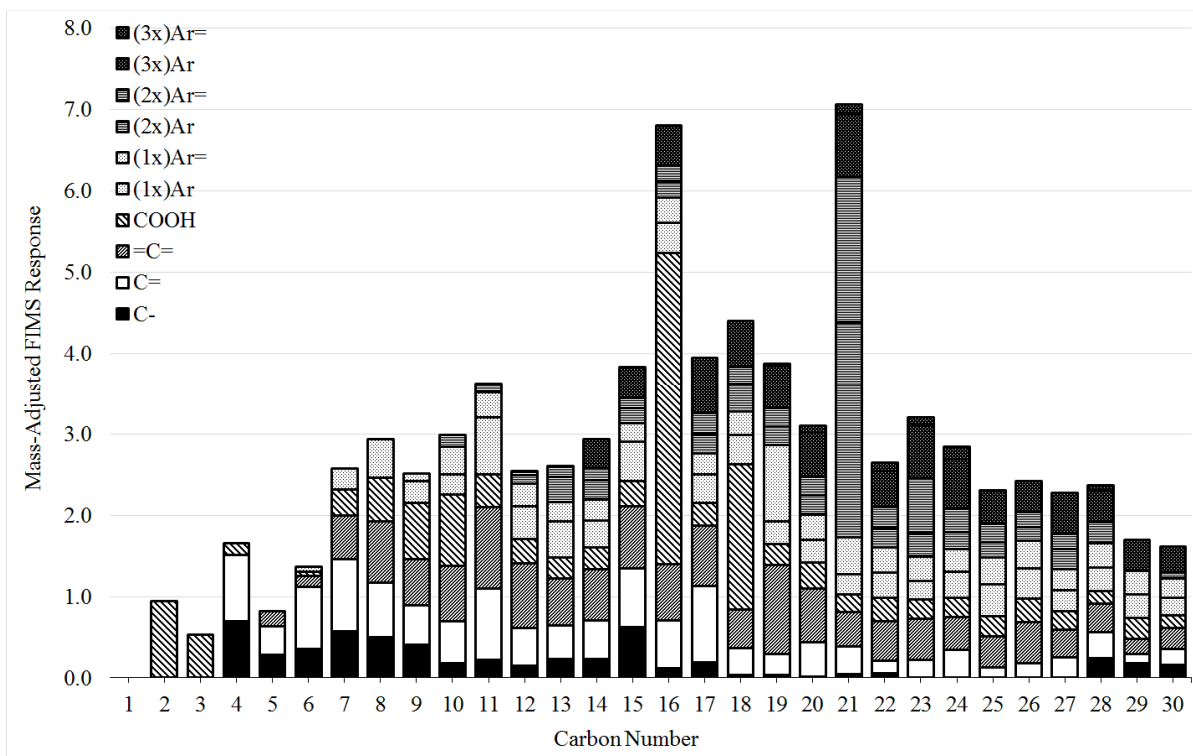
Figure 77. CND (1-30) of C-Soy CTL, mass-adjusted FIMS response

further degrading to a variety of cracked products. This is explainable through the reaction temperature increasing reaction severity.

The correlation of increasing reaction temperature to increase cracking reaction severity is supported by the FTIR analysis of CTL described on page 365. FTIR found that the extent of TAG degradation increased with increasing temperatures at short residence times as determined by the disappearance of residual TAG backbone ester bonds. It is then logical to assume that not only are more fatty acid moieties released from the TAGs, but also more fatty acids moieties are subsequently degraded into cracked products.

VI.B.2.iv. High Temperature, Moderate Residence Time Soybean TAG Cracking

A carbon number distribution is shown in Figure 78 for the CTL from the cracking of soybean TAG at 440 C temperature, 2.9 MPa pressure, and 0.69 h space time, in the 100 mL lab-scale TCR (i.e., sample 'F-Soy' from Table 24) The reaction conditions which the sample were produced are the highest temperature and at a moderate residence time.

What is evident from the carbon number distribution is that the undercracked fatty acid moieties are becoming increasingly less significant. This agrees with previous comments about reaction severity being dependent on time and temperature.

It should also be pointed out that the unsaturated fatty acid moieties appear to be more strongly affected by the operating conditions than the saturated fatty acid moieties. As FIMSDIST is presented herein, it should be reiterated that FIMSDIST was not intended to be used to detect and/or study undercracked fatty acid moieties, and their identity is speculative, although convincing.
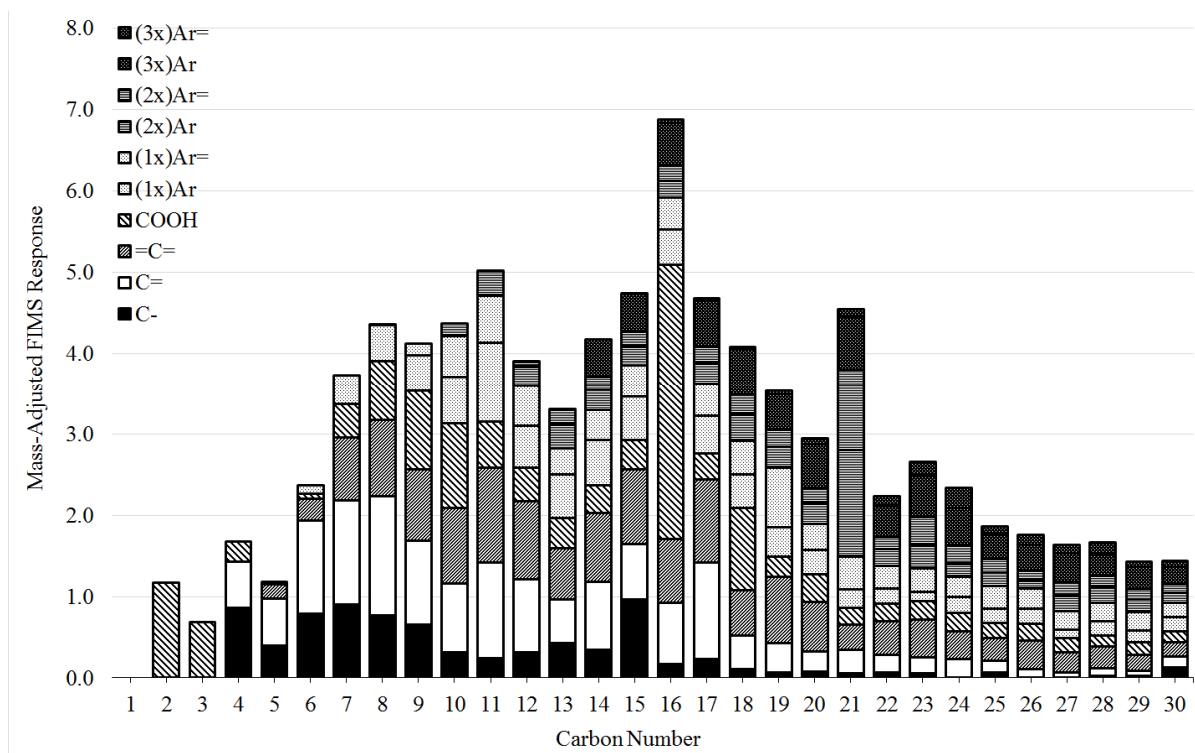
Figure 78. CND (1-30) of F-Soy CTL, mass-adjusted FIMS response

VI.B.2.v. High Temperature, Long Residence Time Soybean TAG Cracking

A carbon number distribution is shown in Figure 79 for the CTL from the cracking of Soybean

TAG at 440 C temperature, 2.9 MPa pressure, and 1.10 h space time in the 100 mL lab-scale

TCR (i.e., sample 'I-Soy' from Table 24) The operating conditions used to produce this sample

were relatively the highest temperature and the longest space time. In comparison to the

previous CND for a moderate residence time, it is apparent that the presence of the ions for

unsaturated fatty acid moieties are completely indistinguishable from the bulk of the sample. In

addition, saturated fatty acid moiety appears to be less prominent as well.

Therefore, it follows that when the temperature is increased to this level, the unsaturated

fatty acid moieties are sufficiently reacted so as to not stand out in the CTL. As a result, any

277
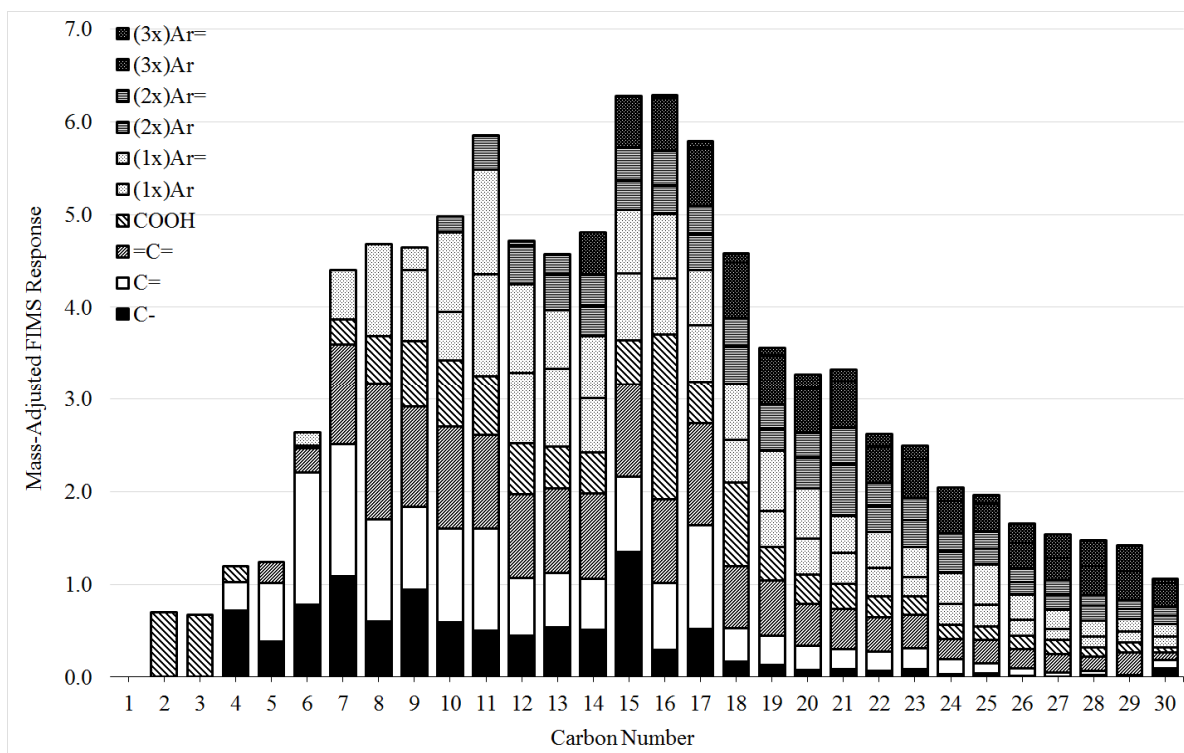
Figure 79. CND (1-30) of I-Soy CTL, mass-adjusted FIMS response

presence of unsaturated fatty acid moieties may be assumed negligible, and the CTL composition

tends to appear closer to the findings of Luo, who reported a lack of unsaturated carboxylic acids

in the CTL.[54] The ultimate outcomes for the data provided by FIMSDIST as presented herein

are these: (1) at milder reaction severity, FIMSDIST speciation may be only valid up to C18 due

to the presence of speculative unsaturated fatty acid moieties in the CTL that were unanticipated;

and (2) at more intense reaction severity, FIMSDIST speciation may be valid up through C30 as

intended due to a lack of unsaturated carboxylic acid moieties in the CTL. This is useful for the

simulation of process yield in a latter section.

In addition to the effects of temperature and space time, pressure was also considered in

samples J-Canola through N-Canola as described by Table 24. Although the mass-adjusted

FIMS response was found to change with pressure, it was not found to do so to a noticeable extent in graphical form. As a result, the mass-adjusted FIMS response CNDs for these samples are included in Appendix I. The effect of pressure is considered on a mass basis in a latter section through the use of statistics.

VI.C. Direct Comparison of Carboxylic Acids in Cracked Triglyceride Liquids Quantified by the FIMSDIST Method and by the Detailed Compositional Analysis

The mass-adjusted FIMS response for various TAGs tended to reveal that the CTLs from TAG cracking contained a significant percentage of undercracked fatty acid moieties. This was true for the TAG that was cracked under reaction conditions of 435 C temperature, 2.9 MPa pressure, and 0.4 h space time in the 100 mL lab-scale TCR. The most significant mass-adjusted ions tended to be carboxylic acids that were directly relatable to the composition of their original TAG feedstocks. This included unsaturated carboxylic acids, which were not found and/or reported in the work of Luo.[54]

The samples of CTL that were characterized by FIMSDIST were also recently characterized for their carboxylic acid composition by Geetla in a master's student thesis presented to UND.[156] Geetla also found up to ~15% unsaturated carboxylic acids (as a mole percentage of the total molar carboxylic acids) in various TAGs. This is helpful to validate the existence of unsaturated carboxylic acids in the CTL studied in the current work using the FIMSDIST method.

One advantageous observation from Geetla's characterization of these CTLs is that all of the unsaturated carboxylic acids in the CTL tended to be C18 and higher, as a direct result of the TAG's fatty acid moieties. No unsaturated short chain carboxylic acid moieties were present in the CTL. This is advantageous for FIMSDIST because the mass error between unsaturated fatty

acids and adjacent ions is too small to resolve and identify the unsaturated carboxylic acids

reliably in this study unless the fatty acids are outliers. Therefore, the utilization of FIMSDIST

below C18 should be considered to be valid, whereas above C18 should be subject to some

questionability of the results. It should also be noted that a higher resolution mass spectrometer

should be capable of resolving the unsaturated carboxylic acids and adjacent ions in future

expansions to this work.

In order to further compare and validate the FIMSDIST approach to CTL

characterization, Geetla's results are presented herein below and furthermore in Appendix G in

graphical form and tabulated form. This also helps identify limitations to FIMSDIST's abilities

and helps fill in previously mentioned gaps in the data FIMSDIST is able to provide.

Figure 80 is a plot of the carbon number distribution (wt. % basis) of saturated carboxylic

acids taken from Geetla and compared to the results of FIMSDIST for sample 'AA-Soy,' which

was prepared according to the specifications in Table 24. Geetla reported her data as the mol %

of total carboxylic acids, so it was necessary to adjust her samples to a mass % and furthermore

adjust that data to normalize the mass percentages to the same range as those provided by

FIMSDIST, as shown. To reiterate, these CND's are based on true-mass results, and they are not

the mass-adjusted FIMS response.

What is apparent from the figure is that the data of Geetla and the data from FIMSDIST

do not agree directly as a result of quantitation, however their trends do agree reasonably well.

The mass of acetic and propionic acid tended to be underestimated by FIMS in relation to that of

Geetla. This was especially true for propionic acid and butyric acid in CTLs from other TAGs

that were tested (Table 24). The masses of C8-C15 tended to agree quite well between Geetla

and the FIMSDIST analysis.
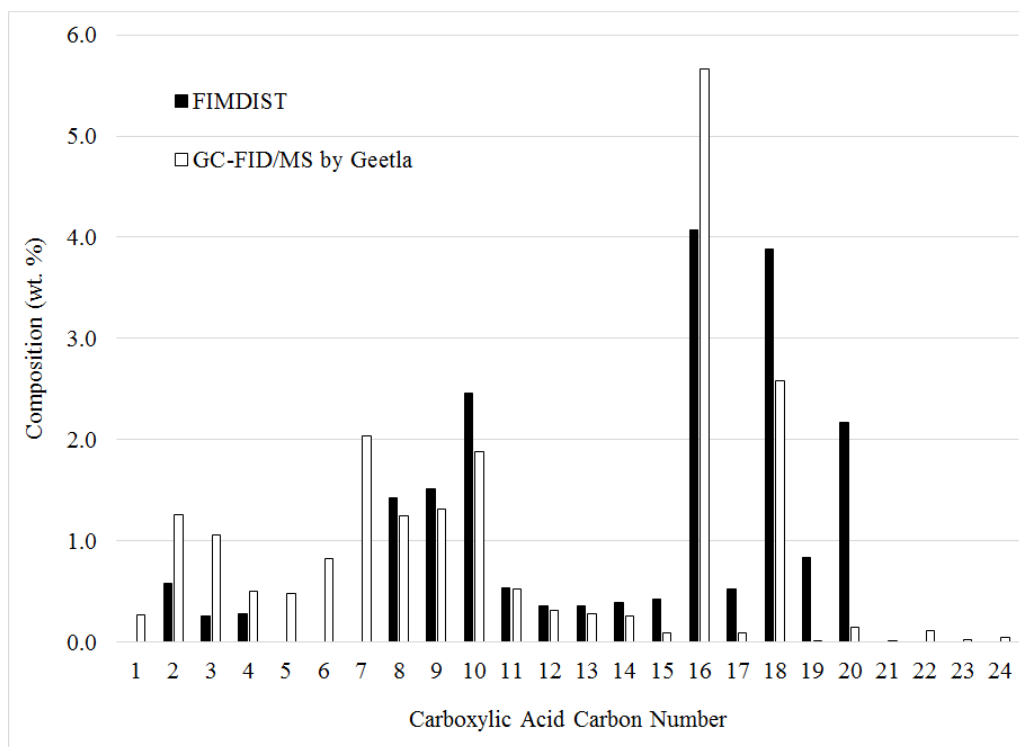
Figure 80. Comparison of carboxylic acid composition for sample AA-Soy
from FIMSDIST compared to data reported by Geetla[156]

FIMSDIST appeared to have falsely identified and/or responded to ions in the range of

C20 and larger. Previously it was considered that FIMSDIST was capable of quantifying

carboxylic acids up to C20. In comparing these data to the data of Geetla, it seems unacceptable

to utilize FIMSDIST to quantify carboxylic acids greater than C18. This was an unforeseen and

unfortunate drawback of using FIMSDIST.

As previously mentioned, FIMSDIST is unsuited for determining the mass percentage of

carboxylic acids between C5-C7 and above C18. This is due to very low response for these

carboxylic acids, leading to large quantitation errors. As a result, it is necessary to utilize

carboxylic acid data from Geetla in order to make up for the missing data that FIMSDIST is unable to provide. In particular, C5-C7 data was obtained from Geetla, whereas the longer chain carboxylic acids were of lesser importance. In addition, data for formic acid was taken from Geetla as well. Geetla's quantitation for a full range of saturated carboxylic acids are included in Appendix G (see Table 67) for seven of the nine TAGs utilized in this study.

VI.D. Composition Data of Cracked Triglyceride Liquid (CTL) Samples by FIMSDIST and Detailed Compositional Analysis of Stavova

This section presents the composition of cracked triglycerides determined by the detailed compositional analysis method (Stavova et al.) and determined by FIMSDIST in order to compare the data that are obtained from the two and to consider the differences in the data formats.

The cracking of soybean TAG in CSTRs was previously investigated by Sander[62] who varied reactor operating parameters such as temperature, pressure, and space time as described in Section V.C.3.i (see Table 21). In addition, several batch cracking experiments were performed utilizing various TAG feedstocks under identical reaction operating conditions in order to observe the effect of the TAG feedstock on the CTL produced. The experimental methodology used to produce these samples are described in Section V.C.3.ii (see Table 22). The composition of the cracked triglyceride liquids from those experiments has been determined using a detailed compositional analysis method developed by Stavova et al.[152] which is described in Section V.B.4.i. All components determined by the detailed compositional analysis are provided in Appendix A (see Table 57 for Sander's work and see Table 58 and Table 59 batch cracking work). Summary tables of their detailed compositions are presented in the following two sections for interpretation and comparison.

In addition, the FIMSDIST method has been used to determine the composition of cracked triglyceride liquid of the experiments performed in tubular cracking reactors under various operating conditions and with various TAG feedstocks (see Section V.C.3).

VI.D.1. Detailed Composition from CSTR Cracked Soybean TAG at Various Operating Conditions by Sander[62]

Triglyceride (TAG) cracking was performed in a bench-scale continuous stirred tank reactor (CSTR) by Sander and published in his master's thesis.[62] Through his work, Sanders examined the products that were generated by cracking soybean TAG in the CSTR under a variety of conditions using a 3 factor, 2 level, full factorial experimental design in temperature, pressure, and space time. The conditions studied are included in Table 21 and further described in Section V.C.3.i. The detailed chemical composition of Sander's CTL samples has also been included in Appendix A for reference. A summary of the information in Appendix A is shown in Table 30 for the CTL samples from Sander's work.[62]

Temperature appears to have a largest effect on the quantities of components in the table. Increasing the temperature appears to lead to a clear increase in nearly all product groups, except for diesel range (C13-C18) carboxylic acids. This is sensible due to the thought that increased temperature leads to greater reaction severity, which leads to a greater extent of TAG cracking and ultimately greater yields of lighter products. Furthermore, the increased temperature will lead to decreased production of long chain carboxylic acids by increasing the rate of decarboxylation.

Likewise, similar effects were observed with increasing space time as with temperature, leading to greater quantities of these products. The main difference was that the effect of space time did not effect diesel range components as strongly as components of a lighter range. The

Table 30. Summary of product analysis from the cracking of soybean oil in a bench-scale continuous-stirred-tank-reactor (CSTR) from the work of Sanders[62]

Sample Designation		CSTR-A	CSTR-B	CSTR-C	CSTR-D	CSTR-E	CSTR-F	CSTR-G	CSTR-H
Reaction Conditions									
TAG Type	-	Soy	Soy	Soy	Soy	Soy	Soy	Soy	Soy
Temperature	(C)	400	420	400	420	400	420	400	420
Pressure	(Mpa)	2.9	2.9	2.9	2.9	1.5	1.5	1.5	1.5
Space Time	(h)	2.4	2.4	1.4	1.4	2.4	2.4	1.4	1.4
CTL Components									
n-Paraffins	(wt. %)								
C3-C8		2.03	4.67	1.71	3.07	2.28	4.64	1.67	3.31
C9-C12		0.73	2.19	0.68	1.31	0.80	2.54	0.57	1.82
C14-C18		1.22	2.89	1.45	2.00	1.31	4.23	1.10	3.82
>C18		0.19	0.33	0.25	0.36	0.42	0.38	0.18	0.46
Isoparaffins	(wt. %)								
C3-C8		0.07	0.14	0.02	0.07	0.02	0.10	0.01	0.06
C9-C13		0.05	0.11	0.03	0.07	0.04	0.12	0.02	0.07
Cyclics	(wt. %)								
C5-C8		0.26	0.83	0.23	0.48	0.29	0.72	0.19	0.46
C9-C13		0.33	0.85	0.34	0.51	0.40	0.92	0.29	0.59
C14-C18		0.16	0.34	0.20	0.24	0.20	0.50	0.15	0.40
Olefins	(wt. %)								
C3-C8		1.01	2.03	0.85	1.56	1.51	2.61	1.17	1.92
C9-C13		0.77	1.70	0.67	1.33	1.09	2.29	0.73	1.69
C14-C18		0.57	1.16	0.60	0.94	0.82	1.90	0.54	1.64
Aromatics	(wt. %)								
C6-C8		0.21	0.58	0.21	0.37	0.21	0.59	0.17	0.42
C9-C12		0.64	1.50	0.61	0.97	0.72	1.64	0.52	1.38
C13-C18		0.28	0.44	0.30	0.35	0.23	0.66	0.25	0.70
Polycyclic Aromatics	(wt. %)								
C9-C12		0.14	0.41	0.13	0.26	0.16	0.44	0.10	0.31
C13-C18		0.10	0.16	0.12	0.18	0.07	0.25	0.06	0.20
Saturated Fatty Acids	(wt. %)								
C1-C5		1.14	2.17	0.73	1.52	1.41	2.00	1.13	1.32
C6-C9		2.03	3.40	1.50	2.55	2.75	3.58	2.06	2.41
C10-C14		1.12	1.41	0.91	1.20	1.31	1.84	1.10	1.24
C15-C18		5.84	2.21	4.48	2.77	4.07	3.73	5.40	2.45
>C18		0.00	0.00	0.00	0.00	0.00	0.00	0.00	0.00
Unsaturated Fatty Acids	(wt. %)								
C18-C22		2.38	1.20	2.26	1.40	2.00	1.16	2.42	1.32
Other		0.00	0.00	0.00	0.00	0.00	0.00	0.00	0.00
Totals	(wt. %)								
Condensed Phase (C.P.) Identified		22.19	33.07	19.07	25.27	23.59	39.85	20.64	30.08
C.P. Unresolved / Non-Eluted		77.81	66.93	80.93	74.73	76.41	60.15	79.36	69.92

effect of pressure is much weaker than either. The most significant effect of increasing pressure was an observed decrease in yield of C14-C18 cyclics and most olefins. These have been thoroughly considered by Sander and are not repeated to the same extent in the present work.[62]

What was evident from Sander's results is that all samples have a substantial quantity of mass that was either unresolved or non-eluted by gas chromatography, indicated at the bottom

of the table.

This may be partially due to unreacted and/or under-reacted feedstock material in the cracked TAG liquid or due to residue formed as a precursor to coke formation. Either way, the result is that between 60 and 81 wt. % of Sander's samples are nondescript. This makes it difficult to estimate the quantity of final fuel products that may be produced through the refinement of Sander's samples with the noncatalytic cracking process (NCP) described in Chapter II. For this reason, the new analytical method known as FIMSDIST was developed herein, described in Section V.B.4.ii.

VI.D.2. Detailed Composition from Batch Cracking of Various TAGs

Several 300 mL aliquots of various TAGs were cracked at 430 C temperature for 30 minutes time in a 500 mL batch reactor, with the experimental methodology described in Section V.C.3.ii. Cracked TAG liquid was collected and its detailed composition was determined according to the method of Stavova et al.[152] A summary of the cracked TAG liquid (CTL) composition is presented in Table 31, and the full detailed composition is also provided in Appendix A (see Table 58 and Table 59). Additionally, the molar concentration of TAG feedstock fatty acid moieties are included in the table, being taken from literature values as described in Section III.F.6.

A greater percentage of n-paraffins are observed in the lightest range (C3-C8), whereas in the heavier ranges the quantity of paraffins are less. A similar observation was true for cyclics and a less dramatic observation for olefins. The reverse was observed for isoparaffins, in that longer isoparaffins were more prevalent.

The quantity of isoparaffins was very low relative to the quantity of isoparaffins. The

285

quantity of olefins was found to be on the order of twice as much as that of cyclics. Aromatics were typically found in lesser concentration than olefins, cyclics, and paraffins. The ratios of these are examined in Section VI.D.4 in more detail.

Saturated fatty acids were also quantified in significant amounts. Additionally, some unsaturated fatty acids were quantified on the order of about 3 to 24 wt. % of the total carboxylic acids. Furthermore, all unsaturated carboxylic acids were longer chain, evidently resulting from undercracked TAG fatty acid moieties.

Concerning differences between the CTL as a result of fatty acid moiety composition of the TAG feedstocks, it is apparent that linseed TAG is producing a reduced quantity of olefins. This may be expected, since linseed TAG has higher bond energies which resistance cracking unless a radical first formed through bisallylic hydrogen abstraction, which may lead to aromatization instead of olefinization. The quantity of aromatic (not polycyclic aromatics) is high in Linseed TAG, which could be considered to result from the high quantity of linolenic acid (COOH 18:3) in the feedstock TAG.

However, VHONO was found to produce only slightly less aromatics, and VHONO contains very little linolenic acid. Then observing that the aromaticity of HONO was the lowest in this series, it is wondered why the aromaticity of VHONO was found to be higher. More work may be necessary to account for this contradiction.

TAGs rich in monounsaturated fatty acids such as HENO, HONO, and VHONO showed higher quantities of unsaturated fatty acids in the product. This might indicate slower cracking speeds of monounsaturated carboxylic acids. In general, the TAGs produce CTL that appears to

Sample Designation		Batch-1*	Batch-2	Batch-3	Batch-4	Batch-5	Batch-6
Reaction Conditions							
TAG Type		Soy	HONO[I]	VHONO[II]	HENO[III]	Cottonseed	Linseed
Volume	(mL)	300	300	300	300	300	300
Temperature	(C)	430	430	430	430	430	430
Reaction Time	(h)	0.5	0.5	0.5	0.5	0.5	0.5
TAG Fatty Acid Moieties	(mol. %)						
Palmitic (16-0)		11.4	3.7	3.2	3.5	23.9	6.0
Stearic (18-0)		4.2	2.0	2.3	1.2	2.4	0.0
Oleic (18-1)		26.1	73.3	84.1	18.5	17.4	17.0
Linoleic (18-2)		50.3	14.8	4.0	13.2	53.4	14.0
Linolenic (18-3)		7.9	2.6	2.6	7.7	0.0	60.0
Erucic (22-1)		0.0	0.0	0.0	41.2	0.0	0.0
CTL Components							
n-Paraffins	(wt. %)						
C3-C8		5.40 (0.10)	6.18	7.33	6.48	6.00	4.87
C9-C13		2.46 (0.18)	3.469	2.329	3.731	2.947	2.038
C14-C18		2.27 (0.19)	1.676	1.739	1.215	3.098	1.792
>C18		0.33 (0.04)	0.38	0.40	0.58	0.36	0.27
Isoparaffins	(wt. %)						
C3-C8		0.07 (0.005)	0.07	0.18	0.19	0.22	0.28
C9-C13		0.15 (0.003)	0.22	0.27	0.22	0.11	0.12
Cyclics	(wt. %)						
C5-C8		1.12 (0.02)	1.22	1.51	1.25	1.08	1.22
C9-C13		0.99 (0.09)	1.411	1.680	1.374	0.821	0.844
C14-C18		0.48 (0.10)	0.966	0.960	0.611	0.383	0.337
Olefins	(wt. %)						
C3-C8		2.14 (0.03)	2.23	2.33	2.18	2.53	1.69
C9-C13		1.77 (0.09)	2.301	2.406	2.301	1.638	1.056
C14-C18		1.43 (0.16)	1.666	1.585	1.097	1.253	0.632
Aromatics	(wt. %)						
C6-C8		0.75 (0.01)	0.61	0.84	0.79	0.61	1.01
C9-C13		1.58 (0.00)	1.201	1.643	1.388	1.393	1.774
C14-C18		0.34 (0.08)	0.428	0.447	0.334	0.316	0.329
Polycyclic Aromatics	(wt. %)						
C9-C13		0.39 (0.02)	0.324	0.438	0.362	0.500	0.600
C14-C18		0.17 (0.02)	0.187	0.188	0.153	0.087	0.759
Saturated Fatty Acids	(wt. %)						
C1-C5		3.08 (0.09)	2.83	3.18	2.79	3.28	4.21
C6-C9		4.90 (0.15)	4.06	4.06	3.26	4.80	5.56
C10-C14		2.42 (0.12)	3.600	3.869	4.314	2.611	2.598
C15-C18		4.10 (0.07)	2.273	1.976	1.703	4.330	2.368
>C18		0.44 (0.001)	0.44	0.41	0.93	0	0
Unsaturated Fatty Acids	(wt. %)						
C18-C22		1.55 (0.28)	4.10	3.38	2.53	0.50	0.97
Other		0.34 (0.02)	0.20	0.20	0.41	0.15	0.15
Totals	(wt. %)						
Identified		42.5 (1.6)	46.1	47.9	44.9	42.2	38.5
Unidentified		8.6 (0.9)	12.3	10.0	9.1	6.8	6.4
Unresolved		44.6 (2.9)	35.5	42.5	41.1	21.9	26.6
Total Accounted Mass	(wt. %)	95.7 (0.4)	93.9	100.4	95.1	70.9	71.5

* Note: Batch-1 noncatalytic cracking data are reported as the mean (standard deviation) of a triplicate sample.
I. HONO is High Oleic Novelty Oil; II. VHONO is Very High Oleic Novelty Oil; III. HENO is High Erucic Novelty Oil

be more alike than dissimilar, which makes it difficult to observe the dependence on TAG fatty

acid moiety composition.

It should be mentioned that a significant concentration in these samples could not be identified or resolved, on the order of > 50 wt. %. This appears to be dominated by unresolved mass, and/or mass that is not accounted for rather than components which could not be identified. In any event, the dominance of all of these masses motivated the pursuit of FIMSDIST.

VI.D.3. FIMSDIST Composition from Cracking in Tubular Reactors

Composition data from FIMSDIST analysis are presented in Table 32 and Table 33 in similar format to tables depicted for the data from detailed compositional analysis, presented in the previous two sections (VI.D.1 and VI.D.2). These data are briefly analyzed herein for comparison between analytical methods, however, they are more thoroughly analyzed in Section VII.E.3 to determine the effects of different operating parameters on yield with the noncatalytic cracking process (NCP). In addition, the data have been truncated to narrow the discussion to relevant data that is comparable between FIMSDIST and detailed methods. Complete data tables are included in Appendix K.

Table 32 shows the composition data from cracking various TAGs in the 100 mL lab-scale TCR. Reaction conditions are included at the top of the table, having been held constant during experimentation. The composition of selected components from the cracked TAG (CT) are shown in the remainder of the table, expressed as a wt. %. The data have been grouped according to the group encoding description shown in Section VI.A.2 (see page 247).

In examining the TAGs, five of the nine TAGs were previously processed in batch reactors, with their compositions described in the last section (VI.D.2). Since the samples were

produced using two different methods (batch reactors vs. tubular cracking reactors) and analyzed

by two different methods also (detailed compositional analysis vs. FIMSDIST), some different

results might be anticipated.

As a result of FIMSDIST (i.e., utilizing normalization, FIMS data, and associated

assumptions) there is no reportable unresolved portion of the analytes and the non-eluted portion

of the analytes is assumed to be negligible, consistent with ASTM D7500.[64]

In examining the composition in Table 32, paraffins (C-) tended to be lower in the jet fuel

range (C9-C13) than either the naptha (C5-C8) or diesel range (C14-C18). A similar effect is

seen in the detailed compositional analysis data from samples produced using the continuous-

stirred-tank-reactor (CSTR) under Sander[62] (see Figure 33). However, the paraffin distribution

was different in batch TAG cracking, which showed a strong decrease of n-paraffins in heavier

fuel fractions.

In Table 32, olefins/cyclics (C=) appeared to be more concentrated in the jet and diesel

ranged than in the naphtha range. This trend was not observed in either CSTRs or batch reactors,

which is a curious result. In Table 32, a likewise effect was observed for diolefins/dicyclics/etc.

(group =C=), having greater fractions in the jet/diesel range than in the naphtha range. However,

the =C= group components were not very apparent in the detailed compositional analysis data.

No explanation is offered for this at the present time.

Concerning aromatics (denoted by various forms of "(…)Ar(…)"), the majority of the

aromatics that were formed were found to be in the jet and diesel ranges, with only minor

amounts of benzene/toluene/xylene (BTX) aromatics being formed. Reduced quantity of BTX

Table 32. Composition data from high throughput analysis (FIMSDIST method) of
CTL produced by the cracking of various TAGs in the lab-scale
tubular cracking reactor

Sample Designation		AA-Soy	BB-VHONO	CC-HENO	DD-Linseed	EE-Camelina	FF-Corn	GG-Cottonseed	HH-Canola	II-HONO
Reaction Conditions										
TAG Feedstock		Soybean	VHONO	HENO	Linseed	Camelina	Corn	Cottonseed	Canola	HONO
Temperature	(C)	435	435	435	435	435	435	435	435	435
Space Time	(h)	0.44	0.44	0.44	0.44	0.44	0.44	0.44	0.44	0.44
Pressure	(MPa)	2.9	2.9	2.9	2.9	2.9	2.9	2.9	2.9	2.9
CT Components										
Group C-	(wt. %)									
C5-C8		1.61	1.79	1.26	1.50	1.89	2.10	1.93	1.97	2.34
C9-C12		0.63	0.77	0.89	0.64	0.88	0.73	0.74	0.90	0.81
C13-C18		1.53	0.60	0.65	1.25	1.25	1.31	2.63	1.03	0.89
Group C=	(wt. %)									
C5-C8		2.06	1.70	1.27	2.14	2.64	3.03	3.05	2.69	2.82
C9-C12		4.34	4.49	4.36	4.10	4.75	4.68	4.13	4.87	5.04
C13-C18		5.27	7.23	5.64	4.63	4.28	4.08	3.77	5.35	6.21
Group =C=	(wt. %)									
C5-C8		1.97	1.57	1.21	2.17	2.58	2.28	2.11	2.26	2.31
C9-C12		3.76	2.82	3.14	4.16	3.93	3.93	3.85	3.65	3.36
C13-C18		5.80	5.37	5.37	5.79	5.30	5.44	4.91	5.78	5.59
Group (1x)Ar / (1x)Ar=	(wt. %)									
C6-C8		0.19	0.11	0.12	0.36	0.31	0.20	0.21	0.23	0.19
C9-C12		1.01	0.43	0.65	1.67	1.36	1.05	1.05	0.80	0.59
C13-C18		1.93	1.01	1.23	3.05	2.16	1.81	1.85	1.74	1.41
All (2x) & (3x) Ar	(wt. %)									
C10-C13		0.40	0.27	0.27	0.60	0.44	0.40	0.40	0.36	0.33
C14-C18		2.13	1.61	1.61	2.79	2.18	2.08	2.20	2.00	1.71
Group COOH	(wt. %)									
C1-C5		2.37	1.46	1.43	2.80	3.38	3.42	2.59	2.21	1.76
C6-C9		7.81	5.10	4.79	9.18	7.70	8.92	7.96	7.44	5.01
C10-C14		3.31	6.97	5.41	3.92	3.58	2.64	2.39	3.34	3.60
C15-C18		8.49	5.20	3.50	7.41	5.02	7.35	11.97	5.73	4.18

aromatics were also observed in the batch reactor data shown in Table 31 and the CSTR data

shown in Table 30. The major difference is that the detailed compositional analysis data did not

show an increase in aromaticity of the diesel fraction from data produced via batch or CSTR,

whereas the FIMSDIST data did with tubular cracking reactors. This might be hypothesized to

result from a lack of chromatography resolution in the diesel fuel range, with many components

overlapping. This might make it difficult to identify and quantify aromatics, however it is

presently difficult to make that claim with certainty.

Concerning carboxylic acids, there is greater variety in their response. In general, it

appears as though the naphtha range and diesel range carboxylic acids were higher than the jet and gaseous fuel range carboxylic acids. What was previously mentioned in Section VI.C should be reiterated—the data of Geetla were utilized to supplement FIMSDIST data for C1 and C5-C7 carboxylic acids. This was done by converting the mole percentage of Geetla's data to a mass form, and then normalizing the resultant data according the sum mass percentage of C2-C4 and C8-C18 carboxylic acids. This was necessary due to the inability of FIMSDIST to identify and quantify C5-C7 carboxylic acids and also C1 (see Section VI.A.2).

Further analysis of the composition of Table 32 are performed in Section VII.E.3 using statistical regression to determine the effects of fatty acid moieties in TAG feedstocks on the distribution and speciation of products with the noncatalytic cracking process (NCP).

Table 33 shows the composition data from cracking soybean TAG in the 100 mL lab-scale TCR under various operating conditions, which are indicated at the top of the table. The composition of selected components from the cracked TAG (CT) are shown in the remainder of the table, expressed as a wt. %. The data have been grouped according to the group encoding description shown in Section VI.A.2 (see page 247). Additional experimental information may be obtained from Section 0.

In examining the composition in Table 33, most mass fractions were found to increase in magnitude substantially with increasing temperature / space time. This is assumed to be a result of increased cracking reaction severity, not unlike that of CSTR cracking which showed a very similar trends in Table 30.

It should be mentioned that the data tables herein are truncated in order to focus the discussion on data that can be compared between FIMSDIST and detailed methods. As a result,

291

fuel oil fractions are not presented in these tables, but they are presented in complete data tables in Appendix K. To briefly describe that trend, the fuel oil fractions are decreased with increasing reaction severity, which coincides with the production of lighter fuel.

Table 33. Composition data from high throughput analysis (FIMSDIST method) of CTL produced by the cracking of soybean TAG in the lab-scale tubular cracking reactor under various operating conditions

Sample Designation		A-Soy	B-Soy	C-Soy	D-Soy	E-Soy	F-Soy	G-Soy	H-Soy	I-Soy
Reaction Conditions										
TAG Feedstock		Soybean	Soybean	Soybean	Soybean	Soybean	Soybean	Soybean	Soybean	Soybean
Temperature	(C)	420	430	440	420	430	440	420	430	440
Space Time	(h)	0.27	0.27	0.27	0.69	0.70	0.69	1.22	1.17	1.10
Pressure	(MPa)	2.9	2.9	2.9	2.9	2.9	2.9	2.9	2.9	2.9
Selected Liquid Components										
Group C-	(wt. %)									
C5-C8		1.13	1.39	1.62	1.80	2.60	2.51	1.77	2.34	2.53
C9-C12		0.42	0.61	0.78	1.12	1.21	1.15	1.08	1.40	1.96
C13-C18		0.90	1.05	1.21	1.88	2.01	1.83	1.91	2.31	3.21
Group C=	(wt. %)									
C5-C8		1.68	2.30	2.62	2.99	3.58	4.00	3.03	3.90	4.49
C9-C12		2.93	3.18	3.56	3.53	6.07	5.99	4.11	4.57	5.33
C13-C18		3.53	3.89	4.12	4.65	5.21	5.04	4.63	4.93	5.86
Group =C=	(wt. %)									
C5-C8		1.42	1.79	2.24	2.63	3.08	2.85	2.61	3.07	3.80
C9-C12		3.21	3.48	3.81	3.65	5.07	4.71	3.95	4.45	4.98
C13-C18		3.99	4.60	4.92	5.82	6.47	5.77	5.81	6.41	7.27
Group (1x)Ar / (1x)Ar=	(wt. %)									
C6-C8		0.15	0.18	0.26	0.30	0.35	0.29	0.26	0.36	0.53
C9-C12		0.67	0.78	0.92	1.34	1.51	1.43	1.33	1.67	2.26
C13-C18		1.14	1.43	1.68	2.38	2.66	2.05	2.18	2.62	3.28
All (2x) & (3x) Ar	(wt. %)									
C10-C13		0.35	0.36	0.36	0.40	0.48	0.47	0.39	0.45	0.62
C14-C18		1.56	1.90	2.02	2.01	2.14	1.92	2.10	2.19	2.28
Group COOH	(wt. %)									
C1-C5		2.37	2.55	2.57	2.32	2.69	2.68	2.43	2.38	2.23
C6-C9		7.48	7.79	7.97	7.52	8.39	8.47	7.74	7.57	7.50
C10-C13		2.28	2.60	2.66	2.49	3.06	3.12	2.69	2.72	2.90
C14-C18		9.75	9.69	8.54	6.86	5.70	6.34	7.45	5.95	4.71

The mass fraction of paraffins (C-) tended to have a trend where jet fuel range paraffins were less in quantity than for the other fuel ranges. This trend was also previously found from FIMSDIST data presented in Table 32 (TCR cracking) and detailed composition data presented in Table 30 (CSTR cracking) but not for the detailed composition data presented in Table 31

(batch cracking).

As with the data presented in Table 32 for TCR cracking of various TAGs, it was apparent that C= and =C= components were more concentrated in the jet and diesel range than in the naphtha range. However, their relatively high concentration in the jet/diesel ranges was less pronounced with increased cracking severity, as a result of a greater increase in the naphtha range C= and =C= components.

Larger sized aromatics tended to be more concentrated in the products than smaller sized aromatics. The same was also true of polycyclic aromatics. This agrees with Table 32 for the cracking of various TAGs by TCR. Reduced concentrations of BTX aromatics were likewise observed in data from detailed analysis (Table 30 and Table 31), but the aromaticity of diesel fuel was contrary to the data from FIMSDIST analysis, being less than the jet range aromatics. This may be due to the inability of the detailed method to resolve all the analytes in the diesel range by chromatography, leading to reduced quantitation, whereas the FIMSDIST method is not hindered by a lack of chromatographic resolution.

Concerning carboxylic acids, the long chain carboxylic acids appear to be decreasing with increased cracking severity, however the concentration of the naphtha, jet, and gaseous range carboxylic acids appear to be unaffected.

Further analyses of the composition of Table 33 are performed in Section VII.E.3 using statistical regression to determine the effects of fatty acid moieties in TAG feedstocks on the distribution and speciation of products with the noncatalytic cracking process (NCP).

VI.D.4. Indirect Ratio Comparison

Characteristic ratios are presented in order to indirectly compare the results of FIMSDIST

and the detailed compositional analysis method described by Stavova et al.[63]. Four ratios are presented. These are considered indirect comparisons because different reactor types were utilized and different analytical methods were utilized. Direct comparisons of carboxylic acids quantified from analyses of cracked TAG liquid (CTL) samples produced in a tubular cracking reactor (TCR) are included in Section VI.C. Direct comparisons of various hydrocarbon components quantified from analyses of CTL samples produced via CSTRs are described in Section VI.D.5.

The first two ratios that were considered were the n-paraffin/isoparaffin ratio and the olefin/cyclic ratio which were only obtainable by the detailed compositional analysis method. This is because the olefins and cyclics have identical exact masses of their molecular ion isotopes. The same is true of n-paraffins and isoparaffins. As a result, FIMSDIST is unable to differentiate between these groups, which was an anticipated weak point of FIMSDIST. These two ratios are presented for various carbon number ranges so that they may be utilized in potential future studies to estimate the quantity of the related constituents in FIMSDIST data (e.g., to estimate the quantity of isoparaffins).

The latter two ratios are the ratio of paraffins to combined olefins/cyclics and the ratio of aromatics to the combined olefins/cyclics/paraffins/isoparaffins/carboxylic acids. These are presented to address some differences between the data produced by the detailed compositional analysis method and the FIMSDIST method.

Table 34 shows characteristic ratios from the composition of CTL that was produced by noncatalytic cracking of various TAGs in batch reactors as described by Section VI.D.2.

For C3-C8 hydrocarbons, the ratio of paraffins to isoparaffins was very large on the order of 18 to 86. This was in contrast to the ratio for C9-C12 hydrocarbons which have a milder ratio of about 7 to 21. There did not appear to be an obvious trend between this ratio and the type of TAG feedstock and/or its fatty acid moiety composition. Also, this is so large that isoparaffins might be considered negligible in many cases. Although unsuccessful attempts were made to utilize PIANO standards to calibrate for isoparaffins in FIMSDIST, it appears as though there was may be little consequence to the lack of isoparaffins standardization for this set of data, due to the overwhelming quantity of n-paraffins vs. isoparaffins. Additionally, the ratio is much larger in the smaller carbon number range (C3-C8) than in the larger carbon number range (C9-C13), indicating that the smaller chain lengths are less likely to undergo rearrangement during cracking.

As shown in Table 34, the ratio of olefins to cyclics was on the order of 1.3 to 2.3. Based on this, it was not be possible to assume that cyclics were negligible, as could be assumed for isoparaffins. For this reason, a lack of cyclic calibration in FIMSDIST should be remedied with additional calibration standards in future experiments, as previously mentioned on page 255.

As previously mentioned, attempts to utilize PIANO standards were unsuccessful due to their excessive dilution, however these would be the ideal mixtures for calibrating a wide range of hydrocarbon types with FIMS in future attempts to reapply the FIMSDIST method for high throughput compositional analysis of CTL or other comparable samples.

The ratio of olefins/cyclics did appear to vary with the different type of TAGs used, but no obvious dependence on fatty acid moiety composition of the TAG feedstock was apparent. The same could likely be said for the paraffins/isoparaffins, however the quantity of isoparaffins

295

was negligible in comparison.

It was furthermore difficult from the olefin/cycle ratios shown in Table 34 to elucidate an
obvious trend of the ratios vs. TAG fatty acid moiety composition.

Table 34. Characteristic ratios from the composition data of detailed analysis (Stavova et al. [63]
method) of CTL produced by the cracking of various TAGs in the batch cracking reactor

Sample Designation		Batch-1[†]	Batch-2	Batch-3	Batch-4	Batch-5	Batch-6
TAG Feedstock	-	Soybean	HONO[I]	VHONO[II]	HENO[III]	Cottonseed	Linseed
n-Paraffin/Isoparaffin Ratio	(wt. % basis)						
C3-C8		74.9 (6.0)	86.5	40.6	33.6	27.3	17.7
C9-C13		16.0 (1.5)	15.5	8.8	17.1	27.7	17.4
Olefin/Cyclic Ratio	(wt. % basis)						
C3-C8		1.9 (0.1)	1.8	1.5	1.7	2.3	1.4
C9-C13		1.8 (0.1)	1.6	1.4	1.7	2.0	1.3
Paraffin/(Olefin+Cyclic) Ratio	(wt. % basis)						
C3-C8		1.7 (0.0)	1.8	2.0	1.9	1.7	1.8
C9-C13		0.9 (0.0)	1.0	0.6	1.1	1.2	1.1
*Aromatics Ratio	(wt. % basis)						
C6-C8		0.055 (0.001)	0.044	0.054	0.059	0.042	0.074
C9-C13		0.203 (0.012)	0.109	0.156	0.116	0.172	0.267

* Note: Aromatics Ratio indicates the quantity of n-alkylaromatics divided by the sum quantity of paraffins, isoparaffins, olefins, cyclics, and saturated carboxylic acids.
† Note: Batch-1 noncatalytic cracking data are reported as the mean (standard deviation) of a triplicate sample.
I. HONO is High Oleic Novelty Oil; II. VHONO is Very High Oleic Novelty Oil; III. HENO is High Erucic Novelty Oil

Table 35 shows characteristic ratios from CSTR cracking described in Section VI.D.1
over various carbon number ranges. What can be observed is that the ratio of paraffins to
isoparaffins is on the order of 16 to 180. This is essentially in direct agreement the data from the
detailed composition data from the cracking of various TAGs in batch reactors presented in
Table 34 and the comments about paraffin/isoparaffins ratio mentioned previously. In
comparison to the batch cracking ratios reported in Table 34 the paraffin/isoparaffins ratios and
the olefin/cyclic ratios appear to have increased compared to batch cracking, on the order of 20-
40 % more. The exception to this appears to be in the C3-C8 range olefins/cyclics ratio, which

was averaged at 4.6 for CSTR cracking and 1.8 for batch cracking. Future mechanistic

considerations could shed light on this phenomenon.

The ratio of olefins to cyclics is on the order of 2 to 6. This is substantially lower than

the ratio of paraffins to isoparaffins. What can be observed from the data is that the ratios for

C3-C8 range hydrocarbons are clearly dependent upon operating conditions. Specifically,

increased temperatures and decreased pressures increase the ratio of olefins to cyclics. It is also

evident that the effect of operating conditions is relatively weak over the range of C9-C13

hydrocarbons. Therefore, a relatively constant ratio of olefins to cyclics may be assumed for C9-

C13, if CSTR data is utilized as a basis.

Table 35. Characteristic ratios from the composition data of detailed analysis (Stavova et al.[63] method) of CTL produced by the cracking of soybean TAGs in the cracking continuous-stirred-tank-reactor by Sander[62] under various operating conditions

Sample Designation		CSTR -A	CSTR -B	CSTR -C	CSTR -D	CSTR -E	CSTR -F	CSTR -G	CSTR -H
Reaction Conditions									
TAG Feedstock		Soybean	Soybean	Soybean	Soybean	Soybean	Soybean	Soybean	Soybean
Temperature	(C)	400	420	400	420	400	420	400	420
Space Time	(h)	2.9	2.9	2.9	2.9	1.5	1.5	1.5	1.5
Pressure	(MPa)	2.4	2.4	1.4	1.4	2.4	2.4	1.4	1.4
n-Paraffin/Isoparaffin Ratio	(wt. % basis)								
C3-C8		28	34	91	43	123	48	180	55
C9-C13		16	20	24	18	22	21	31	27
Olefin/Cyclic Ratio	(wt. % basis)								
C3-C8		3.9	2.4	3.6	3.3	5.2	3.6	6.3	4.2
C9-C13		2.3	2.0	2.0	2.6	2.7	2.5	2.5	2.8
Paraffin/(Olefin + Cyclic) Ratio	(wt. % basis)								
C3-C8		1.7	1.7	1.6	1.5	1.3	1.4	1.2	1.4
C9-C13		0.7	0.9	0.7	0.8	0.6	0.8	0.6	0.8
Aromatics Ratio*	(wt. % basis)								
C6-C8		0.038	0.052	0.048	0.048	0.031	0.051	0.033	0.052
C9-C13		0.069	0.092	0.079	0.084	0.059	0.077	0.062	0.078

* Note: Aromatics Ratio indicates the quantity of n-alkylaromatics divided by the sum quantity of paraffin, isoparaffins, olefin, cyclic, and saturated carboxylic acids.

The ratio of paraffins and isoparaffins to olefins+cyclics (C-/C= ratio) and the ratio of

aromatics to the sum of isoparaffins+paraffins+cyclics+olefins+saturated carboxylic acids (i.e.,

aromatics ratio) can also be used to compare the results of the FIMSDIST method and the detailed compositional analysis method.

In Table 34 and Table 35 (above) the C-/C= ratio over the C3-C8 ranged components is reported on the order of 1.8 for batch cracking and 1.5 for CSTR cracking. These are in agreement. For components in the C9-C13 range, the C-/C= ratio is on the order of 1.0 for batch TAG cracking and 0.7 for CSTR cracking. There appears to be a noticeable dependence of the C-/C= ratio on operating conditions in the CSTR. There is an decrease in the C-/C= ratio for C3-C8 ranged components with increasing space time. The C-/C= ratio for C9-C13 ranged components also increases with increasing temperature and decreases with increasing space time. Despite the dependence, these ratios do not change by more than approximately 25 % over the full range of conditions studied.

In order to enable indirect comparison, the characteristic ratios computed previously in Table 34 and Table 35 (above) for detailed composition data were likewise computed in Table 36 and Table 37 (below) for FIMSDIST method characteristic ratios. These characteristic ratios correspond to the composition data in Table 30 and Table 31 from detailed compositional analysis and to the composition data in Table 32 and Table 33 from the FIMSDIST method, respectively.

In comparing the ratios for detailed compositional analysis to those of the FIMSDIST method, it is evident that FIMSDIST results lead to a lower C-/C= ratio. For FIMSDIST analysis of the CTL from the cracking of various TAGs by TCR (i.e., Table 36), the C-/C= ratio for C3-C8 ranged components is approximately 0.8, and for cracking soybean TAG under a variety of conditions (i.e., Table 37) the ratio is approximately 0.6. This is on the order of half to

one third the C-/C= ratio that would be expected based on the data from detailed compositional analysis. For C9-C13 ranged components, the ratio of paraffins to olefins+cyclics by FIMSDIST is on the order of 0.2 to 0.3, which is approximately one third the quantity that was determined from detailed compositional analysis.

It might have been considered that the C-/C= ratio was a result of differences in the type of reactors utilized to produce the samples. This potential explanation seemed unlikely when examining Figure 106, which shows the mass fraction carbon number distribution (CND) for a sample of jet fuel (i.e., Jet-A-1) produced with the noncatalytic cracking process (NCP). This sample of Jet-A-1 was refined from a sample of soybean TAG processed in batch reactors consistent with sample Batch-1 (see Table 31). In examining the CND, there is a high percentage of C= and =C= components. Yet the detailed composition of Batch-1 (Table 31) does not indicate an unusually high percentage of cyclics or olefins. Furthermore, during deoxygenation, the paraffin content would be expected to increase through the hydrogenation of double bonds on olefins and through the decarboxylation of carboxylic acids to n-paraffins. This is verified by the analysis of 1) the fully deoxygenated products, as shown in Section VII.A for olefin content, indicating olefins in the final products on the order of less than 0.5 wt. %, and 2) the final fuel sample produced by deoxygenation in Section VII.D. As a result, the primary C= and =C= contributors in the final fuel product would be expected to be cyclics, not olefins.

Since it is not well supported that reactor differences are causing an unexpected high concentration of C= and =C= fractions, then it must be due to FIMSDIST calibration. The difference in C-/C= ratio potentially indicates that FIMSDIST is either underrepresenting paraffins or overrepresenting cyclics+olefins. As previously mentioned in this section, n-

paraffins tend to make up the overwhelming majority of the paraffins, whereas isoparaffins are a minor constituent of CTL. It then follows that since n-paraffins were thoroughly calibrated to determine their RIEs with the FIMSDIST method (see Figure 66), it is difficult to conclude that paraffins are being misrepresented by FIMSDIST.

On the other hand, the RIE calibration for olefin+cyclic (C= group) components was already described as being lacking earlier in this section and in Section VI.A.3. If the C= group components are overrepresented by FIMSDIST by a factor of ~3, then the implication is that the RIE for the C= groups is on the order of 1/3 what it really should be. Such an RIE is reasonable because it falls within the range of RIEs utilized in this experiment (see Figure 66), which vary by approximately half an order of magnitude for any given carbon number. The different RIE for C= group components could stem from a variety of issues that could be elucidated by greater standardization utilizing PIANO standards or other similar standards. It was intended for PIANO standards (see Section V.A.7) to provide more thorough calibration data for FIMSDIST, however they were found to be too dilute to utilize in the present work, although they were adequate for the detailed compositional analysis method. Future work should attempt to utilize more concentrated PIANO standards for calibration of the FIMSDIST method.

Some potential explanations should be mentioned that may account for the potential differences in RIE values observed. Sander indicated that the majority of olefins were not α-olefins. Therefore, it is possible that α-olefins and other olefins have different RIEs, leading to a miscalibration in FIMSDIST. Otherwise, cyclics were estimated to account for approximately 1/3 of the C= components. Therefore, misrepresentation may also stem from cyclics potentially having different RIEs than α-olefins. This aligns with the observation of high fractions of C=

300

and =C= groups in the sample of Jet-A-1 that was previously described.   This needs to be verified with more standardization in future utilization of FIMSDIST.

In line with these considerations, it might be considered that =C= group components are also misrepresented by FIMSDIST, since their calibration was likewise based on α-olefins. Furthermore, =C= components are more enigmatic than olefins, in that they have a much greater number of potential formula isomers, and they are resultantly less quantifiable and have less accurate calibrations in analytical methods.

In likeness to CSTR cracking (which was performed under a variety of operating conditions), there appears to be a dependence of the C-/C= ratio for C9-C13 components on the operating conditions for cracking in TCRs, with increasing cracking severity showing an increase in this ratio. One might therefore conclude that FIMSDIST is capable of elucidating the trends in CTL, despite having some potential calibration issues for C= and/or =C= group components.

No dependence was evident for the C3-C8 ratio in the TCR, but there was an observed dependence in the CSTR as a function of space time. This difference may result from reactor differences, whereby the gas phase residence time in the CSTR should be assumed to be relatively very brief. This would potentially effect the C3-C8 in different ways than would be expected for the TCR, which is less prone to phase partitioning.

In examining the aromatics ratios (which were previously defined two pages earlier), the C6-C8 aromatics ratio is on the order of 0.01 to 0.04 in TCR cracking and analysis by the FIMSDIST method (see Table 36 and Table 37). This may be compared to an aromatics ratio ranging from approximately 0.03 to 0.08 from data derived from the detailed compositional

analysis method. In general, it may appear as though aromatics are lower in FIMSDIST data, but not to an alarming extent. This is especially not alarming on account of the reactor differences, and on account of FIMSDIST having an exact calibration for benzene, toluene, and ethylbenzene.

Table 36. Characteristic ratios from the composition data of FIMSDIST method of CTL produced by the cracking of various TAGs in the lab-scale tubular cracking reactor

		AA-Soy	BB-VHONO	CC-HENO	DD-Linseed	EE-Camelina	FF-Corn	GG-Cottonseed	HH-Canola	II-HONO
Paraffin/(Olefin+Cyclic) Ratio	(wt. % basis)									
C3-C8		0.8	1.1	1.0	0.7	0.7	0.7	0.6	0.7	0.8
C9-C13		0.1	0.2	0.2	0.2	0.2	0.2	0.2	0.2	0.2
Aromatics Ratio*	(wt. % basis)									
C6-C8		0.017	0.013	0.017	0.028	0.025	0.015	0.016	0.019	0.019
C9-C13		0.122	0.035	0.061	0.192	0.147	0.130	0.145	0.088	0.062

* Note: Aromatics ratio indicates the quantity of n-alkylaromatics divided by the sum quantity of C-, C=, and COOH components.

The aromatics ratio of C9-C13 components tended to be on the order of 0.12 to 0.22 for FIMSDIST data from the processing of soybean TAG at various temperatures and space times, which was an order of magnitude higher than for C6-C8 components. Detailed compositional analysis of CTL samples from noncatalytic cracking of soybean TAG via CSTR, showing an aromatics ratio components on the order of 0.06 to 0.09. As a result, it appears that the FIMSDIST method is indicating on the order of twice as many aromatics than the detailed method. This may not be alarming, due to the relatively low percentage of aromatics in the overall CTL, in conjunction with the differing types of reactors.

Table 37. Characteristic ratios from the compositional analysis by the FIMSDIST method for CTL produced by the cracking of soybean TAG in the lab-scale tubular cracking reactor under various operating conditions

		A-Soy	B-Soy	C-Soy	D-Soy	E-Soy	F-Soy	G-Soy	H-Soy	I-Soy
Paraffin/(Olefin+Cyclic) Ratio	(wt. % basis)									
C3-C8		0.7	0.6	0.6	0.6	0.7	0.6	0.6	0.6	0.6
C9-C13		0.1	0.2	0.2	0.3	0.2	0.2	0.3	0.3	0.4
Aromatics Ratio*	(wt. % basis)									
C6-C8		0.015	0.015	0.021	0.024	0.024	0.020	0.021	0.026	0.036
C9-C13		0.119	0.122	0.132	0.188	0.146	0.139	0.168	0.192	0.222

* Note: Aromatics Ratio indicates the quantity of n-alkylaromatics divided by the sum quantity of C-, C=, and COOH components.

In examining the comparable aromatics ratio data in Table 36 and Table 34, there appears to be similar dependence of the aromatics ratio on the type of TAG feedstock being used. For detailed composition data of samples produced by noncatalytic cracking in batch reactors (Table 34), the aromatics ratio of C9-C13 ranged components varied from 0.11 to 0.27, with the greatest aromatics resulting from Linseed TAG cracking. Likewise, the FIMSDIST data for the cracking of various TAGs in the TCR (Table 36) indicated aromatics data that varied from as low as 0.03 to as high as 0.19, with the greatest aromaticity resulting from linseed TAG. These numbers appear to be comparable, which helps validate the trends of aromaticity that may be gleaned from FIMSDIST method data.

VI.D.5. Direct Comparison of FIMSDIST Composition Data to Detailed Composition Data for CTL Samples Produced by Sander[62] in a Cracking CSTR

In order to directly cross check the FIMSDIST method with Stavova et al.'s detailed compositional analysis method[152], six of Sander's CSTR samples[62] that were previously analyzed by Stavova et al.'s method were analyzed by FIMSDIST in the present work. A summary of the FIMSDIST rendered composition data is shown in Table 38 for those six samples. Composition data from Stavova et al.'s method is presented in Table 30. The other two samples (CSTR-A and

CSTR-E) from Sander's work[62] were unavailable for FIMSDIST analysis in the present work.

The trends that were observed in the FIMSDIST reported composition as a result of changing operating temperature, space time, and pressure are consistent with those in Table 30 for the detailed compositional analysis.

Table 38. Composition data from high throughput compositional analysis (FIMSDIST method) of CTL produced by the cracking of soybean TAG in a bench-scale continuous-stirred-tank-reactor (CSTR) from the work of Sanders[62]

		CSTR-B	CSTR-C	CSTR-D	CSTR-F	CSTR-G	CSTR-H
Reaction Conditions							
TAG Type	-	Soy	Soy	Soy	Soy	Soy	Soy
Temperature	(C)	420	400	420	420	400	420
Pressure	(Mpa)	2.9	2.9	2.9	1.5	1.5	1.5
Space Time	(h)	2.4	1.4	1.4	2.4	1.4	1.4
CTL Components							
Group C-	(wt. %)						
C5-C8		2.70	0.96	1.89	2.52	0.79	1.81
C9-C13		1.94	0.55	1.24	2.11	0.50	1.32
C14-C18		3.42	1.25	2.48	5.01	1.38	3.28
Group C=	(wt. %)						
C5-C8		2.75	0.89	2.00	3.24	1.04	2.62
C9-C13		6.65	1.99	4.76	7.96	2.61	5.44
C14-C18		5.44	1.96	4.83	8.43	3.03	5.79
Group =C=	(wt. %)						
C5-C8		1.92	0.59	1.76	3.24	0.89	2.19
C9-C13		3.88	1.34	2.90	5.02	1.79	3.64
C14-C18		5.67	2.05	5.20	7.71	3.17	5.88
Group (1x)Ar / (1x)Ar=	(wt. %)						
C6-C8		0.49	0.51	0.41	0.57	0.14	0.34
C9-C13		2.11	2.04	1.90	3.09	0.86	1.98
C14-C18		2.41	2.86	2.69	4.17	1.48	2.91
All (2x) & (3x) Ar	(wt. %)						
C10-C13		0.67	0.78	0.65	1.00	0.30	0.64
C14-C18		2.42	2.92	2.27	2.72	1.50	2.30
Group COOH	(wt. %)						
C1-C5		3.44	2.40	2.58	2.76	2.09	2.56
C6-C9		8.40	6.33	7.83	9.20	7.19	8.37
C10-C14		3.21	1.13	2.68	4.16	1.98	3.22
C15-C18		15.54	10.34	15.19	10.07	18.23	17.39

The FIMSDIST data indicates that increasing reaction temperature results in an increase in the mass fraction of most tabulated groups (i.e., greater yield of various lighter fuel fractions). A similar trend was observed for increasing space time. The effect of pressure was much weaker

than either temperature or space time. Increasing pressure tended to decrease the quantity of C=

and =C= components. These observations agree with previously considered observations that

were mentioned in Section VI.D.1 in regard to data from the method of Stavova et al.[152]

In comparing Table 38 to Table 30, the approximate naphtha range aromatics (C6-C8)

appear to be directly comparable between FIMSDIST and the method of Stavova et al.[152] The

aromatics in the approximate jet range (C9-C13) appear to be less consistent quantitatively,

varying by up to a factor of 2. Nevertheless, the trends in the jet range agree, whereby when the

FIMSDIST reports a high concentration of aromatics, the GC-FID/MS method agrees. The

discrepancy may be due to an increased variety of aromatics, requiring a more diverse set of

calibration compounds used by FIMSDIST, and/or due to the GC-FID/MS method being unable

to resolve and/or identify some aromatics components due to a lack of chromatographic

resolution, which is necessary for that method to quantify components properly.

By summing the quantitified products in Table 38 as compared to Table 30, it appeared

as though the FIMSDIST method was quantifying a greater fraction of Sander's samples.

FIMSDIST quantified between 43 and 81 wt. % of components having carbon numbers below

C18 (inclusive), whereas the detailed compositional analysis method quantified approximately

16 to 35 wt. %. One possible explanation for the greater quantitation in FIMSDIST is that the

detailed method requires gas chromatography resolution, whereas FIMSDIST does not. This

was an expected outcome, and it motivated the development of FIMSDIST.

It should be further clarified that the values reported in Table 38 are not predictions of

yields from the noncatalytic cracking process. In order to provide yields for the noncatalytic

cracking process from FIMDIST data, they must be adjusted for (1) the composition and yield of

gas phase, (2) the effect of catalytic deoxygenation, and (3) the yield of carbon products.

Furthermore, the final fuel yields have a slightly different range, such as for example the jet fuel

range herein is described as C9-C13, whereas the jet fuel range is described as *C9-C13* in

Section VII.E.3.

The sum total of quantified products in approximate fuel range fractions (i.e., naphtha,

jet, and diesel) are presented in the following three figures in order to compare the FIMSDIST

and detailed compositional analysis methods.

Figure 81 shows the quantified naphtha range products for each of the six samples that
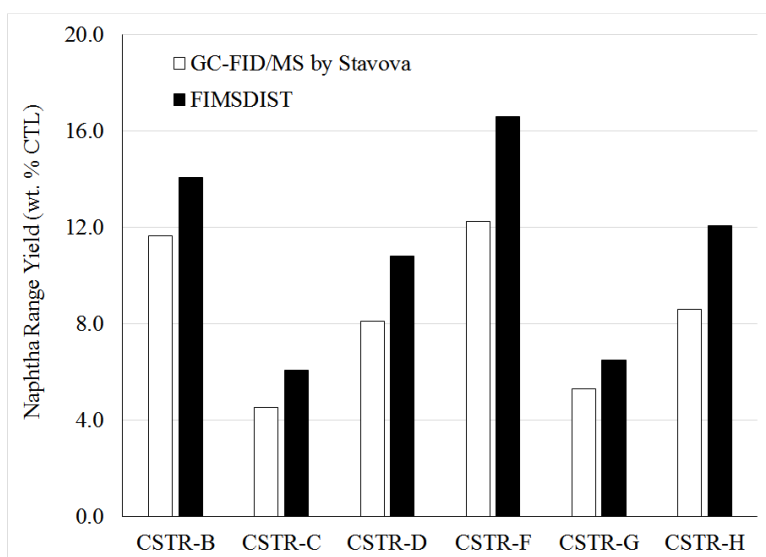
Figure 81. Comparison of approximate naphtha range (C5-C8) quantified products by
FIMSDIST and by detailed compositional analysis of Stavova et al.[152] for cracked TAG distillate
samples produced using the cracking continuous-stirred-tank-reactor by Sander[62]

were considered. What can be observed is a noticeable and similar trend between the FIMSDIST

Note: C9 denotes half the C9 components, and C13* denotes half the C18 components.

method and the detailed GC-FID/MS by Stavova et al. When the detailed method is quantifying

a high fraction of naphtha components, then the FIMSDIST method agrees. Additionally, the

quantified values of the fuels are fairly close, on the order of ±20 wt. % of each other.

Figure 82 shows the quantified products in the estimated jet fuel range (C9-C13). In like

manner to Figure 81, the trend between FIMSDIST and the detailed method are in direct

agreement. Furthermore, the trends in Figure 82 are also matching those of Figure 81, indicating

that when the naphtha fraction is dominant, the jet fuel range fraction will tend to be high as

well. However, the sum total quantitation of the jet fuel components by FIMSDIST are on the

order of twice as high as the detailed GC-FID/MS method, which is in greater disagreement that

for the naphtha range components.
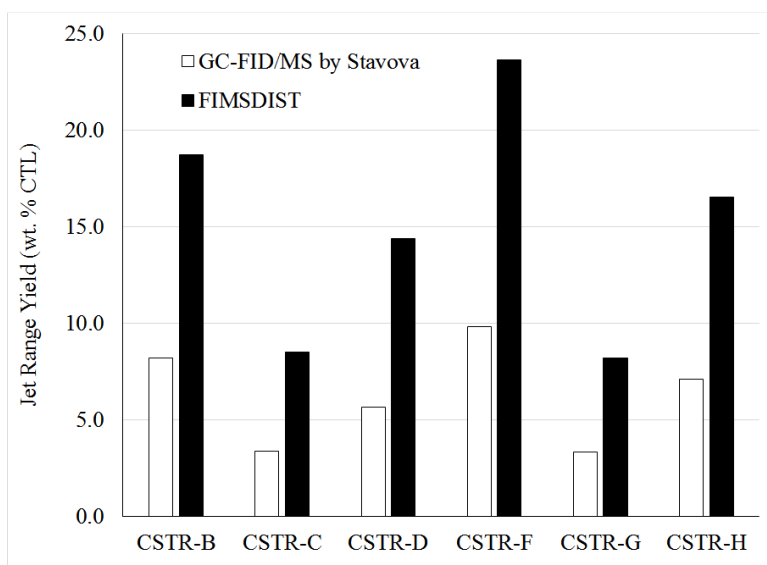
Figure 82. Comparison of approximate jet range (C9-C13) quantified products by FIMSDIST
and by detailed compositional analysis of Stavova et al.[152] for cracked TAG distillate samples
produced using the cracking continuous-stirred-tank-reactor by Sander[62]

This result was expected because the FIMSDIST method represents all mass, whereas the

GC-FID/MS method represents only the mass which can be resolved by gas chromatography. With the greater variety of potential isomers existing at higher carbon numbers, it is expected that as the carbon numbers increase from the naphtha range components to the jet range components, quantitation will decrease for the GC-FID/MS method. Furthermore, greater quantitation of FIMSDIST in the diesel and fuel oil range components is likewise expected, with increasing carbon number.

Figure 83 shows the quantified diesel fuel range products (C14-C18). There may be a slight trend between the FIMSDIST and the detailed method for samples CSTR-F through CSTR-H, however it is not very apparent throughout all samples. In general, the trends in Figure 83 for FIMSDIST match those of Figure 81 and Figure 82 for FIMSDIST. This would imply
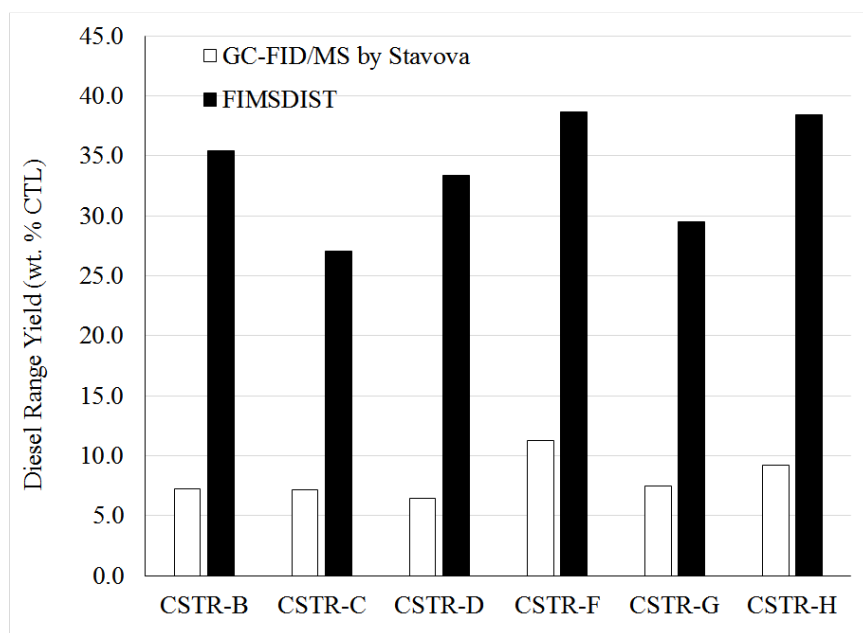
Figure 83. Comparison of approximately diesel range (C14-C18) quantified products by FIMSDIST and by detailed compositional analysis of Stavova et al.[152] for cracked TAG liquid samples produced using the cracking continuous-stirred-tank-reactor by Sander[62]

that when the yield of naphtha is high, it is likewise high for jet and diesel. The sum total

quantitation of the diesel fuel components by FIMSDIST are on the order of threefold to fourfold

greater than the detailed GC-FID/MS method. The explanation for this is the same as for Figure

82 that was described in the previous paragraph.

The ratios of paraffin components (C-) to combined olefin and cyclic components (C=) is

quantified for the naphtha range and jet range below in Table 39 for the detailed method of

Stavova et al.[152] and for the FIMSDIST method. This data has been derived from the data

presented in Table 38 and Table 30. The expectation is that the ratios between the two methods

should be the same regardless of the method used.

Table 39. Ratios of paraffin and isoparaffin components to cyclic and olefin components in the approximate naphtha range (C5-C8) and jet range (C9-C13) for samples produced by Sander[62] and analyzed by the GC-FID/MS method of Stavova et al.[152] and by FIMSDIST

		Ratio of Paraffins and Isoparaffins (C-) to Cyclics and Olefins (C=)					
Range	Analysis	CSTR-B	CSTR-C	CSTR-D	CSTR-F	CSTR-G	CSTR-H
Naphtha (C5-C8)	Detailed GC-FID/MS	1.7	1.6	1.5	1.4	1.2	1.4
	FIMSDIST	1.0	0.8	0.9	0.8	0.8	0.7
Jet (C9-C13)	Detailed GC-FID/MS	0.9	0.7	0.8	0.8	0.6	0.8
	FIMSDIST	0.3	0.2	0.3	0.3	0.2	0.2

However, it appears as though the FIMSDIST method is indicating a reduced quantity of

C- components compared to C= components when compared to the GC-FID/MS method of

Stavova et al.[152] This is shown by Figure 84. The ratio indicated by the FIMSDIST method is

on the order of 60 % that of the GC-FID/MS method for approximate naphtha range (C5-C8)

components. This discrepancy is the same discrepancy that was reported for the ratios from

indirect comparison of samples that were described in Section VI.D.4. The previous explanation

was that the method was inflating the quantity of C= components rather than the reactor. This

direct comparison of the CSTR samples seems to corroborate that explanation. In order to solve

the discrepancy, a greater quantity and variety of calibrants was suggested in Section VI.D.4.
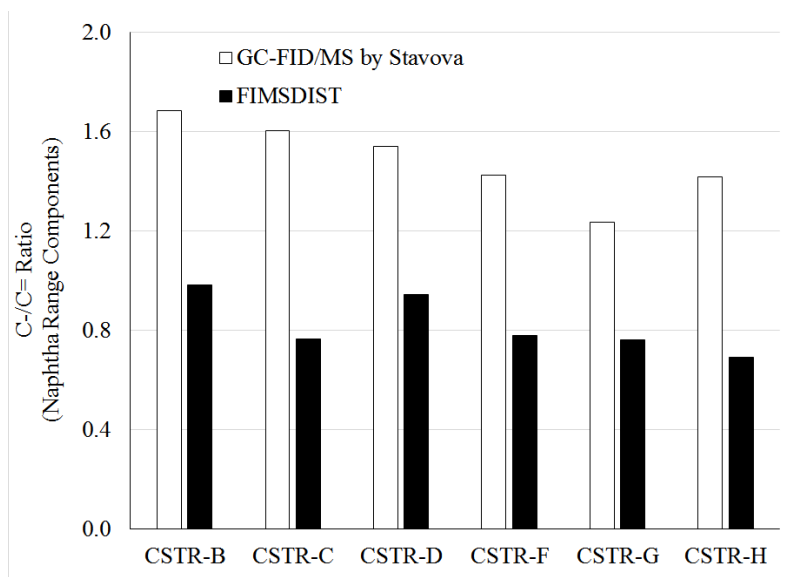
Figure 84. Ratio of paraffin and isoparaffin components to cyclic and olefin components in the approximate jet range (C5-C8) for samples produced by Sander[62] using a cracking CSTR and analyzed by detailed GC-FID/MS method of Stavova et al. and by FIMSDIST[152]

Figure 85 shows the C-/C= ratio for samples quantified by the FIMSDIST method vs. the

GC-FID/MS method for approximate jet range (C9-C13) components. The discrepancy between

FIMSDIST and GC-FID/MS method of Stavova et al.[152] is approximately a factor of 2.5 to 3.0.

In like manner as observed for approximate naphtha range components, discrepancy is the same

discrepancy that was reported for the ratios from indirect sample comparison in Section VI.D.4.

The explanation for the discrepancy is that a greater number of calibration compounds are

necessary so that the response from FIMSDIST is in line with the response from the detailed GC-MS/FID analysis of Stavova et al.[152]
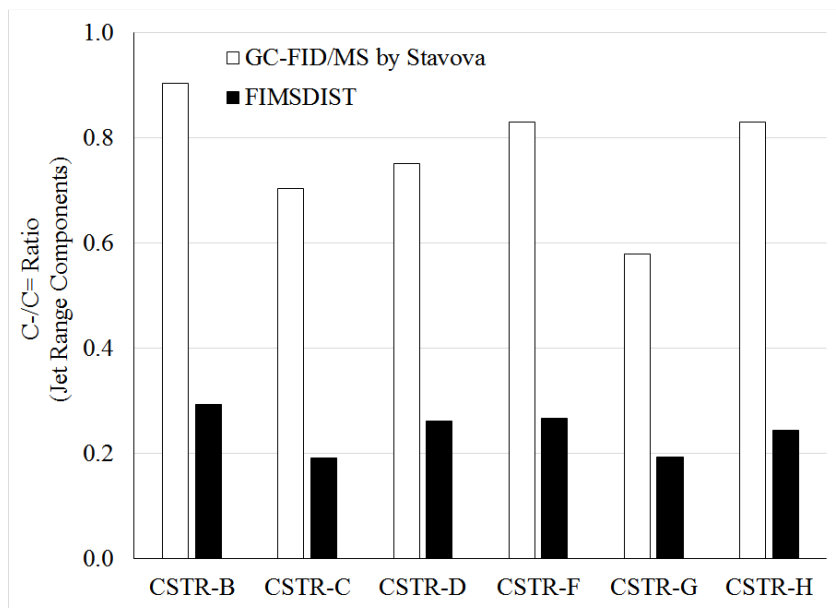
Figure 85. Ratio of paraffin and isoparaffin components to cyclic and olefin components in the approximate jet range (C9-C13) for samples produced by Sander[62] using a cracking CSTR and analyzed by detailed GC-FID/MS method of Stavova et al. and by FIMSDIST[152]

VI.D.6. Summary

The detailed compositional analysis method was used to determine a great quantity and variety of compounds in CTL samples as reported in Appendix A. This is particularly advantageous for (1) mechanistic insights, (2) determining target components, (3) examining ratios of products in various fual fractions. Furthermore, the data from detailed compositional analysis is critical for (1) developing new methods, (2) validating such methods (e.g., FIMSDIST), and (3) providing data to compensate for shortcomings of new methods.

One unfortunate consequence of relying on these detailed composition data is that there is

a large fraction of unresolved, unidentified, or otherwise nondescript sample mass. This complicates the prediction of fuel yields from the NCP if they are based solely on the detailed compositional analysis data because it is not known how the nondescript CTL sample mass should be distributed into fuel products.

As a result, fuel yield estimations from detailed compositional analysis data are strongly subject to the way in which the data were utilized. For example, the preliminary study of noncatalytic cracking process yields utilized the CSTR composition data by normalizing it to the CTL yield (assuming it was representative of the total CTL composition). As a result, no components in the simulation had carbon numbers greater than C25, which may be a very inaccurate representation of what should be expected from the NCP.

This motivated the development of the FIMSDIST method, which does not require chromatographic resolution of analytes and is capable of eluting components with boiling points in excess of 650 C. As a result, problems with unresolved and non-elutable components were mitigated.

The carboxylic acid concentration was considered in Section VI.C, where it was shown that FIMSDIST was suitable for quantifying most of the carboxylic acids up to C18 (inclusive), but not C5-C7 carboxylic acids. It was necessary to use data from other methods (see Section VI.C) to provide information on C5-C7 acids.

Despite some of its attractive features, FIMSDIST is unable to differentiate between cyclics/olefins and paraffins/isoparaffins as they are formula isomers. As a result, the ratios of paraffins/isoparaffins and olefins/cyclics were explicitly reported in this section to be utilized as needed, potentially in future simulation studies. The ratios presented herein could be used to

normalize the FIMSDIST data into a more suitable form, if desired. Since *n*-paraffins were found in such a high concentration, it is believed that isoparaffins may be neglected. As a result, FIMSDIST's quantitation for paraffins should be considered to be accurate, since the calibration utilized a full range of *n*-paraffins. The olefin/cyclic ratio might be assumed on the order of 2 to 6, indicating a much greater quantity of olefins than cyclics.

In addition, other ratios were examined in order to determine the validity of FIMSDIST. The aromatics quantification as evaluated by the indirect comparison of samples from different reactors appeared to be different, but not unreasonable due to the differences in reactor types. The aromatics concentrations in direct comparison of samples analyzed by both methods appeared to be very comparable. The trends in aromaticity tended to agree with those of detailed compositional analysis data. Discrepancies were observed between the ratios of paraffins to cyclics+olefins (C-/C= ratio) from FIMSDIST analysis vs. detailed compositional analysis. The evidence seemed to suggest that the RIE for olefins may need to be 3 times higher, ultimately adjusting the fraction of olefins in the TCL by a factor of approximately 3. This may stem from a variety of possibilities, all of which require additional calibration using concentrated PIANO standard solutions or other specialized standard solutions to confirm the RIEs for a greater number of compounds.

In comparing the data from detailed compositional analysis to that of FIMSDIST, similar trends were observed in the two methods. Increased cracking severity led to an increase of lighter components. This trend was predicted by both analytical methods utilized for compositional analysis. Furthermore, similarities were noticed in the chemistry, such as increased cracking severity led to increased aromatics ratio. Additionally, carboxylic acids and

313

aromatics tended to agree between cracking of various types of TAG and analyzing by

FIMSDIST or by detailed compositional analysis. As a result, the utilization of FIMSDIST for

determining trends in TAG noncatalytic cracking chemistry seems to be supported, but further

standardization and/or adjusting the RIE for C= group components by a factor of 3 should be

strongly considered for quantitative accuracy.

VI.E. Summary of FIMSDIST

Based on these observations, it appears that the FIMSDIST high throughput

compositional analysis of cracked CTL samples is fairly valid in some circumstances and invalid

in other circumstances.

As previously mentioned FIMSDIST is unable to provide reliable data for formic acid,

C5-C7 carboxylic acids and carboxylic acids above C20. This is caused by poor relative

ionization efficiency (RIE) observed for those components in FI mass spectrometry (see Figure

66 on page 255). In order to obtain suitable replacement data required utilizing data from the

work of detailed characterization methods such as Geetla.[156]

In addition, the work of Geetla demonstrated a strong disagreement with the FIMSDIST

reported carboxylic acid C20. Given the nature of the declining RIE of carboxylic acids in the

range of C20, Geetla's data are assumed to be the correct data in this circumstance. This is

indicative that the data from FIMSDIST are potentially only valid up to C18 for carboxylic acids.

In addition, since FIMSDIST was previously developed based on the observations of

Luo,[54] unsaturated carboxylic acids were not anticipated in the CTL. As such, no prior

consideration was made for unsaturated carboxylic acids, and no calibration was developed for

these compounds for use with the FIMSDIST method. As presented herein, FIMSDIST was

unable to confirm the identity of presumed unsaturated carboxylic acids in CTL, and instead it mistakenly identified saturated carboxylic acids as hydrocarbon components.

Geetla likewise found the presence of unsaturated carboxylic acids at up to 15 % (mol carboxylic acids basis) in all seven of the CTLs samples that she worked with (out of the nine total samples considered herein). Geetla was able to show that the unsaturated carboxylic acids were all C18 and greater in size, directly a result of long chain unsaturated fatty acid moieties in the original TAG feedstock. This agrees with speculations herein. Furthermore, FIMSDIST tended to improperly identify those acids as larger carbonaceous compounds (e.g., COOH 18:1 being identified as (2x)Ar 21).

As a result of this, the data from FIMSDIST high throughput compositional analysis of CTL samples appears to be valid up through C18, but no higher. It should also be mentioned that a greater resolution mass spectrometer would be able to overcome some of the resolving limitations of FIMSDIST described herein.

Over the range of carboxylic acids that FIMSDIST was able to accurately quantitate, FIMSDIST appeared to be reasonably consistent with the data of Geetla on a mass basis. This is presented in Section VI.C, with the trends in quantitated carboxylic acids between Geetla and FIMSDIST tended to agree quite well. Additionally, FIMSDIST data appears to be justified for aromatics and paraffins as described in Section VI.D.

Discrepancies in the FIMSDIST data were observed for the C= group components, and speculated for and =C= group components through comparison to detailed compositional analysis data. It may be considered to adjust (increase) the RIEs for C= group components by a factor of 3 in future renditions of the FIMSDIST data, which will consequently decrease the

315

yield of C= and =C= fractions by a factor of ~3. Nevertheless, greater standardization of the FIMSDIST method is highly desired, through the procurement and utilization of more concentrated PIANO standards to provide calibration for a greater diversity of components in FIMSDIST.

FIMSDIST appears to be suitable for elucidating trends in the data, due to the observation that the trends in the composition of the CTL tended to agree with Geetla (Section VI.C) and with the detailed compositional analysis from Sander and from batch work (Section VI.D).

In the Section VII.E.3, FIMSDIST data has been used to produce mass-based data via the FIMS calibration depicted in Figure 66 (see page 255). Then the data were arranged in summation format in order to examine the effects of various cracking parameters on the CTL composition. CTL data from FIMSDIST was also combined with gas phase data and CTL yields that are presented in Chapter VII (see Section VII.B.4 and VII.E.2).

CHAPTER VII

EXPERIMENTAL RESULTS

This chapter presents the results of catalytic deoxygenation experiments, experiments in cracking reactor design, and experiments to determine the yields of triglyceride noncatalytic cracking.

VII.A. Catalytic Deoxygenation Experiments

Since catalytic deoxygenation is necessary to produce fuels meeting the ASTM standard specifications for transportation fuels, these experiments were very important. Preliminary deoxygenation experiments were performed using powdered catalysts in order to prove that acidity could be reduced to international jet fuel specifications by palladium and nickel catalysts. Then screening deoxygenation experiments were performed, by first preparing and testing the properties of several nickel catalyst formulations in comparison to commercial palladium and nickel catalysts. Then the relative activities of the catalysts were determined in batch experiments in order to determine trends and to select catalysts for testing at a larger scale. Finally, a single catalyst was tested in packed bed reactors in order to determine suitable operating conditions that allowed the catalyst to effectively deoxygenate the fuel intermediate with acceptable levels of catalyst activity over a 56 hour period.

VII.A.1. Preliminary Deoxygenation Testing

Preliminary tests of a nickel-based deoxygenation catalyst in comparison to a palladium-

based deoxygenation catalyst were performed in batch reactors as described in Section V.C.1.i. A powdered 5 wt. % palladium on activated carbon catalyst (i.e., Pd/C 5 powder) was compared to a Ni/SiO2 64 powder catalyst. Cracked TAG distillates (CTD) were used as a test feedstock, having been obtained from the noncatalytic cracking of soybean TAG followed by phase separation and fractionation. The yield and total acidity of deoxygenated CTD were determined. The results of this test are shown in Table 40 below.

Table 40. Results of preliminary deoxygenation testing in batch reactors

Deoxygenation System	-	Dual-Purpose Batch Reactor	Dual-Purpose Batch Reactor
Feedstock	-	CTD	CTD
Temperature	(C)	325	325
Pressure	(MPa)	1.8	1.8
Catalyst	ratio (type)	1:50 (Pd/C 5 powder)	1:50 (Ni/SiO2 64 powder)
Batch Cycles	-	4	4
Deoxygenated CTD			
Yield	wt. %	88.2	91.3
Acidity	mgKOH/g	0.002	0.012
Olefins	mol/L	0.014	0.019

A higher yield of deoxygenated CTD was observed for the nickel catalyst in comparison to the palladium catalyst. This may be due to greater reduction during reaction by the nickel catalyst.

Reduction is also evident through the lack of olefins in the deoxygenated CTD as determined by FTIR. Fuel production processes often observe and attempt to limit the quantity of olefins in final fuels so that the fuel has good oxidative stability properties. The mol/L olefins may be used for an estimate of the mass percent olefins through simply comparison to a 5 wt. % 1-tetradecene standard in n-dodecane, whose molar olefin composition was determined at

0.310 mol/L. By comparison, the wt. % of olefins in the product deoxygenated CTD might be estimated at less than 0.5 wt. %. This is well below quality standards for olefins in jet fuel.

The FTIR spectra is shown for CTD (feedstock) and deoxygenated CTD (product) from deoxygenation using Ni/SiO2 64 powder in Figure 86. As pointed out by the arrows, the intensity of the carboxylic acid peak at wavenumber 1710 is negligible after deoxygenation. The FTIR for deoxygenated CTD from reaction using Pd/C 5 powder catalyst is not shown because it is redundant and otherwise indistinguishable from the deoxygenated CTD from reaction using Ni/SiO2 64 powder catalyst.
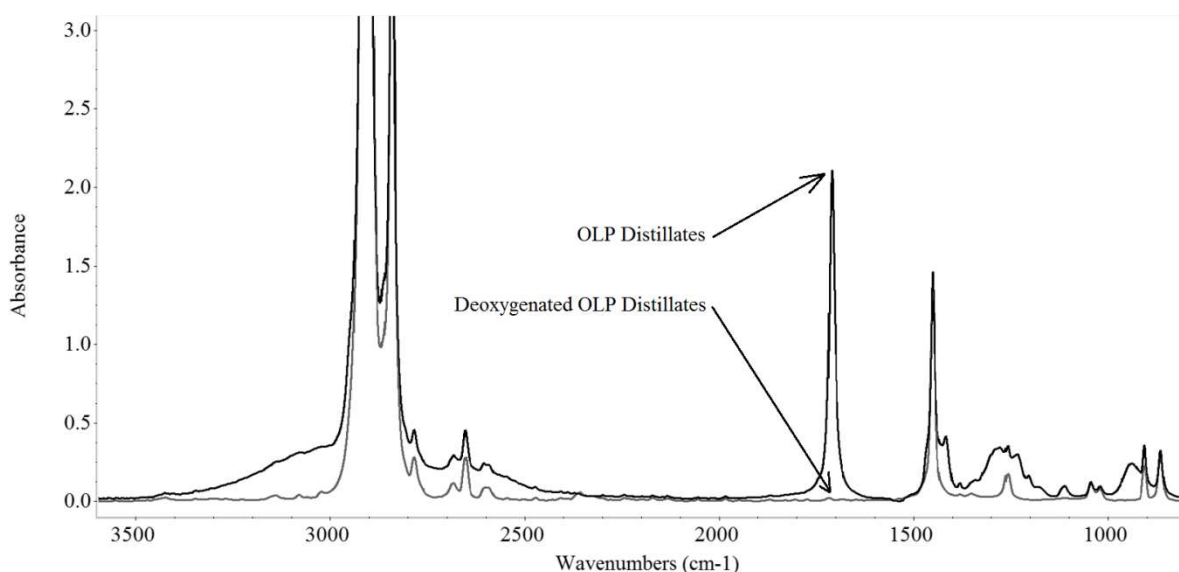
Figure 86. FTIR of feedstock distillates and fully deoxygenated product

VII.A.2. Batch Reactions to Screen Catalyst Activity

The batch reactor was used to screen catalysts for activity as previously described in Section V.B.2.i (see page 210). Samples were taken from the liquid phase of the reactor at various time intervals in order to map the activity of the catalyst using FTIR as an analytical

technique. The FTIR was used to determine the molar concentration of carboxylic acids in the liquid samples for each data point over time. The calibration of the FTIR for oxygenates (both esters and acids) is shown in Appendix E.

The time-based concentration of octanoic acid in the deoxygenation reactor outlet product has been plotted in Figure 87 for several catalysts of interest. The data shown are the average of two experimental replicates for each catalyst. As shown, the molar concentration of octanoic acid decreases steadily as the reaction progresses for each of the catalysts studied. A linear regression is included for each data set in order to help visualize the differences between the catalysts.
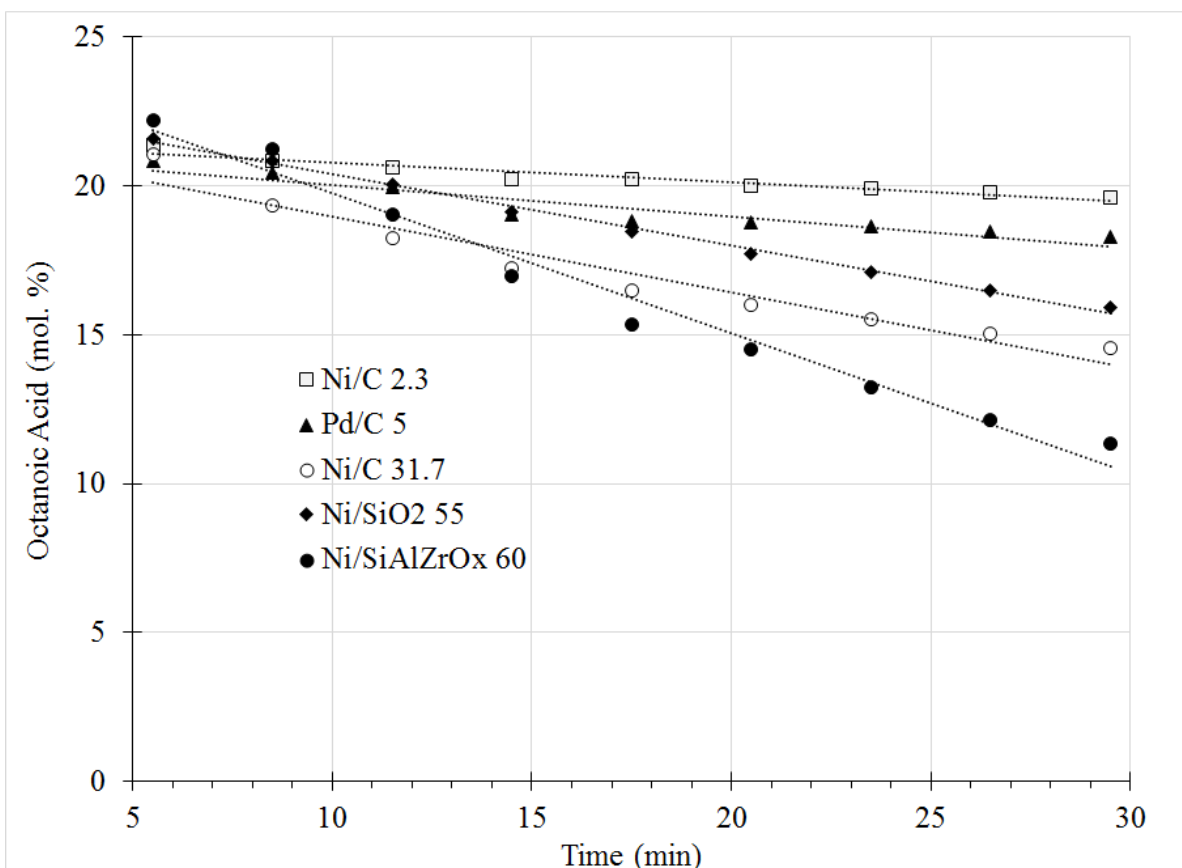
Figure 87. Octanoic acid concentration vs. time for batch catalytic deoxygenation reactions

The most rapid and strongest decline in octanoic acid concentration was observed for the Ni/SiAlZrOx 60 catalyst. This is indicative that Ni/SiAlZrOx 60 has the strongest activity of all the catalysts tested. Without the linear regressions drawn in Figure 87, it might be assumed that the second strongest catalyst is Ni/C 31.7, based on the magnitude of its decent. However, scatter in the data is removed by the linear regression to show that both Ni/SiO2 55 and Ni/C 31.7 have equivalent slopes (indicates by their linear regressions being drawn parallel). As a result, it can be considered that they have essentially the same magnitude of activity towards deoxygenation as studied. Likewise, Pd/C 5 has less activity and Ni/C 2.3 has the lowest activity. In addition, there are 4 additional Ni/C catalysts which were not depicted in Figure 87 so as not to clutter the figure. Data for these are included in Appendix B.

The observed integrated activity of each catalyst was computed as the average millimole reduction in carboxylic acids per time per gram catalyst (on the basis of a 23.4 mol % feedstock and a reaction temperature of 325 C). These have been plotted in Figure 88, and error bars represent the percent difference of two replicates.

In comparing the Ni/C catalysts to three commercial catalysts, it appears that the higher nickel load Ni/C catalysts are capable of at least 2-3 times more activity than the Pd/C 5 catalyst under the conditions studied. Due to the scatter in the data, it is difficult to say whether Ni/C 20 or Ni/C 30 are more active than the commercial catalyst Ni/SiO2 55. In any event, Ni/SiAlZrOx appears to have at least twofold stronger activity than any of the other catalysts considered in this study.

In observing the activity of the Ni/C catalysts, it is apparent that increasing the percentage of nickel in the catalyst formulation led to a direct increase in observed activity up to

at least Ni/C 4.6. Above Ni/C 4.6, diminishing returns start to become noticeable in that the addition of twice as much nickel does not supply twice as much activity. Nevertheless, the addition of nickel to the formula appears to have an increasing effect on the activity up until the point of approximately 20 wt. % nickel. Above 20 wt. % nickel in Ni/C wet impregnated catalysts appears to have the same activity.
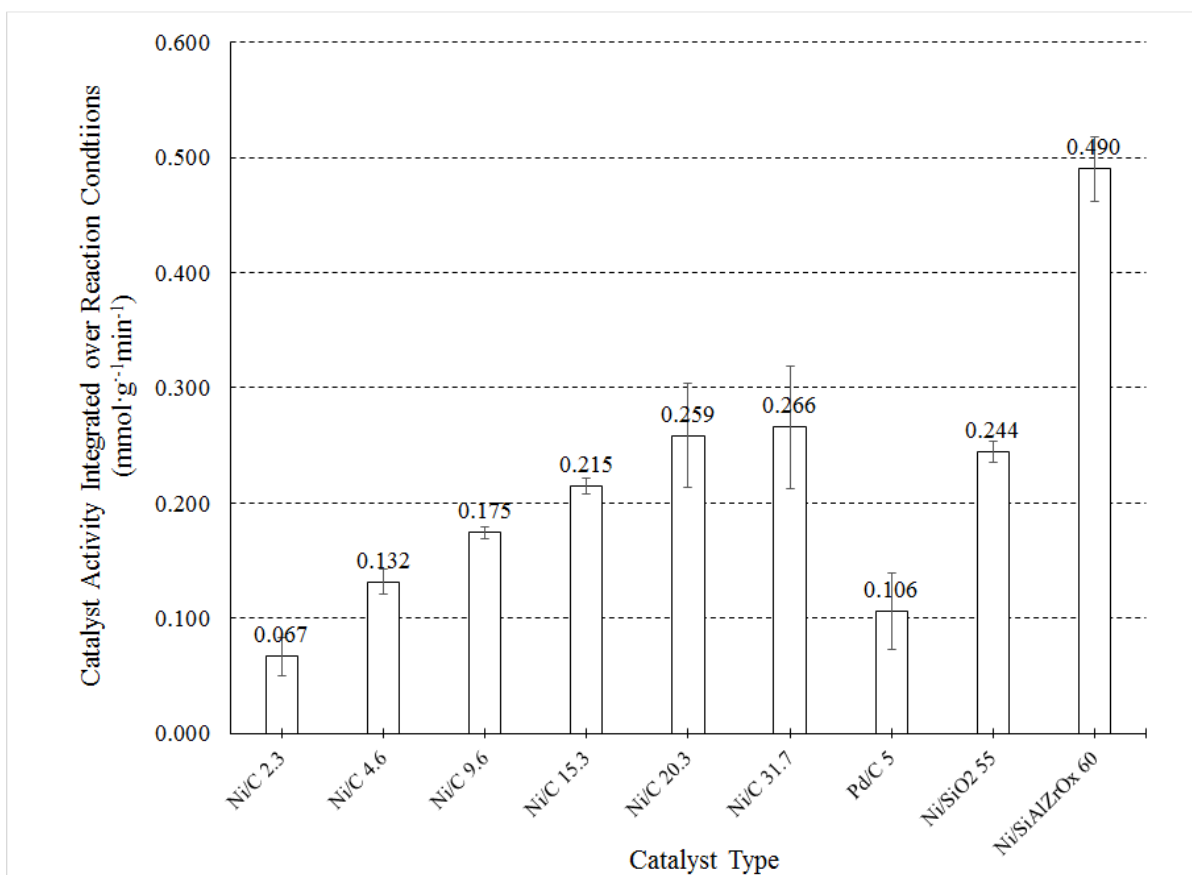
Figure 88. Observed deoxygenation activity of various commercial and prepared catalysts

The liquid samples taken from the use of blank carbon and the empty reactor weren't analyzed by FTIR. Nevertheless, the reactivity of the reactor was found to be negligible and the

activity of the catalyst support is relatively weak in comparison to the catalysts (although minor activity was observed). These observations were gleaned from the gas phase composition data presented in the following subsection.

VII.A.2.i. Analysis of Gas Phase

The gas phase from the batch reactions were analyzed by GC-FID/TCR as previously described in order to determine the concentration of various components. The compositions are presented in Table 41, using mole percentages for lighter components and mass percentages for heavier components. Data are represented as the mean (standard deviation) of their respective units for replicates where applicable. Data have been normalized to 100%, although on a molar basis the recovery was 96% on average and always greater than 90%.

What can be observed from this table is that the mole fraction of hydrogen and the mole fraction of methane are inversely related. Most of the gas phase compositions appear similar, with high concentrations of H_2, modest concentrations of CH_4, and low concentrations of CO and CO_2. An unusual case is observed for Ni/SiAlZrOx 60, which has

Table 41. Gas phase composition from batch deoxygenation screening reactions

Basis	Mole %				Mass %		
Component	H_2	CO	CO_2	CH_4	$(C_2H_X-C_6H_X)$	C_7H_X	C_8H_X
Empty Reactor	99.8	0.01	0.0	0.1	0.0	0.0	0.0
Blank Carbon	99.6	0.2	0.2	0.0	0.0	0.2	0.0
Pd/C 5	97.9 (0.1)	1.9 (0.1)	0.1 (0.0)	0.1 (0.0)	0.1 (0.0)	1.6 (0.3)	0.1 (0.0)
Ni/C 2.3	99.1 (0.1)	0.2 (0.0)	0.1 (0.0)	0.7 (0.1)	0.1 (0.1)	0.4 (0.2)	0.1 (0.1)
Ni/C 4.6	98.3 (0.0)	0.0 (0.0)	0.1 (0.0)	1.6 (0.0)	0.0 (0.0)	1.1 (0.4)	0.1 (0.1)
Ni/C 9.6	97.1 (0.9)	0.0 (0.0)	0.1 (0.0)	2.7 (0.9)	0.1 (0.2)	1.8 (0.2)	0.3 (0.3)
Ni/C 15.3	95.1 (0.6)	0.0 (0.0)	0.1 (0.0)	4.7 (0.5)	0.2 (0.3)	1.5 (0.4)	0.1 (0.1)
Ni/C 20.3	93.0 (2.5)	0.0 (0.0)	0.2 (0.1)	6.7 (2.4)	0.5 (0.4)	2.0 (0.2)	0.0 (0.0)
Ni/C 31.7	n.d.	n.d.	n.d.	n.d.	n.d.	n.d.	n.d.
Ni/SiO2 55	91.1 (2.1)	0.0 (0.0)	0.1 (0.0)	8.7 (2.1)	0.8 (0.0)	1.1 (0.4)	0.1 (0.0)
Ni/SiAlZrOx 60	10.6 (0.7)	0.0 (0.1)	19.7 (0.5)	64.0 (1.2)	9.4 (0.3)	0.9 (0.1)	0.0 (0.0)
Note: n.d. stands for not determined.							

a greatly reduced quantity of hydrogen and greatly increased methane and CO_2 concentrations. Furthermore, CO_2 was only significantly present in reactions with the Ni/SiAlZrOx 60 catalyst. It is also noticeable that the mass fraction of C_2H_X-C_6H_X components is relatively high for the Ni/SiAlZrOx 60. In addition, the mass fraction of C_2H_X-C_6H_X components appears to increase in the various Ni/C catalysts as the nickel content in the catalyst increases.

VII.A.2.ii. Characterization of Catalysts

The catalyst properties were determined for the several internally prepared Ni/C catalysts according to the characterization methods described previously in Section V.C.1.ii (see page 208). The catalyst properties for the commercial catalysts were obtained from their vendors. Properties for all catalysts studied are tabulated in Table 42, with properties such as metal content, estimated surface area, bulk density, fines loss, and observed activity from the batch experiments above.

The nickel content of the various catalysts was determined by UV-VIS as previously described on page 208. What is important to note is that the catalysts that were prepared by wet impregnation were intended to span a wide range of nickel content in order to be able to discern any trends in the catalyst formula that may influence the catalysts' reactivity. According to the metal content verified by UV-VIS, the range of catalysts spanned nickel contents as low as 2.3 to as high as 31.7 wt. %. The palladium content of the palladium catalyst was substantially towards the lower end of the metal contents studied. The Ni/Si(X) variety of catalysts had extremely high nickel contents on the order of 55 to 60 wt. %.

The surface area of the Ni/C catalysts was estimated using a standardized iodine number test as previously described (page 208) and presented in Table 42 as shown. The estimated

Table 42. Properties of the deoxygenation catalysts studied

Designation	Active Metal	Support	Metal Content	Est. Surface Area	Bulk Density	Fines Loss	Observed Activity
-	-	-	wt. %	m²/g	kg/m³	wt. %	mmol·g^{-1}·min^{-1}
Ni/C 2.3	Ni	C	2.3 ± 0.4	1160	476 ± 27	0.0	0.067
Ni/C 4.6	Ni	C	4.6 ± 0.3	1120	492 ± 9	0.1	0.132
Ni/C 9.6	Ni	C	9.6 ± 0.4	1040	527 ± 10	2.1	0.175
Ni/C 15.3	Ni	C	15.3 ± 1.5	820	516 ± 18	3.3	0.215
Ni/C 20.3	Ni	C	20.3 ± 0.6	870	536 ± 15	7.0	0.259
Ni/C 31.7	Ni	C	31.7 ± 1.4	640	502 ± 26	9.0	0.266
Pd/C 5	Pd	C	5	1000	n.d.	n.d.	0.106
Ni/SiO2 55	Ni	SiO$_2$	55	80	1000	n.d.	0.244
Ni/SiAlZrOx 60	Ni	SiO$_2$/Al$_2$O$_3$/ZrO$_3$	60	90	1000	n.d.	0.490

surface area ranged from 1160 to as low as 640 in Ni/C catalysts, whereas in the Ni/Si(X) catalysts, the surface area was an order of magnitude less. The bulk density of the Ni/C catalysts ranged from 476 to 536 kg/m³, increasing slightly with the Ni content of the catalysts. The bulk density of the Ni/Si(X) catalysts were approximately twofold higher. This is likely due to the increased nickel content in conjunction with the less porous supports. Although the bulk density of the Pd/C was not determined, it might be estimated on the order of 475 kg/m³, based on the idea that the carbon was dominating the density in comparison to the density of Ni/C 2.3.

The losses to fines during the production of the Ni/C catalysts was determined using sieve type filter trays as previously described (page 208). The loss to fines ranged from essentially 0.0 to 9.0 wt. %, increasing with nickel content. This is an important consideration, whereas the increased nickel content tends to increase the amount of waste produced during catalyst manufacture.

VII.A.3. Deoxygenation in Continuous Packed Bed Reactors

A single catalyst was selected for testing in lab-scale and batch scale packed bed reactors.

Although Ni/SiAlZrOx 60 appears to be the best choice based on its twofold greater activity, this catalyst was found to have an extremely high molar consumption rate of hydrogen, based on the differences in hydrogen concentration observed from the gas phase exiting the reactor. In addition, Ni/SiAlZrOx 60 yielded an order of magnitude higher concentration of $C_2H_X - C_6H_X$ compounds (i.e., catalytic cracking compounds) during the deoxygenation test reactions described above. For this reason, Ni/SiAlZrOx 60 was not chosen for follow up testing.

Considering the remaining high-activity catalysts, Ni/SiO2 55 was selected for continuous reactor tests above Ni/C because Ni/SiO2 was readily available in large quantities commercially whereas both Ni/C 20.3 and Ni/C 31.7 had to be manufactured via wet impregnation.

As previously described on Section V.C.1.v, several tests were conducted using a packed bed reactor system with either a 0.1 kg or 1.0 kg bed of catalyst. Distillates were prepared from by TAG cracking and distillation as described previously in Section V.A.2. These distillates were co-fed to the packed bed reactor with hydrogen and/or water as described on page 175.

At first, all tests were performed on the 0.1 kg bed system over the temperature range of 250 – 350 C. The initial packed bed reactor commissioning test labeled 'Deoxy-19' in Table 14 was conducted using a model feedstock of 20.9 wt. % octanoic acid in cyclohexane. The catalyst was activated and the reactor was brought to operation for 3 hours with a continuous feed of hydrogen gas and the model compound feedstock. The feedstock and bulk products were analyzed by FTIR as shown in Figure 89 with the feedstock spectrum shown above and the product spectrum shown below.

The octanoic acid peak is very visible in the feedstock near the vicinity of wavenumber

1700 cm^{-1}. However in the product stream, the peak is entirely absent as shown by the arrow.

Standardized titration tests of the effluent by ASTM 974 indicated essentially zero acidity (below

the method's detection limit) to confirm that the deoxygenation was completed to the extent

required in order to produce jet fuel meeting ASTM specifications.[27]

The next series of tests labeled 'Deoxy-20' through 'Deoxy-25' were conducted using a

practical feedstock of CTD obtained from the processing of soybean TAG using equipment to

model the NCP as described in Section V.A.2. To reiterate, the CTD were obtained from the

cracking of soybean TAG to produce cracked TAG (CT), which was followed by phase

separation of cracked TAG gas (CTG) and cracked TAG liquid (CTL), which was then followed

by distillation of the CTL to produce CTD.
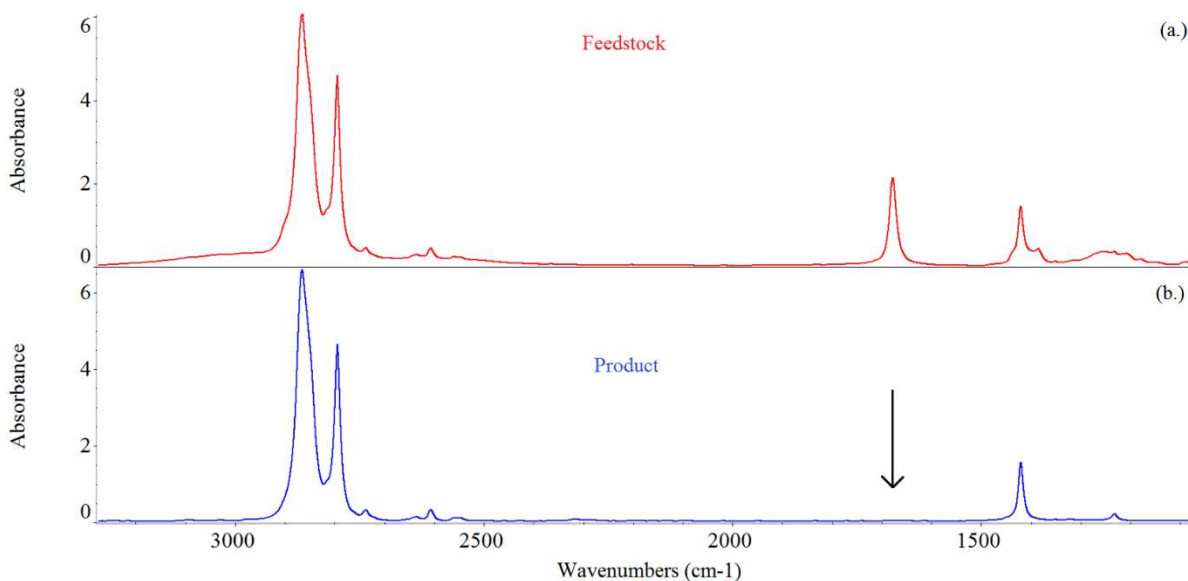
Figure 89. FTIR absorbance spectra from the deoxygenation of octanoic acid in a packed bed
reactor using Ni/SiO2 55 catalyst: a) feedstock and b) product spectra

327

The tests using CTD as a feedstock were carried out in a similar manner as those using a model compound feedstock, first activating the catalyst via the previously described reduction procedure, and then feeding hydrogen and CTD under the specified conditions in Table 14. Product samples were collected from the PBR over several hours each day the reactor was in operation and analyzed by FTIR. An example of one of the FTIR charts is shown below in Figure 90.

Initially, the extent of reaction across 100 grams of catalyst was nearly 70 %, based on FTIR for the first ~1 hour. However, the conversion of deoxygenation dropped steadily
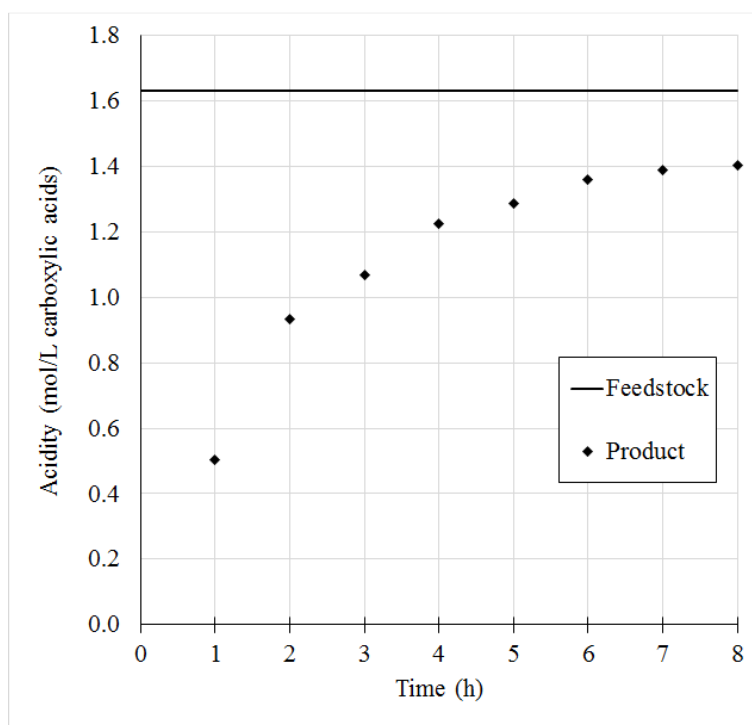
Figure 90. The acidity of CTD before and after deoxygenation in a packed bed reactor using Ni/SiO2 55. Time represents the duration the catalyst is in operation, not the space time of reactants in the reactor.

over the next several hours potentially indicating a loss of activity in the bed. Eventually, the

pressure drop across the bed reached inoperable levels and the reactor was shut down. Upon

shutting down and cooling the reactor, it was decommissioned and the catalyst was examined to

find severely coked catalyst as shown in Figure 91.

Figure 91. Coked bed of Ni/SiO2 55 catalyst

In response to this, attempts were made to adjust the feed ratio of hydrogen to CTD and

especially to adjust the temperature of the bed. Conditions studied are included in Table 14.

Despite these efforts, all of the experiments labeled 'Deoxy-20' through 'Deoxy-22' showed similar deactivation results to Figure 90. After one experiment, the reactor was opened and the catalyst was examined to find that it was impregnated with tarry residue as shown in Figure 92.
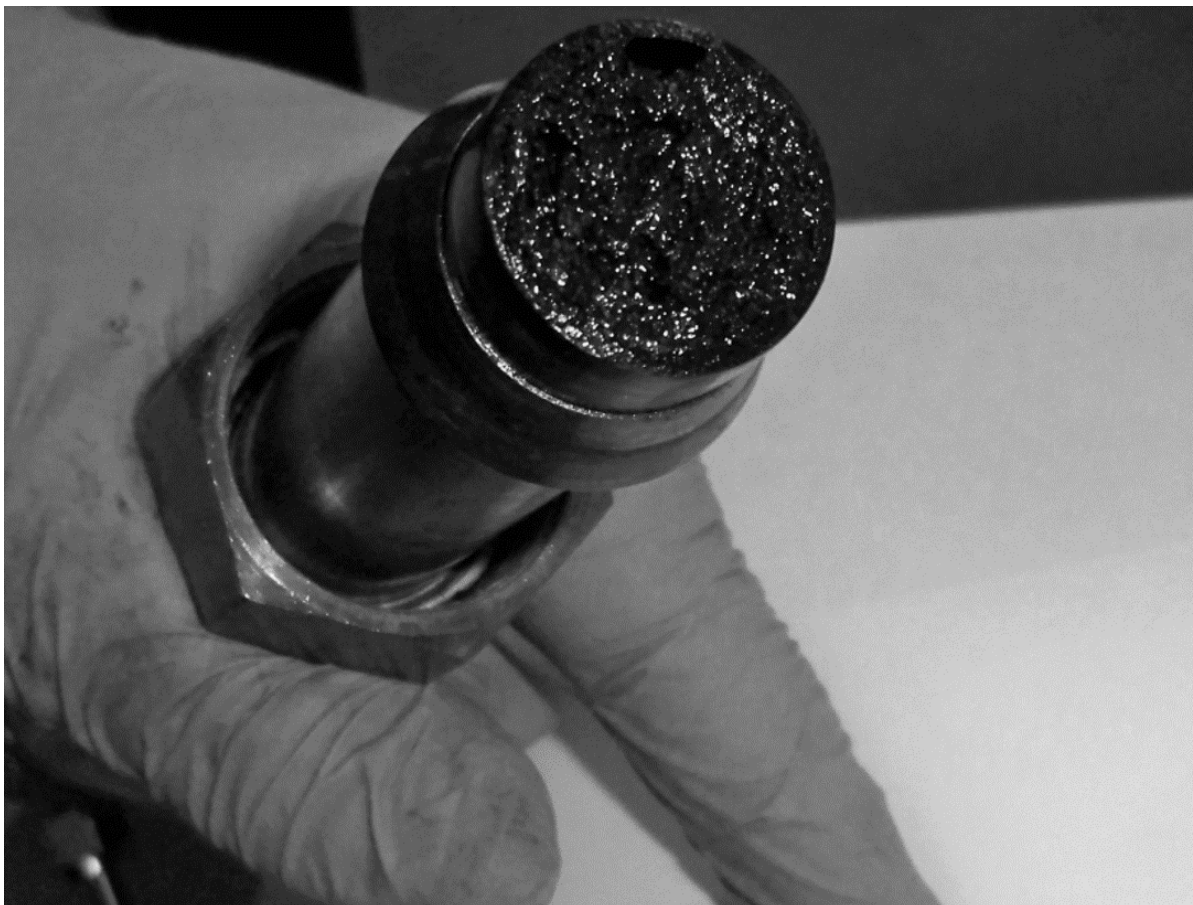
Figure 92. Catalyst impregnated with tarry residue

A previously reviewed publication (see Section I.D.2) by Katikaneni et al.[44] discussed the significance of adding steam to catalytic processes that were notoriously coke prone. Katikaneni observed a positive effect from adding steam to the catalytic cracking of TAG in that the steam prolonged the catalyst life and promoted deoxygenation. Consequently, this same addition of

steam was utilized herein for the catalytic deoxygenation packed bed reactor.

A 1.0 kg sized PBR was loaded with 0.98 kg of new catalyst and operated according to the experimental operating conditions described for 'Deoxy-23' in Table 14 (page 211), utilizing a 1:20 mass ratio of water to CTD. In like manner to previous BPR experiments, product samples were taken from the reactor at regular intervals and their acidity was monitored by FTIR to indicate the activity of the catalyst. A plot of the product acidity over time is shown in Figure 93.
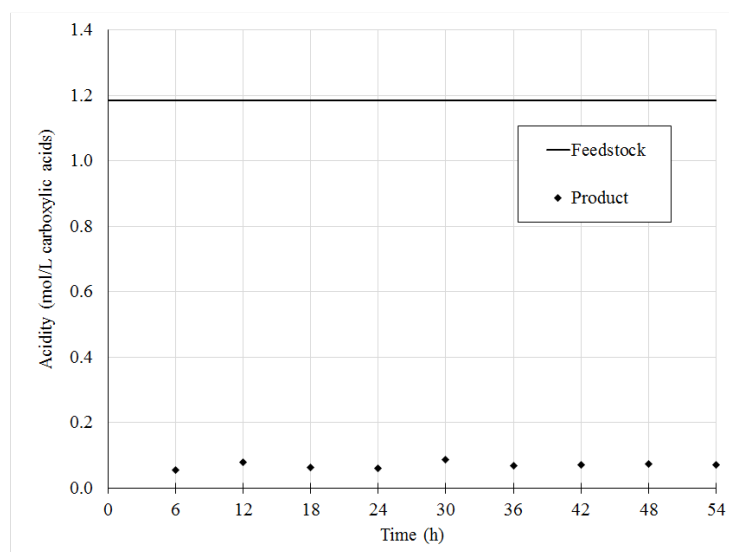
Figure 93. The acidity of CTD before and after deoxygenation in a PBR
using Ni/SiO2 55 supplemented by the minor addition of steam

Through the addition of steam, stable activity was observed for 54 hours continuous operation of the packed bed reactor. The average reduction in acidity over the 54 hour period was a 94% molar reduction in acidity under the conditions studied. At approximately 20 hours into the run, the operating conditions were switched to that of 'Deoxy-24' (Table 14 on page

211), in that the hydrogen feed rate was set to zero. The activity remained stable and unchanged, as shown in Figure 93. At approximately 36 hours into the run, the water feed rate was reduced from 0.05 to 0.03 as described in sample 'Deoxy-25,' and no loss in activity was observed as indicated.

VII.B. Coking and Cracking Reactor Design

In order for the NCP to be commercially relevant, it was also important that the systems studied in the laboratory easily scaled to a commercial sized plant. Because severe coke formation makes it difficult to scale process equipment, experiments were necessary to elucidate coke formation and to design a tubular cracking reactor that was capable of continuously cracking TAG with minimal coke formation.

Experiments performed using the continuous-stirred-tank-cracking reactor (CSTR) indicated that this design was not capable of operating without coke formation. A series of batch reactor experiments were conducted to show that factors such as temperature and residence time had a strong effect on coke formation, and they needed to be well controlled. This led to the design, construction, and testing of a prototype tubular cracking reactor (TCR) that was capable of operating without coke formation.

Based on the success of the prototype TCR, a lab-scale TCR was constructed and operated in order to determine the potential for coking in TCRs. Coking in TCRs was found to be a result of similar conditions in the batch reactor, such as excessive temperature and/or residence time. Observations from the lab-scale TCR eventually led to the design, construction, and testing of a bench-scale TCR unit for TAG cracking that was successfully operated over a 100 hour period without coke formation, proving that the design and scalability of a non-coking

332

TAG cracking reactor was feasible.

VII.B.1. Classifications of Coke Formation

In this section, qualitative observations of coke formation are used to as experimental results. This was done since the quantitation of coke by mass was tedious and challenging to do accurately without a reactor system that has been designed for convenient study of coke formation. On account of the successful ability to counteract coke formation in cracking reactors through the results herein, the inferences that can be obtained from qualitative experimental results were proven effective without quantitation.
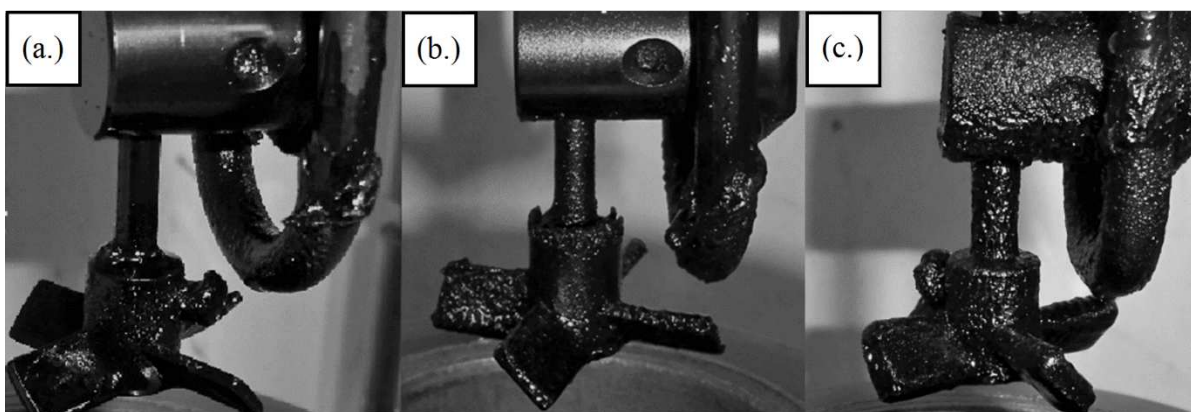
Figure 94. Coke formation qualitative classification: a) flocculating, b) mature, and c) severe

The mildest classification for coke is *flocculating* coke, which is characterized by the formation and agglomeration of small solid amorphous coke particles. These particles eventually stick to and agglomerate on surfaces especially in stagnant areas of flow. This can be seen in Figure 98.a where agglomeration on the surface of an impeller is observed. Flocculating coke is further defined as being able to be removed from a surface simply by wiping and/or agitation and it is therefore filterable from the bulk fluid.

On the other hand, mature coke is more dense and rigid, typically forming at a solid surface, as shown in Figure 98.b. Mature coke forms a rough layer on the metallic surface. Its rigidity makes it difficult to remove, so scraping, brushing, and abrasive action is needed. In a continuous process, mature coke may be removed by steam-air decoking, spalling, or line pigging, but generally it is necessary to shut down the equipment and service it, reducing process efficiency.

Severe coke, shown in Figure 98.c is the propagation of mature coke on a surface, becoming increasingly thick and hazardous to safe operation of equipment. The hazardousness stems from the risk of large particles breaking off and plugging orifices and due to dramatic performance changes in heat transfer.

VII.B.2. Coke Formation in Cracking Continuous Stirred-Tank Reactors

VII.B.2.i. Operating Conditions

As previously described (see Section V.B.1.v), a continuous-stirred-tank-reactor was designed and commissioned during the master's thesis work of Sander for the cracking of TAG at the bench-scale.[62] Sander found that this reactor was an improvement to its predecessor, which was a short/wide tubular cracking reactor (TCR) that was characterized by very severe coke formation. During his thesis work, Sander was able to show that a continuous-stirred-tank-reactor (CSTR) was better for TAG cracking than the short/wide TCR, improving yields and reducing coke formation.

In the present work, attempts were made to continue Sander's work by studying TAG cracking reactions in the cracking CSTR. Various operating conditions were tested, which are summarized by Table 15 on page 214, include varying operating temperature, pressure, and

space time. A schematic of the CSTR and operating procedure is described in Section V.B.1.v (see Figure 33 on page 165).

During these experiments, coke formation was observed in all cases as the inevitable result of using a CSTR for TAG cracking. This included cracking with as mild of conditions as 1 h space time and 400 C. Furthermore the coke was classified as severe, being a thick layer that was hazardous to safe operation. Strong abrasion was necessary to remove the majority of the coke from the walls on a regular basis.

Over an extended period of reactor operation, the coke formation was found to be so severe that it was hazardous to keep the reactor running for more than 15-30 hours without shutting down and cleaning. In one particular extended run (> 40 h), coke formation was observed to nearly cover all of the reactor except for a narrow 6-10 cm central region where the impeller shaft was agitating. Large clumps of cokes were broken from the reactor as shown below in Figure 95. Such severe coke formation is responsible for dangerous reactor plugging as a result of the pressure generated by cracking reactions.

In response to the observance of severe coke, operating times in the cracking CSTR were typically shortened to approximately 10 – 15 h in order to produce results that could conceivably be valid and/or at steady state.

Some extended runs were nonetheless performed carefully as necessary, typically resulting in large quantities of coke. In these cases, temperature fluxuations became significant as the reaction progressed. This is assumed to be caused by increasing thermal lag from the heaters due to thermal resistance from the increasingly thick layer of coke.

Figure 95. A large clump of coke produced during cracking in a severely coked CSTR

The thickness of the coke layer on the walls was variable with the height of the reactor. The thickest region typically resided towards the center of the reactor as indicated by the thickening black walls below in the example Figure 96. In the thickest region, it was typically noticeable between approximately 0.6 mm and 2.0 mm thick after only approximately 10 – 15 hours of operation.

This was the region where the measured temperatures were greatest. Coke formation was also observed on thermocouples and the impellers. Coke formation did appear to cover all surfaces of the reactor, but was dramatically lessened on the top and bottom surfaces where band heaters were not contacting. On those surfaces it was typically less than 2 mm, approaching 0 mm at the base of the reactor.
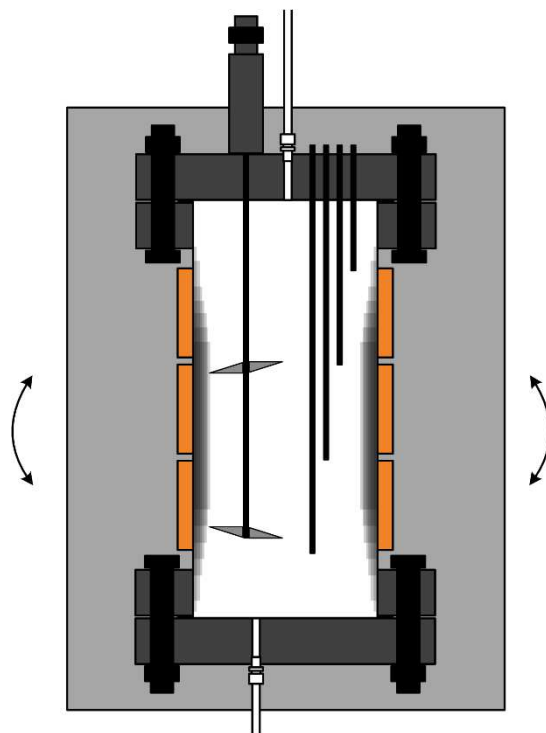
Figure 96. Region of greatest coke formation in the TAG cracking CSTR

In all cases, upon shutting down the reactor and disassembling the vessel, severe coking was found on the surfaces of the reactor. For these reasons and over the conditions studied, operating parameters did not appear to have a significant ability to negate coke formation. The effect of variations in reactor operating parameters on the coke formation was not able to be considered quantitatively. This would require the repeatable removal, isolation, and collection of coke gravimetrically.

In practice, it proved especially difficult to remove the entirety of the coke from the walls of the reactor, and the researchers involved in the work were concerned about the lack of repeatability that would result. Due to the total laboriousness of removing, capturing, and isolating the dry weight of coke, in conjunction with the laboriousness of reactor operation, only

qualitative observations of coke formation were used as experimental outcomes from the CSTR.

VII.B.2.ii. Wall Temperature Measurement

Concerning the adaptation of a strategic thermocouple to measure the wall and/or coke temperature in situ, temperatures in the forming coke were found to be as much as 50 C hotter than in the bulk fluid. By contrast, the wall-contacting thermocouple typically measured within a few degrees of the bulk fluid temperature at the same fluid elevation during the start of the reaction. During the experiment, this temperature was on the order of 410 C. After 5 – 6 h of operating time however, the wall-contacting temperature began to rise steadily over approximately 1 h, eventually leveling off at approximately 460 C. Meanwhile the bulk fluid remained in the vicinity of 410 C, although temperature instability became increasingly worse from 5 – 8 h of operation, fluctuating on the order of ±10 C. Due to the temperature instability, the reactor was shut down after 8 hours of continuous operation to observe any formation of coke. After the reactor was disassembled and examined, it was found that a 4 – 5 mm layer of coke had enclosed the thermocouple's tip.

VII.B.2.iii. Increased Feedstock Oil Preheating Temperature

Increasing the temperature of the preheated oil was expected to reduce the coke formation by reducing the flux through the reactor wall. This would effectively reduce the temperature at the wall–fluid interface. Unfortunately, the additional preheating did not appear to have any effect on coke formation.

VII.B.2.iv. Removal from the Bottom of the Reactor

No substantial reduction in coke formation was observed by the installation and operation of a bottoms draw for the cracking CSTR. Coke particles tended to appear in the filter for the

338

bottoms draw, having an estimated size of 2 mm or smaller, including fine and coarse particles. The filter was swapped out and cleaned approximately every 30-45 minutes in order to mitigate line clogging in the bottoms draw. Nevertheless, line clogging was always a concern, and it happened not infrequently making it difficult to infer success in coke prevention.

VII.B.3. Coke Formation in Batch Reactors

Since the experiments and modifications of the cracking CSTR did not have a significant ability to mitigate coke formation, the use of batch reactors was considered to elucidate coke formation criteria that would be useful to design a continuous, non-coking reactor. Furthermore, small batch reactors are advantageous for studying coke formation factors due to their small size and thoroughly controlled environment, in comparison to the CSTR which was laborious to operate and especially to clean. Coke was not commonly observed during the research group's previous experiences in cracking TAGs in batch reactors. Therefore, batch reactor operating conditions were adjusted from typical (i.e., non-coking) operating conditions in order to elicit coke formation, which could then be explained. A schematic of the reactor and operating procedure for the reactor may be found on page 142 (Figure 27) and an experimental list is shown in Table 17 in Section V.C.2.ii (see page 216).

VII.B.3.i. Reaction Temperature

Two temperatures were used for the study of coke formation in batch reactors: 430 and 445 C. Batch cracking of TAGs showed no evidence of coke formation on the surfaces of the reactor for any of the conditions studied at 430 C with up to 1 hour of reaction time.

By contrast, in all cases where the reactor was operated at 445 C, mature coke appeared in like appearance to Figure 94.b. The mature coke was only found in areas where liquid was in

339

contact with the surface, indicating a liquid phase coke formation reaction rather than a gas phase coke formation reaction, although both mechanisms have been observed in various petroleum processes.

In order to remove the coke from the surfaces of the reactor, a power drill was necessary, equipped with a 5 cm metal wire brush at speeds of approximately 300 – 600 rpm. Coke removal from the 500 mL reactor took approximately 5-10 minutes. It was deemed to be too tedious and/or inaccurate to attempt to measure the quantity of coke that was produced.

VII.B.3.ii. Reaction Time

Since mature coke always formed at 445 C (with a minimum residence time of 0.5 hours), it was important to determine the length of reaction time that soybean TAG could crack at lower temperatures (i.e., 430 C) before mature coke presented. For this reason, soybean TAG was cracked at 430 C for various lengths of time separately, including 0.5, 1.0, 1.5, 2 and 3 hours. It was not necessary to repeat these experiments at 445 C because it had already been shown that 0.5 hours was a sufficient length of time for mature coke to form at that temperature.

From these tests, it was observed that no coke was visibly formed after 1 hour at 430 C. However, at 1.5 hours of reaction time, flocculating coke appeared as small particulate in the liquid phase (see Figure 94.a). The coke appeared to be agglomerating with a tar-like residue that appears to form either within or around the coke particles. This agglomeration was apparent in that the fine coke particles tended to clump together in the liquid phase and on reactor surfaces. When they were wiped off reactor surfaces, the agglomerations smeared thickly onto paper towels and latex gloves. The consistency of the agglomerations was tarry, with fine grit particles in the tar. Nevertheless, the flocculating coke was easily removed from the surfaces by

wiping, and scrubbing/abrading was not needed.

In examining the reactor after 2 hours of operation, the coke would be classified as mature coke. The coke appeared in greater quantity and it was more difficult to remove from the surfaces. For complete removal of the coke, it was necessary to use repeat wipes with paper towels with scrubbing action. It was also necessary to use mixed xylenes as a solvent to help achieve complete coke removal. The particles were similar to flocculating coke although they were growing in size and thoroughly fixed on the surfaces of the reactor as shown in Figure 94.b. In like manner to the mature coke resulting from cracking at 445 C, this coke was only present on surfaces exposed to liquid phase contact, similarly indicating a liquid phase coke formation mechanism.

When the reactor was operated for 3 hours and inspected, the coke formation was classified as severe. There was a large, thick presence of coke that had adhered to the surfaces of the impeller, thermocouple, and reactor walls that were in contact with the liquid phase as shown in Figure 94.c. It proved to be futile to attempt to remove the coke by wiping or simple abrading. Instead, it was necessary to remove the coke using a power drill with an attached metal wire brush. As expected, this coke presented in the liquid regions of the reactor.

VII.B.3.iii. Phase Removal

After observing that thermal cracking could proceed for at least 1 hour without the production of coke, it was important to examine the influence of phase separation on coke formation. The thought is that the removal of volatile "solvents" (i.e. cracking products) from the cracking reactor by phase removal tends to concentrate asphaltenes in the liquid phase. It was anticipated that the concentration of asphaltenes would result in the formation of mature coke on

reactor surfaces. In order to investigate this, two different types of phase separation experiments were performed at 430 C. The first type was the continuous removal of the vapor phase in order to maintain a constant reaction pressure at 1.5 MPa. The second type of phase removal was a sudden flashing of volatile components, achieved by fully opening the effluent valve and permitting the reaction to continue until cracked TAG distillate (CTD) condensation rates were negligible (less than about a tenth of a milliliter per minute).

In both cases, a tar-like residue remained in the reactor. In order to remove the residue, the vapor phase material that had been removed was condensed and recovered, and then added back to the reactor at standard temperature/pressure after the reaction was finished and the gas was vented. With sufficient mixing, the distillates were sufficient to remove all traces of tar-like residue, indicating that no coke was formed in these experiments.

Concerning phase removal, the most important observation was that no coke particles were found to be adhering to the surfaces of the reactor. This was contrary to the hypothesis stated above that increasing the concentration of asphaltenes would promote flocculation of coke. Since coke is a second order reaction by nature, the concentration of asphaltenes would be expected to produce coke. Nevertheless, coke did not present during these phase separation experiments. A large number of papers document studies of TAG cracking via destructive distillation and/or pressurized destructive distillation as in these experiments. Most publications of this type do not make mention of coke. Based on the findings herein, it is reasonable to assume that they did not observe coke during their experiments.

VII.B.3.iv. Other Factors

Both the initial reactor pressure head of nitrogen gas and the volume of oil loaded into the

342

batch TAG cracking reactors tended to affect the mean reaction pressure and max reactor

pressure, as anticipated. These were not shown to influence coke formation in this study.

VII.B.3.v. Summary

After examining the factors that promoted coke formation, higher temperatures and/or

higher reaction times promoted coke formation. Phase separation was expected to cause coke

formation, however that was not found in these experiments. Pressure also did not impact coke

formation.

VII.B.4. Continuous Tubular Cracking Reactors

This section describes the versions of the tubular cracking reactor (TCR) which were

used to crack TAG continuously while mitigating coke formation and determining the operability

range of the reactor.

VII.B.4.i. Prototype Tubular Cracking Reactor

The prototype TCR is depicted in Figure 28 in Section V.B.1.ii. The reactor was only

commissioned briefly, being quickly replaced by a more robust TCR unit. During its short term

of service, it was only operated at the conditions indicated in Table 18 (see Section V.C.2.iii).

No coke formation was observed in the 100 mL tubular reactor volume and no coke particles

were observed in the product stream. There were no restrictions, neither gradual nor sudden, that

would indicate clogging or flow constriction. A list of experimental operating conditions utilized

is described by Table 18.

The CTL from the cracked TAG had a thicker (i.e., less visbroken) appearance than

anticipated, indicating potentially less severe cracking than desired. It was considered that the

TAG may require additional heating to reach oil cracking temperatures. With this qualitative

observation, TAG preheating was implemented on the successor reactor (the 100 mL lab-scale TCR).

VII.B.4.ii. Lab-Scale Tubular Cracking Reactor

The lab-scale TCR was constructed as described in Section V.B.1.iii (see Figure 29 on page 148) in order to permit continuous cracking of TAG in the absence of coke formation based on the success of the prototype TCR. This system included three different reactor configurations, as depicted by Figure 30 (page 155). The lab-scale TCR was operated under a variety of conditions as described in Table 19. This was done in order to examine the reactor yields and to determine what the range of operability would ensure the absence of coke formation or be at risk for coke formation.

The reactors were operated over a wide temperature range as low as 420 C and as high as 470 C. A variety of space times were also tested, ranging from as low as 0.27 hours to as high as 1.28 hours. Only two pressures were examined in this series of experiments (1.5 and 2.9 MPa). The CTL yields from its operation are shown in Table 43. Unless otherwise noted, soybean TAG was used as the feedstock.

One significant observation that was found using the TCRs was the production of agglomerations in the sub-cracking temperature range. When the reactor was originally brought online from ambient conditions, the reactor passed through a lower temperature region on the order of 360 – 400 C. During this temperature range, a rise in reactor pressure was often seen and found to be caused by an increased pressure drop across the filter array (i.e., F-1a/b depicted in Figure 29). Upon changing the filters and inspecting them, a fat-like agglomeration was observed as shown in Figure 97.

Figure 97. Fat-like residue on stainless steel filter during sub-cracking temperatures

This agglomeration was presumed to be TAG oligomers and/or partially reacted glycerides with long chain fatty acids. It presented as a sludge/gelatinous substance as shown in the figure. The sludge did not cause the reactor to plug, however it did cause a rise in pressure across the filter and it also caused problems for the pressure regulating value (i.e., V-6). At reactor temperatures greater than 400 C, this sludge formation was not noticed. Its observance is useful for reactor design considerations discussed in Section VIII.B.

In several experiments involving cracking with the 100 mL lab-scale TCR, steady state was not achieved. Originally, the 100 mL TCR included a preheater that was maintained at a temperature equal to the cracking reactor's temperature. It was thought that this would properly preheat and introduce components to the reactor at the desired reactor operating temperature. However, it was soon found that coking occurred in the preheater, especially when the temperature exceeded 430 C. As a result of these experiments, the preheater temperature was

reduced to 340 C, which was well below the temperature expected to produce cracking based on the observations of Luo.[54]

It was also found that sometimes during reactor operation, the TAG feed pump, i.e. P-1 (see Figure 29 on page 148), would cavitate with an air bubble. As a result, the operator had to work quickly to get the pump re-primed so that the reactor could continue regular operation. In cases when the pump was not feeding for extended periods of time (> 10 – 20 min), coke formation typically resulted in the reactor as a plug. The plug was typically observed by a large pressure rise across the reactor after the pump was eventually restored to operation. The greatly elevated pressure was typically about 5.9 MPa caused by the pressure building action of the pump, whereby 5.9 MPa was the pump's practical limit of operation. For this reason, a feedback control system was implemented on the 200 mL reactor in order to produce an alarm if the pump stopped feeding TAG.

VII.B.4.iii. The impact of operating temperature, pressure, and space time on the yield of cracked TAG liquid (CTL) from the noncatalytic cracking of TAG

In many of the cases however, steady state was reached and a sample of CTL was collected at steady state, determining the liquid yield gravimetrically. A summary of the conditions studied and the CTL yield from the reactor are included in Table 43. The rows in Table 43 represent experiments with data collected at steady-state reactor operation. All of the experiments utilized the 100 mL TCR except for the last row, which utilized the 500 mL TCR. These reactors are closely related in their design and operation although they differ in their geometry, preheating, and the quantity/location of thermocouple probes, as described by page 148.

Table 43. Tubular cracking reactor operating conditions to determine CTL yield

Label	Temperature	Pressure	Reactor Volume	Space Time	CTL Yield
-	(C)	(MPa)	(mL)	(h)	(wt. %)
A-Soy	420	2.9	100	0.27	94.6
B-Soy	430	2.9	100	0.27	93.9
C-Soy	440	2.9	100	0.27	92.4
X1	450	2.9	100	0.27	90.7
X2	460	2.9	100	0.27	89.1
X3	470	2.9	100	0.27	86.6
X4	420	1.5	100	0.27	95.6
X5	430	1.5	100	0.27	94.0
X6	440	1.5	100	0.27	92.3
X7	450	1.5	100	0.27	90.3
X8	470	1.5	100	0.27	86.6
D-Soy	420	2.9	100	0.69	91.2
E-Soy	430	2.9	100	0.70	90.5
F-Soy	440	2.9	100	0.69	87.2
G-Soy	420	2.9	100	1.22	88.9
H-Soy	430	2.9	100	1.17	86.8
I-Soy	440	2.9	100	1.11	85.1
X9	450	2.9	100	1.16	72.5
X10	435	1.8	500	1.28	87.5

What can be observed from these experiments is that the CTL yields were decreasing with increasing temperature and increasing space time in the reactor. This is furthermore shown by the plots of CTL yield for various samples in Figure 98 and Figure 99.

Figure 98 shows the yield of CTL at various temperatures and two operating pressures for low space times (0.27 h). Pressures were investigated at either 1.5 MPa or 2.9 MPa, and temperatures were investigated over the range of 420 to 470 C. CTL yields ranged from as low as 86.6 wt. % to as high as 95.6 wt. %.

What can be seen is a decreasing trend with increasing temperature to as high as 470 C. This is observed for both 1.5 MPa pressure and 2.9 MPa pressure. Furthermore, there does not appear to be a dependence of the CTL yield as a function of pressure since the CTL yield is quite similar at either pressure for any given temperature. The reactor was not operated higher than
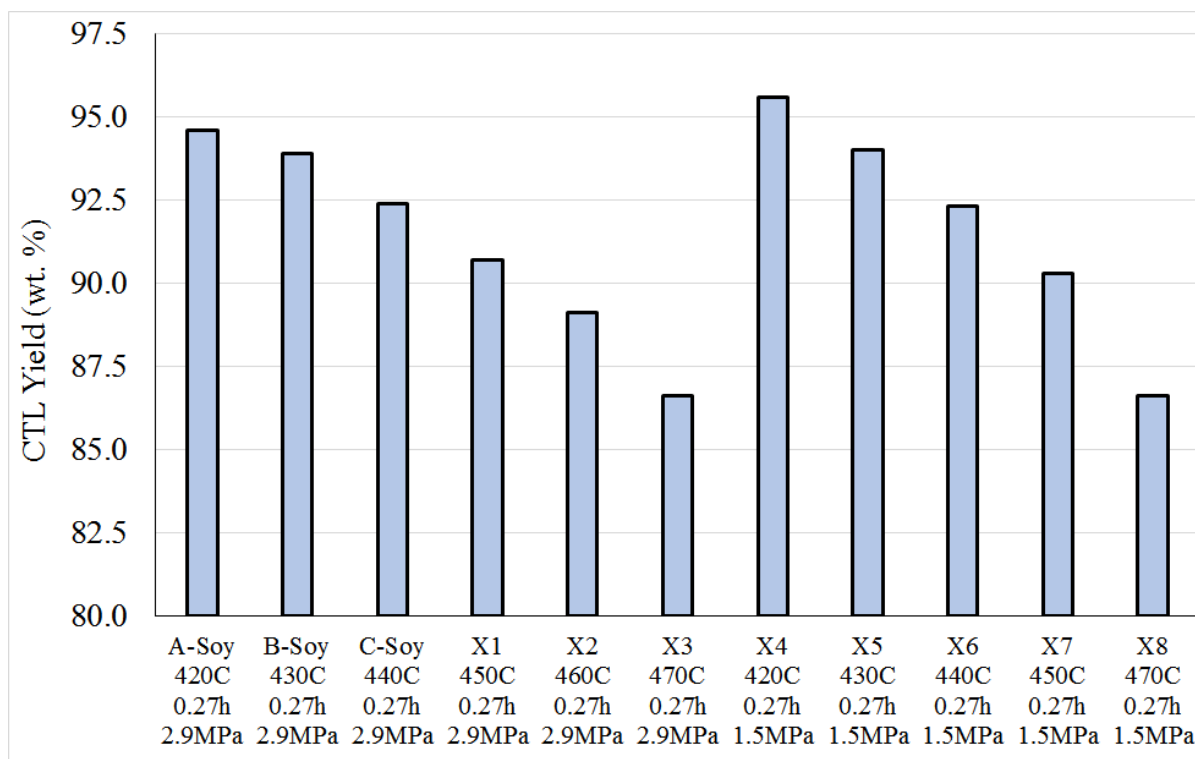
Figure 98. Yield of CTL from the tubular cracking reactor vs. operating
temperature and pressure at low space time for soybean TAG

470 C due to concern about the integrity of the stainless steel reactor parts.

Figure 99 shows the yields of CTL from the tubular cracking reactor vs. operating
temperature at moderate/high space times. Space times in these experiments were either of 0.7
or 1.2 hours on the 100 mL TCR or 1.3 hours on the 500 mL TCR. Temperatures were
investigated over the range of 420 to 450 C. Pressure was kept constant at 2.9 MPa. Larger
deviations in CTL yield were observed ranging from as low as 72.5 wt. % to as high as 91.2 wt.
%.

It is observed that increasing the reaction temperature results in a decrease in yield of
CTL in a similar manner as for Figure 98. Additionally, increasing the space time from the low
space time (0.27 h) shown in Figure 98 to the moderate/high space times shown in Figure 99
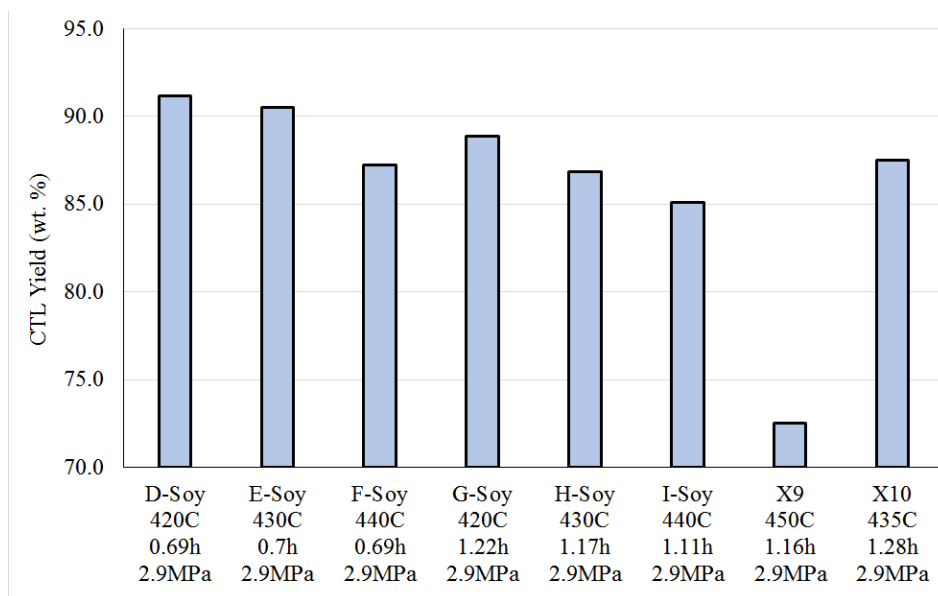
Figure 99. Yield of CTL from tubular cracking reactor vs. operating temperature and moderate/high space time for soybean TAG

leads to a decrease in CTL yield. This is indicative of increased process gas formation, likely resulting from increased extent of the TAG cracking reactions.

From these observations, it appears as though increasing temperature and/or increasing space time results in an increase in the severity of cracking. As indicated in Figure 98, pressure did not appear to increase the severity of cracking.

One clearly exceptional case is sample X9. This sample was operated at 450 C and 1.16 h space time. What was observed was a dramatic decrease in the yield of CTL from the operating case of I-Soy. Additionally, X9 was only operated for a relatively short period of time, on the order of about 2 hours. Afterwards, coke formation was found to result in the reactor from an observed rise in pressure drop across the reactor, i.e. PT 1 – PT 2 (see Figure 29 on page 148). The coke formation resulted in a pressure of about 5.9 MPa at the TAG feed pump, i.e. P-1, causing the pump to stop operating. This plug warranted reactor shut down and the reactor

was discarded for a virtually identical replacement.

X10 was a considerably different case in that X10 was performed using a different reactor (500 mL) from the other samples in this series (100 mL). The reactor was 5x longer reactor, and it also had no preheater. Sample X10 was reacted at conditions that were similar to H-Soy, although it was operated at 5 C hotter temperatures and 0.11 h longer residence times. Despite the elevated operating conditions, the yield of CTL from sample X10 was slightly greater than that of sample H-Soy. Based on this, one might conclude that the longer/thinner reactor has a positive effect on the CTL yield, but this claim is difficult to make without more information.

It was necessary to operate the 500 mL reactor (i.e., experiment X10) at the maximum flow rate of the reactor's TAG feed pump, i.e., P-1 (see Figure 29 on page 148). Prior attempts to operate the reactor at lower pump rates (i.e., increased residence times) resulted in occasional reactor plugs due to coke formation. Plugs were detected through observing increased pressure drop across the reactor, which was measured by two pressure transducers on either side of the reactor, i.e., PT 1 – PT 2.

It was necessary to clean/replace the post-reactor filters regularly during operation of the 500 mL reactor. This was necessary due to a steady increase in the pressure drop across the filter array (i.e., F-1a/b). Filters were changed at least every hour, except when the steady state sample was taken, which lasted approximately 2 hours. When the filters were examined, flocculated asphaltenes mixed with coke particles were observed. These were cleaned from the filters with relative ease using acetone and a sonic bath.

Figure 100. Coke accumulation on stainless steel tee-type filter during over-reaction

Based on appearance of the filters and the changing of them approximately every hour, the asphaltene flocculant formation might be estimated on the order of 0.1 to 0.3 wt. % by comparison to the reactor feed rate.

VII.B.4.iv. The Impact of TAG Composition on Cracked TAG Liquid Yield

The cracked TAG liquid (CTL) and cracked TAG gas (CTG) that results from TAG cracking influences all the processes in the NCP. As a result, it was necessary to determine the effects of various types of TAG and reactor operating conditions on the composition of CTL and CTG. The lab-scale TCR was used to produce samples of CTL and CTG from nine different TAGs in order to determine the effect of TAG composition on the composition of cracked TAG (CT). The reactor was also operated at 5 different pressures, 3 different temperatures, and 3 different space times to examine their effects on the product compositions.

From these tests, the composition of CTG was analyzed and found to be fairly independent of the type of TAG processed. Greater dependence was observed with changing

operating conditions.

In addition to experiments involving the exploration of operating conditions, other experiments were performed on the 100 mL reactor to determine the CTL as described in Table 24 (see Section V.C.3). Some of the CTL yields from these experiments were shown previously in Figure 98 and Figure 99. Additional CTL yields for experiments AA-Soy through II-HONO and J-Canola through N-Canola are shown in Figure 101 and Figure 102.

Figure 101 shows the CTL yields of cracking various TAGs on the 100 mL TCR as described in Table 24 with an operating temperature of 435 C, a pressure of 2.9 MPa, and a space time of 0.4 h. CTL yield was observed to differ within a relatively narrow band among
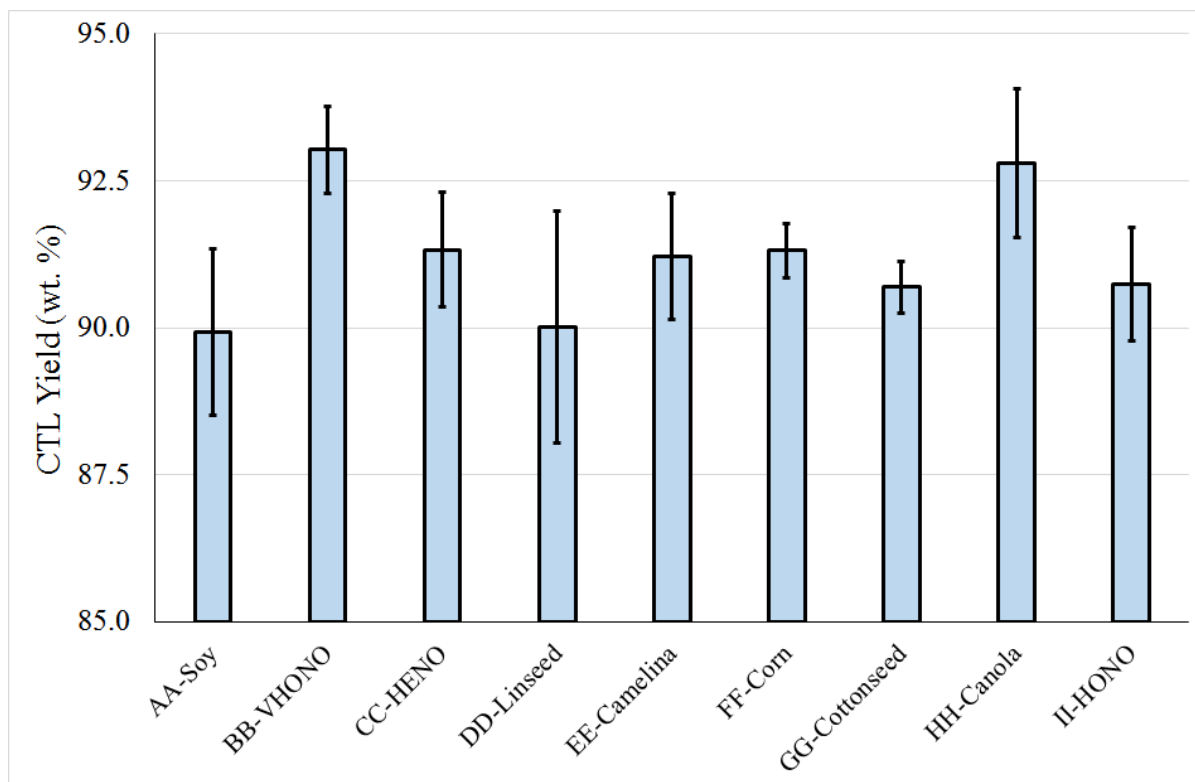
Figure 101. Cracked TAG liquid yield for samples varying triglyceride type. Error bars indicate twice the standard deviation about the mean.

In examining the error bars, there are clear statistical differences between the CTL yields of these TAGs. Nevertheless, the trend is not obvious from these results. In particular, one might conclude that TAGs rich in oleic acid yield higher quantities of CTL on account of observing the CTL yields for VHONO and Canola TAGs. Considering that HONO has a higher oleic acid content than canola TAG but a statistically lower CTL yield, it is not possible to make that statement confidently. Additionally, the fatty acid moiety composition of corn TAG and soybean TAG are relatively similar to each other. However the CTL yield of these two TAGs are clearly statistically different as well. As a result of observations such as these, it is difficult to notice the trends in the yield of CTL for various types of TAG.

Figure 102 shows the CTL yields from cracking canola TAG in the 200 mL TCR as described in Table 24. Canola TAG was cracked over a wide range of pressures in order to determine the effect of operating pressure on the reaction products. The graph of the CTL yields
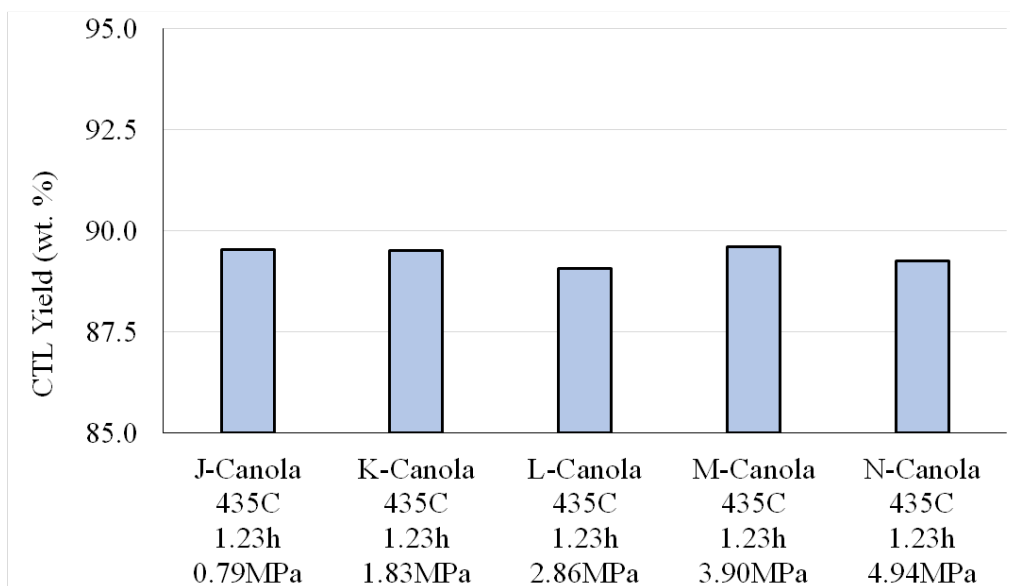
Figure 102. Cracked TAG liquid (CTL) yield for samples with varying pressure

353

show relatively similar values on the order of 89.1 to 89.6 wt. %. One may conclude that the

CTL yield is unaffected by pressure. This could be based on (1) observing no trend of the CTL

yield over a large range of operating pressures, (2) observing a small magnitude of variation of

CTL yield with pressure (i.e., the values are relatively very similar), and (3) apparent trends with

temperature and space time are clear and relatively strong in magnitude.

For cracking in the 200 mL TCR, temperatures remained consistent with standard errors

of about 0.7 C. An approximate thermal profile of the 200 mL tubular cracking reactor is shown

in Figure 103 for the conditions studied over a range of pressures. Except for the entrance
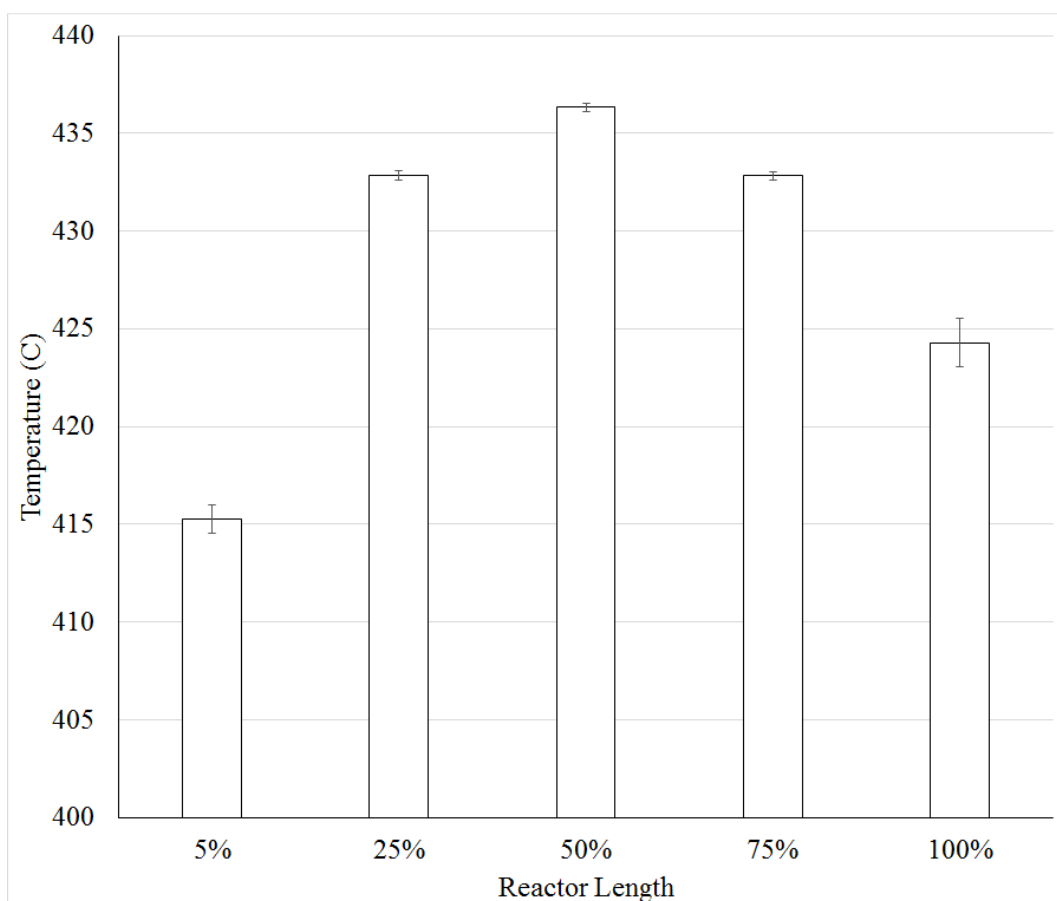
Figure 103. Thermal profile of the 200 mL tubular cracking reactor

temperature, temperatures in the cracking fluid at any point in the reactor tended to be an average of 2.2 C lower than the free air temperature outside the reactor wall, possibly indicating a slightly endothermic reaction.

Due to the endothermicity and due to the entrance/exit effects of the reactor, the reactor volume average temperature was determined to be 430.4 C instead of the set point temperature of 435 C. It may then be considered that all temperatures in this dissertation could be adjusted by some similar factor of about 4.6 C. However, since for the other TCRs, thermocouples to measure the temperature profile was unavailable, the set point temperature has been used consistently for all reactors. However it should be noted that at least for the TCR's, this temperature value likely overstates the averaged reactor temperature by approximately 5 C.

VII.B.4.v. Bench-Scale TCR

The bench-scale TCR was designed and constructed according to Figure 31 and the associated description on page 157 based on previous design information and success of the prototype TCR (Figure 28) and lab-scale TCR (Figure 29). Operation of the bench scale TCR was performed according to Table 20 at approximately 420 C temperature, 0.69 h space time, and 1.9 MPa pressure using soybean oil.

Sensor data from the first four hours of operation are summarized over time in Figure 104, showing the minimum, maximum and average temperatures for the free air of the tube furnace and the cracking fluid. Pressure transducers (PT_1 and PT_2, see Figure 31) are also shown on the secondary axis.

What is immediately evident in Figure 104 is a relatively large spike in pressure at about 2 hours of operation when the temperatures were nearly reaching cracking temperatures.

355

Otherwise the pressures were fairly consistent. This was later determined to be caused by sludge

formation in the sub-cracking temperature range of 380-400 C as previously described on 345

(see Figure 97). Otherwise the pressures remained fairly consistent during reaction, with a

pressure drop across the reactor of approximately 116 kPa and a standard error of 45 kPa.

It is worth noting that the initial pressure spike at about 0.35 h was due to pressurizing the

reactor with N2, and should not be regarded as a significant event.
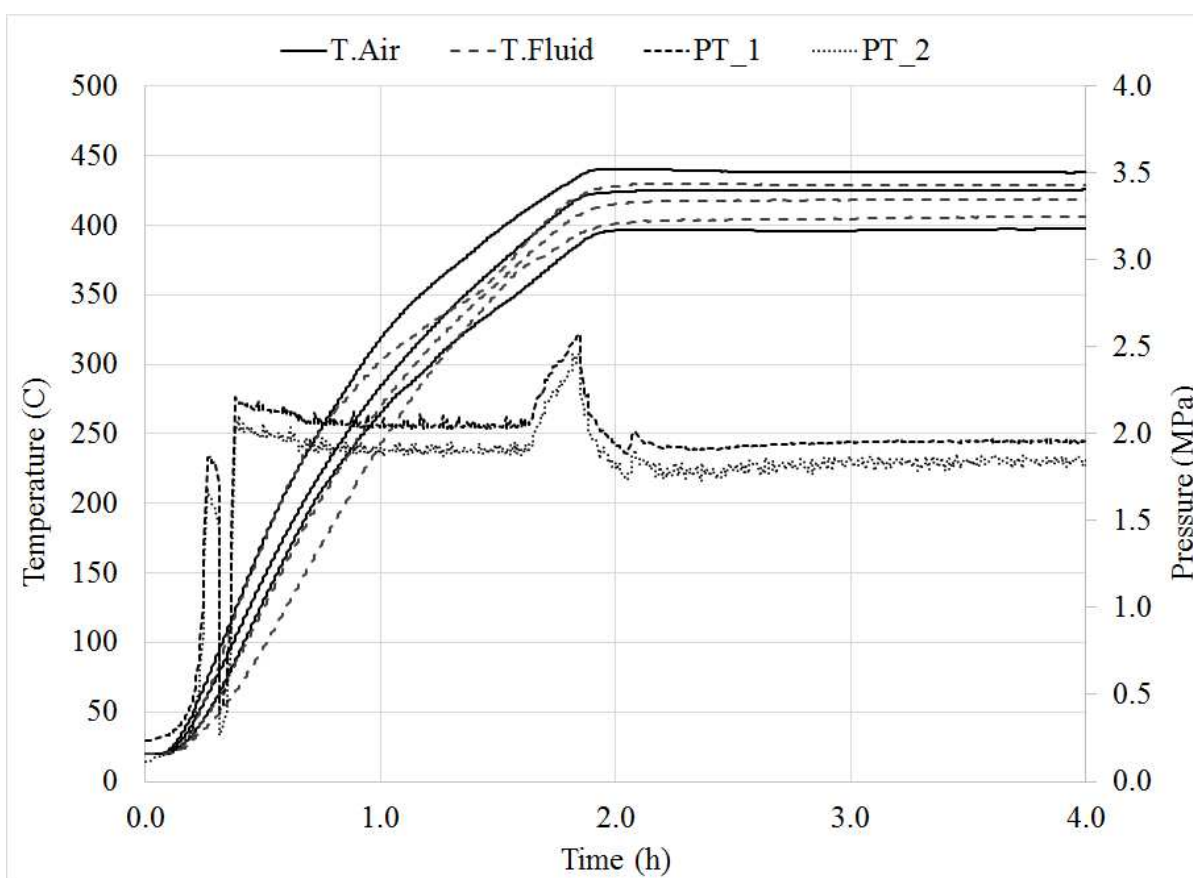
Figure 104. Operating temperature and pressure profile for tubular cracking reactor

The temperature of the oil was preheated to approximately 410 C in the two-stage

preheater shown in Figure 31 before being fed to the reactor. Reactor temperature control was

setup to utilize free air temperatures as process variables instead of fluid temperatures. As a

result, the set point temperature was on the order of 12-18 C higher than the average fluid

temperature (at about 432 C for the lower furnace zone and 438 C for the upper furnace zone).

This elevated free air temperature may also indicate an endothermic cracking reaction as

previously consistent with the observation on page 354.

At steady-steady operation, the bench-scale TCR's fluid temperatures were measured as

low as 406 near the inlet to as high as 428 C towards the central region. This is comparable to

the range of temperatures observed over the length of the 200 mL lab-scale TCR, which varied

from 415 to 436 as indicated in Figure 103 (page 354). For the bench-scale TCR, free air

temperatures in the reactor varied more, ranging from about 397 to about 438 C. This dispersion

is larger than for the lab-scale 200 mL TCR. As a result of the wider temperature range, it was

not desired to run the reactor at hotter temperatures, which might risk coking the reactor (which

was more expensive to replace than the lab-scale version(s)). For this reason, tighter thermal

control is desirable in future tubular cracking reactor designs.

The CTL yield from the reactor was determined to be approximately 89 wt. % which is in

the range of CTL yields observed for cracking in the lab-scale 100 mL TCR shown in Figure 99

(see 349). The composition of the gas phase is shown below in Figure 105. The gas

composition indicates slightly lower H_2 and slightly greater CO than in other comparable

reactions, however the general trend remains consistent.
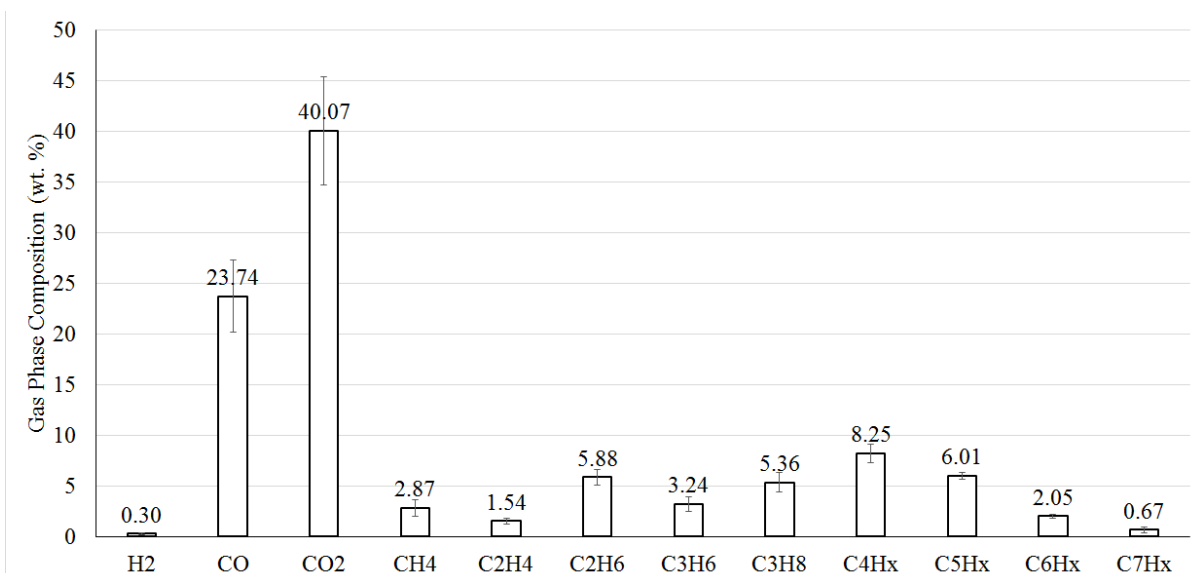
Figure 105. Gas phase composition of bench-scale tubular cracking reactor operation. Data are a triplicate average and error bars indicate two times their standard deviation.

VII.C. Processing to Determine Coke Yields During Residue Processing

Experiments were conducted in order to estimate the coke yield from the NCP as described in Section V.C.4.i. Soybean TAG was used as a feedstock, which was processed in three successive steps: TAG cracking, fractionation, and residue processing. Two sets of experiments were performed in parallel, utilizing different space times during TAG cracking. Otherwise, the process steps were identical for both sets. This was done to see if the severity of TAG cracking affected the coke yield. The results and operating conditions are summarized in Table 44.

A major effect is readily observed by this experimentation. The sample that was processed at shorter space times led to increased production of cracked TAG distillation residue (CTR). However, during coking, a substantially greater portion of the CTR was volatilized. As a result, the true total distillates, gas, and coke yields are shown to be relatively consistent both

conditions.

Table 44. Summary of experimentation to estimate the yield
of dense carbon products formed via the NCP

TAG Cracking			
Feedstock	-	Soybean TAG	Soybean TAG
Temperature	(C)	440	440
Space Time	(h)	0.77	0.43
Pressure	(MPa)	1.5	1.5
CTG	(wt. %)	12.2	7.7
CTL	(wt. %)	87.8	92.3
Distillation			
Feedstock	-	CTL	CTL
Final Temperature	(C)	350	350
Final Pressure	(kPa)	0.8	0.8
CTL Distillates	(wt. %, TAG basis)	75.3	60.3
Residue	(wt. %, TAG basis)	12.5	32.0
Aqueous Phase	(L/kg CTL)	2.4	2.4
Coker			
Feedstock	-	CTR	CTR
Final Temperature	(C)	490	490
Coker Gas	(wt. %, TAG basis)	2.0	4.5
Coker Distillates	(wt. %, TAG basis)	4.8	23.2
Coke	(wt. %, TAG basis)	5.7	4.4
Process Totals			
Total Gas	(wt. %, TAG basis)	14.2	12.1
Total Distillates	(wt. %, TAG basis)	80.1	83.5
Total Coke	(wt. %, TAG basis)	5.7	4.4
Aqueous Phase	(L/ kg TAG)	2.1	2.2

There are subtle differences however. In examining the total gas produced, less gas and more distillates were processed from samples that were cracked at reduced residence times. It appears as though the coke yield increases with increased space time, but more data would be desirable to validate this observation. Also, the coke yield for the NCP appears to be approximately 4 – 6 wt. % over the conditions studied.

359

For the purposes of estimating the yield of products from the noncatalytic cracking process (NCP) in Section VII.E.3.i, coke yield is assumed to be a constant value, equal to 5.05 wt. % (the arithmetic mean of the two observed values in Table 44).

VII.D. Production of Fuel from Triglycerides via the Noncatalytic Cracking Process

Jet fuel was produced in the laboratory from reactive and separations processes according to the experimental methods described in Section V.C.4.ii. These laboratory processes were intended to model the noncatalytic cracking process (NCP) described by Chapter II. Final fuel was prepared and tested for key physical properties in order to ensure the fuel met the international criteria for Jet-A-1 fuel.[27] The properties tested are reported in Table 45. The fuel shall be referred to as 'Soy-Jet-A-1' in this dissertation.

Table 45. Key properties of Jet-A-1 kerosene turbine (jet) fuel derived from soybean TAG utilizing the noncatalytic cracking process

	Units	Specification	NCP Soy-Jet-A-1
Total Acidity[154]	mg KOH/g	≤ 0.015	0.002
Flash Point[158]	C	≥ 38.8	40
Freeze Point[157]	C	≤ -47	-49.3
Density at 15 C[159]	kg/m^3	775 - 840	784
Net Heat of Combustion[160]	MJ / kg	≥42.8	46.0
Olefin Content	est. wt. %	-	0.2

What can be seen is that all properties of Soy-Jet-A-1 were within the specifications for petroleum-derived Jet-A-1 fuel. The total acidity reveals that deoxygenation was virtually complete. The quantity of olefins was approximately 0.2 wt. % by FTIR, which is well below the 5 vol. % olefin maximum that is typically observed for jet fuels and indirectly verifies that the fuel will pass the oxidative stability test. The freeze point is lower than the maximum

tolerable freeze point in order to ensure that the fuel product is safely rated for use in aircraft at

the extreme temperatures which are common. The density is on the lower end of the range of

densities, however it is still within acceptable limits. The heat of combustion shows that the

energy is well above the acceptable lower limit of energy density for the fuel, and the flash point

is above the minimum specification so that the fuel may be handled safely without special

precautionary measures.

The Soy-Jet-A-1 sample was analyzed by FIMSDIST according to the method described

in Section V.B.4.ii. The data was reduced in like manner to that of sample AA-Soy as described

in Section VI.A. The result is a mass-based carbon number distribution (CND) as shown in

Figure 106. A likewise CND was produced for the FIMSDIST analysis of petroleum-derived
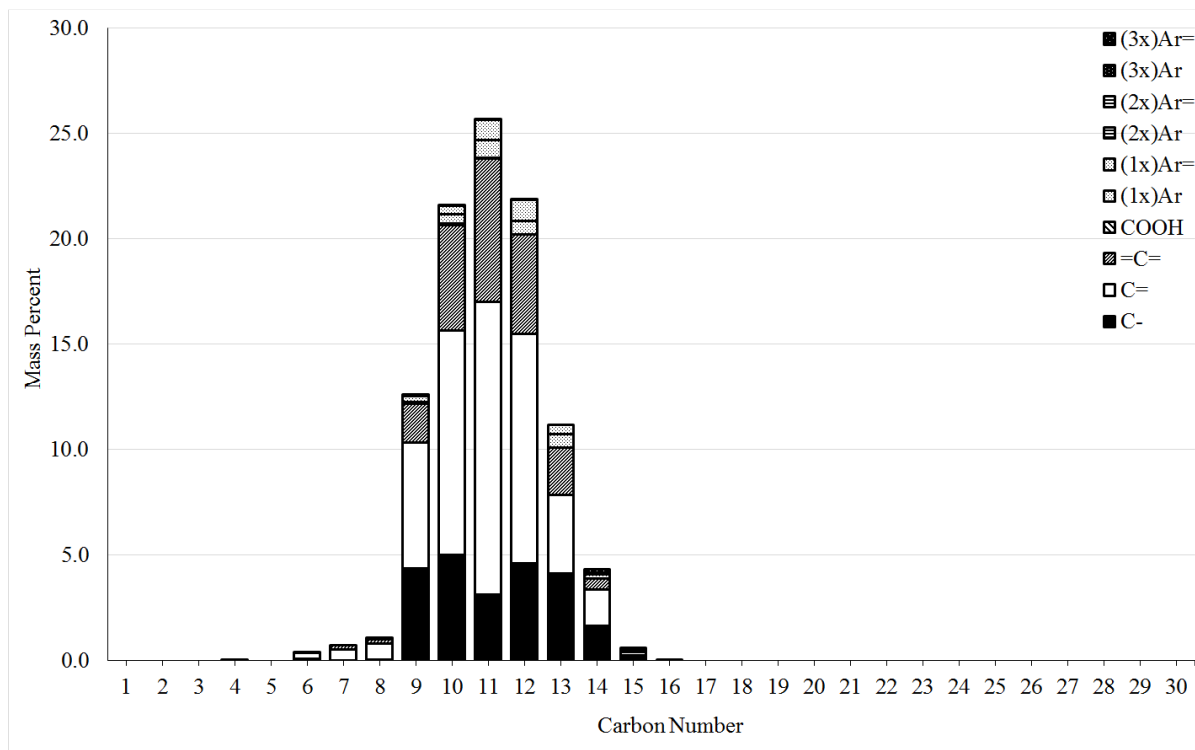
Figure 106. Carbon number distribution of Soy-Jet A-1 turbine fuel

kerosene fuel for comparison, shown in Figure 107. These CND's span carbon numbers C1-C30, which corresponds to the majority of other CNDs in this chapter.

It should be mentioned that the majority of C= and =C= components are cyclics and dicyclics rather than olefins, due to the very low quantitation of olefins in the final fuel products by FTIR. The concentration of cyclics and dicyclics is expected to be over estimated by the FIMSDIST method from the concentration of cyclics/dicyclics derived from the direct method comparison (as described in Section VII.D.5) by approximately a factor of 3

It must be mentioned that the petroleum-derived kerosene fuel's freeze point and flash point corresponded to the requirements of Jet-A-1 fuel, however the fuel was not specified to meet the quality of Jet-A-1 fuel. It was specified as kerosene fuel, potentially due to increased sulfur or other contaminants. Nevertheless, the data that are obtained from the comparison of the Soy-Jet-A-1 and the petroleum-derived kerosene are suitable for consideration.

In comparing these two figures, it can be seen that the Soy-Jet-A-1 has a CND that predominantly spans carbon numbers C9-C13. By contrast, the petroleum-derived kerosene spans carbon numbers C10-C15. This is the most significant difference between the two fuels.

Although virtually no trace carboxylic acids were discovered in the Soy-Jet-A-1 kerosene, there appear to be some components of the petroleum-derived kerosene that were identified as though they were carboxylic acids. It is more likely that they are some other species in smaller amounts that are being mistakenly identified as carboxylic acids. Nevertheless, their contribution is minor.

In comparing the aromaticity of the two fuels, very little aromaticity is found in the Soy-Jet-A-1 fuel, on the order of about 6.4 wt. % total. By contrast, a significant aromatic

362
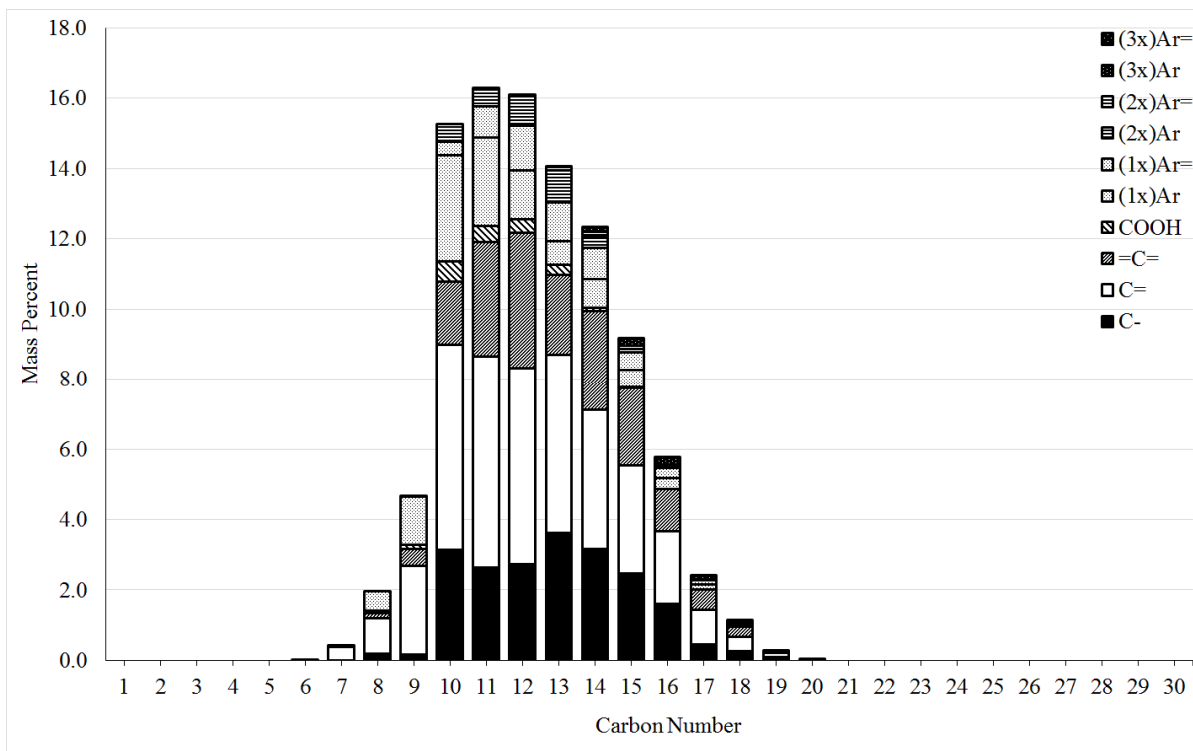
Figure 107. Carbon number distribution of a typical petroleum-derived kerosene fuel

contribution is found in this petroleum-derived kerosene, on the order of about 21.4 wt. %.

Aromaticity may be responsible for some of the differences between the fuels, which is

discussed in Section VIII.E.1.

This petroleum-derived kerosene has a noticeable percentage of bicyclic/polycyclic

aromatics, whereas the Soy-Jet-A-1 has negligible quantities. For this reason, it may also be

assumed that the petroleum-derived kerosene would be at risk for not passing the naphthalenes

test for Jet-A-1 fuel.

In addition to the preparation of fuel, soybean-TAG-derived deoxygenated distillates

were produced and fractioned into various boiling point fractions (BPFs) spanning

approximately 20 C increments from 100 C to 300 C as described in Section V.C.4.ii. Then the

density, freeze point, flash point, pour point, and cloud point were determined for each of the

BPFs. Similar BPFs were prepared from the petroleum-derived kerosene and tests were run on

those BPFs as well. The fractions of the soybean-derived distillates spanned a wider range from

110 to 290 C than the petroleum-derived kerosene distillates, which spanned from 170 to 265 C.

Table 46 presents the results.

Table 46. Physical properties of boiling point fractions from soybean-oil-derived deoxygenated
distillates and petroleum-derived kerosene distillates

Source of Distillates	MABP*	Flash Point	Freeze Point	Pour Point	Cloud Point	Density at 15C
-	(C)	(C)	(C)	(C)	(C)	kg/m^3
Soybean-TAG-Derived	110	17	-53.9	<-75	<-74.4	739
	135	28	-70.5	<-76.0	-43.7	758
	165	46	-53.2	-73	-59.1	781
	190	60	-40.8	-57	-49.1	801
	210	77	-29.7	-45	-38.4	813
	230	90	-24.1	-31	-26.8	822
	250	>110	-7.7	-12	-9.6	819
	270	>110	0.3	-4	-2.9	829
	290	>110	10.1	3	2.9	852
Petroleum-Derived Kerosene	170	45	-74.4	<-76	-47.4	792
	190	55	-66.1	-72	-56.1	802
	210	69	-56.3	-63	-52.9	813
	230	86	-44.5	-51	-44.1	828
	250	104	-33.6	-52	-34.1	838
	265	>110	-22	-37	-26.1	848

*Note: MABP stands for mean average boiling point

Densities were determined for the soybean-derived distillates ranging from 739 to 852

kg/m^3, and in the petroleum-derived distillates from 792 to 848 kg/m^3. Flash points were

determined over the range of 17-90 C and 45-104 C for soybean-derived distillates and petroleum-derived distillates respectively. Most of the flash point and density data were fairly consistent as a function of the MABP regardless of whether or not the BPF was derived from petroleum or from cracking/refinement of soybean TAG.

The major deviation between the soy/petroleum derived BPFs was for properties having to do with the low-temperature behavior of the fuel (e.g., the freeze point, pour point, and cloud point). These properties differed by as much as 20 C, with the petroleum-derived fuel having superior cold weather performance. Differences between these fuels are further discussed in Section VIII.E.1.

VII.E. TAG Processing in Tubular Cracking Reactors

This section describes the results of experiments to determine the composition of various reaction products from triglyceride cracking in the present work and/or related works.

VII.E.1. FTIR Analysis of Cracked TAG Liquid (CTL)

Selected samples of soybean CTL that were produced from TAG cracking in the 100 mL lab-scale TCR (see Table 24) were analyzed by FTIR. The resultant FTIR spectra are shown in Figure 108, which was produced according to the FTIR operation details described in Section V.B.4.iv. The spectra for most CTL samples looked relatively similar, with a large peak at wavenumber 1710 cm^{-1} coinciding with a carboxylic acid functional group.

The height of the carboxylic acid peak tended to be approximately 2.2 to 2.8, with an average height of 2.5. This corresponded to a 1.9 mol/L concentration of carboxylic acid functional groups according to the FTIR calibration described in Appendix E. To add perspective, this is equivalent to mixing 33 grams of octanoic acid with 67 grams of hexadecane

for a total mass of 100 grams, and it gives a fair idea of the concentration of acidity that is expected in CTL.
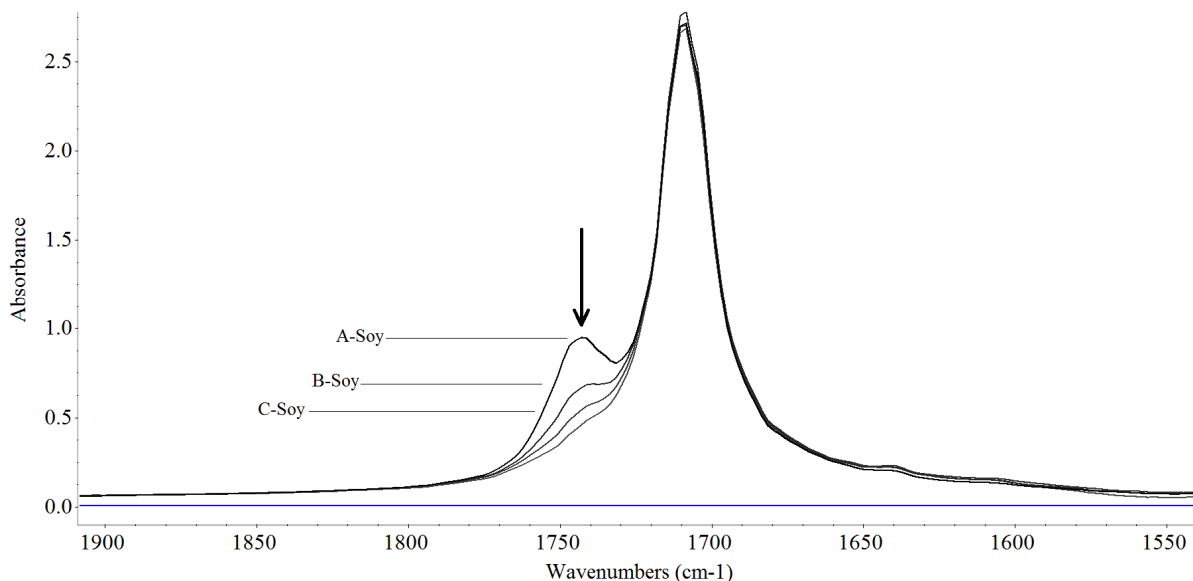
Figure 108. FTIR spectra for cracked soybean oil CTL with
disappearing abundance of residual triglyceride ester bonds

There were some atypical FTIR spectra observed when cracking samples with short residence times (A-Soy, B-Soy, and C-Soy shown in Table 24). In these cases, the FTIR spectra indicated another peak at wavenumber 1747 cm^{-1} as shown in Figure 108. Out of all the samples analyzed by FTIR, only the samples cracked at low residence times observed this peak. Furthermore, the peak was decreasing as the temperature increased.

This peak coincided with the TAG feedstock ester bond according to FTIR calibrations that were performed using soybean TAG. It appears as though the samples with the most brief residence time still contained ester groups. This implies that not all carboxylic acids had been

freed from the TAG molecule backbone. The quantity of ester groups have been computed

below as mol/L. To add perspective, these quantities of ester groups are comparable to 100%

uncracked soybean TAG, having an approximately 3.1 mol/L concentration of ester functional

groups.

Table 47. Residual esters in cracked TAGs

Label	Space Time (h)	Pressure (MPa)	Temperature (C)	Ester Group Concentration (mol/L)
A-Soy	0.27	2.9	420	0.50
B-Soy	0.27	2.9	430	0.21
C-Soy	0.27	2.9	440	0.08

This implied that on the order of $1/6^{th}$ of the TAG backbone bonds are still intact at the

conditions which A-Soy was cracked. This drops to around $1/15^{th}$ and less than $1/30^{th}$ of the

TAG bonds at only 10 and 20 degrees hotter, respectively. As previously stated, for TAGs

cracked at longer space times a significant peak indicating residual TAG ester groups was not

observed.

VII.E.2. Gas Phase Composition

The gas phase product composition (i.e., noncondensable products) was determined for

the cracking of various TAGs and various operating conditions in the 100 mL and 200 mL lab-

scale TCRs as described in Section V.C.3. Gas phase composition was determined according to

the method described in Section V.B.4.iii. Gas phase data are shown in Figure 109 through

Figure 111. Numerical gas composition data are also included in Appendix C (see Table 61 on

page 467), with means/standard deviations where appropriate.

Figure 109 shows the gas phase composition from the cracking of various TAGs according to the experimental list in Table 24 (the samples are AA-Soy through HH-Canola). Data presented are the average of 3 values, however, error bars are not shown so as not to clutter the figure.
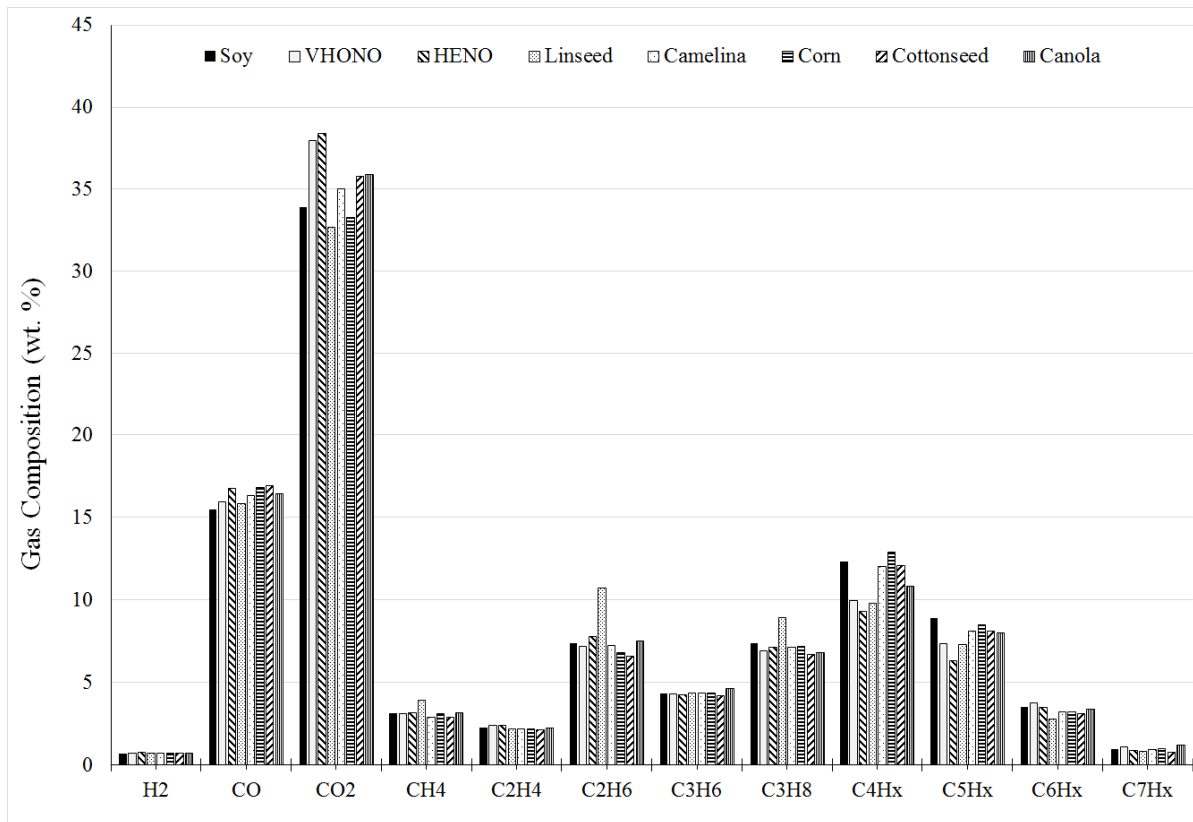
Figure 109. Gaseous product composition from cracking various
types of triglyceride oils in a tubular cracking reactor

What is immediately noticeable is a relatively high mass concentration of carbon dioxide and carbon monoxide. This agrees with the findings of Sander[62] in noncatalytic cracking using CSTRs. The combined percentage of hydrogen and light hydrocarbons is relatively low.

Paraffinic hydrocarbons tend to dominate the gaseous product, based on the observed

ethylene:ethane and propylene:propane ratios. In general, the ratios of light gaseous products

appear fairly consistent between the types of TAG.

Figure 110 shows the gas phase composition for cracking soybean TAG at various

temperatures produced using the 100 mL lab-scale TCR. Experiments were performed

according to the experimental list in Table 24 (these are samples D-Soy, E-Soy, and F-Soy).
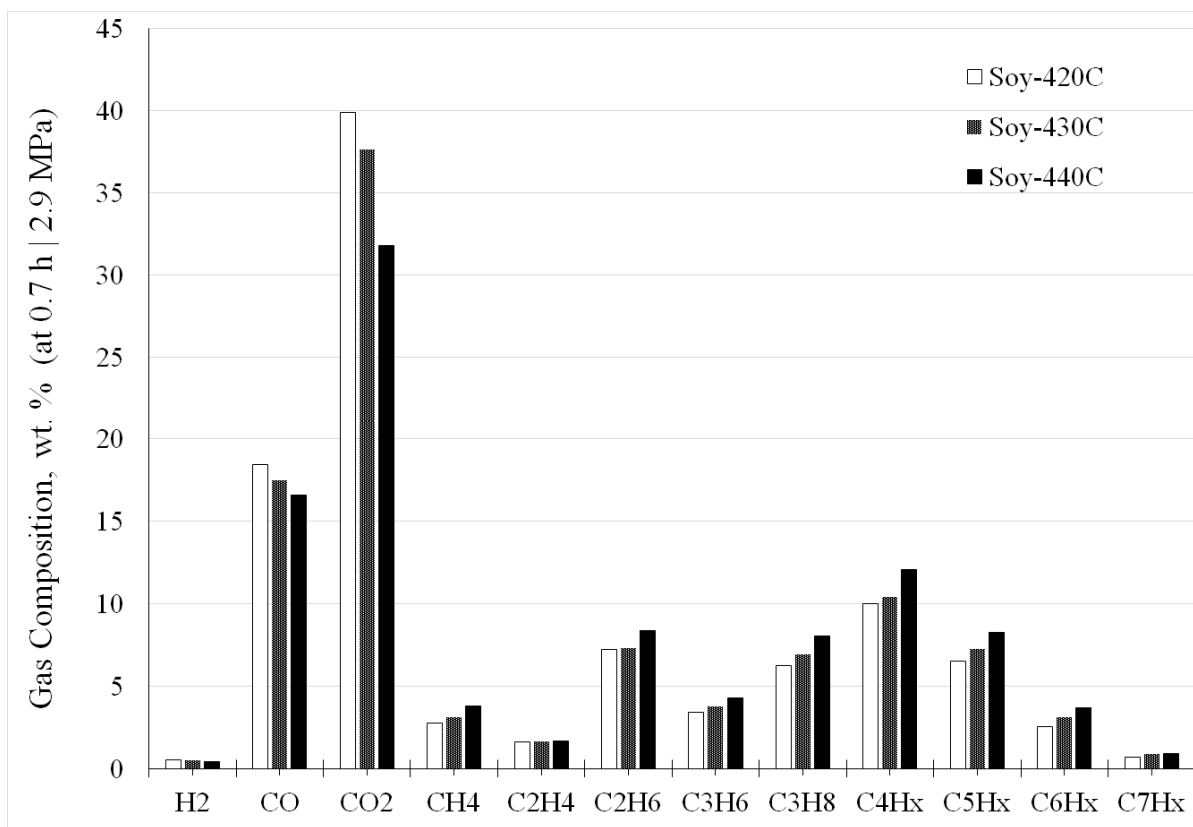
Figure 110. Gas phase composition at various temperatures (at 0.7 h and 2.9 MPa)

Clear trends are observed in the figure for increased operating temperature. The

percentage of CO and CO_2 are decreasing with temperature, relative to the other components in

369

the gas phase. This is indicative of increased cracking reactions at higher temperatures relative

to deoxygenation reactions.

Figure 111 shows the gas phase composition for cracking canola TAG at various

temperatures in the 200 mL lab-scale TCR. Experiments were performed according to the

experimental list in Table 24 (these are samples J-Canola through N-Canola).
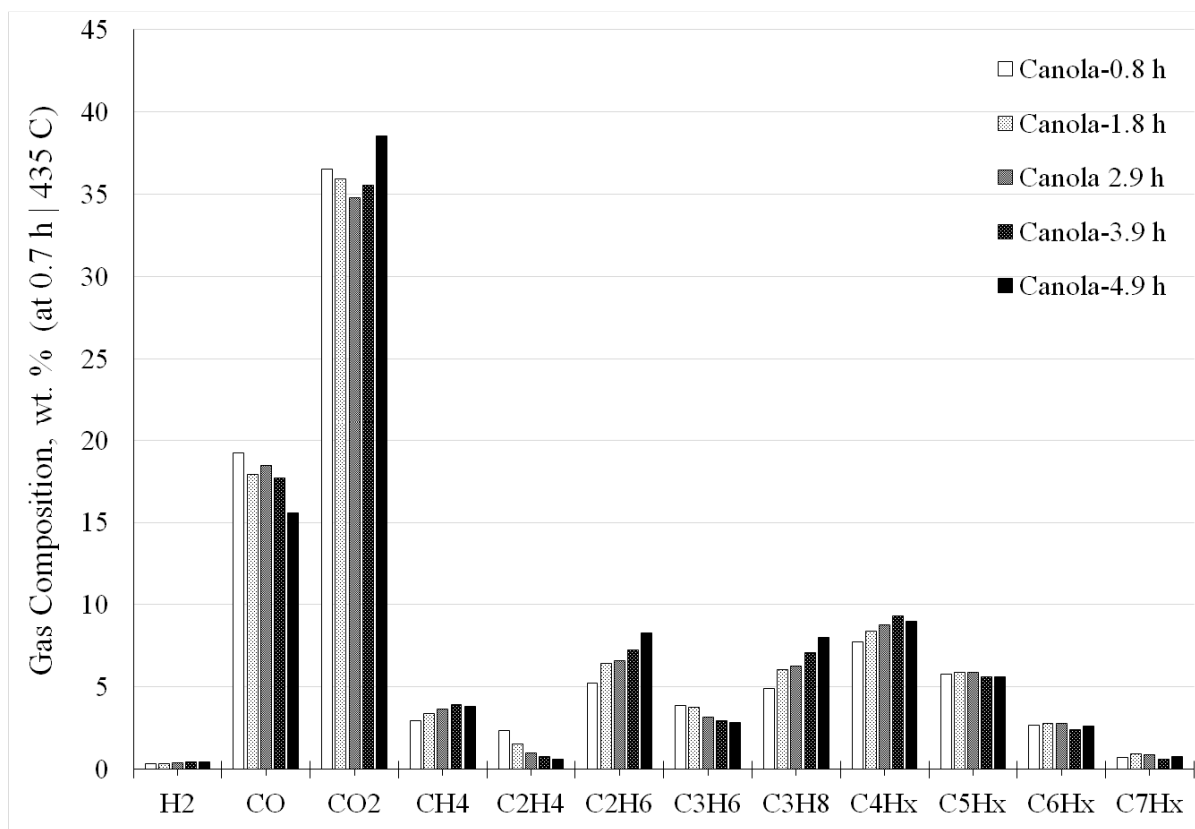
Figure 111. Gas phase composition at various pressures (at 440 C and 0.7 h)

The composition of CO in the gas phase decreasing with increasing pressure. It is not

clear whether CO_2 is increasing or decreasing with increasing pressure. What is interesting is the

clear decrease in the production of gaseous olefins and the increase in the production of gaseous paraffins as the pressure increases.

The effect of space time was not very apparent, so no figure is included to show the gas phase composition across various space times. Tabulated values for gas phase composition with standard deviations (where appropriate) are included in Appendix C. Example chromatograms and calibration plots for the analysis of gaseous products by GC-FID/TCD are shown in Appendix D.

VII.E.3. Effect of TAG Composition and Reaction Conditions on Product Composition

Table 24 summarizes a multitude of samples that were produced in the 100 mL and 200 mL configurations of the lab-scale TCR under various operating conditions (see Section 0). The CTL samples from these experiments were analyzed by FIMSDIST to determine their composition (see Chapter VI), and the gas composition was analyzed by GC-FID/TCD (see Section V.B.4.iii). This produced sufficiently detailed composition data to interpret the effect of various operating parameters on the distribution and quality of products from the noncatalytic cracking process (NCP). CTL composition data from analysis by the FIMSDIST method are included in Appendix K, and gas composition data are included in Appendix C.

VII.E.3.i. Noncatalytic Cracking Process Yield Estimations for Various Operating Conditions of TAG Cracking

In order to estimate the yields from various TAG cracking experiments, data were organized into fuels according to their carbon number groups. C3-C4 ranged components were considered to be products consistent with liquefied process gas (LPG). Flammable components that were lighter than C3 were considered to be burner fuel (e.g., H_2, CO, CH_4, C_2H_4, and C_2H_6), which can be used to substitute for natural gas in process heaters/boilers. Based on that, the

371

equivalent yield of natural gas was calculated and presented in place of the burner fuel in order to simplify the results.

Based on the observed carbon number distribution from the Soy-Jet-A-1 sample that was produced via cracking/refinement (see Section VII.D), the jet fuel range was defined as all of the C10-C12 ranged components and half of the C9 and C13 components. This range is denoted as (*9-13*) in Table 50 through Table 52. In a similar fashion, naphtha was defined as all of the C5-C8 components and half of the C9 components, i.e. (5-9*). Diesel included half of the C13 components and all of the C14-C18 components. The components in the C19-C25 range were considered to be no. 2 fuel oil and remaining components (i.e., the C26-C74 range) were considered to be no. 4 fuel oil.

It was also necessary to account for residue formation and for deoxygenation. Although the present work investigated deoxygenation, it focused on the optimization of catalysts by minimizing catalyst costs and maximizing activity and also determining operable conditions in continuous reactors. Selectivity was not investigated. According to the work described by Snare[31], some deoxygenation catalysts are capable of achieving decarboxylation with selectivity on the order of 99% towards decarboxylation. Based on this, ideal decarboxylation was assumed to be achievable, and this assumption was utilized for the compilation of these data. Thus, every carboxylic acid in the range C1-C18 was converted to an n-paraffin assuming a molar loss of CO_2.

In addition, the yield of residual carbon products was estimated to be approximately 5.05 wt. % (feedstock basis) in Section VII.C. This was determined by the stepwise processing of soybean TAG in cracking reactors, fractionating equipment, and a residue processing furnace

and coincides with observations from the work of Bosquez[66] and unpublished experiments that were ongoing at UND at the time of publication for the production of carbon fiber. As a result, the data have been adjusted by normalizing the CTL formed to account for 5.05 wt. % residue. Although experiments conducted by Bosquez and in the current study both suggest that the formation of coke would lead to formation of process gas, the production of process gas may be expected to be substantially lower if carbon fiber is the sought after product. As a result, gas formation from residue processing has been neglected. This also serves to provide a best-case-scenario estimate.

Finally, the total product value (TPV) was computed according to the price estimates as of July 2014 (see Section II.D.2 on page 51), assuming a 1.0 USD/kg product value for coke and/or carbon products, which is considered to be a conservative estimate. The resultant data have been tabulated in Appendix L and are shown in Figure 112 through Figure 116.

Figure 112 shows the estimated product yields from cracking various TAGs according to the operating conditions provided in Table 24. By estimation, these samples tend to produce on the order of 2-3 wt. % natural gas equivalents, 2-4 wt. % LPG, 7-12 wt. % naphtha, 10-12 wt. % jet fuel, 16 to 23 wt. % diesel, 17-25 wt. % no. 2 fuel oil, and 15-24 wt. % no. 4 fuel oil. Also about 8 wt. % mass was estimated to be lost as CO_2 during cracking and deoxygenation (not depicted, but tabulated in Appendix L).

The greatest estimated producers of jet fuel were linseed TAG and camelina TAG, and the weakest producers of jet fuel were corn TAG and HONO TAG. The greatest producers of naphtha were corn TAG and camelina TAG, and HONO TAG, with the weakest producer of naphtha being HENO TAG. Concerning diesel fuel, HENO produced the least on account of

greater production of combined fuel oils. In contrast, cottonseed TAG produced the most diesel

and the least combined fuel oil.
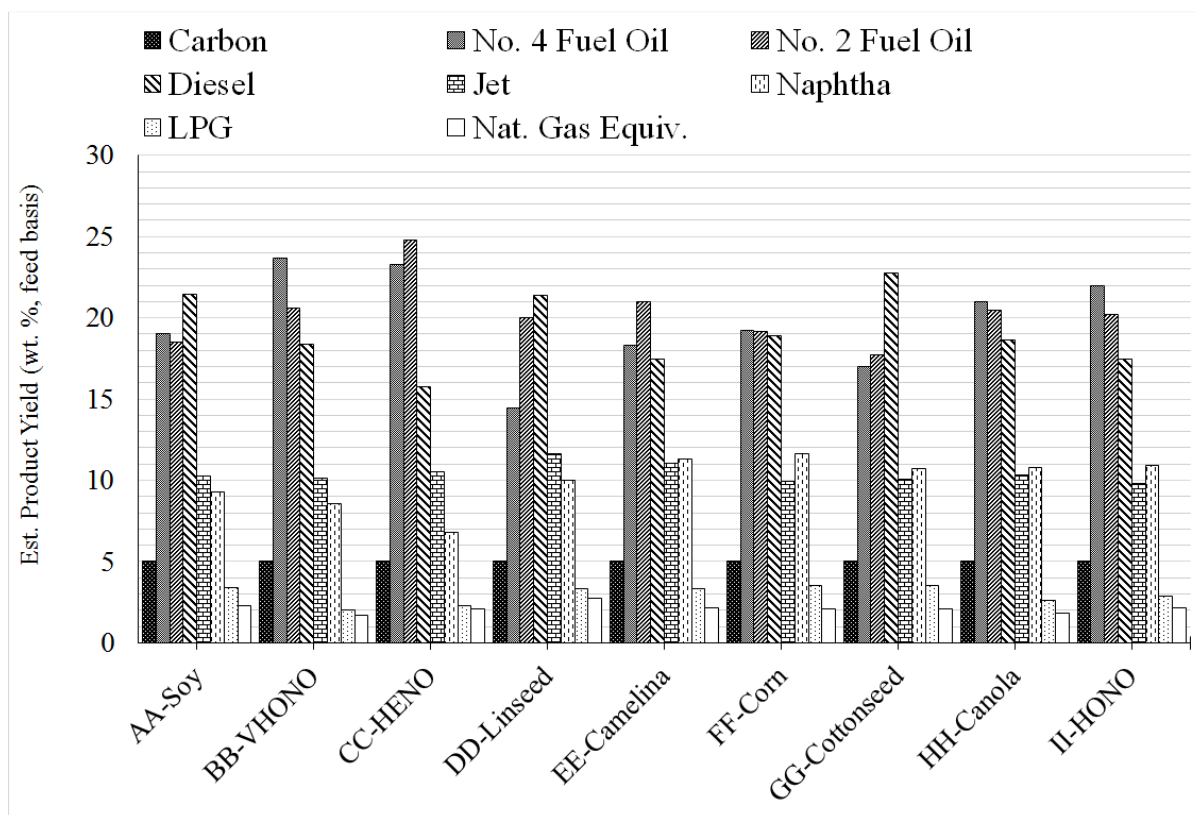
Figure 112. Estimated fuel product yields from cracked samples by varying TAG type

The greatest variability in the fuels was in the heavier fuels, such as diesel and fuel oils.

This is presumed to be an effect of differing concentrations of undercracked fatty acid moieties

in the feedstock TAG.

Figure 113 shows the estimated total product values (TPV) obtained by processing the

various TAGs into fuels with the NCP. It is apparent that the total product value is on the order

of 0.805 USD/kg on a feed basis. The total product value only changed by approximately

±0.015 USD/kg (feed basis) over all the TAGs processed in this manner, i.e., about ±2 percent.
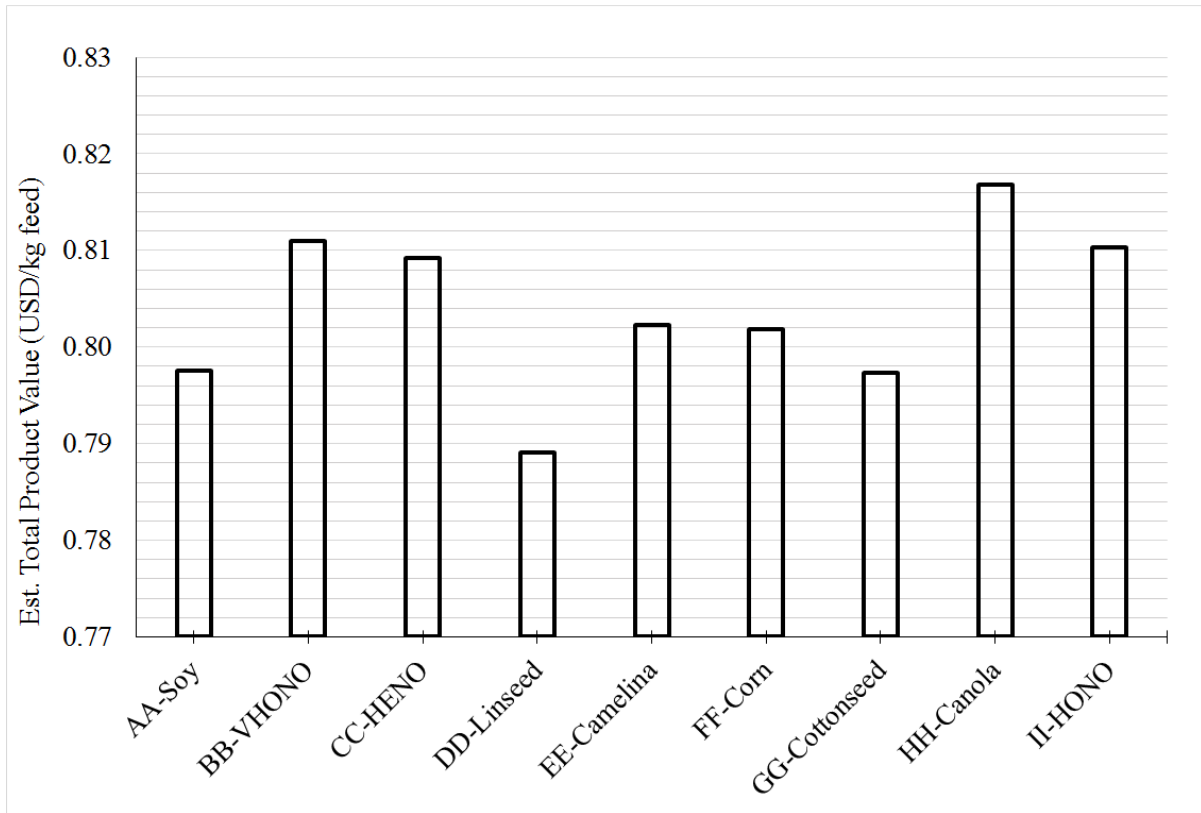
Figure 113. Estimated total product values from cracked samples by varying TAG type

Soybean TAG and canola TAG are suitable reference TAGs by which to compare all other tags. For this reason, the following table presents a summary of the relative estimated fuels yields and total product values from the refinement of each of the TAGs with the NCP in comparison to the refinement of the two reference TAGs.

Table 48. Relative estimated fuel yields and total product value for various TAGs in comparison to soybean TAG and canola TAG as reference TAGs

			Canola	VHONO	HENO	Linseed	Camelina	Corn	Cottonseed	HONO
Relative to Soy TAG	Nat. Gas Equiv.	(rel. wt. %)	-18	-25	-8	21	-5	-8	-8	-4
	LPG		-23	-40	-32	-2	-2	3	4	-16
	Naphtha		16	-8	-26	8	22	25	15	18
	Jet		0	-1	2	13	8	-3	-2	-4
	Diesel		-13	-14	-26	0	-19	-12	6	-18
	No. 2 Fuel Oil		10	11	34	8	13	3	-4	9
	No. 4 Fuel Oil		10	24	22	-24	-4	1	-11	15
	Carbon		0	0	0	0	0	0	0	0
	TPV		2	2	1	-1	1	1	0	2
			Soy	VHONO	HENO	Linseed	Camelina	Corn	Cottonseed	HONO
Relative to Canola TAG	Nat. Gas Equiv.	(rel. wt. %)	23	-9	12	48	17	12	13	18
	LPG		31	-22	-12	28	28	35	36	10
	Naphtha		-14	-21	-37	-7	4	8	-1	1
	Jet		0	-2	2	13	7	-4	-2	-5
	Diesel		15	-2	-15	14	-7	1	22	-6
	No. 2 Fuel Oil		-9	1	21	-2	3	-6	-13	-1
	No. 4 Fuel Oil		-9	13	11	-31	-13	-8	-19	5
	Carbon		0	0	0	0	0	0	0	0
	TPV		-2	-1	-1	-3	-2	-2	-2	-1

The most intriguing aspect of these comparisons is that despite large deviations in the quantities of fuels produced, the total product value remains relatively unaffected on a percentage basis. The implication of this is that despite the quantity of fuels produced, no additional profitability may be expected from the products of the NCP as interpreted as a purely TAG-to-fuel process, and therefore the production of valuable byproducts may be useful.

Based on this interpretation, while the production of lighter fuels is most desirable from TAGs, the cost of feedstocks will dominate the economics of NCP facilities and commercial operators should look for the least expensive feedstocks available. For example, whereas linseed TAG produces a higher quantity of lighter fuels, it will tend to cost more than yellow grease (e.g., waste soybean oil) or distillers corn oil.

Nevertheless, these relative comparisons are useful for predictions about what fuel may be expected from switching from one TAG feedstock to another. For example, switching from

soybean TAG to canola TAG might be expected to produce on the order of: 18 % less burner

fuel, 23 % less LPG, 16 % more naphtha, 13 % less diesel, and a combined 20 % more fuel oil.

The economic advantage of switching from soybean TAG to canola TAG might be an estimated

2 % greater total product value. The increase in total product value gained would be

unimportant, next to a relative feedstock cost increase of over 14 % as a result of switching from

soybean TAG feedstock to canola TAG feedstock (see Figure 5 on page 54).

Figure 114 shows the estimated product yields for soybean TAG cracked in the 100 mL

TCR according to the operating conditions provided in Table 24. What is evident, is much

greater variability in the yields of fuel than in Figure 112, especially for the fuel oils.

No. 4 fuel oil varied from 8 to 24 wt. %, and no. 2 fuel oil varied from 15 to 22 wt. %.

Diesel fuel varied from 18 to 23 wt. %, and jet fuel varied from 7 to 14 wt. %. Naphtha varied

from 7 to 15 wt. %, LPG varied from 2 to 5 wt. %, and natural gas equivalents varied from 1 to 3

wt. %.

Samples 'A-Soy,' 'B-Soy,' and 'C-Soy,' were all produced at 0.27 hours space time,

however their temperatures varied, 'A-Soy' at 420 C, 'B-Soy' at 430 C, and 'C-Soy' at 440 C.

Increasing reactor temperature at low residence times appears to have a beneficial effect,

resulting in decreased fuel oils yields and increased lighter fuel production. This agrees with the

discussion of mass-adjusted FIMS data provided in Section VI.B.2, which also showed that

increasing the reactor temperature shifted the distribution towards lighter products. In addition,

this is in line with the FTIR data presented in Section VII.E.1 which show that increased

temperature promotes the breakdown of residual TAG ester bonds.

377
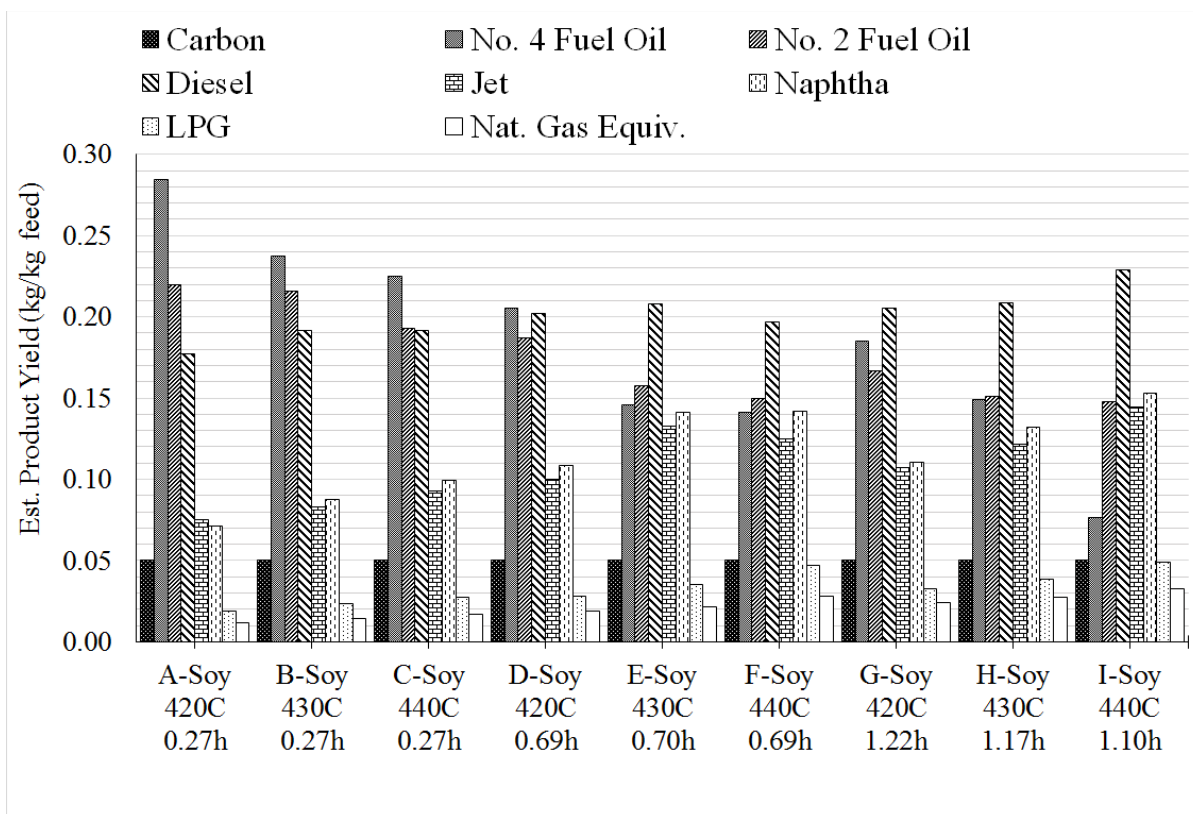
Figure 114. Estimated fuel product yields from cracked samples of soybean TAG
by varying reactor operating temperature and space time

In examining samples 'D-Soy,' 'E-Soy,' and 'F-Soy,' a similar trend is generally seen

with decreased fuel oil and increased lighter fuel production as a result of increased temperature

across the samples. The significant difference between the set of samples A-C and the set D-F is

that the production of light gaseous fuels appears to have a clear positive correlation for set D-F,

whereas in set A-C the trend is not clear. Most likely, the longer space time of the set D-F

experiments provides better resolution of this effect.

A very pronounced reduction in the estimated fuel oil yields is observed over the set of

samples G-I, which were performed at the longer space times, on account of increased

temperature in like manner to sets A-C and D-F. As a result, the yield of lighter fuels is likewise

increased.

Whereas the previous triplicates that were described accounted for increases in

temperature at constant space times, sets such as 'A-Soy,' 'D-Soy,' and 'G-Soy,' are triplicates

representing increasing space times at constant temperature. Set A-D-G is a series with

increasing space time from 0.27 to 1.22 hours at 420 C. This set exhibits a similar trend to the

trends observed for increasing temperature, whereby increased space time in the reactor leads to

increased production of lighter fuels and reduction of fuel oils. Similar trends are also observed

for increasing residence time at 430 C and 440 C according to sets B-E-H and C-F-I,

respectively. Additional insights from these data are provided by the regression analysis in the

next section (see Section VII.E.3.ii).

When the TPV is considered, it is apparent that over the range of experiments conducted

the TPV doesn't vary by more than ± 0.02 USD/kg (feed basis; i.e., about ± 2 %). The mean

value is 0.80 USD/kg on a feed basis. These values are essentially equivalent to the range of

values observed for the various TAG feedstocks studied in Figure 112.

There appears to be a significant decreasing trend in the TPV with increased cracking

severity on account of increased formation of LPG and natural gas equivalents. The magnitude

of the decrease in TPV is about 4.8 % over the range of conditions studied.
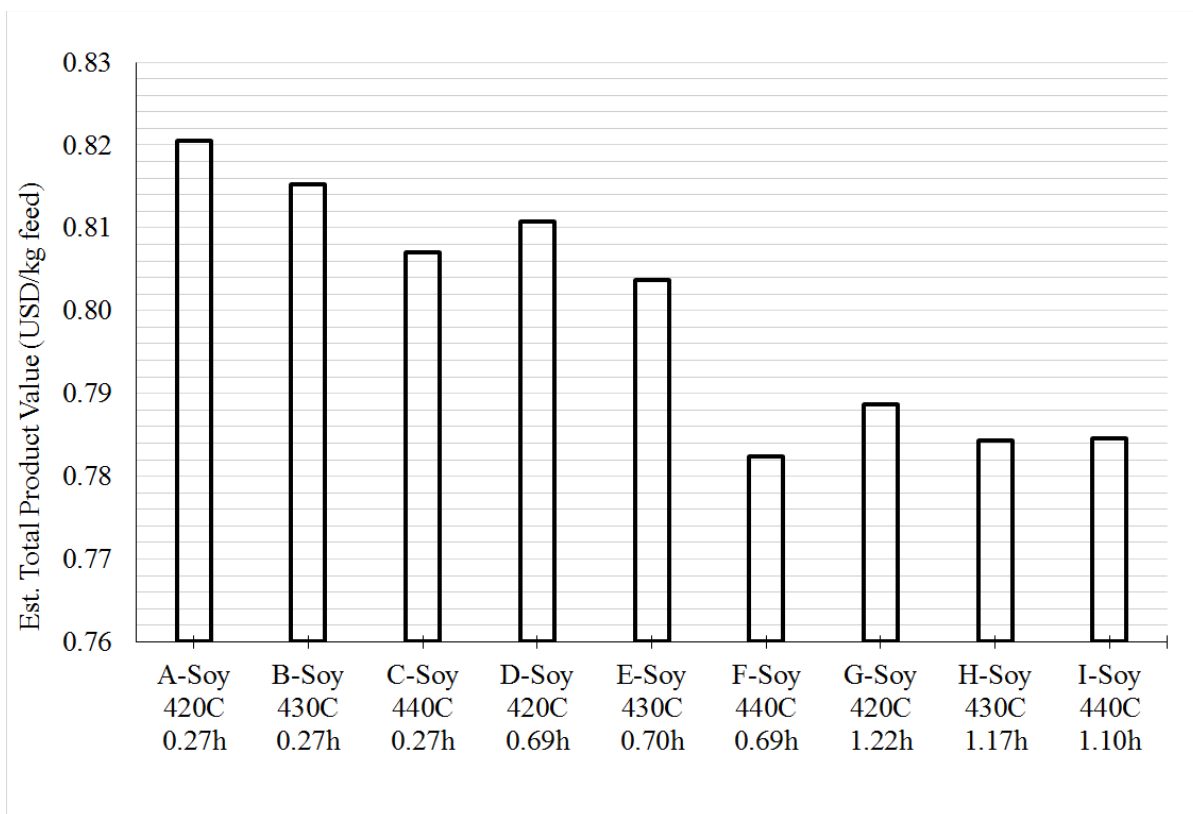
Figure 115. Estimated total product values from cracked samples of soybean TAG
by varying reactor operating temperature and space time

It should be considered that the yield of fuel oils is decreased by more than a factor of
two with the concurrent decrease in TPV of only 4.8 %. Due to the low desirability of fuel oils,
it may not be economically practical to designate optimal reaction conditions on the basis of
TPV alone, whereby the highest TPV coincides with the least production of process gas, and
consequently, the greatest production of fuel oils. Of course, if fuel oil upgrading facilities are
included in the NCP refinery, the trends shown here should be relevant.

Figure 116 shows the estimated product yields for canola TAG cracked in the 200 mL
tubular cracking reactor at various operating pressures (from 0.79 MPa to 4.94 MPa) according

to the operating conditions provided in Table 24. There appears to be greater consistency of samples than for Figure 114 or Figure 112, potentially indicating a minimal effect of pressure. In general, as the pressure is increased, diesel fuel yield appears to decrease and jet/naphtha fuels appear to increase. The yield of no. 2 fuel oil appears to slightly decrease with increasing pressure. However, the yield of no. 4 fuel oil appears to slightly increase.
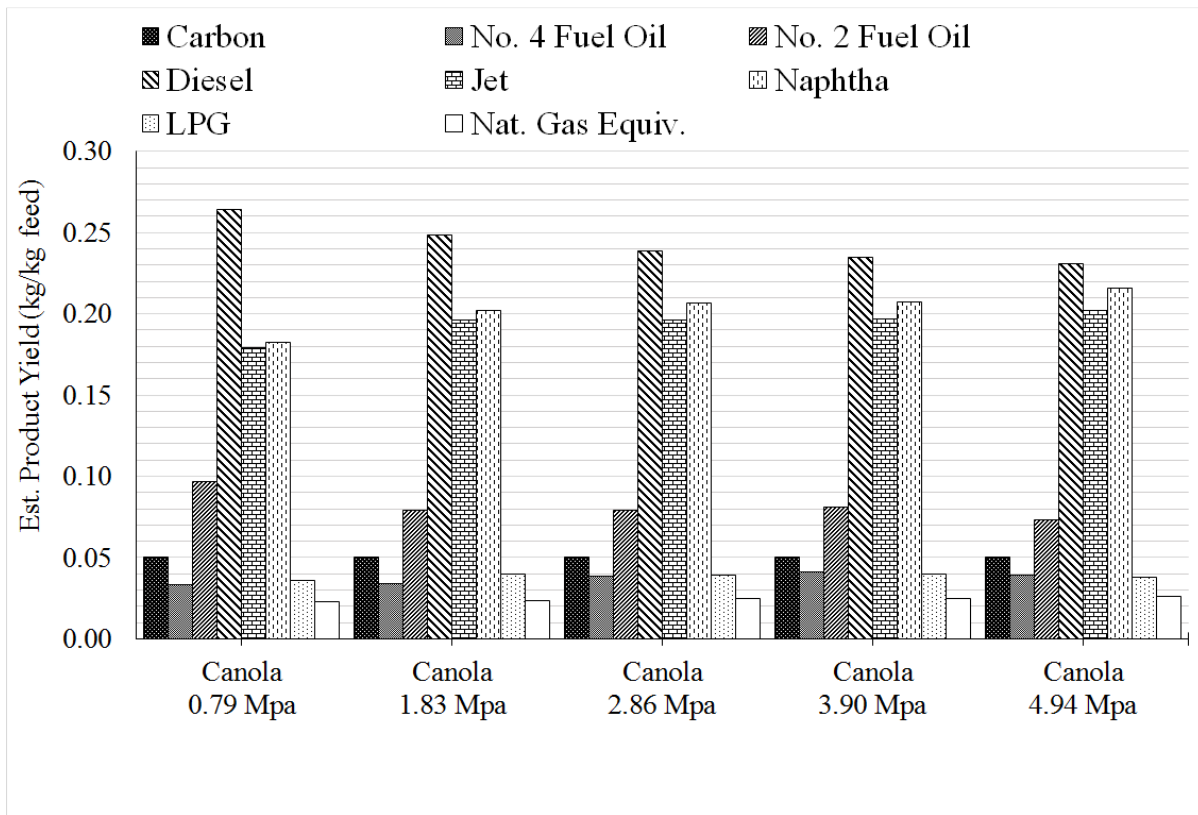
Figure 116. Estimated fuel product yields from cracked samples of canola oil
by varying reactor operating pressure

The total product value for this set of experiments is on the order of 0.795, which is slightly lower that the TPV in the other two cases. Furthermore, the TPV only varies by approximately 0.005 USD/kg (about 1 %).
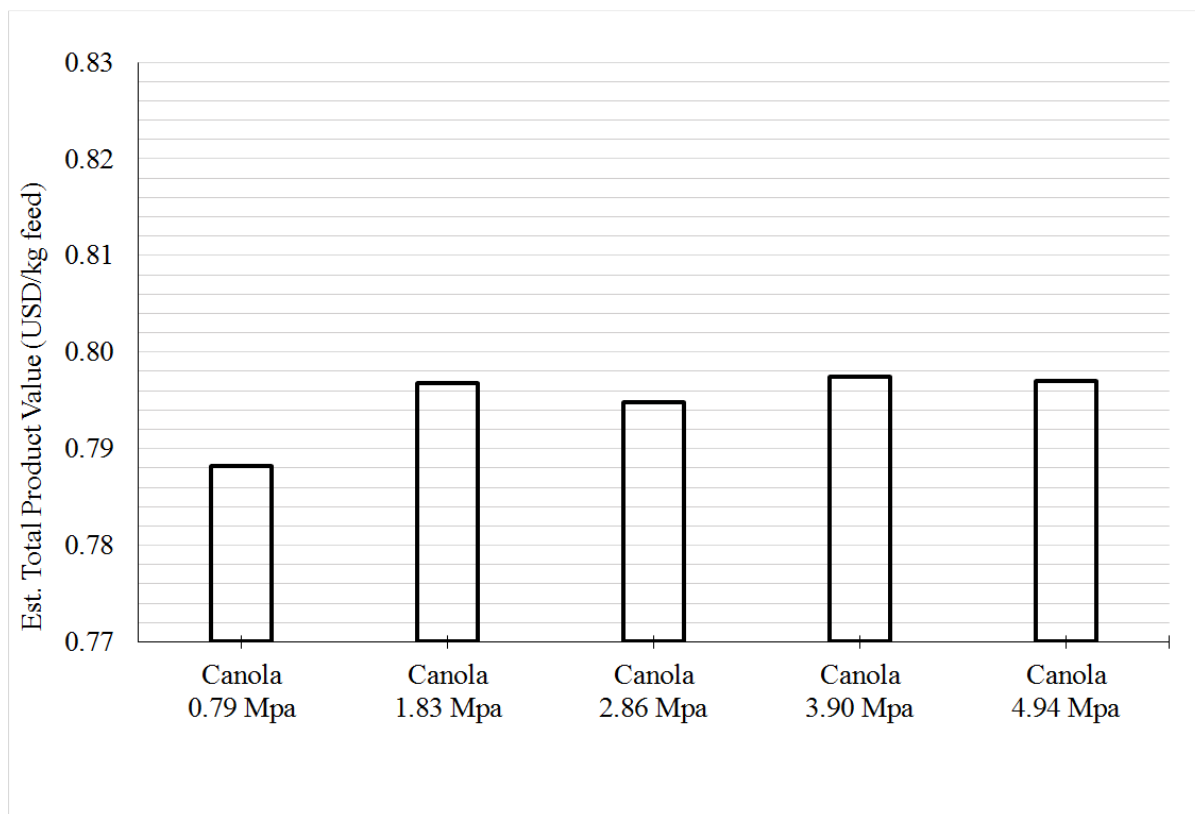
Figure 117. Estimated total product values from cracked samples of canola oil by varying reactor operating pressure

VII.E.3.ii. Statistical Regressions of Noncatalytic Cracking Process Yields to Determine Significant Effects

Regressions were calculated for the data presented in Figure 112 through Figure 117 according to the methods described by Lawson and Erjavec[155] in order to determine the effects of various reactor operating conditions and various fatty acid moieties in the feedstock on the estimated products of fuel refinement with the noncatalytic cracking process (NCP). Regressions were performed on the (1) temperature and space time and (2) the pressure, and the regression results are presented in Table 52 through Table 51, respectively. Each set contains 8 regressions, one for each type of product and also one for the total product value. Residue

products were not regressed because they were set to 5.05 wt. % based on the work on Bosquez[66] as described in Section VII.E.3.i.

In order to regress the data according to the methods of Lawson and Erjavec[155], values for TAG fatty acid moieties were coded from -1 to 1, respective of the mole fraction of each fatty acid in the original TAG feedstock molecules over their experimental domains. Therefore, it should be mentioned that since the mole fraction of fatty acids cannot exceed 100, it is not possible in this instance for all coded fatty acid variables to be 1.0 at the same time. The result of this phenomenon is an asymmetrical regression domain. Nevertheless, the data from the regression based on fatty acid moieties are valid so long as the data are not improperly utilized by assuming that the domain were symmetrical or by extrapolating far outside the experimental domain. Values for temperature, pressure, and space time were coded from -1 to 1 likewise; these have a symmetrical domain. Coded variables are shown in Table 49.

Table 49. Regression variable domain and encoding

Coded Value:			-1	0	1
Uncoded Variable	Unit	Coded Variable			
Palmitic (COOH 16:0)	(mol %)	X1	3.2	13.5	23.9
Stearic (COOH 18:0)	(mol %)	X2	0.0	2.1	4.2
Oleic (COOH 18:1)	(mol %)	X3	13.0	48.6	84.1
Linoleic (COOH 18:2)	(mol %)	X4	4.0	30.8	57.6
Linolenic (COOH 18:3)	(mol %)	X5	0.0	30.0	60.0
Erucic (COOH 22:1)	(mol %)	X6	0.0	20.6	41.2
Temperature	(C)	X7	420	430	440
Space Time	(h)	X8	0.27	0.75	1.22
Pressure	(MPa)	X9	0.79	2.86	4.94

In addition to the linear factors, two-way interaction parameters were also considered for the case of temperature/space time, although none were found to be statistically significant. As a

result, they were omitted and not tabulated. In the case of pressure, a second order term was considered. It was also found to be insignificant in all cases, so it was likewise not tabulated.

Effects that were not significant were systematically eliminated from the regression so that the remaining coefficients were significant to a statistical p-value of 0.05 for temperature and pressure and a p-value of 0.10 for TAG fatty acid moiety composition.[155] The resulting regression coefficients are indicated in Table 52 through Table 51 in units of wt. %, and a coefficient of determination is included for each row. The constant in each row is the mean effect for that row, denoted as B1, B2, or B3 depending on the regression set.

Each coefficient indicates a magnitude change over the half experimental domain (due to the coded experimental domain being from -1 to 1). In Table 50, for example, coefficient X4 by the product LPG indicates an increase of LPG yield by 1.0 wt. % (feedstock TAG basis) in the products as a result of increasing the linoleic acid content in the feed from a coded value of -1 (4 mole %) to a coded value of 1 (57.6 mole %). In addition to the coefficients in the regression, the coefficient of determination must be considered, whereas a coefficient of determination indicates the quantity of error explained by the model.

Table 50 is the result of statistical regression of Figure 112 and Figure 113 to determine the effect of TAG fatty acid moiety composition on the distribution of products from the NCP. The mole percent of each fatty acid moiety was encoded from -1 to 1 over the experimental domain as variable X1 through X6 according to Table 49. Table 50 indicates the regression coefficients which are statistically significant to a p-value of 0.10, corresponding to a 90 % confidence interval. It was desirable to use a reduced confidence interval in order to observe any marginally significant statistical effects, due to the complexity and asymmetry of the

384

experimental domain.

It is evident that the effect of stearic acid was found to be negligible for any of the fuels produced. This is expected, because the molar concentration of stearic acid in the feedstocks was estimated to only be present in the range of less than 5 mole % (see composition data in Table 1).

Palmitic acid was found to only have a statistically significant effect on the production of diesel and fuel oils. This is expected because the bonds on the carbon chain of the fatty acid moiety are fully saturated, thereby not promoting chain scission reactions which would otherwise influence lighter fuels.

Observing the coefficients of determination, the fatty acid linear regression model was found to poorly fit the estimated yields for natural gas equivalents and for naphtha. As a result, the statistical conclusions about naphtha and burner fuel should be taken with less consideration than statistical conclusions about other fuels (e.g., no. 2 fuel oil has a 0.99 coefficient of determination).

Oleic acid was correlated to reduced yields of all product fuels except for no. 4 fuel oil. Erucic acid was similarly correlated to reduced yields of lighter fuels, however increased yields of fuel oils. This is an undesired effect due to the reduced salability and value of fuel oils.

The yield of lighter fuels was found to statistically increase with increasing concentration of linoleic acid and, to a greater extent, linolenic acid. Furthermore, fuel oil yield was reduced for these fatty acid moieties. This is desirable due to the improved salability of lighter liquid fuels.

Table 50. Regression coefficients showing the statistically significant effects
of various triglyceride fatty acid moieties on the distribution of end products
from the noncatalytic cracking process

TAG Composition	(COOH 16:0)	(COOH 18:0)	(COOH 18:1)	(COOH 18:2)	(COOH 18:3)	(COOH 22:1)	Const	Coeff. Det.
Coded Variable	X1	X2	X3	X4	X5	X6	B1	R^2
Effect Coefficients (wt. %)								
Nat. Gas Equiv.	-	-	-0.2	-	0.2	-	2.1	0.59
LPG (3-4)	-	-	-0.2	0.5	0.3	-0.2	3.0	0.90
Naphtha (5-9*)	-	-	-	0.9	0.8	-1.0	10.0	0.52
Jet (*9-13*)	-	-	-0.4	-0.3	0.4	-	10.4	0.93
Diesel (*13-18)	2.2	-	-	-	-	-1.5	19.1	0.72
No. 2 Fuel Oil (19-25)	-1.3	-	-0.7	-0.9	-0.6	1.7	20.3	0.99
No. 4 Fuel Oil (26-74)	-1.5	-	1.6	-	-2.2	1.9	19.8	0.96
Carbon	-	-	-	-	-	-	5.1	1.00
TPV (USD/kg)	-0.004	-	0.005	-	-0.005	0.004	0.804	0.78

It appeared as though some of the fatty acid moieties had a statistically significant effect on the TPV. Increasing the oleic acid and/or erucic acid in the TAG feedstock would be expected to improve the profitability of the process, albeit slightly. The consequence of increasing palmitic acid or linolenic acid in the process would be slightly reduced process profitability. This may be related to the yield of process gas that coincides with reduced TPV. Process gas yield was lower for TAGs rich in oleic acid and erucic acid (see Section VII.B.4.ii).

Table 51 is the result of statistical regression of Figure 114 and Figure 115 to determine the effect of reactor operating temperature and space time on the distribution of products from the NCP. Temperature has been encoded as X7 and space time has been encoded as X8 according to Table 49. As previously mentioned, a two-way interaction parameter was also included but was not significant in any cases and was removed from the regression. Table 51 indicates the regression coefficients which are statistically significant to a p-value of 0.05.

What can be seen is that the yields of all the products are statistically dependent upon temperature and/or space time except for the formation of carbon products and LPG. The yield of no. 4 fuel oil is also dependent upon the 2-way interaction parameter. The coefficient of

determination for all products is on the order of 0.8 or better for all regressions except for diesel, indicating that about 80 % of the error in the system is described by the model in most cases. Additionally, the regression for the TPV was found to be statistically significant, albeit miniscule in effect.

By observing the coefficients for various fuels, it appears that operating at increased temperature and pressure results in an increase to such fuel yields as: natural gas equivalents, naphtha, and jet. Likewise, increasing temperature leads to a statistical decrease in no. 2 fuel oil and no. 4 fuel oil. The yield of diesel was statistically found to increase with increased space time but not with increasing temperature.

The total product value (TPV) was found to decrease with temperature and/or space time over the experiments. This was visually determined in Figure 114 as well. The statistical magnitude of change in the TPV is on the order of 0.046 USD/kg over the full range of conditions studied (i.e., about 5.8%). This is likely a consequence of increased formation of process gas formation at higher temperatures and pressures, which has reduced value compared to liquid fuels.

Table 51. Regression coefficients showing the statistically significant effects of operating temperature and space time on the distribution of end products from the noncatalytic cracking process

Operating Condition(s) Coded Variable		Temperature X7	Space Time X8	Const B2	Coeff. Det. R^2
Effect Coefficients	(wt. %)				
Nat. Gas Equiv.		0.4	0.7	2.2	0.95
LPG (3-4)		0.8	0.9	3.3	-
Naphtha (5-9*)		1.8	2.3	11.6	0.78
Jet (*9-13*)		1.4	2.1	10.9	0.77
Diesel (*13-18)		-	1.4	20.1	0.61
No. 2 Fuel Oil (19-25)		-1.5	-2.8	17.6	0.85
No. 4 Fuel Oil (26-74)		-4.1	-5.8	18.3	0.86
Carbon		-	-	5.1	1.00
TPV	(USD/kg)	-0.008	-0.015	0.800	0.90

Table 52 is the result of statistical regression of Figure 116 and Figure 117 to determine the effect of reactor operating pressure on the distribution of products from the NCP. Reactor operating pressure has been encoded as variable X9. As previously mentioned, a 2nd order term was included (i.e., X9·X9) but found to be significant in no cases. Table 52 indicates the regression coefficients which are statistically significant to a p-value of 0.05.

The strongest effects are the increased production of naphtha and jet fuel and the decreased production of diesel and no. 2 fuel oil. It appears that as the pressure increases from the minimum pressure of 0.79 MPa to the maximum pressure of 4.94 MPa, the yield of naphtha increases by approximately 3 wt. %, which is a relative increase of about 15 %. Jet fuel yield increased by approximately 1.8 wt. %, which is a relative increase of about 10 %. At the same time, the yield of diesel and no. 2 fuel oil decreased by 3.2 wt. % and 1.8 wt. % respectively, which corresponds to relative reductions of about 13 % and 22 % respectively. As a result of increased pressure, the decreased fuel oil yield and increased jet and naphtha yields is desirable. However, diesel fuel yield is consequentially reduced, which is undesired due to the high value and salability of diesel.

On a statistical basis, it appears as though operating at various pressures has no benefit economically, as long as the downstream fuel intermediates are hydrogenated to increase fuel stability via olefin conversion to paraffins. Therefore, operating pressures might be considered that minimize the cost of the reactor and the operating cost. As a result, only the mean value is reported for the total product value (TPV).

Minor effects include the increase of natural gas equivalents (burner fuels) with increasing pressure and increased yield of no. 4 fuel oil with increasing pressure.

388

Table 52. Regression coefficients showing the statistically significant effects
of operating pressure on the distribution of end products
from the noncatalytic cracking process

Operating Condition(s)		P	Const	Coeff. Det.
Coded Variable		X9	B3	R^2
Effect Coefficients	wt. %			
Nat. Gas Equiv.		0.1	2.4	0.94
LPG (3-4)		-	3.9	-
Naphtha (5-9*)		1.5	20.3	0.84
Jet (*9-13*)		0.9	19.4	0.71
Diesel (*13-18)		-1.6	24.3	0.91
No. 2 Fuel Oil (19-25)		-0.9	8.2	0.66
No. 4 Fuel Oil (26-74)		0.4	3.7	0.79
Carbon		-	5.1	1.00
TPV	(USD/kg)	-	0.795	-

The effect of pressure on LPG was not found to be significant. As previously described,

there was no regression performed on the yield of carbon product, however the mathematical

equivalent of a regression is depicted with a coefficient of determination of 1.

VII.E.3.iii. Statistical Regressions of Functional Group Speciation in the Products of the Noncatalytic Cracking Process

Composition data that was used to produce the estimated process yields in the prior two

sections has been used to produce the data in Table 123 through Table 125 in Appendix N. This

data is similar to the process yield data that was presented in the prior two sections, however, the

percentage of different functional groups is determined for each fuel product. This is beneficial

for observing the effect of a certain operating parameter on, for instance, the aromaticity of the

jet fuel fraction. The data are sufficiently detailed that their interpretation requires statistical

regression. For this reason, the data have been placed in Appendix N.

For these data, the jet fuel range is defined by the carbon number range 9-13 in these

tables for the sake of simplicity (not the partial carbon number range, *9-13*, as previously

described in Section VII.E.3.i). Naphtha and diesel fuel ranges are consequently adjusted to 5-8

and 14-18, as indicated in Table 123 through Table 125 (Appendix N).

Regressions were performed on the data according to the methods of Lawson and Erjavec[155] in like manner as in the previous section (VII.E.3.ii). This was done in order to determine the effects of various reaction parameters on the distribution of functional groups in each fuel product. The results are tabulated in Appendix O (see Table 126 through Table 128).

Table 53 through Table 55 are reduced versions of Table 126 through Table 128, showing only statistically significant coefficients with coefficients of determination equal to 0.65 or better. This narrows the discussion to only the regression data that is meaningful and reasonably well correlated.

Table 53 indicates the regression coefficients which are reflective of the effect of various TAG fatty acid moieties on the distribution of functional groups in the products from the NCP.

Linoleic acid and linolenic acid were correlated to reduced quantities of H, CO, and CO_2 in the process gas that was produced from TAG processing. In contrast, Erucic acid is correlated to increased quantities of the same species. This may be interesting from a mechanistic standpoint, however it does not pose a significant advantage or disadvantage when it comes to the production of fuel.

The quantities of paraffins and aromatics in the naphtha product were found to be statistically correlated to fatty acid moieties in the TAG feedstock. Specifically, linolenic acid was correlated to decrease the paraffin content and increase aromatic content of the naphtha range. Oleic acid was found to have the opposite effect, and linoleic acid was correlated to decrease aromaticity and paraffin content of naphtha. The effect on aromaticity tended to be on the order of about 0.3 to 0.8 % over the full magnitude of the experimental domain, whereas the

effect on paraffin content was on the order of 2 to 4 %. Although the increased aromaticity

might be considered to improve the octane rating of the naphtha, the effect would be minimal

due to the low magnitude of the change in aromaticity.

The only functional groups that were significantly affected and well correlated were

aromatics and carboxylic acids. These were statistically influenced by all fatty acids except for

palmitic acid.

Table 53. Regression coefficients showing the effect of various triglyceride fatty acid moieties on the distribution of products from triglyceride cracking in tubular cracking reactors

TAG Composition	(COOH 16:0)	(COOH 18:0)	(COOH 18:1)	(COOH 18:2)	(COOH 18:3)	(COOH 22:1)	Const	Coeff. Det.
Coded Variable	X1	X2	X3	X4	X5	X6	B1	R^2
Effect Coefficients (wt. %)								
Gaseous Fuel Range (1-4)								
H_2/Range	-	-	-	-0.03	-0.04	0.04	0.57	0.69
CO/Range	-	-	-	-0.54	-0.77	0.69	13.20	0.73
CO_2/Range	-	-	-	-2.86	-2.86	2.21	29.03	0.78
Naphtha Range (5-8)								
C-/Range	-	-	1.98	-1.09	-1.49	-	13.71	0.81
(1x)Ar(=)/Range	-	-	-0.19	-0.16	0.38	-0.15	1.56	0.91
Jet Range (9-13)								
(1x)Ar(=)/Range	-	-0.96	-1.40	1.67	2.47	-1.32	8.14	0.99
(2/3x)Ar(=)/Range	-	-0.38	-	0.54	0.57	-0.39	2.55	0.94
COOH/Range	-	-	-	-6.63	-3.19	2.88	28.15	0.65
Diesel Range (14-18)								
C-/Range	1.88	-	-0.92	-	-	-0.89	4.98	0.91
C=/Range	-	-	2.91	-6.48	-4.09	2.85	23.55	0.94
=C=/Range	-3.81	-	-	-	-	2.45	24.27	0.91
(1x)Ar(=)/Range	-	-	-1.08	-	2.10	-0.90	7.52	0.90
(2/3x)Ar(=)/Range	-0.64	-	-0.77	-	1.18	-	10.09	0.85
COOH/Range	8.83	-	-	-	-	-5.13	29.59	0.88

Aromaticity increased in the jet fuel range by as much as 6 % for increasing linolenic

acid moiety content and by as much as 4 % for increasing linoleic acid moiety content in the

TAG feedstock. Both of these fatty acid moieties were correlated to reduced acidity of the jet

fuel range. Therefore, after deoxygenation, this may coincide with reduced paraffin content of

the jet fuel range due to the lesser quantity of n-paraffins being formed by decarboxylation. This may be helpful for widening the jet fuel range or improving the quality of the jet fuel.

Erucic acid and stearic acid were correlated to reduced aromaticity of the jet fuel range. Furthermore, erucic acid was correlated to increased acidity in the jet fuel range. It is interesting to observe the statistical effect of stearic acid on the jet fuel range, due to its absence of double bonds on the carbon chain. The statistical effect may be due to the asymmetric experimental domain, whereby increasing the stearic acid content of the TAG feedstock likewise results in a decrease of other fatty acid moieties. Otherwise this may simply be a statistical artifact in the data due to chance.

The diesel fuel range was not affected by stearic acid, which was unexpected. Based on the interpretations from the bond energies of stearic acid that were discussed in Section III.F.4, stearic acid would be expected to produce long chain n-paraffin or carboxylic acids in the product, which would resultantly increase the paraffin content or carboxylic acid content of diesel. In examining the composition of the various TAGs (see Section III.F.4) that were utilized to produce the data in Table 53, it is apparent that stearic acid may only be present on the order of 0 to 5 mol % in the TAGs processed in this dissertation. Due to its minor presence in the TAG feedstocks, it may be difficult to determine the statistical influence of stearic acid on the products of TAG cracking. Future experiments could consider processing saturated TAG feedstocks (e.g., fully saturated soybean TAG) in order to have a better experimental domain for determining the influence of stearic acid on the products from TAG cracking.

The diesel range showed a well-correlated statistical dependence of various TAGs on distribution of C= and =C= group components, which was not observed in the other fuels.

Furthermore, the effects on functional groups in the diesel range were substantially stronger in magnitude that the effects for other fuels. Monounsaturated fatty acid moieties (COOH 18:1 and COOH 22:1) were shown to have an increasing effect on C= components in the diesel range, whereas polyunsaturated fatty acid moieties (COOH 18:2 and COOH 18:3) had the opposite effect.

Palmitic acid was statistically correlated to cause an increase in the acidity of the diesel fuel. This is expected due to the unsaturated nature of palmitic acid, whereby it does not have C=C bonds on the fatty acid chain to promote mid-chain cracking reactions.

Linolenic acid was correlated to an increase in aromaticity of the diesel, potentially leading to a better quality product. Oleic acid, palmitic acid, and erucic acid were shown to have a decreasing effect on the aromaticity of the diesel fuel range, potentially having the opposite effect on quality.

Data are presented in Table 54 for the second regression with the independent variables being temperature, space time, and their two-way interaction for the 100 mL lab-scale TCR. In examining the magnitude of the effects, an increase in space time appears to have approximately twofold stronger influence on the distribution of functional groups in the fuel products than an increase in temperature over the conditions studied. This may indicate an advantage to cracking reactors at longer space times and reduced temperatures.

It is apparent that the increase of temperature and space time leads to a statistically strong reduction in the acidity of all the fuel products. This is expected, indicative of increased deoxygenation with increased cracking severity. Interestingly, the increased cracking severity was not well correlated to increase the content of CO and CO_2 in the gaseous fuel range. This

393

may be due to simply an increased magnitude of the gaseous fuel, without shifting the distribution of CO and CO_2. Otherwise, no explanation for this lack of CO/CO_2 is offered.

What stands out is the increased aromaticity of the jet fuel range with increased cracking space time (however not temperature). This may be due to a need of additional time for dehydrogenation/aromatization reactions to occur. A similar increase in aromaticity of the diesel fuel was observed for both temperature and space time.

Table 54. Regression coefficients showing the effect of temperature and space time on the distribution of products from triglyceride cracking in tubular cracking reactors

Operating Condition(s)		T	Tau	T×Tau	Const	Coeff. Det.
Coded Variable		X7	X8	X7·X8	B2	R^2
Effect Coefficients	(wt. %)					
Gaseous Fuel Range (1-4)						
C-/Range		3.0	2.5	-	23.3	0.77
C=/Range		1.2	1.5	-	11.0	0.74
COOH/Range		-2.5	-6.3	-	21.4	0.94
Naphtha Range (5-8)						
C=/Range		1.8	2.9	-	19.6	0.89
=C=/Range		-	2.4	-	16.2	0.66
COOH/Range		-4.0	-7.1	-	50.2	0.84
Jet Range (9-13)						
C-/Range		-	2.1	-	8.6	0.68
(1x)Ar(=)/Range		-	2.1	-	10.7	0.70
COOH/Range		-1.1	-2.5	-1.0	20.7	0.86
Diesel Range (14-18)						
C-/Range		1.1	2.7	1.1	7.2	0.89
(2/3x)Ar(=)/Range		0.3	0.5	-0.4	9.5	0.70
COOH/Range		-4.6	-9.8	-	32.7	0.76

Data are presented in Table 55 for the third regression with the independent variable being the pressure for the 100 mL lab-scale TCR. As mentioned, the second-order pressure term was also included in the regression but removed after it was found to be not significant in all cases.

It is apparent that the increase of pressure leads to an increase in the hydrogen content of

the gaseous fuel range. This agrees with an observed statistical increase of the concentration of aromatics in all the other fuel products. As a result, increased fuel quality may be expected from an increase in operating pressure of TAG cracking reactors.

Additionally, the acidity of the jet fuel range was found to decrease strongly with increased pressure. This might indicate increased decarboxylation at higher operating pressures, but it doesn't agree well with the decrease in carbon monoxide in the gaseous fuel range.

Table 55. Regression coefficients showing the effect of pressure on the distribution
of products from triglyceride cracking in tubular cracking reactors

Operating Condition Coded Variable	Pressure X9	Const B3	Coeff. Det. R^2
Effect Coefficients (wt. %)			
Gaseous Fuel Range (1-4)			
H/Range	0.04	0.31	0.78
CO/Range	-1.3	13.8	0.70
C-/Range	0.9	24.7	0.68
Naphtha Range (5-8)			
C-/Range	1.0	16.8	0.87
(1x)Ar(=)/Range	0.7	2.2	0.95
COOH/Range	-1.2	35.3	0.83
Jet Range (9-13)			
C-/Range	1.1	9.6	0.88
=C=/Range	1.5	26.3	0.85
(1x)Ar(=)/Range	1.7	9.2	0.89
(2/3x)Ar(=)/Range	0.4	2.2	0.72
COOH/Range	-4.0	20.4	0.69
Diesel Range (14-18)			
C-/Range	0.8	6.3	0.69
C=/Range	-2.6	34.9	0.90
(1x)Ar(=)/Range	1.5	10.7	0.73

It is interesting to observe a negative effect of C= group components in the diesel range with increased operating pressure. It is difficult to explain this observation from a mechanistic standpoint, due to the lack of identification of C= as an olefin or a cyclic product.

VII.E.3.iv. Differing Cracking Efficiency of Tubular Cracking Reactors

It was expected that the 100 mL lab-scale TCR and 200 mL lab-scale TCR configurations

would have similar performance. However, in examining the yield data in Section VII.E.3.i, it is apparent that canola TAG cracking in the 200 mL lab-scale TCR had less than half the fuel oil yield than that of soybean TAG cracking in the 100 mL lab-scale TCR. The yield of lighter fuels was likewise greater in the 200 mL configuration, indicating better performance.

This is evidence that the reactor redesign to the 200 mL cracking reactor was beneficial and important to the production of renewable transportation fuels. Major changes to the reactor between the 100 mL configuration and the 200 mL configuration included (1) increasing reactor length, (2) removing the preheater, (3) an upright configuration of the cracking coil, and (4) the dual-zone cracking tube heater configuration, all of which are indicated in Section V.B.1.iii.

Although the temperature distribution of the 100 mL lab-scale TCR was not well characterized, due to a lack of thermocouples, the 200 mL lab-scale TCR had a very uniform and well characterized thermal profile as indicated in VII.B.4.ii. It is probable that the 100 mL lab-scale TCR had less uniform thermal profile, due to only single-zone heater control. However, not enough thermocouples were used to confirm this during its operation.

VII.E.3.v. Summary

What can be generally observed from the statistical regressions is that increasing temperature and space time, and to a lesser extent, pressure improves the yield of lighter fuels and reduces the yield of residual fuels (i.e., no. 4 fuel oil and no. 2 fuel oil). Increasing these operating parameters can be described as increased cracking severity. Residual fuel yields were decreased from as high as ~45 wt. % to as low as ~14 wt. % under the best operating conditions. This is beneficial due to the increased salability of lighter fuels, whereby fuel oil usage in the US only accounts for a miniscule fraction of the total petroleum usage as described in Section II.D.3

Over the conditions studied, the total product value (TPV) tended to vary on the order of ±0.02 USD/kg with a mean value on the order of 0.8 USD/kg. Statistical correlations showed very minimal effect on the TPV with the experimental factors studied. Although gaseous fuel tended to increase as a result of increased cracking severity, it did not have a substantial negative impact on the TPV. Due to the increased salability of lighter fuels, it is then considered that cracking at the most severe conditions over the range studied is optimal.

Increasing the cracking severity led to an increase in aromaticity of the products. This potentially leads to better fuel quality and/or wider fuel carbon number ranges. This is discussed in greater detail in Section VIII.E.2. Additionally, aromaticity was increased in products as a result of polyunsaturated fatty acid moieties in the feedstock. This is sensible in light of related literature that is discussed in Section VIII.E.2.

Exceeding the operating temperature, pressure, and space time investigated in this dissertation is not recommended due to the onset of coke formation. As previously noted in Section VII.B.4.ii, there is substantial concern for coking if the temperature exceeds 440 C and if the space time exceeds approximately 1.3 hours. With these practical limitations on what temperatures and what pressures can be utilized, it appears that 440 C temperature and 1.3 hour space time at 4.9 MPa is a safe and reasonably optimal operating condition.

CHAPTER VIII

DISCUSSION

This chapter discusses the findings of this dissertation in light of published literature and the noncatalytic cracking process.

VIII.A. Deoxygenation

The results of batch reactor experiments to determine a suitable catalyst for deoxygenation are described in this section, followed by the results of continuous packed bed reactor deoxygenation.

VIII.A.1. Batch Screening Experiments

Batch catalytic deoxygenation experiments indicated that several nickel catalysts were capable of outperforming the activated carbon supported palladium catalyst (Pd/C 5) for the deoxygenation of carboxylic acids present in the CTL from noncatalytically cracked TAG. This is shown in Figure 88 on page 322. Furthermore, all tested catalysts outperformed Pd/C 5 except for the catalyst with the lowest content of nickel (Ni/C 2.3), which was made via wet impregnation. The potential superior activity of nickel based catalysts relative to palladium is advantageous due to the substantially reduced cost of nickel relative to palladium. Further, palladium is a rare metal, leading one to assume that widespread utilization of palladium in catalytic processes may become hindered by an inability to source palladium.

In examining the activity of the catalysts (Figure 88 on page 322), it was apparent that

Ni/SiAlZrOx 60 had twofold stronger activity than its nearest three competitors (Ni/SiO2 55; Ni/C 31.7; and Ni/C 20.3). Although this appeared desirable, the mass consumption of H_2 appeared to be very high for Ni/SiAlZrOx 60 relative to its activity (see Table 41 on page 323). In addition, the gas phase composition from Ni/SiAlZrOx 60 contained a substantial concentration of cracked components (Table 41), indicating increased cracking relative to other catalysts. The increased cracking and increased hydrogen consumption are disadvantages for the noncatalytic cracking process. Cracking leads to generation of lower value smaller carbon chain compounds while the increased use of hydrogen adds cost.

Ni/SiO2 55, Ni/C 20.3, and Ni/C 31.7 were all shown to have statistically similar activity (see Figure 88) on the order of 0.25 mmol·g^{-1}·min^{-1} under the conditions studied. This makes it beneficial to compare their features and notice any trends. In examining the gas phase composition data, it is noticeable that the hydrogen consumption increases with the production of methane for all nickel catalysts. CO and CO_2 were not produced in large quantities, potentially indicating a reduction of product carbon oxides into methane. This is an undesirable condition for fuel production, whereby the reactor utilizes hydrogen gas, adding cost.

The surface area of the catalysts should be considered for the scale-up of this process (see Table 42). The Ni/C catalysts have on the order of 8-14 times the surface area of the Ni/SiO2 55 catalyst. Since the catalyst size typically increases for packed bed reactors as they are scaled up to commercial size, there is greater possibility for the reaction to become limited by the rate of internal diffusion, rather than by the rate of reaction. In a severely diffusion limited scenario, Ni/C catalyst could potentially have better performance on the order of the square root of the relative surface area (i.e., 3-4 times better performance) according to effectiveness factor

correlations in Fogler.[161] In a more appropriate scenario however, the various Ni/C catalyst

particles could simply be larger in size, having otherwise equal performance to that of Ni/SiO$_2$

catalyst. The increased size would enable more favorable reactor dimensions.

The findings from the batch reactor selectivity experiments of this work may be

compared to a similar study conducted by Snare et al.,[31] who studied 20 catalysts in batch

reactors for the deoxygenation of stearic acid diluted in n-dodecane. In contrast to the results

herein, Snare found that precious metal catalysts outperformed the inexpensive base metal

catalysts, such as nickel. Systematic experimental differences between the present work and

Snare's work may help explain the discrepancy in catalyst performance.

The present work utilized high temperature/pressure introduction of reactants to an

already preheated reactor as described by page 171 (see Figure 35). This provided a practically

instantaneous reaction start time. By contrast, Snare added catalysts and reactants to the reactor

at room temperature and then heated the contents up afterwards, similar to a more basic

procedure utilized in other experiments of this dissertation (see page 181 and Figure 37).

Additionally, experiments herein were performed under a reducing atmosphere of hydrogen at

higher pressures (3.6 MPa), whereas Snare performed the reactions under helium (non-reducing)

at lower pressures (0.6 kPa).

Of the 20 catalysts studied by Snare,[31] the most active catalysts included rare metal

catalysts such as Pd/C 5, Ru/MgO 5[*], Pt/C 5, and Pd·Pt/C 8·2 which were found to be active on

the order of 62 to 100 % (based on conversion over six hours). Nickel catalysts however were

---

[*] All catalyst names are presented following the same nomenclature

found to be active only on the order of 8-18 %, including Ni/SiO_2, Ni/Cr_2O_3, Ni/Al_2O_3, Raney-Nickel, and a nickel-molybdenum catalyst. Based on his findings, Snare indicated that catalytic deoxygenation is 'preferably carried out over palladium and platinum supported catalysts.' Snare added that palladium was characterized by decarboxylation and platinum was characterized by decarbonylation thereby increasing the potential for hydrogen consumption.

In the work herein, the Pd/C was found to produce large amounts of CO and smaller amounts of CO_2 as indicated in Table 41. This may indicate a decarbonylation mechanism dominating the reaction with palladium. Decarbonylation consumes additional hydrogen as the reaction is completed through the production of water, as indicated by Snare.[31] This is a disadvantage due to increased consumption (and cost) of hydrogen.

The work herein showed that nearly all the nickel catalysts were stronger acting than Palladium for the first half hour. This may be due to the rapid start time of reaction, mitigating the effect of deactivations that can take place during the preparation and warm-up time for Snare's work. A likely explanation is that the increased performance of nickel is due to the high partial pressure of hydrogen gas, whereby Snare's did work without hydrogen.

VIII.A.2. Packed Bed Reactors

A continuous packed bed reactor (PBR) system with a 0.1 kg bed of Ni/SiO2 55 was successfully used for deoxygenating a model compound feedstock (20.5 wt. % octanoic acid in cyclohexane) due to rapid and complete deoxygenation in a single pass through the bed. By contrast, the attempts to utilize the PBR with the cracked TAG distillates (CTD) were originally found to be unsuccessful at achieving steady state or at deoxygenating. This was due to coking and/or plugging in the reactor as indicated on page 329 (see Figure 91) or otherwise due to

deactivation of the catalyst as shown by Figure 90.

Adjusting the quantity of hydrogen gas did not seem to counteract the deactivation of the catalyst bed. As previously mentioned in Section I.D.1 for triglyceride hydrotreatment processes, high partial pressures of hydrogen gas are necessary for proper function (Guzman[33]). Since triglyceride hydrotreatment and catalytic deoxygenation are similar processes, it stands to reason that increasing the partial pressure of hydrogen in the deoxygenation reactor might help improve reactor performance. This was not the case over the range of conditions studied, however.

Comparisons can also be made to hydroisomerization processes, which operate using catalytic reactors over a similar range of temperatures and pressures. Raseev indicates that increasing the pressure of hydrogen in hydroisomerization processes is beneficial for reducing undesired hydrocracking and coking reactions.[34] Since coke and tar formations were observed on catalysts in this study, it stood to reason that increasing the hydrogen partial pressure may have potential benefit for this process as well. Raseev furthermore adds that the relative molar feed rate of hydrogen to reactants is on the order of 2-6 for lower alkanes (<C7) and on the order of 8-20 for oils. For the experiments performed herein with the model compound feedstock, the molar relative feed rate of hydrogen to liquid feedstocks was computed to be on the order of 0.4, which was relatively low.

The experiments with the PBR that utilized the CTD feedstock were performed using higher molecular weight compounds, formed from the distillation and vacuum distillation of cracked TAG liquid (CTL) as described in Section V.A.2. It is estimated that the molecular weight of the CTD are 2-3 times higher than the model compounds. Furthermore, the hydrogen

402

feed quantity was increased from 100 mL/min to 500 mL/min in some of the experiments

described in Table 14 (see page 211). The total effect of these adjustments might make for a

molar feed rate of H_2 to reactants on the order of 5, which is still relatively low compared to

ratios of 8-20 seen in hydroisomerization processes of oils. From this, it might stand to reason

that increasing the hydrogen feed rate from 500 mL/min to 2000 mL/min might be able to reduce

the amount of coke formed on the catalysts and preserve their activity. Furthermore, increasing

the pressure has also been shown to have a positive effect for reducing coke formation in

hydroisomerization reactors.[34] However, equipment restrictions prevented operating at higher

pressures than 3.6 MPa.

Due to the onset of coke on the catalyst surfaces, and based on the observed dependence

of coke formation with temperature in Section VII.B.3 for triglyceride cracking in batch reactors,

it was considered that reduced temperatures might reduce the coke formation on catalyst

surfaces. This was not shown to be the case. This is not an unexpected outcome, since coke

formation on the surfaces of catalysts may proceed through different mechanisms.

Fortunately, the addition of steam was found to be the critical factor for preserving

catalyst activity, as described on page 331 (Figure 93). After adding steam at a relative mass

feed rate of at least 0.03, catalyst activity was found to be stable over a 56 hour period. Similar

effects have been shown by Katikaneni et al.[44] for the catalytic cracking of triglycerides (TAG),

a process which is notoriously coke prone as described in Section I.D.2 (see page 13).

Katikaneni observed that the addition of steam prolonged the catalyst life through a reduction in

coke deposition. The reduction in coke deposition was explained by the competitive adsorption

between coke precursors and water molecules on the acid site of the catalysts, and/or the partial

gasification of coke deposits by steam. Pansing offers a similar statement about diluting the

reactant feed to catalytic cracking with steam, stating that 'steam increases […catalytic reaction

rates…] by reducing chemisorption of reaction products which compete for chemisorption [on

active sites]'.[162]

Future experiments should consider a study of the effect of steam/hydrogen/reactant ratio

on the catalyst activity and reaction yield. It could be assumed that the addition of steam should

be minimized to prevent extraneous gasification of reactant. This should be verified with

additional studies. Future research should also consider the catalytic effect on other species such

as olefins, cyclics, aromatics, and oxygenates such as alcohols and ketones which may be formed

during the reaction. Catalytic effects such as hydrogenation, dehydrogenation, cyclization,

aromatization, and others may have an important influence on fuel production with the

noncatalytic cracking process (NCP).

VIII.B. Coking in Triglyceride Cracking Reactors

Severe coke formation has been shown to cause multiple problems in TAG noncatalytic

cracking reactors, such as (1) untimely shutdowns and laborious cleaning efforts, (2) process

upsets due to sudden particulate plugging, (3) a reduction of desirable product yields, and (4)

increased resistance to heat transfer. After reviewing numerous studies involving the cracking of

triglycerides, the only substantial studies targeting the reduction and/or elimination of coke

formation involve those prolonging catalyst life in TAG catalytic cracking (Katikaneni[44]), which

is important but not applicable to TAG noncatalytic cracking.

It was not practical to study coke formation during triglyceride (TAG) cracking in the

bench-scale continuous stirred tank reactor (CSTR) due to its large heat-up / cool-down and

assembly/disassembly times and also due to concern about the accuracy of coke quantitation. Nevertheless, TAG cracking in CSTRs was found to be significantly hindered by coke formation and attempts to alleviate the coke formation by reactor modifications were unsuccessful, including increased feed preheating (see Section VII.B.2.iii) and the removal of products from the bottom of the unit (see Section VII.B.2.iv). Attempts to measure the temperature of the wall in the reactor during coke formation crudely indicated that the wall temperature might be on the order of 40 degrees higher than that of the bulk fluid (see Section VII.B.2.ii). This implies that when operating the reactor at 400 C or 420 C, the reactor wall temperature may on the order of 440 C or 460 C, respectively.

Batch reactor coke formation was more easily studied and it provided helpful insights into the conditions promoting coke formation. Mature coke formed on the surfaces of reactor walls in contact with the liquid phase at shorter residence times when the temperature of reaction was high; on the order of less than 30 minutes at 445 C (see Section VII.B.3.i). In comparing the batch reactor temperature to the wall temperatures of the cracking CSTR unit's wall temperatures, it is sensible that coke formation might be expected to occur quickly in CSTRs. Greater heat transfer area to volume ratio is therefore desired in TAG cracking reactors in order to reduce the flux through the wall and minimize the wall temperature. One might therefore conclude that a longer/thinner CSTR with even heating might have exhibited slower coking rates, or likewise a CSTR with imbedded heat transfer coils providing sufficient surface area.

In addition, mature coke formation was observed in batch reactors at lower temperatures and longer residence times, on the order of 120 minutes at 430 C (see Section VII.B.3.ii). By comparison to reactions at 445 C which exhibited mature coke formation after only 30 minutes

405

(see Section VII.B.3.i), this suggests that coke formation is on the order of at least 4 times slower at 430 C than at 445 C. Considering that Luo[54] and the present work were able to sufficiently crack at lower temperatures (see Section VI.B.2), it would appear that operating at elevated temperatures is not necessary and potentially risky from a coke formation standpoint.

From this, one might also conclude that coke formation is an inevitable end product of cracking TAG. This conclusion was reached by Raseev, who explains that 'the formation of coke doesn't take place directly, but it takes place through several steps.' These steps are generally accepted as the thermal transformation of hydrocarbons → resins → asphaltenes → flocculated asphaltenes → coke.[34] Raseev mentioned that the flocculation of asphaltenes must take place before advanced coke formation can occur and adds, 'Thus, in processes […] which target liquid products, the reaction conditions are selected such that […] the reaction is stopped before reaching the conversion corresponding to the flocculation of asphaltenes.'

It may then be considered that an ideal CSTR is a poor choice for a TAG cracking reactor when coke formation is an operating concern. This is due to the residence time distribution of an ideal CSTR, which implies that at least an finite amount of feed molecules experience very long residence times (see Fogler[161]). As a result, at least some feed molecules will lead to coke formation, which will accumulate over time. By comparison, a reactor having ideal plug flow, turbulent pipe flow, and/or multiphase flow is expected to have a more favorable residence time distribution with a non-infinite domain. It may be considered that laminar flow reactors have an infinite domain not unlike CSTRs, but this does not readily apply to TAG cracking whereby gas bubble formation in cracking reactors result in mixing action.

Based on these observations, temperature and residence time control are highly desirable

in TAG cracking reactors. For this reason, a long/thin prototype tubular cracking reactor (TCR) was designed, tested, and found to be able to crack TAG without the formation of coke as described on page 343 (see Section VII.B.4.i). This was sensible for two reasons: (1) a definite and narrow residence time distribution and (2) increased heat transfer surface area to volume ratio. The former reason enables precise targeting of reaction time before the flocculation of asphaltenes, and the latter enables reduced flux, leading to cooler wall temperatures to mitigate coke formation at the wall/liquid interface.

The prototype TCR was upgraded to a more robust lab-scale version, and furthermore shown to be scalable to the bench-scale sized TCR (2-10 kg/h). Operation of the bench-scale TCR at lower temperatures and moderate residence times was shown to be sustainable without the onset of coke formation as described in Section VII.B.4.v. Since it was not desired to 'push the limits' of the bench-scale TCR to coking conditions, the majority of coke elucidation experiments were conducted using the 100 mL and 500 mL versions of the lab-scale TCR.

The lab-scale TCR system was designed and constructed according to Figure 29 (see Section V.B.1.iii) and the results of its operation which pertain to this discussion are included on page 343 (see Section VII.B.4.ii). The 100 mL lab-scale TCR's preheater consisted of a 3 m long section of tube that was heated conductively by having a resistive heating cord wrapped around it.

The preheater was intended to be operated at the temperature of the reactor during cracking experiments, and during initial experiments this was attempted (see remarks on page 147). As a result, coking was soon found to be a major issue in the preheater. In order to counteract this, the preheater temperature was reduced to 340 C, which is below the point of

cracking. It was considered that uneven heating and especially uneven heat loss may have caused the coking in the preheater, leading to the formation of hot spots. These hot spots would be difficult to study using thermocouples, due to the heat transfer losses on account of the thermocouple probes themselves.

The preheater was eventually abandoned in latter versions of the lab-scale TCR, such as the 500 mL and 200 mL lab-scale TCR versions as it was shown to be unnecessary. The fluid temperature in the 200 mL lab-scale TCR was within 20 degrees of its set point after traversing as little as 5% of the reaction chamber's volume (see Figure 103 on page 354').

Preheating in the bench-scale TCR was successfully achieved at a temperature of around 410 C, but no higher due to the fear of coke formation.

Cracking in TCRs at temperatures greater than 440 C resulted in coke formation and as a result, it was difficult to keep reactors in operation for extended periods of time while cracking in that temperature range. For this reason, there was a lack of steady-state data generated during these experiments. At these elevated temperatures, the detection of coke formation was sudden and was observed indirectly as an inability of the feed pump to operate correctly. Filterable coke was less evident in those cases, indicating that the coke was likely forming on the walls, analogous to the majority of the CSTR coke formation (see Section VII.B.2). Further, the formation of wall coke implies that excessive wall temperatures were the initiating factor rather than residence time at temperature being too excessive.

The exception was for very brief residence times, in which the cracking reactors were able to operate without coke formation at temperatures as high as 470 C as indicated in Figure 98 (see page 348). Clearly both residence time and temperature are critical parameters for coke

formation.

The operation of the 500 mL lab-scale TCR was quite the opposite of excessive temperatures and very brief residence times. Its operation elucidated a point of asphaltene flocculation at reaction conditions of about 435 C temperature, 1.3 h space time, and 2.9 MPa pressure. Under these conditions, it appeared as though the flocculant was filtered out from the effluent of the reactor. According to Raseev's description that was quoted three pages earlier, the point of flocculation is essentially the limit of operation for processes that want to avoid coke formation and produce liquid products.

The ability to pump TAG was a substantial concern during operation of the lab-scale TCR. As previously mentioned in Section VII.B.4.ii, the TAG feed pump would occasionally cavitate with air and require immediate attention so that pump operation could be restored. A lack of ability to pump the TAG for extended periods of time tended to result in coke formation. Part of the reason this was a problem was that the reactor was typically operated at conditions that were near the onset of coke formation.

The ability to pump a TAG oil is probably less of a concern for scaled-up reactors because of differences in the operation of the pumps, leading to more reliable operation at larger scale. Furthermore, during TAG processing at the bench-scale pump cavitation problems were never encountered. Nevertheless, some TAG feedstocks have high melt points and/or contain particulates—this is especially true of waste TAG feedstocks and/or TAGs that would not be considered food grade. Pumping such TAGs may require TAG pre-filtering, preheating and/or other precautions before pumping into the reactor in order to ensure proper pump operation. Such precautions are especially necessary when the reactor is operated at conditions (reaction

temperature, residence time) near those where onset of coke formation occurs.

It was previously mentioned that during operation, the fluid temperature within the cracking tubes was about 2.2 C lower than the temperature in the free air immediately outside of the cracking tubes for the 200 mL lab-scale TCR. Similarly for the bench-scale TCR, the average fluid temperature was about 18 C lower than the average free air temperature. This is an indication of the endothermic nature of the reaction, whereby the temperature drop across the thicker-walled, larger diameter tubes of the bench-scale reactor is larger than the lab-scale reactor (which has thinner-walled, smaller diameter tubes).

Using the composition of samples from the 200 mL lab-scale TCR operation, the heat of reaction was estimated using ChemCAD according to the simulation conditions described on page 49 (see Section II.C). The observed heat of reaction will depend on the operating conditions, especially pressure, due to the enthalpy of evaporation for the products. The heat of reaction was estimated to be as low as 381 kJ/kg at higher pressures (4.94 MPa) and as high as 441 kJ/kg at lower pressures (0.79 MPa). The endothermic nature of the reaction may promote using thinner walled tubes in order to mitigate resistance to heat transfer throughout, leading to smaller deviations in temperature across the reactor.

As previously shown on page 345 (see Figure 97), operating reactors at temperatures that are just below cracking (i.e., 380-400 C) led to the formation of a sludge that tended to cause filter and valve clogging. This temperature range of operation is typically encountered when reactors are being brought online from ambient conditions (see Figure 104 on page 356). This should be taken into account when reactors are designed, installing piping to bypass pipeline filtration and valves during process startup.

One consideration that should be addressed is the potential effect on product quality due to the operating constraint that coke must not form at significant rates in TCRs.

VIII.B.1.i. Summary

From the results of operating batch, CSTR, and tubular cracking reactors it appears as though cracking reactors with high surface area to volume ratio are most suitable for processing TAG for reduced resistance to heat transfer and a narrow residence time distribution. For this reason, a long/thin tubular cracking reactor is a desirable reactor type for cracking TAG. A shell and tube type reactor might be a good configuration, with the TAG cracking occurring in the tube-side fluids. However, this would depend on the heating media utilized. Another possibility is a fired heater type reactor as long as the hot air temperature and distribution can be very carefully controlled.

It appears as though operating without hot spots and/or points in the reactor above a temperature of 440 C is beneficial for preventing coke formation, thereby ensuring continuous operation. If there must be an exposed portion of the reactor subject to temperature above 440 C (e.g., a 450 C wall temperature in the preheating zone of the reactor), then it should be utilized only at the beginning of the reactor, where it is less risky to do so. This is based on the ability to operate the reactor at excessively high temperatures (i.e., 470 C temperature) for brief periods of time (i.e., 0.27 h space time) and also based on Raseev's description of coke formation as a stepwise reaction mechanism.[34]

The operating condition that corresponds to asphaltene flocculation should be approached during operation but not reached or coke formation will result. Results from experiments using the 500 mL TCR estimated a point of flocculation on the order of 435 C temperature, 1.3 h space

time, and 1.9 MPa pressure. Special attention must be paid to the residence time and/or residence time distribution in tubular cracking reactors as the reactors are scaled up to commercial scale. Larger diameter tubes are commonly used at larger scales in order to decrease cost of materials of construction. Therefore, reactors should be iteratively scaled up towards commercial scale in order to mitigate unforeseen reactor heating/coking limitations as a result of larger diameter tubes.

VIII.C. The Effectiveness of FIMSDIST Data

The equipment and setup of the high throughput compositional analysis of CTL (regarded as FIMSDIST) is described in Section V.B.4.ii, and the background leading to its creation is described in Chapter IV. The method used for the reduction of FIMSDIST data is described on page 230. FIMSDIST was shown to be effective for providing a good overall picture of CTL, especially for insights into fuel production. However it was not able to provide information on all components, and other methods must be used to fill in the gaps in the data.

VIII.C.1. Crude Distillation Methods

In Sander's work,[62] the CTL from TAG cracking in a continuous-stirred-tank-reactor (CSTR) was characterized using ASTM D86 distillation[93] in order to draw conclusions about cracking by CSTR. Sander specifically described, "[That the D86 distillation method] proved difficult [...] with these liquid product samples. At vapor temperature levels above 250°C, the non-vaporized liquid sample appeared to undergo further noncatalytic cracking degradation from the heat being applied to the boiling flask."

As a result, Sander's findings were limited in that they could not provide information on components more volatile than 250 C. This is part way into the diesel range, and a large

percentage of CTL boils above this temperature. Although it was possible for Sander to derive meaningful conclusions from that data, it was not possible to obtain a complete picture of CTL from those efforts. Furthermore, it was difficult to estimate or approximate the yield of fuel from the noncatalytic cracking process (NCP) based on these limited data. As a result, overall optimization of the NCP was difficult to perform from Sander's work.

VIII.C.2. Detailed Compositional Analytical Methods

It should be noted that the detailed compositional analysis by GC-FID/MS published in Stavova et al.[152] utilized a 100 m long column, which was well suited for resolving a variety of components in the middle distillate range. From this, hundreds of components were quantified in CTL as described in Appendix A.

However, what the 100 m long column gains in resolution, it suffers in poor elutability of low volatility analytes. Based on the calibration of the detailed method, one may assume that the method is not able to provide significant information about analytes with greater volatility than a boiling point above about 400 C (consistent with the normal boiling point of n-pentacosane, $C_{25}H_{52}$, at around 402 C). Furthermore resolving limitations of CTL samples was likely a problem much lower than 400 C, increasing the ambiguity of the data. As a result, typically as much as 50 % of a sample's mass was nondescript (see page 260). This likewise made it difficult to optimize the overall noncatalytic cracking process based on this data.

VIII.C.3. FIMSDIST

FIMSDIST was conceived based on a combination of (1) the ASTM D7500[64] SimDist method and (2) a field ionization mass spectrometer (FIMS) connected in parallel to the FID detector. These features were intended to at least provide (1) excellent elutability of analytes and

(2) a distribution of the functional groups present in the CTL, respectively.

The elutability of the analytes was indeed possible to a boiling point in excess of 650 C. This provided a complete picture of the volatility distribution of products in CTL. The consequence of such strong elutability was a lack of GC resolution, so that many compounds were coeluting and the data would be impossible to deconvolute with conventional methods. Nevertheless, FIMS was able to provide functional group data on many of the analytes. Since the FIMS detector does not rely on the resolving power of the GC, there is a significant motivation for its utilization.

One obvious consequence of utilizing FIMSDIST was an inability to differentiate between formula isomers, since their molecular ions have identical masses (e.g., 1-hexene and cyclohexane). It was necessary therefore to examine the detailed composition data provided by Stavova's method[152] in order to provide an estimation for the concentration of cyclics/olefins and paraffins/isoparaffins, as described in Section VI.B.

Whereas carboxylic acids made up a significant portion of CTL, one unexpected consequence of using FIMSDIST was that the relative ionization efficiency (RIE) for a few specific carboxylic acids was very weak relative to the RIE for hydrocarbon analytes. Specifically, carboxylic acids C5-C7 and greater than C20 had very weak RIEs. As a result, it was not possible to quantify those species in CTL. The reason for this has not been clarified in the literature, potentially on account of a lack of publications utilizing FIMSDIST. Therefore, it was necessary to use the detailed compositional analysis work of Geetla[156] in order to provide data to compensate for the missing data from FIMSDIST, negating at least some of the data processing efficiency of the FIMSDIST method.

414

In addition, the presence of unsaturated carboxylic acids was not previously found in cracked TAG distillates (CTD) that were studied through the work of Luo,[54] which led to much of this methodology. As a result, they were not anticipated in the CTL samples produced in the present work. However, in the analysis of these samples through the completion of Geetla's work[156], unsaturated carboxylic acids were found in these samples in significant quantities. These were mistakenly identified by FIMSDIST as hydrocarbon components due to a lack of their anticipation in the CTL. As a result, it was inappropriate to quantify them with FIMSDIST, and they were lumped into the data for carbon numbers greater than C18. Future work on the FIMSDIST method should incorporate unsaturated carboxylic acids into the available chemical set for use during automated analyses.

Nevertheless, Geetla showed that the unsaturated carboxylic acids in the CTL were almost entirely as a direct result of degradation of the TAG molecule backbone ester bonds, releasing free fatty acids into the CTL. Therefore these were not a result of carboxylic acid degradation, and more importantly they were all longer chain ($\geq$C18).

The resolution of the mass spectrometer employed in this work was a limiting factor for using exact masses to identify and quantify analytes. For this reason, it was difficult to confirm the identity of an unsaturated carboxylic acid, which had very near exact mass to hydrocarbon components, as shown in Table 28.

Furthermore, as the molecular weight becomes increasingly large, there are a greater number of potential analytes that could be present in the CTL. This puts practical constraints on the ability of FIMS to identify all components with exact masses. As previously described on page 116, the resolution of FIMS is less than EIMS for otherwise identical ion transduction

equipment, adding to the difficulty of exact mass identification. Despite this, FIMS instruments have been studied with resolution in excess of 30,000 (see page 116), so better equipment could potentially overcome some of the FIMS limitations herein, but not all of them.

Due to the inability to quantify unsaturated carboxylic acids, FIMSDIST was considered to be valid for the functional group speciation of carbon numbers up to approximately C18 and to be fairly valid as a predictor of carbon number above C18, as described in Section VI.E. It was furthermore shown that as TAG samples are cracked at increased temperatures and increased space times, the CTL has a reduction in unsaturated carboxylic acids. As a result, FIMSDIST becomes more valid as the samples are produced at higher cracking severity.

One feature worth mentioning is the intensity of reduction in data processing efforts that were necessary for FIMSDIST in comparison to that of the detailed compositional analytical method of Stavova.[152] In private communications with analytical chemists, the detailed methods require many hours of data processing per sample analyzed. FIMSDIST on the other hand can be automated so that sample analysis is on the order of minutes. It should be cautioned however that without greatly improved equipment, errors in the data were only noticeable by observing outliers in the data, as in Section VI.B.1.

FIMSDIST was also found to improperly quantify the ratio of paraffins/isoparaffins to olefins/cyclics. This was found to be a result of the analytical method, not the type of reactor being used to produce the samples (see Section VI.D.5). As a result, additional calibration compounds were recommended to further improve the accuracy of the RIEs for the FIMSDIST method for olefins and cyclics. This is furthermore recommended for diolefins and dicyclics.

VIII.C.4. Recommendations for Further Use

A mass spectrometer with improved resolution may help overcome some of the mass resolving limitations of FIMSDIST for components greater than C18, and be able to confidently identify unsaturated carboxylic acids and other such longer-chain species in the CTL. Such instruments are typically much higher cost. In addition, specialized software would need to be written and/or procured in order to process the FIMSDIST data in an effective manner.

A triple photoionization source / triple detector mass spectrometer could be considered for determining quantities of olefins and cyclics in CTL. At the current state of photoionization mass spectrometry technology, there are few commercial instruments to choose from, if any. As a result, such instruments would have to be custom designed, which would significantly increase the cost of the instrument. There would also be added complexity, with an increased need for software to be developed. The benefits of photoionization mass spectrometry were previously described in Section IV.E, but they haven't been proven more effective than FIMS. It's therefore possible that such improvements to this method may not provide significant benefit to warrant their pursuit.

One consideration that was taken into account in Chapter IV (see page 116) was the utilization of retention index data for determining the identity of analyte ions in the FIMSDIST data. This was not taken into account due to (1) the very low separation of GC components by the FIMSDIST method and (2) a lack of suitable software for handling this type of concerted information. As a result, future adaptions to this method could consider a longer/thinner column to increase the separation of analytes by gas chromatography. Then if more specialized software were available, it would be possible to determine the identity of analyte ions with greater

information (e.g., n-paraffins vs. isoparaffins). If this were attempted, the decreased analyte elutability resulting from using a longer/thinner column could be offset by using all-metal GC components to increase the maximum temperature of the FIMSDIST method to 400 C or greater. In this study, 380 C was the maximum temperature due to the stability of fused silica capillaries, on account of metal columns being incompatible with this particular FIMS instrument (not all FIMS instruments).

VIII.C.5. Summary

In summary, FIMSDIST was capable of eluting analytes in excess of 650 C so that it might produce data that completely represents CTL samples. This complete representation had advantages in comparison to other methods such as D86 distillation and detailed composition methods for the estimation of fuel yields by the noncatalytic cracking process. Nevertheless, FIMSDIST was based upon the predecessor work of detailed compositional methods. Without such information, FIMSDIST couldn't have been conceived. Furthermore, when FIMSDIST is employed, data from detailed methods such as those described by Stavova[152] and Geetla[156] are required for a complete profile of the CTL sample. As a result, there is a clear need for a multitude of analytical methods for the study and optimization of fuel refinement processes.

VIII.D. Cracking Mechanisms and Reaction Sets

TAG cracking reaction mechanisms are mentioned and discussed in several papers and summarized by Maher and Bressler[57] who compiled the mechanisms from various authors and discussed them in light of their own work. Mechanisms included in Maher and Bressler's work include Chang and Wan, 1947[163]; Nawar, 1969[164]; Alencar et al., 1983[165]; Schwab et al., 1988[50]; and others. It should be mentioned that the majority of mechanisms are specified as being

provided as either examples or representations. A multitude of authors simply describe the decomposition of triglycerides by the simple release of fatty acids from the TAG backbone by cleavage of the ester bond, followed by cracking of the free fatty acids. However, some authors additionally describe that approximately up to 1/3 of the fatty acid moieties are released as ketenes, with the triglyceride backbone being degraded as acrolein. This comes from the mechanism proposed by Chang and Wan,[163] shown in Figure 118. The ketenes and acrolein further degrade so that each of them will release carbon monoxide.

Decomposition of the glyceride

$$
\begin{array}{l}
CH_2OCOR' \\
| \\
CHOCOCH_2R'' \\
| \\
CH_2OCOR'''
\end{array}
\longrightarrow
\begin{array}{l}
CH_2 \\
| \\
CH \\
| \\
CHO
\end{array}
+ \ R'COOH \ + \ R'''COOH \ + \ R''CH=CO
$$
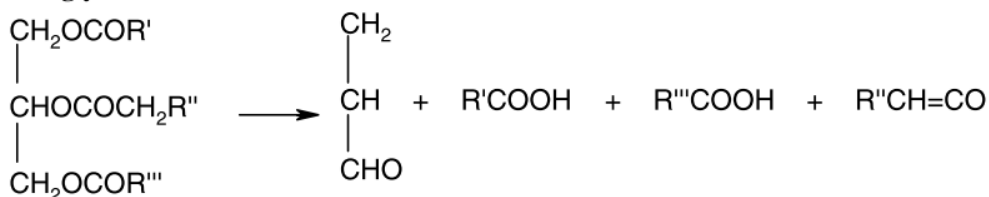
Figure 118. Initial triglyceride decomposition step explained by Chang and Wan[163]

Inconsistency between the proposed mechanisms may be a result of how the experiments used in their formulation (e.g., reaction in the potential presence of moisture, air, etc.) were performed, which could have a significant affect on the products obtained. Furthermore, inconsistency may result from the simplicity (or rigor) with which products were characterized. Unfortunately, the mechanisms proposed by various authors are insufficient to describe the extensive set of reactions that take place during triglyceride cracking. Furthermore, it is difficult from the data that are available to determine which reactions are dominant. Kubatova et al.[22] explains some of the inconsistency as resulting from, "the inherent complexity of the diverse

suite of reactions that can occur and the wide variety of experimental setups employed."

The findings of the present work were tailored towards overcoming obstacles to producing fuel from TAGs via the Noncatalytic Cracking Process, NCP (see the introduction to Chapter V), rather than mechanism investigation, so the data are only speculative from a mechanistic standpoint. Nevertheless, in examining the mass-adjusted FIMS response data for the cracking of various TAGs (see Section VI.B.1) there appeared to be a high concentration and variety of fatty acids, both unsaturated and saturated, in the cracked TAG (CT). Furthermore, Geetla[156] confirms that the unsaturated fatty acids were all longer chain, a direct result of a TAG molecules fatty acid moieties being cleaved at the TAG molecule backbone.

It was interesting that the unidentified ions in Table 29 (page 267) appeared in such large quantities in the CTL's derived from VHONO and HENO TAG, which have a high quantity of oleic acid and erucic acid moieties, respectively. These data are reproduced in Table 56 for the sake of their discussion. These species were identified by FIMSDIST as long chain dienes, however there was no simple explanation for why long chain dienes would result from either oleic acid or erucic acid decomposition in VHONO or HENO, respectively.

It was previously thought that 'Unidentified Species 1' might be a decomposition product of 'Unidentified Species 2.' A variety of oxygenates were considered in an attempt to identify

Table 56. Unidentified ions of mechanistic significance in VHONO and HENO cracked TAG liquid

TAG Type	VHONO	HENO
Dominant Fatty Acid Moiety	COOH 18:1	COOH 22:1
Unidentified Species 1 (*m/z*)	264.3	320.4
Unidentified Species 2 (*m/z*)	362.4	418.5

the unknown ions, however no suitable oxygenate matches were found that would explain 'Unidentified Species 1' as a product of decomposition of 'Unidentified Species 2.'

In examining the work of Nawar[164], a credible explanation was found for 'Unidentified Species 2.' In Nawar's explanation, the 'Unidentified Species 2' ions are identified as long chain dienes. Nawar explained that the long chain dienes (specifically 9,17-hexacosadiene) are the result of a recombination of fatty acid fragments, shown by Figure 119 (taken from Nawar[164]). This observation is based on composition data from the products of very long (i.e., 65 hour) exposure of methyl oleate to temperatures of 280 C by Sen Gupta[166] (although Nawar[164] clarified the mechanism).

Concerning 'Unidentified Species 1', these are presently thought to be unrelated to 'Unidentified Species 2.' The identity of *m/z* 320.3 and *m/z* 264.3 is closely matched to an unsaturated ketene. The ions may be identified as the ketene versions of erucic acid (COOH 22:1) and oleic acid (COOH 22:0) moieties, respectively. This explanation comes from the initial TAG molecule degradation mechanism proposed by Chang and Wan (see Figure 118 on page 419), whereby up to 1/3 of TAG fatty acid moieties are degraded into ketenes, with the TAG backbone being degraded as acrolein. This helps validate (in part) the degradation mechanism of Chang and Wan. Future experiments might elucidate the extent to which triglycerides are degraded to ketenes vs. free fatty acids.

One unusual occurrence observed was that the degradation of linseed TAG (see Section VI.B.1.iv) produced a high quantity of an ion (*m/z* 278.2) that was noted as potentially being a fourfold unsaturated carboxylic acid, i.e., octadecatetraenoic acid (COOH 18:4). This stems from the high concentration of linolenic acid (COOH 18:3) moieties in the linseed TAG
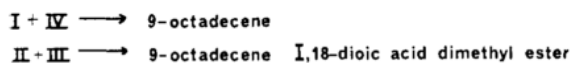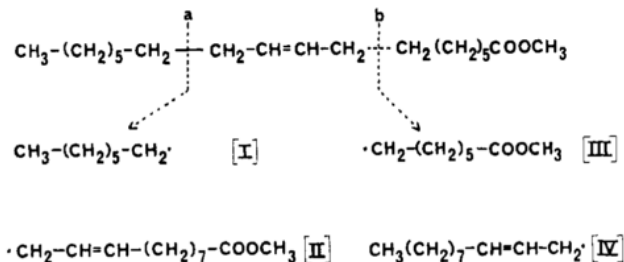
Figure 7. Splitting at positions beta to the double bond
(Nawar and Dubravcic, 1968)
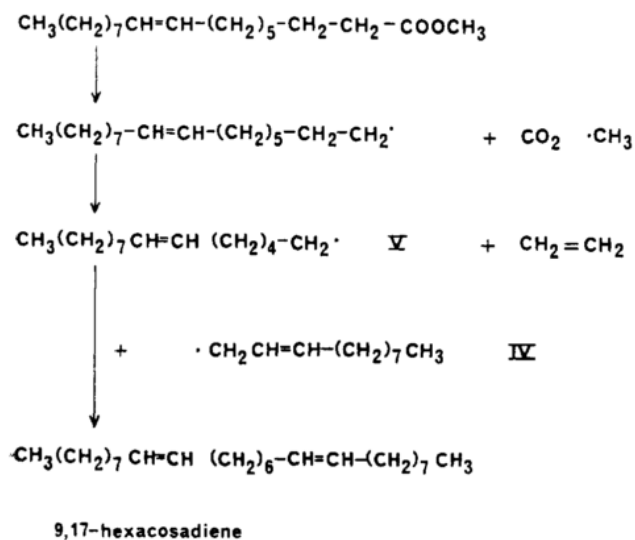
9,17-hexacosadiene

Figure 119. Methyl oleate degradation to produce hexacosadiene
(taken from and described by Nawar[164])

feedstock. This may be a precursor for aromatic formation, or potentially an aromatic carboxylic

acid already. In either case, it could be hypothesized that m/z 278.2 results from the dehydration

and/or cyclization of linolenic acid in the Linseed TAG feedstock. The high aromaticity

observed in the Linseed CTL relative to other CTLs (see Section VII.E.3.i) supports the

hypothesis that linolenic acid is an aromatic precursor. Furthermore, Li et al.[45] have published

422

data on the pyrolysis of tung oil—which is rich in a conjugated COOH 18:3—that leads to an increased formation of aromatic hydrocarbons in the CTL, not unlike that of linseed TAG pyrolysis.

Decanoic acid (COOH 10:0) was found to be produced in higher concentrations in the CTLs from TAG feedstocks that were rich in oleic acid moieties (e.g., canola oil, HONO, VHONO TAG) and also erucic acid moieties (HENO TAG). This is a difficult result to explain because it implies that C-C bond scission is occurring directly adjacent to a C=C bond which is disfavored (see Section III.B.2). Geetla[156] offers one explanation that this may be due to a radical propagation reaction (see Section III.C.3), with hydrogenation of the double bond by atomic hydrogen, leading to cleavage in the vicinity of the double bond due to excess kinetic energy and bond destabilization.

Unfortunately, Geetla's explanation does not explain the high concentration of decanoic acid (COOH 10:0) in the CTL from the cracking of HENO or the lack of tetradecanoic acid (COOH 14:0) that results in HENO CTL. As a result, further investigation into decanoic acid formation is justified.

Due to the complexity of triglyceride cracking reaction mechanisms, a reaction simulation approach may be justified, taking into account the discussion of bond energies, reaction sets, and kinetic observations presented throughout Chapter III. This is recommended for future exploration of TAG cracking.

VIII.E. Fuel Refinement and Yields

VIII.E.1. Comparison of Noncatalytic Cracking Process Fuel to Petroleum Fuel

A sample of jet fuel (a.k.a. Soy-Jet-A-1) was produced from soybean TAG in the

laboratory using reaction and separation operations to model the noncatalytic cracking process (NCP) as described in Section VII.D. In examining the properties of the Soy-Jet-A-1 sample, it appears to meet five critical specifications for Jet-A-1 aviation turbine fuel (see Table 45). As a result of these tests, it is suitable to believe that fuel can be prepared by the NCP with acceptable heating value, density, fire hazard safety, cold weather performance, and corrosivity of petroleum derived fuels.

Additional tests were not performed on the Soy-Jet-A-1 due to the availability of test equipment and the quantity of Soy-Jet-A-1 that was available. Based on the FIMSDIST results of the fuel, it would be expected to pass the following additional tests if they had been performed: D86 distillation[93], aromatic content (max 25%), and naphthalene content (max 3%). Considering that the fuel was derived from a TAG that is virtually free of sulfur, the fuel would also be expected to pass the requirements for total sulfur, mercaptan sulfur, and the copper strip corrosion test.

A similar study was published in the literature by the present author and associates (Linnen et al.),[59] for the production of fuel from microbial TAG via the NCP. The product fuel was very similar to Soy-Jet-A-1, and it was demonstrated that it can be prepared from waste biomass sources (e.g., glycerol). In this case, microbes were utilized for bioconversion of waste biomass into TAG biomass, which was compatible as a feedstock for the NCP. Then fuel was refined in like manner to Soy-Jet-A-1 refinement. The study compared fuel refinement from a fully-refined microbial TAG source and a crude microbial TAG source. That study found no barriers to the production of fuel from the crude microbial TAG. The study also demonstrated that low grade and/or waste TAG sources are suitable feedstocks for fuel refinement with the

NCP in addition to fully-refined TAG feedstocks. Such a result also has important implications for the development of algal lipids as a feedstock. A process that can tolerate impurities, such as cellular debris, in the feed has an inherent advantage over competing processes that require near food grade quality material.

The carbon number profiles of the Soy-Jet-A-1 sample and a petroleum-derived kerosene are shown in Figure 106 and Figure 107. These fuel samples have similar freeze point, flash points, and densities, with both meeting the specifications for Jet-A-1 fuel. In comparing their carbon number distributions, it is evident that the carbon number range is smaller for the Soy-Jet-A-1 sample than for the petroleum-derived sample. The consequence of this smaller carbon number range is that the distribution of molecules in the jet fuel produced by the NCP is narrower than for petroleum. As a result one may assume that for 'equivalent' barrels of petroleum and soybean CTL, more jet fuel could be refined from the petroleum sample than from the CTL sample.

The reason for the smaller carbon number range of jet fuel from the NCP appears to be due to decreased cold weather properties in the soy-derived sample. This is evident from comparing the physical properties of various boiling point fractions (BPFs) spanning 100 to 300 C in increments of approximately 20 C for both petroleum-derived and soybean-derived distillates (see Table 46). Although the flash point and density of the petroleum / soybean BPFs were fairly similar, the cold weather property points were different. Specifically, the freeze point, pour point, and cloud point of the soybean-derived distillates were on the order of 20 C higher than the petroleum-derived distillates. This explains the narrower carbon number distribution of the Soy-Jet-A-1, as it was not possible to incorporate the lengthier carbon number

425

molecules into the Soy-Jet-A-1 and still comply with the cold weather specifications of Jet-A-1.

The explanation for this observation is in the aromaticity of the two fuels. A plot of freeze points vs. carbon number is shown in Figure 120 for various n-paraffins, 2-methylalkenes, α-olefins, n-alkylcyclopentanes, and n-alkylbenzenes. What is immediately noticeable is that the n-alkylaromatics tend to have the lowest freeze point on the basis of carbon number. By contrast, n-paraffins tend to have the highest freeze point by carbon number, with other functional groups in between, as shown. In examining the Soy-Jet-A-1 composition, the aromaticity is relatively low, on the order of 6.4 wt. % total. By contrast, a significant aromatic contribution is found in the petroleum-derived kerosene sample used in this comparison (it should be noted that other kerosenes have much lower aromaticity, depending on the process configuration of the refinery that produced the kerosene), on the order of about 21.4 wt. %. The increased aromaticity in the petroleum-derived fuel is therefore responsible for the ability to incorporate a larger carbon number range for this petroleum kerosene fuel relative to the Soy-Jet-A-1 fuel. The improvement of aromaticity on fuel quality is mentioned in the literature by Li[45].

As a result of this, NCP facilities should be designed which preserve the aromaticity during the refinement into the final fuel. For example, it is not currently known whether the deoxygenation catalysts are capable of hydrogenating aromatic rings. Future research should investigate to see if aromatic rings are hydrogenated during deoxygenation, and to what extent. It may be desirable to use aromatic extraction processes (as described in Section II.B.3) to preserve the aromatics for final fuel blending. In addition, aromatic reformation processes may be important as well. For example, the high concentration of olefins in the non-condensible gases generated in the NCP may be reformed into additional aromatics (Fegade[70]).
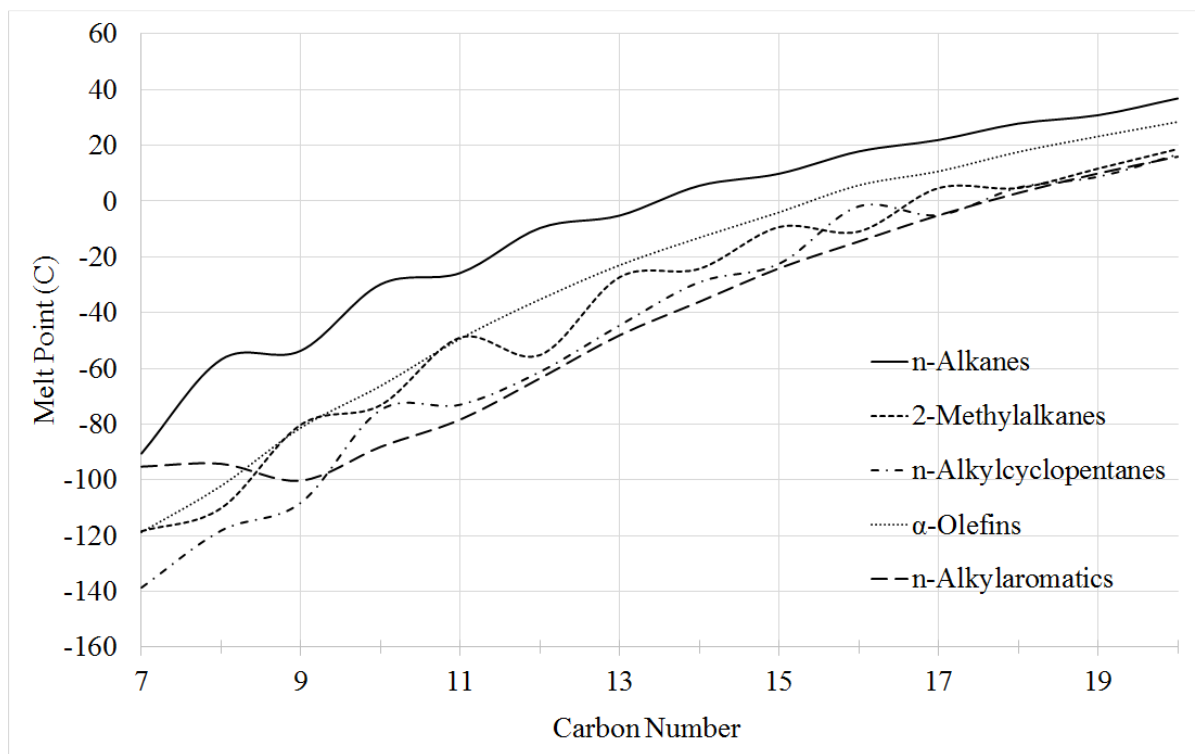
Figure 120. Freeze point vs. carbon number for various functional hydrocarbon groups

VIII.E.2. Effect of Refinement Parameters on Fuel Yield

VIII.E.2.i. Definition and Limitations of Experimental Optima

One consideration that was previously mentioned in this chapter was that the point of asphaltene flocculation (leading to coke formation) should be approached but not reached. As a result of this, optimal cracking conditions are those that maximize cracking reaction severity while still low enough to avoid coke formation.

The optimal operating temperature is recommended not to exceed 440 C, a temperature that experiments have shown is the near-maximum temperature suitable for avoiding coke formation (see Section VII.B.4.ii), so long as residence times are not excessive.

The optimal operating space time is recommended not to greatly exceed 1.3 h because one tubular cracking reactor experiment using the 500 mL TCR at 435 C and 1.3 h space time resulted in the continuous appearance of asphaltene flocculant and bits of coke in the effluent, indicating the onset of asphaltene flocculation in the vicinity that reaction temperature/space time combination. In any event, conditions should be monitored for the commissioning of any cracking reactor such that the point of coke formation is approached but not reached, as described by Section VII.B.4.iii.

The total product value of the fuels produced by the process remained relatively constant (approximately ± 2 %) despite great variations in the quantities of the various fuel products. This may be explained by the fact that most of the fuels have similar values when compared on a mass basis (except for gaseous fuels). It should also be mentioned that the price of fuels may vary by as much as 2 % or more in a single day, so it might therefore be considered that from an economic standpoint, these results have not showed any significant change in the total product value despite the conditions studied.

As previously noted in Section II.D.3 the market for heavy fuels, such as fuel oil numbers 4 and 6, in the US is very small. Therefore, since the economics are only minimally affected but the fuel yields are substantially affected, optimal reactor operation should coincide with the minimization of fuel oil yields, for which there is little market. As an alternative, heavy oil upgrading facilities that are based on existing petroleum refining technologies may be incorporated into a NCP-based biorefinery to increase the yield of middle distillate fuel products.

VIII.E.2.ii. Cracking Reaction Temperature and Space Time

Over the range of conditions studied in Table 24, the strongest effects for the decrease of

fuel oil yield was observed with increasing temperature and increasing space time, as shown in

see Section VII.E.3.ii. Compared to operation at 420 C and 0.27 h space time, operating at 20 C

hotter and fivefold greater space time may be statistically expected to reduce the yield of no. 4

fuel oil from about 22 wt. % to less than 6 wt. %. The yield of no. 2 fuel oil is similarly reduced

from about 21 wt. % to about 12 wt %, and the yield of lighter fuels are consequently increased.

One consequence of operating a reactor at increased space time is that the reactor will

have reduced operating capacity vs. capital cost. Therefore, the reactor designed for optimal

conditions would cost around 2.5 times more than the poorly designed reactor for the same

capacity (based on the sixth-tenths rule of equipment costing by Turton et al.[167]). However,

since the economics of NCP facilities are expected to be dominated by feedstock costs, this

additional capital cost is likely to be justified.

VIII.E.2.iii. Type of TAG Feedstock

Various TAGs were investigated in order to establish a link between the composition of

the TAG feedstock and the products of TAG processing by the NCP. As a result, a large

variation was observed in the estimated quantity of the fuels produced for each of the nine tested

TAG feedstocks (see Table 24). Nevertheless, the total product value of the products from TAG

refinement remained virtually unaffected by the large deviations in fuel product yields. As a

result, the process is best optimized economically not by choosing a TAG feedstock in order to

produce certain target products, but rather by choosing a TAG feedstock due to its low cost.

This was demonstrated on page 356, which showed that switching from soybean TAG to canola

TAG would lead to a substantial change in the yields of various fuels, but only provide an

estimated 2 % greater profitability at the expense of 14 % increased feedstock costs

429

VIII.E.2.iv. Cracking Reactor Pressure

The optimal reactor operating pressure in triglyceride cracking from a fuel production standpoint could not be determined in this study, as the best CTL production and quality occurred at the highest pressure condition that could be achieved in the experimental systems utilized. As a result of increasing the operating pressure of the cracking reactor, heavier fuels will be reduced and lighter fuels will be concurrently increased, which have better salability. Furthermore, increased pressure has been shown to increase hydrogen production and increase the aromaticity of products. This may have other benefits for fuel product quality. Additional optimization at higher pressure is recommended in future studies.

Operating at increased pressure will increase the capital and operating costs of the process. More importantly, if the tube wall thickness in the TCR becomes too great, heat transfer may be hindered, causing additional concerns for reactor design and coke formation as higher utility fluid temperature would be required. However, as long as the inside tube wall temperature is still maintained at the proper temperature, this will not be a concern. But this highlights that operating at increased pressure is something that should be considered with respect to reactor design.

One caveat to this conclusion is that higher pressure also appears to lead to an increase in the production of olefins in a TCR type reactor at the expense of paraffins in the CTL, which is the opposite of previous work with CSTR reactors. This is not a concern as long as the olefins are adequately hydrogenated in the downstream deoxygenation reactor. Additional studies are required as the present work has not specifically addressed this issue.

VIII.E.3. Other Considerations

It was also noticed that there appeared to be differences in the efficiency of the various TCRs utilized for the production of fuels. The 100 mL TCR operated with soybean TAG was found to produce on the order of 23 wt. % fuel oils under optimal conditions, whereas the 200 mL TCR operated with canola TAG was found to produce on the order of 11 to 13 wt. % fuel oils. Based on a comparison of the fuel yields from processing soybean TAG and canola TAG in the 100 mL lab-scale TCR (see Table 123), soybean TAG actually produced a lower quantity of fuel oils than canola TAG. As a result of this it is believed that the 200 mL lab-scale TCR is more efficient than the 100 mL lab-scale TCR on account of better thermal design. Future experiments should consider cracking all TAGs at the approximate optimal operating conditions on the 200 mL lab-scale TCR in order to better confirm the fuel yields.

It should be mentioned that naphtha is produced by this process, not gasoline. Therefore, alkylation or reformation may be necessary for the sale of naphtha as gasoline. Nevertheless, the price of naphtha and the price of gasoline are relatively similar, so that the price of naphtha has been the assumed price of gasoline in the present work.

VIII.E.4. Consideration of the Maximum Theoretical Yield

Triolein may be considered to be a model TAG compound for estimating the economic impact of oxygen in the feedstock of the noncatalytic cracking process (NCP). Examining the molecular weight (i.e., 885.4 g/mol) and molecular formula (i.e., $C_{57}H_{104}O_6$) of triolein, it can be shown that the oxygen mass in triolein accounts for about 10.8 wt. % of triolein's total weight. Thus CTL is estimated to have around 11 wt. % oxygen. This oxygen may be partially eliminated during cracking as a result of concurrent decarboxylation / decarbonylation reactions

with cracking reactions as CO_2, indicated by the gas phase composition data in Section VII.E.2. As observed by Luo[54] and confirmed in the detailed composition data presented on page 285, carboxylic acids account for essentially all of the residual oxygen in the CTL at about 1.9 mol/L (see Section VII.E.1). The oxygen can be fully removed from the process via catalytic deoxygenation, either being eliminated as water or as carbon dioxide, depending on whether or not a reductive deoxygenation is employed.

The removal of oxygen from the process as CO_2 accounts for a total mass loss from the original TAG feedstock of about 14.9 wt. %, whereas the removal of oxygen from the process as water only accounts for 12.2 wt. % based on triolein. Therefore, the mass yield of fuels cannot be expected to exceed about 88 wt. % for a reductive process and about 85 wt. % for a decarboxylative process. Additionally, the TAG backbone accounts for approximately 4.7 wt. % of the TAG's mass, which may be assumed to exit the process as propylene in a highly idealized case (i.e., in a real case, significant backbone degradation should be anticipated via acrolein decomposition). Imperfections in the process lead to the formation of excess process gas which is valued on the basis of natural gas.

The sum total mass of fuels from the best case reactor operation (Figure 116) were found to be on the order of about 81 wt. % (see Section VII.E.3.i) This is a seemingly inflated statistic when considering the mass loss of oxygen as CO_2 in conjunction with extraneous efficiency losses due to C1-C2 gas formation. Reasons for overestimation may partly be explained by the assumptions used to compute the process fuel yields, including (1) assuming ideal decarboxylation and (2) assuming that residue processing doesn't account for gas formation, or for other assumptions as described on page 389. Therefore, adjustments to the predicted yields

are called for, but not presently available.

One adjustment may be made considering the quantity of carboxylic acids. It is considered that for experiments using the TCR, the concentration of carboxylic acids in the CTL that was estimated by FIMSDIST tended to be on the order of 13 to 18 wt. % according to Table 123 through Table 125 (see page 578). This is in line with the 13 to 15 wt. % carboxylic acids determined by detailed compositional analysis of batch-process CTL shown in Table 31 (see page 286). In the estimation of final fuel products for each experiment (see Section VII.E.3.i), the estimation took into account the CO_2 mass that would be eliminated by ideal decarboxylation of the FIMSDIST composition. The mass elimination was only about 4-5 wt. % of the total CTL. By contrast, the FTIR analysis of CTL (see page 365) shows a molar concentration of acids at about 1.9 mol/L. This computationally accounts for 9.5 wt. % CO_2 losses during ideal decarboxylation, based on a typical CTL specific gravity of 0.88.

One might therefore think to reduce the yield of all liquid fuels by a factor of about 4 wt. %, which would make the fuel mass estimations more in line with the expected maximum theoretical yield. Nevertheless, these yields are useful for elucidating process trends. Additionally, the sum total value of the products were estimated at about 0.795 ± 0.02 USD/kg TAG, regardless of the feedstock used or operating conditions utilized over the range of experiments tested in Table 24 (see page 224). This is helpful for considering the economics of TAG-to-fuel processes and relating that importance to the noncatalytic cracking process (NCP).

VIII.E.5. Economic Considerations

The wholesale spot price of gasoline and jet fuels (dotted lines) has been plotted over time against the price of soybean oil and yellow grease (solid lines) in Figure 121 to show the

trend of economics pertaining to the NCP. Also, the wholesale spot prices of B100 biodiesel[80]

and E100 fuel ethanol[168] in Iowa, USA have been adjusted for their heating values relative to

diesel (8%) and gasoline (30%), respectively and also plotted in Figure 121 for reference.
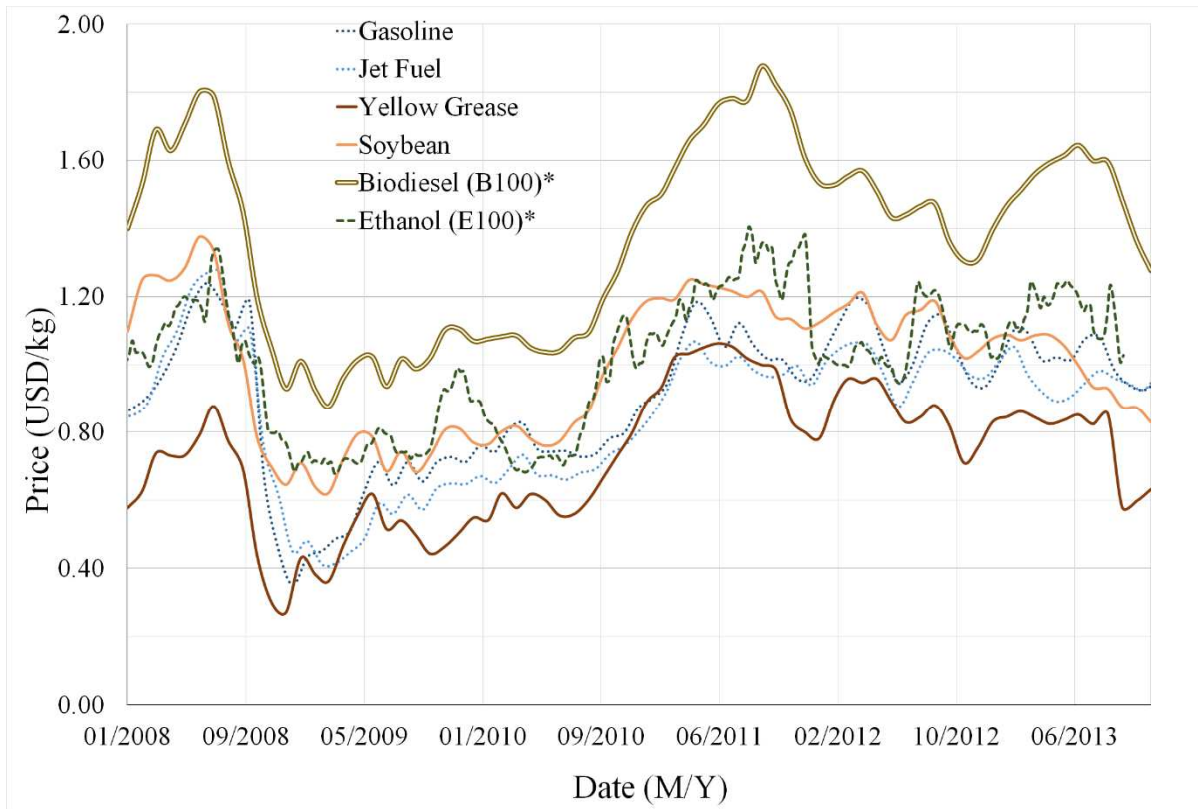
Figure 121. Historical price of fossil fuels, triglyceride feedstocks, and renewable fuels[*]

What can be immediately recognized from the figure is that the value of fuel ethanol,

fossil fuels, and TAG tend to coincide together over time. Whether this is a natural or artificial

---

[*] Historical prices of fuel ethanol (E100) and biodiesel (B100) adjusted by their heating values
relative to gasoline and diesel fuel respectively.

result of supply/demand is not clear. But what seems to be apparent is that in the coming years, the cost of TAG and the price of fuels will probably be fairly consistent on a mass basis. Interestingly, the price of biodiesel tends to be 1/3 higher than the other prices. This is a curious observation, potentially explaining the small contribution of biodiesel processes in comparison to fuel ethanol processes in the US economy.

Based on the maximum theoretical process yield, it is clear that the profit margin from the NCP process as a purely TAG-to-fuel process is relatively weak, perhaps even nonexistent. This is especially evident when considering (1) the oxygen in TAG detracting from the fuel yield via deoxygenation and (2) inherent process imperfections detracting from the fuel yield. As a result, the purification of valuable byproducts from the NCP is most likely a necessity for the process to be economical.

The byproducts which can be purified from the NCP were discussed previously on page 44 (see Section II.B). Some examples of byproducts that have been considered include carboxylic acids and aromatics. These have significant potential to elevate the TPV above that of the TAG feedstock costs and make the NCP profitable.

In particular, the production of carbon fiber is one byproduct with lucrative potential from the processing of residual material, since carbon fiber is worth between 5 and 20 times its weight in fuel. This residual material was only described as 'Carbon' in the present work, due to the ongoing nature of the carbon fiber research (see page 371). Furthermore, its value was very conservatively estimated in the present work at 1.0 USD / kg, which was a loose estimate of the sale value of coke based on Bosquez.[66]

The historical prices of byproducts are less available than the historical prices for TAGs

and fuels. As a result, the prices of byproducts are not considered in this dissertation, beyond the

observation that byproducts have a significant potential to elevate the profit potential of the NCP.

CHAPTER IX

CONCLUSIONS

IX.A. Analysis of Cracked Triglyceride Liquid (CTL) by the FIMSDIST Method

Using the high throughput compositional speciation analysis by GC-FID/FIMS (a.k.a. FIMSDIST) for various CTL samples, it was found that for the instrumentation used herein, FIMSDIST data are only valid up to C18 carbon chain lengths at TAG cracking severities in the region of interest for the production of renewable fuels. This is due to the presence of a significant fraction of undercracked unsaturated fatty acid moieties in the CTL, which were not anticipated based on previous literature. However at increased cracking severity, FIMSDIST data may be valid to quantify compounds of greater carbon chain length than C18, due to the disappearance of undercracked unsaturated fatty acid moieties from the CTL.

Additionally, FIMSDIST was unable to quantify carboxylic acids C5-C7 and above C22 due to reduced ionization response. Furthermore, FIMSDIST quantifications for > C20 carboxylic acids were found to disagree with published data from detailed compositional analysis methods. Otherwise, the trends in FIMSDIST carboxylic acid data were reasonably consistent with the data from detailed compositional analysis methods.

A higher resolution FIMS instrument may be able to overcome some of the limitations of FIMSDIST that were encountered, due to better exact mass differentiation of analytes. Other method optimizations could consider all-metallic GC components to permit increased analysis

temperatures and therefore the utilization of columns with greater separation of analytes. In addition, specialized software may be useful to improving the capabilities of FIMSDIST by quantifying components by residence time and exact mass. PIMS may also provide additional benefits, such as the differentiation of analytes by their photoionization energy (e.g., functional groups), but more developments into the field of PIMS are necessary.

IX.B. Deoxygenation of Cracked Triglyceride Distillates (TCD) by Nickel Catalysts

From the deoxygenation studies, it was concluded that nickel catalysts were capable of outperforming the palladium catalysts under the conditions studied. This was true with respect to both the yield of liquid product and the speed of reaction. Furthermore, from the perspective of catalyst cost, nickel is substantially more attractive than palladium.

It was apparent that the higher concentration wet impregnated nickel catalysts (i.e., activated carbon supported) were capable of similar activity to that of the silica supported nickel catalyst (55 wt. %) that was procured from a commercial source. However, the commercially available silica/zirconia/alumina supported nickel catalyst (60 wt. %) showed at least twice the activity of all other catalysts. Unfortunately, it was also shown to have a very high consumption of hydrogen gas and a high production of gaseous product components, which was indicative of hydrocracking type reactions.

Due to its commercial availability, the silica supported nickel catalyst (55 wt. %) was selected for continuous testing, however a carbon supported nickel catalyst could likewise have been chosen. Silica supported nickel catalyst (55 wt. %) was tested in packed bed reactors in order to determine suitable operating conditions for continuous deoxygenation.

Many conditions were shown to be problematic for operation due to the formation of

residue on the catalyst, leading to coke formation and reactor plugging. The addition of steam was found to be necessary to prevent coking of the catalyst. The addition of steam was shown to preserve activity for on the order of 56 hours, with steam feed rates of as low as 1:33 weight ratio of steam:distillates, even in the absence of hydrogen gas. After experimentation, it was also concluded that at least a fourfold increase in hydrogen gas may be necessary to preserve catalyst activity when operating without steam.

Due to the low cost and ease of producing the wet impregnated nickel catalyst, future NCP endeavors could consider the cost of purchasing a commercial nickel catalyst against the cost of manufacturing the catalyst via wet impregnation.

IX.C. Fuel Production by the NCP

Efforts to produce a high quality, drop-in compatible jet fuel meeting the international specifications for Jet-A-1 (ASTM D) were successful. The jet fuel carbon number range was shown to be narrower than for petroleum-derived kerosene fuel with a high aromatic concentration. As a result, it was concluded that increasing the aromaticity of products in the NCP will enable higher yields of lighter fuels. Special consideration should be given to aromatics in future fuel production activities, especially including the catalytic effect of the deoxygenation catalyst on aromatics. It may be beneficial to consider aromatic extraction and/or reforming technologies to preserve and/or increase the aromaticity of fuel products. Related literature studies by the author of the present work and associates also indicated that jet fuel can be produced by the NCP while utilizing waste and/or impure TAG feedstocks with no observable drawbacks to the fuel quality.

IX.D. Reactor Design and Coke Formation in TAG Cracking Reactors

From the batch experiments, it was concluded that coke formation was observed during TAG cracking as a result of increased temperatures and/or increased residence time. Furthermore, it was concluded that TAG cracking at 445 C results in coke formation in approximately ¼ the residence time of 430 C.

It was concluded that tubular cracking reactors (TCRs) were capable of operating with the absence of coke formation under suitable operating conditions for cracking TAGs. It was furthermore learned that the point of asphaltene flocculation is a critical operating parameter that can be approached, but should not be reached during operating of TAG cracking reactors—if asphaltene flocculation occurs, coke formation can result.

Experiments showed that under relatively brief space times (~0.3 hours) it was possible to operate a TCR at temperatures of 470 C. However for most of the residence times studied, coke formation was observed when the temperature of the reactor was increased above 440 C.

The tubular cracking reactor design was shown to be scalable to a 2-10 kg/h unit. This bench-scale TCR was found to be capable of cracking TAG without coking over at least a 100 hour operating period. Endothermicity was observed in TAG cracking, which had a greater effect in the bench-scale TCR than in the lab-scale TCR. This may be an important factor in commercial TCR designs.

IX.E. Effect of Operating Parameters on Fuel Yields from the NCP

From the efforts to determine optimal operation parameters of the TAG cracking reactor, it was concluded that greater cracking reaction temperature and space time were optimal for producing the greatest yield of lighter fuels over the experimental domain that was studied. As a

result, reactors should be operated at approximately 440 C and 1.2 h space time. Furthermore, the point of asphaltene flocculation should be approached in order to observe the greatest production of lighter fuels, which are more desirable. The effect of pressure was found to be less influential on coke formation than the effect of temperature and space time.

The effect of cracking reaction temperature was strongest for influencing the distribution of fuel products in the noncatalytic cracking process. However, the effect of space time was stronger than temperature for influencing the distribution of functional groups within the fuel products. TAGs containing higher quantities of polyunsaturated fatty acids were shown to produce greater yields of lighter fuels and greater aromaticity in fuel products. Higher pressure also shifted the production distribution towards lighter, more valuable fuels and additional studies beyond the limits of the present study should be considered for future work.

From an economic standpoint, very little change (approximately ± 2 %) was observed in the total value of products from the NCP. The TPV was relatively stable despite large changes in fuel yields over the conditions studied. Therefore, it is concluded that the pursuit of low cost feedstocks should be a priority, rather than selecting a feedstock that produces relatively desirable products. Additionally, technology for the production of valuable byproducts such as aromatics, carboxylic acids, or carbon fiber should be considered to improve the economics of noncatalytic cracking processes.

APPENDICES

Appendix A.
Detailed Composition Data from Noncatalytic Cracking of TAG in Batch and CSTRs

This appendix contains tabulated data from the detailed compositional analysis of

cracked triglyceride (TAG) liquid (CTL) samples from batch TAG noncatalytic cracking (see

Section V.C.3.ii) and TAG noncatalytic cracking by continuous-stirred-tank-reactor, CSTR (see

Section V.C.3.i). Conditions for operation are also described at the top of the tables.

Data reflect concentrations of the CTL, denoted by wt. %. Summary information is

presented toward the top of the table, including the total mass of CTL produced, total cracked

TAG gaseous (CTG) product produced, etc. Component concentration data are presented below

the summary information.

Component naming codes are used instead of component names due to size restrictions

for the data tables. These naming codes were devised by Stavova[152] as she described below:

"A compound labeling system was developed to facilitate data processing in terms of

analyte sorting, handling, etc. Each label consisted of the following parameters in the written

order: abbreviation for a class of compound (AA for alkanes, AE for alkenes, AR for aromatics),

a number of carbon atoms in the main chain/class, colon, a number of double bonds and their

position in a parenthesis, underscore, a number of carbon atoms in the branch with their type,

position, and isomer indication in a parenthesis (e.g., 3-Me or 4-Et,t). For instance, AA_cyclo

05_C3(1,2,3-Me) represented 1,2,3-trimethylcyclopentane, and AE 08:1(2c) cis-2-octene. The

species identified tentatively were labeled with a "T" sign and no specification of functionality

position was provided. Analyte identification was based on the retention time and mass spectra

matching the standards. If no standard was available, the tentative identification of unknown

peaks was performed by their mass spectra matching the standard reference mass spectra of the

National Institute of Standards and Technology (NIST) library, version 05.[169] The required

match with the reference mass spectrum was at least 80% and confirmed visually for the major

ions present."

Table 57. Detailed composition of cracked soybean TAG liquid samples via bench-scale CSTR

Bench-Scale CSTR Cracking Sample		A	B	C	D	E	F	G	H
TAG Type	-	Soy	Soy	Soy	Soy	Soy	Soy	Soy	Soy
Temperature	(C)	400	420	400	420	400	420	400	420
Pressure	(Mpa)	2.9	2.9	2.9	2.9	1.5	1.5	1.5	1.5
Space Time	(h)	2.4	2.4	1.4	1.4	2.4	2.4	1.4	1.4
Summary Information	wt. %								
Total Cracked TAG Liquid (CTL)		10.0	13.7	6.2	9.6	6.8	20.0	7.2	14.0
Total Cracked TAG Gas (CTG)		90.0	86.3	93.8	90.4	93.2	80.0	92.8	86.0
Total Identified Components	wt. %	34.6	48.4	30.3	37.9	35.2	59.8	32.3	45.0
Total Identified Carboxylic Acids		13.89	12.05	10.56	10.44	12.38	15.38	13.09	10.18
Total Identified Hydrocarbons		14.1	31.0	13.6	22.0	16.6	38.5	12.8	29.2
Total Unidentified Carboxylic Acids		8.26	7.25	8.97	7.41	8.58	10.55	7.68	8.65
Total Unresolved Mass		3.80	5.34	8.39	7.79	6.28	5.30	9.87	7.83
Total Non-Elutables		53.34	39.02	52.30	46.92	49.89	24.37	50.13	38.49
Total Linear Paraffins		6.73	14.69	6.47	10.06	7.31	17.66	5.71	5.71
Total Branched Paraffins		0.12	0.28	0.05	0.16	0.05	0.29	0.03	0.03
Total Mono-Cyclic Paraffins		0.85	2.28	0.81	1.36	0.92	2.59	0.66	0.66
Total Poly-Cyclic Paraffins		0.02	0.05	0.01	0.03	0.03	0.06	0.01	0.01
Total Linear Olefins		4.15	8.05	4.25	6.77	5.71	10.65	4.43	4.43
Total Branched Olefins		0.08	0.19	0.06	0.13	0.10	0.21	0.07	0.07
Total Terminal Olefins		0.00	0.04	0.00	0.02	0.01	0.04	0.00	0.00
Total Mono-Cyclic Olefins		0.49	1.14	0.36	0.82	0.72	1.62	0.53	0.53
Total Poly-Cyclic Olefins		0.00	0.01	0.00	0.01	0.01	0.01	0.01	0.01
Total Mono-Cyclic Aromatics		1.34	3.47	1.31	2.13	1.43	4.33	1.09	1.09
Total Poly-Cyclic Aromatics		0.28	0.71	0.27	0.49	0.28	0.93	0.20	0.20

Table 57. cont.

Bench-Scale CSTR Cracking Sample	(wt. %)	A	B	C	D	E	F	G	H
FAS 01 Formic Acid, TMS		0.00	0.00	0.00	0.00	0.00	0.00	0.00	0.00
FAS 02 Acetic Acid, TMS		0.66	1.04	0.43	0.78	0.73	0.86	0.66	0.64
FAS 03 Propanoic Acid, TMS		0.16	0.43	0.09	0.28	0.25	0.42	0.17	0.25
FAS 04 Butanoic Acid, TMS		0.13	0.30	0.08	0.19	0.19	0.30	0.13	0.18
FAS 05 Pentanoic Acid, TMS		0.20	0.40	0.12	0.27	0.24	0.42	0.18	0.26
FAS 06 Hexanoic Acid, TMS		0.34	0.63	0.22	0.42	0.42	0.64	0.31	0.40
FAS 07 Heptanoic Acid, TMS		0.63	1.04	0.47	0.80	0.92	1.02	0.71	0.72
FAS 08 Octanoic Acid, TMS		0.52	0.88	0.40	0.68	0.71	0.93	0.53	0.64
FAS 09 Nonanoic Acid, TMS		0.54	0.85	0.41	0.64	0.70	0.98	0.51	0.65
FAS 10 Decanoic Acid, TMS		0.60	0.77	0.46	0.63	0.75	0.83	0.63	0.63
FAS 11 Undecanoic Acid, TMS		0.30	0.38	0.25	0.33	0.33	0.46	0.27	0.36
FAS 12 Dodecanoic Acid, TMS		0.22	0.26	0.20	0.24	0.23	0.28	0.20	0.25
FAS 13 Tridecanoic Acid, TMS		0.00	0.00	0.00	0.00	0.00	0.26	0.00	0.00
FAS 14 Tetradecanoic Acid, TMS		0.00	0.00	0.00	0.00	0.00	0.00	0.00	0.00
FAS 15 Pentadecanoic Acid		0.00	0.00	0.00	0.00	0.00	0.00	0.00	0.00
FAS 16 Hexadecanoic Acid, TMS		3.48	1.35	2.61	1.73	2.59	2.20	3.40	1.38
FAS 17 Heptadecanoic Acid, TMS		0.00	0.00	0.00	0.00	0.00	0.00	0.00	0.00
FAS 18 Octadecanoic Acid, TMS		2.36	0.85	1.88	1.04	1.48	1.53	2.00	1.07
FAS 20 Eicosanoic Acid, TMS		0.00	0.00	0.00	0.00	0.00	0.00	0.00	0.00
FAS 22 Docosanoic Acid, TMS		0.00	0.00	0.00	0.00	0.00	0.00	0.00	0.00
FAU 18:1 11-Octadecenoic Acid, TMS		1.56	0.72	1.46	0.88	1.25	0.74	1.42	0.80
FAU 18:1 9-Octadecenoic Acid, TMS		0.82	0.47	0.80	0.52	0.75	0.42	1.00	0.52
FAU 18:2 9,12-Octadecadienoic Acid, TMS		0.00	0.00	0.00	0.00	0.00	0.00	0.00	0.00
FAU 20:11 Eicosenoic Acid, TMS		0.00	0.00	0.00	0.00	0.00	0.00	0.00	0.00
AA 03		0.04	0.04	0.05	0.05	0.05	0.04	0.04	0.05
AA 04		0.20	0.33	0.20	0.26	0.23	0.30	0.19	0.24
AA 05		0.48	0.98	0.39	0.68	0.53	0.90	0.40	0.65
AA 06		0.47	1.11	0.37	0.72	0.53	1.10	0.38	0.75
AA 07		0.43	1.10	0.35	0.69	0.48	1.12	0.33	0.80
AA 08		0.42	1.10	0.36	0.68	0.47	1.17	0.32	0.83
AA 09		0.29	0.81	0.24	0.49	0.34	0.90	0.23	0.63
AA 10		0.17	0.53	0.16	0.31	0.19	0.62	0.13	0.44
AA 11		0.14	0.47	0.15	0.28	0.15	0.55	0.11	0.40
AA 12		0.13	0.39	0.13	0.24	0.13	0.47	0.09	0.35
AA 13		0.15	0.43	0.15	0.29	0.18	0.53	0.12	0.38
AA 14		0.16	0.43	0.17	0.29	0.19	0.54	0.15	0.40
AA 15		0.49	1.17	0.56	0.80	0.57	1.70	0.47	1.38
AA 16		0.14	0.32	0.15	0.23	0.14	0.43	0.11	0.39
AA 17		0.39	0.86	0.52	0.60	0.37	1.43	0.32	1.51
AA 18		0.05	0.10	0.06	0.08	0.05	0.13	0.04	0.13
AA 19		0.05	0.09	0.06	0.08	0.06	0.13	0.04	0.13
AA 20		0.03	0.05	0.04	0.05	0.06	0.06	0.03	0.07
AA 21		0.04	0.06	0.05	0.09	0.10	0.06	0.04	0.08
AA 22		0.02	0.03	0.02	0.05	0.08	0.03	0.02	0.05
AA 23		0.02	0.03	0.03	0.03	0.04	0.04	0.02	0.05
AA 24		0.02	0.03	0.04	0.03	0.04	0.02	0.02	0.03
AA 25		0.01	0.02	0.01	0.02	0.03	0.02	0.01	0.03
AA 26		0.02	0.02	0.02	0.02	0.02	0.02	0.01	0.03
AA 05_C1(2-Me)		0.01	0.02	0.01	0.01	0.00	0.02	0.00	0.01
AA 05_C1(3-Me)		0.01	0.02	0.00	0.01	0.00	0.01	0.00	0.01
AA 05_C2 (2,3-Me)		0.00	0.01	0.00	0.01	0.00	0.01	0.00	0.01
AA 06_C1(2-Me)		0.00	0.03	0.00	0.01	0.00	0.02	0.00	0.01
AA 06_C1(3-Me)		0.01	0.03	0.01	0.02	0.01	0.02	0.01	0.01
AA 07_C1(3-Me)		0.01	0.03	0.00	0.02	0.01	0.02	0.00	0.01
AA 07_C1(4-Me)		0.04	0.02	0.00	0.00	0.00	0.02	0.00	0.01
AA 07_C2(2,3-Me)		0.01	0.01	0.01	0.01	0.01	0.02	0.01	0.01
AA 07_C2(3-Et)		0.02	0.01	0.00	0.01	0.00	0.01	0.00	0.00
AA 08_C1(3-Me)		0.00	0.01	0.00	0.01	0.00	0.01	0.00	0.01
AA 08_C2(2,2-Me)		0.00	0.00	0.00	0.00	0.00	0.01	0.00	0.00
AA 08_C2(3,3-Me)		0.00	0.01	0.00	0.00	0.00	0.01	0.00	0.00
AA 08_C2(3-Et)		0.00	0.00	0.00	0.01	0.00	0.00	0.00	0.00
AA 09_C1(2-Me)		0.01	0.03	0.01	0.01	0.01	0.02	0.00	0.02

Table 57. cont.

Bench-Scale CSTR Cracking Sample	(wt. %)	A	B	C	D	E	F	G	H
AA 09_C1(3-Me)		0.01	0.02	0.01	0.01	0.01	0.02	0.01	0.01
AA 10_C1(2-Me) T		0.00	0.02	0.00	0.01	0.01	0.02	0.00	0.02
AA 11_C1(2-Me) T		0.00	0.02	0.00	0.01	0.00	0.02	0.00	0.01
AA decahydro naphthalene T		0.00	0.02	0.00	0.01	0.01	0.02	0.00	0.01
AA decahydro naphthalene_C1(Me) T		0.01	0.02	0.01	0.01	0.01	0.02	0.01	0.01
AA decahydro naphthalene_C1(Me) T		0.01	0.02	0.00	0.01	0.01	0.02	0.00	0.00
AA_cyclo 05		0.03	0.08	0.03	0.05	0.03	0.06	0.02	0.05
AA_cyclo 05_C1(Me)		0.03	0.10	0.03	0.06	0.03	0.09	0.02	0.06
AA_cyclo 05_C10(n-De) T		0.02	0.04	0.02	0.03	0.02	0.05	0.01	0.03
AA_cyclo 05_C11(n-Un) T		0.01	0.02	0.01	0.01	0.01	0.02	0.00	0.03
AA_cyclo 05_C12(n-Do) T		0.01	0.03	0.02	0.02	0.01	0.05	0.01	0.04
AA_cyclo 05_C2(1,2-Me)		0.01	0.02	0.00	0.01	0.01	0.02	0.00	0.01
AA_cyclo 05_C2(1,3-Me,c)		0.00	0.01	0.00	0.00	0.00	0.01	0.00	0.00
AA_cyclo 05_C2(1,3-Me,t)		0.00	0.02	0.00	0.01	0.00	0.02	0.00	0.01
AA_cyclo 05_C2(Et) T		0.03	0.09	0.02	0.05	0.03	0.07	0.02	0.04
AA_cyclo 05_C3(1-Et,2-Me)		0.01	0.03	0.01	0.02	0.01	0.02	0.01	0.01
AA_cyclo 05_C3(1-Et,2-Me,t)		0.02	0.05	0.02	0.03	0.02	0.04	0.01	0.03
AA_cyclo 05_C3(1-Et,3-Me,t)		0.00	0.01	0.00	0.00	0.00	0.00	0.00	0.00
AA_cyclo 05_C3(1-Me,2-Pr) T		0.01	0.03	0.01	0.02	0.01	0.03	0.01	0.02
AA_cyclo 05_C3(n-Pr)		0.02	0.06	0.02	0.04	0.02	0.06	0.01	0.03
AA_cyclo 05_C4(n-Bu)		0.02	0.06	0.02	0.04	0.03	0.06	0.02	0.04
AA_cyclo 05_C5(n-Pe) T		0.03	0.07	0.03	0.05	0.04	0.07	0.03	0.05
AA_cyclo 05_C6(n-Hex) T		0.05	0.09	0.05	0.06	0.05	0.10	0.03	0.07
AA_cyclo 05_C7(n-Hep) T		0.02	0.02	0.02	0.00	0.00	0.04	0.01	0.01
AA_cyclo 05_C9(n-No) T		0.02	0.05	0.02	0.04	0.03	0.06	0.02	0.04
AA_cyclo 06		0.01	0.04	0.01	0.03	0.02	0.04	0.01	0.03
AA_cyclo 06_C1(Me)		0.05	0.13	0.04	0.08	0.06	0.12	0.04	0.08
AA_cyclo 06_C10(n-De) T		0.02	0.04	0.02	0.03	0.03	0.07	0.02	0.06
AA_cyclo 06_C11(n-Un) T		0.04	0.07	0.05	0.05	0.04	0.10	0.04	0.09
AA_cyclo 06_C2(1,2-Me,cis)		0.01	0.03	0.01	0.02	0.01	0.02	0.01	0.02
AA_cyclo 06_C2(1,2-Me,t)		0.02	0.04	0.02	0.03	0.02	0.04	0.02	0.03
AA_cyclo 06_C2(1,3-Me,c)		0.00	0.01	0.00	0.00	0.00	0.00	0.00	0.00
AA_cyclo 06_C2(1,4-Me,t)		0.00	0.00	0.00	0.00	0.00	0.00	0.00	0.00
AA_cyclo 06_C2(Et)		0.04	0.09	0.03	0.05	0.04	0.08	0.02	0.05
AA_cyclo 06_C3(1,2,4-Me, ctt)		0.00	0.00	0.00	0.00	0.00	0.00	0.00	0.00
AA_cyclo 06_C3(1c,2t,4t-Me)		0.00	0.00	0.00	0.00	0.00	0.00	0.00	0.00
AA_cyclo 06_C3(Et,Me) T		0.02	0.04	0.01	0.03	0.02	0.04	0.01	0.03
AA_cyclo 06_C3(Et,Me) T		0.01	0.02	0.01	0.01	0.01	0.02	0.00	0.01
AA_cyclo 06_C3(i-Pr)		0.01	0.00	0.00	0.00	0.02	0.03	0.01	0.00
AA_cyclo 06_C3(n-Pr) T		0.03	0.07	0.02	0.05	0.03	0.07	0.02	0.05
AA_cyclo 06_C4(1-Me,2-Pr) T		0.00	0.01	0.00	0.01	0.01	0.02	0.00	0.01
AA_cyclo 06_C4(n-Bu)		0.02	0.05	0.02	0.04	0.02	0.06	0.02	0.03
AA_cyclo 06_C5(1-Et,2-Pr) T		0.01	0.02	0.01	0.01	0.01	0.02	0.01	0.02
AA_cyclo 06_C5(Et,Pr) T		0.01	0.02	0.02	0.01	0.01	0.00	0.02	0.01
AA_cyclo 06_C5(n-Pe) T		0.05	0.10	0.05	0.07	0.05	0.12	0.04	0.09
AA_cyclo 06_C6 T		0.01	0.03	0.01	0.03	0.02	0.04	0.01	0.03
AA_cyclo 06_C6(n-Hex) T		0.02	0.09	0.04	0.03	0.03	0.07	0.03	0.05
AA_cyclo 06_C7(n-Hep) T		0.04	0.09	0.04	0.06	0.05	0.11	0.04	0.09
AA_cyclo 06_C8(n-Oc) T		0.02	0.02	0.03	0.02	0.02	0.06	0.02	0.05
AA_cyclo 06_C9(n-No) T		0.04	0.07	0.04	0.05	0.05	0.09	0.04	0.06
AE 03 T		0.01	0.02	0.02	0.02	0.02	0.02	0.02	0.03
AE 04 T		0.04	0.06	0.04	0.06	0.07	0.10	0.06	0.08
AE 04:1(2c) T		0.02	0.03	0.02	0.03	0.03	0.03	0.02	0.03
AE 04:1(2t) T		0.03	0.04	0.02	0.04	0.04	0.04	0.03	0.03
AE 04_C1(2-Me)		0.07	0.15	0.06	0.10	0.08	0.14	0.06	0.09
AE 05		0.07	0.16	0.07	0.14	0.14	0.24	0.11	0.17
AE 05:1(2)_C1(2-Me)		0.00	0.01	0.00	0.01	0.01	0.02	0.00	0.01
AE 05:1(2)_C1(3-Me) T		0.00	0.01	0.00	0.01	0.00	0.01	0.00	0.01
AE 05:1(2c)		0.02	0.03	0.02	0.02	0.02	0.03	0.02	0.03
AE 05:1(2t)		0.04	0.07	0.03	0.05	0.04	0.06	0.03	0.04
AE 06		0.07	0.19	0.07	0.14	0.14	0.31	0.11	0.22
AE 06:1(2c)		0.03	0.06	0.02	0.05	0.04	0.06	0.02	0.04

Table 57. cont.

Bench-Scale CSTR Cracking Sample	(wt. %)	A	B	C	D	E	F	G	H
AE 06:1(2t)		0.05	0.12	0.04	0.09	0.07	0.13	0.05	0.09
AE 06:1(3) T		0.02	0.03	0.01	0.03	0.02	0.04	0.01	0.03
AE 06:2(1,4)_C2(2,3-Me) T		0.00	0.03	0.00	0.02	0.01	0.03	0.00	0.02
AE 06:2(1,4)_C2(3-Et) T		0.00	0.01	0.00	0.00	0.00	0.01	0.00	0.00
AE 07		0.09	0.22	0.08	0.15	0.16	0.32	0.13	0.24
AE 07:1(2c)		0.05	0.07	0.03	0.05	0.06	0.09	0.05	0.06
AE 07:1(2t)		0.08	0.14	0.07	0.10	0.11	0.16	0.08	0.12
AE 07:1(3t)		0.04	0.07	0.03	0.05	0.04	0.07	0.03	0.05
AE 07_C1(2-Me) T		0.00	0.00	0.00	0.00	0.00	0.01	0.00	0.00
AE 08		0.05	0.12	0.05	0.10	0.09	0.20	0.07	0.15
AE 08:1(2c)		0.06	0.09	0.06	0.08	0.08	0.12	0.07	0.09
AE 08:1(2t)		0.11	0.16	0.09	0.14	0.16	0.22	0.14	0.17
AE 08:1(3) T		0.05	0.08	0.04	0.06	0.06	0.09	0.04	0.07
AE 08:1(4) T		0.02	0.04	0.02	0.03	0.02	0.04	0.01	0.03
AE 08:1(4) T		0.01	0.03	0.01	0.02	0.01	0.02	0.01	0.02
AE 09		0.05	0.10	0.04	0.08	0.07	0.18	0.06	0.13
AE 09:1(2c)		0.03	0.05	0.02	0.04	0.04	0.07	0.03	0.05
AE 09:1(2t)		0.05	0.09	0.03	0.06	0.06	0.11	0.05	0.08
AE 09:1(3c)		0.02	0.03	0.02	0.03	0.03	0.04	0.02	0.03
AE 09:1(3t)		0.04	0.07	0.03	0.05	0.04	0.08	0.03	0.06
AE 09:1(4) T		0.02	0.03	0.02	0.04	0.03	0.05	0.02	0.03
AE 10		0.03	0.07	0.02	0.05	0.05	0.12	0.03	0.09
AE 10:1(2c) T		0.03	0.05	0.02	0.05	0.05	0.08	0.03	0.05
AE 10:1(2t) T		0.05	0.09	0.04	0.06	0.06	0.12	0.04	0.09
AE 10:1(3c) T		0.01	0.01	0.00	0.01	0.01	0.02	0.00	0.01
AE 10:1(3t) T		0.02	0.05	0.02	0.04	0.03	0.06	0.02	0.05
AE 10:1(X) T		0.01	0.04	0.01	0.03	0.01	0.05	0.01	0.03
AE 10:1(X) T		0.00	0.01	0.00	0.01	0.01	0.01	0.00	0.01
AE_cyclo 06_C4(Bu) T		0.02	0.05	0.02	0.04	0.03	0.06	0.02	0.04
AE 11		0.05	0.09	0.04	0.07	0.06	0.14	0.05	0.10
AE 11:1(2c) T		0.03	0.05	0.03	0.05	0.04	0.08	0.04	0.07
AE 11:1(2t) T		0.05	0.09	0.05	0.08	0.07	0.13	0.06	0.10
AE 11:1(3c) T		0.01	0.03	0.01	0.03	0.02	0.04	0.01	0.03
AE 11:1(3t) T		0.03	0.05	0.02	0.05	0.04	0.07	0.03	0.05
AE 11:1(X) T		0.01	0.03	0.01	0.02	0.01	0.02	0.01	0.02
AE 11:1(X) T		0.01	0.03	0.01	0.02	0.02	0.03	0.01	0.03
AE 11:1(X) T		0.01	0.02	0.01	0.02	0.01	0.02	0.01	0.02
AE 12		0.04	0.09	0.04	0.07	0.06	0.14	0.04	0.10
AE 12:1(2c) T		0.02	0.04	0.02	0.04	0.02	0.06	0.02	0.04
AE 12:1(2t) T		0.02	0.04	0.02	0.04	0.03	0.06	0.02	0.04
AE 12:1(3) T		0.02	0.03	0.01	0.02	0.02	0.03	0.01	0.03
AE 12:1(4) T		0.01	0.04	0.01	0.03	0.02	0.05	0.01	0.03
AE 12:1(X) T		0.03	0.05	0.03	0.04	0.03	0.06	0.03	0.04
AE 13		0.05	0.11	0.05	0.08	0.07	0.15	0.04	0.11
AE 13:1(2) T		0.01	0.03	0.01	0.02	0.01	0.02	0.00	0.02
AE 13:1(3) T		0.01	0.02	0.01	0.02	0.01	0.02	0.00	0.02
AE 13:1(X) T		0.00	0.01	0.00	0.01	0.01	0.01	0.00	0.01
AE 13:1(X) T		0.02	0.03	0.02	0.03	0.03	0.03	0.02	0.03
AE 13:1(X) T		0.02	0.03	0.01	0.02	0.04	0.03	0.01	0.03
AE 13:1(X) T		0.01	0.04	0.01	0.03	0.02	0.05	0.00	0.03
AE 14		0.05	0.09	0.04	0.07	0.07	0.12	0.06	0.09
AE 14:1(X) T		0.02	0.03	0.02	0.03	0.03	0.03	0.02	0.03
AE 14:1(X) T		0.01	0.02	0.01	0.02	0.02	0.02	0.01	0.02
AE 14:1(X) T		0.01	0.03	0.01	0.03	0.02	0.04	0.01	0.03
AE 15		0.03	0.08	0.04	0.06	0.05	0.13	0.03	0.10
AE 15:1(X) T		0.03	0.04	0.03	0.05	0.05	0.06	0.04	0.05
AE 15:1(X) T		0.00	0.01	0.00	0.01	0.02	0.02	0.00	0.02
AE 15:1(X) T		0.01	0.04	0.00	0.03	0.02	0.06	0.00	0.04
AE 15:1(X) T		0.00	0.03	0.00	0.02	0.01	0.04	0.00	0.03
AE 16		0.03	0.06	0.03	0.05	0.04	0.08	0.03	0.07
AR 9H-fluorene T		0.04	0.05	0.03	0.05	0.05	0.07	0.04	0.06
AE 16:1(X) T		0.01	0.03	0.01	0.03	0.01	0.05	0.00	0.03

Table 57. cont.

Bench-Scale CSTR Cracking Sample	(wt. %)	A	B	C	D	E	F	G	H
AE 16:1(X) T		0.01	0.03	0.01	0.03	0.02	0.04	0.01	0.03
AE 16:1(X) T		0.02	0.03	0.01	0.02	0.02	0.04	0.01	0.03
AR naphthalene_C4(2-Bu) T		0.02	0.04	0.01	0.03	0.03	0.06	0.01	0.04
AE 17		0.05	0.09	0.07	0.07	0.06	0.17	0.04	0.15
AE 17:1(8) T		0.08	0.09	0.09	0.09	0.13	0.29	0.12	0.29
AE 17:1(X) T		0.05	0.10	0.07	0.08	0.07	0.18	0.05	0.16
AE 17:1(X) T		0.04	0.06	0.04	0.05	0.04	0.10	0.03	0.09
AE 17:1(X) T		0.02	0.04	0.03	0.03	0.03	0.08	0.02	0.08
AE 17:1(X) T		0.02	0.04	0.03	0.04	0.03	0.08	0.02	0.07
AE 17:1(X) T		0.02	0.03	0.02	0.03	0.02	0.06	0.00	0.06
AE 17:1(X) T		0.02	0.03	0.02	0.03	0.02	0.05	0.01	0.04
AE 18		0.01	0.02	0.01	0.02	0.01	0.02	0.01	0.02
AE 18:1(X) T		0.00	0.00	0.00	0.00	0.00	0.00	0.00	0.00
AE 18:1(X) T		0.00	0.02	0.00	0.02	0.00	0.00	0.00	0.00
AE 19		0.01	0.02	0.00	0.02	0.02	0.02	0.00	0.03
AE 20		0.01	0.01	0.01	0.02	0.00	0.00	0.00	0.02
AE hexahydro indene T		0.00	0.01	0.00	0.01	0.01	0.01	0.01	0.01
AE_cyclo 05 T		0.09	0.15	0.08	0.14	0.17	0.21	0.13	0.16
AE_cyclo 05_C1(Me) T		0.00	0.01	0.00	0.01	0.01	0.02	0.00	0.01
AE_cyclo 05_C1(Me) T		0.02	0.06	0.02	0.04	0.01	0.07	0.02	0.03
AE_cyclo 05_C2(3,5-Me) T		0.00	0.02	0.00	0.01	0.01	0.02	0.00	0.01
AE_cyclo 05_C2(3-Et) T		0.00	0.01	0.00	0.01	0.01	0.01	0.00	0.01
AE_cyclo 05_C2(Et) T		0.01	0.03	0.01	0.02	0.01	0.03	0.01	0.03
AE_cyclo 05_C2(Me) T		0.01	0.03	0.00	0.02	0.01	0.04	0.01	0.02
AE_cyclo 05_C3(1-Et,5-Me) T		0.01	0.03	0.00	0.02	0.01	0.03	0.00	0.02
AE_cyclo 05_C3(1-Pr) T		0.01	0.03	0.01	0.02	0.02	0.04	0.01	0.03
AE_cyclo 05_C3(Pr) T		0.01	0.01	0.00	0.01	0.01	0.02	0.01	0.01
AE_cyclo 05_C5(1-Pe) T		0.01	0.04	0.02	0.04	0.03	0.04	0.02	0.03
AE_cyclo 05_C6(1-Hex) T		0.02	0.03	0.00	0.00	0.00	0.04	0.02	0.03
AE_cyclo 05_C7(1-Hep) T		0.01	0.03	0.01	0.03	0.02	0.05	0.01	0.03
AE_cyclo 05_C8(1-Oc) T		0.01	0.03	0.01	0.02	0.03	0.05	0.01	0.03
AE_cyclo 06 T		0.03	0.05	0.02	0.05	0.05	0.06	0.03	0.04
AE_cyclo 06_C1(4-Me) T		0.01	0.01	0.00	0.01	0.01	0.01	0.00	0.01
AE_cyclo 06_C1(Me) T		0.01	0.03	0.01	0.02	0.01	0.02	0.01	0.02
AE_cyclo 06_C1(Me) T		0.02	0.09	0.03	0.06	0.06	0.10	0.04	0.07
AE_cyclo 06_C2(1,4-Me) T		0.00	0.00	0.00	0.00	0.00	0.01	0.00	0.00
AE_cyclo 06_C2(3,5-Me) T		0.01	0.00	0.00	0.00	0.00	0.00	0.00	0.00
AE_cyclo 06_C2(Et) T		0.01	0.02	0.00	0.01	0.01	0.02	0.01	0.02
AE_cyclo 06_C2(Et) T		0.02	0.04	0.02	0.04	0.03	0.06	0.02	0.04
AE_cyclo 06_C2(Me) T		0.01	0.03	0.01	0.02	0.02	0.03	0.01	0.02
AE_cyclo 06_C2(Me) T		0.02	0.03	0.01	0.03	0.03	0.04	0.02	0.03
AE_cyclo 06_C3(1-Pr) T		0.02	0.02	0.01	0.01	0.00	0.04	0.01	0.02
AE_cyclo 06_C4(1-Bu) T		0.01	0.02	0.01	0.02	0.02	0.02	0.01	0.02
AE_cyclo 06_C4(4-Me,1-MeEt) T		0.00	0.01	0.00	0.01	0.01	0.02	0.00	0.01
AE_cyclo 06_C5(1-Pe) T		0.03	0.03	0.02	0.04	0.04	0.06	0.03	0.04
AE_cyclo 06_C6(Hex) T		0.01	0.02	0.00	0.02	0.02	0.02	0.01	0.02
AE_cyclo 06_C7(1-Hep) T		0.01	0.02	0.01	0.02	0.02	0.02	0.01	0.02
AE_cyclo 06_C8(1-Oc) T		0.01	0.03	0.01	0.02	0.02	0.03	0.01	0.02
AON 06_(3) T		0.01	0.01	0.00	0.00	0.00	0.01	0.00	0.00
AON 07_(2) T		0.01	0.03	0.01	0.02	0.01	0.03	0.01	0.03
AON 08_(2) T		0.01	0.03	0.01	0.02	0.02	0.04	0.01	0.03
AON 08_(3) T		0.01	0.02	0.00	0.01	0.01	0.02	0.00	0.01
AON 09_(3) T		0.01	0.03	0.01	0.02	0.01	0.04	0.01	0.03
AON 10_(2) T		0.01	0.03	0.01	0.03	0.02	0.05	0.01	0.03
AON 11_(2) T		0.02	0.05	0.02	0.04	0.02	0.06	0.01	0.04
AON 12_(2) T		0.01	0.02	0.00	0.01	0.01	0.02	0.01	0.02
AON 16(2) T		0.00	0.00	0.00	0.02	0.00	0.04	0.00	0.00
AON 17_(2) T		0.04	0.06	0.04	0.05	0.05	0.08	0.03	0.07
AON 18_(3) T		0.03	0.03	0.03	0.04	0.05	0.04	0.03	0.03
AON 19_(2) T		0.04	0.06	0.04	0.08	0.09	0.06	0.03	0.06
AON 20_(3) T		0.02	0.03	0.02	0.05	0.10	0.02	0.01	0.03
AON_cyclo 05(2-Me) T		0.00	0.01	0.00	0.01	0.00	0.02	0.00	0.01

Table 57. cont.

Bench-Scale CSTR Cracking Sample	(wt. %)	A	B	C	D	E	F	G	H
AON_cyclo 06 T		0.02	0.03	0.00	0.04	0.04	0.06	0.02	0.04
AR 06 benzene		0.00	0.00	0.00	0.00	0.00	0.00	0.00	0.00
AR 06_C1(Me) toluene		0.08	0.22	0.08	0.14	0.09	0.21	0.06	0.15
AR 06_C10 T		0.02	0.00	0.02	0.02	0.01	0.01	0.03	0.03
AR 06_C10(1-MeNo) T		0.06	0.09	0.08	0.08	0.03	0.16	0.07	0.15
AR 06_C10(n-De) T		0.02	0.01	0.01	0.01	0.01	0.01	0.01	0.05
AR 06_C11 T		0.03	0.06	0.03	0.05	0.03	0.10	0.02	0.11
AR 06_C11(1-MeDe) T		0.03	0.04	0.04	0.04	0.03	0.06	0.03	0.07
AR 06_C11(n-Un) T		0.03	0.03	0.03	0.03	0.03	0.05	0.03	0.05
AR 06_C13(n-Tri) T		0.01	0.01	0.01	0.01	0.00	0.01	0.01	0.01
AR 06_C15(n-Pe) T		0.00	0.00	0.00	0.03	0.05	0.01	0.00	0.01
AR 06_C2(1,2-Me) o-xylene		0.06	0.17	0.06	0.11	0.06	0.18	0.05	0.15
AR 06_C2(1,3-Me) m-xylene		0.01	0.05	0.02	0.04	0.01	0.06	0.01	0.02
AR 06_C2(1,4-Me) p-xylene		0.01	0.03	0.01	0.02	0.01	0.02	0.01	0.01
AR 06_C2(Et)		0.05	0.11	0.05	0.07	0.05	0.12	0.04	0.09
AR 06_C3(1,2,3-Me) T		0.01	0.03	0.01	0.02	0.01	0.03	0.01	0.02
AR 06_C3(1,2,4-Me)		0.01	0.03	0.01	0.02	0.01	0.04	0.00	0.03
AR 06_C3(1-Et,2-Me)		0.05	0.11	0.04	0.07	0.04	0.13	0.03	0.10
AR 06_C3(1Me,3-Et)		0.01	0.03	0.01	0.02	0.01	0.03	0.01	0.02
AR 06_C3(1Me,4-Et)		0.01	0.03	0.00	0.01	0.01	0.02	0.00	0.02
AR 06_C3(1-Me,Et)		0.01	0.03	0.01	0.02	0.01	0.02	0.01	0.02
AR 06_C3(1-Pr)		0.05	0.13	0.05	0.09	0.07	0.14	0.05	0.10
AR 06_C4(1,2-Et) T		0.01	0.03	0.01	0.02	0.01	0.02	0.01	0.02
AR 06_C4(1,2-Me,4-Et)		0.00	0.02	0.01	0.01	0.01	0.02	0.00	0.02
AR 06_C4(1,3-Me,2-Et)		0.00	0.01	0.00	0.01	0.00	0.01	0.00	0.01
AR 06_C4(1,4-Me,2-Et)		0.00	0.01	0.00	0.01	0.00	0.01	0.00	0.01
AR 06_C4(1-Me,2-Pr)		0.03	0.09	0.03	0.01	0.04	0.10	0.03	0.08
AR 06_C4(1-Me,3-iPr)		0.00	0.01	0.00	0.00	0.00	0.01	0.00	0.00
AR 06_C4(1-Me,3-Pr)		0.01	0.03	0.01	0.02	0.01	0.03	0.01	0.02
AR 06_C4(1-Me,4-iPr)		0.01	0.02	0.01	0.01	0.01	0.02	0.01	0.01
AR 06_C4(1-Me,EtMe) T		0.02	0.05	0.02	0.04	0.02	0.06	0.01	0.04
AR 06_C4(n-Bu)		0.05	0.06	0.05	0.05	0.04	0.08	0.04	0.09
AR 06_C5(1-Me,4-MePr) T		0.00	0.02	0.00	0.01	0.01	0.02	0.00	0.01
AR 06_C5(1-MeBu) T		0.05	0.11	0.05	0.07	0.06	0.14	0.04	0.13
AR 06_C5(n-Pe)		0.09	0.13	0.08	0.12	0.10	0.07	0.08	0.15
AR 06_C6 T		0.02	0.03	0.01	0.03	0.02	0.05	0.01	0.04
AR 06_C6 T		0.01	0.03	0.01	0.02	0.02	0.03	0.01	0.02
AR 06_C6 T		0.01	0.03	0.01	0.02	0.01	0.04	0.01	0.03
AR 06_C6(1-MePe) T		0.05	0.10	0.05	0.07	0.06	0.14	0.04	0.12
AR 06_C6(Et) T		0.00	0.03	0.00	0.00	0.00	0.01	0.00	0.00
AR 06_C6(n-Hex)		0.04	0.09	0.04	0.06	0.05	0.10	0.04	0.09
AR 06_C7(1-Me,3-Hex) T		0.03	0.05	0.02	0.04	0.03	0.05	0.02	0.03
AR 06_C7(1-Me,Hex) T		0.01	0.02	0.01	0.01	0.01	0.02	0.01	0.02
AR 06_C7(1-Me,Hex) T		0.02	0.03	0.02	0.03	0.02	0.04	0.01	0.03
AR 06_C7(1-MeHex) T		0.03	0.06	0.03	0.05	0.03	0.08	0.03	0.07
AR 06_C7(n-Hep) T		0.04	0.06	0.04	0.05	0.04	0.09	0.03	0.07
AR 06_C8 T		0.01	0.02	0.01	0.01	0.01	0.02	0.00	0.02
AR 06_C8(1-MeHep) T		0.03	0.06	0.03	0.04	0.03	0.08	0.02	0.07
AR 06_C8(1-Oct)		0.02	0.04	0.02	0.03	0.02	0.06	0.02	0.04
AR 06_C9(1-MeOc) T		0.03	0.05	0.03	0.04	0.03	0.07	0.02	0.06
AR 06_C9(n-No) T		0.02	0.03	0.02	0.03	0.02	0.05	0.01	0.04
AR 9H-fluorene_C1(Me) T		0.01	0.03	0.01	0.02	0.01	0.03	0.01	0.03
AR 9H-fluorene_C1(Me) T		0.01	0.03	0.01	0.02	0.01	0.03	0.00	0.03
AR indane		0.03	0.06	0.02	0.04	0.03	0.06	0.02	0.05
AR indane_C1(Me) T		0.00	0.02	0.00	0.01	0.00	0.02	0.00	0.01
AR indane_C1(Me) T		0.02	0.07	0.02	0.04	0.02	0.07	0.01	0.04
AR indane_C1(Me) T		0.02	0.06	0.02	0.03	0.02	0.06	0.01	0.04
AR indane_C1(Me) T		0.00	0.04	0.02	0.00	0.01	0.05	0.00	0.03
AR indane_C2(2-Et) T		0.02	0.04	0.02	0.04	0.02	0.06	0.02	0.03
AR indane_C2(Me) T		0.00	0.03	0.00	0.02	0.00	0.03	0.00	0.02
AR indane_C2(Me) T		0.00	0.02	0.00	0.00	0.00	0.02	0.00	0.01
AR indane_C2(Me) T		0.02	0.04	0.02	0.04	0.02	0.07	0.01	0.04

Table 57. cont.

Bench-Scale CSTR Cracking Sample	(wt. %)	A	B	C	D	E	F	G	H
AR phenanthrene/anthracene_C1(Me) T		0.00	0.02	0.00	0.00	0.00	0.02	0.00	0.02
AR phenol_C1(2-Me) T		0.02	0.02	0.00	0.00	0.00	0.02	0.00	0.00
AR tetrahydro naphthalene T		0.00	0.02	0.00	0.00	0.00	0.02	0.00	0.01
AR tetrahydro naphthalene_C2(Et) T		0.00	0.02	0.00	0.00	0.00	0.02	0.00	0.02
AR tetrahydro naphthalene_C2(Et) T		0.00	0.02	0.00	0.00	0.00	0.02	0.00	0.00
AR indane_C2(Me) T		0.00	0.02	0.00	0.00	0.00	0.02	0.00	0.00
AR indane_C3(Me) T		0.02	0.06	0.02	0.04	0.02	0.06	0.01	0.04
AR indene_C2(Me) T		0.02	0.05	0.02	0.04	0.03	0.06	0.02	0.04
AR indene_C2(Me) T		0.02	0.06	0.02	0.05	0.02	0.06	0.01	0.04
AR indene_C3(Me) T		0.02	0.03	0.02	0.04	0.02	0.06	0.02	0.04
AR indene_C3(Me) T		0.01	0.03	0.01	0.02	0.01	0.03	0.01	0.02
AR naphthalene		0.00	0.01	0.00	0.01	0.00	0.01	0.00	0.01
AR naphthalene_C1(Me) T		0.01	0.02	0.01	0.01	0.01	0.02	0.01	0.01
AR naphthalene_C1(Me) T		0.01	0.03	0.01	0.02	0.01	0.02	0.01	0.02
AR naphthalene_C2(Et) T		0.00	0.01	0.00	0.01	0.00	0.02	0.00	0.01
AR naphthalene_C2(Et) T		0.02	0.03	0.01	0.00	0.02	0.03	0.01	0.02
AR naphthalene_C2(Me) T		0.01	0.03	0.01	0.02	0.01	0.02	0.01	0.02
AR naphthalene_C2(Me) T		0.00	0.02	0.00	0.01	0.01	0.02	0.00	0.02
AR naphthalene_C2(Me) T		0.00	0.01	0.00	0.00	0.00	0.01	0.00	0.01
AR naphthalene_C2(Me) T		0.01	0.03	0.01	0.02	0.01	0.02	0.00	0.02
AR naphthalene_C2(Me) T		0.01	0.02	0.01	0.02	0.01	0.02	0.00	0.02
AR naphthalene_C2(Me) T		0.01	0.02	0.01	0.02	0.01	0.04	0.01	0.04
AR naphthalene_C3(Me) T		0.02	0.01	0.01	0.02	0.00	0.02	0.01	0.02
AR naphthalene_C3(Me) T		0.01	0.01	0.02	0.03	0.00	0.03	0.01	0.03
AR naphthalene_C3(n-Pr) T		0.00	0.02	0.03	0.01	0.01	0.02	0.00	0.01
AR naphthalene_C6(n-Hex) T		0.05	0.06	0.04	0.06	0.03	0.09	0.02	0.06
AR naphthalene_C7(n-Hep) T		0.01	0.02	0.01	0.02	0.01	0.02	0.01	0.02
AR phenanthrene T		0.00	0.01	0.00	0.01	0.01	0.01	0.00	0.01

Table 58. Detailed composition of various cracked TAGs via batch reactor

Component (wt. %)	Soybean*	HONO[I]	VHONO[II]	HENO[III]
AA 03	0.18 (0.02)	0.15	0.21	0.23
AA 04	0.67 (0.02)	0.46	0.58	0.60
AA 05	1.09 (0.09)	0.71	0.88	0.94
AA 06	1.24 (0.03)	1.27	1.42	1.31
AA 07	1.10 (0.06)	1.70	1.97	1.63
AA 08	1.12 (0.09)	1.88	2.28	1.77
AA 09	0.83 (0.08)	1.67	0.20	1.67
AA 10	0.44 (0.02)	0.58	0.72	0.72
AA 11	0.38 (0.02)	0.49	0.59	0.57
AA 12	0.35 (0.01)	0.36	0.42	0.44
AA 13	0.45 (0.04)	0.36	0.39	0.34
AA 14	0.39 (0.02)	0.27	0.31	0.23
AA 15	1.03 (0.10)	0.60	0.57	0.42
AA 16	0.25 (0.02)	0.23	0.26	0.18
AA 17	0.52 (0.05)	0.46	0.46	0.25
AA 18	0.09 (0.01)	0.11	0.14	0.13
AA 19	0.09 (0.01)	0.12	0.14	0.17
AA 20	0.05 (0.00)	0.05	0.05	0.10
AA 21	0.06 (0.01)	0.06	0.06	0.16
AA 22	0.03 (0.00)	0.03	0.03	0.03
AA 23	0.04 (0.01)	0.04	0.04	0.04
AA 24	0.03 (0.01)	0.03	0.03	0.03
AA 25	0.02 (0.00)	0.02	0.02	0.02
AA 26 T	0.02 (0.00)	0.03	0.03	0.02
AA 27 T	0.01 (0.00)	0.01	0.01	0.01
AA 03_C1(Me)	0.00 (0.00)	0.00	0.01	0.01
AA 04_C1(2-Me)	0.02 (0.00)	0.02	0.04	0.03
AA 05_C1(2-Me)	0.02 (0.00)	0.02	0.05	0.07
AA 05_C1(3-Me)	0.02 (0.00)	0.02	0.07	0.08
AA 05_C3(2-Me,3-Et)	0.01 (0.00)	0.01	0.01	0.01
AA 06_C1(2-Me)	0.02 (0.00)	0.02	0.03	0.03
AA 06_C1(3-Me)	0.02 (0.01)	0.01	0.04	0.03
AA 06_C2(3-Et)	0.01 (0.00)	0.00	0.01	0.01
AA 07_C1(3-Me)	0.02 (0.00)	0.02	0.03	0.02
AA 08_C1(3-Me)	0.03 (0.00)	0.04	0.05	0.04
AA 08_C1(4-Me)	0.02 (0.00)	0.02	0.03	0.02
AA 08_C2(3,3-Me)	0.00 (0.00)	0.00	0.00	0.00
AA 08_C2(4-Et) T	0.01 (0.00)	0.02	0.02	0.02
AA 09_C1(2-Me)	0.02 (0.00)	0.03	0.04	0.03
AA 09_C1(3-Me)	0.03 (0.00)	0.03	0.04	0.03
AA 09_C1(4-Me) T	0.01 (0.01)	0.03	0.01	0.03
AA 10_C1(2-Me) T	0.02 (0.00)	0.03	0.03	0.02
AA 10_C1(4-Me) T	0.02 (0.00)	0.02	0.02	0.02
AA 11_C1(2-Me) T	0.01 (0.00)	0.02	0.03	0.02
AA 11_C1(3-Me) T	0.02 (0.00)	0.03	0.04	0.03
AA naphthalene decahydro T	0.02 (0.00)	0.02	0.02	0.01
AA naphthalene decahydro_C1(Me) T	0.02 (0.00)	0.02	0.03	0.02
AA naphthalene decahydro_C2(Me) T	0.02 (0.00)	0.01	0.01	0.01
AA pentalene octahydro T	0.01 (0.01)	0.03	0.02	0.02
AA_cyclo 05	0.05 (0.00)	0.04	0.07	0.05
AA_cyclo 05_C1(Me)	0.13 (0.00)	0.15	0.19	0.16
AA_cyclo 05_C10(n-De) T	0.05 (0.01)	0.07	0.09	0.06
AA_cyclo 05_C2(1,2-Me,c)	0.02 (0.00)	0.02	0.02	0.02
AA_cyclo 05_C2(1,2-Me,t), AE 07	0.11 (0.00)	0.11	0.12	0.13
AA_cyclo 05_C2(1,3-Me,c)	0.01 (0.00)	0.01	0.01	0.01
AA_cyclo 05_C2(1,3-Me,t)	0.02 (0.00)	0.02	0.02	0.02
AA_cyclo 05_C2(Et) T	0.11 (0.00)	0.13	0.16	0.13
AA_cyclo 05_C3(1-Et,2-Me)	0.03 (0.00)	0.03	0.04	0.03
AA_cyclo 05_C3(1-Et,2-Me,t)	0.08 (0.00)	0.09	0.10	0.09
AA_cyclo 05_C3(1-Et,3-Me,t)	0.01 (0.00)	0.01	0.01	0.01
AA_cyclo 05_C3(Me) T	0.00 (0.00)	0.00	0.00	0.00
AA_cyclo 05_C3(n-Pr)	0.07 (0.00)	0.09	0.12	0.10

451

Table 58. cont.

Component	(wt. %)	Soybean*	HONO[I]	VHONO[II]	HENO[III]
AA_cyclo 05_C4 T		0.01 (0.00)	0.06	0.03	0.01
AA_cyclo 05_C4(1-Me,2-Pr) T		0.05 (0.00)	0.06	0.08	0.07
AA_cyclo 05_C4(1-Me,2-Pr) T		0.02 (0.00)	0.03	0.03	0.03
AA_cyclo 05_C4(n-Bu)		0.07 (0.00)	0.10	0.14	0.11
AA_cyclo 05_C5(n-Pe) T		0.07 (0.00)	0.08	0.10	0.08
AA_cyclo 05_C6(n-Hex) T		0.08 (0.01)	0.07	0.07	0.07
AA_cyclo 05_C7 T		0.02 (0.00)	0.04	0.04	0.04
AA_cyclo 05_C7(n-Hep) T		0.02 (0.01)	0.07	0.08	0.06
AA_cyclo 05_C9(n-No) T		0.07 (0.02)	0.20	0.23	0.15
AA_cyclo 06		0.05 (0.00)	0.06	0.08	0.06
AA_cyclo 06_C1(Me)		0.15 (0.00)	0.15	0.18	0.15
AA_cyclo 06_C10 T		0.02 (0.00)	0.04	0.05	0.03
AA_cyclo 06_C10(n-De) T		0.04 (0.01)	0.07	0.08	0.07
AA_cyclo 06_C11 T		0.05 (0.01)	0.06	0.05	0.03
AA_cyclo 06_C11 T		0.02 (0.00)	0.03	0.02	0.01
AA_cyclo 06_C11(n-Un) T		0.05 (0.01)	0.07	0.07	0.04
AA_cyclo 06_C13(n-Tri) T		0.00 (0.00)	0.01	0.02	0.02
AA_cyclo 06_C2(1,2-Me,c)		0.01 (0.00)	0.01	0.02	0.01
AA_cyclo 06_C2(1,2-Me,cis)		0.03 (0.00)	0.03	0.04	0.03
AA_cyclo 06_C2(1,2-Me,t)		0.07 (0.00)	0.06	0.08	0.06
AA_cyclo 06_C2(1,3-Me,c)		0.01 (0.00)	0.01	0.01	0.01
AA_cyclo 06_C2(Et)		0.13 (0.01)	0.17	0.21	0.16
AA_cyclo 06_C2(Me) T		0.00 (0.00)	0.00	0.00	0.00
AA_cyclo 06_C2(Me) T		0.02 (0.00)	0.04	0.04	0.03
AA_cyclo 06_C3(Et,Me) T		0.07 (0.00)	0.09	0.11	0.09
AA_cyclo 06_C3(Et,Me) T		0.03 (0.00)	0.04	0.05	0.04
AA_cyclo 06_C3(n-Pr)		0.07 (0.01)	0.12	0.15	0.12
AA_cyclo 06_C4 T		0.02 (0.00)	0.03	0.03	0.03
AA_cyclo 06_C4(1-Me,2-Pr) T		0.02 (0.00)	0.02	0.03	0.02
AA_cyclo 06_C4(i-Bu)		0.02 (0.01)	0.06	0.02	0.02
AA_cyclo 06_C4(n-Bu)		0.06 (0.00)	0.09	0.12	0.10
AA_cyclo 06_C5 T		0.03 (0.00)	0.04	0.02	0.03
AA_cyclo 06_C5 T		0.02 (0.01)	0.04	0.06	0.05
AA_cyclo 06_C5 T		0.02 (0.00)	0.03	0.04	0.03
AA_cyclo 06_C5(1-Et,2-Pr) T		0.02 (0.00)	0.05	0.06	0.05
AA_cyclo 06_C5(n-Pe) T		0.04 (0.01)	0.06	0.07	0.07
AA_cyclo 06_C6 T		0.02 (0.01)	0.02	0.02	0.01
AA_cyclo 06_C6 T		0.05 (0.00)	0.06	0.08	0.07
AA_cyclo 06_C6(n-Hex) T		0.05 (0.01)	0.05	0.06	0.05
AA_cyclo 06_C7 T		0.09 (0.01)	0.09	0.19	0.14
AA_cyclo 06_C8 T		0.02 (0.00)	0.02	0.02	0.02
AA_cyclo 06_C8(n-Oc) T		0.04 (0.03)	0.12	0.03	0.01
AA_cyclo 06_C9 T		0.03 (0.00)	0.04	0.04	0.03
AA_cyclo 06_C9(n-No) T		0.11 (0.02)	0.24	0.28	0.16
AE 03 T		0.02 (0.00)	0.02	0.02	0.03
AE 04 T		0.08 (0.01)	0.04	0.06	0.07
AE 04_C1(3-Me)		0.01 (0.00)	0.00	0.01	0.01
AE 05		0.10 (0.01)	0.05	0.08	0.10
AE 05_C1(2-Me) T		0.00 (0.00)	0.00	0.01	0.01
AE 05_C1(3-Me) T		0.00 (0.00)	0.00	0.00	0.00
AE 05_C1(4-Me)		0.00 (0.00)	0.00	0.00	0.00
AE 06		0.11 (0.01)	0.05	0.09	0.11
AE 07_C1(2-Me) T		0.00 (0.00)	0.01	0.01	0.01
AE 08		0.06 (0.00)	0.07	0.07	0.08
AE 09		0.08 (0.00)	0.10	0.11	0.12
AE 10		0.04 (0.00)	0.03	0.03	0.05
AE 11		0.09 (0.00)	0.12	0.13	0.12
AE 13		0.12 (0.00)	0.11	0.12	0.12
AE 14		0.07 (0.00)	0.05	0.05	0.05
AE 15		0.14 (0.01)	0.05	0.06	0.05
AE 16		0.02 (0.01)	0.01	0.03	0.02
AE 17		0.05 (0.03)	0.07	0.02	0.03

452

Table 58. cont.

Component	(wt. %) Soybean*	HONO[I]	VHONO[II]	HENO[III]
AE 18	0.03 (0.02)	0.05	0.06	0.05
AE 19	0.03 (0.00)	0.03	0.03	0.04
AE 04:1(2) T	0.10 (0.03)	0.12	0.08	0.08
AE 04:1(2) T	0.07 (0.01)	0.05	0.07	0.08
AE 05:1(2)_C1(2-Me)	0.00 (0.00)	0.01	0.04	0.03
AE 05:1(2)_C1(Me) T	0.01 (0.01)	0.02	0.02	0.02
AE 05:1(2)_C1(Me) T	0.01 (0.00)	0.02	0.02	0.02
AE 05:1(2c)	0.10 (0.00)	0.08	0.09	0.09
AE 05:1(2t)	0.21 (0.02)	0.17	0.19	0.22
AE 06:1(2)_C1(4-Me) T	0.01 (0.00)	0.01	0.01	0.01
AE 06:1(2)_C1(Me) T	0.03 (0.01)	0.03	0.01	0.02
AE 06:1(2c)	0.12 (0.00)	0.13	0.12	0.12
AE 06:1(2t)	0.19 (0.02)	0.17	0.18	0.15
AE 06:1(3) T	0.04 (0.03)	0.11	0.02	0.01
AE 06:1(3) T	0.02 (0.01)	0.03	0.01	0.01
AE 07:1(2)_C1(Me) T	0.01 (0.00)	0.01	0.01	0.01
AE 07:1(2c)	0.08 (0.00)	0.10	0.10	0.09
AE 07:1(2t)	0.15 (0.00)	0.18	0.17	0.16
AE 07:1(3c)	0.02 (0.02)	0.01	0.05	0.01
AE 07:1(3t)	0.11 (0.01)	0.15	0.15	0.12
AE 08:1(2c)	0.10 (0.00)	0.12	0.12	0.11
AE 08:1(2t)	0.16 (0.01)	0.20	0.19	0.17
AE 08:1(X) T	0.11 (0.01)	0.14	0.15	0.12
AE 08:1(X) T	0.03 (0.00)	0.04	0.06	0.04
AE 08:1(X)	0.07 (0.01)	0.09	0.10	0.08
AE 09:1(2c)	0.08 (0.00)	0.11	0.11	0.11
AE 09:1(2t)	0.12 (0.00)	0.19	0.18	0.18
AE 09:1(3c)	0.04 (0.00)	0.06	0.07	0.05
AE 09:1(3t)	0.10 (0.01)	0.17	0.18	0.14
AE 09:1(4) T	0.05 (0.01)	0.10	0.12	0.08
AE 10:1(2c) T	0.07 (0.00)	0.09	0.09	0.09
AE 10:1(2t) T	0.08 (0.01)	0.09	0.09	0.11
AE 10:1(3c) T	0.02 (0.00)	0.03	0.02	0.02
AE 10:1(3t) T	0.04 (0.00)	0.06	0.06	0.06
AE 10:1(4) T	0.02 (0.00)	0.02	0.03	0.02
AE 10:1(x) T	0.07 (0.00)	0.09	0.11	0.10
AE 11:1(2c) T	0.06 (0.00)	0.07	0.07	0.07
AE 11:1(2t) T	0.06 (0.01)	0.09	0.08	0.09
AE 11:1(X) T	0.03 (0.00)	0.07	0.08	0.07
AE 11:1(X) T	0.03 (0.00)	0.05	0.05	0.04
AE 11:1(X) T	0.03 (0.00)	0.04	0.04	0.03
AE 11:1(X) T	0.05 (0.00)	0.08	0.07	0.07
AE 11:1(X) T	0.03 (0.01)	0.04	0.05	0.03
AE 12:1(2c) T	0.06 (0.00)	0.06	0.06	0.07
AE 12:1(2t) T	0.06 (0.00)	0.06	0.06	0.08
AE 12:1(3) T	0.04 (0.01)	0.05	0.05	0.05
AE 12:1(X) T	0.06 (0.00)	0.08	0.09	0.08
AE 12:1(X) T	0.06 (0.00)	0.06	0.07	0.06
AE 12:1(X) T	0.04 (0.00)	0.04	0.05	0.05
AE 13:1(2) T	0.04 (0.00)	0.03	0.03	0.04
AE 13:1(X) T	0.03 (0.00)	0.04	0.04	0.04
AE 13:1(X) T	0.05 (0.00)	0.06	0.07	0.06
AE 14:1(X) T	0.03 (0.02)	0.05	0.06	0.04
AE 14:1(X) T	0.03 (0.00)	0.05	0.02	0.04
AE 14:1(X) T	0.02 (0.00)	0.03	0.03	0.02
AE 14:1(X) T	0.05 (0.00)	0.06	0.07	0.05
AE 15:1(X) T	0.11 (0.01)	0.07	0.06	0.05
AE 15:1(X) T	0.05 (0.00)	0.03	0.03	0.02
AE 15:1(X) T	0.10 (0.00)	0.05	0.04	0.03
AE 16:1(X) T	0.04 (0.00)	0.06	0.06	0.04
AE 16:1(X) T	0.02 (0.00)	0.04	0.05	0.02
AE 16:1(X) T	0.03 (0.01)	0.04	0.03	0.03

Table 58. cont.

Component	(wt. %)	Soybean*	HONO[I]	VHONO[II]	HENO[III]
AE 16:1(X) T		0.03 (0.00)	0.04	0.04	0.03
AE 16:1(X) T		0.04 (0.00)	0.04	0.05	0.03
AE 17:1(8) T		0.04 (0.01)	0.05	0.05	0.02
AE 17:1(X) T		0.08 (0.02)	0.17	0.16	0.07
AE 17:1(X) T		0.07 (0.01)	0.14	0.13	0.06
AE 17:1(X) T		0.07 (0.04)	0.08	0.09	0.04
AE 17:1(X) T		0.11 (0.02)	0.14	0.12	0.06
AE 17:1(X) T		0.05 (0.01)	0.06	0.05	0.03
AE 17:1(X) T		0.04 (0.01)	0.07	0.07	0.04
AE 17:1(X) T		0.06 (0.00)	0.05	0.04	0.02
AE 18:1(X) T		0.02 (0.00)	0.06	0.07	0.08
AE 18:1(X) T		0.00 (0.00)	0.02	0.02	0.03
AE 19:1(X) T		0.02 (0.00)	0.04	0.05	0.02
AE 20:1(X) T		0.01 (0.00)	0.02	0.03	0.04
AE 20:1(X) T		0.00 (0.00)	0.02	0.02	0.04
AE 20:1(X) T		0.00 (0.00)	0.02	0.01	0.05
AE 20:1(X) T		0.00 (0.00)	0.01	0.00	0.02
AE 21:1(X) T		0.00 (0.00)	0.02	0.03	0.09
AE 21:1(X) T		0.02 (0.00)	0.00	0.00	0.05
AE 21:1(X) T		0.00 (0.00)	0.02	0.01	0.06
AE 21:1(X) T		0.00 (0.00)	0.01	0.00	0.07
AE 21:1(X) T		0.00 (0.01)	0.00	0.00	0.06
AE 21:1(X) T		0.02 (0.00)	0.02	0.02	0.05
AE 06:2(1,3)_C3(3-Et,2-Me) T		0.03 (0.00)	0.03	0.03	0.03
AE 06:2(1,3)_C3(Et,Me) T		0.01 (0.00)	0.02	0.02	0.02
AE 06:2(1,4)_C2(3-Et) T		0.01 (0.00)	0.01	0.02	0.01
AE 06:2(1,4)_C2(Me) T		0.05 (0.00)	0.05	0.07	0.05
AE pentalene hexahydro T		0.01 (0.00)	0.01	0.01	0.01
AE_cyclo 05 T		0.06 (0.01)	0.05	0.06	0.06
AE_cyclo 05_C1(1-Pr) T		0.04 (0.00)	0.05	0.06	0.05
AE_cyclo 05_C1(Me) T		0.02 (0.00)	0.01	0.02	0.02
AE_cyclo 05_C1(Me) T		0.01 (0.00)	0.01	0.01	0.01
AE_cyclo 05_C2(1-Et) T		0.04 (0.00)	0.04	0.05	0.04
AE_cyclo 05_C2(3-Et) T		0.01 (0.00)	0.01	0.02	0.01
AE_cyclo 05_C2(Et) T		0.01 (0.00)	0.01	0.01	0.01
AE_cyclo 05_C2(Me) T		0.02 (0.00)	0.02	0.03	0.02
AE_cyclo 05_C2(Me) T		0.04 (0.00)	0.05	0.06	0.05
AE_cyclo 05_C3(Me,Et) T		0.04 (0.00)	0.05	0.06	0.05
AE_cyclo 05_C3(Pr) T		0.01 (0.00)	0.01	0.02	0.01
AE_cyclo 05_C4(Bu) T		0.01 (0.00)	0.01	0.01	0.01
AE_cyclo 05_C5(1-Pe) T		0.04 (0.00)	0.04	0.05	0.04
AE_cyclo 05_C6(1-Hex) T		0.03 (0.00)	0.03	0.03	0.03
AE_cyclo 05_C7(1-Hep) T		0.05 (0.00)	0.06	0.06	0.06
AE_cyclo 05_C8(1-Oc) T		0.03 (0.00)	0.05	0.05	0.04
AE_cyclo 06 T		0.07 (0.00)	0.08	0.08	0.06
AE_cyclo 06_C1(Me) T		0.02 (0.00)	0.03	0.03	0.03
AE_cyclo 06_C1(Me) T		0.02 (0.00)	0.02	0.02	0.02
AE_cyclo 06_C1(Me) T		0.10 (0.00)	0.11	0.14	0.12
AE_cyclo 06_C10(1-De) T		0.02 (0.00)	0.05	0.05	0.04
AE_cyclo 06_C2(3,5-Me) T		0.01 (0.00)	0.01	0.01	0.02
AE_cyclo 06_C2(Et) T		0.01 (0.00)	0.01	0.02	0.01
AE_cyclo 06_C2(Et) T		0.02 (0.00)	0.02	0.02	0.02
AE_cyclo 06_C2(Et) T		0.02 (0.00)	0.03	0.03	0.03
AE_cyclo 06_C2(Et) T		0.05 (0.02)	0.07	0.08	0.07
AE_cyclo 06_C2(Me) T		0.01 (0.00)	0.01	0.01	0.01
AE_cyclo 06_C2(Me) T		0.01 (0.00)	0.01	0.02	0.01
AE_cyclo 06_C2(Me) T		0.03 (0.00)	0.03	0.04	0.03
AE_cyclo 06_C2(Me) T		0.05 (0.00)	0.06	0.06	0.06
AE_cyclo 06_C3(1-Pr) T		0.04 (0.00)	0.05	0.06	0.05
AE_cyclo 06_C4 T		0.02 (0.00)	0.02	0.02	0.02
AE_cyclo 06_C4(1-Bu) T		0.02 (0.00)	0.03	0.04	0.03
AE_cyclo 06_C5(1-Pe) T		0.00 (0.00)	0.00	0.00	0.00

Table 58. cont.

Component	(wt. %)	Soybean*	HONO[I]	VHONO[II]	HENO[III]
AE_cyclo 06_C8(1-Oc) T		0.03 (0.00)	0.05	0.05	0.04
AE_cyclo 06_C9(1-No) T		0.03 (0.02)	0.06	0.06	0.04
AOL 29 tocopherol (vitamin E) T		0.00 (0.00)	0.00	0.00	0.00
AON 06_(2) T		0.02 (0.00)	0.00	0.02	0.01
AON 07_(2) T		0.03 (0.02)	0.03	0.01	0.04
AON 08_(2) T		0.05 (0.00)	0.05	0.06	0.04
AON 08_(3) T		0.01 (0.01)	0.00	0.00	0.00
AON 09_(2), AA10_C1(3-Me) T		0.07 (0.01)	0.10	0.09	0.07
AON 10_(2), AR indene_C2(Me) T		0.05 (0.00)	0.06	0.08	0.06
AON 11_(2) T		0.07 (0.01)	0.15	0.20	0.16
AON 12_(2) T		0.02 (0.00)	0.03	0.03	0.04
AON 12_(3) T		0.02 (0.00)	0.04	0.05	0.06
AON 17_(2) T		0.10 (0.02)	0.05	0.05	0.07
AON 18_(3) T		0.04 (0.00)	0.02	0.02	0.00
AON 19_(2) T		0.05 (0.01)	0.03	0.06	0.00
AON_cyclo 05_C1(2-Me) T		0.00 (0.00)	0.00	0.00	0.00
AON_cyclo 06 T		0.05 (0.01)	0.05	0.06	0.05
AR 06 benzene		0.11 (0.00)	0.00	0.11	0.11
AR 06_C1(Me) toluene		0.25 (0.01)	0.23	0.28	0.26
AR 06_C2(1,2-Me) o-xylene		0.14 (0.00)	0.12	0.15	0.14
AR 06_C2(1,3-Me) m-xylene		0.08 (0.00)	0.08	0.11	0.09
AR 06_C2(1,4-Me) p-xylene		0.05 (0.00)	0.05	0.06	0.05
AR 06_C2(Et)		0.12 (0.00)	0.11	0.14	0.13
AR 06_C10(1-MeNo) T		0.06 (0.01)	0.10	0.09	0.06
AR 06_C10(n-De) T		0.03 (0.03)	0.02	0.02	0.02
AR 06_C11(1-MeDe) T		0.02 (0.01)	0.04	0.03	0.02
AR 06_C11(n-Un) T		0.02 (0.00)	0.02	0.03	0.02
AR 06_C13(n-Tri) T		0.01 (0.00)	0.01	0.01	0.01
AR 06_C14(n-Tet) T		0.01 (0.00)	0.01	0.00	0.00
AR 06_C15(n-Pen) T		0.01 (0.00)	0.01	0.01	0.01
AR 06_C3(1,2,3-Me) T		0.03 (0.00)	0.04	0.04	0.04
AR 06_C3(1,2,4-Me)		0.04 (0.00)	0.04	0.05	0.04
AR 06_C3(1,3,5-Me)		0.01 (0.00)	0.01	0.03	0.03
AR 06_C3(1-Et,2-Me)		0.08 (0.00)	0.07	0.08	0.08
AR 06_C3(1-Me,3-Et)		0.05 (0.00)	0.05	0.07	0.06
AR 06_C3(1-Me,4-Et)		0.03 (0.00)	0.02	0.03	0.03
AR 06_C3(1-MeEt)		0.02 (0.00)	0.02	0.03	0.02
AR 06_C3(n-Pr)		0.14 (0.00)	0.14	0.15	0.15
AR 06_C4 T		0.01 (0.00)	0.01	0.02	0.02
AR 06_C4 T		0.01 (0.00)	0.01	0.01	0.01
AR 06_C4 T		0.00 (0.00)	0.00	0.00	0.00
AR 06_C4 (tert-Bu)		0.00 (0.00)	0.00	0.00	0.00
AR 06_C4(1,2-Et)		0.01 (0.00)	0.01	0.01	0.01
AR 06_C4(1,2-Et) T		0.02 (0.00)	0.02	0.02	0.02
AR 06_C4(1,2-Me,4-Et)		0.02 (0.00)	0.02	0.02	0.02
AR 06_C4(1,4-Me,2-Et)		0.01 (0.00)	0.01	0.02	0.01
AR 06_C4(1-Me,2-iPr)		0.02 (0.01)	0.00	0.11	0.03
AR 06_C4(1-Me,2-Pr)		0.01 (0.00)	0.05	0.05	0.05
AR 06_C4(1-Me,3-iPr)		0.01 (0.00)	0.01	0.01	0.01
AR 06_C4(1-Me,3-Pr)		0.04 (0.00)	0.04	0.04	0.04
AR 06_C4(1-Me,4-iPr)		0.01 (0.00)	0.02	0.08	0.02
AR 06_C4(1-Me,EtMe) T		0.03 (0.00)	0.01	0.08	0.01
AR 06_C4(1-MePr) T		0.03 (0.00)	0.03	0.03	0.03
AR 06_C4(n-Bu)		0.11 (0.00)	0.08	0.08	0.08
AR 06_C5 T		0.02 (0.01)	0.01	0.08	0.03
AR 06_C5 T		0.05 (0.01)	0.02	0.03	0.04
AR 06_C5(1,1-Me,Pr) T		0.02 (0.01)	0.02	0.02	0.01
AR 06_C5(1-Me,4-MePr) T		0.02 (0.00)	0.01	0.02	0.01
AR 06_C5(1-Me,MePr) T		0.01 (0.00)	0.01	0.01	0.01
AR 06_C5(1-MeBu) T		0.07 (0.00)	0.04	0.04	0.05
AR 06_C5(n-Pe)		0.13 (0.03)	0.04	0.02	0.06
AR 06_C5, AE_cyclo 06_C5(1-Pe) T		0.04 (0.00)	0.04	0.04	0.04

Table 58. cont.

Component	(wt. %)	Soybean*	HONO[I]	VHONO[II]	HENO[III]
AR 06_C6 T		0.01 (0.00)	0.01	0.01	0.01
AR 06_C6 T		0.05 (0.00)	0.03	0.03	0.03
AR 06_C6(1-Me,Hex) T		0.05 (0.00)	0.03	0.03	0.03
AR 06_C6(1-MePe), AR naphthalene tetrahydro_C1(Me) T		0.09 (0.00)	0.06	0.06	0.06
AR 06_C6(n-Hex)		0.10 (0.00)	0.08	0.06	0.06
AR 06_C7(1-Me,3-Hex) T		0.06 (0.01)	0.02	0.02	0.05
AR 06_C7(1-MeHex) T		0.05 (0.00)	0.04	0.04	0.04
AR 06_C7(n-Hep) T		0.05 (0.00)	0.05	0.06	0.04
AR 06_C8 T		0.03 (0.01)	0.03	0.03	0.03
AR 06_C8 T		0.02 (0.00)	0.02	0.02	0.02
AR 06_C8(1-MeHep) T		0.05 (0.01)	0.06	0.07	0.05
AR 06_C8(n-Oct)		0.04 (0.00)	0.05	0.06	0.05
AR 06_C9(1-MeOc) T		0.03 (0.00)	0.04	0.04	0.03
AR 06_C9(n-No) T		0.03 (0.00)	0.04	0.05	0.04
AR 06_phenol_C3(Pr) T		0.02 (0.00)	0.02	0.02	0.01
AR 06 phenol T		0.00 (0.00)	0.00	0.00	0.00
AR 06 phenol_C1(Me) T		0.04 (0.00)	0.04	0.05	0.04
AR 06 phenol_C12(3-Do) T		0.02 (0.00)	0.02	0.02	ND
AR 06 phenol_C2(3-Et) T		0.02 (0.01)	0.03	0.04	0.03
AR 06 phenol_C2(Me) T		0.00 (0.00)	0.00	0.00	0.00
AR 06 phenol_C3 T		0.01 (0.00)	0.01	0.01	0.01
AR indane		0.07 (0.00)	0.07	0.09	0.07
AR indane_C1(Me) T		0.09 (0.01)	0.09	0.11	0.08
AR indane_C1(Me) T		0.06 (0.00)	0.06	0.07	0.05
AR indane_C1(Me) T		0.07 (0.00)	0.07	0.09	0.05
AR indane_C2(2-Et) T		0.05 (0.00)	0.04	0.05	0.04
AR indane_C2(Et), AE 12 T		0.07 (0.00)	0.06	0.07	0.08
AR indane_C2(Me) T		0.02 (0.00)	0.02	0.02	0.02
AR indane_C2(Me) T		0.03 (0.01)	0.02	0.03	0.02
AR indane_C2(Me) T		0.04 (0.00)	0.04	0.05	0.04
AR indane_C2(Me) T		0.02 (0.00)	0.01	0.02	0.02
AR indane_C2(Me) T		0.06 (0.00)	0.07	0.08	0.08
AR indane_C2(Me) T		0.02 (0.00)	0.02	0.03	0.02
AR indane_C3(Me) T		0.02 (0.01)	0.02	0.02	0.02
AR indane_C3(Me) T		0.01 (0.01)	0.02	0.01	0.01
AR indane_C3(Me) T		0.02 (0.00)	0.01	0.01	0.01
AR indane_C3(Me) T		0.01 (0.01)	0.02	0.02	0.02
AR indene		0.01 (0.00)	0.00	0.01	0.01
AR indene_C1(Me) T		0.02 (0.00)	0.01	0.04	0.04
AR indene_C2(Me) T		0.02 (0.00)	0.02	0.03	0.02
AR indene_C2(Me) T		0.03 (0.01)	0.02	0.03	0.02
AR indene_C3(Me) T		0.01 (0.00)	0.02	0.02	0.01
AR indene_C3(Me) T		0.02 (0.00)	0.02	0.02	0.02
AR naphthalene		0.04 (0.00)	0.03	0.04	0.04
AR naphthalene tetrahydro T		0.07 (0.01)	0.07	0.07	0.06
AR naphthalene tetrahydro_C1(Me) T		0.02 (0.00)	0.02	0.02	0.02
AR naphthalene tetrahydro_C2(Et) T		0.01 (0.00)	0.01	0.01	0.01
AR naphthalene_C1(Me) T		0.06 (0.00)	0.06	0.07	0.06
AR naphthalene_C1(Me) T		0.06 (0.00)	0.05	0.06	0.05
AR naphthalene_C2(Et) T		0.02 (0.00)	0.02	0.03	0.02
AR naphthalene_C2(Et), AE 14:1(X) T		0.07 (0.00)	0.03	0.07	0.06
AR naphthalene_C2(Me) T		0.01 (0.01)	0.01	0.00	0.01
AR naphthalene_C2(Me) T		0.03 (0.00)	0.02	0.03	0.02
AR naphthalene_C2(Me) T		0.01 (0.00)	0.01	0.02	0.01
AR naphthalene_C2(Me) T		0.01 (0.00)	0.02	0.03	0.02
AR naphthalene_C3(Me) T		0.01 (0.00)	0.01	0.01	0.01
AR naphthalene_C3(Me) T		0.02 (0.01)	0.02	0.02	0.01
AR naphthalene_C3(n-Pr) T		0.02 (0.00)	0.01	0.03	0.01
AR naphthalene_C4(Bu) T		0.01 (0.01)	0.01	0.03	0.02
AR naphthalene_C6(2-Hex) T		0.03 (0.01)	0.02	0.01	0.01
AR naphthalene_C6(Hex) T		0.01 (0.00)	0.01	0.01	0.00
AR acenapthene/naphthalene_C2(ethenyl) T		0.02 (0.00)	0.02	0.02	0.01

Table 58. cont.

Component	(wt. %)	Soybean*	HONO[I]	VHONO[II]	HENO[III]
AR 9H-fluorene T		0.01 (0.00)	0.01	0.02	0.01
AR 9H-fluorene_C1(Me) T		0.02 (0.00)	0.03	0.04	0.03
AR 9H-fluorene_C1(Me) T		0.03 (0.01)	0.03	0.04	0.03
AR 9H-fluorene_C2(Me) T		0.03 (0.01)	0.03	0.03	0.02
AR phenanthrene T		0.02 (0.00)	0.02	0.02	0.02
AR anthracene/phenanthrene_C1(Me) T		0.01 (0.01)	0.03	0.00	0.01
AR fluoranthene/pyrene T		0.01 (0.00)	0.01	0.02	0.02
FAS 01 Formic Acid, TMS		0.00 (0.00)	0.00	0.00	0.00
FAS 02 Acetic Acid, TMS		1.56 (0.04)	1.46	1.61	1.45
FAS 03 Propanoic Acid, TMS		0.48 (0.03)	0.46	0.55	0.47
FAS 03_C1(2-Me), TMS T		0.00 (0.00)	0.00	0.00	0.00
FAS 04 Butanoic Acid, TMS		0.46 (0.02)	0.41	0.47	0.42
FAS 04_C1(3-Me), TMS T		0.00 (0.00)	0.00	0.00	0.00
FAS 05 Pentanoic Acid, TMS		0.59 (0.02)	0.49	0.54	0.45
FAS 05_C1(Me), TMS T		0.00 (0.00)	0.00	0.00	0.00
FAS 06 Hexanoic Acid, TMS		0.97 (0.03)	0.77	0.80	0.61
FAS 07 Heptanoic Acid, TMS		1.62 (0.04)	1.13	1.03	0.89
FAS 08 Octanoic Acid, TMS		1.22 (0.03)	0.97	0.97	0.85
FAS 09 Nonanoic Acid, TMS		1.09 (0.06)	1.18	1.24	0.92
FAS 10 Decanoic Acid, TMS		1.16 (0.09)	2.42	2.67	2.20
FAS 11 Undecanoic Acid, TMS		0.41 (0.01)	0.43	0.46	0.76
FAS 12 Dodecanoic Acid, TMS		0.30 (0.01)	0.28	0.29	0.55
FAS 13 Tridecanoic Acid, TMS		0.28 (0.00)	0.24	0.23	0.52
FAS 14 Tetradecanoic Acid, TMS		0.26 (0.00)	0.23	0.22	0.28
FAS 15 Pentadecanoic Acid, TMS		0.29 (0.00)	0.26	0.25	0.29
FAS 16 Hexadecanoic Acid, TMS		2.29 (0.04)	0.79	0.60	0.61
FAS 17 Heptadecanoic Acid, TMS		0.30 (0.00)	0.26	0.25	0.26
FAS 18 Octadecanoic Acid, TMS		1.23 (0.02)	0.96	0.88	0.55
FAS 19 Nonadecanoic Acid, TMS T		0.00 (0.00)	0.00	0.00	0.00
FAS 20 Eicosanoic Acid, TMS T		0.44 (0.00)	0.44	0.41	0.46
FAS 21 Heneicosanoic Acid, TMS T		0.00 (0.00)	0.00	0.00	0.00
FAS 22 Docosanoic Acid, TMS T		0.00 (0.00)	0.00	0.00	0.47
FAS 23 Tricosanoic Acid, TMS T		0.00 (0.00)	0.00	0.00	0.00
FAS 24 Tetracosanoic Acid, TMS T		0.00 (0.00)	0.00	0.00	0.00
FAS 25 Pentacosanoic Acid, TMS T		0.00 (0.00)	0.00	0.00	0.00
FAS 26 Hexacosanoic Acid, TMS T		0.00 (0.00)	0.00	0.00	0.00
FAS_cyclo 05, TMS T		0.00 (0.00)	0.00	0.00	0.00
FAS_cyclo 06, TMS T		0.01 (0.01)	0.01	0.02	0.00
FAU 05:1, TMS T		0.00 (0.00)	0.00	0.00	0.00
FAU 06:1, TMS T		0.00 (0.00)	0.00	0.00	0.00
FAU 06:1, TMS T		0.00 (0.00)	0.00	0.00	0.00
FAU 06:1, TMS T		0.00 (0.00)	0.00	0.00	0.00
FAU 07:1, TMS T		0.00 (0.00)	0.00	0.00	0.00
FAU 07:1, TMS T		0.00 (0.00)	0.00	0.00	0.00
FAU 08:1, TMS T		0.04 (0.01)	0.05	0.05	0.03
FAU 08:1, TMS T		0.01 (0.01)	0.00	0.00	0.00
FAU 08:1, TMS T		0.00 (0.00)	0.00	0.00	0.00
FAU 08:1, TMS T		0.01 (0.01)	0.00	0.00	0.00
FAU 08:1, TMS T		0.00 (0.00)	0.00	0.00	0.00
FAU 09:1, TMS T		0.06 (0.00)	0.05	0.05	0.05
FAU 09:1, TMS T		0.06 (0.00)	0.06	0.05	0.05
FAU 09:1, TMS T		0.05 (0.00)	0.05	0.04	0.05
FAU 10:1, TMS T		0.00 (0.00)	0.00	0.00	0.00
FAU 10:1, TMS T		0.11 (0.00)	0.00	0.00	0.10
FAU 10:1, TMS T		0.00 (0.00)	0.00	0.00	0.00
FAU 11:1, TMS T		0.00 (0.00)	0.00	0.00	0.00
FAU 11:1, TMS T		0.00 (0.00)	0.00	0.00	0.00
FAU 11:1, TMS T		0.00 (0.00)	0.00	0.00	0.00
FAU 11:1, TMS T		0.00 (0.00)	0.00	0.00	0.00
FAU 11:1, TMS T		0.00 (0.00)	0.00	0.00	0.00
FAU 12:1, TMS T		0.00 (0.00)	0.00	0.00	0.00
FAU 12:1, TMS T		0.00 (0.00)	0.00	0.00	0.00

Table 58. cont.

Component	(wt. %)	Soybean*	HONO[I]	VHONO[II]	HENO[III]
FAU 12:1, TMS T		0.00 (0.00)	0.00	0.00	0.00
FAU 13:1, TMS T		0.00 (0.00)	0.00	0.00	0.18
FAU 14:1, TMS T		0.00 (0.00)	0.00	0.00	0.00
FAU 18:1(11), TMS T		0.00 (0.00)	0.40	0.00	0.00
FAU 18:1(11), TMS T		0.50 (0.02)	0.71	0.64	0.42
FAU 18:1(9), TMS T		0.46 (0.00)	0.50	0.42	0.00
FAU 18:1(9), TMS T		0.15 (0.25)	0.41	0.38	0.00
FAU 18:1, TMS T		0.45 (0.01)	0.47	0.43	0.00
FAU 18:1, TMS T		0.00 (0.00)	0.41	0.38	0.00
FAU 18:1, TMS T		0.00 (0.00)	0.40	0.00	0.00
FAU 18:1, TMS T		0.00 (0.00)	0.40	0.37	0.00
FAU 18:2(9,12), TMS T		0.00 (0.00)	0.00	0.00	0.00
FAU 18:2, TMS T		0.00 (0.00)	0.00	0.00	0.00
FAU 20:1, TMS T		0.00 (0.00)	0.00	0.00	0.00
FAU 20:1, TMS T		0.00 (0.00)	0.00	0.00	0.00
FAU 20:1, TMS T		0.00 (0.00)	0.00	0.00	0.00
FAU 20:1, TMS T		0.00 (0.00)	0.00	0.00	0.00
FAU 20:1, TMS T		0.00 (0.00)	0.00	0.00	0.00
FAU 20:1, TMS T		0.00 (0.00)	0.00	0.00	0.00
FAU 20:1, TMS T		0.00 (0.00)	0.00	0.00	0.39
FAU 20:1, TMS T		0.00 (0.00)	0.00	0.00	0.00
FAU 20:1, TMS T		0.00 (0.00)	0.00	0.38	0.00
FAU 20:1, TMS T		0.00 (0.00)	0.40	0.38	0.00
FAU 20:1, TMS T		0.00 (0.00)	0.00	0.00	0.00
FAU 22:1, TMS T		0.00 (0.00)	0.00	0.00	0.41
FAU 22:1, TMS T		0.00 (0.00)	0.00	0.00	0.39
FAU 22:1, TMS T		0.00 (0.00)	0.00	0.00	0.00
FAU 22:1, TMS T		0.00 (0.00)	0.00	0.00	0.00
FAU 22:1, TMS T		0.00 (0.00)	0.00	0.00	0.46
FAU 22:1, TMS T		0.00 (0.00)	0.00	0.00	0.45
FAU 22:1, TMS T		0.00 (0.00)	0.00	0.00	0.00
FAU 22:1, TMS T		0.00 (0.00)	0.00	0.00	0.00
FAU 22:1, TMS T		0.00 (0.00)	0.00	0.00	0.00
FAU 24:1, TMS T		0.00 (0.00)	0.00	0.00	0.00
FAU 24:1, TMS T		0.00 (0.00)	0.00	0.00	0.00
diFAS 09, TMS T		0.08 (0.01)	0.06	0.05	0.04
diFAS 10, TMS T		0.37 (0.04)	0.29	0.27	0.19
diFAS 11, TMS T		0.16 (0.00)	0.14	0.13	0.13
diFAS 12, TMS T		0.20 (0.00)	0.18	0.17	0.21
diFAS 13, TMS T		0.00 (0.00)	0.00	0.00	0.18
diFAS 14, TMS T		0.00 (0.00)	0.00	0.00	0.32
diFAS 15, TMS T		0.00 (0.00)	0.00	0.00	0.00
diFAS 16, TMS T		0.00 (0.00)	0.00	0.00	0.00

* Note: Soybean cracked TAG liquid (CTL) composition is reported as mean (standard deviation) of a triplicate sample.
I. HONO is High Oleic Novelty Oil; II. VHONO is Very High Oleic Novelty Oil; III. HENO is High Erucic Novelty Oil

Table 59. Detailed composition of various cracked TAG liquid samples via batch reactor

Component	(wt. %)	Cottonseed	Linseed
AA 03		0.31	0.25
AA 04		0.94	0.59
AA 05		1.45	1.01
AA 06		1.24	0.99
AA 07		1.03	1.02
AA 08		1.03	1.01
AA 09		0.80	0.74
AA 10		0.50	0.40
AA 11		0.47	0.34
AA 12		0.47	0.27
AA 13		0.72	0.29
AA 14		0.59	0.30
AA 15		1.79	0.64
AA 16		0.23	0.24
AA 17		0.40	0.53
AA 18		0.10	0.08
AA 19		0.10	0.07
AA 20		0.05	0.05
AA 21		0.06	0.03
AA 22		0.05	0.03
AA 23		0.04	0.03
AA 24		0.04	0.02
AA 25		0.02	0.02
AA 26 T		0.01	0.02
AA 27 T		0.01	0.01
AA 03_C1(Me)		0.01	0.02
AA 04_C1(2-Me)		0.05	0.06
AA 05_C1(2-Me)		0.03	0.05
AA 05_C1(3-Me)		0.03	0.04
AA 05_C3(2-Me,3-Et)		0.01	0.01
AA 06_C1(2-Me)		0.02	0.04
AA 06_C1(3-Me)		0.03	0.04
AA 06_C2(3-Et)		0.01	0.00
AA 07_C1(3-Me)		0.03	0.02
AA 08_C1(3-Me)		0.03	0.03
AA 08_C1(4-Me)		0.01	0.01
AA 08_C2(3,3-Me)		0.00	0.00
AA 09_C1(2-Me)		0.02	0.03
AA 09_C1(3-Me)		0.02	0.02
AA 11_C1(3-Me) T		0.02	0.02
AA naphthalene decahydro T		0.02	0.02
AA naphthalene decahydro_C1...		0.02	0.01
AA pentalene octahydro T		0.02	0.03
AA_cyclo 05		0.07	0.10
AA_cyclo 05_C1(Me)		0.13	0.17
AA_cyclo 05_C10(n-De) T		0.04	0.04
AA_cyclo 05_C2(1,2-Me,c)		0.02	0.02
AA_cyclo 05_C2(1,2-Me,t), A...		0.11	0.09
AA_cyclo 05_C2(1,3-Me,c)		0.01	0.02
AA_cyclo 05_C2(1,3-Me,t)		0.02	0.02
AA_cyclo 05_C2(Et) T		0.11	0.14
AA_cyclo 05_C3(1-Et,2-Me)		0.02	0.02
AA_cyclo 05_C3(1-Et,2-Me,t)		0.08	0.07
AA_cyclo 05_C3(1-Et,3-Me,t)		0.01	0.01
AA_cyclo 05_C3(n-Pr)		0.06	0.12
AA_cyclo 05_C4 T		0.01	0.02
AA_cyclo 05_C4(1-Me,2-Pr) T		0.05	0.07
AA_cyclo 05_C4(1-Me,2-Pr) T		0.02	0.02
AA_cyclo 05_C4(n-Bu)		0.06	0.08
AA_cyclo 05_C5(n-Pe) T		0.07	0.06
AA_cyclo 05_C6(n-Hex) T		0.06	0.05
AA_cyclo 05_C7(n-Hep) T		0.01	0.04

Table 59. cont.

Component	(wt. %)	Cottonseed	Linseed
AA_cyclo 05_C9(n-No) T		0.06	0.05
AA_cyclo 06		0.05	0.06
AA_cyclo 06_C1(Me)		0.14	0.13
AA_cyclo 06_C10 T		0.02	0.02
AA_cyclo 06_C10(n-De) T		0.07	0.04
AA_cyclo 06_C11 T		0.04	0.04
AA_cyclo 06_C11(n-Un) T		0.04	0.05
AA_cyclo 06_C2(1,2-Me,c)		0.01	0.01
AA_cyclo 06_C2(1,2-Me,cis)		0.03	0.02
AA_cyclo 06_C2(1,2-Me,t)		0.07	0.04
AA_cyclo 06_C2(1,3-Me,c)		0.01	0.01
AA_cyclo 06_C2(Et)		0.12	0.13
AA_cyclo 06_C2(Me) T		0.02	0.02
AA_cyclo 06_C3(Et,Me) T		0.07	0.05
AA_cyclo 06_C3(Et,Me) T		0.02	0.02
AA_cyclo 06_C3(n-Pr)		0.07	0.08
AA_cyclo 06_C4 T		0.03	0.02
AA_cyclo 06_C4(1-Me,2-Pr) T		0.01	0.01
AA_cyclo 06_C4(i-Bu)		0.01	0.02
AA_cyclo 06_C4(n-Bu)		0.05	0.06
AA_cyclo 06_C5 T		0.02	0.01
AA_cyclo 06_C5(1-Et,2-Pr) T		0.03	0.02
AA_cyclo 06_C5(n-Pe) T		0.04	0.03
AA_cyclo 06_C6 T		0.04	0.04
AA_cyclo 06_C6(n-Hex) T		0.06	0.05
AA_cyclo 06_C7 T		0.09	0.09
AA_cyclo 06_C8 T		0.03	0.02
AA_cyclo 06_C8(n-Oc) T		0.01	0.02
AA_cyclo 06_C9 T		0.03	0.02
AA_cyclo 06_C9(n-No) T		0.09	0.08
AE 03 T		0.05	0.02
AE 04 T		0.11	0.06
AE 04_C1(3-Me)		0.02	0.01
AE 05		0.12	0.07
AE 05_C1(2-Me) T		0.01	0.01
AE 05_C1(3-Me) T		0.00	0.00
AE 05_C1(4-Me)		0.00	0.00
AE 06		0.09	0.07
AE 08		0.05	0.03
AE 09		0.06	0.06
AE 10		0.03	0.01
AE 11		0.09	0.06
AE 13		0.12	
AE 14		0.18	0.04
AE 15		0.18	0.04
AE 16		0.02	0.01
AE 17		0.05	0.03
AE 18		0.02	0.02
AE 19		0.02	
AE 04:1(2) T		0.14	0.08
AE 04:1(2) T		0.11	0.06
AE 05:1(2)_C1(2-Me)		0.03	0.02
AE 05:1(2)_C1(Me) T		0.01	0.01
AE 05:1(2)_C1(Me) T		0.02	0.02
AE 05:1(2c)		0.15	0.10
AE 05:1(2t)		0.29	0.20
AE 06:1(2)_C1(4-Me) T		0.01	0.01
AE 06:1(2)_C1(Me) T		0.01	0.01
AE 06:1(2c)		0.12	0.08
AE 06:1(2t)		0.22	0.16
AE 06:1(3) T		0.10	0.04
AE 06:1(3) T		0.04	0.01

Table 59. cont.

Component	(wt. %)	Cottonseed	Linseed
AE 07:1(2)_C1(Me),AE 06:2(1...		0.01	0.01
AE 07:1(2c)		0.07	0.06
AE 07:1(2t)		0.13	0.10
AE 07:1(3c)		0.05	0.03
AE 07:1(3t)		0.12	0.08
AE 08:1(2c)		0.08	0.07
AE 08:1(2t)		0.13	0.09
AE 08:1(X) T		0.11	0.07
AE 08:1(X) T		0.02	0.02
AE 08:1(X), AE 06:2(1,3)_C2...		0.09	0.07
AE 09:1(2c)		0.06	0.04
AE 09:1(2t)		0.09	0.06
AE 09:1(3c)		0.04	0.02
AE 09:1(3t)		0.11	0.05
AE 09:1(4) T		0.07	0.04
AE 10:1(2c) T		0.06	0.06
AE 10:1(2t) T		0.06	0.05
AE 10:1(3c) T		0.02	0.01
AE 10:1(3t) T		0.06	0.05
AE 10:1(4) T		0.05	0.03
AE 10:1(x) T		0.06	0.07
AE 11:1(2c) T		0.04	0.03
AE 11:1(2t) T		0.08	0.05
AE 11:1(X) T		0.03	0.02
AE 11:1(X) T		0.03	0.02
AE 11:1(X) T		0.05	0.03
AE 11:1(X) T		0.02	0.02
AE 11:1(X), AR phenol_C2(Me...		0.03	0.03
AE 12:1(2c) T		0.04	0.02
AE 12:1(2t) T		0.05	0.03
AE 12:1(3) T		0.05	0.03
AE 12:1(X) T		0.06	0.05
AE 12:1(X) T		0.06	0.07
AE 12:1(X) T		0.04	0.02
AE 13:1(2) T		0.04	0.02
AE 13:1(X) T		0.03	0.02
AE 13:1(X) T		0.02	0.00
AE 14:1(X) T		0.03	0.00
AE 14:1(X) T		0.03	0.00
AE 15:1(X) T		0.17	0.05
AE 15:1(X) T		0.07	0.03
AE 15:1(X) T		0.14	0.03
AE 16:1(X) T		0.02	0.03
AE 17:1(8) T		0.03	0.02
AE 17:1(X) T		0.05	0.07
AE 17:1(X) T		0.05	0.05
AE 17:1(X) T		0.04	0.02
AE 17:1(X) T		0.08	0.08
AE 17:1(X) T		0.03	0.04
AE 17:1(X) T		0.04	0.04
AE 18:1(X) T		0.02	0.02
AE 06:2(1,3)_C3(3-Et,2-Me) T		0.02	0.03
AE 06:2(1,3)_C3(Et,Me) T		0.01	0.01
AE 06:2(1,4)_C2(3-Et) T		0.01	0.01
AE 06:2(1,4)_C2(Me) T		0.05	0.05
AE pentalene hexahydro T		0.01	0.01
AE_cyclo 05 T		0.07	0.06
AE_cyclo 05_C1(1-Pr) T		0.04	0.05
AE_cyclo 05_C1(Me) T		0.02	0.02
AE_cyclo 05_C1(Me) T		0.01	0.01
AE_cyclo 05_C2(1-Et) T		0.04	0.04
AE_cyclo 05_C2(3-Et) T		0.01	0.01

Table 59. cont.

Component	(wt. %)	Cottonseed	Linseed
AE_cyclo 05_C2(Et) T		0.01	0.00
AE_cyclo 05_C2(Me) T		0.02	0.02
AE_cyclo 05_C2(Me) T		0.04	0.05
AE_cyclo 05_C3(Me,Et) T		0.04	0.04
AE_cyclo 05_C4(Bu) T		0.01	0.01
AE_cyclo 05_C5(1-Pe) T		0.03	0.03
AE_cyclo 05_C6(1-Hex) T		0.06	0.05
AE_cyclo 05_C7(1-Hep) T		0.02	0.03
AE_cyclo 05_C8(1-Oc) T		0.02	0.02
AE_cyclo 06 T		0.05	0.05
AE_cyclo 06_C1(Me) T		0.02	0.02
AE_cyclo 06_C1(Me) T		0.02	0.01
AE_cyclo 06_C1(Me) T		0.09	0.09
AE_cyclo 06_C2(3,5-Me) T		0.01	0.02
AE_cyclo 06_C2(Et) T		0.01	0.01
AE_cyclo 06_C2(Et) T		0.02	0.02
AE_cyclo 06_C2(Et) T		0.06	0.02
AE_cyclo 06_C2(Me) T		0.01	0.01
AE_cyclo 06_C2(Me) T		0.01	0.01
AE_cyclo 06_C2(Me) T		0.03	0.02
AE_cyclo 06_C2(Me) T		0.04	0.03
AE_cyclo 06_C3(1-Pr) T		0.02	0.02
AE_cyclo 06_C4 T		0.01	0.01
AE_cyclo 06_C4(1-Bu) T		0.02	0.01
AE_cyclo 06_C5(1-Pe) T		0.02	0.01
AOL 29 tocopherol (vitamin ...		0.00	0.00
AON 06_(2) T		0.03	0.03
AON 07_(2) T		0.04	0.04
AON 08_(2) T		0.06	0.04
AON 09_(2) T		0.07	0.06
AON 10_(2) T		0.02	0.03
AON 11_(2) T		0.06	0.07
AON 12_(2) T		0.02	0.02
AON 17_(2) T		0.17	0.05
AON 18_(3) T		0.06	0.03
AON 19_(2) T		0.02	0.06
AON_cyclo 05_C1(2-Me) T		0.01	0.01
AON_cyclo 06 T		0.02	0.02
AR 06 benzene		0.00	0.14
AR 06_C1(Me) toluene		0.24	0.32
AR 06_C2(1,2-Me) o-xylene		0.12	0.19
AR 06_C2(1,3-Me) m-xylene		0.09	0.10
AR 06_C2(1,4-Me) p-xylene		0.05	0.06
AR 06_C2(Et)		0.11	0.21
AR 06_C10(1-MeNo) T		0.05	0.05
AR 06_C10(n-De) T		0.03	0.02
AR 06_C11(1-MeDe) T		0.03	0.03
AR 06_C11(n-Un) T		0.02	0.02
AR 06_C13(n-Tri) T		0.01	0.01
AR 06_C14(n-Tet) T		0.02	0.00
AR 06_C15(n-Pen) T		0.02	0.00
AR 06_C3(1,2,3-Me) T		0.03	0.04
AR 06_C3(1,2,4-Me)		0.04	0.05
AR 06_C3(1,3,5-Me)		0.01	0.01
AR 06_C3(1-Et,2-Me)		0.07	0.15
AR 06_C3(1-Me,3-Et)		0.05	0.08
AR 06_C3(1-Me,4-Et)		0.04	0.06
AR 06_C3(1-MeEt)		0.03	0.03
AR 06_C3(n-Pr)		0.11	0.18
AR 06_C4 T		0.01	0.01
AR 06_C4 T		0.00	0.00
AR 06_C4 (tert-Bu)		0.00	0.00

Table 59. cont.

Component	(wt. %)	Cottonseed	Linseed
AR 06_C4(1,2-Et)		0.00	0.01
AR 06_C4(1,2-Et) T		0.02	0.03
AR 06_C4(1,2-Me,4-Et)		0.03	0.04
AR 06_C4(1,4-Me,2-Et)		0.01	0.02
AR 06_C4(1-Me,2-iPr)		0.02	0.01
AR 06_C4(1-Me,2-Pr)		0.05	0.10
AR 06_C4(1-Me,3-iPr)		0.01	0.01
AR 06_C4(1-Me,3-Pr)		0.03	0.06
AR 06_C4(1-Me,4-iPr)		0.01	0.01
AR 06_C4(1-Me,EtMe) T		0.02	0.01
AR 06_C4(1-MePr) T		0.03	0.04
AR 06_C4(n-Bu)		0.09	0.09
AR 06_C5 T		0.01	0.01
AR 06_C5 T		0.01	0.02
AR 06_C5, AE_cyclo 06_C5(1-Pe) T		0.03	0.03
AR 06_C5(1,1-Me,Pr) T		0.01	0.07
AR 06_C5(1-Me,4-MePr) T		0.01	0.03
AR 06_C5(1-Me,MePr) T		0.02	0.02
AR 06_C5(1-MeBu) T		0.05	0.07
AR 06_C5(n-Pe)		0.20	0.10
AR 06_C6 T		0.01	0.01
AR 06_C6 T		0.03	0.02
AR 06_C6(1-Me,Hex) T		0.04	0.03
AR 06_C6(1-MePe) T		0.06	0.09
AR 06_C6(n-Hex)		0.08	0.07
AR 06_C7(1-Me,3-Hex) T		0.05	0.04
AR 06_C7(1-MeHex) T		0.04	0.05
AR 06_C7(n-Hep) T		0.05	0.05
AR 06_C8 T		0.05	0.02
AR 06_C8(1-MeHep) T		0.05	0.06
AR 06_C8(n-Oct)		0.04	0.04
AR 06_C9(1-MeOc) T		0.03	0.04
AR 06_C9(n-No) T		0.03	0.04
AR 9H-fluorene T		0.01	0.02
AR 9H-fluorene_C1(Me) T		0.04	0.05
AR 9H-fluorene_C1(Me) T		0.04	0.04
AR 9H-fluorene_C2(Me) T		0.04	0.02
AR indane		0.06	0.09
AR indane_C1(Me) T		0.08	0.12
AR indane_C1(Me) T		0.05	0.08
AR indane_C1(Me) T		0.07	0.10
AR indane_C2(2-Et) T		0.03	0.07
AR indane_C2(Et), AE 12 T		0.09	0.07
AR indane_C2(Me) T		0.01	0.02
AR indane_C2(Me) T		0.04	0.06
AR indane_C2(Me) T		0.01	0.02
AR indane_C2(Me) T		0.05	0.08
AR indane_C2(Me) T		0.01	0.04
AR indane_C3(Me) T		0.01	0.03
AR indane_C3(Me) T		0.02	0.04
AR indene		0.01	0.01
AR indene_C1(Me) T		0.02	0.02
AR indene_C2(Me) T		0.02	0.01
AR indene_C2(Me) T		0.01	0.02
AR indene_C2(Me) T		0.01	0.03
AR indene_C3(Me) T		0.01	0.02
AR indene_C3(Me) T		0.02	0.02
AR acenapthene/naphthalene_...		0.03	0.02
AR naphthalene		0.04	0.06
AR naphthalene tetrahydro T		0.05	0.05
AR naphthalene tetrahydro_C...		0.02	0.03
AR naphthalene tetrahydro_C...		0.01	0.02

Table 59. cont.

Component	(wt. %)	Cottonseed	Linseed
AR naphthalene_C1(Me) T		0.05	0.07
AR naphthalene_C2(Et) T		0.02	0.03
AR naphthalene_C2(Et), AE 1...		0.09	0.05
AR naphthalene_C2(Me) T		0.06	0.10
AR naphthalene_C2(Me) T		0.02	0.03
AR naphthalene_C2(Me) T		0.03	0.04
AR naphthalene_C2(Me) T		0.01	0.02
AR naphthalene_C2(Me) T		0.02	0.02
AR naphthalene_C3(Me) T		0.01	0.02
AR naphthalene_C3(Me) T		0.01	0.01
AR naphthalene_C3(n-Pr) T		0.03	0.03
AR naphthalene_C4(Bu) T		0.01	0.69
AR naphthalene_C6(2-Hex) T		0.03	0.02
AR naphthalene_C6(Hex) T		0.01	0.01
AR anthracene/phenanthrene_...		0.01	0.01
AR phenanthrene T		0.02	0.02
AR fluoranthene/pyrene T		0.01	0.01
AR phenol T		0.00	0.00
AR phenol_C1(Me) T		0.04	0.03
AR phenol_C12(3-Do) T		0.01	0.01
AR phenol_C2(3-Et) T		0.03	0.01
AR phenol_C3 T		0.02	0.02
FAS 01 Formic Acid, TMS		0.00	0.00
FAS 02 Acetic Acid, TMS		1.65	1.73
FAS 03 Propanoic Acid, TMS		0.53	0.78
FAS 03_C1(2-Me), TMS T		0.00	0.00
FAS 04 Butanoic Acid, TMS		0.47	0.86
FAS 04_C1(3-Me), TMS T		0.00	0.00
FAS 05 Pentanoic Acid, TMS		0.63	0.84
FAS 05_C1(Me), TMS T		0.00	0.00
FAS 06 Hexanoic Acid, TMS		1.00	1.15
FAS 07 Heptanoic Acid, TMS		1.68	1.52
FAS 08 Octanoic Acid, TMS		1.09	1.51
FAS 09 Nonanoic Acid, TMS		1.04	1.35
FAS 10 Decanoic Acid, TMS		1.09	1.17
FAS 11 Undecanoic Acid, TMS		0.41	0.50
FAS 12 Dodecanoic Acid, TMS		0.34	0.35
FAS 13 Tridecanoic Acid, TMS		0.32	0.31
FAS 14 Tetradecanoic Acid, TMS		0.45	0.27
FAS 15 Pentadecanoic Acid, TMS		0.32	0.30
FAS 16 Hexadecanoic Acid, TMS		2.94	1.09
FAS 17 Heptadecanoic Acid, TMS		0.32	0.00
FAS 18 Octadecanoic Acid, TMS		0.76	0.98
FAS 19 Nonadecanoic Acid, TMS T		0.00	0.00
FAS 20 Eicosanoic Acid, TMS T		0.00	0.00
FAS 21 Heneicosanoic Acid, TMS T		0.00	0.00
FAS 22 Docosanoic Acid, TMS T		0.00	0.00
FAS 23 Tricosanoic Acid, TMS T		0.00	0.00
FAS 24 Tetracosanoic Acid, TMS T		0.00	0.00
FAS 25 Pentacosanoic Acid, TMS T		0.00	0.00
FAS 26 Hexacosanoic Acid, TMS T		0.00	0.00
FAS_cyclo 05, TMS T		0.00	0.00
FAS_cyclo 06, TMS T		0.00	0.02
FAU 05:1, TMS T		0.00	0.00
FAU 06:1, TMS T		0.00	0.00
FAU 06:1, TMS T		0.00	0.00
FAU 06:1, TMS T		0.00	0.00
FAU 07:1, TMS T		0.00	0.00
FAU 07:1, TMS T		0.00	0.00
FAU 08:1, TMS T		0.04	0.05
FAU 08:1, TMS T		0.00	0.00
FAU 08:1, TMS T		0.00	0.00

Table 59. cont.

Component	(wt. %)	Cottonseed	Linseed
FAU 08:1, TMS T		0.00	0.00
FAU 08:1, TMS T		0.00	0.00
FAU 09:1, TMS T		0.05	0.05
FAU 09:1, TMS T		0.06	0.05
FAU 09:1, TMS T		0.00	0.00
FAU 10:1, TMS T		0.00	0.00
FAU 10:1, TMS T		0.00	0.00
FAU 10:1, TMS T		0.00	0.00
FAU 11:1, TMS T		0.00	0.00
FAU 11:1, TMS T		0.00	0.00
FAU 11:1, TMS T		0.00	0.00
FAU 11:1, TMS T		0.00	0.00
FAU 11:1, TMS T		0.00	0.00
FAU 12:1, TMS T		0.00	0.00
FAU 12:1, TMS T		0.00	0.00
FAU 12:1, TMS T		0.00	0.00
FAU 13:1, TMS T		0.00	0.00
FAU 14:1, TMS T		0.00	0.00
FAU 18:1(11), TMS T		0.00	0.00
FAU 18:1(11), TMS T		0.50	0.50
FAU 18:1(9), TMS T		0.00	0.00
FAU 18:1(9), TMS T		0.00	0.00
FAU 18:1, TMS T		0.00	0.47
FAU 18:1, TMS T		0.00	0.00
FAU 18:1, TMS T		0.00	0.00
FAU 18:1, TMS T		0.00	0.00
FAU 18:2(9,12), TMS T		0.00	0.00
FAU 18:2, TMS T		0.00	0.00
FAU 20:1, TMS T		0.00	0.00
FAU 20:1, TMS T		0.00	0.00
FAU 20:1, TMS T		0.00	0.00
FAU 20:1, TMS T		0.00	0.00
FAU 20:1, TMS T		0.00	0.00
FAU 20:1, TMS T		0.00	0.00
FAU 20:1, TMS T		0.00	0.00
FAU 20:1, TMS T		0.00	0.00
FAU 20:1, TMS T		0.00	0.00
FAU 20:1, TMS T		0.00	0.00
FAU 20:1, TMS T		0.00	0.00
FAU 22:1, TMS T		0.00	0.00
FAU 22:1, TMS T		0.00	0.00
FAU 22:1, TMS T		0.00	0.00
FAU 22:1, TMS T		0.00	0.00
FAU 22:1, TMS T		0.00	0.00
FAU 22:1, TMS T		0.00	0.00
FAU 22:1, TMS T		0.00	0.00
FAU 22:1, TMS T		0.00	0.00
FAU 22:1, TMS T		0.00	0.00
FAU 24:1, TMS T		0.00	0.00
FAU 24:1, TMS T		0.00	0.00
diFAS 09, TMS T		0.07	0.08
diFAS 10, TMS T		0.35	0.27
diFAS 11, TMS T		0.16	0.17
diFAS 12, TMS T		0.00	0.00
diFAS 13, TMS T		0.00	0.00
diFAS 14, TMS T		0.00	0.00
diFAS 15, TMS T		0.00	0.00
diFAS 16, TMS T		0.00	0.00

Data from Deoxygenation Catalyst Screening in Batch Reactors

Table 60. Mole percent of octanoic acid vs. time for deoxygenation utilizing various catalysts during screening tests in batch reactors

Time				Catalyst Designation*						
	Pd/C 5	Ni/C 31.7	Ni/SiO2 55	Ni/SiAlZrOx 60	Ni/C 2.3	Ni/C 4.6	Ni/C 9.6	Ni/C 15.3	Ni/C 20.3	Ni/C 31.7
(min)										
5.5	20.8 (0.0)	21.1 (1.7)	21.6 (0.2)	22.2 (0.7)	21.4 (0.7)	21.7 (0.2)	20.9 (0.8)	22.2 (0.7)	21.9 (0.1)	21.1 (1.7)
8.5	20.4 (0.1)	19.4 (0.9)	20.9 (0.1)	21.3 (1.3)	20.9 (0.2)	21.1 (0.2)	20.3 (0.6)	20.8 (0.7)	21.0 (0.5)	19.4 (0.9)
11.5	20.0 (0.1)	18.3 (0.9)	20.1 (0.0)	19.0 (2.2)	20.6 (0.4)	20.6 (0.0)	19.5 (0.3)	20.2 (0.5)	19.9 (0.1)	18.3 (0.9)
14.5	19.0 (0.7)	17.2 (0.7)	19.1 (0.1)	17.0 (1.5)	20.2 (0.2)	20.1 (0.1)	19.0 (0.6)	19.4 (0.9)	18.9 (0.1)	17.2 (0.7)
17.5	18.8 (0.8)	16.5 (0.5)	18.5 (0.0)	15.3 (0.6)	20.2 (0.4)	19.7 (0.0)	18.5 (0.7)	18.8 (0.3)	18.2 (0.3)	16.5 (0.5)
20.5	18.8 (0.7)	16.0 (0.4)	17.7 (0.3)	14.5 (1.3)	20.0 (0.2)	19.3 (0.1)	18.0 (0.6)	18.3 (0.6)	17.6 (0.1)	16.0 (0.4)
23.5	18.6 (0.7)	15.5 (0.4)	17.1 (0.3)	13.2 (1.3)	19.9 (0.4)	19.0 (0.1)	17.6 (0.7)	17.9 (0.5)	16.8 (0.6)	15.5 (0.4)
26.5	18.4 (0.7)	15.0 (0.4)	16.5 (0.3)	12.1 (1.0)	19.8 (0.1)	18.8 (0.0)	17.1 (0.7)	17.4 (0.8)	16.4 (0.7)	15.0 (0.4)
29.5	18.3 (0.7)	14.5 (0.4)	15.9 (0.2)	11.4 (0.8)	19.6 (0.1)	18.5 (0.0)	16.8 (0.8)	16.7 (0.5)	15.8 (0.6)	14.5 (0.4)

* Note: data reported in columns are mole percent carboxylic acids, as mean (deviation) of two samples

This appendix contains tabulated values obtained for the gaseous composition from cracking various triglycerides (TAGs) by the tubular cracking reactor (TCR). Samples were produced according to Section 0.

Table 61. Gas phase composition vs. triglyceride type via tubular cracking reactor

Sample	H_2	CO	CO_2	CH_4	C_2H_4	C_2H_6	C_3H_6	C_3H_8	C_4H_X	C_5H_X	C_6H_X	C_7H_X
AA-Soy	0.7(0.1)	15.5(0.7)	33.9(1.1)	3.1(0.1)	2.2(0.1)	7.4(0.5)	4.3(0.3)	7.4(0.6)	12.3(0.4)	8.9(0.5)	3.5(0.3)	1.0(0.1)
BB-VHONO	0.7(0.03)	15.9(0.9)	38.0(1.6)	3.1(0.1)	2.4(0.1)	7.2(0.3)	4.3(0.2)	6.9(0.3)	9.9(0.3)	7.3(0.2)	3.7(0.1)	1.1(0.04)
CC-HENO	0.8(0.04)	16.8(1.6)	38.4(1.7)	3.2(0.1)	2.4(0.1)	7.8(0.2)	4.2(0.1)	7.1(0.1)	9.3(0.1)	6.3(0.05)	3.5(0.04)	0.9(0.02)
DD-Linseed	0.7(0.05)	15.8(0.4)	32.7(0.4)	3.9(0.1)	2.2(0.2)	10.7(1.1)	4.4(0.3)	8.9(1.0)	9.8(0.2)	7.3(0.1)	2.8(0.1)	0.8(0.1)
EE-Camelina	0.7(0.1)	16.3(0.7)	35.0(2.1)	2.9(0.2)	2.2(0.1)	7.2(0.4)	4.4(0.2)	7.1(0.3)	12.0(0.7)	8.1(0.5)	3.2(0.2)	0.9(0.1)
FF-Corn	0.7(0.1)	16.8(0.8)	33.3(0.7)	3.1(0.1)	2.2(0.1)	6.8(0.4)	4.3(0.2)	7.2(0.4)	12.9(0.4)	8.5(0.6)	3.2(0.2)	1.0(0.03)
GG-Cottonseed	0.7(0.03)	16.9(0.8)	35.8(1.9)	2.9(0.2)	2.1(0.1)	6.6(0.1)	4.2(0.1)	6.7(0.1)	12.1(0.6)	8.1(0.6)	3.1(0.3)	0.8(0.1)
HH-Canola	0.7(0.1)	16.4(0.4)	35.9(0.7)	3.2(0.1)	2.2(0.1)	7.5(0.2)	4.6(0.1)	6.8(0.4)	10.8(0.2)	8.0(0.2)	3.4(0.1)	1.2(0.02)

Notes: Data are reported as mean(standard deviation) of an experimental triplicate. Data for II-HONO were not determined.

Table 62. Gas phase composition vs. operating conditions via tubular cracking reactor

Sample	H_2	CO	CO_2	CH_4	C_2H_4	C_2H_6	C_3H_6	C_3H_8	C_4H_X	C_5H_X	C_6H_X	C_7H_X
A-Soy	0.6	17.7	46.1	1.8	2.0	4.9	2.6	4.3	8.4	6.7	2.8	2.0
B-Soy	0.6	17.1	42.2	2.1	2.1	5.5	3.2	5.1	9.2	7.3	2.9	2.5
C-Soy	0.6	16.6	41.5	2.4	2.3	6.0	3.8	5.9	10.0	7.2	2.6	1.1
D-Soy	0.5	17.0	39.0	2.7	1.7	6.6	3.5	6.2	10.6	8.1	3.1	0.9
E-Soy	0.5	16.1	36.4	3.1	1.7	7.4	3.9	7.3	11.2	8.1	3.3	1.0
F-Soy	0.4	14.7	32.9	3.5	1.8	8.0	4.4	8.4	12.2	8.9	3.8	1.1
G-Soy	0.5	18.4	39.9	2.8	1.6	7.2	3.4	6.3	10.0	6.5	2.5	0.7
H-Soy	0.5	17.5	37.6	3.1	1.7	7.3	3.8	6.9	10.4	7.2	3.1	0.9
I-Soy	0.4	16.6	31.8	3.8	1.7	8.4	4.3	8.0	12.1	8.3	3.7	0.9
J-Canola	0.4	19.2	36.5	2.9	2.3	5.3	3.9	4.9	7.7	5.8	2.7	0.7
K-Canola	0.4	17.9	35.9	3.4	1.6	6.4	3.8	6.0	8.4	5.9	2.8	0.9
L-Canola	0.4	18.4	34.8	3.7	1.0	6.6	3.2	6.3	8.8	5.9	2.8	0.9
M-Canola	0.4	17.7	35.5	3.9	0.8	7.3	2.9	7.1	9.3	5.6	2.4	0.6
N-Canola	0.4	15.5	38.5	3.8	0.6	8.3	2.8	8.0	9.0	5.6	2.6	0.8

Appendix D.
Gas Phase Compositional Analysis Details

This appendix provides example chromatograms, calibration plots, and retention time tables for the gas phase analysis.

An example FID chromatogram is shown below. Light gaseous compounds are labeled. Reasonable peak separation is achieved for the majority of components up until C_4H_X. At which point, components are integrated in groups.
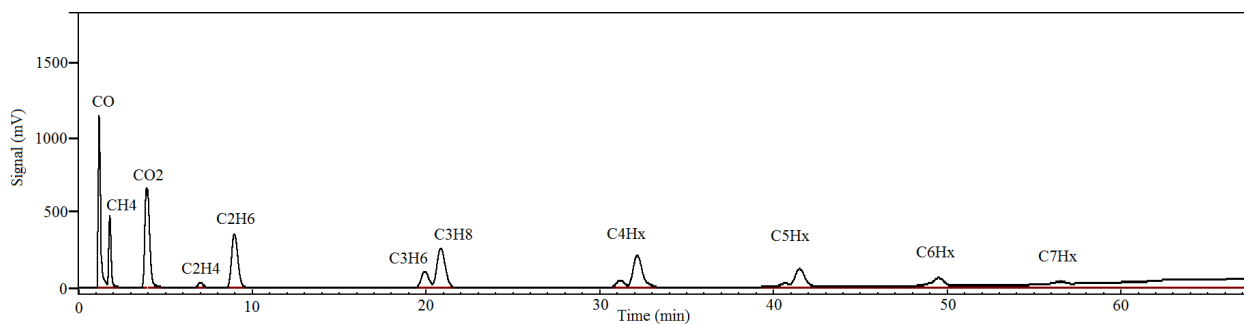
Figure 122. Example FID chromatogram

An example chromatogram for the TCD is shown below. Hydrogen is the only peak quantified by the TCD, due to its absence on the FID detector. Hydrogen is the first peak at 0.8 minutes, quickly followed by the elution of N_2, O_2, and CO, which co-elute.
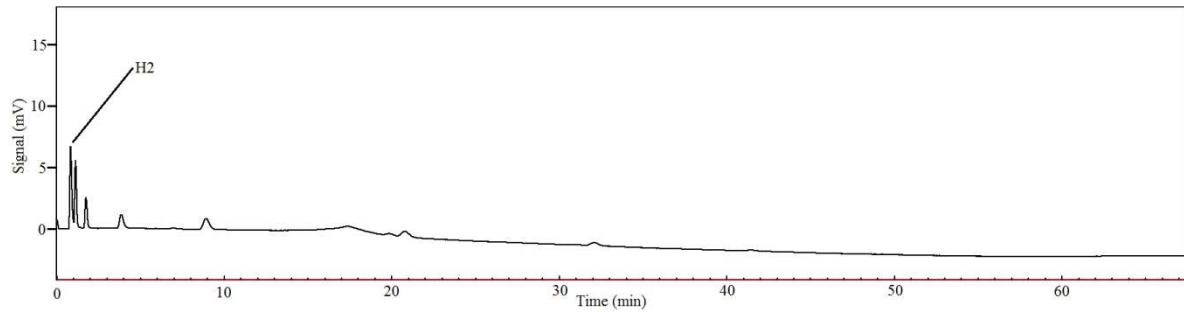
Figure 123. Example TCD chromatogram

The following table described the elution time of the various peaks that are identified in the chromatograms. Hydrogen is reported as the elution time via the TCD, whereas the remainder are reported as the elution time via the FID. The first several peaks are integrated alone, whereas the latter five peaks are integrated as the total of all peaks. This is due to a lack of isomeric separation and identification.

Table 63. Peak elution table for GC-FID/TCD

Analyte	Elution Time (min)
H_2	0.8
CO	1.13
CH_4	1.76
CO_2	3.9
C_2H_4	7.0
C_2H_6	9.0
C_3H_6	19.9
C_3H_8	20.9
C_4H_X	24.0 - 33.0
C_5H_X	33.0 - 43.5
C_6H_X	43.5 - 52.5
C_7H_X	52.5 - 59.1
C_8H_X	59.1 - 66.0

The following plot is a calibration of the FID response verse the microliters injected, normalized to the moles of carbon in each molecule. C_2H_4 calibration was used to quantify all light hydrocarbon components detected by the GC-FID/TCD, whereas CO and CO_2 calibration were used directly for their quantitation.
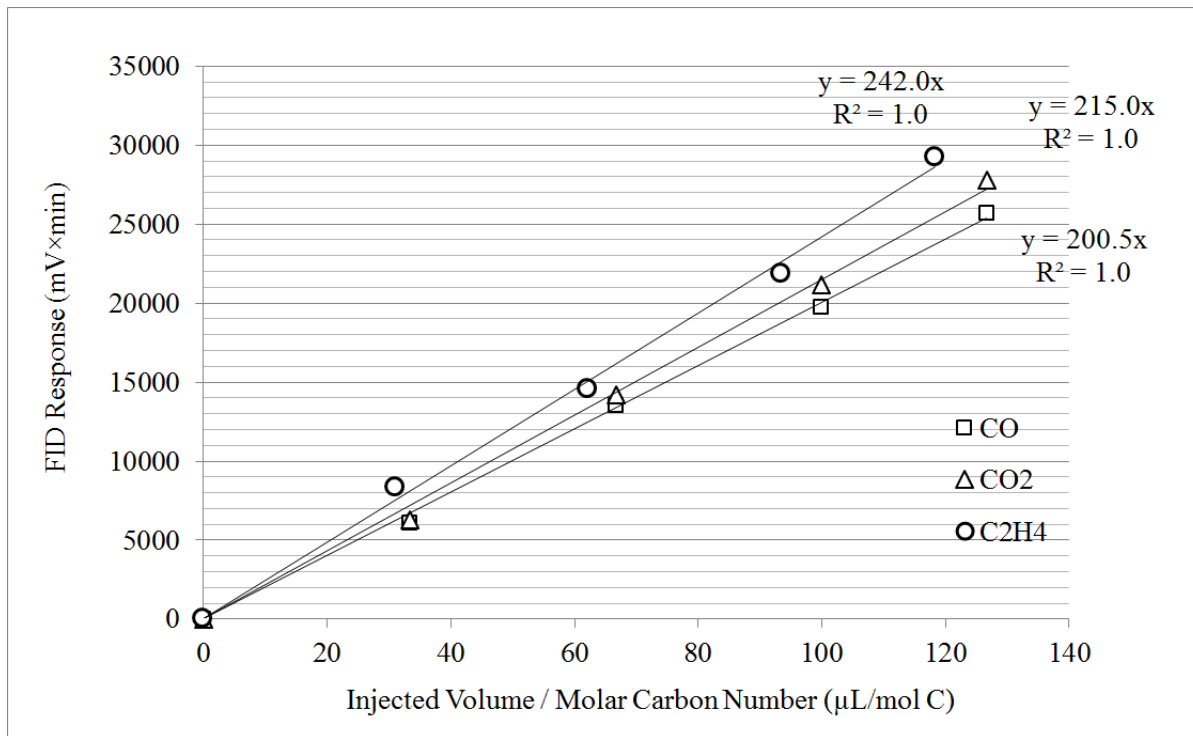
Figure 124. FID calibration plot of light carbonaceous compounds on GC-FID/TCD

The following calibration plot shows the TCD response as a function of the volume of injected hydrogen. Hydrogen was the only component which utilized the TCD response for quantitation.
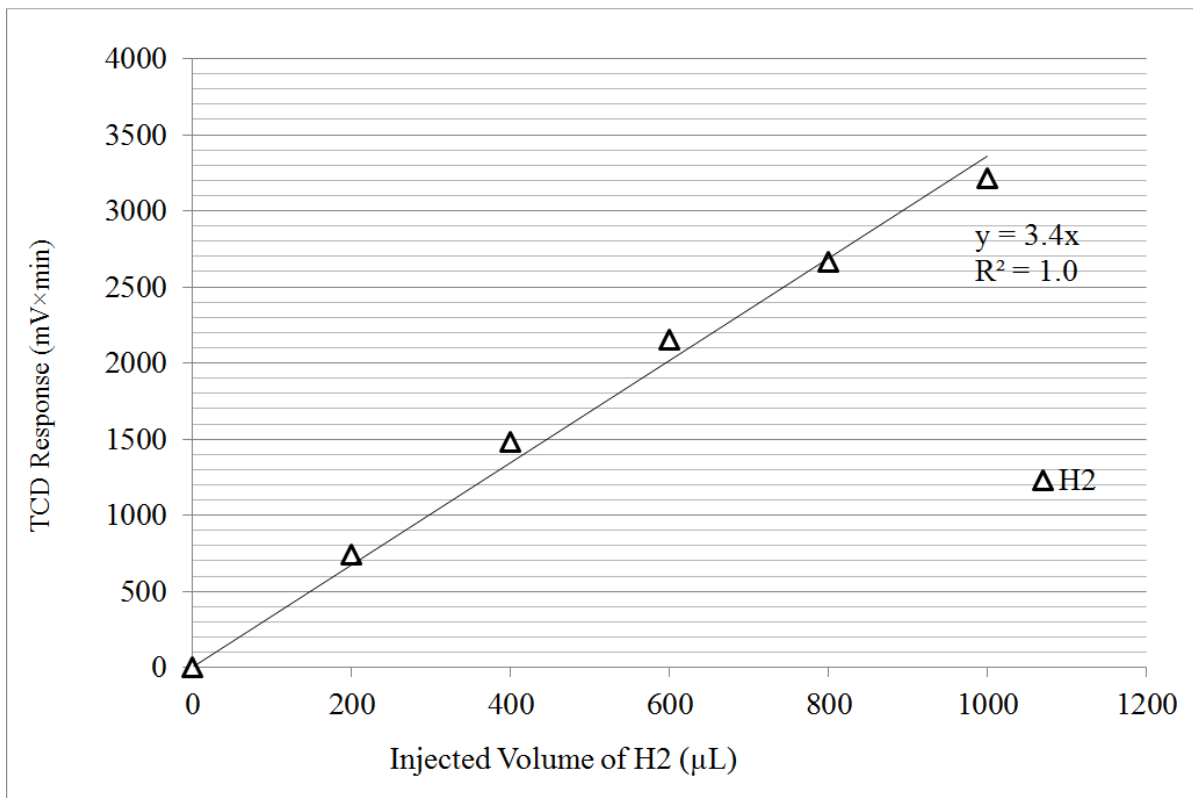
Figure 125. TCD calibration plot of hydrogen on GC-FID/TCD

Appendix E.
FTIR Calibration Spectra

Standards for calibration of the FTIR were prepared as according to Section V.A.5.

The overlaid FTIR absorbance spectra of standards 0 to 35 vol. % octanoic acid in n-decane are depicted in Figure 126 in gray, with darker shades of gray indicating more concentrated standards. The baseline spectra is a blank of the clean ATR trough.

This array of spectra indicated a relatively strong absorbance of the C=O bond at an approximately wavenumber of 1710 cm^{-1} that was relatively isolated from other absorbances. These interpretations of the spectra are in good agreement with the guidelines for interpreting FTIR spectra by Coates.[170] The region of absorbance near 1710 cm^{-1} was used for quantification of carboxylic acids by FTIR throughout this dissertation, and the region has been magnified in the figure due to its importance.

The peak absorbance at wavenumber 1710 ± 2 cm^{-1} was plotted against molar concentrations of carboxylic acid functional groups, depicted in Figure 129. The linear range was acceptable to approximately (35 vol. %) for an absorbance of approximately 3.0 that corresponds to a concentration of 2.23 $mol \cdot L^{-1}$ carboxylic acid functional groups. The molar absorptivity coefficient for carbonyl groups of carboxylic acids was found to be 1.35 $A_{1710}/(mol \cdot L^{-1})$ in this experiment, as indicated in Figure 129. Gray points show standard solutions that are above the linear range and prone to error, where Beer's law does not apply.
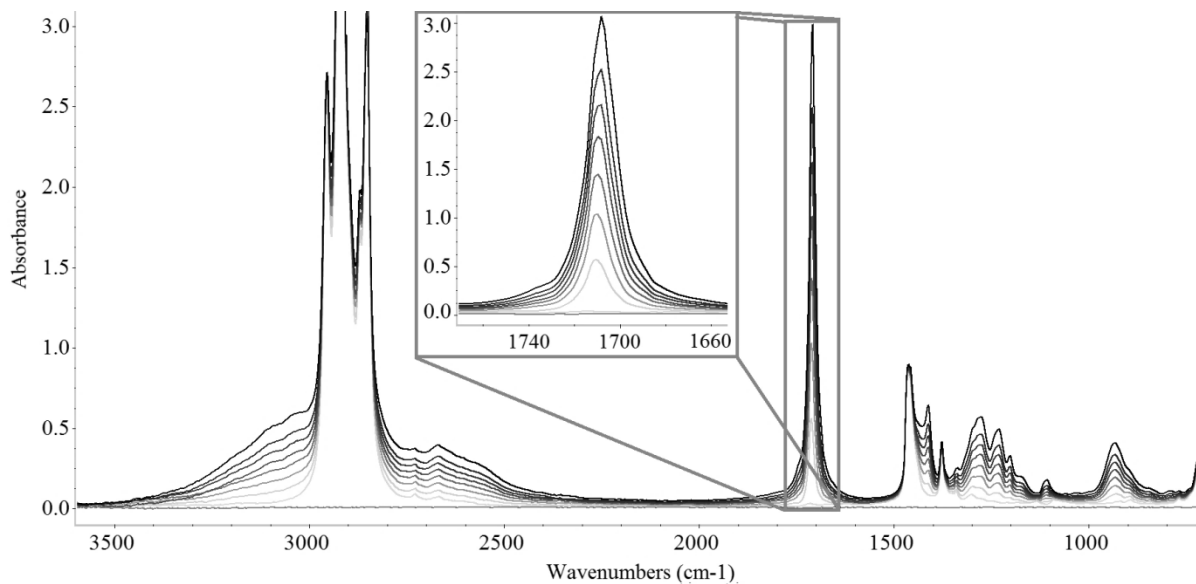
Figure 126. FTIR spectra for calibration solutions of octanoic
acid diluted in n-decane described in the text

The overlaid FTIR absorbance spectra of calibration standards for carboxylic acids and
unreacted triglyceride esters are depicted in Figure 127, with darker shades of color indicating
more concentrated standards. The black spectra is a blank of the clean ATR trough. This array
of spectra indicated relatively strong absorbances for the carboxylic acid C=O bond at 1710 cm^{-1}
wavenumber and for the triglyceride ester C=O bond at 1747 cm^{-1} wavenumber. These intense
and highly localized absorbances are in good agreement with the guidelines for interpreting
FTIR spectra by Coates.[170]
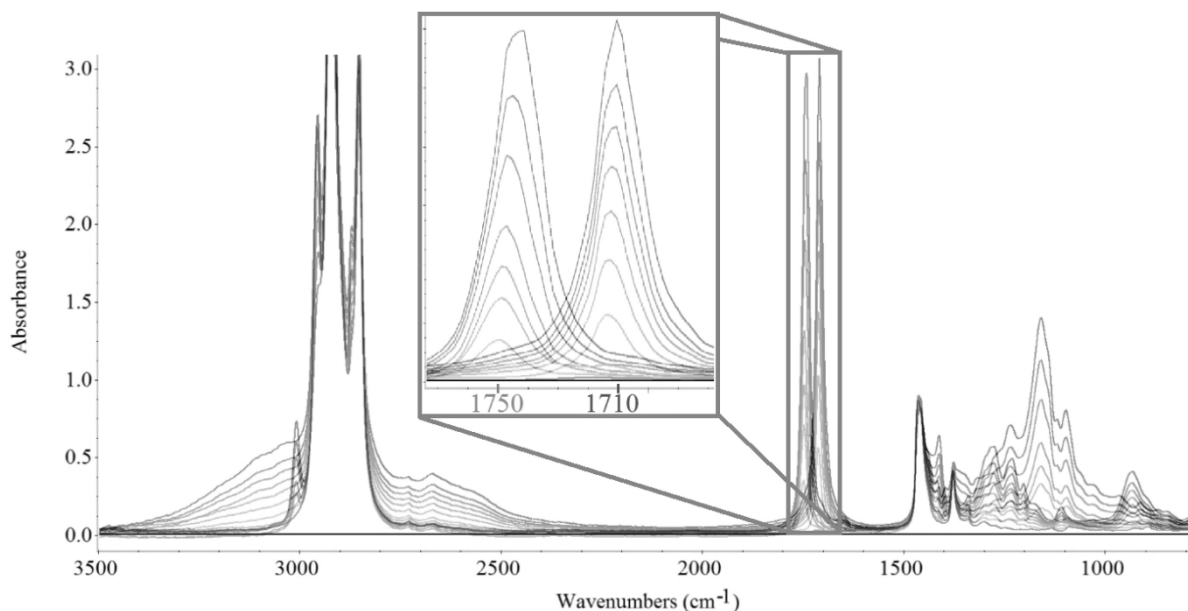
Figure 127. FTIR spectra for calibration solutions of octanoic acid diluted
in n-decane and soybean TAG diluted in n-decane described in the text

Although the valley's between the peaks of these two absorbances overlap, it was possible to intuitively partition the absorbances for CTL assuming that the carboxylic acid absorbance peak is dominant and unaffected by the smaller triglyceride absorbance peak, depicted in Figure 127. The region has been magnified in the figure due to its importance.

The molar absorptivity coefficient for carbonyl groups of TAG ester bonds was found to be 0.98 $A_{1747}/(mol \cdot L^{-1})$ as indicated in Figure 129.

The overlaid FTIR absorbance spectra of standards 0 to 100 wt. % 1-tetradecene in n-dodecane are depicted in Figure 128 in gray, with darker shades of gray indicating more concentrated standards. Olefin spectra were done in reference to a background spectrum using n-dodecane, instead of the clean ATR trough as for carbonyl group absorbance. The bottom spectra is a blank using n-dodecane. The molar absorptivity coefficient for carbonyl groups of

carboxylic acids was found to be 0.21 $A_{1710}/(mol \cdot L^{-1})$ in this experiment, as indicated in Figure 128.
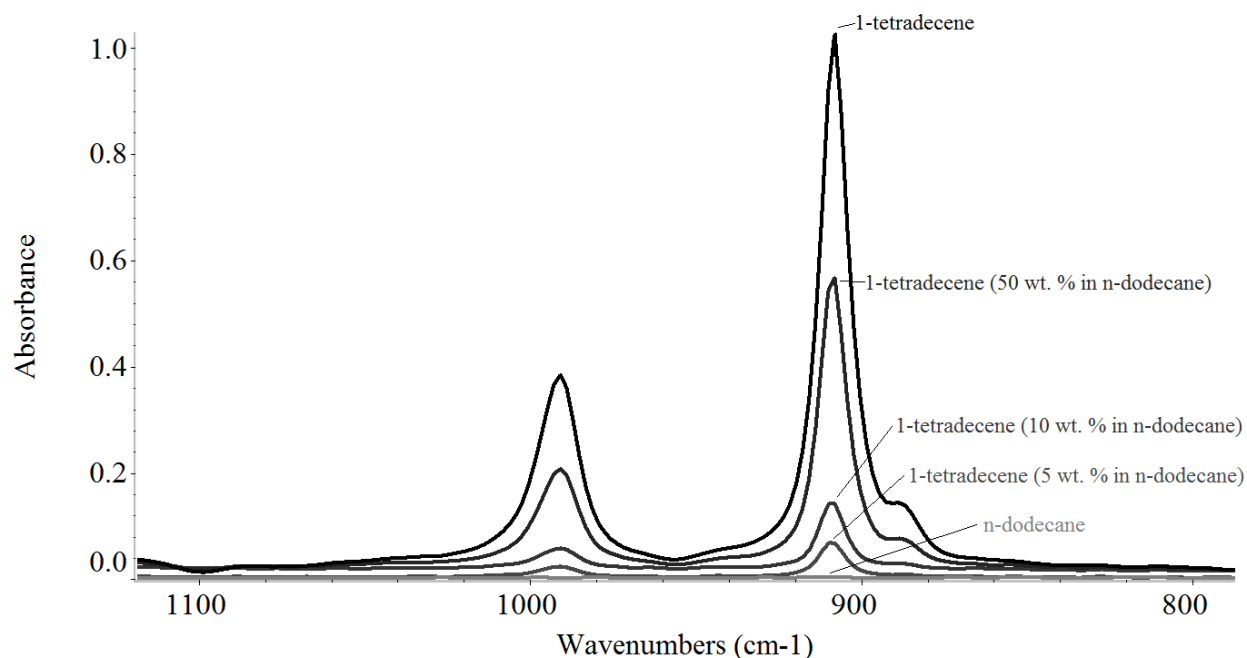
Figure 128. FTIR spectra for calibration solutions of 1-tetradecene diluted in n-dodecane described in the text

The peak absorbance at these wavenumbers were plotted against the molar concentrations of the functional groups, depicted in Figure 129. The linear range was acceptable with minor deviations to approximately 3.0 absorbance units as shown. For this ATR trough, the molar absorptivity coefficient was found to be 1.35 for carboxylic acids and 0.98 for triglyceride esters in units of absorbance units per concentration (mol/L). This was based on the assumption that free fatty acids in the fully refined soybean oil were negligible. Additionally, the calibration for olefin groups (based on 1-tetradecene) indicated a molar absorptivity coefficient of 0.21.
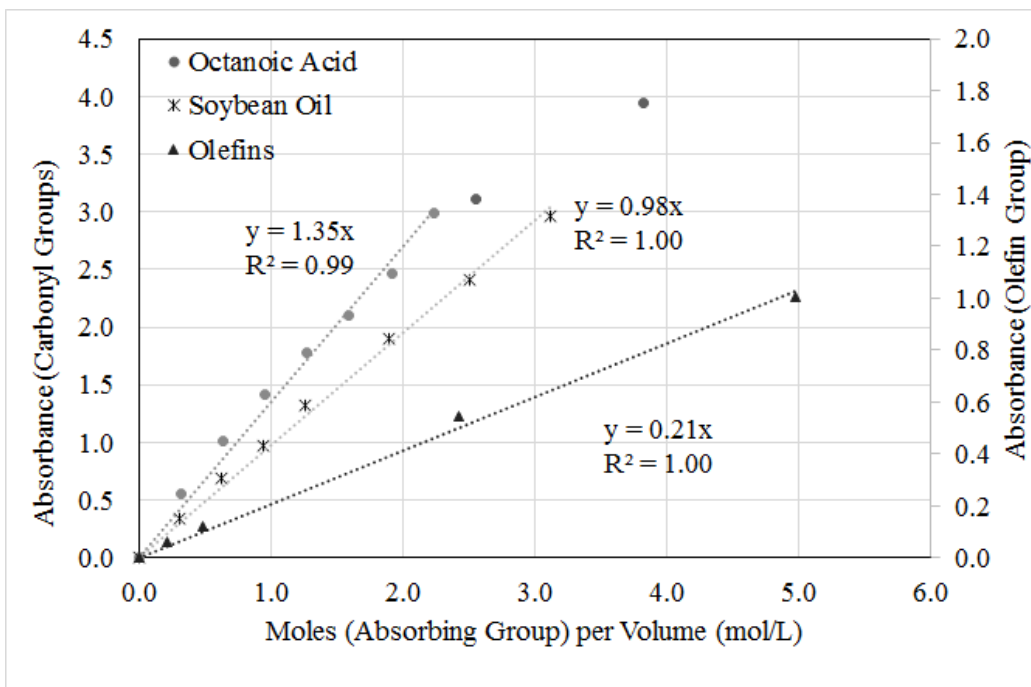
Figure 129. Linear range of FTIR absorbance for carboxylic acids (1710 cm^{-1}),
triglyceride esters (1747 cm^{-1}), and olefin groups (908 cm^{-1})

This appendix contains supplementary information, tables, data, and charts which are important to the FIMSDIST method.

Table 64. Parameters for FIMS boiling point fractions

Temperature (C)	Time (min)	FID Flow (%)
Ambient - 100	0.00 - 3.69	77.5
100 - 150	3.69 - 6.68	77.3
150 - 200	6.68 - 9.81	77.2
200 - 250	9.81 - 13.05	77.0
250 - 300	13.05 - 16.33	76.8
300 - 350	16.33 - 19.65	76.7
350 - 400	19.65 - 22.98	76.5
400 - 450	22.98 - 26.34	76.3
450 - 500	26.34 - 29.77	76.2
500 - 550	29.77 - 33.33	76.0
550 - 600	33.33 - 37.21	75.8
600 - 650	37.21 - 41.79	75.7
650 - Residual	41.79 - 75.00	75.6

Table 65. Exact masses for solvents and the internal standard

Carbon Disulfide		Dichloromethane		2-Bromobutane	
m/z	Abundance	*m/z*	Abundance	*m/z*	Abundance
75.944	100.0	83.953	100.0	57.070	100.0
77.940	9.1	85.950	63.9	58.074	4.4
76.945	2.7	84.957	1.1	59.077	0.1
78.942	0.2	86.954	0.7	60.081	0.0

Table 66. Analytical Standard 'STDx56' for D-FIMS and FIMSDIST

Type	Reagent	Exact Mass	Mass Percent	Vendor	Purity
Solvent	Dichloromethane	(multiple)	85.7%	Omnisolve	99.9
Paraffin	Pentane	72.094	0.13%	Aldrich	98
Paraffin	Hexane	86.110	0.20%	Aldrich	99
Paraffin	Heptane	100.125	0.22%	Acros	99
Paraffin	Octane	114.141	0.22%	Fluka	99
Paraffin	Nonane	128.157	0.22%	Lancaster	99
Paraffin	Decane	142.172	0.27%	Acros	99
Paraffin	Undecane	156.188	0.23%	TCI	99
Paraffin	Dodecane	170.203	0.23%	Fluka	-
Paraffin	Tridecane	184.219	0.23%	Fluka	-
Paraffin	Tetradecane	198.235	0.24%	Fluka	-
Paraffin	Pentadecane	212.250	0.24%	Fluka	-
Paraffin	Hexadecane	226.266	0.24%	Fluka	99.8
Paraffin	Heptadecane	240.282	0.30%	K&K	99
Paraffin	Octadecane	254.297	0.37%	Fluka	-
Paraffin	Nonadecane	268.313	0.25%	Alfa Aesar	99
Paraffin	Eicosane	282.329	0.27%	Acros	99
Paraffin	Tricosane	324.376	0.26%	K&K	-
Olefin	1-Hexene	84.094	0.20%	Fluka	99.8
Olefin	1-Octene	112.125	0.22%	Aldrich	98
Olefin	1-Nonene	126.141	0.23%	Aldrich	-
Olefin	1-Undecene	154.172	0.23%	Aldrich	-
Olefin	1-Dodecene	168.188	0.24%	TCI	93
Olefin	1-Tridecene	182.203	0.24%	K&K	-
Olefin	1-Tetradecene	196.219	0.24%	K&K	-
Olefin	1-Pentadecene	210.235	0.24%	K&K	-
Olefin	1-Hexadecene	224.250	0.24%	K&K	-
Olefin	1-Heptadecene	238.266	0.25%	K&K	-
Olefin	1-Octadecene	252.282	0.24%	Fluka	99.5
Olefin	1-Nonadecane	266.297	0.33%	K&K	-
Olefin	1-Eicosene	280.313	0.31%	K&K	-
Aromatic	Benzene	78.047	0.27%	Aldrich	99
Aromatic	Toluene	92.063	0.27%	Aldrich	99
Aromatic	Ethylbenzene	106.078	0.27%	Aldrich	99
Aromatic	Butylbenzene	134.110	0.27%	Aldrich	99
Aromatic	Hexylbenzene	162.141	0.27%	Fluka	98
Aromatic	Octylbenzene	190.172	0.26%	Aldrich	98
Aromatic x2	Naphthalene	128.063	0.21%	Aldrich	98
Aromatic x3	Anthracene	178.078	0.19%	Fluka	99
Aromatic x4	Pyrene	202.078	0.17%	Fluka	99
Carboxylic Acid	Acetic Acid	60.021	0.33%	Fisher	100
Carboxylic Acid	Propanoic Acid	74.037	0.31%	Aldrich	99.5
Carboxylic Acid	Butyric Acid	88.052	0.30%	Acros	99
Carboxylic Acid	Pentanoic Acid	102.068	0.29%	Acros	99
Carboxylic Acid	Hexanoic Acid	116.084	0.22%	Aldrich	98
Carboxylic Acid	Heptanoic Acid	130.099	0.29%	Aldrich	99
Carboxylic Acid	Octanoic Acid	144.115	0.29%	Acros	99
Carboxylic Acid	Nonanoic Acid	158.131	0.28%	Fluka	-
Carboxylic Acid	Decanoic Acid	172.146	0.26%	Acros	99
Carboxylic Acid	Undecanoic Acid	186.162	0.26%	Acros	99
Carboxylic Acid	Dodecanoic Acid	200.178	0.44%	Alfa Aesar	99.5
Carboxylic Acid	Tetradecanoic Acid	228.209	0.30%	Fluka	-
Carboxylic Acid	Hexadecanoic Acid	256.240	0.24%	Acros	90
Carboxylic Acid	Octadecanoic Acid	284.272	0.25%	Acros	91
Carboxylic Acid	Eicosanoic Acid	312.303	0.27%	Acros	99
Carboxylic Acid	Docosanoic Acid	340.334	0.24%	Aldrich	99
Carboxylic Acid	Tetracosanoic Acid	368.365	0.27%	Acros	99

Figure 130. Mass spectrum of hydrocarbon window defining standard
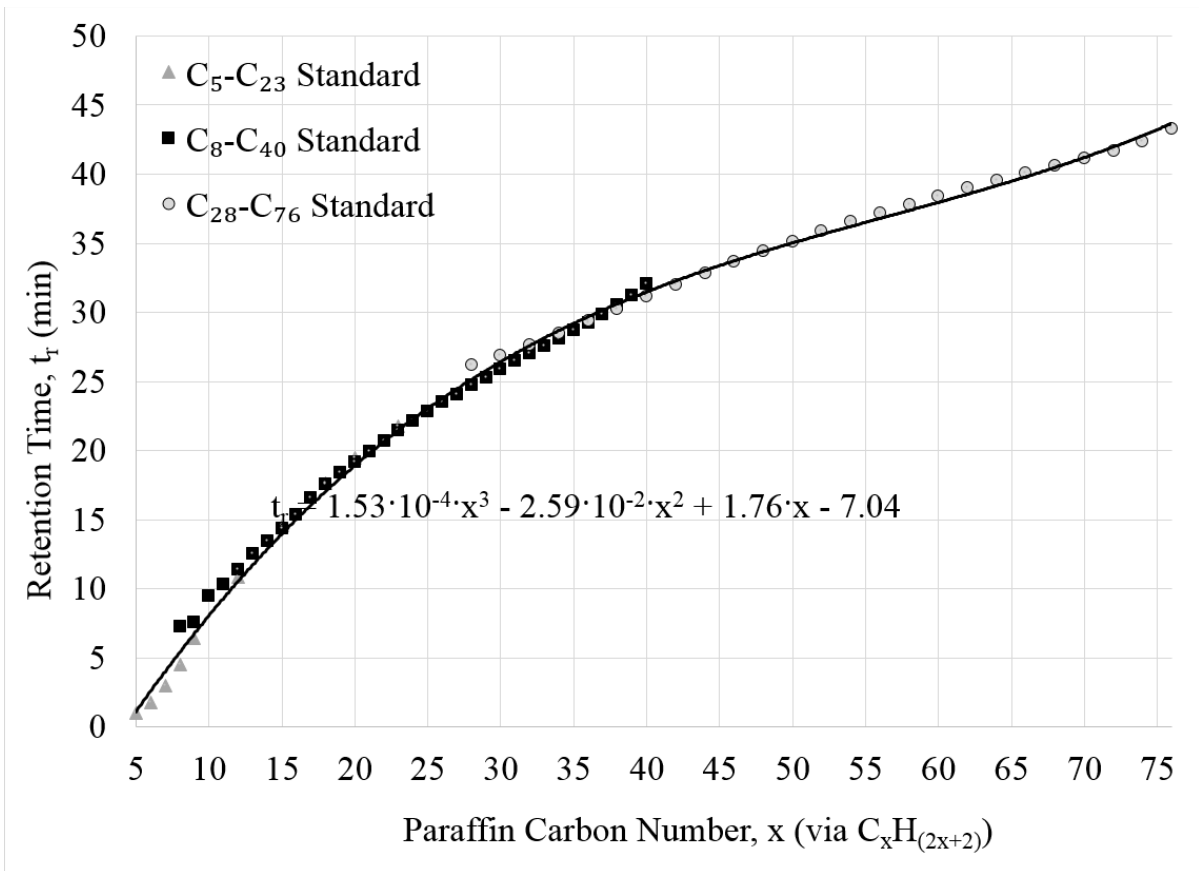
Figure 131. Linearity of elution during FIMSDIST analysis

481
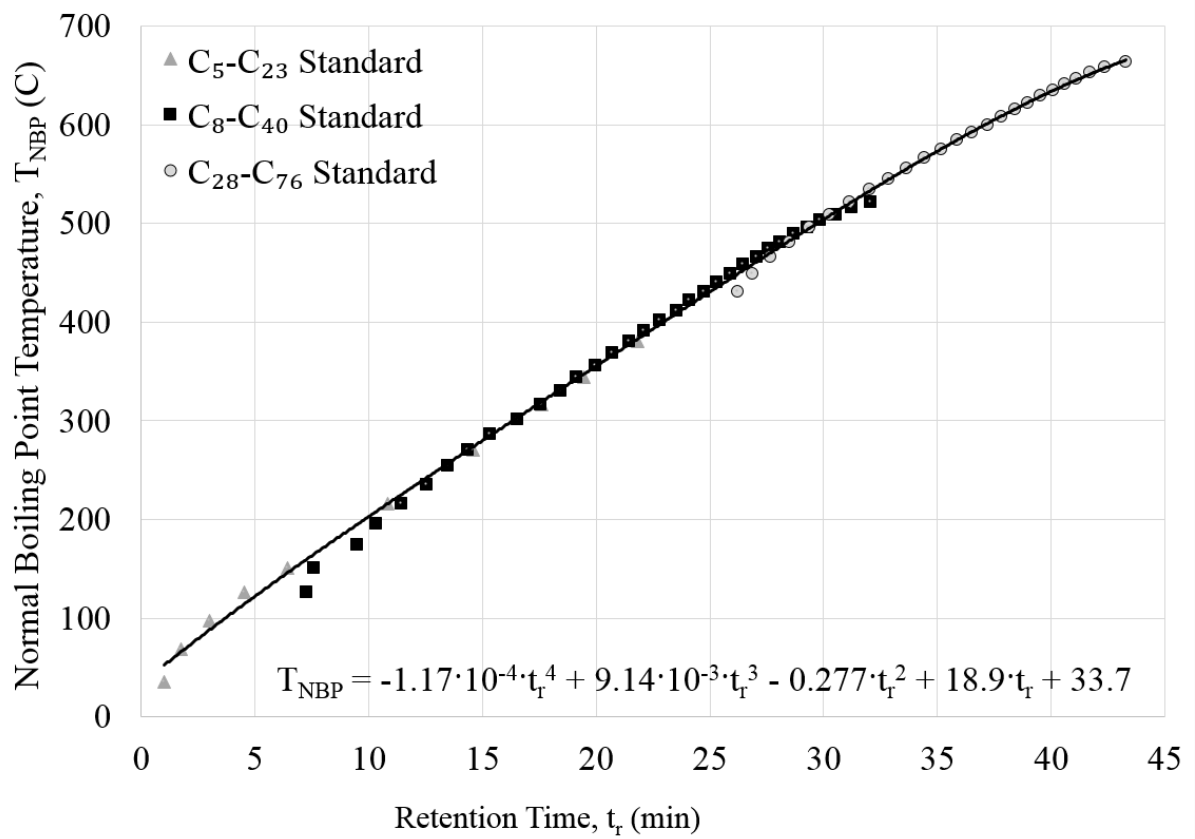
Figure 132. Correlating between normal boiling point temperature and retention time

Appendix G.
Comparison of Literature Reported Acid Composition of Cracked TAGs to FIMSDIST

This appendix contains a comparison of the acid compositions from CTL derived from six different types of TAGs. The CTLs were produced during this study according to Section 0, but they acid compositions were determined by Geetla.[156] The CTL samples were derived from Soybean TAG, Canola TAG, Linseed TAG, Corn TAG, Cottonseed TAG, Camelina TAG, and High Oleic Novelty Oil (HONO) TAG, and the literature reported carboxylic acid composition are tabulated in this appendix and graphically compared to the values found in the present work via the FIMSDIST method.
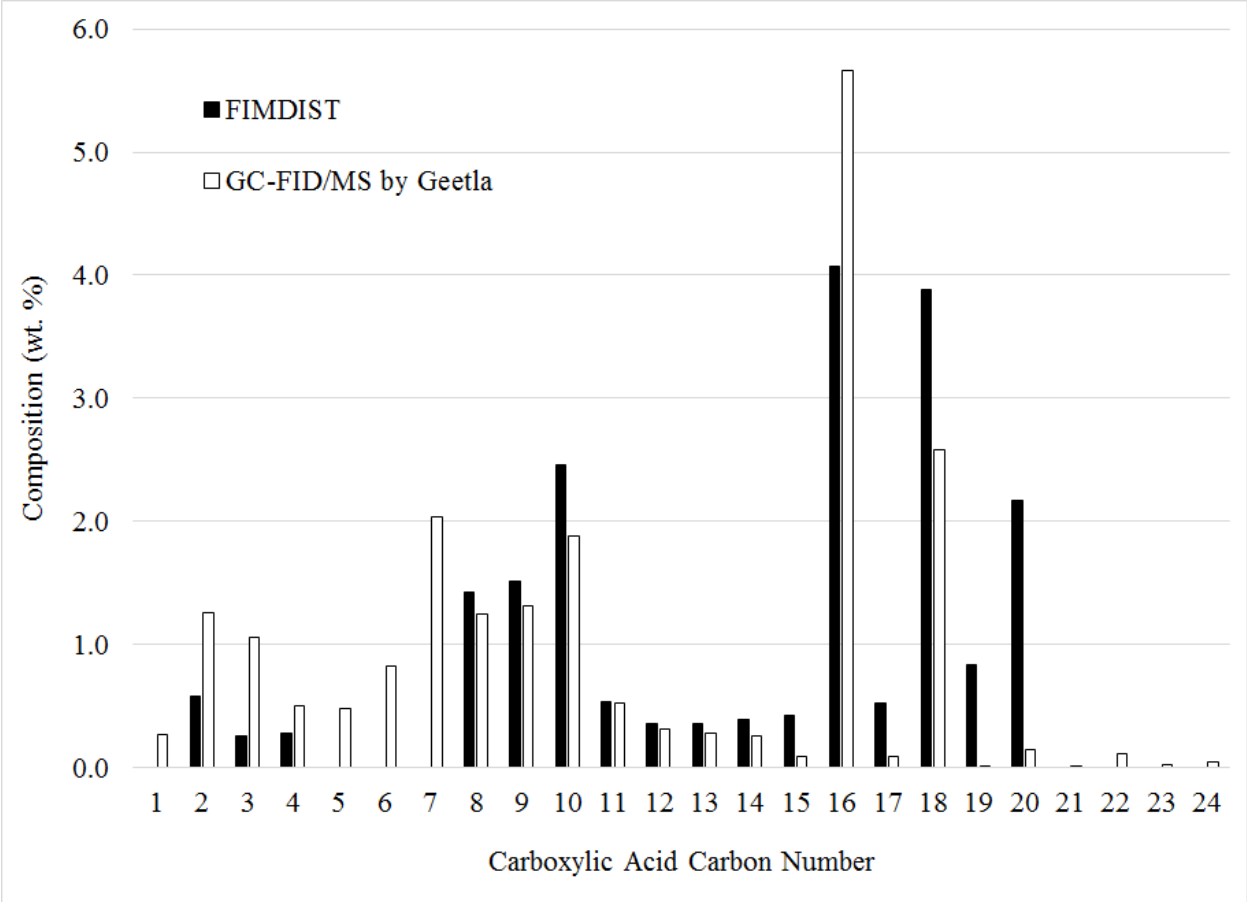
Figure 133. AA-Soy CTL acid composition compared to literature data
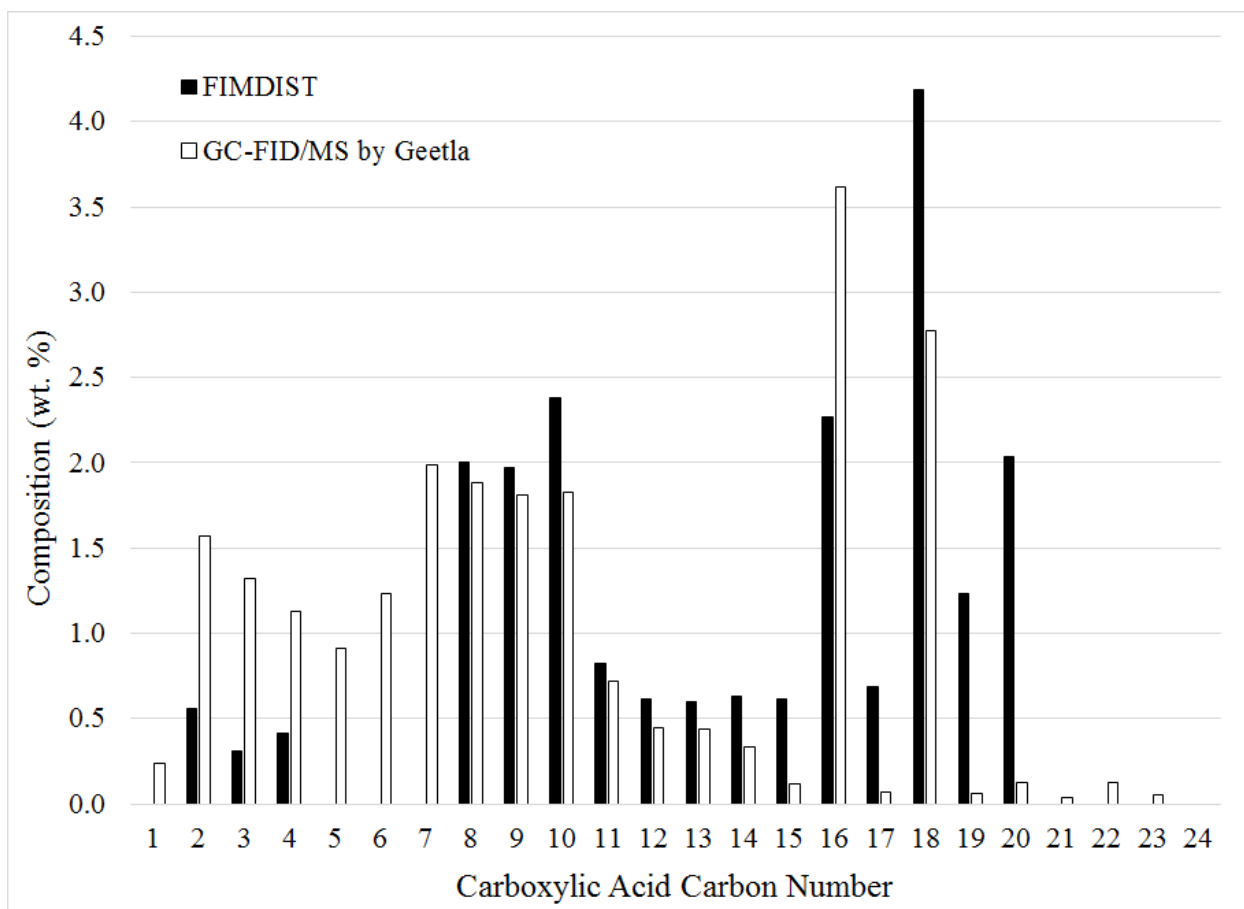
Figure 134. DD-Linseed CTL acid composition compared to literature data
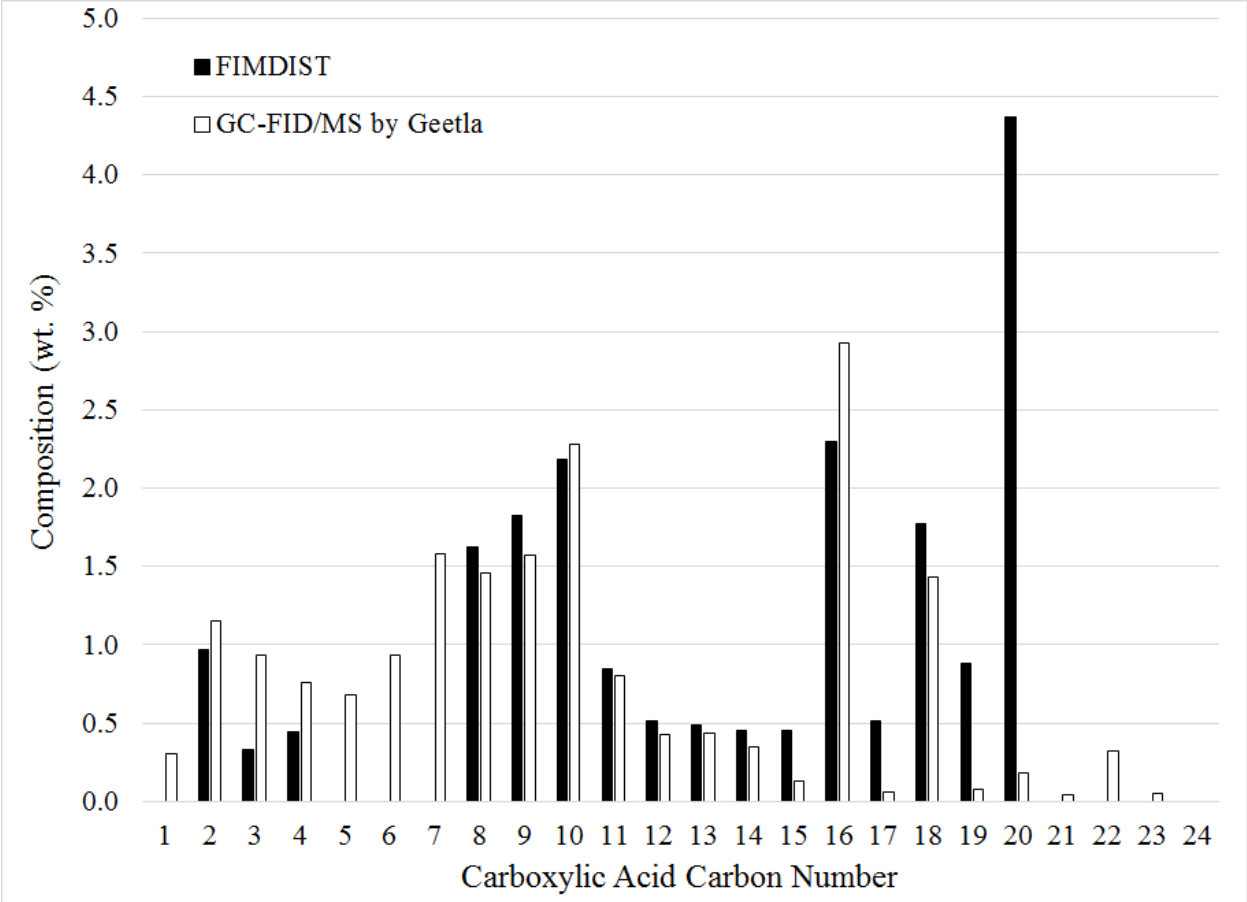
Figure 135. EE-Camelina CTL acid composition compared to literature data
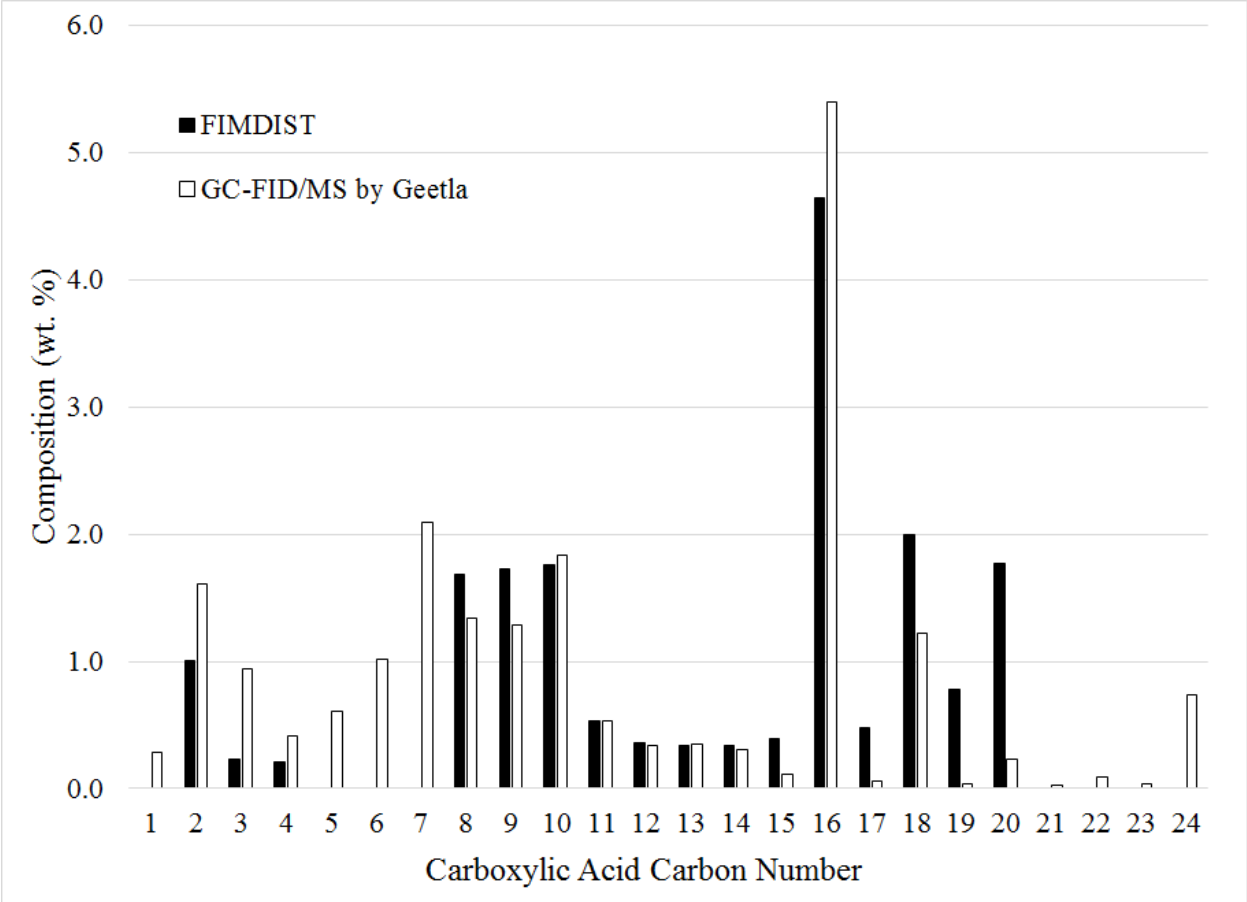
Figure 136. FF-Corn CTL acid composition compared to literature data
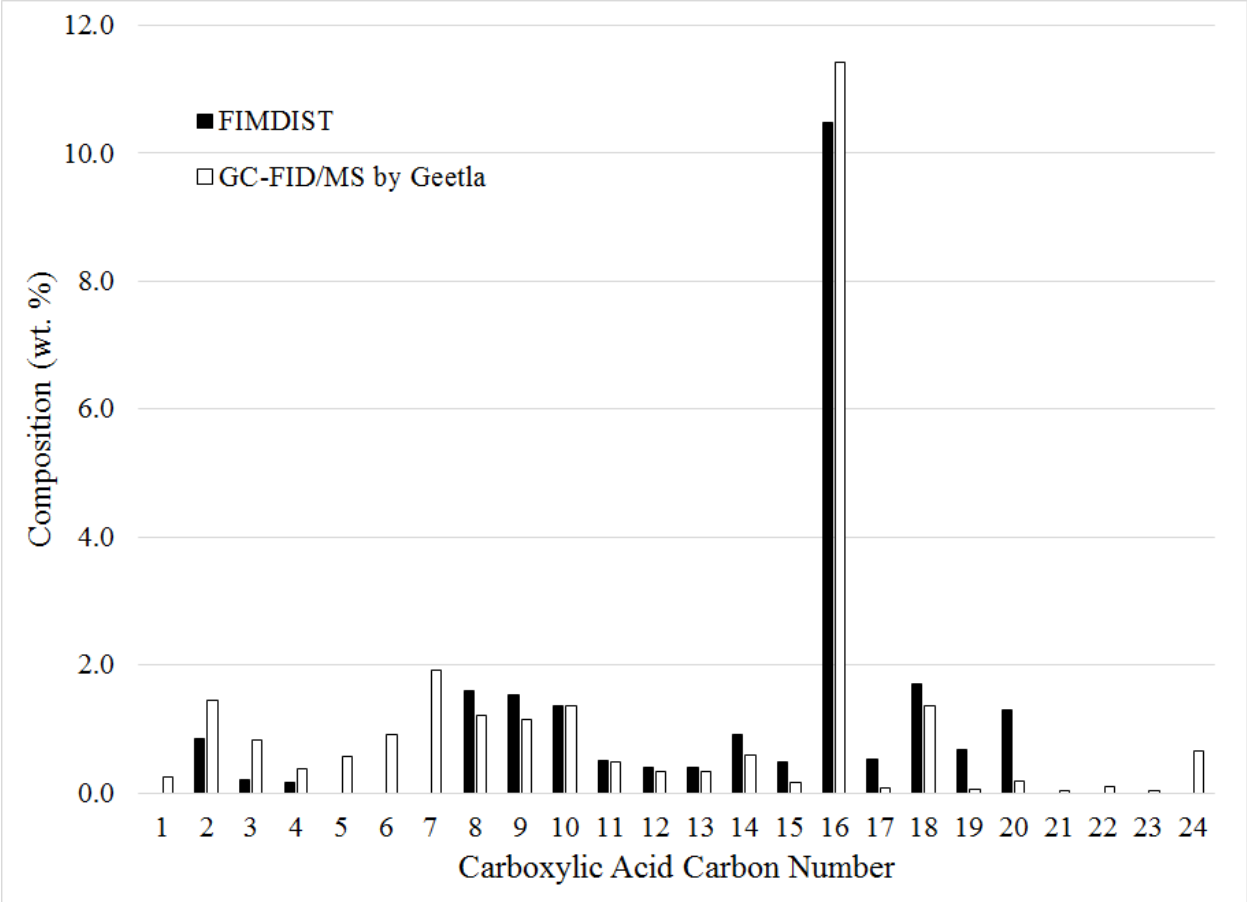
Figure 137. GG-Cottonseed CTL acid composition compared to literature data
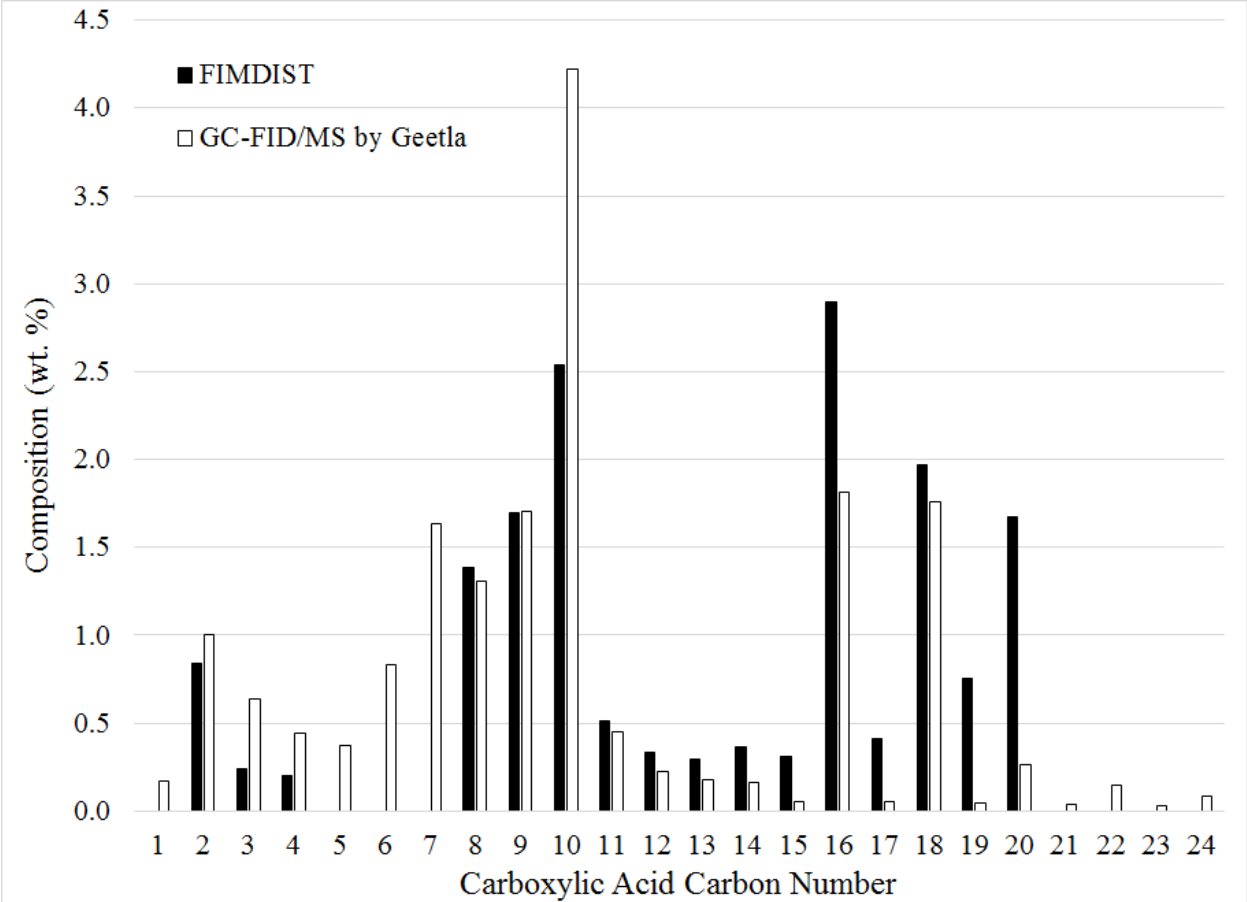
Figure 138. HH-Canola CTL acid composition compared to literature data
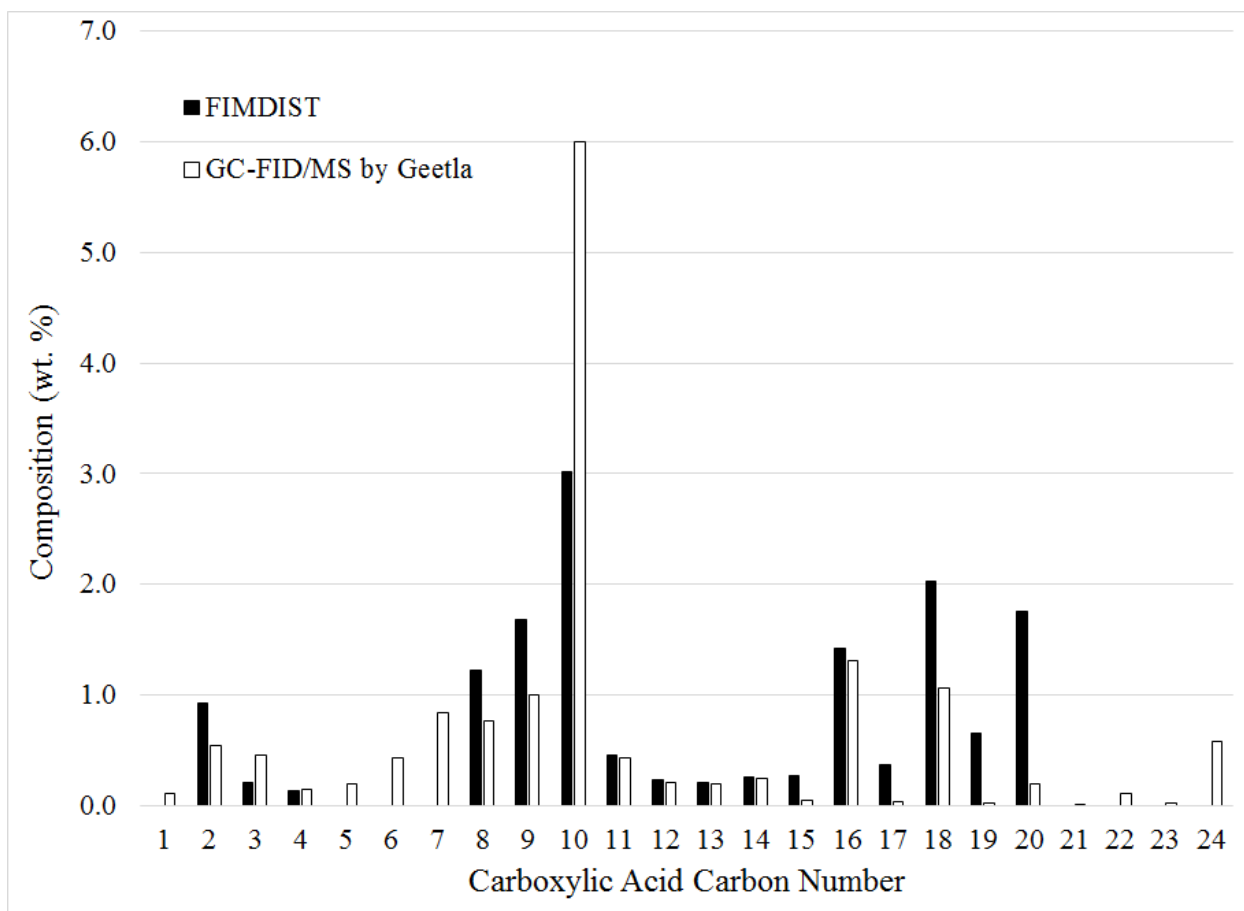
Figure 139. II-HONO CTL acid composition compared to literature data

The following is a table of the mass concentrations of various carboxylic acids determined by Geetla[156], having been converted from mol % to mass % through normalizing the mass % data to the composition of carboxylic acids confidently determined by FIMSDIST (i.e., the sum of C2-C4 and C8-C18 carboxylic acids). C5-C7 and C1 data was taken from this table and utilized to fill gaps in the CTL composition produced from the TAGs listed below. Data are reported as the weight percent of carboxylic acids.

Table 67. Saturated carboxylic acids composition in CTL by detailed characterization

C#	AA-Soy	DD-Linseed	EE-Camelina	FF-Corn	GG-Cottonseed	HH-Canola	II-HONO
1	0.28	0.29	0.31	0.24	0.25	0.17	0.11
2	1.26	1.60	1.15	1.57	1.44	1.00	0.54
3	1.06	0.94	0.94	1.32	0.83	0.63	0.46
4	0.51	0.41	0.76	1.13	0.37	0.44	0.15
5	0.49	0.61	0.68	0.91	0.56	0.37	0.20
6	0.83	1.02	0.93	1.23	0.92	0.83	0.43
7	2.03	2.09	1.58	1.99	1.92	1.63	0.84
8	1.25	1.34	1.46	1.88	1.20	1.30	0.76
9	1.31	1.28	1.57	1.81	1.15	1.70	1.00
10	1.88	1.84	2.28	1.83	1.35	4.22	5.99
11	0.53	0.53	0.80	0.72	0.48	0.45	0.42
12	0.32	0.34	0.43	0.45	0.33	0.22	0.21
13	0.28	0.35	0.43	0.44	0.33	0.18	0.19
14	0.26	0.30	0.35	0.33	0.59	0.16	0.24
15	0.09	0.12	0.13	0.12	0.15	0.06	0.05
16	5.66	5.40	2.93	3.62	11.42	1.81	1.31
17	0.09	0.06	0.06	0.07	0.08	0.05	0.03
18	2.59	1.22	1.43	2.77	1.36	1.76	1.06
19	0.02	0.04	0.07	0.06	0.04	0.05	0.03
20	0.15	0.23	0.18	0.13	0.18	0.26	0.20
21	0.01	0.03	0.04	0.04	0.03	0.04	0.02
22	0.12	0.09	0.32	0.12	0.10	0.14	0.11
23	0.02	0.03	0.05	0.05	0.04	0.03	0.02
24	0.05	0.73	0.00	0.00	0.66	0.09	0.59

This appendix contains the boiling point fractions (BPFs) from various samples that were

analyzed by the FIMSDIST method. Samples are labeled according to their sample name.

Operating parameters used to generate these samples are described in 0 (see Table 24).

Table 68. Boiling point fractions from FID data of FIMSDIST for CTLs
from the cracking of various TAGs in the 100 mL lab-scale TCR

BPF		AA-Soy	BB-VHONO	CC-HENO	DD-Linseed	EE-Camelina	FF-Corn	GG-Cottonseed	HH-Canola	II-HONO
0-100	~ wt. %	0.3	0.2	0.3	0.2	2.5	3.1	1.6	2.8	2.7
100-150		3.3	2.7	2.9	3.3	5.7	5.8	5.7	5.2	5.9
150-200		4.8	4.8	4.7	5.8	5.7	4.7	4.4	4.9	4.9
200-250		8.2	6.2	6.0	8.8	7.5	7.3	7.0	6.7	6.2
250-300		13.2	11.9	10.4	13.6	11.0	10.7	10.7	10.8	10.3
300-350		12.6	14.2	13.2	13.3	12.3	10.6	9.7	11.9	12.3
350-400		17.8	13.9	12.5	13.4	12.5	14.4	18.3	13.2	11.7
400-450		16.5	20.6	18.6	17.1	16.0	16.5	16.2	17.7	19.1
450-500		10.9	10.9	14.5	10.3	10.4	10.4	10.2	10.4	10.5
500-550		7.5	8.2	8.5	7.4	7.6	7.7	7.6	7.7	7.7
550-600		3.7	4.2	5.0	4.1	4.5	4.5	4.5	4.5	4.5
600-650		0.6	1.3	1.9	1.6	2.8	2.8	2.8	2.8	2.8
>650		0.7	0.9	1.4	1.1	1.5	1.6	1.4	1.5	1.5

Table 69. Boiling point fractions from FID data of FIMSDIST for CTLs from cracking soybean
TAG under various operating temperatures and space times in the 100 mL lab-scale TCR

BPF		A-Soy	B-Soy	C-Soy	D-Soy	E-Soy	F-Soy	G-Soy	H-Soy	I-Soy
0-100	~ wt. %	1.6	2.5	2.8	3.2	4.6	4.8	3.3	4.3	5.7
100-150		3.2	3.9	4.6	5.3	7.1	6.8	5.7	7.0	8.0
150-200		3.2	3.6	4.4	4.8	6.8	6.9	5.4	6.6	8.4
200-250		5.2	5.8	6.6	7.3	9.7	9.7	7.9	9.3	11.6
250-300		7.9	9.0	10.1	11.0	13.6	13.5	12.0	13.1	15.4
300-350		7.8	9.3	10.1	10.9	13.2	12.8	11.8	13.1	14.6
350-400		13.3	14.4	14.0	13.7	13.1	13.2	13.5	13.2	13.0
400-450		18.0	19.1	17.3	15.4	12.1	12.1	14.5	12.4	10.1
450-500		10.3	11.0	10.5	10.3	8.1	8.0	9.6	8.2	6.1
500-550		9.5	8.3	8.3	7.9	5.6	5.7	7.2	5.9	3.7
550-600		7.3	5.5	5.4	5.0	3.3	3.4	4.4	3.5	1.9
600-650		6.8	4.3	3.7	3.4	1.9	2.2	2.8	2.1	1.1
>650		5.8	3.3	2.2	1.9	1.0	1.1	1.7	1.3	0.5

Table 70. Boiling point fractions from FID data of FIMSDIST for CTLs from the cracking of canola TAG under various operating pressures on the 200 mL lab-scale TCR

BPF		J-Canola	K-Canola	L-Canola	M-Canola	N-Canola
0-100	~ wt. %	8.4	9.6	9.9	10.4	10.2
100-150		8.8	10.8	11.1	11.0	11.6
150-200		9.6	11.3	11.8	11.9	12.1
200-250		12.9	14.5	14.5	14.4	15.0
250-300		21.6	22.4	21.7	21.2	21.6
300-350		21.8	17.8	17.1	16.6	16.2
350-400		10.9	7.7	7.4	7.5	6.5
400-450		3.2	2.7	2.9	3.0	2.9
450-500		1.4	1.4	1.6	1.8	1.8
500-550		0.7	0.8	1.0	1.1	1.1
550-600		0.4	0.5	0.6	0.7	0.6
600-650		0.2	0.2	0.3	0.3	0.3
>650		0.1	0.2	0.2	0.2	0.2

Appendix I.
Mass-Adjusted FIMS Response Carbon Number Distributions

This appendix contains mass-adjusted FIMS response carbon number distributions determined by FIMSDIST in this study ranging from C1-C30 for various CTLs that were produced and not included in the text.
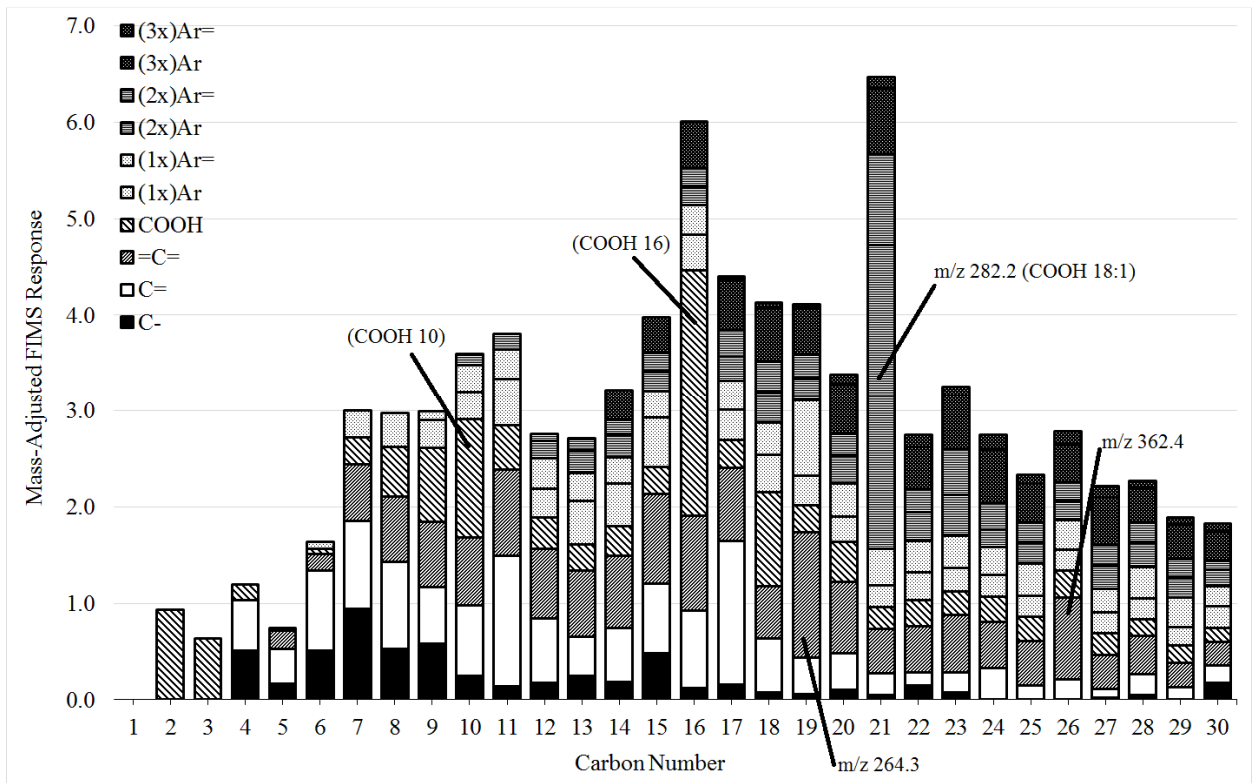
Figure 140. CND (1-30) of HH-Canola CTL, mass adjusted FIMS response
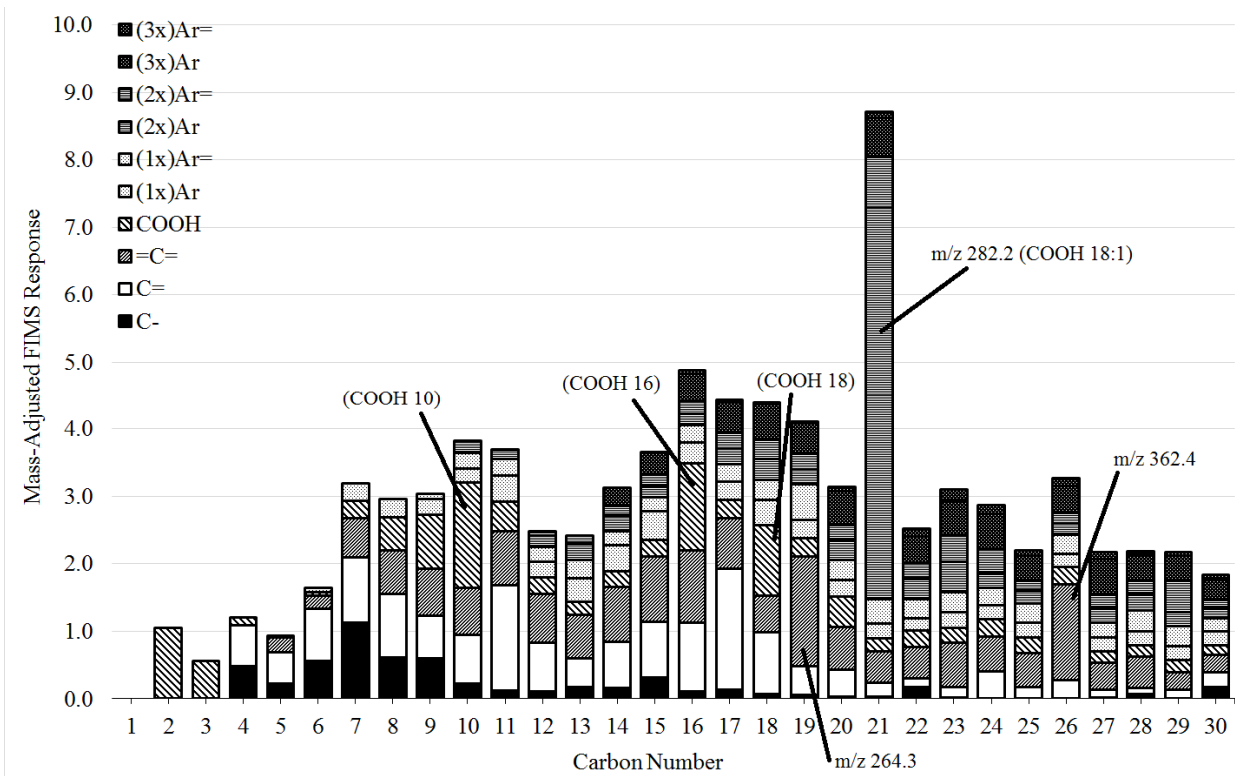
Figure 141. CND (1-30) of II-HONO CTL, mass adjusted FIMS response
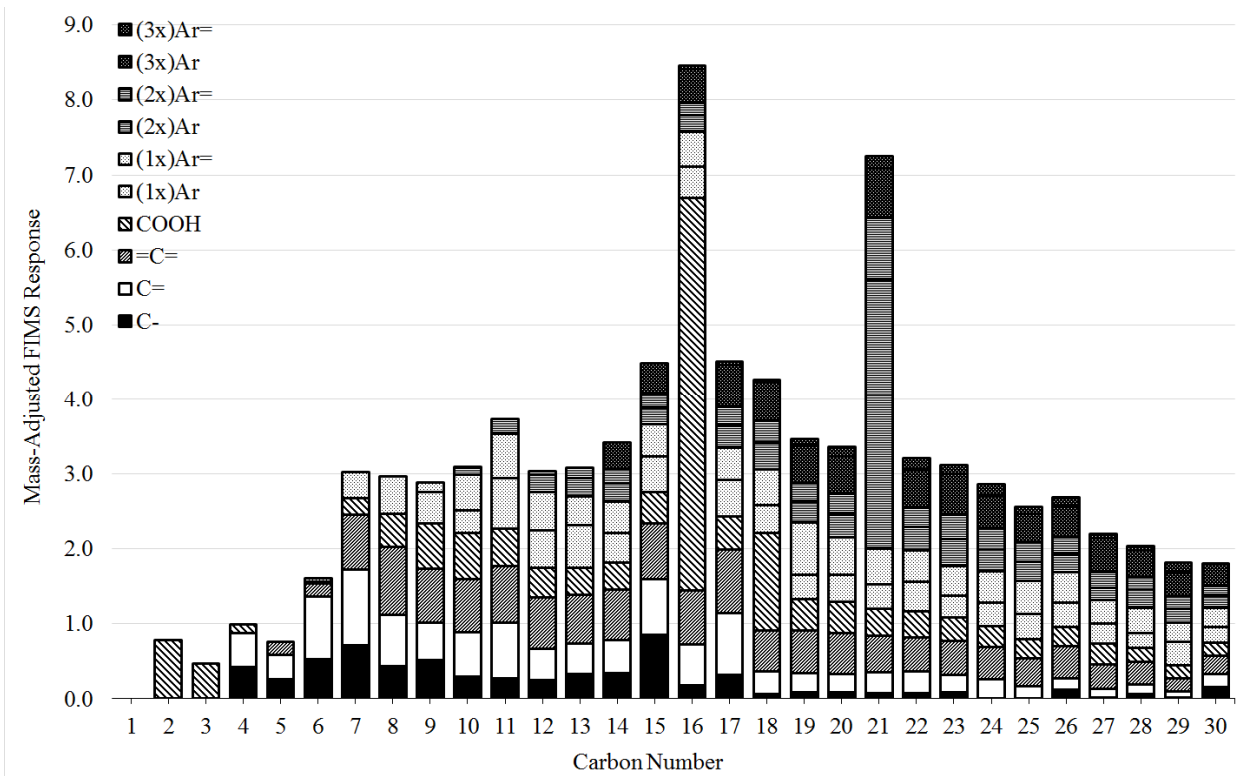
Figure 142. CND (1-30) of D-Soy CTL, mass adjusted FIMS response
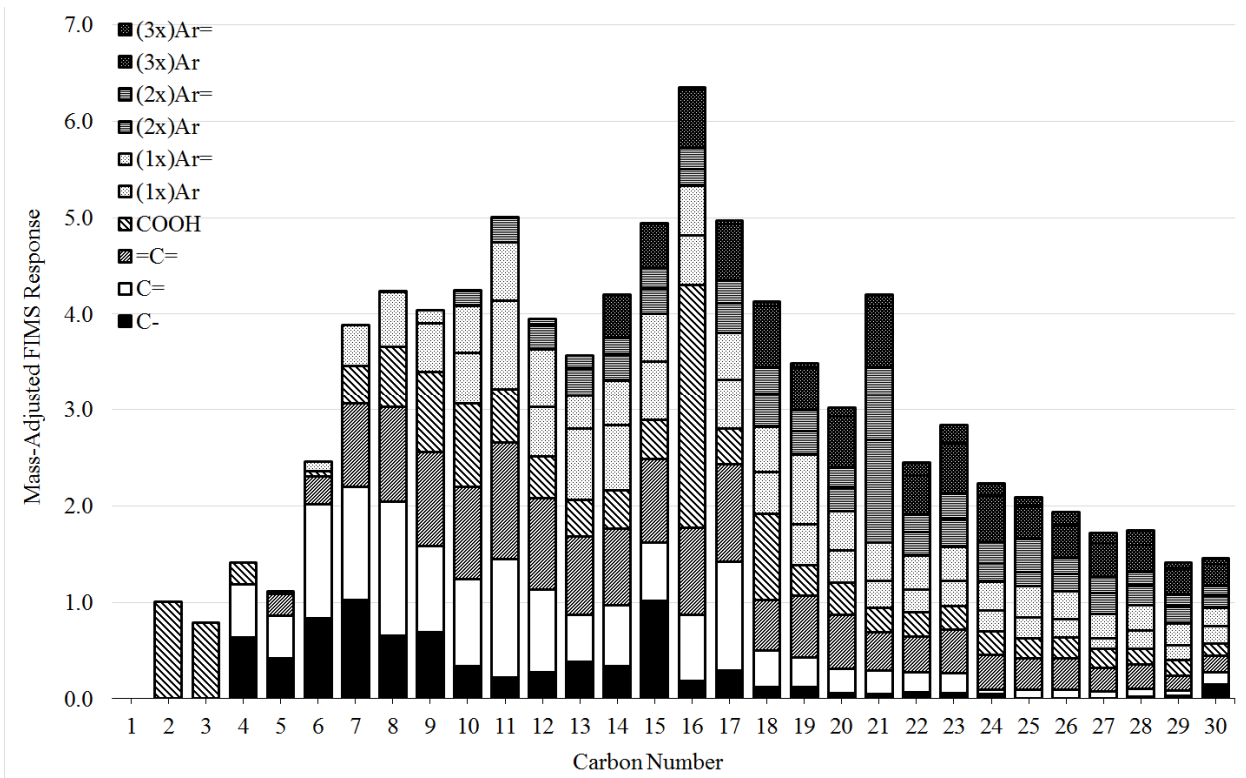
Figure 143. CND (1-30) of E-Soy CTL, mass adjusted FIMS response
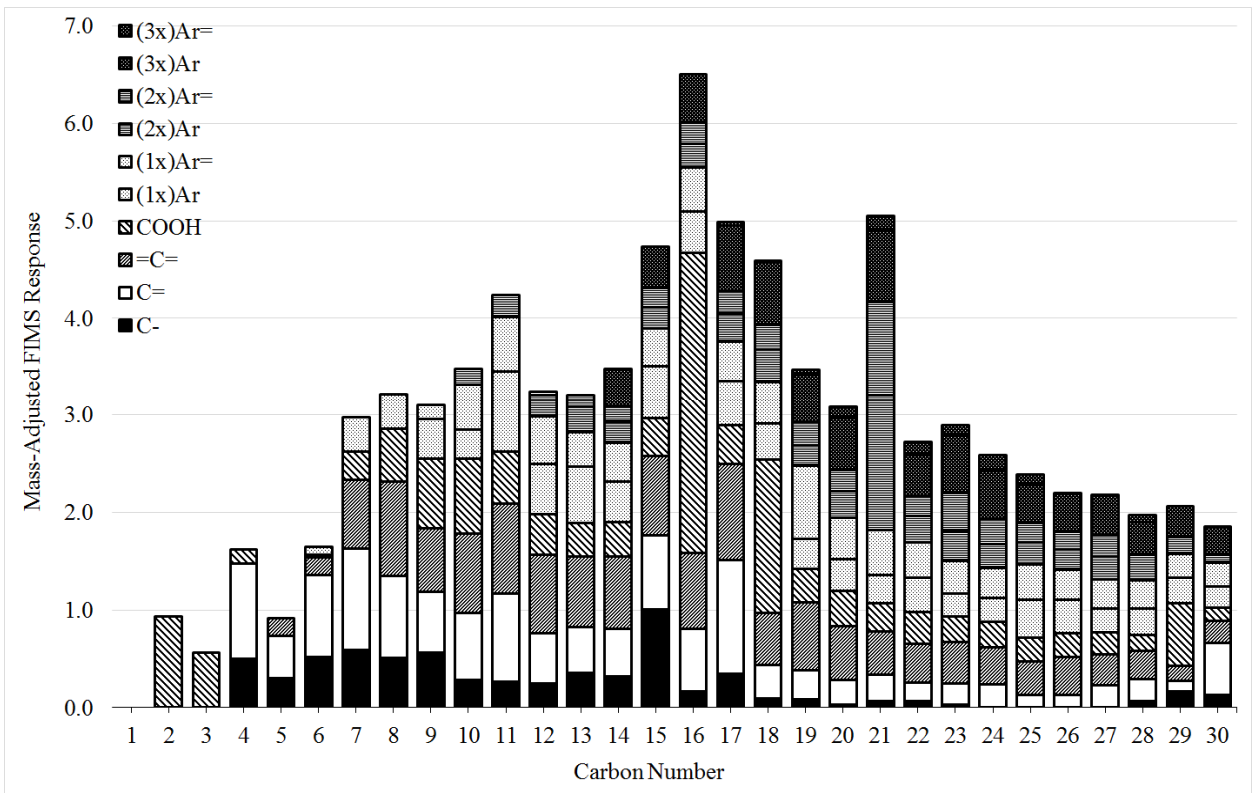
Figure 144. CND (1-30) of G-Soy CTL, mass adjusted FIMS response
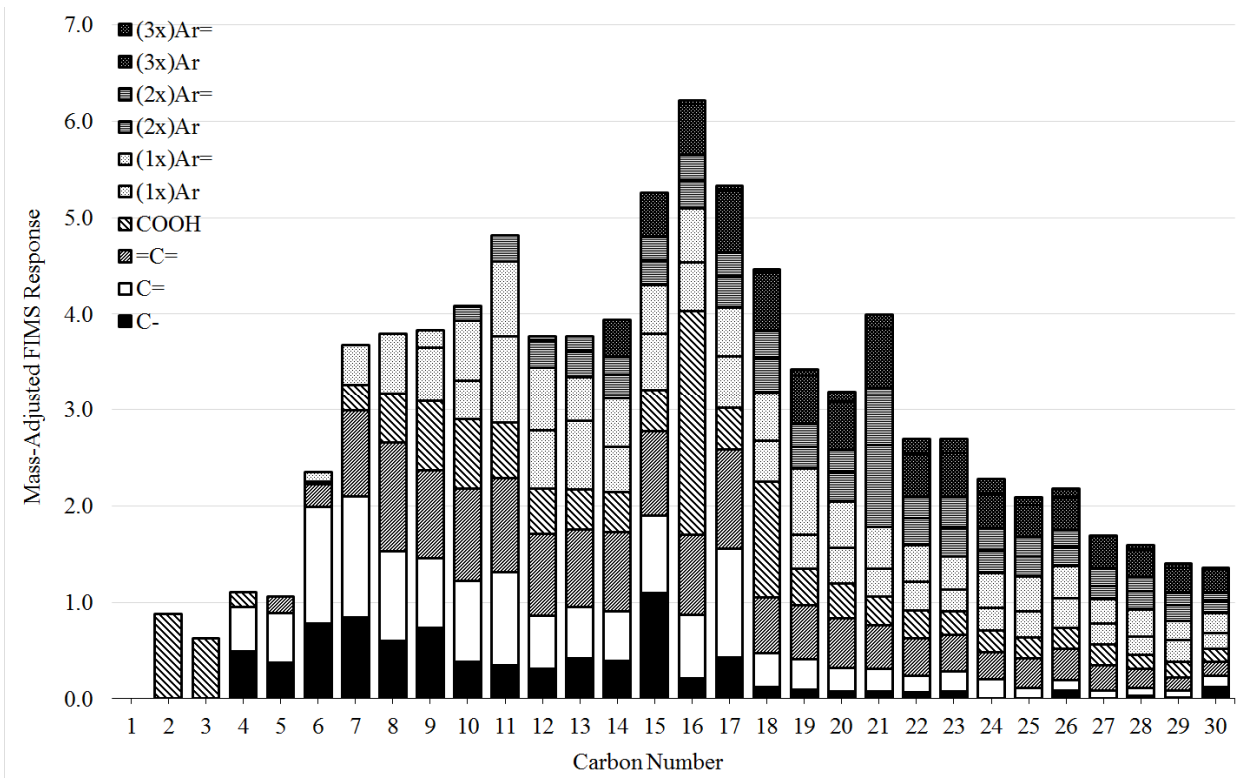
Figure 145. CND (1-30) of H-Soy CTL, mass adjusted FIMS response
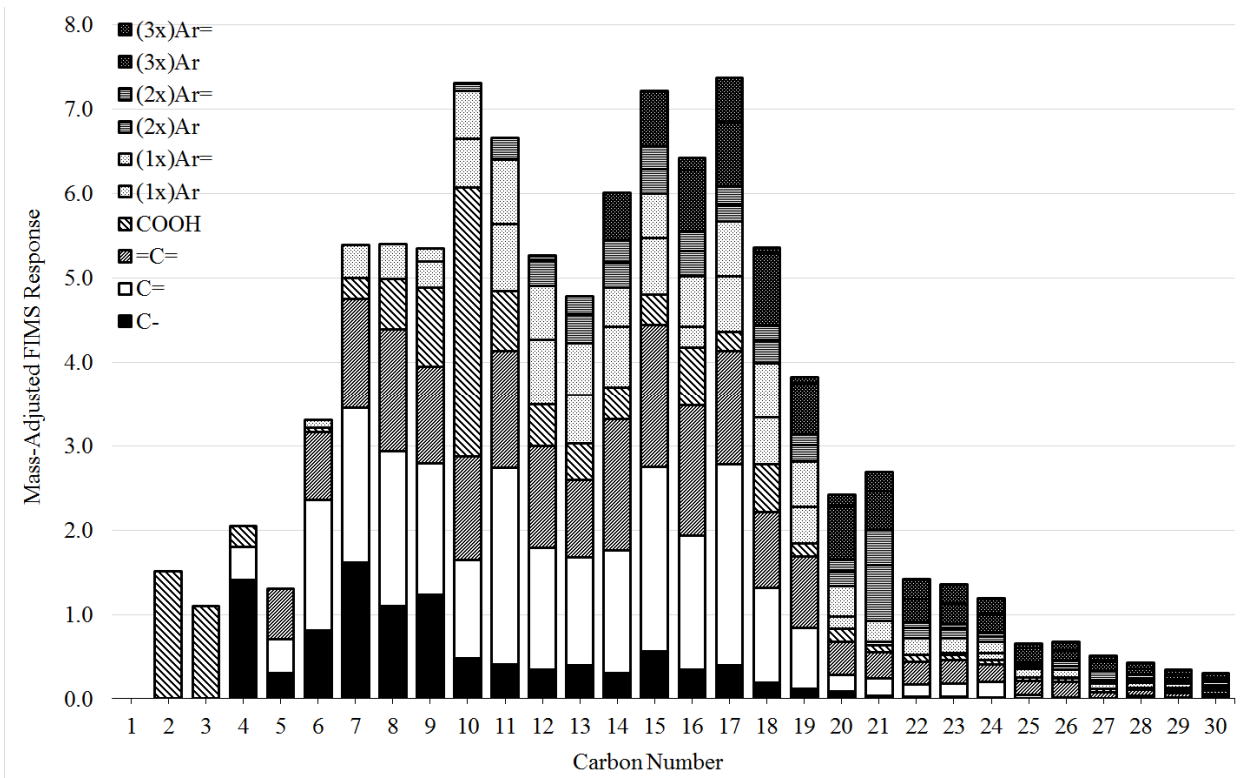
Figure 146. CND (1-30) of J-Canola CTL, mass adjusted FIMS response
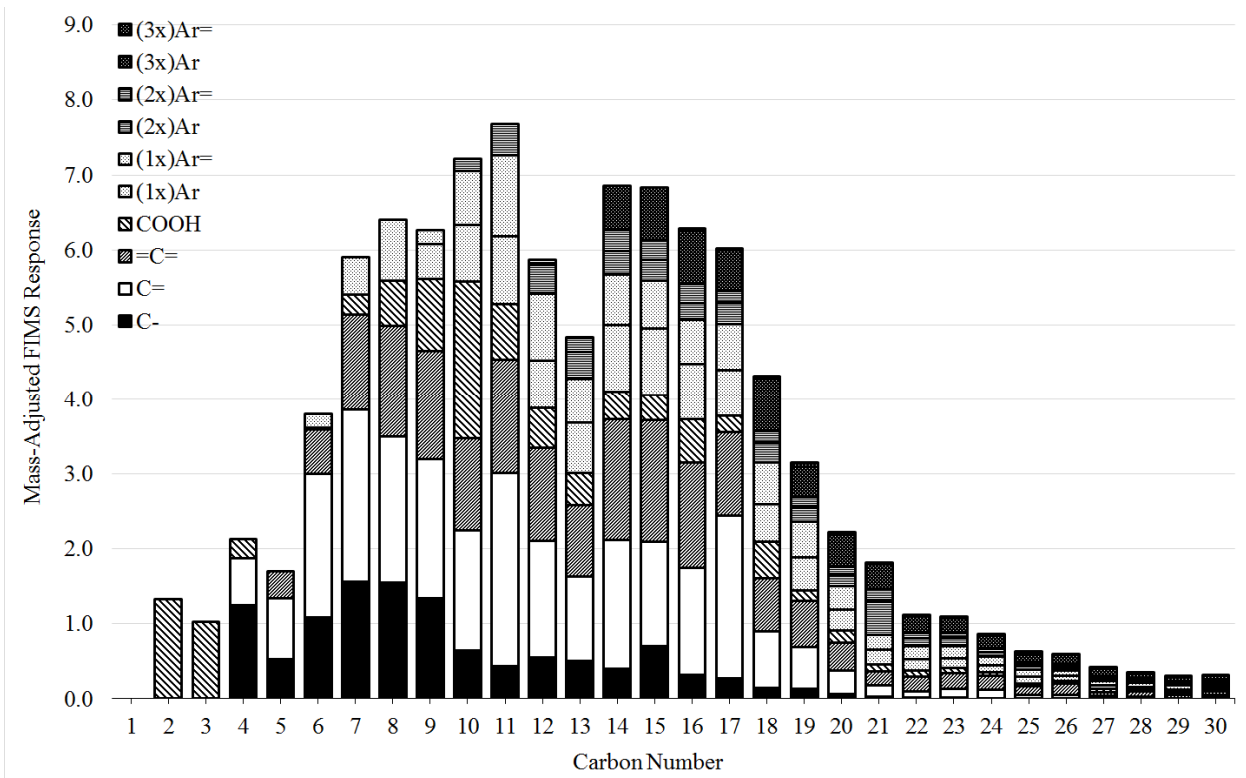
Figure 147. CND (1-30) of K-Canola CTL, mass adjusted FIMS response
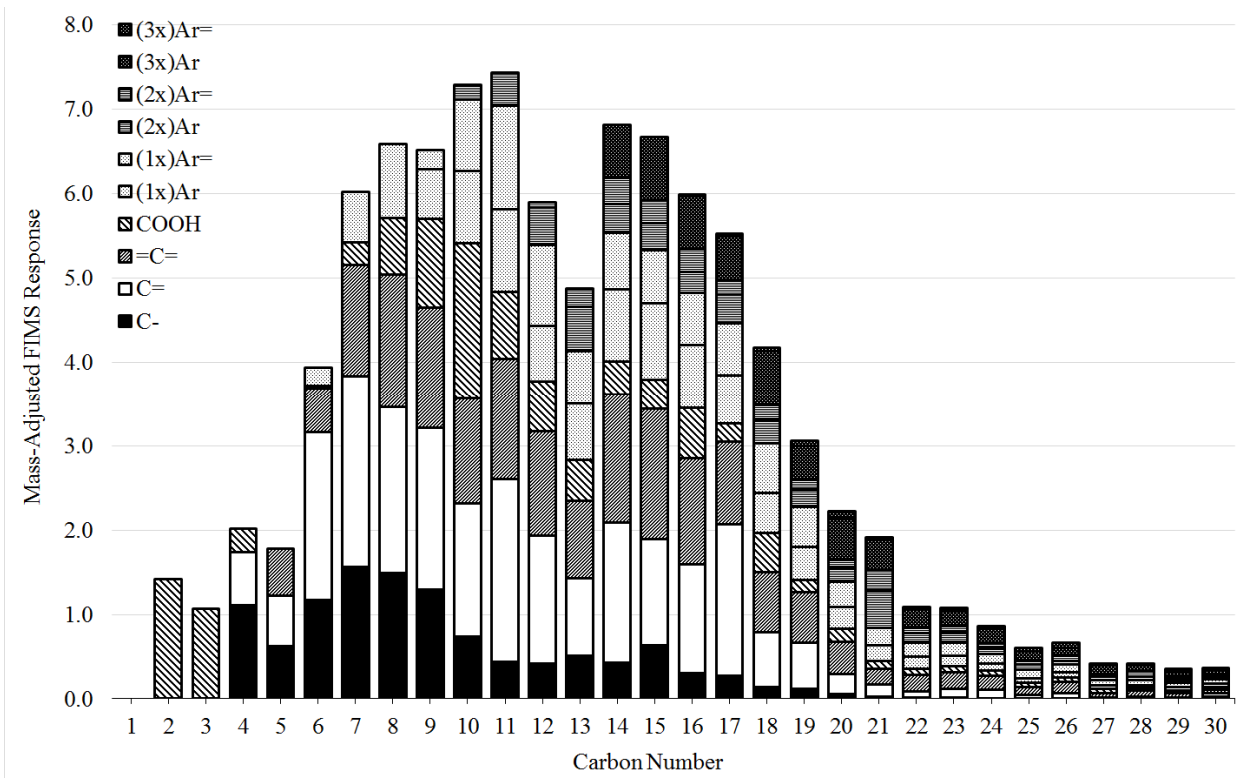
Figure 148. CND (1-30) of L-Canola CTL, mass adjusted FIMS response
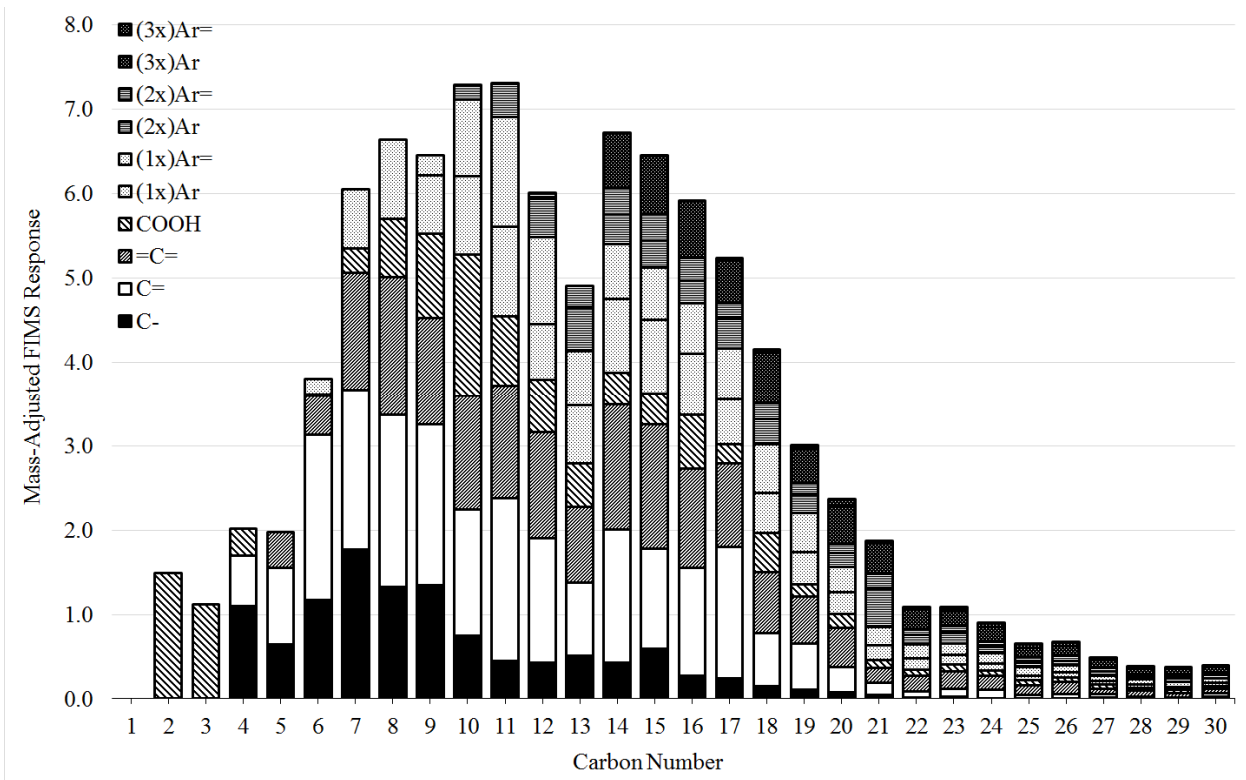
Figure 149. CND (1-30) of M-Canola CTL, mass adjusted FIMS response
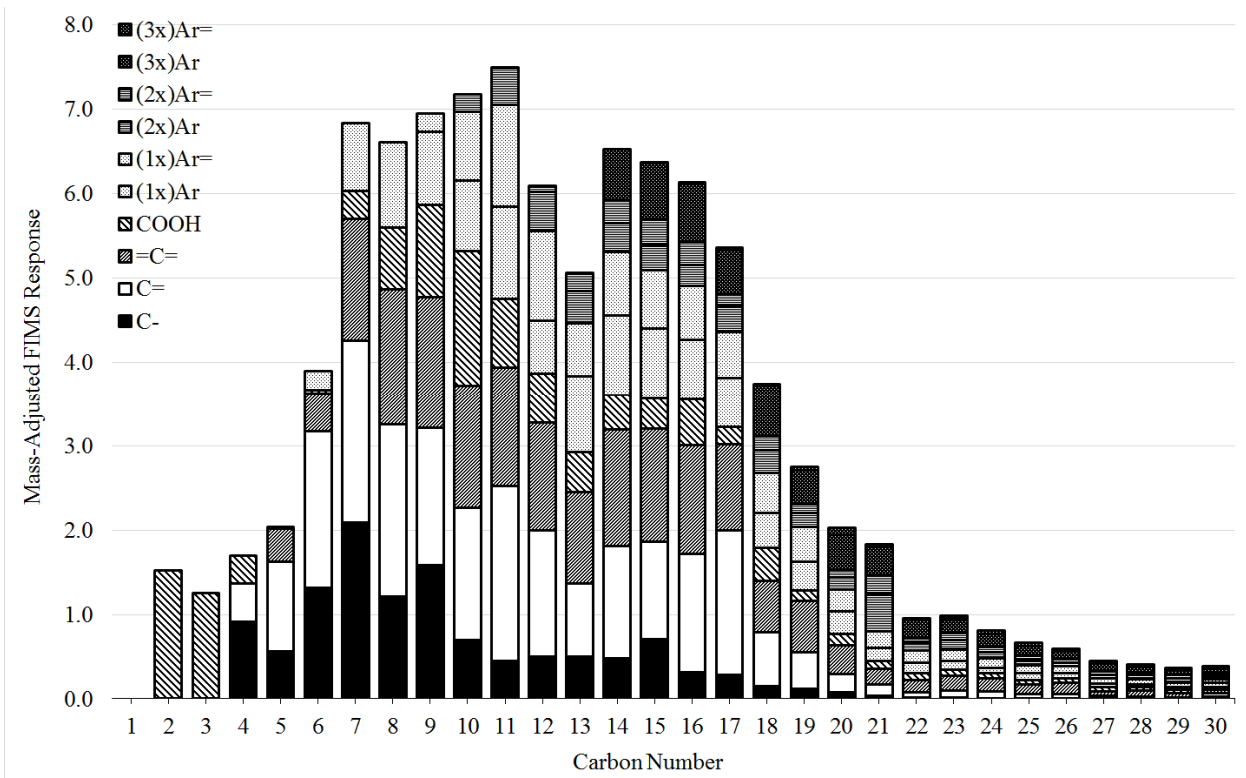
Figure 150. CND (1-30) of N-Canola CTL, mass adjusted FIMS response
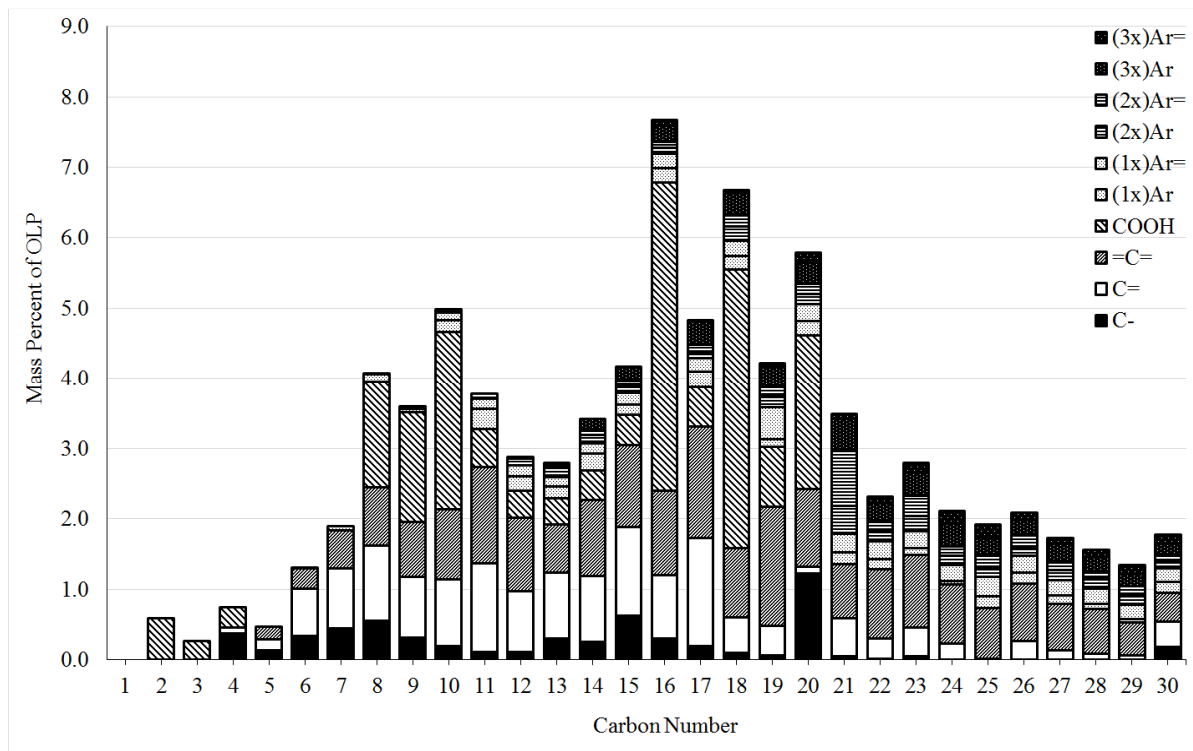
Figure 151. Mass-based carbon number distribution for C1-C30
components from sample 'AA-Soy' CTL
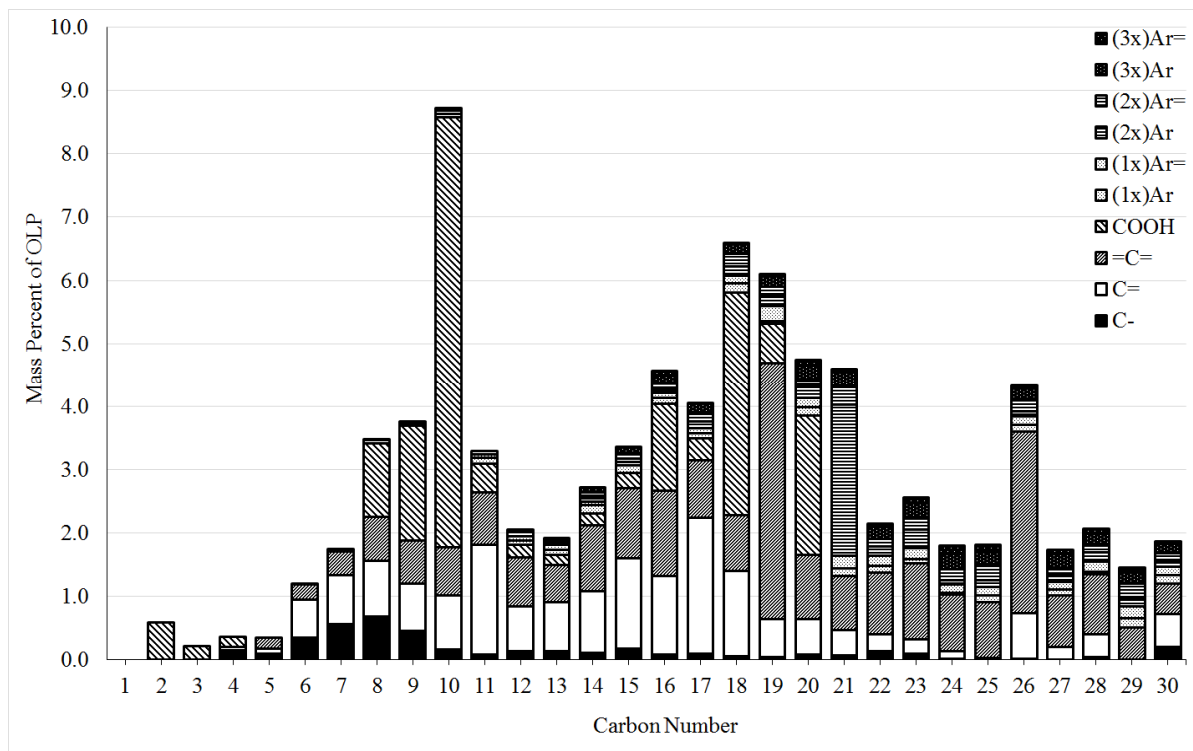
Figure 152. Mass-based carbon number distribution for C1-C30 components from sample 'BB-VHONO' CTL
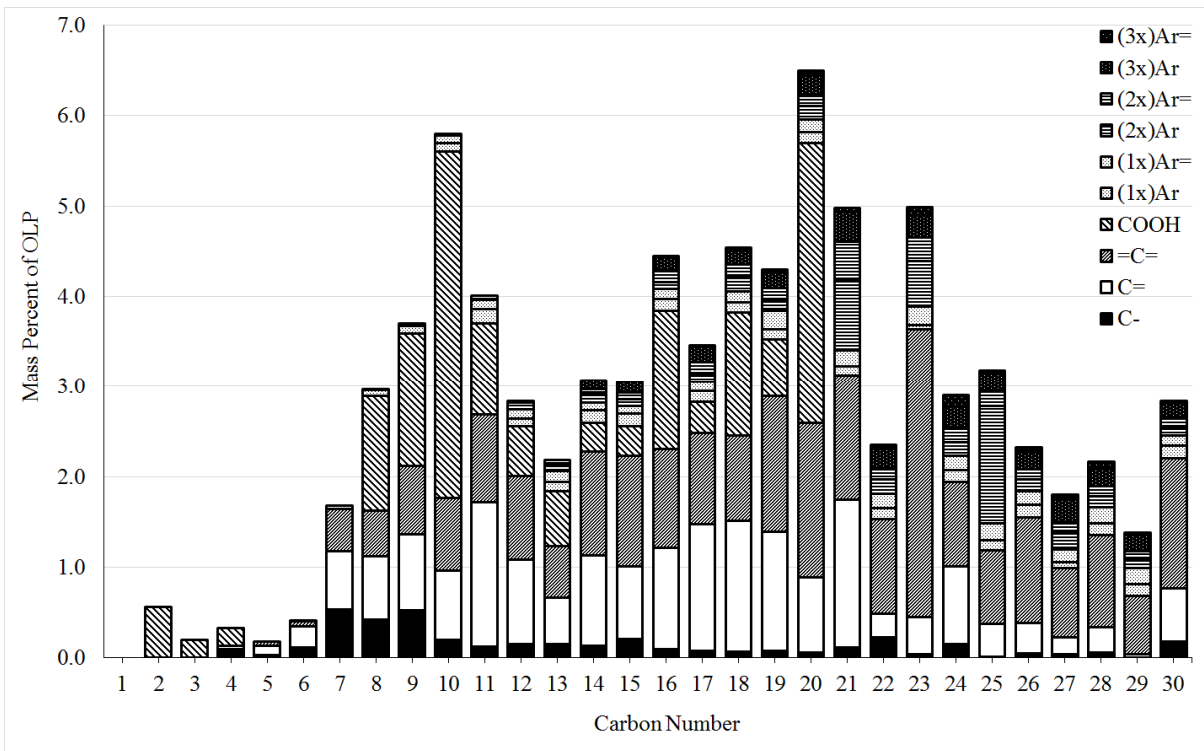
Figure 153. Mass-based carbon number distribution for C1-C30
components from sample 'CC-HENO' CTL
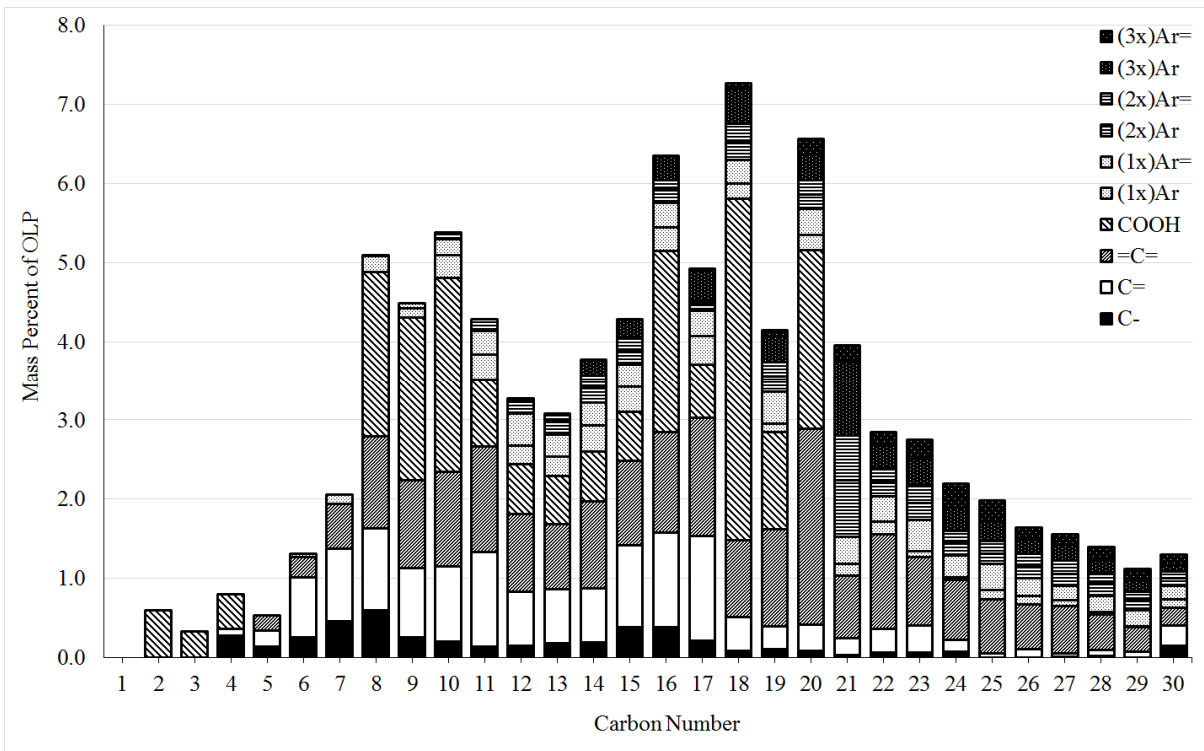
Figure 154. Mass-based carbon number distribution for C1-C30
components from sample 'DD-Linseed' CTL
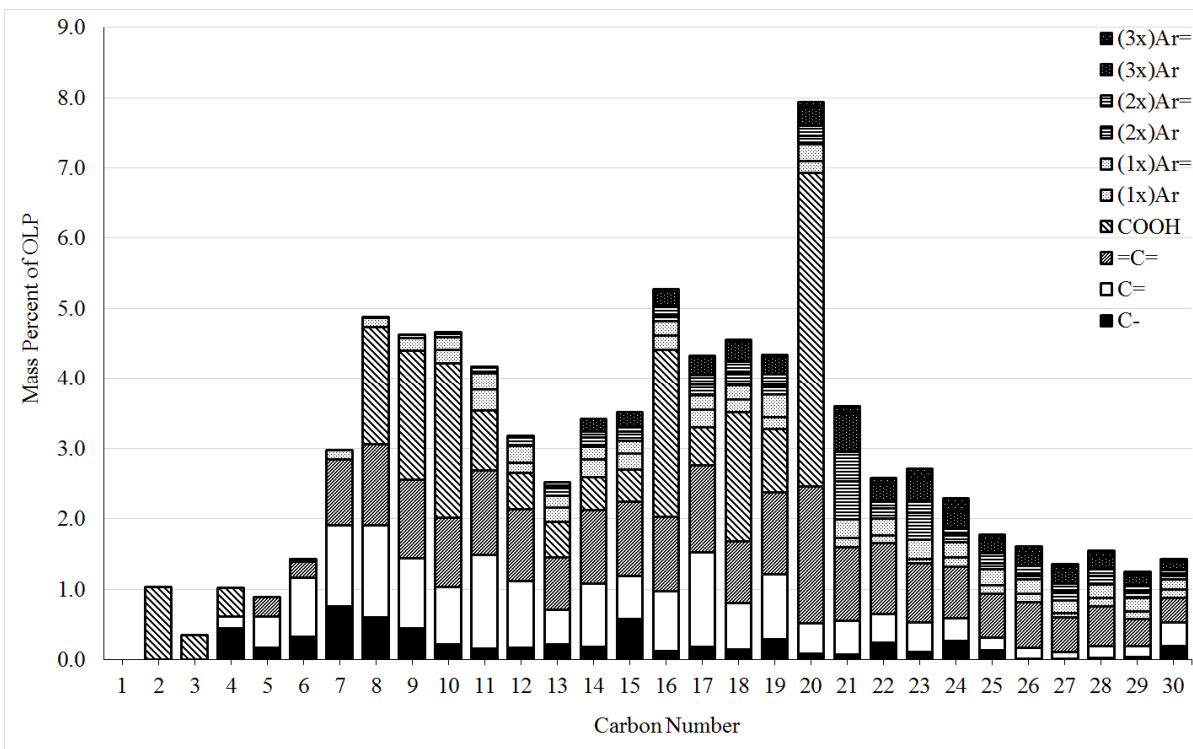
Figure 155. Mass-based carbon number distribution for C1-C30
components from sample 'EE-Camelina' CTL
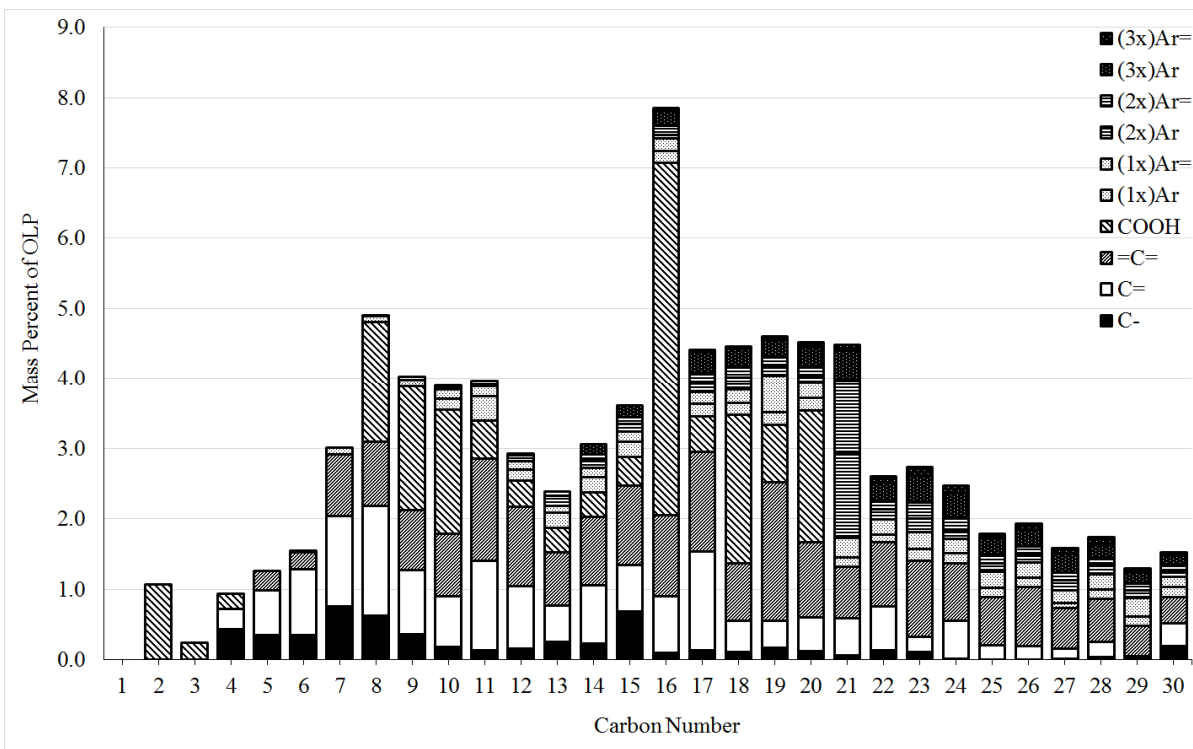
Figure 156. Mass-based carbon number distribution for C1-C30
components from sample 'FF-Corn' CTL
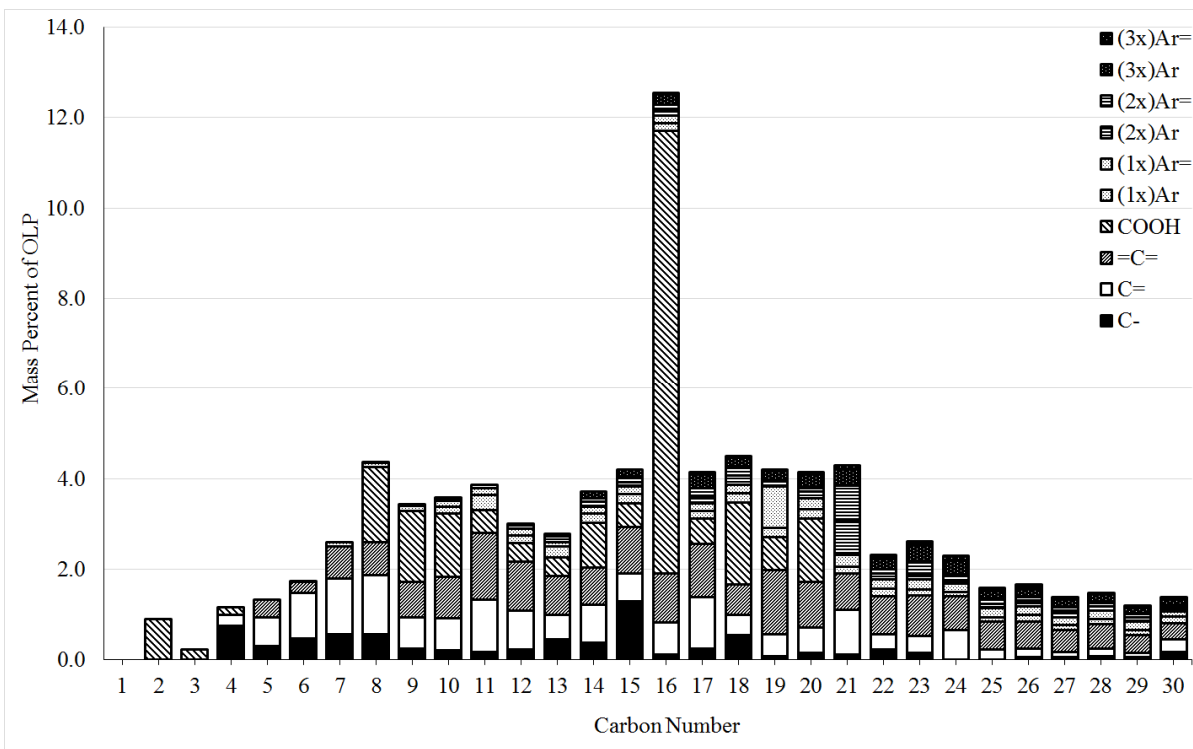
Figure 157. Mass-based carbon number distribution for C1-C30
components from sample 'GG-Cottonseed' CTL
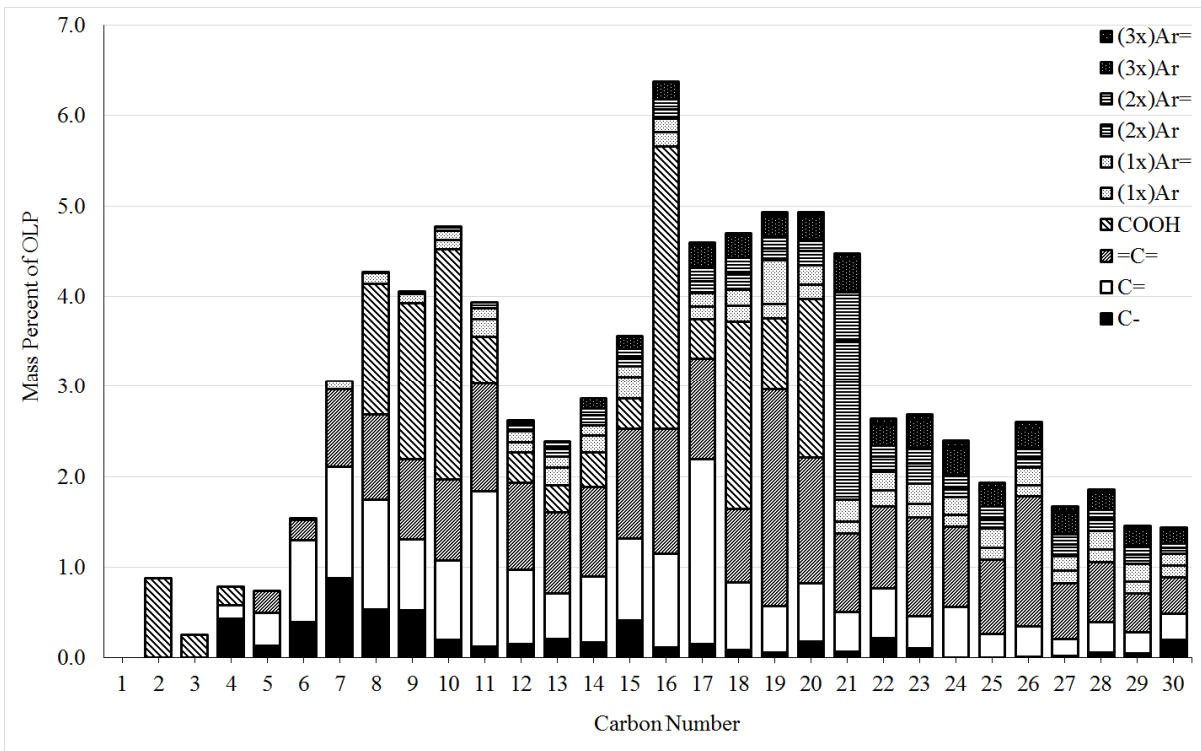
Figure 158. Mass-based carbon number distribution for C1-C30
components from sample 'HH-Canola' CTL
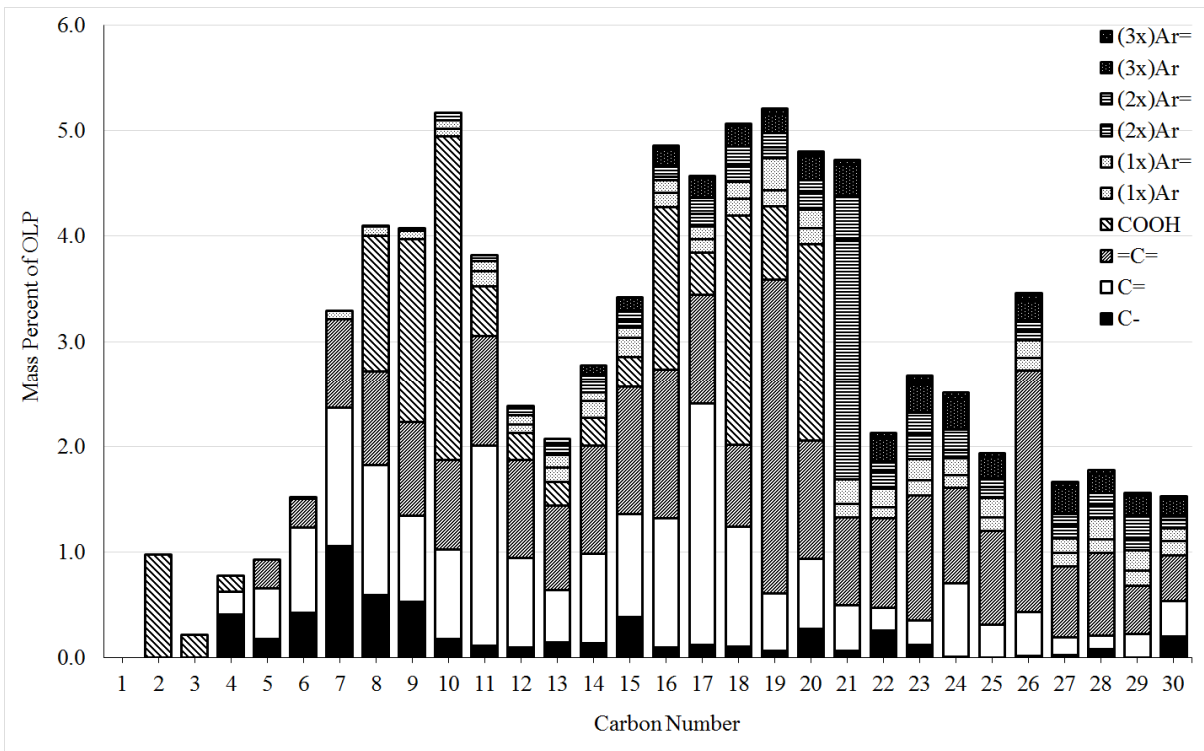
Figure 159. Mass-based carbon number distribution for C1-C30 components from sample 'II-HONO' CTL
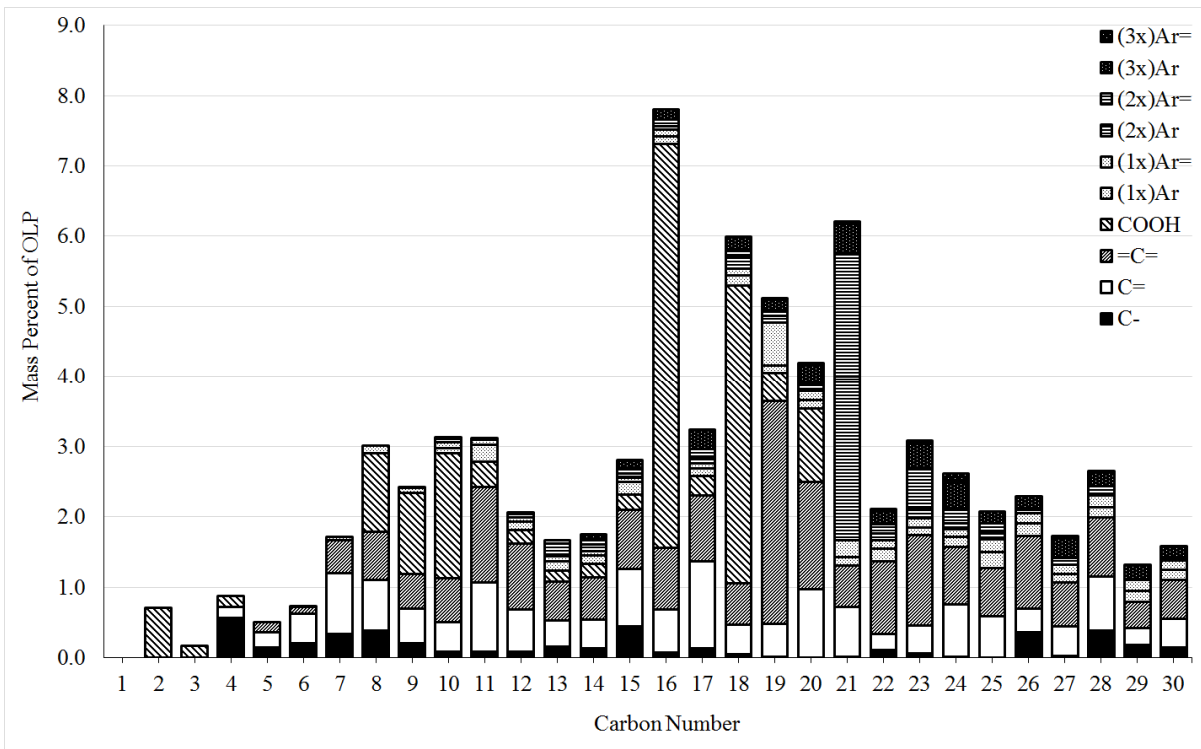
Figure 160. Mass-based carbon number distribution for C1-C30
components from sample 'A-Soy' CTL
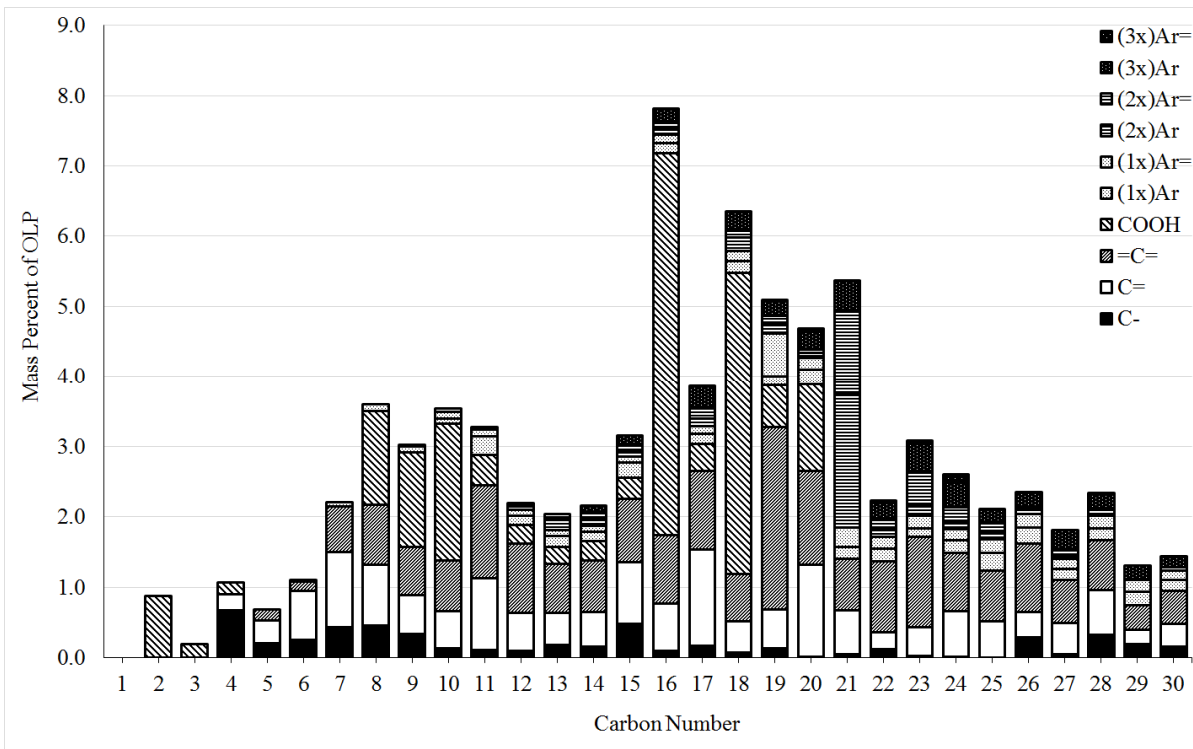
Figure 161. Mass-based carbon number distribution for C1-C30
components from sample 'B-Soy' CTL
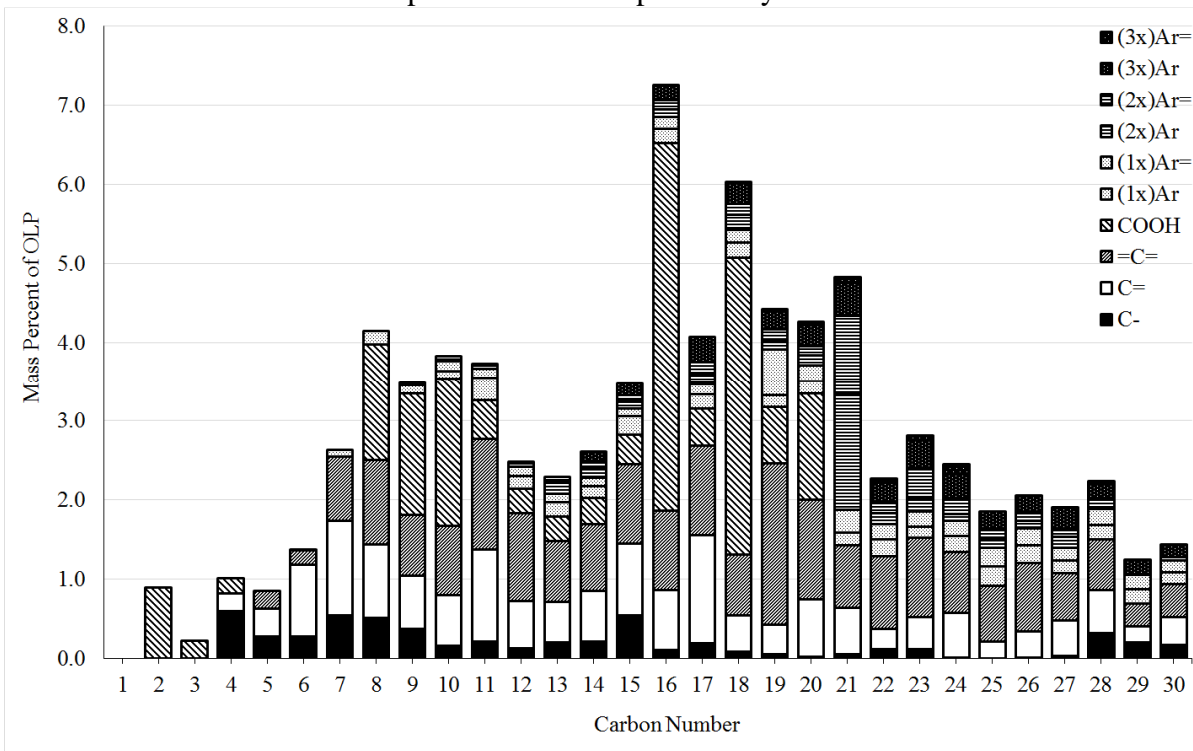
Figure 162. Mass-based carbon number distribution for C1-C30
components from sample 'C-Soy' CTL
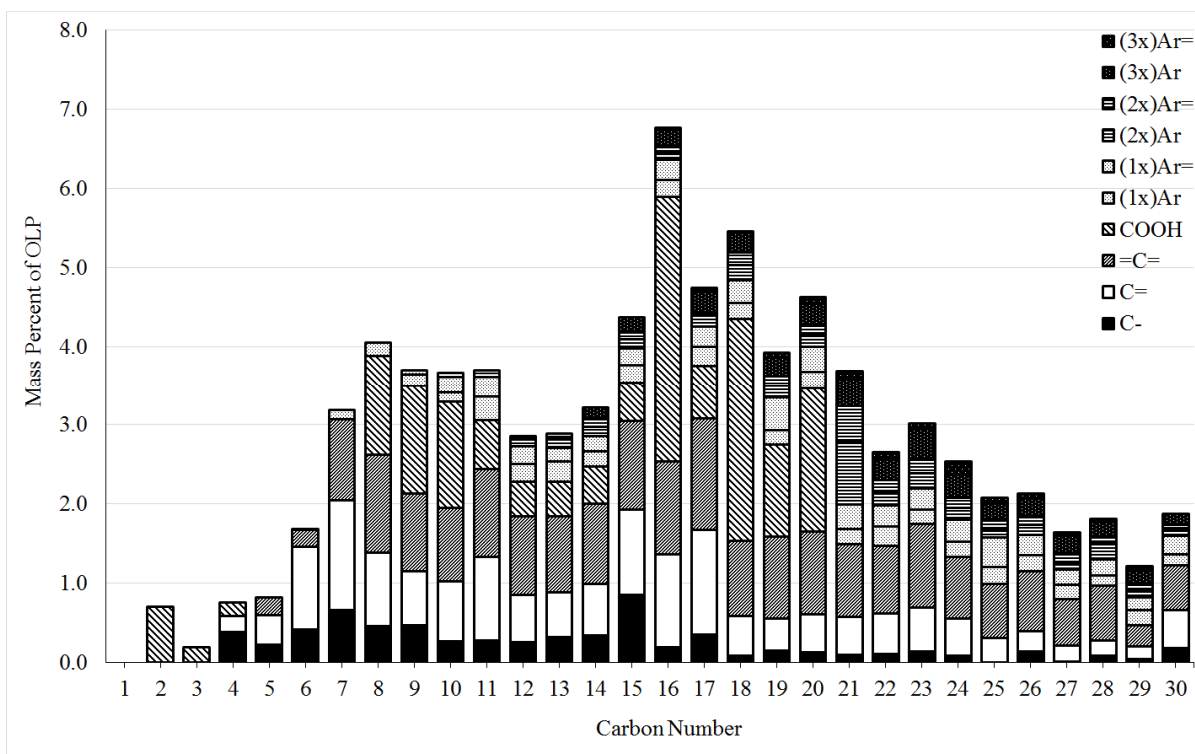
Figure 163. Mass-based carbon number distribution for C1-C30
components from sample 'D-Soy' CTL
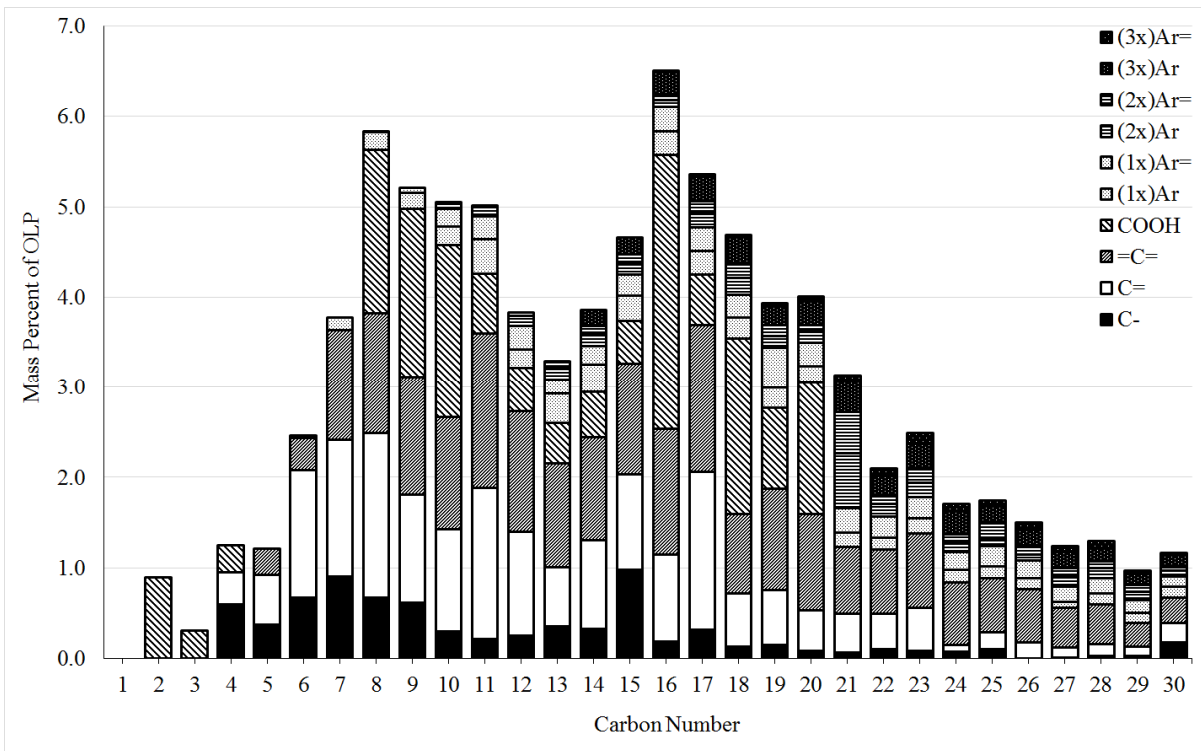
Figure 164. Mass-based carbon number distribution for C1-C30
components from sample 'E-Soy' CTL
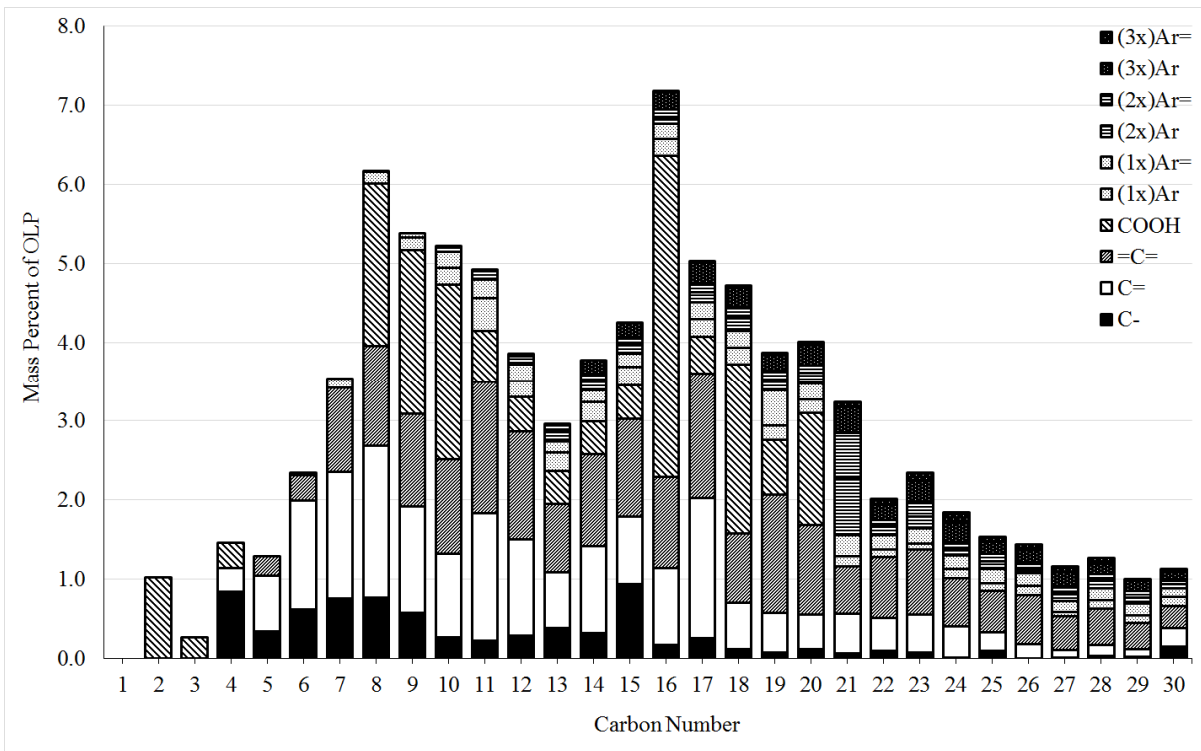
Figure 165. Mass-based carbon number distribution for C1-C30 components from sample 'F-Soy' CTL
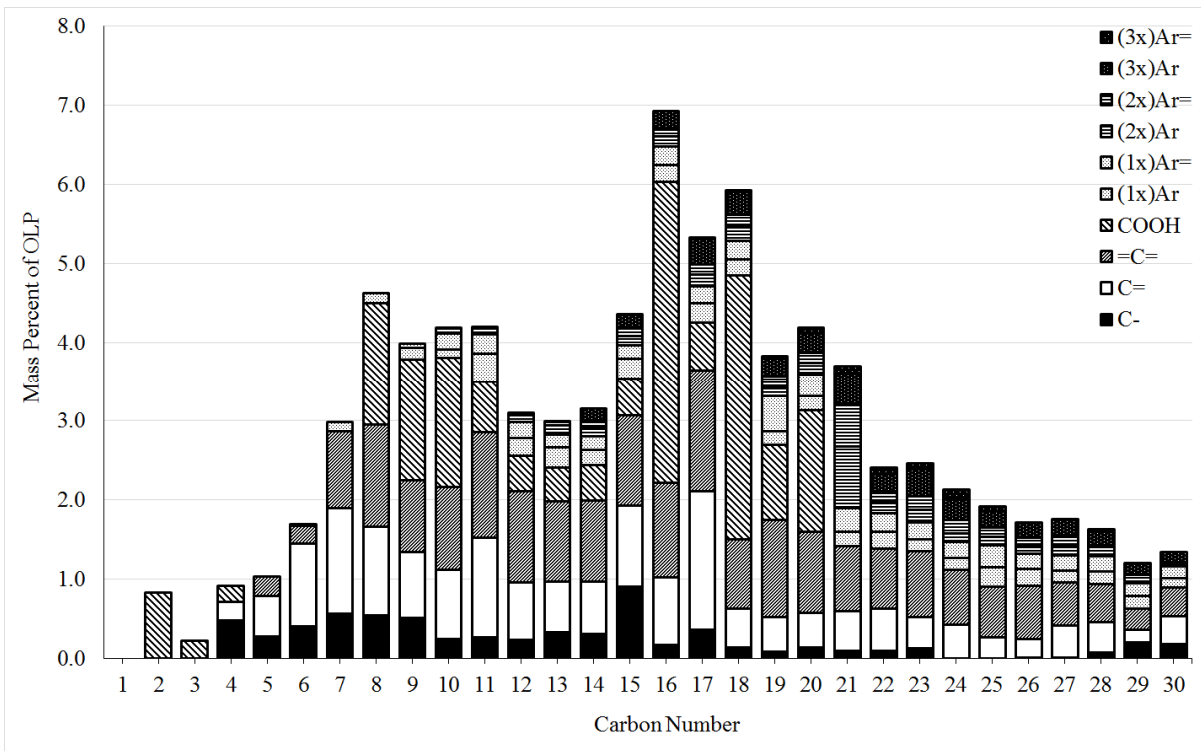
Figure 166. Mass-based carbon number distribution for C1-C30
components from sample 'G-Soy' CTL
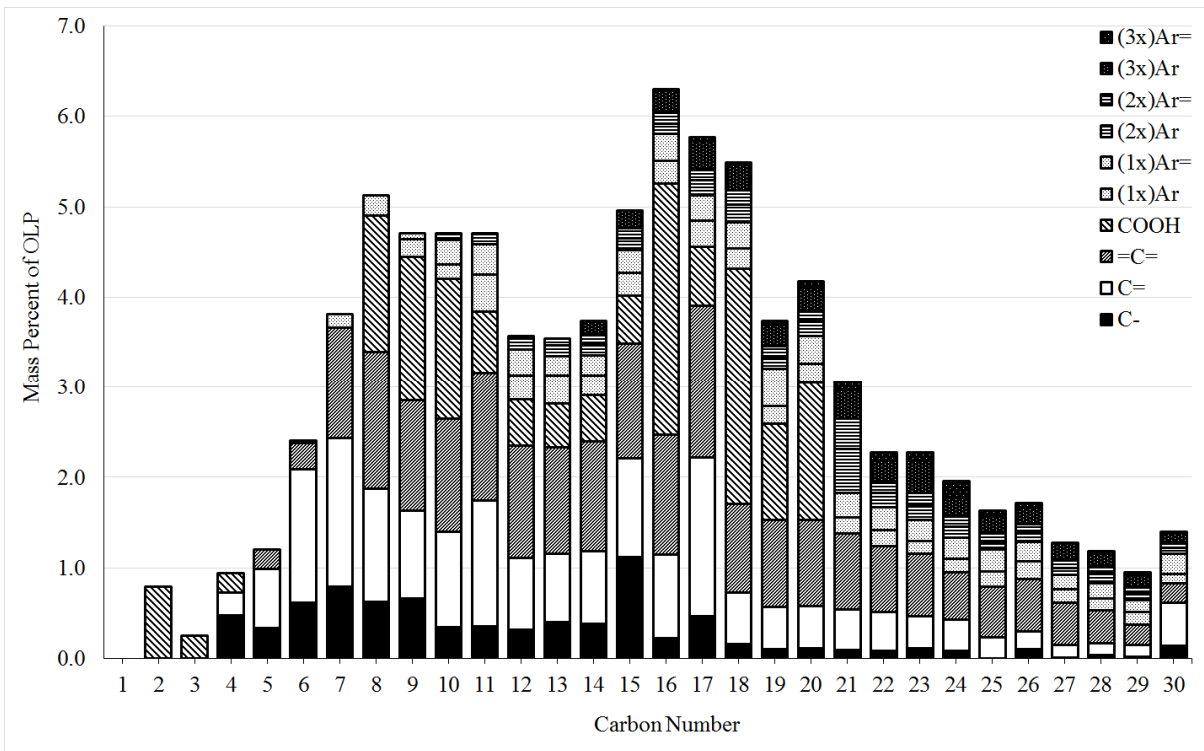
Figure 167. Mass-based carbon number distribution for C1-C30
components from sample 'H-Soy' CTL
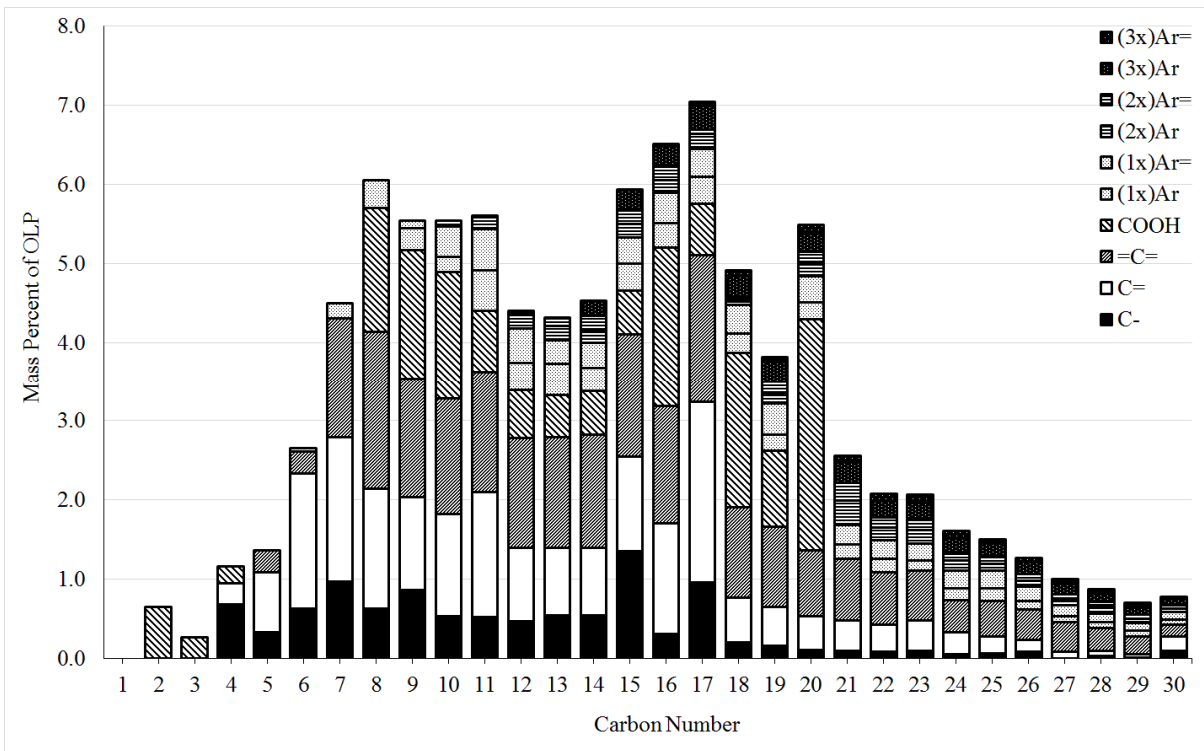
Figure 168. Mass-based carbon number distribution for C1-C30
components from sample 'I-Soy' CTL
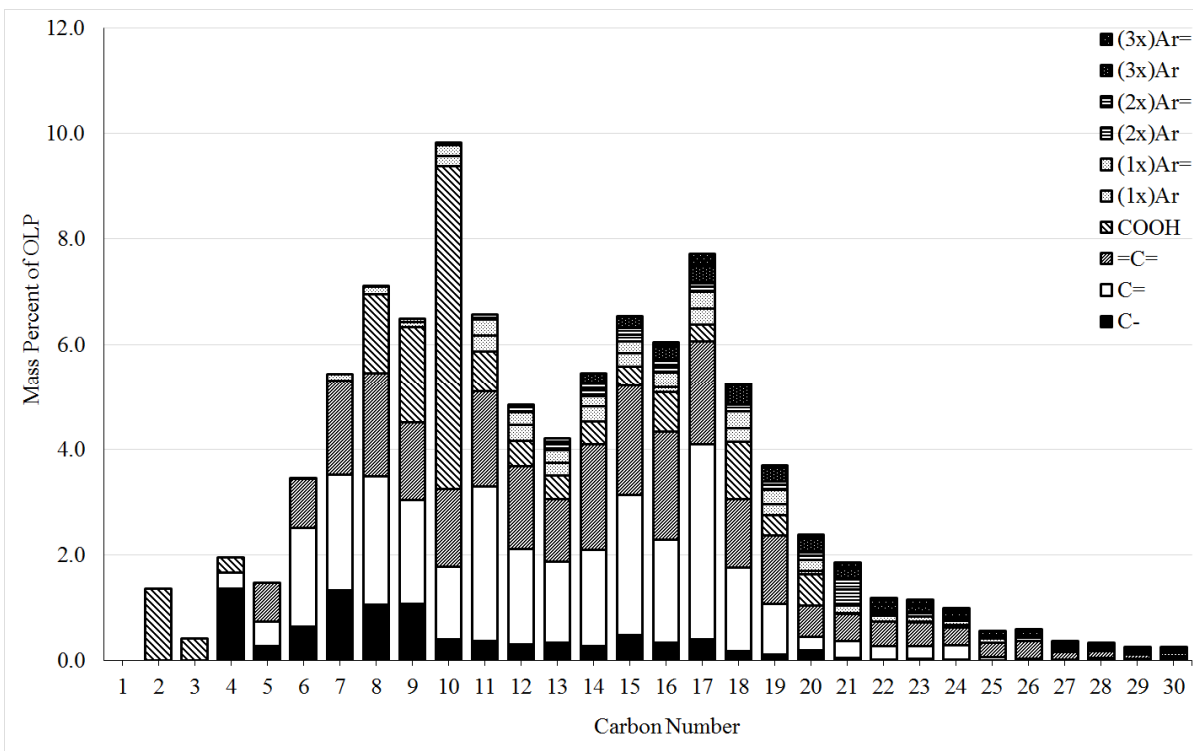
Figure 169. Mass-based carbon number distribution for C1-C30
components from sample 'J-Canola' CTL
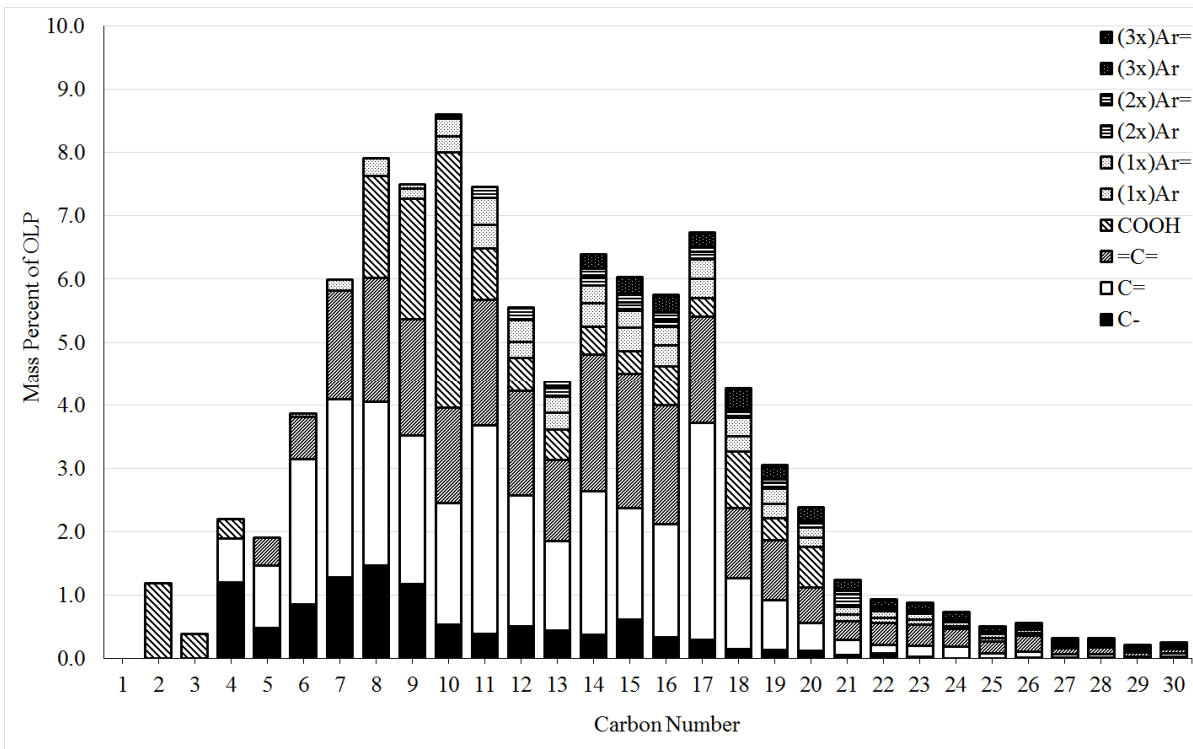
Figure 170. Mass-based carbon number distribution for C1-C30
components from sample 'K-Canola' CTL
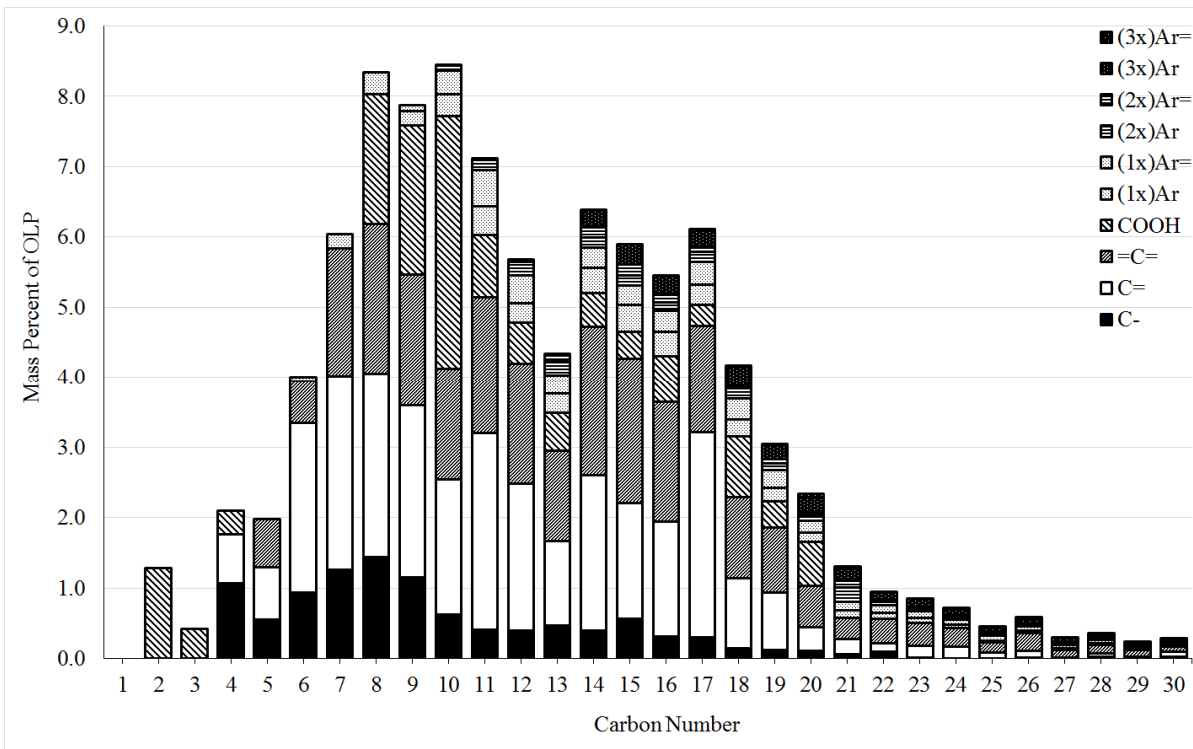
Figure 171. Mass-based carbon number distribution for C1-C30
components from sample 'L-Canola' CTL
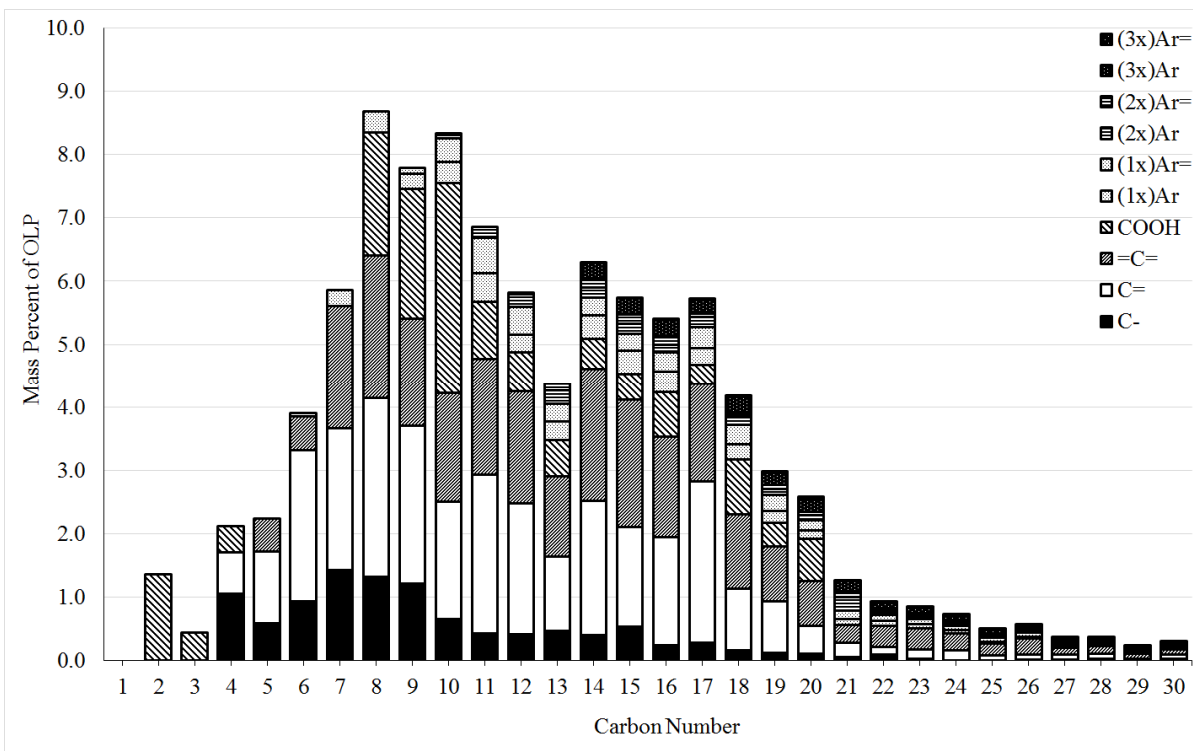
Figure 172. Mass-based carbon number distribution for C1-C30
components from sample 'M-Canola' CTL
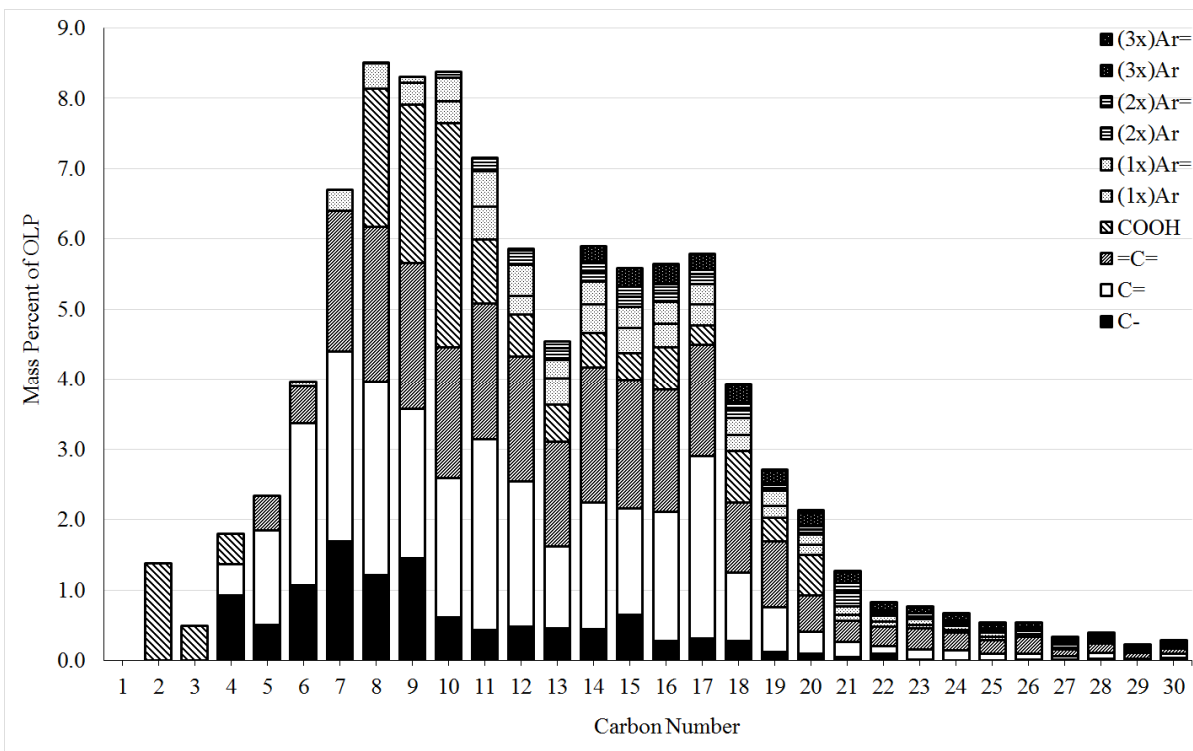
Figure 173. Mass-based carbon number distribution for C1-C30
components from sample 'N-Canola' CTL

Appendix K.
Mass-Based FIMSDIST Data

Table 71. Mass-based FIMSDIST speciation data for C1-C30
components of sample 'AA-Soy' CTL

C#	C-	C=	=C=	COOH	(1x)Ar	(1x)Ar=	(2x)Ar	(2x)Ar=	(3x)Ar	(3x)Ar=
1	0.00	0.00	0.00	0.28	0.00	0.00	0.00	0.00	0.00	0.00
2	0.00	0.00	0.00	0.57	0.00	0.00	0.00	0.00	0.00	0.00
3	0.00	0.00	0.00	0.26	0.00	0.00	0.00	0.00	0.00	0.00
4	0.36	0.08	0.00	0.28	0.00	0.00	0.00	0.00	0.00	0.00
5	0.13	0.14	0.18	0.49	0.00	0.00	0.00	0.00	0.00	0.00
6	0.33	0.65	0.27	0.83	0.02	0.00	0.00	0.00	0.00	0.00
7	0.43	0.82	0.52	2.03	0.06	0.00	0.00	0.00	0.00	0.00
8	0.54	1.03	0.80	1.46	0.10	0.01	0.00	0.00	0.00	0.00
9	0.30	0.83	0.75	1.50	0.05	0.04	0.00	0.00	0.00	0.00
10	0.19	0.92	0.96	2.43	0.17	0.11	0.04	0.00	0.00	0.00
11	0.10	1.22	1.32	0.53	0.27	0.13	0.08	0.00	0.00	0.00
12	0.10	0.83	1.01	0.37	0.20	0.15	0.09	0.03	0.00	0.00
13	0.29	0.91	0.66	0.36	0.17	0.13	0.14	0.06	0.00	0.00
14	0.24	0.90	1.04	0.41	0.23	0.14	0.12	0.08	0.13	0.00
15	0.60	1.22	1.11	0.43	0.14	0.16	0.10	0.09	0.17	0.00
16	0.29	0.86	1.16	4.24	0.19	0.19	0.09	0.07	0.22	0.08
17	0.18	1.48	1.54	0.54	0.21	0.19	0.07	0.12	0.30	0.02
18	0.10	0.48	0.95	3.83	0.18	0.21	0.19	0.17	0.30	0.04
19	0.06	0.40	1.63	0.83	0.10	0.44	0.16	0.15	0.25	0.06
20	1.18	0.09	1.07	2.11	0.19	0.23	0.15	0.13	0.29	0.14
21	0.05	0.51	0.75	0.00	0.16	0.25	0.38	0.77	0.41	0.07
22	0.02	0.28	0.95	0.00	0.14	0.24	0.16	0.12	0.25	0.08
23	0.05	0.40	1.00	0.00	0.09	0.23	0.20	0.28	0.33	0.12
24	0.00	0.22	0.81	0.00	0.04	0.22	0.13	0.13	0.31	0.17
25	0.00	0.01	0.70	0.00	0.16	0.26	0.12	0.20	0.22	0.18
26	0.00	0.26	0.78	0.00	0.16	0.22	0.12	0.18	0.20	0.09
27	0.00	0.13	0.63	0.00	0.12	0.20	0.14	0.12	0.24	0.09
28	0.00	0.08	0.62	0.00	0.06	0.21	0.14	0.11	0.19	0.10
29	0.00	0.06	0.45	0.00	0.04	0.20	0.13	0.12	0.18	0.11
30	0.17	0.35	0.39	0.00	0.16	0.18	0.10	0.10	0.15	0.12

Table 72. Mass-based FIMSDIST Z-Table data for C30-C74
components of sample 'AA-Soy' CTL

C#	Z+2	Z+2	Z-2	Z-4	Z-6	Z-8	Z-10
30	0.00	0.00	0.00	0.34	0.00	0.00	0.00
31	0.20	0.22	0.26	0.29	0.29	0.29	0.00
32	0.19	0.18	0.23	0.26	0.28	0.26	0.00
33	0.15	0.16	0.18	0.24	0.24	0.24	0.00
34	0.15	0.15	0.17	0.19	0.21	0.19	0.20
35	0.11	0.13	0.14	0.16	0.18	0.16	0.17
36	0.12	0.12	0.13	0.16	0.17	0.15	0.14
37	0.09	0.12	0.11	0.12	0.15	0.13	0.12
38	0.10	0.08	0.10	0.12	0.11	0.14	0.11
39	0.08	0.08	0.09	0.10	0.10	0.12	0.10
40	0.07	0.08	0.07	0.09	0.09	0.10	0.09
41	0.07	0.07	0.05	0.08	0.08	0.08	0.08
42	0.07	0.06	0.05	0.06	0.06	0.08	0.08
43	0.04	0.06	0.05	0.05	0.07	0.06	0.05
44	0.04	0.05	0.05	0.04	0.05	0.06	0.05
45	0.05	0.04	0.03	0.04	0.04	0.05	0.04
46	0.03	0.03	0.03	0.03	0.03	0.03	0.04
47	0.02	0.03	0.03	0.03	0.04	0.04	0.03
48	0.03	0.03	0.03	0.02	0.02	0.02	0.02
49	0.02	0.02	0.02	0.02	0.02	0.02	0.03
50	0.02	0.02	0.02	0.02	0.02	0.02	0.02
51	0.02	0.02	0.01	0.02	0.02	0.02	0.02
52	0.02	0.02	0.01	0.01	0.01	0.01	0.02
53	0.01	0.01	0.01	0.01	0.01	0.02	0.02
54	0.01	0.01	0.01	0.02	0.01	0.01	0.01
55	0.01	0.00	0.00	0.01	0.01	0.01	0.01
56	0.01	0.01	0.01	0.01	0.01	0.01	0.01
57	0.01	0.00	0.01	0.01	0.01	0.00	0.00
58	0.01	0.01	0.01	0.01	0.00	0.00	0.01
59	0.00	0.00	0.01	0.01	0.00	0.00	0.01
60	0.00	0.00	0.00	0.01	0.01	0.00	0.00
61	0.00	0.00	0.00	0.00	0.00	0.01	0.00
62	0.00	0.01	0.00	0.00	0.00	0.00	0.01
63	0.00	0.00	0.00	0.00	0.00	0.00	0.00
64	0.00	0.00	0.00	0.00	0.00	0.00	0.00
65	0.00	0.00	0.00	0.00	0.00	0.00	0.00
66	0.00	0.00	0.00	0.00	0.00	0.00	0.00
67	0.00	0.00	0.00	0.00	0.00	0.00	0.00
68	0.00	0.00	0.00	0.00	0.00	0.00	0.00
69	0.00	0.00	0.00	0.00	0.00	0.00	0.00
70	0.00	0.00	0.00	0.00	0.00	0.00	0.00
71	0.00	0.00	0.00	0.00	0.00	0.00	0.00
72	0.00	0.00	0.00	0.00	0.00	0.00	0.00
73	0.00	0.00	0.00	0.00	0.00	0.00	0.00
74	0.00	0.00	0.00	0.00	0.00	0.00	0.00

Table 73. Mass-based FIMSDIST speciation data for C1-C30 components of sample 'BB-VHONO' CTL

C#	C-	C=	=C=	COOH	(1x)Ar	(1x)Ar=	(2x)Ar	(2x)Ar=	(3x)Ar	(3x)Ar=
1	0.00	0.00	0.00	0.11	0.00	0.00	0.00	0.00	0.00	0.00
2	0.00	0.00	0.00	0.58	0.00	0.00	0.00	0.00	0.00	0.00
3	0.00	0.00	0.00	0.22	0.00	0.00	0.00	0.00	0.00	0.00
4	0.15	0.05	0.00	0.15	0.00	0.00	0.00	0.00	0.00	0.00
5	0.09	0.08	0.17	0.20	0.00	0.00	0.00	0.00	0.00	0.00
6	0.34	0.59	0.24	0.43	0.01	0.00	0.00	0.00	0.00	0.00
7	0.55	0.76	0.37	0.84	0.04	0.00	0.00	0.00	0.00	0.00
8	0.67	0.86	0.68	1.15	0.06	0.00	0.00	0.00	0.00	0.00
9	0.45	0.74	0.67	1.79	0.04	0.02	0.00	0.00	0.00	0.00
10	0.16	0.84	0.75	6.70	0.06	0.05	0.03	0.00	0.00	0.00
11	0.08	1.69	0.81	0.45	0.09	0.06	0.05	0.00	0.00	0.00
12	0.13	0.69	0.76	0.20	0.06	0.07	0.06	0.03	0.00	0.00
13	0.13	0.77	0.57	0.16	0.08	0.08	0.06	0.05	0.00	0.00
14	0.11	0.95	1.02	0.19	0.12	0.05	0.08	0.07	0.08	0.00
15	0.18	1.39	1.10	0.24	0.11	0.06	0.06	0.09	0.09	0.00
16	0.08	1.22	1.32	1.35	0.10	0.07	0.06	0.11	0.12	0.07
17	0.09	2.12	0.89	0.33	0.09	0.08	0.11	0.12	0.15	0.01
18	0.05	1.32	0.87	3.48	0.14	0.11	0.16	0.19	0.16	0.02
19	0.04	0.59	3.99	0.61	0.04	0.24	0.15	0.14	0.17	0.03
20	0.08	0.55	1.00	2.16	0.13	0.15	0.17	0.11	0.22	0.09
21	0.07	0.40	0.84	0.00	0.12	0.19	2.35	0.28	0.25	0.03
22	0.14	0.26	0.96	0.00	0.10	0.15	0.15	0.11	0.20	0.04
23	0.09	0.23	1.18	0.00	0.06	0.16	0.30	0.18	0.24	0.07
24	0.02	0.11	0.88	0.00	0.02	0.13	0.07	0.17	0.25	0.11
25	0.00	0.02	0.87	0.00	0.11	0.13	0.10	0.25	0.18	0.12
26	0.01	0.71	2.82	0.00	0.11	0.13	0.08	0.19	0.17	0.05
27	0.01	0.19	0.81	0.00	0.08	0.12	0.11	0.11	0.22	0.05
28	0.04	0.35	0.93	0.00	0.04	0.16	0.14	0.12	0.18	0.07
29	0.00	0.01	0.49	0.00	0.14	0.18	0.13	0.23	0.17	0.08
30	0.20	0.50	0.48	0.00	0.13	0.13	0.08	0.14	0.16	0.02

Table 74. Mass-based FIMSDIST Z-Table data for C30-C74
components of sample 'BB-VHONO' CTL

C#	Z+2	Z+2	Z-2	Z-4	Z-6	Z-8	Z-10
30	0.00	0.00	0.00	0.35	0.00	0.00	0.00
31	0.18	0.25	0.28	0.32	0.25	0.22	0.00
32	0.16	0.22	0.26	0.27	0.25	0.20	0.00
33	0.11	0.17	0.24	0.29	0.23	0.19	0.00
34	0.12	0.16	0.27	0.38	0.22	0.15	0.15
35	0.09	0.15	0.18	0.20	0.19	0.14	0.14
36	0.12	0.15	0.24	0.24	0.18	0.14	0.11
37	0.08	0.12	0.15	0.16	0.17	0.12	0.08
38	0.09	0.09	0.15	0.15	0.12	0.14	0.10
39	0.08	0.09	0.12	0.12	0.12	0.12	0.09
40	0.06	0.08	0.08	0.11	0.10	0.11	0.08
41	0.05	0.06	0.06	0.10	0.10	0.09	0.07
42	0.07	0.05	0.06	0.09	0.08	0.09	0.07
43	0.04	0.06	0.07	0.07	0.08	0.07	0.05
44	0.04	0.05	0.06	0.07	0.06	0.07	0.05
45	0.05	0.04	0.04	0.06	0.06	0.06	0.04
46	0.03	0.03	0.04	0.05	0.05	0.04	0.04
47	0.02	0.02	0.03	0.05	0.05	0.04	0.03
48	0.03	0.03	0.03	0.03	0.03	0.03	0.03
49	0.02	0.02	0.02	0.02	0.03	0.03	0.03
50	0.02	0.02	0.02	0.03	0.03	0.03	0.02
51	0.02	0.02	0.02	0.02	0.03	0.03	0.03
52	0.02	0.02	0.02	0.02	0.02	0.02	0.02
53	0.01	0.01	0.01	0.02	0.02	0.03	0.02
54	0.02	0.01	0.02	0.02	0.03	0.02	0.01
55	0.01	0.01	0.01	0.01	0.02	0.02	0.02
56	0.01	0.01	0.01	0.01	0.02	0.02	0.02
57	0.01	0.01	0.01	0.02	0.01	0.00	0.01
58	0.01	0.01	0.01	0.01	0.00	0.01	0.01
59	0.01	0.01	0.01	0.01	0.00	0.01	0.01
60	0.00	0.01	0.00	0.01	0.01	0.00	0.01
61	0.00	0.00	0.01	0.00	0.01	0.01	0.00
62	0.00	0.01	0.00	0.00	0.00	0.00	0.01
63	0.00	0.00	0.00	0.01	0.00	0.00	0.00
64	0.00	0.01	0.00	0.00	0.00	0.00	0.00
65	0.00	0.00	0.00	0.00	0.00	0.00	0.00
66	0.00	0.00	0.00	0.00	0.00	0.00	0.00
67	0.00	0.00	0.00	0.00	0.00	0.00	0.00
68	0.00	0.00	0.00	0.00	0.00	0.00	0.00
69	0.00	0.00	0.00	0.00	0.00	0.00	0.00
70	0.00	0.00	0.00	0.00	0.00	0.00	0.00
71	0.00	0.00	0.00	0.00	0.00	0.00	0.00
72	0.00	0.00	0.00	0.00	0.00	0.00	0.00
73	0.00	0.00	0.00	0.00	0.00	0.00	0.00
74	0.00	0.00	0.00	0.00	0.00	0.00	0.00

Table 75. Mass-based FIMSDIST speciation data for C1-C30
components of sample 'CC-HENO' CTL

C#	C-	C=	=C=	COOH	(1x)Ar	(1x)Ar=	(2x)Ar	(2x)Ar=	(3x)Ar	(3x)Ar=
1	0.00	0.00	0.00	0.11	0.00	0.00	0.00	0.00	0.00	0.00
2	0.00	0.00	0.00	0.55	0.00	0.00	0.00	0.00	0.00	0.00
3	0.00	0.00	0.00	0.19	0.00	0.00	0.00	0.00	0.00	0.00
4	0.09	0.04	0.00	0.20	0.00	0.00	0.00	0.00	0.00	0.00
5	0.03	0.10	0.05	0.20	0.00	0.00	0.00	0.00	0.00	0.00
6	0.11	0.22	0.06	0.43	0.01	0.00	0.00	0.00	0.00	0.00
7	0.52	0.63	0.46	0.84	0.04	0.00	0.00	0.00	0.00	0.00
8	0.41	0.69	0.50	1.25	0.06	0.00	0.00	0.00	0.00	0.00
9	0.51	0.83	0.74	1.45	0.08	0.02	0.00	0.00	0.00	0.00
10	0.19	0.76	0.78	3.78	0.09	0.08	0.02	0.00	0.00	0.00
11	0.12	1.57	0.95	1.01	0.15	0.10	0.05	0.00	0.00	0.00
12	0.15	0.92	0.91	0.54	0.08	0.10	0.07	0.02	0.00	0.00
13	0.15	0.51	0.56	0.59	0.10	0.11	0.08	0.05	0.00	0.00
14	0.13	0.98	1.13	0.31	0.14	0.08	0.09	0.06	0.10	0.00
15	0.21	0.79	1.20	0.32	0.14	0.08	0.07	0.08	0.12	0.00
16	0.09	1.11	1.08	1.51	0.13	0.11	0.08	0.12	0.14	0.02
17	0.08	1.38	0.99	0.34	0.11	0.10	0.10	0.13	0.17	0.01
18	0.07	1.42	0.92	1.35	0.11	0.12	0.16	0.14	0.15	0.03
19	0.08	1.29	1.48	0.62	0.11	0.20	0.11	0.13	0.17	0.04
20	0.06	0.82	1.68	3.06	0.12	0.14	0.15	0.12	0.20	0.06
21	0.11	1.61	1.36	0.00	0.10	0.17	0.76	0.43	0.32	0.04
22	0.22	0.27	1.02	0.00	0.12	0.15	0.16	0.12	0.20	0.05
23	0.04	0.40	3.14	0.00	0.05	0.20	0.49	0.26	0.24	0.09
24	0.14	0.85	0.92	0.00	0.12	0.16	0.15	0.16	0.22	0.13
25	0.01	0.36	0.80	0.00	0.11	0.18	1.28	0.17	0.19	0.04
26	0.05	0.33	1.15	0.00	0.13	0.15	0.13	0.11	0.19	0.05
27	0.04	0.18	0.75	0.00	0.06	0.14	0.19	0.11	0.24	0.05
28	0.05	0.27	1.01	0.00	0.12	0.18	0.12	0.11	0.19	0.08
29	0.00	0.04	0.63	0.00	0.13	0.18	0.09	0.09	0.18	0.03
30	0.17	0.58	1.42	0.00	0.14	0.12	0.08	0.12	0.16	0.02

Table 76. Mass-based FIMSDIST Z-Table data for C30-C74
components of sample 'CC-HENO' CTL

C#	Z+2	Z+2	Z-2	Z-4	Z-6	Z-8	Z-10
30	0.00	0.00	0.00	0.41	0.00	0.00	0.00
31	0.17	0.28	0.39	0.33	0.26	0.23	0.00
32	0.16	0.31	0.37	0.28	0.24	0.22	0.00
33	0.14	0.20	0.28	0.27	0.22	0.19	0.00
34	0.14	0.19	0.23	0.23	0.21	0.16	0.16
35	0.11	0.16	0.18	0.19	0.18	0.15	0.14
36	0.13	0.15	0.17	0.20	0.17	0.13	0.12
37	0.08	0.11	0.14	0.15	0.16	0.13	0.10
38	0.09	0.09	0.14	0.16	0.13	0.13	0.10
39	0.08	0.07	0.11	0.13	0.12	0.11	0.10
40	0.07	0.09	0.12	0.15	0.11	0.11	0.09
41	0.06	0.07	0.07	0.10	0.11	0.09	0.08
42	0.07	0.06	0.08	0.12	0.08	0.08	0.08
43	0.04	0.05	0.07	0.08	0.08	0.08	0.06
44	0.04	0.04	0.07	0.07	0.07	0.07	0.06
45	0.05	0.05	0.05	0.06	0.06	0.07	0.05
46	0.04	0.03	0.04	0.05	0.06	0.04	0.04
47	0.03	0.03	0.03	0.05	0.06	0.05	0.04
48	0.03	0.04	0.04	0.04	0.05	0.04	0.03
49	0.03	0.03	0.03	0.04	0.04	0.04	0.04
50	0.03	0.03	0.03	0.03	0.04	0.04	0.03
51	0.03	0.02	0.03	0.03	0.03	0.03	0.03
52	0.02	0.02	0.02	0.03	0.03	0.03	0.03
53	0.02	0.02	0.02	0.03	0.03	0.03	0.03
54	0.02	0.02	0.02	0.03	0.02	0.02	0.02
55	0.01	0.01	0.01	0.02	0.02	0.02	0.02
56	0.02	0.02	0.01	0.02	0.02	0.02	0.02
57	0.01	0.01	0.02	0.02	0.01	0.01	0.01
58	0.01	0.01	0.01	0.01	0.01	0.01	0.02
59	0.01	0.01	0.01	0.01	0.01	0.01	0.01
60	0.01	0.01	0.01	0.01	0.00	0.01	0.01
61	0.00	0.01	0.00	0.00	0.01	0.00	0.00
62	0.01	0.01	0.00	0.01	0.00	0.01	0.01
63	0.00	0.00	0.00	0.01	0.00	0.01	0.00
64	0.00	0.00	0.00	0.00	0.00	0.01	0.00
65	0.00	0.00	0.00	0.00	0.00	0.00	0.00
66	0.00	0.00	0.00	0.00	0.00	0.00	0.00
67	0.00	0.00	0.00	0.00	0.00	0.00	0.00
68	0.00	0.00	0.00	0.00	0.00	0.00	0.00
69	0.00	0.00	0.00	0.00	0.00	0.00	0.00
70	0.00	0.00	0.00	0.00	0.00	0.00	0.00
71	0.00	0.00	0.00	0.00	0.00	0.00	0.00
72	0.00	0.00	0.00	0.00	0.00	0.00	0.00
73	0.00	0.00	0.00	0.00	0.00	0.00	0.00
74	0.00	0.00	0.00	0.00	0.00	0.00	0.00

Table 77. Mass-based FIMSDIST speciation data for C1-C30
components of sample 'DD-Linseed' CTL

C#	C-	C=	=C=	COOH	(1x)Ar	(1x)Ar=	(2x)Ar	(2x)Ar=	(3x)Ar	(3x)Ar=
1	0.00	0.00	0.00	0.29	0.00	0.00	0.00	0.00	0.00	0.00
2	0.00	0.00	0.00	0.57	0.00	0.00	0.00	0.00	0.00	0.00
3	0.00	0.00	0.00	0.32	0.00	0.00	0.00	0.00	0.00	0.00
4	0.27	0.08	0.00	0.42	0.00	0.00	0.00	0.00	0.00	0.00
5	0.14	0.19	0.19	0.61	0.00	0.00	0.00	0.00	0.00	0.00
6	0.25	0.73	0.25	1.02	0.04	0.00	0.00	0.00	0.00	0.00
7	0.44	0.88	0.54	2.09	0.11	0.00	0.00	0.00	0.00	0.00
8	0.58	0.99	1.12	2.00	0.20	0.01	0.00	0.00	0.00	0.00
9	0.24	0.85	1.07	1.99	0.11	0.07	0.00	0.00	0.00	0.00
10	0.19	0.91	1.15	2.37	0.27	0.19	0.08	0.00	0.00	0.00
11	0.13	1.15	1.28	0.82	0.31	0.28	0.15	0.00	0.00	0.00
12	0.15	0.65	0.95	0.60	0.23	0.39	0.15	0.04	0.00	0.00
13	0.18	0.66	0.79	0.58	0.23	0.27	0.16	0.09	0.00	0.00
14	0.18	0.65	1.06	0.61	0.32	0.28	0.20	0.14	0.19	0.00
15	0.37	0.99	1.02	0.59	0.31	0.28	0.17	0.16	0.21	0.00
16	0.37	1.15	1.21	2.22	0.28	0.30	0.17	0.10	0.29	0.01
17	0.20	1.28	1.43	0.66	0.35	0.30	0.10	0.04	0.35	0.03
18	0.08	0.42	0.93	4.16	0.18	0.29	0.22	0.22	0.43	0.06
19	0.11	0.27	1.18	1.18	0.10	0.38	0.20	0.17	0.31	0.09
20	0.08	0.32	2.37	2.18	0.18	0.32	0.17	0.18	0.31	0.20
21	0.03	0.20	0.76	0.00	0.14	0.33	0.69	0.54	0.91	0.20
22	0.06	0.28	1.15	0.00	0.15	0.31	0.19	0.17	0.26	0.17
23	0.06	0.33	0.83	0.00	0.07	0.38	0.20	0.21	0.32	0.24
24	0.07	0.15	0.72	0.00	0.03	0.27	0.16	0.14	0.28	0.30
25	0.00	0.06	0.65	0.00	0.11	0.32	0.13	0.15	0.25	0.25
26	0.00	0.10	0.54	0.00	0.11	0.21	0.15	0.14	0.18	0.15
27	0.01	0.04	0.57	0.00	0.07	0.18	0.14	0.17	0.18	0.13
28	0.02	0.07	0.43	0.00	0.03	0.19	0.17	0.11	0.15	0.16
29	0.00	0.07	0.30	0.00	0.02	0.19	0.12	0.10	0.13	0.14
30	0.15	0.25	0.21	0.00	0.10	0.16	0.09	0.08	0.08	0.12

Table 78. Mass-based FIMSDIST Z-Table data for C30-C74
components of sample 'DD-Linseed' CTL

C#	Z+2	Z+2	Z-2	Z-4	Z-6	Z-8	Z-10
30	0.00	0.00	0.00	0.24	0.00	0.00	0.00
31	0.17	0.17	0.17	0.20	0.21	0.24	0.00
32	0.25	0.20	0.16	0.18	0.26	0.25	0.00
33	0.11	0.18	0.13	0.22	0.21	0.26	0.00
34	0.12	0.16	0.10	0.10	0.14	0.12	0.20
35	0.08	0.11	0.13	0.10	0.15	0.10	0.17
36	0.09	0.09	0.07	0.08	0.14	0.19	0.09
37	0.06	0.09	0.07	0.06	0.17	0.12	0.07
38	0.07	0.06	0.06	0.07	0.05	0.08	0.08
39	0.05	0.06	0.06	0.06	0.05	0.07	0.06
40	0.05	0.06	0.05	0.05	0.04	0.06	0.06
41	0.05	0.05	0.02	0.06	0.05	0.05	0.03
42	0.05	0.04	0.03	0.04	0.02	0.05	0.05
43	0.03	0.04	0.04	0.03	0.04	0.03	0.02
44	0.01	0.07	0.04	0.03	0.03	0.04	0.02
45	0.07	0.03	0.02	0.02	0.03	0.03	0.02
46	0.01	0.02	0.03	0.02	0.01	0.01	0.05
47	0.00	0.01	0.06	0.07	0.02	0.02	0.02
48	0.02	0.02	0.02	0.01	0.00	0.00	0.00
49	0.00	0.01	0.01	0.00	0.00	0.01	0.05
50	0.00	0.00	0.00	0.00	0.00	0.00	0.00
51	0.00	0.00	0.00	0.00	0.00	0.00	0.00
52	0.04	0.03	0.00	0.00	0.00	0.00	0.00
53	0.00	0.00	0.00	0.00	0.00	0.00	0.04
54	0.00	0.00	0.00	0.04	0.04	0.04	0.00
55	0.00	0.00	0.00	0.00	0.00	0.00	0.00
56	0.00	0.00	0.00	0.00	0.00	0.00	0.04
57	0.00	0.00	0.00	0.00	0.00	0.00	0.00
58	0.00	0.00	0.00	0.00	0.00	0.00	0.00
59	0.00	0.00	0.00	0.00	0.00	0.00	0.00
60	0.00	0.00	0.00	0.00	0.00	0.00	0.00
61	0.00	0.00	0.00	0.00	0.00	0.00	0.00
62	0.00	0.00	0.00	0.00	0.00	0.00	0.00
63	0.00	0.00	0.00	0.00	0.00	0.00	0.00
64	0.00	0.00	0.00	0.00	0.00	0.00	0.00
65	0.00	0.00	0.00	0.00	0.00	0.00	0.00
66	0.00	0.00	0.00	0.00	0.00	0.00	0.00
67	0.00	0.00	0.00	0.00	0.00	0.00	0.00
68	0.00	0.00	0.00	0.00	0.00	0.00	0.00
69	0.00	0.00	0.00	0.00	0.00	0.00	0.00
70	0.00	0.00	0.00	0.00	0.00	0.00	0.00
71	0.00	0.00	0.00	0.00	0.00	0.00	0.00
72	0.00	0.00	0.00	0.00	0.00	0.00	0.00
73	0.00	0.00	0.00	0.00	0.00	0.00	0.00
74	0.00	0.00	0.00	0.00	0.00	0.00	0.00

Table 79. Mass-based FIMSDIST speciation data for C1-C30
components of sample 'EE-Camelina' CTL

C#	C-	C=	=C=	COOH	(1x)Ar	(1x)Ar=	(2x)Ar	(2x)Ar=	(3x)Ar	(3x)Ar=
1	0.00	0.00	0.00	0.31	0.00	0.00	0.00	0.00	0.00	0.00
2	0.00	0.00	0.00	1.00	0.00	0.00	0.00	0.00	0.00	0.00
3	0.00	0.00	0.00	0.33	0.00	0.00	0.00	0.00	0.00	0.00
4	0.43	0.16	0.00	0.40	0.00	0.00	0.00	0.00	0.00	0.00
5	0.16	0.43	0.27	0.68	0.00	0.00	0.00	0.00	0.00	0.00
6	0.31	0.81	0.22	0.93	0.04	0.00	0.00	0.00	0.00	0.00
7	0.73	1.11	0.90	1.58	0.13	0.00	0.00	0.00	0.00	0.00
8	0.58	1.26	1.12	1.62	0.12	0.01	0.00	0.00	0.00	0.00
9	0.43	0.96	1.07	1.78	0.17	0.05	0.00	0.00	0.00	0.00
10	0.21	0.79	0.94	2.13	0.19	0.18	0.06	0.00	0.00	0.00
11	0.15	1.29	1.16	0.82	0.29	0.23	0.10	0.00	0.00	0.00
12	0.16	0.91	0.98	0.50	0.15	0.23	0.11	0.03	0.00	0.00
13	0.21	0.48	0.71	0.48	0.21	0.15	0.12	0.07	0.00	0.00
14	0.18	0.87	1.01	0.46	0.24	0.18	0.12	0.09	0.17	0.00
15	0.55	0.59	1.02	0.45	0.22	0.18	0.12	0.08	0.18	0.00
16	0.12	0.82	1.02	2.31	0.20	0.19	0.07	0.13	0.21	0.03
17	0.18	1.29	1.20	0.52	0.24	0.20	0.14	0.14	0.25	0.02
18	0.14	0.64	0.85	1.77	0.17	0.20	0.17	0.16	0.27	0.03
19	0.28	0.90	1.11	0.87	0.17	0.31	0.14	0.15	0.23	0.04
20	0.09	0.41	1.88	4.32	0.16	0.23	0.12	0.13	0.26	0.06
21	0.07	0.47	1.00	0.00	0.13	0.26	0.52	0.40	0.53	0.09
22	0.23	0.40	0.97	0.00	0.11	0.23	0.14	0.10	0.22	0.10
23	0.10	0.41	0.80	0.00	0.07	0.26	0.37	0.18	0.27	0.15
24	0.26	0.32	0.70	0.00	0.13	0.21	0.11	0.09	0.23	0.18
25	0.12	0.18	0.61	0.00	0.11	0.22	0.09	0.13	0.19	0.08
26	0.01	0.16	0.62	0.00	0.12	0.20	0.06	0.11	0.18	0.09
27	0.01	0.09	0.48	0.00	0.06	0.17	0.13	0.11	0.19	0.08
28	0.03	0.15	0.54	0.00	0.12	0.19	0.12	0.10	0.15	0.10
29	0.04	0.14	0.38	0.00	0.10	0.18	0.10	0.08	0.14	0.04
30	0.19	0.32	0.34	0.00	0.12	0.13	0.07	0.05	0.12	0.04

Table 80. Mass-based FIMSDIST Z-Table data for C30-C74
components of sample 'EE-Camelina' CTL

C#	Z+2	Z+2	Z-2	Z-4	Z-6	Z-8	Z-10
30	0.00	0.00	0.00	0.27	0.00	0.00	0.00
31	0.18	0.19	0.21	0.23	0.23	0.24	0.00
32	0.17	0.17	0.19	0.20	0.22	0.22	0.00
33	0.15	0.15	0.17	0.19	0.20	0.19	0.00
34	0.14	0.13	0.15	0.17	0.18	0.17	0.18
35	0.12	0.13	0.14	0.13	0.16	0.16	0.16
36	0.13	0.11	0.12	0.15	0.15	0.14	0.13
37	0.09	0.11	0.11	0.12	0.14	0.13	0.11
38	0.11	0.09	0.11	0.11	0.10	0.13	0.11
39	0.09	0.08	0.09	0.10	0.09	0.10	0.10
40	0.08	0.09	0.08	0.09	0.08	0.10	0.09
41	0.07	0.08	0.06	0.08	0.08	0.08	0.08
42	0.07	0.07	0.07	0.07	0.06	0.07	0.07
43	0.05	0.07	0.07	0.05	0.06	0.07	0.06
44	0.04	0.05	0.06	0.05	0.05	0.06	0.06
45	0.05	0.05	0.04	0.05	0.05	0.06	0.05
46	0.04	0.04	0.05	0.04	0.04	0.03	0.04
47	0.03	0.03	0.04	0.04	0.05	0.05	0.04
48	0.04	0.04	0.04	0.04	0.04	0.03	0.03
49	0.03	0.03	0.03	0.03	0.03	0.03	0.04
50	0.03	0.03	0.03	0.03	0.03	0.03	0.03
51	0.03	0.03	0.03	0.03	0.03	0.03	0.03
52	0.03	0.03	0.02	0.02	0.03	0.03	0.03
53	0.02	0.02	0.02	0.02	0.03	0.03	0.03
54	0.02	0.02	0.03	0.03	0.02	0.02	0.01
55	0.01	0.01	0.01	0.02	0.02	0.02	0.02
56	0.02	0.02	0.01	0.02	0.02	0.02	0.02
57	0.01	0.01	0.02	0.02	0.01	0.01	0.01
58	0.01	0.01	0.02	0.00	0.00	0.01	0.01
59	0.00	0.01	0.01	0.01	0.00	0.01	0.01
60	0.01	0.00	0.00	0.01	0.00	0.00	0.01
61	0.00	0.00	0.00	0.00	0.00	0.00	0.00
62	0.00	0.01	0.00	0.00	0.00	0.00	0.01
63	0.00	0.00	0.00	0.00	0.00	0.00	0.00
64	0.00	0.00	0.00	0.00	0.00	0.00	0.00
65	0.00	0.00	0.00	0.00	0.00	0.00	0.00
66	0.00	0.00	0.00	0.00	0.00	0.00	0.00
67	0.00	0.00	0.00	0.00	0.00	0.00	0.00
68	0.00	0.00	0.00	0.00	0.00	0.00	0.00
69	0.00	0.00	0.00	0.00	0.00	0.00	0.00
70	0.00	0.00	0.00	0.00	0.00	0.00	0.00
71	0.00	0.00	0.00	0.00	0.00	0.00	0.00
72	0.00	0.00	0.00	0.00	0.00	0.00	0.00
73	0.00	0.00	0.00	0.00	0.00	0.00	0.00
74	0.00	0.00	0.00	0.00	0.00	0.00	0.00

Table 81. Mass-based FIMSDIST speciation data for C1-C30
components of sample 'FF-Corn' CTL

C#	C-	C=	=C=	COOH	(1x)Ar	(1x)Ar=	(2x)Ar	(2x)Ar=	(3x)Ar	(3x)Ar=
1	0.00	0.00	0.00	0.24	0.00	0.00	0.00	0.00	0.00	0.00
2	0.00	0.00	0.00	1.02	0.00	0.00	0.00	0.00	0.00	0.00
3	0.00	0.00	0.00	0.24	0.00	0.00	0.00	0.00	0.00	0.00
4	0.42	0.27	0.00	0.20	0.00	0.00	0.00	0.00	0.00	0.00
5	0.34	0.61	0.26	0.91	0.00	0.00	0.00	0.00	0.00	0.00
6	0.34	0.89	0.23	1.23	0.03	0.00	0.00	0.00	0.00	0.00
7	0.73	1.23	0.84	1.99	0.09	0.00	0.00	0.00	0.00	0.00
8	0.59	1.49	0.88	1.64	0.08	0.01	0.00	0.00	0.00	0.00
9	0.35	0.87	0.82	1.68	0.10	0.04	0.00	0.00	0.00	0.00
10	0.18	0.69	0.85	1.69	0.14	0.13	0.06	0.00	0.00	0.00
11	0.13	1.21	1.39	0.52	0.34	0.14	0.08	0.00	0.00	0.00
12	0.15	0.86	1.08	0.35	0.15	0.12	0.08	0.03	0.00	0.00
13	0.25	0.49	0.72	0.33	0.20	0.10	0.13	0.06	0.00	0.00
14	0.21	0.80	0.92	0.34	0.21	0.12	0.11	0.07	0.14	0.00
15	0.65	0.64	1.07	0.40	0.20	0.15	0.10	0.10	0.16	0.00
16	0.09	0.78	1.10	4.81	0.17	0.17	0.05	0.12	0.21	0.03
17	0.13	1.34	1.36	0.48	0.18	0.16	0.13	0.15	0.29	0.02
18	0.10	0.42	0.78	2.02	0.16	0.18	0.18	0.16	0.23	0.03
19	0.17	0.36	1.88	0.79	0.17	0.50	0.13	0.14	0.22	0.05
20	0.12	0.45	1.03	1.79	0.17	0.21	0.10	0.13	0.28	0.06
21	0.05	0.51	0.70	0.00	0.13	0.25	1.16	1.00	0.42	0.06
22	0.13	0.60	0.87	0.00	0.11	0.21	0.14	0.12	0.24	0.08
23	0.10	0.21	1.03	0.00	0.16	0.23	0.18	0.22	0.35	0.13
24	0.01	0.52	0.78	0.00	0.14	0.20	0.09	0.20	0.33	0.10
25	0.00	0.19	0.66	0.00	0.13	0.22	0.11	0.13	0.20	0.07
26	0.00	0.18	0.80	0.00	0.14	0.20	0.11	0.12	0.21	0.10
27	0.02	0.14	0.55	0.00	0.07	0.17	0.14	0.11	0.24	0.08
28	0.04	0.20	0.59	0.00	0.13	0.21	0.14	0.09	0.17	0.10
29	0.04	0.01	0.41	0.00	0.12	0.25	0.11	0.09	0.16	0.04
30	0.18	0.31	0.36	0.00	0.14	0.13	0.07	0.10	0.13	0.04

Table 82. Mass-based FIMSDIST Z-Table data for C30-C74
components of sample 'FF-Corn' CTL

C#	Z+2	Z+2	Z-2	Z-4	Z-6	Z-8	Z-10
30	0.00	0.00	0.00	0.31	0.00	0.00	0.00
31	0.17	0.21	0.24	0.27	0.25	0.25	0.00
32	0.16	0.17	0.22	0.22	0.23	0.23	0.00
33	0.15	0.15	0.18	0.21	0.21	0.20	0.00
34	0.14	0.13	0.17	0.19	0.21	0.18	0.19
35	0.11	0.13	0.15	0.15	0.18	0.17	0.16
36	0.12	0.11	0.14	0.17	0.17	0.15	0.14
37	0.09	0.12	0.12	0.13	0.15	0.14	0.12
38	0.10	0.08	0.10	0.11	0.11	0.14	0.12
39	0.09	0.07	0.09	0.10	0.10	0.12	0.11
40	0.07	0.08	0.08	0.09	0.09	0.11	0.09
41	0.07	0.07	0.05	0.08	0.09	0.08	0.08
42	0.07	0.06	0.06	0.07	0.06	0.07	0.08
43	0.04	0.06	0.07	0.06	0.07	0.07	0.05
44	0.04	0.05	0.05	0.05	0.05	0.07	0.06
45	0.05	0.05	0.04	0.04	0.05	0.06	0.05
46	0.04	0.04	0.04	0.04	0.04	0.03	0.04
47	0.03	0.02	0.03	0.04	0.05	0.05	0.04
48	0.04	0.04	0.04	0.03	0.03	0.03	0.03
49	0.03	0.03	0.03	0.03	0.03	0.03	0.04
50	0.03	0.03	0.03	0.03	0.03	0.03	0.03
51	0.02	0.02	0.02	0.02	0.03	0.03	0.03
52	0.03	0.02	0.02	0.02	0.02	0.02	0.02
53	0.01	0.02	0.02	0.02	0.03	0.03	0.03
54	0.02	0.02	0.03	0.02	0.02	0.01	0.01
55	0.01	0.01	0.01	0.02	0.01	0.02	0.02
56	0.02	0.02	0.01	0.01	0.01	0.02	0.02
57	0.01	0.01	0.02	0.02	0.01	0.00	0.01
58	0.01	0.01	0.01	0.01	0.00	0.01	0.01
59	0.00	0.01	0.01	0.01	0.00	0.01	0.01
60	0.01	0.00	0.00	0.01	0.00	0.00	0.01
61	0.00	0.00	0.00	0.00	0.01	0.00	0.00
62	0.00	0.00	0.00	0.00	0.00	0.00	0.01
63	0.00	0.00	0.00	0.00	0.00	0.00	0.00
64	0.00	0.00	0.00	0.00	0.00	0.00	0.00
65	0.00	0.00	0.00	0.00	0.00	0.00	0.00
66	0.00	0.00	0.00	0.00	0.00	0.00	0.00
67	0.00	0.00	0.00	0.00	0.00	0.00	0.00
68	0.00	0.00	0.00	0.00	0.00	0.00	0.00
69	0.00	0.00	0.00	0.00	0.00	0.00	0.00
70	0.00	0.00	0.00	0.00	0.00	0.00	0.00
71	0.00	0.00	0.00	0.00	0.00	0.00	0.00
72	0.00	0.00	0.00	0.00	0.00	0.00	0.00
73	0.00	0.00	0.00	0.00	0.00	0.00	0.00
74	0.00	0.00	0.00	0.00	0.00	0.00	0.00

Table 83. Mass-based FIMSDIST speciation data for C1-C30
components of sample 'GG-Cottonseed' CTL

C#	C-	C=	=C=	COOH	(1x)Ar	(1x)Ar=	(2x)Ar	(2x)Ar=	(3x)Ar	(3x)Ar=
1	0.00	0.00	0.00	0.24	0.00	0.00	0.00	0.00	0.00	0.00
2	0.00	0.00	0.00	1.02	0.00	0.00	0.00	0.00	0.00	0.00
3	0.00	0.00	0.00	0.24	0.00	0.00	0.00	0.00	0.00	0.00
4	0.42	0.27	0.00	0.20	0.00	0.00	0.00	0.00	0.00	0.00
5	0.34	0.61	0.26	0.91	0.00	0.00	0.00	0.00	0.00	0.00
6	0.34	0.89	0.23	1.23	0.03	0.00	0.00	0.00	0.00	0.00
7	0.73	1.23	0.84	1.99	0.09	0.00	0.00	0.00	0.00	0.00
8	0.59	1.49	0.88	1.64	0.08	0.01	0.00	0.00	0.00	0.00
9	0.35	0.87	0.82	1.68	0.10	0.04	0.00	0.00	0.00	0.00
10	0.18	0.69	0.85	1.69	0.14	0.13	0.06	0.00	0.00	0.00
11	0.13	1.21	1.39	0.52	0.34	0.14	0.08	0.00	0.00	0.00
12	0.15	0.86	1.08	0.35	0.15	0.12	0.08	0.03	0.00	0.00
13	0.25	0.49	0.72	0.33	0.20	0.10	0.13	0.06	0.00	0.00
14	0.21	0.80	0.92	0.34	0.21	0.12	0.11	0.07	0.14	0.00
15	0.65	0.64	1.07	0.40	0.20	0.15	0.10	0.10	0.16	0.00
16	0.09	0.78	1.10	4.81	0.17	0.17	0.05	0.12	0.21	0.03
17	0.13	1.34	1.36	0.48	0.18	0.16	0.13	0.15	0.29	0.02
18	0.10	0.42	0.78	2.02	0.16	0.18	0.18	0.16	0.23	0.03
19	0.17	0.36	1.88	0.79	0.17	0.50	0.13	0.14	0.22	0.05
20	0.12	0.45	1.03	1.79	0.17	0.21	0.10	0.13	0.28	0.06
21	0.05	0.51	0.70	0.00	0.13	0.25	1.16	1.00	0.42	0.06
22	0.13	0.60	0.87	0.00	0.11	0.21	0.14	0.12	0.24	0.08
23	0.10	0.21	1.03	0.00	0.16	0.23	0.18	0.22	0.35	0.13
24	0.01	0.52	0.78	0.00	0.14	0.20	0.09	0.20	0.33	0.10
25	0.00	0.19	0.66	0.00	0.13	0.22	0.11	0.13	0.20	0.07
26	0.00	0.18	0.80	0.00	0.14	0.20	0.11	0.12	0.21	0.10
27	0.02	0.14	0.55	0.00	0.07	0.17	0.14	0.11	0.24	0.08
28	0.04	0.20	0.59	0.00	0.13	0.21	0.14	0.09	0.17	0.10
29	0.04	0.01	0.41	0.00	0.12	0.25	0.11	0.09	0.16	0.04
30	0.18	0.31	0.36	0.00	0.14	0.13	0.07	0.10	0.13	0.04

Table 84. Mass-based FIMSDIST Z-Table data for C30-C74
components of sample 'GG-Cottonseed' CTL

C#	Z+2	Z+2	Z-2	Z-4	Z-6	Z-8	Z-10
30	0.00	0.00	0.00	0.31	0.00	0.00	0.00
31	0.17	0.21	0.24	0.27	0.25	0.25	0.00
32	0.16	0.17	0.22	0.22	0.23	0.23	0.00
33	0.15	0.15	0.18	0.21	0.21	0.20	0.00
34	0.14	0.13	0.17	0.19	0.21	0.18	0.19
35	0.11	0.13	0.15	0.15	0.18	0.17	0.16
36	0.12	0.11	0.14	0.17	0.17	0.15	0.14
37	0.09	0.12	0.12	0.13	0.15	0.14	0.12
38	0.10	0.08	0.10	0.11	0.11	0.14	0.12
39	0.09	0.07	0.09	0.10	0.10	0.12	0.11
40	0.07	0.08	0.08	0.09	0.09	0.11	0.09
41	0.07	0.07	0.05	0.08	0.09	0.08	0.08
42	0.07	0.06	0.06	0.07	0.06	0.07	0.08
43	0.04	0.06	0.07	0.06	0.07	0.07	0.05
44	0.04	0.05	0.05	0.05	0.05	0.07	0.06
45	0.05	0.05	0.04	0.04	0.05	0.06	0.05
46	0.04	0.04	0.04	0.04	0.04	0.03	0.04
47	0.03	0.02	0.03	0.04	0.05	0.05	0.04
48	0.04	0.04	0.04	0.03	0.03	0.03	0.03
49	0.03	0.03	0.03	0.03	0.03	0.03	0.04
50	0.03	0.03	0.03	0.03	0.03	0.03	0.03
51	0.02	0.02	0.02	0.02	0.03	0.03	0.03
52	0.03	0.02	0.02	0.02	0.02	0.02	0.02
53	0.01	0.02	0.02	0.02	0.03	0.03	0.03
54	0.02	0.02	0.03	0.02	0.02	0.01	0.01
55	0.01	0.01	0.01	0.02	0.01	0.02	0.02
56	0.02	0.02	0.01	0.01	0.01	0.02	0.02
57	0.01	0.01	0.02	0.02	0.01	0.00	0.01
58	0.01	0.01	0.01	0.01	0.00	0.01	0.01
59	0.00	0.01	0.01	0.01	0.00	0.01	0.01
60	0.01	0.00	0.00	0.01	0.00	0.00	0.01
61	0.00	0.00	0.00	0.00	0.01	0.00	0.00
62	0.00	0.00	0.00	0.00	0.00	0.00	0.01
63	0.00	0.00	0.00	0.00	0.00	0.00	0.00
64	0.00	0.00	0.00	0.00	0.00	0.00	0.00
65	0.00	0.00	0.00	0.00	0.00	0.00	0.00
66	0.00	0.00	0.00	0.00	0.00	0.00	0.00
67	0.00	0.00	0.00	0.00	0.00	0.00	0.00
68	0.00	0.00	0.00	0.00	0.00	0.00	0.00
69	0.00	0.00	0.00	0.00	0.00	0.00	0.00
70	0.00	0.00	0.00	0.00	0.00	0.00	0.00
71	0.00	0.00	0.00	0.00	0.00	0.00	0.00
72	0.00	0.00	0.00	0.00	0.00	0.00	0.00
73	0.00	0.00	0.00	0.00	0.00	0.00	0.00
74	0.00	0.00	0.00	0.00	0.00	0.00	0.00

Table 85. Mass-based FIMSDIST speciation data for C1-C30
components of sample 'HH-Canola' CTL

C#	C-	C=	=C=	COOH	(1x)Ar	(1x)Ar=	(2x)Ar	(2x)Ar=	(3x)Ar	(3x)Ar=
1	0.00	0.00	0.00	0.17	0.00	0.00	0.00	0.00	0.00	0.00
2	0.00	0.00	0.00	0.85	0.00	0.00	0.00	0.00	0.00	0.00
3	0.00	0.00	0.00	0.25	0.00	0.00	0.00	0.00	0.00	0.00
4	0.42	0.15	0.00	0.20	0.00	0.00	0.00	0.00	0.00	0.00
5	0.12	0.36	0.24	0.37	0.00	0.00	0.00	0.00	0.00	0.00
6	0.38	0.88	0.21	0.83	0.02	0.00	0.00	0.00	0.00	0.00
7	0.85	1.20	0.83	1.63	0.09	0.00	0.00	0.00	0.00	0.00
8	0.52	1.18	0.91	1.41	0.12	0.00	0.00	0.00	0.00	0.00
9	0.51	0.75	0.86	1.68	0.10	0.03	0.00	0.00	0.00	0.00
10	0.19	0.85	0.87	2.48	0.10	0.10	0.05	0.00	0.00	0.00
11	0.12	1.67	1.16	0.50	0.19	0.11	0.07	0.00	0.00	0.00
12	0.15	0.79	0.93	0.33	0.11	0.12	0.08	0.03	0.00	0.00
13	0.20	0.49	0.87	0.29	0.18	0.12	0.10	0.06	0.00	0.00
14	0.17	0.70	0.96	0.37	0.18	0.11	0.11	0.07	0.11	0.00
15	0.40	0.87	1.18	0.32	0.24	0.12	0.09	0.10	0.14	0.00
16	0.11	1.00	1.34	3.04	0.16	0.14	0.10	0.11	0.18	0.00
17	0.15	1.98	1.09	0.43	0.14	0.14	0.13	0.15	0.23	0.02
18	0.08	0.72	0.80	2.02	0.17	0.17	0.17	0.17	0.23	0.03
19	0.06	0.50	2.32	0.77	0.16	0.47	0.12	0.13	0.21	0.05
20	0.17	0.63	1.35	1.71	0.15	0.21	0.16	0.12	0.24	0.05
21	0.06	0.43	0.84	0.00	0.13	0.24	1.71	0.52	0.35	0.07
22	0.20	0.53	0.88	0.00	0.17	0.20	0.16	0.12	0.22	0.07
23	0.10	0.34	1.06	0.00	0.14	0.22	0.22	0.18	0.29	0.06
24	0.00	0.54	0.86	0.00	0.13	0.18	0.09	0.15	0.28	0.09
25	0.00	0.25	0.80	0.00	0.13	0.21	0.11	0.12	0.21	0.05
26	0.01	0.32	1.39	0.00	0.13	0.19	0.10	0.11	0.20	0.08
27	0.02	0.19	0.60	0.00	0.13	0.15	0.13	0.11	0.24	0.06
28	0.05	0.33	0.65	0.00	0.13	0.20	0.13	0.09	0.18	0.03
29	0.05	0.22	0.41	0.00	0.12	0.19	0.11	0.10	0.17	0.04
30	0.19	0.28	0.38	0.00	0.13	0.13	0.06	0.04	0.14	0.03

Table 86. Mass-based FIMSDIST Z-Table data for C30-C74
components of sample 'HH-Canola' CTL

C#	Z+2	Z+2	Z-2	Z-4	Z-6	Z-8	Z-10
30	0.00	0.00	0.00	0.31	0.00	0.00	0.00
31	0.18	0.22	0.25	0.27	0.24	0.24	0.00
32	0.14	0.17	0.22	0.23	0.22	0.23	0.00
33	0.15	0.15	0.19	0.21	0.21	0.19	0.00
34	0.14	0.14	0.19	0.23	0.21	0.18	0.18
35	0.11	0.14	0.15	0.15	0.18	0.16	0.16
36	0.13	0.12	0.15	0.19	0.17	0.14	0.13
37	0.10	0.12	0.12	0.13	0.15	0.13	0.11
38	0.10	0.07	0.12	0.12	0.11	0.14	0.10
39	0.09	0.08	0.10	0.10	0.11	0.11	0.10
40	0.07	0.09	0.08	0.10	0.08	0.12	0.09
41	0.07	0.08	0.05	0.08	0.10	0.09	0.09
42	0.07	0.06	0.05	0.08	0.06	0.08	0.09
43	0.04	0.06	0.07	0.06	0.08	0.08	0.05
44	0.04	0.05	0.06	0.06	0.06	0.07	0.06
45	0.06	0.06	0.05	0.05	0.06	0.07	0.05
46	0.04	0.04	0.04	0.05	0.05	0.03	0.04
47	0.03	0.03	0.03	0.04	0.05	0.05	0.05
48	0.04	0.04	0.04	0.04	0.04	0.04	0.03
49	0.03	0.03	0.03	0.03	0.03	0.03	0.04
50	0.04	0.03	0.03	0.03	0.04	0.04	0.04
51	0.03	0.03	0.03	0.03	0.03	0.04	0.04
52	0.03	0.02	0.02	0.02	0.02	0.03	0.03
53	0.02	0.02	0.02	0.03	0.03	0.03	0.03
54	0.02	0.03	0.03	0.03	0.02	0.02	0.01
55	0.01	0.01	0.02	0.02	0.02	0.01	0.02
56	0.02	0.02	0.01	0.01	0.02	0.03	0.02
57	0.01	0.01	0.02	0.02	0.00	0.00	0.02
58	0.01	0.01	0.02	0.00	0.00	0.01	0.02
59	0.00	0.01	0.01	0.00	0.00	0.01	0.01
60	0.01	0.00	0.00	0.01	0.00	0.00	0.01
61	0.00	0.00	0.00	0.00	0.01	0.00	0.00
62	0.00	0.01	0.00	0.00	0.00	0.00	0.01
63	0.00	0.00	0.00	0.00	0.00	0.00	0.00
64	0.00	0.00	0.00	0.00	0.00	0.00	0.00
65	0.00	0.00	0.00	0.00	0.00	0.00	0.00
66	0.00	0.00	0.00	0.00	0.00	0.00	0.00
67	0.00	0.00	0.00	0.00	0.00	0.00	0.00
68	0.00	0.00	0.00	0.00	0.00	0.00	0.00
69	0.00	0.00	0.00	0.00	0.00	0.00	0.00
70	0.00	0.00	0.00	0.00	0.00	0.00	0.00
71	0.00	0.00	0.00	0.00	0.00	0.00	0.00
72	0.00	0.00	0.00	0.00	0.00	0.00	0.00
73	0.00	0.00	0.00	0.00	0.00	0.00	0.00
74	0.00	0.00	0.00	0.00	0.00	0.00	0.00

Table 87. Mass-based FIMSDIST speciation data for C1-C30
components of sample 'II-HONO' CTL

C#	C-	C=	=C=	COOH	(1x)Ar	(1x)Ar=	(2x)Ar	(2x)Ar=	(3x)Ar	(3x)Ar=
1	0.00	0.00	0.00	0.11	0.00	0.00	0.00	0.00	0.00	0.00
2	0.00	0.00	0.00	0.96	0.00	0.00	0.00	0.00	0.00	0.00
3	0.00	0.00	0.00	0.21	0.00	0.00	0.00	0.00	0.00	0.00
4	0.40	0.21	0.00	0.15	0.00	0.00	0.00	0.00	0.00	0.00
5	0.18	0.47	0.27	0.20	0.00	0.00	0.00	0.00	0.00	0.00
6	0.42	0.79	0.26	0.43	0.02	0.00	0.00	0.00	0.00	0.00
7	1.04	1.29	0.84	0.84	0.08	0.00	0.00	0.00	0.00	0.00
8	0.58	1.22	0.88	1.26	0.09	0.00	0.00	0.00	0.00	0.00
9	0.52	0.80	0.87	1.72	0.08	0.03	0.00	0.00	0.00	0.00
10	0.17	0.84	0.83	3.03	0.07	0.08	0.07	0.00	0.00	0.00
11	0.11	1.86	1.03	0.47	0.14	0.09	0.06	0.00	0.00	0.00
12	0.09	0.84	0.91	0.25	0.08	0.08	0.06	0.03	0.00	0.00
13	0.15	0.48	0.79	0.22	0.14	0.11	0.10	0.05	0.00	0.00
14	0.13	0.84	1.01	0.26	0.16	0.08	0.10	0.07	0.09	0.00
15	0.38	0.96	1.19	0.29	0.18	0.09	0.08	0.09	0.12	0.00
16	0.10	1.20	1.39	1.51	0.14	0.11	0.03	0.11	0.15	0.03
17	0.12	2.25	1.02	0.40	0.12	0.12	0.12	0.15	0.19	0.01
18	0.10	1.12	0.76	2.15	0.16	0.15	0.16	0.17	0.20	0.02
19	0.06	0.54	2.93	0.69	0.14	0.31	0.10	0.13	0.18	0.05
20	0.26	0.65	1.11	1.84	0.14	0.18	0.16	0.12	0.22	0.04
21	0.06	0.42	0.82	0.00	0.12	0.23	2.25	0.41	0.28	0.05
22	0.25	0.21	0.84	0.00	0.10	0.17	0.16	0.11	0.20	0.06
23	0.12	0.23	1.17	0.00	0.14	0.20	0.23	0.21	0.26	0.09
24	0.01	0.68	0.89	0.00	0.12	0.16	0.08	0.19	0.27	0.07
25	0.00	0.31	0.87	0.00	0.12	0.19	0.10	0.08	0.19	0.04
26	0.01	0.42	2.26	0.00	0.12	0.17	0.09	0.10	0.19	0.06
27	0.02	0.16	0.66	0.00	0.12	0.13	0.12	0.11	0.24	0.06
28	0.08	0.12	0.77	0.00	0.13	0.19	0.13	0.11	0.18	0.03
29	0.00	0.22	0.45	0.00	0.14	0.19	0.10	0.23	0.17	0.03
30	0.20	0.33	0.43	0.00	0.13	0.12	0.08	0.05	0.15	0.02

Table 88. Mass-based FIMSDIST Z-Table data for C30-C74
components of sample 'II-HONO' CTL

C#	Z+2	Z+2	Z-2	Z-4	Z-6	Z-8	Z-10
30	0.00	0.00	0.00	0.33	0.00	0.00	0.00
31	0.19	0.24	0.27	0.29	0.24	0.23	0.00
32	0.14	0.19	0.25	0.24	0.22	0.22	0.00
33	0.14	0.16	0.21	0.23	0.21	0.18	0.00
34	0.13	0.14	0.23	0.29	0.22	0.17	0.17
35	0.11	0.14	0.17	0.16	0.19	0.15	0.15
36	0.12	0.13	0.19	0.21	0.17	0.14	0.12
37	0.09	0.12	0.13	0.15	0.16	0.13	0.10
38	0.10	0.07	0.13	0.13	0.11	0.15	0.11
39	0.09	0.08	0.11	0.11	0.12	0.12	0.10
40	0.07	0.09	0.08	0.11	0.09	0.12	0.09
41	0.07	0.07	0.05	0.09	0.11	0.09	0.08
42	0.07	0.06	0.06	0.09	0.08	0.08	0.09
43	0.04	0.06	0.07	0.07	0.08	0.08	0.05
44	0.03	0.05	0.07	0.07	0.06	0.07	0.06
45	0.06	0.06	0.05	0.06	0.06	0.07	0.05
46	0.04	0.03	0.04	0.06	0.05	0.04	0.04
47	0.02	0.02	0.03	0.05	0.06	0.06	0.05
48	0.04	0.04	0.04	0.04	0.05	0.04	0.04
49	0.03	0.03	0.03	0.03	0.03	0.03	0.04
50	0.04	0.04	0.04	0.04	0.04	0.04	0.04
51	0.03	0.03	0.03	0.03	0.04	0.04	0.04
52	0.02	0.02	0.02	0.02	0.03	0.03	0.03
53	0.02	0.02	0.02	0.03	0.04	0.03	0.03
54	0.02	0.03	0.03	0.03	0.02	0.02	0.02
55	0.01	0.01	0.02	0.02	0.03	0.02	0.02
56	0.02	0.02	0.01	0.02	0.03	0.03	0.02
57	0.01	0.01	0.02	0.02	0.00	0.01	0.02
58	0.01	0.02	0.02	0.00	0.00	0.02	0.02
59	0.00	0.01	0.01	0.00	0.00	0.02	0.01
60	0.01	0.00	0.00	0.01	0.00	0.00	0.01
61	0.00	0.00	0.00	0.00	0.01	0.00	0.00
62	0.00	0.00	0.00	0.00	0.00	0.00	0.00
63	0.00	0.00	0.00	0.00	0.00	0.00	0.00
64	0.00	0.00	0.00	0.00	0.00	0.00	0.00
65	0.00	0.00	0.00	0.00	0.00	0.00	0.00
66	0.00	0.00	0.00	0.00	0.00	0.00	0.00
67	0.00	0.00	0.00	0.00	0.00	0.00	0.00
68	0.00	0.00	0.00	0.00	0.00	0.00	0.00
69	0.00	0.00	0.00	0.00	0.00	0.00	0.00
70	0.00	0.00	0.00	0.00	0.00	0.00	0.00
71	0.00	0.00	0.00	0.00	0.00	0.00	0.00
72	0.00	0.00	0.00	0.00	0.00	0.00	0.00
73	0.00	0.00	0.00	0.00	0.00	0.00	0.00
74	0.00	0.00	0.00	0.00	0.00	0.00	0.00

Table 89. Mass-based FIMSDIST speciation data for C1-C30
components of sample 'A-Soy' CTL

C#	C-	C=	=C=	COOH	(1x)Ar	(1x)Ar=	(2x)Ar	(2x)Ar=	(3x)Ar	(3x)Ar=
1	0.00	0.00	0.00	0.28	0.00	0.00	0.00	0.00	0.00	0.00
2	0.00	0.00	0.00	0.68	0.00	0.00	0.00	0.00	0.00	0.00
3	0.00	0.00	0.00	0.16	0.00	0.00	0.00	0.00	0.00	0.00
4	0.55	0.15	0.00	0.15	0.00	0.00	0.00	0.00	0.00	0.00
5	0.14	0.21	0.14	0.49	0.00	0.00	0.00	0.00	0.00	0.00
6	0.20	0.41	0.09	0.83	0.01	0.00	0.00	0.00	0.00	0.00
7	0.33	0.83	0.45	2.03	0.04	0.00	0.00	0.00	0.00	0.00
8	0.37	0.69	0.66	1.08	0.10	0.00	0.00	0.00	0.00	0.00
9	0.19	0.47	0.48	1.10	0.07	0.01	0.00	0.00	0.00	0.00
10	0.09	0.41	0.59	1.72	0.07	0.08	0.06	0.00	0.00	0.00
11	0.09	0.94	1.30	0.35	0.23	0.07	0.03	0.00	0.00	0.00
12	0.08	0.58	0.90	0.19	0.11	0.06	0.05	0.02	0.00	0.00
13	0.15	0.37	0.52	0.16	0.12	0.07	0.17	0.04	0.00	0.00
14	0.13	0.39	0.57	0.19	0.11	0.06	0.10	0.07	0.07	0.00
15	0.43	0.79	0.81	0.21	0.17	0.06	0.06	0.08	0.11	0.00
16	0.07	0.60	0.84	5.55	0.11	0.09	0.05	0.09	0.14	0.00
17	0.13	1.18	0.91	0.26	0.10	0.07	0.07	0.13	0.25	0.01
18	0.05	0.41	0.56	4.09	0.14	0.10	0.16	0.10	0.18	0.00
19	0.02	0.45	3.05	0.40	0.10	0.58	0.10	0.09	0.15	0.01
20	0.00	0.94	1.47	1.00	0.12	0.12	0.09	0.04	0.24	0.03
21	0.02	0.67	0.58	0.00	0.11	0.23	2.26	1.70	0.39	0.03
22	0.11	0.21	1.00	0.00	0.16	0.12	0.09	0.12	0.19	0.02
23	0.06	0.38	1.24	0.00	0.09	0.14	0.12	0.55	0.35	0.04
24	0.01	0.73	0.78	0.00	0.14	0.11	0.07	0.21	0.35	0.13
25	0.00	0.57	0.66	0.00	0.22	0.18	0.08	0.14	0.16	0.00
26	0.35	0.33	0.99	0.00	0.18	0.14	0.06	0.00	0.17	0.00
27	0.02	0.40	0.60	0.00	0.12	0.12	0.00	0.09	0.28	0.02
28	0.37	0.74	0.81	0.00	0.15	0.16	0.12	0.00	0.19	0.03
29	0.18	0.23	0.36	0.00	0.15	0.14	0.01	0.00	0.20	0.00
30	0.15	0.39	0.53	0.00	0.14	0.13	0.00	0.04	0.16	0.00

Table 90. Mass-based FIMSDIST Z-Table data for C30-C74
components of sample 'A-Soy' CTL

C#	Z+2	Z+2	Z-2	Z-4	Z-6	Z-8	Z-10
30	0.00	0.00	0.00	0.42	0.00	0.00	0.00
31	0.19	0.31	0.39	0.42	0.26	0.22	0.00
32	0.17	0.21	0.23	0.30	0.28	0.25	0.00
33	0.21	0.24	0.25	0.29	0.28	0.22	0.00
34	0.20	0.18	0.22	0.25	0.31	0.24	0.29
35	0.17	0.23	0.20	0.16	0.27	0.24	0.28
36	0.23	0.20	0.24	0.42	0.32	0.18	0.19
37	0.19	0.25	0.27	0.29	0.31	0.22	0.15
38	0.17	0.05	0.28	0.24	0.25	0.30	0.19
39	0.19	0.13	0.28	0.25	0.25	0.19	0.17
40	0.05	0.20	0.13	0.24	0.12	0.25	0.14
41	0.11	0.13	0.08	0.10	0.22	0.10	0.15
42	0.05	0.12	0.06	0.14	0.10	0.06	0.20
43	0.04	0.06	0.17	0.13	0.07	0.16	0.06
44	0.04	0.03	0.10	0.12	0.06	0.08	0.11
45	0.04	0.11	0.09	0.05	0.05	0.11	0.09
46	0.04	0.03	0.03	0.09	0.09	0.05	0.02
47	0.03	0.01	0.01	0.02	0.07	0.12	0.10
48	0.02	0.03	0.06	0.07	0.08	0.07	0.04
49	0.07	0.02	0.02	0.02	0.02	0.03	0.02
50	0.09	0.09	0.08	0.08	0.07	0.08	0.08
51	0.06	0.04	0.06	0.06	0.07	0.09	0.09
52	0.01	0.00	0.00	0.00	0.01	0.04	0.05
53	0.00	0.00	0.04	0.05	0.04	0.04	0.04
54	0.04	0.04	0.06	0.03	0.00	0.00	0.00
55	0.00	0.00	0.02	0.00	0.00	0.00	0.04
56	0.06	0.00	0.00	0.00	0.05	0.04	0.00
57	0.00	0.00	0.06	0.03	0.00	0.00	0.04
58	0.00	0.03	0.03	0.00	0.00	0.00	0.00
59	0.00	0.00	0.03	0.00	0.00	0.00	0.00
60	0.00	0.00	0.00	0.00	0.00	0.00	0.00
61	0.00	0.00	0.00	0.00	0.00	0.00	0.00
62	0.00	0.00	0.00	0.00	0.00	0.00	0.04
63	0.00	0.00	0.00	0.00	0.00	0.00	0.00
64	0.00	0.00	0.00	0.00	0.00	0.00	0.00
65	0.00	0.00	0.00	0.00	0.00	0.00	0.00
66	0.00	0.00	0.00	0.00	0.00	0.00	0.00
67	0.00	0.00	0.00	0.00	0.00	0.00	0.00
68	0.00	0.00	0.00	0.00	0.00	0.00	0.00
69	0.00	0.00	0.00	0.00	0.00	0.00	0.00
70	0.00	0.00	0.00	0.00	0.00	0.00	0.00
71	0.00	0.00	0.00	0.00	0.00	0.00	0.00
72	0.00	0.00	0.00	0.00	0.00	0.00	0.00
73	0.00	0.00	0.00	0.00	0.00	0.00	0.00
74	0.00	0.00	0.00	0.00	0.00	0.00	0.00

Table 91. Mass-based FIMSDIST speciation data for C1-C30
components of sample 'B-Soy' CTL

C#	C-	C=	=C=	COOH	(1x)Ar	(1x)Ar=	(2x)Ar	(2x)Ar=	(3x)Ar	(3x)Ar=
1	0.00	0.00	0.00	0.28	0.00	0.00	0.00	0.00	0.00	0.00
2	0.00	0.00	0.00	0.85	0.00	0.00	0.00	0.00	0.00	0.00
3	0.00	0.00	0.00	0.19	0.00	0.00	0.00	0.00	0.00	0.00
4	0.65	0.22	0.00	0.16	0.00	0.00	0.00	0.00	0.00	0.00
5	0.20	0.32	0.14	0.49	0.00	0.00	0.00	0.00	0.00	0.00
6	0.24	0.67	0.13	0.83	0.02	0.00	0.00	0.00	0.00	0.00
7	0.42	1.03	0.61	2.03	0.06	0.00	0.00	0.00	0.00	0.00
8	0.44	0.84	0.82	1.28	0.09	0.00	0.00	0.00	0.00	0.00
9	0.33	0.53	0.65	1.29	0.08	0.03	0.00	0.00	0.00	0.00
10	0.12	0.51	0.70	1.87	0.07	0.10	0.04	0.00	0.00	0.00
11	0.11	0.98	1.28	0.41	0.25	0.09	0.04	0.00	0.00	0.00
12	0.09	0.53	0.95	0.25	0.13	0.08	0.06	0.03	0.00	0.00
13	0.18	0.44	0.67	0.23	0.15	0.09	0.15	0.06	0.00	0.00
14	0.16	0.46	0.70	0.27	0.13	0.08	0.11	0.07	0.10	0.00
15	0.47	0.84	0.86	0.29	0.20	0.08	0.08	0.09	0.13	0.00
16	0.09	0.65	0.94	5.25	0.13	0.12	0.08	0.10	0.17	0.00
17	0.17	1.32	1.08	0.37	0.14	0.10	0.10	0.15	0.29	0.01
18	0.07	0.43	0.64	4.14	0.17	0.14	0.18	0.12	0.24	0.00
19	0.13	0.54	2.50	0.58	0.13	0.59	0.12	0.11	0.21	0.01
20	0.02	1.26	1.29	1.19	0.20	0.16	0.08	0.05	0.25	0.04
21	0.05	0.60	0.70	0.00	0.16	0.27	1.83	1.16	0.41	0.01
22	0.12	0.22	0.98	0.00	0.17	0.17	0.12	0.14	0.22	0.02
23	0.02	0.39	1.24	0.00	0.12	0.17	0.14	0.48	0.36	0.05
24	0.01	0.63	0.79	0.00	0.18	0.15	0.10	0.20	0.33	0.12
25	0.00	0.49	0.69	0.00	0.25	0.19	0.09	0.13	0.19	0.00
26	0.28	0.35	0.93	0.00	0.22	0.19	0.08	0.02	0.20	0.00
27	0.05	0.43	0.60	0.00	0.15	0.14	0.03	0.10	0.27	0.00
28	0.32	0.61	0.68	0.00	0.16	0.17	0.11	0.00	0.18	0.03
29	0.19	0.20	0.33	0.00	0.18	0.16	0.01	0.00	0.18	0.00
30	0.15	0.32	0.45	0.00	0.14	0.13	0.00	0.04	0.15	0.00

Table 92. Mass-based FIMSDIST Z-Table data for C30-C74
components of sample 'B-Soy' CTL

C#	Z+2	Z+2	Z-2	Z-4	Z-6	Z-8	Z-10
30	0.00	0.00	0.00	0.38	0.00	0.00	0.00
31	0.19	0.26	0.32	0.31	0.26	0.24	0.00
32	0.15	0.18	0.20	0.25	0.26	0.24	0.00
33	0.19	0.19	0.21	0.26	0.25	0.21	0.00
34	0.16	0.15	0.19	0.21	0.27	0.22	0.25
35	0.14	0.18	0.16	0.17	0.23	0.21	0.24
36	0.18	0.15	0.19	0.31	0.25	0.15	0.16
37	0.14	0.19	0.20	0.23	0.24	0.18	0.12
38	0.13	0.05	0.21	0.18	0.18	0.23	0.13
39	0.13	0.05	0.20	0.17	0.18	0.14	0.13
40	0.05	0.14	0.09	0.17	0.07	0.19	0.08
41	0.06	0.08	0.05	0.05	0.16	0.07	0.11
42	0.03	0.10	0.04	0.10	0.07	0.06	0.14
43	0.04	0.03	0.11	0.05	0.06	0.11	0.05
44	0.04	0.03	0.07	0.09	0.05	0.07	0.06
45	0.02	0.09	0.04	0.04	0.04	0.09	0.05
46	0.04	0.02	0.02	0.08	0.08	0.04	0.03
47	0.02	0.02	0.01	0.02	0.07	0.09	0.07
48	0.02	0.02	0.06	0.06	0.06	0.06	0.03
49	0.06	0.04	0.01	0.02	0.02	0.02	0.02
50	0.07	0.07	0.06	0.07	0.07	0.07	0.06
51	0.04	0.05	0.05	0.05	0.06	0.05	0.07
52	0.00	0.00	0.00	0.00	0.01	0.04	0.03
53	0.00	0.03	0.04	0.05	0.04	0.02	0.00
54	0.04	0.05	0.05	0.02	0.00	0.00	0.00
55	0.00	0.00	0.02	0.02	0.00	0.00	0.03
56	0.03	0.00	0.00	0.00	0.04	0.03	0.00
57	0.00	0.00	0.04	0.00	0.00	0.00	0.03
58	0.00	0.00	0.00	0.00	0.00	0.00	0.00
59	0.00	0.00	0.00	0.00	0.00	0.00	0.00
60	0.00	0.00	0.00	0.00	0.00	0.00	0.00
61	0.00	0.00	0.00	0.00	0.00	0.00	0.00
62	0.00	0.00	0.00	0.00	0.00	0.00	0.00
63	0.00	0.00	0.00	0.00	0.00	0.00	0.00
64	0.00	0.00	0.00	0.00	0.00	0.00	0.00
65	0.00	0.00	0.00	0.00	0.00	0.00	0.00
66	0.00	0.00	0.00	0.00	0.00	0.00	0.00
67	0.00	0.00	0.00	0.00	0.00	0.00	0.00
68	0.00	0.00	0.00	0.00	0.00	0.00	0.00
69	0.00	0.00	0.00	0.00	0.00	0.00	0.00
70	0.00	0.00	0.00	0.00	0.00	0.00	0.00
71	0.00	0.00	0.00	0.00	0.00	0.00	0.00
72	0.00	0.00	0.00	0.00	0.00	0.00	0.00
73	0.00	0.00	0.00	0.00	0.00	0.00	0.00
74	0.00	0.00	0.00	0.00	0.00	0.00	0.00

Table 93. Mass-based FIMSDIST speciation data for C1-C30
components of sample 'C-Soy' CTL

C#	C-	C=	=C=	COOH	(1x)Ar	(1x)Ar=	(2x)Ar	(2x)Ar=	(3x)Ar	(3x)Ar=
1	0.00	0.00	0.00	0.28	0.00	0.00	0.00	0.00	0.00	0.00
2	0.00	0.00	0.00	0.87	0.00	0.00	0.00	0.00	0.00	0.00
3	0.00	0.00	0.00	0.21	0.00	0.00	0.00	0.00	0.00	0.00
4	0.57	0.22	0.00	0.18	0.00	0.00	0.00	0.00	0.00	0.00
5	0.27	0.34	0.22	0.49	0.00	0.00	0.00	0.00	0.00	0.00
6	0.26	0.88	0.17	0.83	0.02	0.00	0.00	0.00	0.00	0.00
7	0.52	1.16	0.78	2.03	0.08	0.00	0.00	0.00	0.00	0.00
8	0.50	0.89	1.03	1.42	0.16	0.00	0.00	0.00	0.00	0.00
9	0.36	0.65	0.74	1.49	0.10	0.04	0.00	0.00	0.00	0.00
10	0.15	0.62	0.84	1.81	0.09	0.12	0.06	0.00	0.00	0.00
11	0.20	1.12	1.34	0.48	0.27	0.12	0.05	0.00	0.00	0.00
12	0.12	0.58	1.06	0.31	0.15	0.11	0.05	0.02	0.00	0.00
13	0.20	0.49	0.75	0.29	0.18	0.11	0.14	0.06	0.00	0.00
14	0.20	0.62	0.81	0.32	0.15	0.10	0.11	0.08	0.12	0.00
15	0.52	0.87	0.97	0.35	0.22	0.10	0.09	0.07	0.15	0.00
16	0.11	0.73	0.97	4.49	0.17	0.14	0.10	0.11	0.19	0.00
17	0.19	1.32	1.09	0.45	0.17	0.12	0.12	0.15	0.31	0.00
18	0.08	0.44	0.74	3.64	0.18	0.15	0.19	0.13	0.25	0.01
19	0.05	0.36	1.96	0.69	0.15	0.56	0.12	0.13	0.23	0.02
20	0.02	0.70	1.21	1.30	0.16	0.19	0.12	0.12	0.26	0.05
21	0.05	0.56	0.76	0.00	0.15	0.29	1.41	0.97	0.40	0.07
22	0.12	0.24	0.89	0.00	0.20	0.19	0.13	0.14	0.24	0.06
23	0.12	0.38	0.97	0.00	0.13	0.19	0.15	0.38	0.33	0.05
24	0.01	0.54	0.74	0.00	0.20	0.18	0.09	0.19	0.30	0.12
25	0.00	0.20	0.68	0.00	0.24	0.23	0.10	0.13	0.21	0.00
26	0.01	0.31	0.83	0.00	0.22	0.20	0.09	0.11	0.20	0.00
27	0.03	0.43	0.58	0.00	0.15	0.15	0.13	0.11	0.26	0.00
28	0.31	0.52	0.62	0.00	0.17	0.19	0.13	0.00	0.18	0.03
29	0.20	0.19	0.28	0.00	0.18	0.17	0.01	0.00	0.18	0.00
30	0.16	0.35	0.40	0.00	0.14	0.15	0.00	0.04	0.15	0.00

Table 94. Mass-based FIMSDIST Z-Table data for C30-C74
components of sample 'C-Soy' CTL

C#	Z+2	Z+2	Z-2	Z-4	Z-6	Z-8	Z-10
30	0.00	0.00	0.00	0.33	0.00	0.00	0.00
31	0.20	0.27	0.28	0.30	0.26	0.25	0.00
32	0.16	0.19	0.19	0.24	0.26	0.25	0.00
33	0.18	0.20	0.22	0.26	0.26	0.23	0.00
34	0.16	0.13	0.18	0.19	0.28	0.22	0.25
35	0.13	0.16	0.17	0.16	0.23	0.21	0.23
36	0.18	0.12	0.16	0.29	0.24	0.14	0.14
37	0.11	0.19	0.18	0.20	0.22	0.15	0.09
38	0.12	0.05	0.18	0.15	0.12	0.21	0.10
39	0.11	0.05	0.16	0.11	0.14	0.12	0.05
40	0.05	0.14	0.06	0.14	0.07	0.16	0.09
41	0.06	0.09	0.05	0.06	0.14	0.08	0.08
42	0.05	0.07	0.05	0.07	0.07	0.06	0.13
43	0.04	0.04	0.10	0.05	0.06	0.11	0.05
44	0.04	0.03	0.08	0.09	0.06	0.07	0.06
45	0.03	0.09	0.07	0.04	0.04	0.09	0.05
46	0.04	0.03	0.03	0.08	0.07	0.04	0.03
47	0.02	0.02	0.01	0.04	0.08	0.09	0.07
48	0.02	0.02	0.06	0.07	0.06	0.05	0.03
49	0.06	0.04	0.04	0.01	0.02	0.02	0.02
50	0.07	0.07	0.07	0.07	0.07	0.07	0.06
51	0.05	0.05	0.05	0.06	0.06	0.07	0.07
52	0.02	0.00	0.00	0.00	0.00	0.03	0.04
53	0.00	0.03	0.04	0.05	0.04	0.03	0.00
54	0.05	0.05	0.05	0.03	0.00	0.00	0.00
55	0.00	0.00	0.02	0.02	0.00	0.00	0.00
56	0.03	0.00	0.00	0.00	0.05	0.03	0.00
57	0.00	0.00	0.04	0.00	0.00	0.00	0.03
58	0.00	0.03	0.02	0.00	0.00	0.00	0.00
59	0.00	0.00	0.00	0.00	0.00	0.00	0.00
60	0.00	0.00	0.00	0.00	0.00	0.00	0.00
61	0.00	0.00	0.00	0.00	0.00	0.00	0.00
62	0.00	0.00	0.00	0.00	0.00	0.00	0.00
63	0.00	0.00	0.00	0.00	0.00	0.00	0.00
64	0.00	0.00	0.00	0.00	0.00	0.00	0.00
65	0.00	0.00	0.00	0.00	0.00	0.00	0.00
66	0.00	0.00	0.00	0.00	0.00	0.00	0.00
67	0.00	0.00	0.00	0.00	0.00	0.00	0.00
68	0.00	0.00	0.00	0.00	0.00	0.00	0.00
69	0.00	0.00	0.00	0.00	0.00	0.00	0.00
70	0.00	0.00	0.00	0.00	0.00	0.00	0.00
71	0.00	0.00	0.00	0.00	0.00	0.00	0.00
72	0.00	0.00	0.00	0.00	0.00	0.00	0.00
73	0.00	0.00	0.00	0.00	0.00	0.00	0.00
74	0.00	0.00	0.00	0.00	0.00	0.00	0.00

Table 95. Mass-based FIMSDIST speciation data for C1-C30
components of sample 'D-Soy' CTL

C#	C-	C=	=C=	COOH	(1x)Ar	(1x)Ar=	(2x)Ar	(2x)Ar=	(3x)Ar	(3x)Ar=
1	0.00	0.00	0.00	0.28	0.00	0.00	0.00	0.00	0.00	0.00
2	0.00	0.00	0.00	0.68	0.00	0.00	0.00	0.00	0.00	0.00
3	0.00	0.00	0.00	0.18	0.00	0.00	0.00	0.00	0.00	0.00
4	0.37	0.20	0.00	0.16	0.00	0.00	0.00	0.00	0.00	0.00
5	0.22	0.36	0.21	0.49	0.00	0.00	0.00	0.00	0.00	0.00
6	0.40	1.01	0.20	0.83	0.02	0.00	0.00	0.00	0.00	0.00
7	0.64	1.33	0.99	2.03	0.11	0.00	0.00	0.00	0.00	0.00
8	0.44	0.89	1.19	1.21	0.17	0.00	0.00	0.00	0.00	0.00
9	0.45	0.66	0.94	1.32	0.15	0.05	0.00	0.00	0.00	0.00
10	0.26	0.72	0.89	1.30	0.11	0.20	0.05	0.00	0.00	0.00
11	0.26	1.02	1.07	0.59	0.29	0.25	0.08	0.00	0.00	0.00
12	0.25	0.57	0.96	0.42	0.21	0.22	0.11	0.02	0.00	0.00
13	0.31	0.55	0.92	0.42	0.25	0.17	0.11	0.07	0.00	0.00
14	0.33	0.62	0.98	0.45	0.19	0.19	0.12	0.10	0.13	0.00
15	0.82	1.04	1.09	0.47	0.21	0.20	0.11	0.10	0.16	0.00
16	0.18	1.14	1.13	3.23	0.21	0.24	0.10	0.08	0.19	0.03
17	0.34	1.27	1.36	0.64	0.25	0.24	0.15	0.03	0.26	0.03
18	0.08	0.48	0.91	2.72	0.19	0.27	0.19	0.15	0.24	0.02
19	0.14	0.39	1.00	1.11	0.18	0.40	0.15	0.13	0.24	0.05
20	0.12	0.46	1.01	1.75	0.20	0.30	0.15	0.14	0.25	0.08
21	0.10	0.46	0.89	0.00	0.18	0.29	0.77	0.44	0.34	0.10
22	0.10	0.50	0.83	0.00	0.23	0.26	0.16	0.15	0.25	0.09
23	0.13	0.53	1.02	0.00	0.17	0.25	0.19	0.18	0.37	0.07
24	0.09	0.45	0.75	0.00	0.18	0.27	0.15	0.12	0.30	0.15
25	0.00	0.29	0.66	0.00	0.20	0.36	0.10	0.13	0.20	0.06
26	0.13	0.25	0.73	0.00	0.19	0.25	0.12	0.11	0.21	0.06
27	0.01	0.19	0.56	0.00	0.17	0.19	0.09	0.12	0.22	0.04
28	0.09	0.18	0.67	0.00	0.12	0.20	0.19	0.08	0.18	0.03
29	0.04	0.16	0.26	0.00	0.18	0.16	0.09	0.08	0.16	0.06
30	0.18	0.46	0.55	0.00	0.13	0.22	0.08	0.06	0.13	0.00

Table 96. Mass-based FIMSDIST Z-Table data for C30-C74
components of sample 'D-Soy' CTL

C#	Z+2	Z+2	Z-2	Z-4	Z-6	Z-8	Z-10
30	0.00	0.00	0.00	0.45	0.00	0.00	0.00
31	0.20	0.42	0.42	0.48	0.22	0.25	0.00
32	0.15	0.16	0.19	0.38	0.41	0.38	0.00
33	0.15	0.29	0.32	0.39	0.32	0.18	0.00
34	0.15	0.13	0.16	0.15	0.18	0.17	0.19
35	0.12	0.14	0.13	0.13	0.15	0.16	0.29
36	0.13	0.11	0.10	0.14	0.14	0.13	0.13
37	0.10	0.12	0.11	0.11	0.12	0.12	0.12
38	0.11	0.06	0.10	0.10	0.10	0.13	0.11
39	0.09	0.07	0.10	0.09	0.10	0.10	0.10
40	0.06	0.09	0.07	0.09	0.08	0.11	0.07
41	0.07	0.08	0.06	0.07	0.09	0.08	0.09
42	0.05	0.07	0.05	0.07	0.06	0.06	0.09
43	0.04	0.04	0.07	0.06	0.06	0.07	0.05
44	0.03	0.03	0.18	0.06	0.05	0.05	0.05
45	0.17	0.18	0.04	0.04	0.04	0.05	0.05
46	0.03	0.03	0.02	0.04	0.04	0.03	0.02
47	0.02	0.01	0.01	0.02	0.03	0.16	0.04
48	0.02	0.02	0.02	0.02	0.03	0.03	0.02
49	0.02	0.01	0.01	0.01	0.01	0.01	0.01
50	0.14	0.02	0.02	0.01	0.02	0.02	0.02
51	0.00	0.01	0.01	0.01	0.15	0.02	0.15
52	0.00	0.00	0.00	0.00	0.00	0.00	0.00
53	0.00	0.00	0.00	0.00	0.00	0.00	0.00
54	0.00	0.00	0.13	0.00	0.00	0.00	0.00
55	0.00	0.00	0.00	0.00	0.00	0.00	0.00
56	0.00	0.00	0.00	0.00	0.00	0.00	0.00
57	0.00	0.00	0.00	0.00	0.00	0.00	0.00
58	0.00	0.00	0.00	0.00	0.00	0.00	0.00
59	0.00	0.00	0.00	0.00	0.00	0.00	0.00
60	0.00	0.00	0.00	0.00	0.00	0.00	0.00
61	0.00	0.00	0.00	0.00	0.00	0.00	0.00
62	0.00	0.00	0.00	0.00	0.00	0.00	0.00
63	0.00	0.00	0.00	0.00	0.00	0.00	0.00
64	0.00	0.00	0.00	0.00	0.00	0.00	0.00
65	0.00	0.00	0.00	0.00	0.00	0.00	0.00
66	0.00	0.00	0.00	0.00	0.00	0.00	0.00
67	0.00	0.00	0.00	0.00	0.00	0.00	0.00
68	0.00	0.00	0.00	0.00	0.00	0.00	0.00
69	0.00	0.00	0.00	0.00	0.00	0.00	0.00
70	0.00	0.00	0.00	0.00	0.00	0.00	0.00
71	0.00	0.00	0.00	0.00	0.00	0.00	0.00
72	0.00	0.00	0.00	0.00	0.00	0.00	0.00
73	0.00	0.00	0.00	0.00	0.00	0.00	0.00
74	0.00	0.00	0.00	0.00	0.00	0.00	0.00

Table 97. Mass-based FIMSDIST speciation data for C1-C30 components of sample 'E-Soy' CTL

C#	C-	C=	=C=	COOH	(1x)Ar	(1x)Ar=	(2x)Ar	(2x)Ar=	(3x)Ar	(3x)Ar=
1	0.00	0.00	0.00	0.28	0.00	0.00	0.00	0.00	0.00	0.00
2	0.00	0.00	0.00	0.87	0.00	0.00	0.00	0.00	0.00	0.00
3	0.00	0.00	0.00	0.30	0.00	0.00	0.00	0.00	0.00	0.00
4	0.58	0.35	0.00	0.28	0.00	0.00	0.00	0.00	0.00	0.00
5	0.36	0.53	0.28	0.49	0.00	0.00	0.00	0.00	0.00	0.00
6	0.65	1.36	0.34	0.83	0.03	0.00	0.00	0.00	0.00	0.00
7	0.87	1.46	1.17	2.03	0.14	0.00	0.00	0.00	0.00	0.00
8	0.65	1.75	1.29	1.75	0.19	0.01	0.00	0.00	0.00	0.00
9	0.59	1.15	1.26	1.80	0.17	0.05	0.00	0.00	0.00	0.00
10	0.29	1.09	1.20	1.84	0.19	0.19	0.08	0.00	0.00	0.00
11	0.21	1.61	1.66	0.63	0.37	0.25	0.11	0.00	0.00	0.00
12	0.24	1.11	1.29	0.46	0.20	0.25	0.12	0.03	0.00	0.00
13	0.34	0.63	1.11	0.44	0.32	0.15	0.13	0.07	0.00	0.00
14	0.32	0.94	1.10	0.49	0.29	0.20	0.13	0.09	0.17	0.00
15	0.94	1.01	1.19	0.46	0.27	0.23	0.12	0.08	0.19	0.00
16	0.18	0.93	1.34	2.94	0.25	0.25	0.08	0.06	0.25	0.01
17	0.31	1.68	1.57	0.54	0.25	0.25	0.15	0.13	0.27	0.02
18	0.13	0.57	0.84	1.88	0.22	0.25	0.18	0.15	0.28	0.02
19	0.14	0.59	1.08	0.86	0.22	0.42	0.13	0.12	0.21	0.03
20	0.08	0.43	1.03	1.40	0.19	0.25	0.12	0.07	0.25	0.05
21	0.06	0.42	0.71	0.00	0.16	0.25	0.59	0.44	0.33	0.07
22	0.10	0.38	0.68	0.00	0.13	0.22	0.13	0.10	0.21	0.08
23	0.08	0.46	0.79	0.00	0.16	0.23	0.15	0.15	0.27	0.11
24	0.08	0.07	0.66	0.00	0.13	0.19	0.10	0.08	0.25	0.08
25	0.10	0.18	0.57	0.00	0.13	0.21	0.07	0.19	0.17	0.06
26	0.00	0.17	0.57	0.00	0.12	0.19	0.06	0.09	0.17	0.07
27	0.01	0.11	0.42	0.00	0.06	0.16	0.11	0.09	0.18	0.06
28	0.03	0.12	0.42	0.00	0.12	0.16	0.10	0.07	0.14	0.07
29	0.03	0.10	0.25	0.00	0.10	0.14	0.09	0.07	0.13	0.03
30	0.17	0.21	0.27	0.00	0.11	0.11	0.06	0.05	0.11	0.03

Table 98. Mass-based FIMSDIST Z-Table data for C30-C74
components of sample 'E-Soy' CTL

C#	Z+2	Z+2	Z-2	Z-4	Z-6	Z-8	Z-10
30	0.00	0.00	0.00	0.23	0.00	0.00	0.00
31	0.15	0.16	0.19	0.21	0.20	0.21	0.00
32	0.13	0.13	0.16	0.17	0.18	0.20	0.00
33	0.12	0.12	0.14	0.16	0.16	0.16	0.00
34	0.11	0.10	0.13	0.14	0.16	0.15	0.15
35	0.09	0.10	0.11	0.11	0.13	0.12	0.13
36	0.10	0.08	0.09	0.12	0.12	0.11	0.11
37	0.07	0.09	0.09	0.09	0.11	0.10	0.08
38	0.08	0.06	0.08	0.08	0.07	0.10	0.09
39	0.07	0.06	0.07	0.07	0.07	0.08	0.08
40	0.06	0.06	0.06	0.06	0.06	0.08	0.07
41	0.05	0.06	0.04	0.06	0.07	0.06	0.06
42	0.05	0.05	0.05	0.05	0.04	0.06	0.06
43	0.04	0.05	0.04	0.04	0.05	0.05	0.04
44	0.03	0.04	0.04	0.04	0.04	0.05	0.04
45	0.04	0.04	0.03	0.03	0.04	0.04	0.04
46	0.03	0.03	0.03	0.03	0.03	0.03	0.03
47	0.02	0.02	0.03	0.03	0.04	0.04	0.03
48	0.03	0.03	0.03	0.03	0.03	0.03	0.02
49	0.02	0.02	0.02	0.02	0.02	0.02	0.03
50	0.02	0.02	0.02	0.02	0.02	0.02	0.02
51	0.02	0.02	0.02	0.02	0.02	0.02	0.02
52	0.02	0.02	0.02	0.02	0.02	0.02	0.02
53	0.01	0.01	0.02	0.02	0.02	0.02	0.02
54	0.01	0.02	0.02	0.02	0.02	0.01	0.01
55	0.00	0.01	0.01	0.01	0.01	0.01	0.01
56	0.01	0.01	0.01	0.01	0.01	0.01	0.01
57	0.00	0.01	0.01	0.01	0.00	0.00	0.01
58	0.00	0.01	0.01	0.00	0.00	0.01	0.01
59	0.00	0.00	0.01	0.00	0.00	0.01	0.00
60	0.00	0.00	0.00	0.01	0.00	0.00	0.00
61	0.00	0.00	0.00	0.00	0.01	0.00	0.00
62	0.00	0.00	0.00	0.00	0.00	0.00	0.00
63	0.00	0.00	0.00	0.00	0.00	0.00	0.00
64	0.00	0.00	0.00	0.00	0.00	0.00	0.00
65	0.00	0.00	0.00	0.00	0.00	0.00	0.00
66	0.00	0.00	0.00	0.00	0.00	0.00	0.00
67	0.00	0.00	0.00	0.00	0.00	0.00	0.00
68	0.00	0.00	0.00	0.00	0.00	0.00	0.00
69	0.00	0.00	0.00	0.00	0.00	0.00	0.00
70	0.00	0.00	0.00	0.00	0.00	0.00	0.00
71	0.00	0.00	0.00	0.00	0.00	0.00	0.00
72	0.00	0.00	0.00	0.00	0.00	0.00	0.00
73	0.00	0.00	0.00	0.00	0.00	0.00	0.00
74	0.00	0.00	0.00	0.00	0.00	0.00	0.00

Table 99. Mass-based FIMSDIST speciation data for C1-C30
components of sample 'F-Soy' CTL

C#	C-	C=	=C=	COOH	(1x)Ar	(1x)Ar=	(2x)Ar	(2x)Ar=	(3x)Ar	(3x)Ar=
1	0.00	0.00	0.00	0.28	0.00	0.00	0.00	0.00	0.00	0.00
2	0.00	0.00	0.00	0.98	0.00	0.00	0.00	0.00	0.00	0.00
3	0.00	0.00	0.00	0.26	0.00	0.00	0.00	0.00	0.00	0.00
4	0.81	0.29	0.00	0.31	0.00	0.00	0.00	0.00	0.00	0.00
5	0.33	0.68	0.24	0.49	0.00	0.00	0.00	0.00	0.00	0.00
6	0.59	1.33	0.32	0.83	0.03	0.00	0.00	0.00	0.00	0.00
7	0.73	1.54	1.03	2.03	0.11	0.00	0.00	0.00	0.00	0.00
8	0.74	1.84	1.23	1.99	0.14	0.01	0.00	0.00	0.00	0.00
9	0.56	1.29	1.14	2.00	0.15	0.05	0.00	0.00	0.00	0.00
10	0.26	1.02	1.15	2.13	0.21	0.20	0.07	0.00	0.00	0.00
11	0.22	1.55	1.61	0.63	0.40	0.23	0.12	0.00	0.00	0.00
12	0.28	1.17	1.31	0.42	0.20	0.20	0.11	0.03	0.00	0.00
13	0.37	0.67	0.84	0.40	0.22	0.13	0.13	0.08	0.00	0.00
14	0.30	1.06	1.12	0.40	0.24	0.15	0.12	0.08	0.17	0.00
15	0.90	0.83	1.18	0.41	0.23	0.17	0.11	0.09	0.17	0.00
16	0.16	0.94	1.11	3.93	0.20	0.19	0.07	0.11	0.20	0.02
17	0.25	1.71	1.52	0.46	0.22	0.20	0.13	0.12	0.24	0.02
18	0.11	0.56	0.84	2.07	0.20	0.21	0.17	0.13	0.24	0.02
19	0.07	0.49	1.44	0.66	0.18	0.43	0.12	0.11	0.20	0.02
20	0.11	0.42	1.09	1.37	0.16	0.19	0.13	0.10	0.25	0.04
21	0.06	0.49	0.57	0.00	0.13	0.26	0.70	0.54	0.33	0.05
22	0.09	0.41	0.73	0.00	0.10	0.17	0.11	0.08	0.19	0.06
23	0.08	0.45	0.80	0.00	0.07	0.18	0.15	0.18	0.26	0.10
24	0.01	0.38	0.59	0.00	0.11	0.16	0.08	0.08	0.24	0.13
25	0.09	0.22	0.50	0.00	0.10	0.18	0.09	0.09	0.15	0.06
26	0.00	0.18	0.59	0.00	0.11	0.16	0.05	0.07	0.15	0.07
27	0.01	0.10	0.40	0.00	0.06	0.13	0.10	0.08	0.17	0.06
28	0.03	0.14	0.44	0.00	0.11	0.14	0.10	0.07	0.13	0.07
29	0.02	0.09	0.32	0.00	0.09	0.14	0.08	0.07	0.12	0.03
30	0.15	0.22	0.28	0.00	0.11	0.10	0.06	0.05	0.10	0.03

Table 100. Mass-based FIMSDIST Z-Table data for C30-C74
components of sample 'F-Soy' CTL

C#	Z+2	Z+2	Z-2	Z-4	Z-6	Z-8	Z-10
30	0.00	0.00	0.00	0.23	0.00	0.00	0.00
31	0.14	0.16	0.19	0.21	0.20	0.20	0.00
32	0.13	0.14	0.17	0.17	0.18	0.18	0.00
33	0.11	0.12	0.14	0.17	0.17	0.16	0.00
34	0.11	0.10	0.13	0.15	0.17	0.15	0.15
35	0.10	0.10	0.11	0.12	0.14	0.13	0.13
36	0.10	0.08	0.10	0.13	0.13	0.11	0.11
37	0.07	0.09	0.10	0.10	0.12	0.10	0.09
38	0.08	0.06	0.08	0.08	0.09	0.10	0.09
39	0.06	0.06	0.07	0.08	0.08	0.09	0.08
40	0.06	0.06	0.06	0.07	0.07	0.08	0.07
41	0.05	0.06	0.04	0.06	0.07	0.06	0.06
42	0.06	0.05	0.04	0.05	0.05	0.06	0.06
43	0.03	0.05	0.05	0.04	0.05	0.05	0.04
44	0.03	0.04	0.04	0.04	0.04	0.05	0.05
45	0.04	0.04	0.03	0.03	0.04	0.04	0.04
46	0.03	0.03	0.03	0.03	0.03	0.03	0.03
47	0.02	0.02	0.03	0.03	0.04	0.04	0.03
48	0.03	0.03	0.03	0.03	0.03	0.03	0.02
49	0.02	0.02	0.02	0.02	0.02	0.02	0.03
50	0.02	0.02	0.02	0.02	0.02	0.02	0.02
51	0.02	0.02	0.02	0.02	0.02	0.02	0.02
52	0.02	0.02	0.02	0.02	0.02	0.02	0.02
53	0.01	0.01	0.01	0.02	0.02	0.02	0.02
54	0.02	0.02	0.02	0.02	0.01	0.01	0.01
55	0.01	0.01	0.01	0.01	0.01	0.01	0.01
56	0.01	0.01	0.01	0.01	0.01	0.01	0.01
57	0.00	0.01	0.01	0.01	0.00	0.00	0.01
58	0.01	0.01	0.01	0.00	0.00	0.01	0.01
59	0.00	0.01	0.01	0.00	0.00	0.01	0.01
60	0.01	0.00	0.00	0.01	0.00	0.00	0.00
61	0.00	0.00	0.00	0.00	0.01	0.00	0.00
62	0.00	0.00	0.00	0.00	0.00	0.00	0.00
63	0.00	0.00	0.00	0.00	0.00	0.00	0.00
64	0.00	0.00	0.00	0.00	0.00	0.00	0.00
65	0.00	0.00	0.00	0.00	0.00	0.00	0.00
66	0.00	0.00	0.00	0.00	0.00	0.00	0.00
67	0.00	0.00	0.00	0.00	0.00	0.00	0.00
68	0.00	0.00	0.00	0.00	0.00	0.00	0.00
69	0.00	0.00	0.00	0.00	0.00	0.00	0.00
70	0.00	0.00	0.00	0.00	0.00	0.00	0.00
71	0.00	0.00	0.00	0.00	0.00	0.00	0.00
72	0.00	0.00	0.00	0.00	0.00	0.00	0.00
73	0.00	0.00	0.00	0.00	0.00	0.00	0.00
74	0.00	0.00	0.00	0.00	0.00	0.00	0.00

Table 101. Mass-based FIMSDIST speciation data for C1-C30
components of sample 'G-Soy' CTL

C#	C-	C=	=C=	COOH	(1x)Ar	(1x)Ar=	(2x)Ar	(2x)Ar=	(3x)Ar	(3x)Ar=
1	0.00	0.00	0.00	0.28	0.00	0.00	0.00	0.00	0.00	0.00
2	0.00	0.00	0.00	0.80	0.00	0.00	0.00	0.00	0.00	0.00
3	0.00	0.00	0.00	0.21	0.00	0.00	0.00	0.00	0.00	0.00
4	0.46	0.22	0.00	0.19	0.00	0.00	0.00	0.00	0.00	0.00
5	0.26	0.49	0.24	0.49	0.00	0.00	0.00	0.00	0.00	0.00
6	0.39	1.01	0.21	0.83	0.03	0.00	0.00	0.00	0.00	0.00
7	0.54	1.29	0.94	2.03	0.11	0.00	0.00	0.00	0.00	0.00
8	0.53	1.08	1.24	1.49	0.12	0.00	0.00	0.00	0.00	0.00
9	0.49	0.81	0.87	1.49	0.14	0.05	0.00	0.00	0.00	0.00
10	0.24	0.84	1.01	1.58	0.11	0.19	0.07	0.00	0.00	0.00
11	0.25	1.22	1.29	0.62	0.35	0.23	0.09	0.00	0.00	0.00
12	0.23	0.69	1.12	0.43	0.21	0.20	0.10	0.02	0.00	0.00
13	0.32	0.61	0.98	0.41	0.24	0.15	0.11	0.06	0.00	0.00
14	0.30	0.64	0.99	0.43	0.18	0.17	0.11	0.09	0.14	0.00
15	0.88	0.98	1.10	0.45	0.25	0.17	0.11	0.10	0.17	0.00
16	0.16	0.83	1.15	3.68	0.20	0.23	0.12	0.11	0.20	0.00
17	0.35	1.68	1.49	0.58	0.23	0.21	0.14	0.13	0.31	0.02
18	0.13	0.48	0.84	3.23	0.19	0.23	0.18	0.14	0.28	0.01
19	0.08	0.42	1.18	0.92	0.16	0.44	0.11	0.13	0.23	0.03
20	0.13	0.42	0.98	1.48	0.18	0.26	0.14	0.12	0.25	0.06
21	0.09	0.48	0.80	0.00	0.17	0.28	0.76	0.53	0.37	0.08
22	0.09	0.52	0.73	0.00	0.21	0.23	0.14	0.12	0.23	0.07
23	0.13	0.38	0.80	0.00	0.14	0.21	0.16	0.16	0.34	0.06
24	0.00	0.41	0.66	0.00	0.14	0.20	0.11	0.16	0.25	0.12
25	0.00	0.25	0.62	0.00	0.24	0.26	0.11	0.11	0.20	0.06
26	0.01	0.22	0.64	0.00	0.21	0.18	0.10	0.10	0.19	0.00
27	0.01	0.39	0.52	0.00	0.15	0.18	0.12	0.13	0.20	0.00
28	0.07	0.37	0.46	0.00	0.16	0.18	0.14	0.00	0.16	0.03
29	0.19	0.16	0.25	0.00	0.16	0.15	0.10	0.00	0.15	0.00
30	0.18	0.34	0.34	0.00	0.12	0.14	0.00	0.04	0.13	0.00

Table 102. Mass-based FIMSDIST Z-Table data for C30-C74
components of sample 'G-Soy' CTL

C#	Z+2	Z+2	Z-2	Z-4	Z-6	Z-8	Z-10
30	0.00	0.00	0.00	0.28	0.00	0.00	0.00
31	0.20	0.25	0.23	0.30	0.22	0.24	0.00
32	0.16	0.14	0.17	0.23	0.27	0.28	0.00
33	0.18	0.20	0.20	0.25	0.26	0.23	0.00
34	0.12	0.10	0.14	0.14	0.24	0.15	0.24
35	0.10	0.19	0.14	0.10	0.17	0.17	0.22
36	0.17	0.08	0.09	0.24	0.19	0.11	0.11
37	0.08	0.15	0.08	0.12	0.14	0.10	0.09
38	0.09	0.05	0.15	0.09	0.09	0.16	0.09
39	0.08	0.05	0.13	0.08	0.09	0.08	0.09
40	0.05	0.12	0.06	0.08	0.07	0.15	0.08
41	0.06	0.06	0.05	0.06	0.09	0.07	0.08
42	0.08	0.06	0.04	0.05	0.06	0.05	0.13
43	0.03	0.07	0.10	0.05	0.05	0.07	0.05
44	0.03	0.03	0.10	0.05	0.04	0.04	0.05
45	0.07	0.10	0.04	0.04	0.03	0.08	0.04
46	0.03	0.02	0.02	0.07	0.03	0.03	0.02
47	0.02	0.01	0.01	0.05	0.09	0.10	0.04
48	0.02	0.06	0.06	0.07	0.06	0.02	0.02
49	0.06	0.02	0.01	0.01	0.01	0.01	0.01
50	0.08	0.09	0.09	0.08	0.08	0.07	0.02
51	0.05	0.05	0.06	0.07	0.07	0.08	0.08
52	0.00	0.00	0.00	0.00	0.00	0.01	0.01
53	0.00	0.00	0.05	0.05	0.05	0.04	0.00
54	0.04	0.07	0.05	0.03	0.00	0.00	0.00
55	0.00	0.00	0.00	0.00	0.00	0.00	0.00
56	0.00	0.00	0.00	0.00	0.04	0.00	0.00
57	0.00	0.00	0.00	0.00	0.00	0.00	0.00
58	0.00	0.00	0.00	0.00	0.00	0.00	0.00
59	0.00	0.00	0.00	0.00	0.00	0.00	0.00
60	0.00	0.00	0.00	0.00	0.00	0.00	0.00
61	0.00	0.00	0.00	0.00	0.00	0.00	0.00
62	0.00	0.00	0.00	0.00	0.00	0.00	0.00
63	0.00	0.00	0.00	0.00	0.00	0.00	0.00
64	0.00	0.00	0.00	0.00	0.00	0.00	0.00
65	0.00	0.00	0.00	0.00	0.00	0.00	0.00
66	0.00	0.00	0.00	0.00	0.00	0.00	0.00
67	0.00	0.00	0.00	0.00	0.00	0.00	0.00
68	0.00	0.00	0.00	0.00	0.00	0.00	0.00
69	0.00	0.00	0.00	0.00	0.00	0.00	0.00
70	0.00	0.00	0.00	0.00	0.00	0.00	0.00
71	0.00	0.00	0.00	0.00	0.00	0.00	0.00
72	0.00	0.00	0.00	0.00	0.00	0.00	0.00
73	0.00	0.00	0.00	0.00	0.00	0.00	0.00
74	0.00	0.00	0.00	0.00	0.00	0.00	0.00

Table 103. Mass-based FIMSDIST speciation data for C1-C30
components of sample 'H-Soy' CTL

C#	C-	C=	=C=	COOH	(1x)Ar	(1x)Ar=	(2x)Ar	(2x)Ar=	(3x)Ar	(3x)Ar=
1	0.00	0.00	0.00	0.28	0.00	0.00	0.00	0.00	0.00	0.00
2	0.00	0.00	0.00	0.77	0.00	0.00	0.00	0.00	0.00	0.00
3	0.00	0.00	0.00	0.24	0.00	0.00	0.00	0.00	0.00	0.00
4	0.46	0.25	0.00	0.21	0.00	0.00	0.00	0.00	0.00	0.00
5	0.32	0.63	0.21	0.49	0.00	0.00	0.00	0.00	0.00	0.00
6	0.60	1.42	0.28	0.83	0.03	0.00	0.00	0.00	0.00	0.00
7	0.77	1.58	1.19	2.03	0.14	0.00	0.00	0.00	0.00	0.00
8	0.60	1.20	1.47	1.46	0.21	0.00	0.00	0.00	0.00	0.00
9	0.64	0.94	1.18	1.53	0.19	0.07	0.00	0.00	0.00	0.00
10	0.33	1.02	1.20	1.51	0.16	0.26	0.07	0.00	0.00	0.00
11	0.34	1.34	1.37	0.66	0.39	0.33	0.11	0.00	0.00	0.00
12	0.31	0.76	1.20	0.50	0.25	0.28	0.12	0.02	0.00	0.00
13	0.39	0.73	1.13	0.47	0.30	0.21	0.12	0.07	0.00	0.00
14	0.37	0.77	1.17	0.49	0.22	0.22	0.12	0.10	0.14	0.00
15	1.08	1.05	1.23	0.51	0.25	0.24	0.13	0.11	0.19	0.00
16	0.21	0.89	1.28	2.69	0.24	0.29	0.11	0.14	0.22	0.02
17	0.45	1.70	1.63	0.63	0.28	0.27	0.16	0.13	0.29	0.03
18	0.15	0.55	0.94	2.52	0.22	0.28	0.19	0.15	0.28	0.02
19	0.10	0.45	0.93	1.03	0.19	0.41	0.12	0.12	0.24	0.04
20	0.11	0.45	0.92	1.46	0.21	0.30	0.16	0.12	0.24	0.07
21	0.09	0.43	0.81	0.00	0.17	0.27	0.46	0.33	0.31	0.08
22	0.09	0.41	0.70	0.00	0.17	0.24	0.15	0.13	0.22	0.09
23	0.11	0.34	0.67	0.00	0.13	0.23	0.15	0.14	0.34	0.09
24	0.08	0.33	0.50	0.00	0.14	0.23	0.12	0.13	0.18	0.18
25	0.00	0.23	0.54	0.00	0.16	0.23	0.09	0.10	0.17	0.05
26	0.10	0.19	0.56	0.00	0.19	0.20	0.10	0.09	0.17	0.05
27	0.01	0.13	0.45	0.00	0.14	0.15	0.07	0.10	0.17	0.00
28	0.04	0.13	0.35	0.00	0.12	0.16	0.10	0.07	0.14	0.03
29	0.02	0.12	0.22	0.00	0.13	0.13	0.08	0.06	0.13	0.03
30	0.14	0.46	0.20	0.00	0.10	0.22	0.06	0.05	0.11	0.01

Table 104. Mass-based FIMSDIST Z-Table data for C30-C74
components of sample 'H-Soy' CTL

C#	Z+2	Z+2	Z-2	Z-4	Z-6	Z-8	Z-10
30	0.00	0.00	0.00	0.40	0.00	0.00	0.00
31	0.15	0.37	0.19	0.42	0.18	0.20	0.00
32	0.12	0.13	0.14	0.33	0.35	0.35	0.00
33	0.12	0.12	0.30	0.32	0.15	0.14	0.00
34	0.12	0.10	0.12	0.12	0.14	0.14	0.14
35	0.10	0.10	0.09	0.10	0.12	0.12	0.13
36	0.10	0.08	0.07	0.11	0.10	0.10	0.11
37	0.07	0.09	0.08	0.08	0.09	0.08	0.08
38	0.08	0.05	0.08	0.08	0.07	0.09	0.08
39	0.07	0.05	0.07	0.06	0.07	0.07	0.08
40	0.04	0.07	0.05	0.07	0.06	0.08	0.07
41	0.05	0.05	0.04	0.04	0.07	0.06	0.06
42	0.04	0.05	0.04	0.04	0.05	0.04	0.06
43	0.02	0.03	0.05	0.04	0.04	0.05	0.03
44	0.03	0.02	0.03	0.04	0.04	0.04	0.04
45	0.19	0.19	0.03	0.03	0.03	0.03	0.03
46	0.02	0.02	0.02	0.03	0.03	0.02	0.02
47	0.01	0.01	0.01	0.01	0.19	0.03	0.02
48	0.01	0.01	0.02	0.02	0.02	0.02	0.02
49	0.01	0.01	0.01	0.01	0.01	0.01	0.01
50	0.18	0.01	0.18	0.17	0.01	0.01	0.01
51	0.01	0.01	0.01	0.00	0.01	0.01	0.18
52	0.00	0.00	0.00	0.00	0.00	0.00	0.00
53	0.00	0.00	0.00	0.00	0.00	0.00	0.00
54	0.00	0.00	0.00	0.00	0.00	0.00	0.00
55	0.00	0.00	0.00	0.00	0.00	0.00	0.00
56	0.00	0.00	0.00	0.00	0.00	0.00	0.00
57	0.00	0.00	0.00	0.00	0.00	0.00	0.00
58	0.00	0.00	0.00	0.00	0.00	0.00	0.00
59	0.00	0.00	0.00	0.00	0.00	0.00	0.00
60	0.00	0.00	0.00	0.00	0.00	0.00	0.00
61	0.00	0.00	0.00	0.00	0.00	0.00	0.00
62	0.00	0.00	0.00	0.00	0.00	0.00	0.00
63	0.00	0.00	0.00	0.00	0.00	0.00	0.00
64	0.00	0.00	0.00	0.00	0.00	0.00	0.00
65	0.00	0.00	0.00	0.00	0.00	0.00	0.00
66	0.00	0.00	0.00	0.00	0.00	0.00	0.00
67	0.00	0.00	0.00	0.00	0.00	0.00	0.00
68	0.00	0.00	0.00	0.00	0.00	0.00	0.00
69	0.00	0.00	0.00	0.00	0.00	0.00	0.00
70	0.00	0.00	0.00	0.00	0.00	0.00	0.00
71	0.00	0.00	0.00	0.00	0.00	0.00	0.00
72	0.00	0.00	0.00	0.00	0.00	0.00	0.00
73	0.00	0.00	0.00	0.00	0.00	0.00	0.00
74	0.00	0.00	0.00	0.00	0.00	0.00	0.00

Table 105. Mass-based FIMSDIST speciation data for C1-C30
components of sample 'I-Soy' CTL

C#	C-	C=	=C=	COOH	(1x)Ar	(1x)Ar=	(2x)Ar	(2x)Ar=	(3x)Ar	(3x)Ar=
1	0.00	0.00	0.00	0.28	0.00	0.00	0.00	0.00	0.00	0.00
2	0.00	0.00	0.00	0.63	0.00	0.00	0.00	0.00	0.00	0.00
3	0.00	0.00	0.00	0.26	0.00	0.00	0.00	0.00	0.00	0.00
4	0.66	0.25	0.00	0.21	0.00	0.00	0.00	0.00	0.00	0.00
5	0.32	0.73	0.26	0.49	0.00	0.00	0.00	0.00	0.00	0.00
6	0.60	1.64	0.27	0.83	0.04	0.00	0.00	0.00	0.00	0.00
7	0.94	1.76	1.46	2.03	0.19	0.00	0.00	0.00	0.00	0.00
8	0.61	1.46	1.92	1.52	0.34	0.00	0.00	0.00	0.00	0.00
9	0.83	1.14	1.44	1.58	0.27	0.09	0.00	0.00	0.00	0.00
10	0.51	1.25	1.41	1.55	0.19	0.37	0.08	0.00	0.00	0.00
11	0.50	1.53	1.47	0.76	0.49	0.50	0.16	0.00	0.00	0.00
12	0.45	0.90	1.33	0.59	0.34	0.42	0.19	0.02	0.00	0.00
13	0.52	0.82	1.35	0.52	0.39	0.29	0.17	0.10	0.00	0.00
14	0.52	0.82	1.37	0.54	0.28	0.31	0.15	0.18	0.19	0.00
15	1.31	1.15	1.51	0.53	0.33	0.33	0.16	0.18	0.24	0.00
16	0.30	1.35	1.42	1.94	0.30	0.37	0.15	0.18	0.25	0.02
17	0.93	2.19	1.80	0.63	0.32	0.34	0.18	0.06	0.29	0.05
18	0.20	0.55	1.10	1.89	0.24	0.35	0.05	0.03	0.28	0.05
19	0.16	0.47	0.97	0.93	0.20	0.38	0.13	0.14	0.25	0.05
20	0.10	0.41	0.81	2.82	0.21	0.32	0.16	0.14	0.23	0.10
21	0.10	0.36	0.75	0.00	0.18	0.24	0.30	0.22	0.25	0.08
22	0.08	0.33	0.64	0.00	0.16	0.23	0.15	0.13	0.20	0.08
23	0.10	0.36	0.61	0.00	0.12	0.21	0.16	0.13	0.21	0.09
24	0.05	0.27	0.39	0.00	0.14	0.21	0.12	0.10	0.18	0.09
25	0.06	0.21	0.43	0.00	0.15	0.22	0.09	0.09	0.15	0.05
26	0.08	0.15	0.37	0.00	0.10	0.17	0.07	0.08	0.14	0.05
27	0.00	0.08	0.36	0.00	0.07	0.13	0.06	0.08	0.13	0.05
28	0.03	0.07	0.27	0.00	0.07	0.11	0.08	0.06	0.10	0.06
29	0.01	0.04	0.22	0.00	0.07	0.09	0.05	0.05	0.09	0.05
30	0.10	0.17	0.14	0.00	0.07	0.09	0.04	0.04	0.07	0.03

Table 106. Mass-based FIMSDIST Z-Table data for C30-C74
components of sample 'I-Soy' CTL

C#	Z+2	Z+2	Z-2	Z-4	Z-6	Z-8	Z-10
30	0.00	0.00	0.00	0.16	0.00	0.00	0.00
31	0.10	0.13	0.11	0.14	0.12	0.15	0.00
32	0.09	0.11	0.12	0.12	0.13	0.11	0.00
33	0.09	0.09	0.09	0.11	0.10	0.09	0.00
34	0.08	0.08	0.09	0.07	0.09	0.08	0.09
35	0.04	0.08	0.07	0.06	0.07	0.07	0.10
36	0.07	0.05	0.03	0.06	0.07	0.06	0.06
37	0.03	0.07	0.03	0.03	0.05	0.05	0.03
38	0.05	0.02	0.05	0.04	0.03	0.07	0.03
39	0.04	0.01	0.04	0.04	0.04	0.05	0.03
40	0.01	0.05	0.03	0.04	0.01	0.05	0.02
41	0.02	0.03	0.00	0.02	0.04	0.01	0.03
42	0.00	0.03	0.01	0.03	0.01	0.00	0.03
43	0.00	0.00	0.03	0.01	0.01	0.03	0.00
44	0.00	0.00	0.02	0.00	0.00	0.00	0.02
45	0.00	0.02	0.01	0.00	0.00	0.02	0.01
46	0.00	0.00	0.00	0.00	0.00	0.00	0.00
47	0.00	0.00	0.00	0.00	0.00	0.02	0.00
48	0.00	0.00	0.00	0.00	0.00	0.00	0.00
49	0.00	0.00	0.00	0.00	0.00	0.00	0.00
50	0.00	0.00	0.00	0.00	0.00	0.00	0.00
51	0.00	0.00	0.00	0.00	0.00	0.00	0.00
52	0.00	0.00	0.00	0.00	0.00	0.00	0.00
53	0.00	0.00	0.00	0.00	0.00	0.00	0.00
54	0.00	0.00	0.00	0.00	0.00	0.00	0.00
55	0.00	0.00	0.00	0.00	0.00	0.00	0.00
56	0.00	0.00	0.00	0.00	0.00	0.00	0.00
57	0.00	0.00	0.00	0.00	0.00	0.00	0.00
58	0.00	0.00	0.00	0.00	0.00	0.00	0.00
59	0.00	0.00	0.00	0.00	0.00	0.00	0.00
60	0.00	0.00	0.00	0.00	0.00	0.00	0.00
61	0.00	0.00	0.00	0.00	0.00	0.00	0.00
62	0.00	0.00	0.00	0.00	0.00	0.00	0.00
63	0.00	0.00	0.00	0.00	0.00	0.00	0.00
64	0.00	0.00	0.00	0.00	0.00	0.00	0.00
65	0.00	0.00	0.00	0.00	0.00	0.00	0.00
66	0.00	0.00	0.00	0.00	0.00	0.00	0.00
67	0.00	0.00	0.00	0.00	0.00	0.00	0.00
68	0.00	0.00	0.00	0.00	0.00	0.00	0.00
69	0.00	0.00	0.00	0.00	0.00	0.00	0.00
70	0.00	0.00	0.00	0.00	0.00	0.00	0.00
71	0.00	0.00	0.00	0.00	0.00	0.00	0.00
72	0.00	0.00	0.00	0.00	0.00	0.00	0.00
73	0.00	0.00	0.00	0.00	0.00	0.00	0.00
74	0.00	0.00	0.00	0.00	0.00	0.00	0.00

Table 107. Mass-based FIMSDIST speciation data for C1-C30
components of sample 'J-Canola' CTL

C#	C-	C=	=C=	COOH	(1x)Ar	(1x)Ar=	(2x)Ar	(2x)Ar=	(3x)Ar	(3x)Ar=
1	0.00	0.00	0.00	0.17	0.00	0.00	0.00	0.00	0.00	0.00
2	0.00	0.00	0.00	1.32	0.00	0.00	0.00	0.00	0.00	0.00
3	0.00	0.00	0.00	0.40	0.00	0.00	0.00	0.00	0.00	0.00
4	1.32	0.29	0.00	0.29	0.00	0.00	0.00	0.00	0.00	0.00
5	0.26	0.46	0.70	0.37	0.00	0.00	0.00	0.00	0.00	0.00
6	0.62	1.81	0.90	0.83	0.03	0.00	0.00	0.00	0.00	0.00
7	1.30	2.11	1.74	1.63	0.12	0.00	0.00	0.00	0.00	0.00
8	1.03	2.36	1.91	1.45	0.14	0.01	0.00	0.00	0.00	0.00
9	1.04	1.90	1.43	1.76	0.10	0.05	0.00	0.00	0.00	0.00
10	0.39	1.33	1.44	5.94	0.19	0.21	0.04	0.00	0.00	0.00
11	0.35	2.84	1.76	0.74	0.30	0.29	0.10	0.00	0.00	0.00
12	0.29	1.76	1.52	0.46	0.29	0.24	0.12	0.02	0.00	0.00
13	0.33	1.49	1.15	0.44	0.22	0.24	0.13	0.08	0.00	0.00
14	0.27	1.76	1.94	0.42	0.28	0.18	0.13	0.12	0.19	0.00
15	0.47	2.56	2.02	0.36	0.25	0.21	0.13	0.12	0.22	0.00
16	0.33	1.88	1.99	0.74	0.09	0.27	0.13	0.10	0.26	0.06
17	0.39	3.59	1.91	0.31	0.30	0.31	0.08	0.10	0.29	0.22
18	0.18	1.53	1.27	1.05	0.26	0.30	0.13	0.02	0.34	0.03
19	0.11	0.93	1.25	0.38	0.19	0.27	0.09	0.06	0.25	0.04
20	0.19	0.25	0.57	0.58	0.06	0.19	0.09	0.07	0.25	0.07
21	0.05	0.32	0.49	0.00	0.01	0.14	0.29	0.20	0.20	0.11
22	0.02	0.24	0.45	0.00	0.01	0.11	0.06	0.04	0.12	0.11
23	0.03	0.23	0.43	0.00	0.01	0.10	0.05	0.04	0.11	0.10
24	0.02	0.26	0.33	0.00	0.04	0.07	0.03	0.03	0.10	0.08
25	0.00	0.06	0.27	0.00	0.00	0.06	0.02	0.02	0.08	0.02
26	0.02	0.01	0.32	0.00	0.01	0.06	0.02	0.04	0.05	0.05
27	0.01	0.00	0.15	0.00	0.00	0.04	0.02	0.06	0.06	0.03
28	0.00	0.05	0.12	0.00	0.00	0.04	0.02	0.03	0.03	0.04
29	0.00	0.03	0.07	0.00	0.02	0.03	0.02	0.01	0.03	0.03
30	0.03	0.05	0.06	0.00	0.02	0.03	0.01	0.01	0.02	0.01

Table 108. Mass-based FIMSDIST Z-Table data for C30-C74
components of sample 'J-Canola' CTL

C#	Z+2	Z+2	Z-2	Z-4	Z-6	Z-8	Z-10
30	0.00	0.00	0.00	0.05	0.00	0.00	0.00
31	0.02	0.03	0.04	0.04	0.04	0.04	0.00
32	0.03	0.03	0.03	0.04	0.04	0.04	0.00
33	0.02	0.02	0.03	0.03	0.03	0.03	0.00
34	0.02	0.02	0.03	0.02	0.03	0.02	0.02
35	0.01	0.02	0.02	0.02	0.02	0.02	0.02
36	0.02	0.02	0.02	0.02	0.02	0.02	0.02
37	0.01	0.02	0.02	0.01	0.02	0.02	0.01
38	0.01	0.01	0.01	0.02	0.01	0.02	0.01
39	0.01	0.01	0.01	0.01	0.01	0.02	0.01
40	0.01	0.01	0.01	0.01	0.01	0.01	0.01
41	0.01	0.01	0.00	0.01	0.01	0.01	0.01
42	0.01	0.00	0.00	0.01	0.00	0.08	0.01
43	0.00	0.10	0.00	0.00	0.01	0.01	0.00
44	0.00	0.09	0.00	0.00	0.00	0.00	0.00
45	0.11	0.07	0.00	0.00	0.00	0.00	0.00
46	0.00	0.00	0.00	0.00	0.00	0.00	0.00
47	0.00	0.00	0.00	0.11	0.10	0.00	0.00
48	0.00	0.00	0.00	0.00	0.00	0.00	0.00
49	0.00	0.00	0.00	0.00	0.00	0.00	0.00
50	0.00	0.00	0.00	0.00	0.00	0.00	0.00
51	0.00	0.00	0.00	0.00	0.00	0.00	0.00
52	0.00	0.00	0.00	0.00	0.00	0.00	0.00
53	0.00	0.00	0.00	0.00	0.00	0.00	0.00
54	0.00	0.00	0.00	0.00	0.00	0.00	0.00
55	0.00	0.00	0.00	0.00	0.00	0.00	0.00
56	0.00	0.00	0.00	0.00	0.00	0.00	0.00
57	0.00	0.00	0.00	0.00	0.00	0.00	0.00
58	0.00	0.00	0.00	0.00	0.00	0.00	0.00
59	0.00	0.00	0.00	0.00	0.00	0.00	0.00
60	0.00	0.00	0.00	0.00	0.00	0.00	0.00
61	0.00	0.00	0.00	0.00	0.00	0.00	0.00
62	0.00	0.00	0.00	0.00	0.00	0.00	0.00
63	0.00	0.00	0.00	0.00	0.00	0.00	0.00
64	0.00	0.00	0.00	0.00	0.00	0.00	0.00
65	0.00	0.00	0.00	0.00	0.00	0.00	0.00
66	0.00	0.00	0.00	0.00	0.00	0.00	0.00
67	0.00	0.00	0.00	0.00	0.00	0.00	0.00
68	0.00	0.00	0.00	0.00	0.00	0.00	0.00
69	0.00	0.00	0.00	0.00	0.00	0.00	0.00
70	0.00	0.00	0.00	0.00	0.00	0.00	0.00
71	0.00	0.00	0.00	0.00	0.00	0.00	0.00
72	0.00	0.00	0.00	0.00	0.00	0.00	0.00
73	0.00	0.00	0.00	0.00	0.00	0.00	0.00
74	0.00	0.00	0.00	0.00	0.00	0.00	0.00

Table 109. Mass-based FIMSDIST speciation data for C1-C30
components of sample 'K-Canola' CTL

C#	C-	C=	=C=	COOH	(1x)Ar	(1x)Ar=	(2x)Ar	(2x)Ar=	(3x)Ar	(3x)Ar=
1	0.00	0.00	0.00	0.17	0.00	0.00	0.00	0.00	0.00	0.00
2	0.00	0.00	0.00	1.15	0.00	0.00	0.00	0.00	0.00	0.00
3	0.00	0.00	0.00	0.38	0.00	0.00	0.00	0.00	0.00	0.00
4	1.17	0.67	0.00	0.29	0.00	0.00	0.00	0.00	0.00	0.00
5	0.46	0.96	0.43	0.37	0.00	0.00	0.00	0.00	0.00	0.00
6	0.83	2.21	0.65	0.83	0.05	0.00	0.00	0.00	0.00	0.00
7	1.24	2.73	1.69	1.63	0.17	0.00	0.00	0.00	0.00	0.00
8	1.42	2.51	1.91	1.57	0.27	0.00	0.00	0.00	0.00	0.00
9	1.14	2.28	1.80	1.85	0.16	0.07	0.00	0.00	0.00	0.00
10	0.52	1.86	1.46	3.92	0.25	0.28	0.07	0.00	0.00	0.00
11	0.38	3.18	1.95	0.79	0.36	0.42	0.16	0.00	0.00	0.00
12	0.49	2.01	1.60	0.51	0.24	0.34	0.17	0.03	0.00	0.00
13	0.43	1.37	1.24	0.46	0.26	0.24	0.14	0.08	0.00	0.00
14	0.36	2.19	2.11	0.43	0.36	0.28	0.13	0.13	0.21	0.00
15	0.60	1.71	2.06	0.35	0.36	0.27	0.13	0.14	0.25	0.00
16	0.32	1.73	1.82	0.61	0.33	0.28	0.10	0.12	0.26	0.01
17	0.29	3.32	1.64	0.28	0.30	0.30	0.12	0.07	0.21	0.01
18	0.14	1.09	1.06	0.87	0.24	0.28	0.12	0.03	0.28	0.02
19	0.13	0.77	0.92	0.34	0.21	0.24	0.09	0.06	0.17	0.03
20	0.11	0.44	0.53	0.63	0.14	0.16	0.07	0.05	0.17	0.02
21	0.05	0.23	0.29	0.00	0.10	0.12	0.19	0.08	0.13	0.02
22	0.08	0.13	0.34	0.00	0.09	0.09	0.04	0.04	0.10	0.01
23	0.03	0.17	0.33	0.00	0.07	0.09	0.03	0.04	0.09	0.02
24	0.01	0.18	0.27	0.00	0.04	0.07	0.03	0.03	0.08	0.02
25	0.01	0.08	0.18	0.00	0.05	0.06	0.03	0.02	0.05	0.02
26	0.01	0.10	0.24	0.00	0.04	0.05	0.02	0.03	0.05	0.01
27	0.01	0.05	0.09	0.00	0.03	0.04	0.02	0.01	0.05	0.01
28	0.02	0.05	0.11	0.00	0.02	0.04	0.02	0.01	0.03	0.01
29	0.00	0.02	0.08	0.00	0.02	0.03	0.01	0.01	0.03	0.01
30	0.03	0.05	0.06	0.00	0.02	0.02	0.01	0.01	0.02	0.01

Table 110. Mass-based FIMSDIST Z-Table data for C30-C74
components of sample 'K-Canola' CTL

C#	Z+2	Z+2	Z-2	Z-4	Z-6	Z-8	Z-10
30	0.00	0.00	0.00	0.05	0.00	0.00	0.00
31	0.03	0.04	0.04	0.04	0.04	0.04	0.00
32	0.03	0.02	0.03	0.03	0.03	0.03	0.00
33	0.02	0.02	0.03	0.03	0.03	0.03	0.00
34	0.02	0.02	0.02	0.02	0.03	0.02	0.03
35	0.02	0.02	0.02	0.02	0.02	0.02	0.02
36	0.02	0.02	0.02	0.02	0.02	0.02	0.02
37	0.01	0.02	0.02	0.02	0.02	0.02	0.02
38	0.01	0.01	0.02	0.02	0.01	0.02	0.02
39	0.01	0.01	0.01	0.02	0.01	0.02	0.01
40	0.01	0.01	0.01	0.01	0.01	0.02	0.01
41	0.01	0.01	0.01	0.02	0.01	0.01	0.01
42	0.01	0.01	0.01	0.01	0.01	0.01	0.01
43	0.01	0.01	0.01	0.01	0.01	0.01	0.01
44	0.01	0.01	0.01	0.01	0.01	0.01	0.01
45	0.01	0.01	0.01	0.01	0.01	0.01	0.01
46	0.01	0.01	0.01	0.01	0.01	0.00	0.00
47	0.00	0.00	0.01	0.01	0.01	0.01	0.01
48	0.01	0.01	0.01	0.01	0.01	0.00	0.00
49	0.00	0.00	0.00	0.00	0.00	0.01	0.00
50	0.00	0.00	0.00	0.00	0.00	0.00	0.00
51	0.00	0.00	0.00	0.00	0.00	0.00	0.00
52	0.00	0.00	0.00	0.00	0.00	0.00	0.00
53	0.00	0.00	0.00	0.00	0.00	0.00	0.00
54	0.00	0.00	0.00	0.00	0.00	0.00	0.00
55	0.00	0.00	0.00	0.00	0.00	0.00	0.00
56	0.00	0.00	0.00	0.00	0.00	0.00	0.18
57	0.00	0.00	0.00	0.20	0.00	0.00	0.00
58	0.00	0.00	0.00	0.00	0.00	0.00	0.00
59	0.00	0.00	0.00	0.00	0.00	0.00	0.00
60	0.00	0.00	0.00	0.00	0.00	0.00	0.00
61	0.00	0.00	0.00	0.00	0.00	0.00	0.00
62	0.00	0.00	0.00	0.00	0.00	0.00	0.00
63	0.00	0.00	0.00	0.00	0.00	0.00	0.00
64	0.00	0.00	0.00	0.00	0.00	0.00	0.00
65	0.00	0.00	0.00	0.00	0.00	0.00	0.00
66	0.00	0.00	0.00	0.00	0.00	0.00	0.00
67	0.00	0.00	0.00	0.00	0.00	0.00	0.00
68	0.00	0.00	0.00	0.00	0.00	0.00	0.00
69	0.00	0.00	0.00	0.00	0.00	0.00	0.00
70	0.00	0.00	0.00	0.00	0.00	0.00	0.00
71	0.00	0.00	0.00	0.00	0.00	0.00	0.00
72	0.00	0.00	0.00	0.00	0.00	0.00	0.00
73	0.00	0.00	0.00	0.00	0.00	0.00	0.00
74	0.00	0.00	0.00	0.00	0.00	0.00	0.00

Table 111. Mass-based FIMSDIST speciation data for C1-C30
components of sample 'L-Canola' CTL

C#	C-	C=	=C=	COOH	(1x)Ar	(1x)Ar=	(2x)Ar	(2x)Ar=	(3x)Ar	(3x)Ar=
1	0.00	0.00	0.00	0.17	0.00	0.00	0.00	0.00	0.00	0.00
2	0.00	0.00	0.00	1.25	0.00	0.00	0.00	0.00	0.00	0.00
3	0.00	0.00	0.00	0.40	0.00	0.00	0.00	0.00	0.00	0.00
4	1.04	0.67	0.00	0.33	0.00	0.00	0.00	0.00	0.00	0.00
5	0.53	0.72	0.67	0.37	0.00	0.00	0.00	0.00	0.00	0.00
6	0.90	2.34	0.58	0.83	0.06	0.00	0.00	0.00	0.00	0.00
7	1.22	2.68	1.76	1.63	0.20	0.00	0.00	0.00	0.00	0.00
8	1.40	2.54	2.07	1.79	0.30	0.00	0.00	0.00	0.00	0.00
9	1.12	2.37	1.82	2.06	0.20	0.08	0.00	0.00	0.00	0.00
10	0.61	1.86	1.53	3.50	0.29	0.33	0.07	0.00	0.00	0.00
11	0.40	2.71	1.88	0.86	0.40	0.50	0.16	0.00	0.00	0.00
12	0.38	2.02	1.67	0.58	0.26	0.38	0.19	0.03	0.00	0.00
13	0.45	1.17	1.24	0.52	0.27	0.26	0.20	0.09	0.00	0.00
14	0.38	2.14	2.07	0.46	0.35	0.28	0.14	0.15	0.23	0.00
15	0.55	1.59	2.01	0.37	0.37	0.27	0.15	0.15	0.27	0.00
16	0.30	1.58	1.65	0.64	0.34	0.30	0.12	0.12	0.23	0.01
17	0.29	2.82	1.49	0.29	0.28	0.31	0.14	0.08	0.21	0.01
18	0.14	0.96	1.12	0.83	0.24	0.29	0.13	0.04	0.27	0.02
19	0.12	0.78	0.91	0.35	0.19	0.24	0.10	0.06	0.18	0.03
20	0.10	0.33	0.56	0.61	0.13	0.16	0.08	0.05	0.20	0.04
21	0.06	0.21	0.29	0.00	0.09	0.12	0.20	0.11	0.16	0.02
22	0.09	0.12	0.34	0.00	0.08	0.10	0.05	0.04	0.09	0.02
23	0.02	0.16	0.32	0.00	0.06	0.09	0.03	0.04	0.09	0.02
24	0.00	0.16	0.26	0.00	0.04	0.07	0.04	0.03	0.08	0.02
25	0.00	0.07	0.15	0.00	0.03	0.07	0.03	0.02	0.05	0.02
26	0.01	0.10	0.24	0.00	0.04	0.05	0.03	0.03	0.05	0.03
27	0.01	0.00	0.10	0.00	0.03	0.04	0.02	0.02	0.05	0.01
28	0.02	0.04	0.12	0.00	0.02	0.04	0.02	0.03	0.04	0.01
29	0.00	0.03	0.08	0.00	0.02	0.03	0.01	0.01	0.03	0.01
30	0.03	0.06	0.07	0.00	0.03	0.03	0.02	0.01	0.03	0.01

Table 112. Mass-based FIMSDIST Z-Table data for C30-C74
components of sample 'L-Canola' CTL

C#	Z+2	Z+2	Z-2	Z-4	Z-6	Z-8	Z-10
30	0.00	0.00	0.00	0.06	0.00	0.00	0.00
31	0.03	0.04	0.05	0.05	0.04	0.04	0.00
32	0.03	0.03	0.04	0.04	0.05	0.04	0.00
33	0.03	0.03	0.03	0.10	0.04	0.04	0.00
34	0.02	0.03	0.03	0.03	0.03	0.03	0.03
35	0.02	0.02	0.02	0.03	0.03	0.03	0.03
36	0.02	0.02	0.02	0.03	0.03	0.02	0.02
37	0.01	0.02	0.02	0.02	0.03	0.02	0.02
38	0.02	0.01	0.02	0.02	0.02	0.02	0.02
39	0.01	0.02	0.01	0.02	0.01	0.02	0.02
40	0.01	0.01	0.01	0.01	0.01	0.02	0.01
41	0.01	0.01	0.01	0.02	0.01	0.02	0.01
42	0.02	0.01	0.01	0.01	0.01	0.01	0.02
43	0.01	0.01	0.01	0.01	0.01	0.01	0.01
44	0.01	0.01	0.01	0.01	0.01	0.01	0.01
45	0.01	0.01	0.01	0.01	0.01	0.01	0.01
46	0.01	0.01	0.01	0.01	0.01	0.00	0.00
47	0.00	0.00	0.01	0.01	0.01	0.01	0.01
48	0.01	0.01	0.01	0.01	0.01	0.00	0.00
49	0.00	0.00	0.00	0.00	0.00	0.00	0.01
50	0.00	0.01	0.00	0.00	0.01	0.01	0.01
51	0.00	0.00	0.00	0.00	0.00	0.01	0.01
52	0.00	0.00	0.00	0.00	0.00	0.00	0.00
53	0.00	0.00	0.00	0.00	0.00	0.00	0.00
54	0.00	0.00	0.00	0.06	0.06	0.00	0.00
55	0.00	0.00	0.00	0.00	0.00	0.00	0.00
56	0.00	0.00	0.00	0.00	0.00	0.06	0.00
57	0.00	0.00	0.00	0.07	0.00	0.00	0.00
58	0.00	0.00	0.07	0.00	0.00	0.00	0.00
59	0.00	0.00	0.00	0.00	0.00	0.00	0.00
60	0.00	0.00	0.00	0.06	0.00	0.00	0.00
61	0.00	0.00	0.00	0.00	0.00	0.00	0.00
62	0.00	0.00	0.00	0.00	0.00	0.00	0.00
63	0.00	0.00	0.00	0.00	0.00	0.00	0.00
64	0.00	0.00	0.00	0.00	0.00	0.00	0.00
65	0.00	0.00	0.00	0.00	0.00	0.00	0.00
66	0.00	0.00	0.00	0.00	0.00	0.00	0.00
67	0.00	0.00	0.00	0.00	0.00	0.00	0.00
68	0.00	0.00	0.00	0.00	0.00	0.00	0.00
69	0.00	0.00	0.00	0.00	0.00	0.00	0.00
70	0.00	0.00	0.00	0.00	0.00	0.00	0.00
71	0.00	0.00	0.00	0.00	0.00	0.00	0.00
72	0.00	0.00	0.00	0.00	0.00	0.00	0.00
73	0.00	0.00	0.00	0.00	0.00	0.00	0.00
74	0.00	0.00	0.00	0.00	0.00	0.00	0.00

Table 113. Mass-based FIMSDIST speciation data for C1-C30
components of sample 'M-Canola' CTL

C#	C-	C=	=C=	COOH	(1x)Ar	(1x)Ar=	(2x)Ar	(2x)Ar=	(3x)Ar	(3x)Ar=
1	0.00	0.00	0.00	0.17	0.00	0.00	0.00	0.00	0.00	0.00
2	0.00	0.00	0.00	1.33	0.00	0.00	0.00	0.00	0.00	0.00
3	0.00	0.00	0.00	0.43	0.00	0.00	0.00	0.00	0.00	0.00
4	1.03	0.63	0.00	0.39	0.00	0.00	0.00	0.00	0.00	0.00
5	0.57	1.10	0.50	0.37	0.00	0.00	0.00	0.00	0.00	0.00
6	0.90	2.32	0.51	0.83	0.05	0.00	0.00	0.00	0.00	0.00
7	1.38	2.18	1.89	1.63	0.24	0.00	0.00	0.00	0.00	0.00
8	1.28	2.74	2.19	1.89	0.32	0.00	0.00	0.00	0.00	0.00
9	1.18	2.42	1.65	1.99	0.24	0.09	0.00	0.00	0.00	0.00
10	0.63	1.80	1.67	3.23	0.32	0.36	0.08	0.00	0.00	0.00
11	0.41	2.43	1.78	0.88	0.44	0.54	0.17	0.00	0.00	0.00
12	0.40	2.00	1.73	0.60	0.27	0.42	0.20	0.03	0.00	0.00
13	0.46	1.13	1.22	0.56	0.29	0.27	0.21	0.10	0.00	0.00
14	0.39	2.06	2.02	0.47	0.36	0.28	0.15	0.15	0.24	0.00
15	0.52	1.52	1.95	0.40	0.36	0.26	0.15	0.15	0.26	0.00
16	0.24	1.65	1.54	0.68	0.33	0.29	0.13	0.13	0.25	0.01
17	0.27	2.47	1.50	0.30	0.27	0.31	0.17	0.06	0.20	0.01
18	0.15	0.95	1.14	0.84	0.24	0.29	0.14	0.04	0.26	0.02
19	0.11	0.79	0.85	0.35	0.19	0.24	0.10	0.06	0.18	0.02
20	0.10	0.43	0.69	0.64	0.13	0.16	0.08	0.05	0.19	0.04
21	0.05	0.22	0.28	0.00	0.09	0.12	0.22	0.09	0.15	0.02
22	0.09	0.11	0.32	0.00	0.08	0.10	0.05	0.04	0.10	0.02
23	0.02	0.15	0.33	0.00	0.06	0.08	0.03	0.05	0.09	0.02
24	0.01	0.14	0.27	0.00	0.04	0.07	0.04	0.03	0.08	0.02
25	0.00	0.07	0.19	0.00	0.02	0.07	0.03	0.03	0.05	0.03
26	0.01	0.09	0.24	0.00	0.04	0.05	0.03	0.03	0.05	0.03
27	0.02	0.07	0.10	0.00	0.03	0.04	0.03	0.02	0.05	0.01
28	0.02	0.08	0.12	0.00	0.02	0.04	0.02	0.01	0.04	0.01
29	0.00	0.02	0.08	0.00	0.02	0.04	0.01	0.01	0.03	0.01
30	0.03	0.06	0.08	0.00	0.02	0.03	0.02	0.02	0.03	0.01

Table 114. Mass-based FIMSDIST Z-Table data for C30-C74
components of sample 'M-Canola' CTL

C#	Z+2	Z+2	Z-2	Z-4	Z-6	Z-8	Z-10
30	0.00	0.00	0.00	0.06	0.00	0.00	0.00
31	0.04	0.04	0.05	0.05	0.05	0.05	0.00
32	0.04	0.04	0.04	0.04	0.05	0.05	0.00
33	0.03	0.03	0.04	0.05	0.04	0.04	0.00
34	0.03	0.03	0.03	0.03	0.03	0.03	0.03
35	0.02	0.03	0.03	0.03	0.03	0.03	0.03
36	0.03	0.02	0.02	0.03	0.03	0.03	0.02
37	0.02	0.09	0.02	0.02	0.12	0.02	0.02
38	0.02	0.02	0.02	0.02	0.02	0.03	0.02
39	0.01	0.02	0.02	0.02	0.02	0.02	0.02
40	0.02	0.02	0.02	0.01	0.01	0.02	0.02
41	0.01	0.01	0.01	0.02	0.02	0.02	0.01
42	0.02	0.01	0.01	0.02	0.01	0.02	0.02
43	0.01	0.02	0.01	0.01	0.01	0.01	0.01
44	0.01	0.01	0.01	0.01	0.01	0.01	0.01
45	0.01	0.01	0.01	0.01	0.01	0.01	0.01
46	0.01	0.01	0.01	0.01	0.01	0.00	0.01
47	0.00	0.00	0.01	0.01	0.01	0.01	0.01
48	0.01	0.01	0.01	0.01	0.01	0.00	0.00
49	0.00	0.00	0.00	0.00	0.00	0.00	0.00
50	0.01	0.01	0.00	0.00	0.01	0.01	0.00
51	0.00	0.00	0.00	0.00	0.00	0.00	0.01
52	0.00	0.00	0.00	0.00	0.00	0.00	0.00
53	0.00	0.00	0.00	0.00	0.00	0.00	0.00
54	0.00	0.00	0.00	0.00	0.00	0.00	0.00
55	0.00	0.00	0.00	0.00	0.00	0.00	0.00
56	0.00	0.00	0.00	0.00	0.00	0.00	0.07
57	0.00	0.00	0.00	0.07	0.00	0.00	0.00
58	0.00	0.00	0.07	0.00	0.00	0.00	0.00
59	0.00	0.00	0.00	0.00	0.00	0.00	0.00
60	0.00	0.00	0.00	0.07	0.00	0.00	0.00
61	0.00	0.00	0.00	0.00	0.00	0.00	0.00
62	0.00	0.00	0.00	0.00	0.00	0.00	0.00
63	0.00	0.00	0.00	0.00	0.00	0.00	0.00
64	0.00	0.00	0.00	0.00	0.00	0.00	0.00
65	0.00	0.00	0.00	0.00	0.00	0.00	0.00
66	0.00	0.00	0.00	0.00	0.00	0.00	0.00
67	0.00	0.00	0.00	0.00	0.00	0.00	0.00
68	0.00	0.00	0.00	0.00	0.00	0.00	0.00
69	0.00	0.00	0.00	0.00	0.00	0.00	0.00
70	0.00	0.00	0.00	0.00	0.00	0.00	0.00
71	0.00	0.00	0.00	0.00	0.00	0.00	0.00
72	0.00	0.00	0.00	0.00	0.00	0.00	0.00
73	0.00	0.00	0.00	0.00	0.00	0.00	0.00
74	0.00	0.00	0.00	0.00	0.00	0.00	0.00

Table 115. Mass-based FIMSDIST speciation data for C1-C30
components of sample 'N-Canola' CTL

C#	C-	C=	=C=	COOH	(1x)Ar	(1x)Ar=	(2x)Ar	(2x)Ar=	(3x)Ar	(3x)Ar=
1	0.00	0.00	0.00	0.17	0.00	0.00	0.00	0.00	0.00	0.00
2	0.00	0.00	0.00	1.34	0.00	0.00	0.00	0.00	0.00	0.00
3	0.00	0.00	0.00	0.48	0.00	0.00	0.00	0.00	0.00	0.00
4	0.89	0.44	0.00	0.41	0.00	0.00	0.00	0.00	0.00	0.00
5	0.49	1.30	0.47	0.37	0.00	0.00	0.00	0.00	0.00	0.00
6	1.04	2.23	0.51	0.83	0.06	0.00	0.00	0.00	0.00	0.00
7	1.64	2.63	1.94	1.63	0.28	0.00	0.00	0.00	0.00	0.00
8	1.17	2.68	2.14	1.91	0.35	0.01	0.00	0.00	0.00	0.00
9	1.40	2.07	2.02	2.18	0.30	0.08	0.00	0.00	0.00	0.00
10	0.59	1.93	1.81	3.09	0.30	0.33	0.09	0.00	0.00	0.00
11	0.41	2.63	1.89	0.88	0.45	0.50	0.19	0.00	0.00	0.00
12	0.47	2.00	1.73	0.58	0.26	0.43	0.19	0.03	0.00	0.00
13	0.45	1.12	1.45	0.51	0.37	0.26	0.16	0.09	0.00	0.00
14	0.44	1.74	1.88	0.47	0.39	0.31	0.15	0.13	0.22	0.00
15	0.63	1.46	1.78	0.38	0.34	0.29	0.14	0.14	0.26	0.00
16	0.27	1.78	1.68	0.60	0.32	0.30	0.12	0.13	0.27	0.01
17	0.31	2.51	1.54	0.28	0.29	0.28	0.14	0.06	0.21	0.01
18	0.27	0.95	0.96	0.71	0.21	0.24	0.12	0.08	0.25	0.01
19	0.12	0.62	0.91	0.32	0.16	0.21	0.03	0.06	0.18	0.02
20	0.10	0.30	0.50	0.56	0.13	0.14	0.07	0.05	0.18	0.04
21	0.05	0.21	0.29	0.00	0.09	0.11	0.22	0.11	0.15	0.01
22	0.10	0.10	0.26	0.00	0.07	0.09	0.04	0.03	0.09	0.02
23	0.02	0.14	0.29	0.00	0.05	0.08	0.03	0.04	0.08	0.02
24	0.00	0.14	0.24	0.00	0.04	0.06	0.04	0.03	0.07	0.02
25	0.00	0.09	0.19	0.00	0.05	0.06	0.03	0.03	0.05	0.02
26	0.01	0.08	0.24	0.00	0.04	0.05	0.03	0.02	0.05	0.01
27	0.02	0.04	0.10	0.00	0.02	0.04	0.02	0.02	0.05	0.01
28	0.02	0.09	0.12	0.00	0.03	0.04	0.02	0.02	0.04	0.01
29	0.00	0.02	0.08	0.00	0.02	0.04	0.01	0.01	0.03	0.01
30	0.03	0.06	0.07	0.00	0.03	0.03	0.02	0.02	0.03	0.01

Table 116. Mass-based FIMSDIST Z-Table data for C30-C74
components of sample 'N-Canola' CTL

C#	Z+2	Z+2	Z-2	Z-4	Z-6	Z-8	Z-10
30	0.00	0.00	0.00	0.06	0.00	0.00	0.00
31	0.03	0.04	0.05	0.05	0.05	0.05	0.00
32	0.03	0.04	0.04	0.04	0.04	0.05	0.00
33	0.03	0.03	0.03	0.04	0.04	0.04	0.00
34	0.03	0.03	0.03	0.03	0.04	0.03	0.04
35	0.02	0.03	0.03	0.03	0.03	0.03	0.03
36	0.03	0.02	0.02	0.03	0.03	0.03	0.02
37	0.01	0.20	0.02	0.02	0.26	0.02	0.02
38	0.02	0.01	0.02	0.02	0.02	0.02	0.02
39	0.01	0.01	0.01	0.02	0.02	0.02	0.02
40	0.01	0.01	0.01	0.02	0.01	0.02	0.02
41	0.01	0.01	0.01	0.02	0.02	0.02	0.01
42	0.01	0.01	0.01	0.01	0.01	0.01	0.02
43	0.01	0.01	0.01	0.01	0.01	0.01	0.01
44	0.01	0.01	0.01	0.01	0.01	0.01	0.01
45	0.01	0.01	0.01	0.01	0.01	0.01	0.01
46	0.01	0.01	0.01	0.01	0.01	0.01	0.00
47	0.00	0.00	0.01	0.01	0.01	0.01	0.01
48	0.01	0.01	0.01	0.01	0.01	0.01	0.00
49	0.00	0.00	0.00	0.00	0.00	0.00	0.00
50	0.01	0.01	0.00	0.01	0.01	0.01	0.01
51	0.00	0.00	0.00	0.00	0.00	0.01	0.00
52	0.00	0.00	0.00	0.00	0.00	0.00	0.00
53	0.00	0.00	0.00	0.00	0.00	0.00	0.00
54	0.00	0.00	0.00	0.00	0.00	0.00	0.00
55	0.00	0.00	0.00	0.00	0.00	0.00	0.00
56	0.00	0.00	0.00	0.00	0.00	0.00	0.00
57	0.00	0.00	0.00	0.00	0.00	0.00	0.00
58	0.00	0.00	0.00	0.00	0.00	0.00	0.00
59	0.00	0.00	0.00	0.00	0.00	0.00	0.00
60	0.00	0.00	0.00	0.00	0.00	0.00	0.00
61	0.00	0.00	0.00	0.00	0.00	0.00	0.00
62	0.00	0.00	0.00	0.00	0.00	0.00	0.00
63	0.00	0.00	0.00	0.00	0.00	0.00	0.00
64	0.00	0.00	0.00	0.00	0.00	0.00	0.00
65	0.00	0.00	0.00	0.00	0.00	0.00	0.00
66	0.00	0.00	0.00	0.00	0.00	0.00	0.00
67	0.00	0.00	0.00	0.00	0.00	0.00	0.00
68	0.00	0.00	0.00	0.00	0.00	0.00	0.00
69	0.00	0.00	0.00	0.00	0.00	0.00	0.00
70	0.00	0.00	0.00	0.00	0.00	0.00	0.00
71	0.00	0.00	0.00	0.00	0.00	0.00	0.00
72	0.00	0.00	0.00	0.00	0.00	0.00	0.00
73	0.00	0.00	0.00	0.00	0.00	0.00	0.00
74	0.00	0.00	0.00	0.00	0.00	0.00	0.00

Appendix L.
Estimated Fuel and Product Yields from the NCP

This appendix contains the estimated yields from the noncatalytic cracking process as calculated according to the yield estimation description in Section VII.E.3.i. Samples used to derive these data were processed in two configurations of the lab-scale TCR according to the operating parameters included in Table 24 (see Section 0).

All data are expressed on a TAG feedstock basis. TPV stands for total product value, computed as described in Section VII.E.3.i. The yield of carbon is estimated from data in Section VII.C. The jet fuel cut contains half of the C9 compounds and half of the C13 compounds, indicated in the tables by [9*-13*] rather than [9-13].

Natural gas equivalents is the equivalent are adapted from the net heating value of the burner fuel (provided in MJ/kg TAG). Therefore, when this data is utilized in future endeavors, care should be taken so that the burner fuel is not counted twice (once as burner fuel and once as nat. gas. Equivalents). Both are included however for a complete portrayal of the results.

Table 117. Noncatalytic cracking process estimated yields for various TAG samples processed on the 100 ml lab-scale TCR

		AA-Soy	BB-VHONO	CC-HENO	DD-Linseed	EE-Camelina	FF-Corn	GG-Cottonseed	HH-Canola	II-HONO
Burner Fuel Heat	(MJ/kg)	1.08	0.80	0.99	1.30	1.03	0.98	0.99	0.88	1.03
Burner Fuel	(wt. %)	2.28	1.70	2.09	2.75	2.17	2.08	2.10	1.86	2.18
CO_2		3.49	2.60	3.24	3.98	3.30	3.25	3.34	2.81	3.35
Nat. Gas. Equiv.		8.45	7.37	7.29	8.72	8.15	8.22	8.94	7.24	7.47
LPG [3-4]		3.40	2.04	2.30	3.32	3.33	3.51	3.54	2.60	2.87
Naphtha [5-9*]		9.28	8.55	6.83	10.01	11.28	11.61	10.69	10.80	10.91
Jet [9*-13*]		10.28	10.13	10.52	11.64	11.07	9.96	10.08	10.33	9.82
Diesel [13*-18]		21.45	18.34	15.78	21.37	17.44	18.89	22.73	18.67	17.49
No. 2 Fuel Oil [19-25]		18.53	20.57	24.79	19.98	21.01	19.17	17.71	20.45	20.23
No. 4 Fuel Oil [26-74]		19.01	23.64	23.28	14.48	18.28	19.21	17.00	20.97	21.94
Carbon		5.05	5.05	5.05	5.05	5.05	5.05	5.05	5.05	5.05
TPV	(USD/kg)	0.798	0.811	0.809	0.789	0.802	0.802	0.797	0.817	0.810

Table 118. Noncatalytic cracking process estimated yields for soybean TAG samples processed at various temperatures / space times on the 100 ml lab-scale TCR

		A-Soy	B-Soy	C-Soy	D-Soy	E-Soy	F-Soy	G-Soy	H-Soy	I-Soy
Burner Fuel Heat	(MJ/kg)	0.56	0.67	0.81	0.88	1.03	1.32	1.13	1.30	1.53
Burner Fuel	(wt. %)	2.00	2.28	2.74	3.09	3.40	4.27	4.03	4.56	5.20
CO_2		7.52	7.84	8.31	7.99	8.40	9.27	9.29	9.47	8.95
Nat. Gas. Equiv.		1.19	1.41	1.71	1.87	2.17	2.79	2.39	2.74	3.25
LPG [3-4]		1.93	2.35	2.72	2.81	3.50	4.71	3.29	3.88	4.92
Naphtha [5-9*]		7.14	8.76	9.93	10.85	14.09	14.17	11.03	13.22	15.28
Jet [9*-13*]		7.48	8.29	9.28	10.02	13.27	12.51	10.70	12.16	14.46
Diesel [13*-18]		17.70	19.16	19.15	20.18	20.77	19.65	20.50	20.84	22.88
No. 2 Fuel Oil [19-25]		21.94	21.59	19.30	18.71	15.76	14.96	16.69	15.09	14.76
No. 4 Fuel Oil [26-74]		28.47	23.74	22.52	20.55	14.57	14.10	18.53	14.89	7.68
Carbon		5.05	5.05	5.05	5.05	5.05	5.05	5.05	5.05	5.05
TPV	(USD/kg)	0.820	0.815	0.807	0.811	0.804	0.782	0.789	0.784	0.785

Table 119. Noncatalytic cracking process estimated yields for canola TAG samples processed at various pressures on the 200 ml lab-scale TCR

		J-Canola	K-Canola	L-Canola	M-Canola	N-Canola
Burner Fuel Heat	(MJ/kg)	1.09	1.11	1.16	1.17	1.23
Burner Fuel	(wt. %)	3.97	3.88	4.10	3.96	3.94
CO_2		9.14	8.77	8.70	8.70	9.17
Nat. Gas. Equiv.		2.32	2.34	2.46	2.47	2.59
LPG [3-4]		3.57	4.00	3.94	3.96	3.81
Naphtha [5-9*]		18.22	20.20	20.64	20.76	21.57
Jet [9*-13*]		17.92	19.62	19.60	19.70	20.19
Diesel [13*-18]		26.40	24.85	23.87	23.47	23.08
No. 2 Fuel Oil [19-25]		9.70	7.93	7.90	8.10	7.29
No. 4 Fuel Oil [26-74]		3.34	3.42	3.84	4.11	3.94
Carbon		5.05	5.05	5.05	5.05	5.05
TPV	(USD/kg)	0.788	0.797	0.795	0.797	0.797

Table 120. Summary of triglyceride compositions and cracked product compositions from the cracking of various triglycerides in the 100 mL lab-scale tubular cracking reactor

		Soybean	VHONO	HENO	Linseed	Camelina	Corn	Cottonseed	Canola	HONO
TAG Fatty Acid Moieties	wt. %									
Palmitic (COOH 16:0)		11.4	3.2	3.5	6.0	6.0	11.4	23.9	3.6	3.7
Stearic (COOH 18:0)		4.2	2.3	1.2	0.0	2.0	1.7	2.4	1.5	2.0
Oleic (COOH 18:1)		26.1	84.1	18.5	17.0	13.0	26.6	17.4	61.6	73.3
Linoleic (COOH 18:2)		50.3	4.0	13.2	14.0	16.0	57.6	53.4	21.7	14.8
Linolenic (COOH 18:3)		7.9	2.6	7.7	60.0	39.0	1.0	0.0	9.6	2.6
Erucic (COOH 22:1)		0.0	0.0	41.2	0.0	4.0	0.0	0.0	0.2	0.0
Other		0.1	3.8	13.6	3.0	20.0	1.7	3.0	1.8	3.7
Product Composition										
Gaseous Fuel Range (1-4)	wt. %									
H_2		0.07	0.05	0.07	0.07	0.06	0.06	0.07	0.05	0.06
CO		1.56	1.11	1.46	1.58	1.43	1.46	1.57	1.18	1.48
CO_2		3.42	2.65	3.33	3.27	3.08	2.89	3.33	2.59	3.51
[1-4]C-		3.13	1.85	2.22	3.36	2.68	2.54	3.01	2.22	2.56
[1-4]C=		1.28	0.91	1.13	1.34	1.26	1.53	1.34	1.06	1.42
[1-5]COOH		2.37	1.46	1.43	2.80	3.38	3.42	2.59	2.21	1.76
Total		11.83	8.02	9.62	12.41	11.89	11.90	11.92	9.31	10.79
Naphtha Range (5-8)	wt. %									
[5-8]C-		1.61	1.79	1.26	1.50	1.89	2.10	1.93	1.97	2.34
[5-8]C=		2.06	1.70	1.27	2.14	2.64	3.03	3.05	2.69	2.82
[5-8]=C=		1.97	1.57	1.21	2.17	2.58	2.28	2.11	2.26	2.31
[6-8] (1x)Ar(=)		0.19	0.11	0.12	0.36	0.31	0.20	0.21	0.23	0.19
[6-9]COOH		7.81	5.10	4.79	9.18	7.70	8.92	7.96	7.44	5.01
Total		13.64	10.26	8.64	15.36	15.10	16.53	15.25	14.59	12.68
Jet Range (9-13)	wt. %									
[9-13]C-		0.88	0.89	1.03	0.81	1.07	0.96	1.13	1.09	0.94
[9-13]C=		4.23	4.40	4.19	3.80	4.04	3.77	3.47	4.23	4.38
[9-13]=C=		4.22	3.31	3.60	4.71	4.44	4.43	4.46	4.35	4.02
[9-13] (1x)Ar(=)		1.27	0.58	0.85	2.12	1.68	1.32	1.34	1.08	0.81
[10-13] (2/3x)Ar(=)		0.40	0.27	0.27	0.60	0.44	0.40	0.40	0.36	0.33
[10-14]COOH		3.68	7.15	5.69	4.47	4.00	2.95	3.24	3.69	3.84
Total		14.68	16.59	15.62	16.51	15.67	13.83	14.05	14.79	14.32
Diesel Range (14-18)	wt. %									
[14-18]C-		1.27	0.48	0.52	1.09	1.06	1.09	2.24	0.84	0.76
[14-18]C=		4.45	6.51	5.18	4.04	3.84	3.63	3.29	4.90	5.77
[14-18]=C=		5.21	4.83	4.86	5.09	4.65	4.78	4.16	4.98	4.87
[14-18] (1x)Ar(=)		1.67	0.87	1.03	2.60	1.84	1.54	1.56	1.45	1.19
[14-18] (2/3x)Ar(=)		2.13	1.61	1.61	2.79	2.18	2.08	2.20	2.00	1.71
[15-18]COOH		8.12	5.02	3.22	6.86	4.60	7.04	11.12	5.39	3.94
Total		22.86	19.32	16.41	22.46	18.17	20.16	24.57	19.56	18.24
Fuel Oils (>C18)	wt. %									
[19-25] (No. 2 Fuel Oil)		19.63	21.75	26.24	21.17	22.24	20.30	18.76	21.63	21.42
[26-36] (No. 4 Fuel Oil)		14.38	18.07	17.12	11.79	12.57	13.72	12.22	14.98	15.89
[37-55] (No. 4 Fuel Oil)		5.52	6.55	7.04	3.51	6.45	6.31	5.57	6.82	6.98
[56-74] (No. 4 Fuel Oil)		0.24	0.38	0.47	0.04	0.33	0.30	0.21	0.37	0.37
Total		39.77	46.74	50.88	36.51	41.59	40.63	36.76	43.80	44.65

Table 121. Summary of cracked product compositions from the cracking of soybean oil in the 100 mL lab-scale tubular cracking reactor at various temperatures and space times

		A-Soy	B-Soy	C-Soy	D-Soy	E-Soy	F-Soy	G-Soy	H-Soy	I-Soy
Temperature	(C)	420	430	440	420	430	440	420	430	440
Space Time	(h)	0.27	0.27	0.27	0.69	0.70	0.69	1.22	1.17	1.10
Product Composition										
Gaseous Fuel Range (1-4)	wt. %									
H_2		0.03	0.04	0.04	0.05	0.05	0.05	0.06	0.07	0.07
CO		0.96	1.05	1.27	1.51	1.53	1.87	2.05	2.30	2.47
CO_2		2.49	2.58	3.16	3.45	3.46	4.20	4.45	4.95	4.74
[1-4]C-		1.47	1.82	2.17	2.33	2.87	4.40	2.98	3.56	4.87
[1-4]C=		0.58	0.81	1.07	1.20	1.55	1.89	1.43	1.83	2.17
[1-5]COOH		2.37	2.55	2.57	2.32	2.69	2.68	2.43	2.38	2.23
Total		7.91	8.85	10.27	10.85	12.14	15.10	13.40	15.07	16.55
Naphtha Range (5-8)	wt. %									
[5-8]C-		1.13	1.39	1.62	1.80	2.60	2.51	1.77	2.34	2.53
[5-8]C=		1.68	2.30	2.62	2.99	3.58	4.00	3.03	3.90	4.49
[5-8]=C=		1.42	1.79	2.24	2.63	3.08	2.85	2.61	3.07	3.80
[6-8] (1x)Ar(=)		0.15	0.18	0.26	0.30	0.35	0.29	0.26	0.36	0.53
[6-9]COOH		7.48	7.79	7.97	7.52	8.39	8.47	7.74	7.57	7.50
Total		11.86	13.44	14.70	15.24	18.01	18.12	15.40	17.24	18.85
Jet Range (9-13)	wt. %									
[9-13]C-		0.56	0.78	0.96	1.40	1.51	1.47	1.37	1.74	2.40
[9-13]C=		2.62	2.80	3.19	3.21	5.05	4.97	3.70	4.16	4.79
[9-13]=C=		3.60	3.99	4.37	4.37	5.89	5.27	4.68	5.28	5.96
[9-13] (1x)Ar(=)		0.85	1.00	1.19	1.72	1.93	1.74	1.68	2.11	2.84
[10-13] (2/3x)Ar(=)		0.35	0.36	0.36	0.40	0.48	0.47	0.39	0.45	0.62
[10-14]COOH		2.46	2.85	2.95	2.90	3.50	3.47	3.08	3.15	3.36
Total		10.45	11.78	13.02	14.00	18.36	17.41	14.90	16.89	19.98
Diesel Range (14-18)	wt. %									
[14-18]C-		0.76	0.89	1.03	1.60	1.70	1.50	1.62	1.97	2.77
[14-18]C=		3.18	3.48	3.67	4.15	4.64	4.45	4.09	4.30	5.16
[14-18]=C=		3.50	3.97	4.23	4.98	5.47	5.04	4.94	5.43	6.13
[14-18] (1x)Ar(=)		0.96	1.21	1.41	2.00	2.24	1.74	1.82	2.17	2.70
[14-18] (2/3x)Ar(=)		1.56	1.90	2.02	2.01	2.14	1.92	2.10	2.19	2.28
[15-18]COOH		9.57	9.44	8.24	6.45	5.27	5.99	7.07	5.52	4.25
Total		19.52	20.89	20.60	21.18	21.46	20.64	21.65	21.58	23.28
Fuel Oils (>C18)	wt. %									
[19-25] (No. 2 Fuel Oil)		23.18	22.81	20.41	19.81	16.69	15.88	17.69	16.02	15.69
[26-36] (No. 4 Fuel Oil)		18.31	16.57	15.80	15.75	10.47	10.06	13.23	11.34	6.87
[37-55] (No. 4 Fuel Oil)		11.37	8.37	7.82	6.00	4.80	4.71	6.38	4.47	1.29
[56-74] (No. 4 Fuel Oil)		0.39	0.16	0.20	0.00	0.17	0.20	0.04	0.00	0.00
Total		53.25	47.91	44.23	41.56	32.12	30.84	37.34	31.83	23.85

576

Table 122. Summary of product compositions from the cracking of canola oil
in the 200 mL lab-scale tubular cracking reactor at various pressures

		J-Canola	K-Canola	L-Canola	M-Canola	N-Canola
Pressure	(MPa)	0.79	1.83	2.86	3.90	4.94
Product Composition						
Gaseous Fuel Range (1-4)	wt. %					
H_2		0.04	0.04	0.05	0.05	0.05
CO		2.01	1.87	2.01	1.84	1.67
CO_2		3.82	3.76	3.80	3.69	4.14
[1-4]C-		3.22	3.26	3.32	3.42	3.61
[1-4]C=		1.36	1.83	1.83	1.73	1.49
[1-5]COOH		2.78	2.98	2.73	2.90	2.96
Total		13.23	13.75	13.74	13.62	13.92
Naphtha Range (5-8)	wt. %					
[5-8]C-		3.08	3.74	3.85	3.92	4.13
[5-8]C=		4.34	5.77	5.63	5.45	5.97
[5-8]=C=		5.02	4.41	4.80	4.79	4.75
[6-8] (1x)Ar(=)		0.28	0.45	0.52	0.57	0.65
[6-9]COOH		7.29	8.17	7.81	7.89	8.05
Total		20.01	22.54	22.61	22.63	23.55
Jet Range (9-13)	wt. %					
[9-13]C-		2.15	2.63	2.64	2.76	2.97
[9-13]C=		8.35	9.52	9.02	8.77	8.70
[9-13]=C=		6.53	7.17	7.25	7.22	7.95
[9-13] (1x)Ar(=)		1.91	2.33	2.66	2.90	2.92
[10-13] (2/3x)Ar(=)		0.44	0.58	0.66	0.70	0.67
[10-14]COOH		7.17	5.43	5.26	5.14	4.94
Total		26.55	27.66	27.50	27.49	28.15
Diesel Range (14-18)	wt. %					
[14-18]C-		1.46	1.52	1.49	1.41	1.71
[14-18]C=		10.14	8.94	8.10	7.75	7.54
[14-18]=C=		8.18	7.74	7.42	7.30	6.99
[14-18] (1x)Ar(=)		2.19	2.65	2.70	2.68	2.66
[14-18] (2/3x)Ar(=)		2.40	2.09	2.21	2.26	2.19
[15-18]COOH		2.19	1.88	1.91	1.99	1.76
Total		26.56	24.82	23.81	23.39	22.84
Fuel Oils (>C18)	wt. %					
[19-25] (No. 2 Fuel Oil)		10.28	8.40	8.37	8.58	7.73
[26-36] (No. 4 Fuel Oil)		2.51	2.36	2.73	2.88	2.77
[37-55] (No. 4 Fuel Oil)		1.03	0.92	1.12	1.23	1.40
[56-74] (No. 4 Fuel Oil)		0.00	0.34	0.22	0.25	0.00
Total		13.82	12.03	12.44	12.94	11.90

Table 123. Summary of functional group distributions in fuel products from the cracking of various triglycerides in the 100 mL lab-scale tubular cracking reactor

		Soybean	VHONO	HENO	Linseed	Camelina	Corn	Cottonseed	Canola	HONO
TAG Fatty Acid Moieties	wt. %									
Palmitic (COOH 16:0)		11.4	3.2	3.5	6.0	6.0	11.4	23.9	3.6	3.7
Stearic (COOH 18:0)		4.2	2.3	1.2	0.0	2.0	1.7	2.4	1.5	2.0
Oleic (COOH 18:1)		26.1	84.1	18.5	17.0	13.0	26.6	17.4	61.6	73.3
Linoleic (COOH 18:2)		50.3	4.0	13.2	14.0	16.0	57.6	53.4	21.7	14.8
Linolenic (COOH 18:3)		7.9	2.6	7.7	60.0	39.0	1.0	0.0	9.6	2.6
Erucic (COOH 22:1)		0.0	0.0	41.2	0.0	4.0	0.0	0.0	0.2	0.0
Other		0.1	3.8	13.6	3.0	20.0	1.7	3.0	1.8	3.7
Product Composition										
Gaseous Fuel Range (1-4)	wt. %									
H_2/Range		0.59	0.59	0.69	0.55	0.53	0.50	0.55	0.57	0.58
CO/Range		13.21	13.85	15.12	12.72	12.04	12.26	13.20	12.69	13.67
CO_2/Range		28.88	32.99	34.59	26.32	25.86	24.31	27.96	27.78	32.57
C-/Range		26.45	23.07	23.05	27.06	22.56	21.36	25.30	23.83	23.71
C=/Range		10.84	11.28	11.72	10.77	10.57	12.85	11.26	11.36	13.12
COOH/Range		20.04	18.22	14.83	22.57	28.44	28.72	21.74	23.78	16.35
Range/Total		11.83	8.02	9.62	12.41	11.89	11.90	11.92	9.31	10.79
Naphtha Range (5-8)	wt. %									
C-/Range		11.83	17.44	14.59	9.78	12.49	12.70	12.63	13.53	18.43
C=/Range		15.09	16.52	14.65	13.92	17.47	18.31	19.98	18.43	22.28
=C=/Range		14.43	15.28	13.95	14.16	17.05	13.81	13.86	15.48	18.25
(1x)Ar(=)/Range		1.41	1.10	1.42	2.37	2.02	1.23	1.37	1.59	1.50
COOH/Range		57.23	49.67	55.39	59.78	50.96	53.95	52.17	50.97	39.54
Range/Total		13.64	10.26	8.64	15.36	15.10	16.53	15.25	14.59	12.68
Jet Range (9-13)	wt. %									
C-/Range		6.01	5.34	6.57	4.88	6.82	6.94	8.05	7.35	6.59
C=/Range		28.81	26.52	26.84	23.01	25.77	27.23	24.72	28.58	30.56
=C=/Range		28.77	19.95	23.04	28.51	28.36	32.03	31.76	29.39	28.06
(1x)Ar(=)/Range		8.65	3.47	5.41	12.84	10.74	9.57	9.54	7.32	5.69
(2/3x)Ar(=)/Range		2.70	1.62	1.71	3.66	2.80	2.87	2.84	2.42	2.31
COOH/Range		25.06	43.11	36.43	27.09	25.51	21.36	23.09	24.93	26.78
Range/Total		14.68	16.59	15.62	16.51	15.67	13.83	14.05	14.79	14.32
Diesel Range (14-18)	wt. %									
C-/Range		5.57	2.46	3.16	4.84	5.85	5.39	9.13	4.28	4.14
C=/Range		19.47	33.70	31.55	18.00	21.14	18.00	13.39	25.04	31.66
=C=/Range		22.79	25.01	29.62	22.64	25.57	23.70	16.93	25.45	26.71
(1x)Ar(=)/Range		7.30	4.48	6.28	11.55	10.10	7.64	6.36	7.43	6.51
(2/3x)Ar(=)/Range		9.33	8.35	9.79	12.42	12.02	10.32	8.95	10.25	9.38
COOH/Range		35.53	26.00	19.61	30.55	25.32	34.95	45.24	27.55	21.60
Range/Total		22.86	19.32	16.41	22.46	18.17	20.16	24.57	19.56	18.24
Fuel Oils (>C18)	wt. %									
[19-25]/Range		49.36	46.52	51.57	57.98	53.47	49.95	51.03	49.38	47.97
[26-36]/Range		36.15	38.67	33.66	32.30	30.22	33.77	33.24	34.20	35.57
[37-55]/Range		13.88	14.01	13.84	9.62	15.52	15.53	15.16	15.58	15.62
[56-74]/Range		0.61	0.80	0.92	0.10	0.79	0.75	0.57	0.85	0.84
Range/Total		39.77	46.74	50.88	36.51	41.59	40.63	36.76	43.80	44.65

Table 124. Summary of functional group distributions in fuel products from
the cracking of soybean oil in the 100 mL lab-scale tubular
cracking reactor at various temperatures and space times

		A-Soy	B-Soy	C-Soy	D-Soy	E-Soy	F-Soy	G-Soy	H-Soy	I-Soy
Temperature	(C)	420	430	440	420	430	440	420	430	440
Space Time	(h)	0.27	0.27	0.27	0.69	0.70	0.69	1.22	1.17	1.10
Product Composition										
Gaseous Fuel Range (1-4)	wt. %									
H_2/Range		0.43	0.41	0.42	0.44	0.39	0.35	0.46	0.44	0.39
CO/Range		12.12	11.83	12.33	13.88	12.60	12.40	15.32	15.23	14.95
CO_2/Range		31.52	29.22	30.76	31.76	28.47	27.81	33.17	32.85	28.65
C-/Range		18.59	20.54	21.08	21.44	23.64	29.17	22.24	23.59	29.41
C=/Range		7.36	9.19	10.38	11.07	12.73	12.52	10.67	12.11	13.12
COOH/Range		29.98	28.82	25.04	21.40	22.17	17.75	18.14	15.78	13.48
Range/Total		7.91	8.85	10.27	10.85	12.14	15.10	13.40	15.07	16.55
Naphtha Range (5-8)	wt. %									
C-/Range		9.49	10.37	11.01	11.80	14.45	13.86	11.48	13.55	13.43
C=/Range		14.17	17.08	17.80	19.61	19.87	22.07	19.66	22.61	23.80
=C=/Range		11.98	13.32	15.22	17.27	17.11	15.73	16.97	17.83	20.16
(1x)Ar(=)/Range		1.29	1.30	1.75	1.96	1.96	1.62	1.68	2.09	2.80
COOH/Range		63.06	57.93	54.22	49.37	46.60	46.72	50.21	43.93	39.80
Range/Total		11.86	13.44	14.70	15.24	18.01	18.12	15.40	17.24	18.85
Jet Range (9-13)	wt. %									
C-/Range		5.37	6.60	7.36	10.00	8.24	8.46	9.17	10.31	12.03
C=/Range		25.11	23.79	24.53	22.96	27.51	28.58	24.81	24.61	23.98
=C=/Range		34.45	33.86	33.56	31.19	32.08	30.30	31.42	31.26	29.82
(1x)Ar(=)/Range		8.17	8.46	9.12	12.30	10.53	10.00	11.29	12.52	14.22
(2/3x)Ar(=)/Range		3.35	3.09	2.74	2.83	2.60	2.70	2.65	2.66	3.12
COOH/Range		23.55	24.21	22.70	20.72	19.03	19.96	20.67	18.63	16.84
Range/Total		10.45	11.78	13.02	14.00	18.36	17.41	14.90	16.89	19.98
Diesel Range (14-18)	wt. %									
C-/Range		3.88	4.25	4.98	7.56	7.91	7.29	7.49	9.13	11.88
C=/Range		16.30	16.66	17.82	19.57	21.64	21.58	18.90	19.94	22.17
=C=/Range		17.91	19.01	20.52	23.52	25.48	24.41	22.82	25.15	26.31
(1x)Ar(=)/Range		4.91	5.80	6.85	9.42	10.44	8.41	8.42	10.07	11.59
(2/3x)Ar(=)/Range		7.98	9.11	9.82	9.48	9.99	9.28	9.72	10.14	9.80
COOH/Range		49.03	45.17	40.01	30.44	24.53	29.03	32.65	25.57	18.25
Range/Total		19.52	20.89	20.60	21.18	21.46	20.64	21.65	21.58	23.28
Fuel Oils (>C18)	wt. %									
[19-25]/Range		43.53	47.62	46.14	47.66	51.95	51.48	47.38	50.34	65.79
[26-36]/Range		34.39	34.58	35.72	37.90	32.58	32.62	35.42	35.62	28.80
[37-55]/Range		21.36	17.47	17.68	14.43	14.93	15.26	17.10	14.04	5.41
[56-74]/Range		0.73	0.33	0.46	0.00	0.53	0.64	0.10	0.00	0.00
Range/Total		53.25	47.91	44.23	41.56	32.12	30.84	37.34	31.83	23.85

Table 125. Summary of functional group distributions in fuel products from the cracking of canola oil in the 200 mL lab-scale tubular cracking reactor at various pressures

		J-Canola	K-Canola	L-Canola	M-Canola	N-Canola
Pressure	(MPa)	0.79	1.83	2.86	3.90	4.94
Product Composition						
Gaseous Fuel Range (1-4)	wt. %					
H_2/Range		0.28	0.28	0.34	0.34	0.34
CO/Range		15.18	13.63	14.66	13.50	12.01
CO_2/Range		28.88	27.34	27.66	27.10	29.75
C-/Range		24.34	23.72	24.15	25.12	25.93
C=/Range		10.31	13.32	13.31	12.67	10.69
COOH/Range		21.00	21.70	19.89	21.28	21.28
Range/Total		13.23	13.75	13.74	13.62	13.92
Naphtha Range (5-8)	wt. %					
C-/Range		15.39	16.61	17.01	17.35	17.53
C=/Range		21.70	25.60	24.91	24.09	25.37
=C=/Range		25.10	19.55	21.23	21.16	20.16
(1x)Ar(=)/Range		1.39	2.00	2.29	2.53	2.78
COOH/Range		36.43	36.24	34.56	34.87	34.17
Range/Total		20.01	22.54	22.61	22.63	23.55
Jet Range (9-13)	wt. %					
C-/Range		8.10	9.51	9.61	10.05	10.54
C=/Range		31.46	34.42	32.82	31.90	30.91
=C=/Range		24.61	25.91	26.36	26.25	28.25
(1x)Ar(=)/Range		7.18	8.42	9.67	10.55	10.37
(2/3x)Ar(=)/Range		1.66	2.09	2.40	2.54	2.38
COOH/Range		26.99	19.65	19.14	18.71	17.55
Range/Total		26.55	27.66	27.50	27.49	28.15
Diesel Range (14-18)	wt. %					
C-/Range		5.50	6.14	6.25	6.01	7.48
C=/Range		38.18	36.01	34.01	33.14	32.99
=C=/Range		30.78	31.20	31.15	31.23	30.62
(1x)Ar(=)/Range		8.25	10.67	11.32	11.45	11.63
(2/3x)Ar(=)/Range		9.04	8.40	9.26	9.68	9.60
COOH/Range		8.26	7.58	8.00	8.50	7.68
Range/Total		26.56	24.82	23.81	23.39	22.84
Fuel Oils (>C18)	wt. %					
[19-25]/Range		74.39	69.84	67.28	66.32	64.92
[26-36]/Range		18.17	19.66	21.94	22.30	23.29
[37-55]/Range		7.44	7.69	9.01	9.47	11.78
[56-74]/Range		0.00	2.81	1.77	1.91	0.00
Range/Total		13.82	12.03	12.44	12.94	11.90

Table 126. Regression coefficients showing the effect of various
triglyceride fatty acid moieties on the distribution of products
from triglyceride cracking in tubular cracking reactors

TAG Composition	(COOH 16:0)	(COOH 18:0)	(COOH 18:1)	(COOH 18:2)	(COOH 18:3)	(COOH 22:1)	Const	Coeff. Det. R^2
Coded Variable	X1	X2	X3	X4	X5	X6	B1	
Effect Coefficients wt. %								
Gaseous Fuel Range (1-4)								
H_2/Range	-	-	-	-0.03	-0.04	0.04	0.57	0.69
CO/Range	-	-	-	-0.54	-0.77	0.69	13.20	0.73
CO_2/Range	-	-	-	-2.86	-2.86	2.21	29.03	0.78
C-/Range	-	-	-	-	-	-	24.04	-
C=/Range	-	-1.00	0.63	0.63	-0.50	-	11.53	0.55
COOH/Range	-	-	-	2.98	3.15	-2.52	21.63	0.49
Range/Total	-	-	-0.79	0.98	0.95	-0.51	10.86	0.83
Naphtha Range (5-8)								
C-/Range	-	-	1.98	-1.09	-1.49	-	13.71	0.81
C=/Range	-	-	-	-	-	-	17.40	-
=C=/Range	-	-	-	-	-	-	15.14	-
(1x)Ar(=)/Range	-	-	-0.19	-0.16	0.38	-0.15	1.56	0.91
COOH/Range	-	-	-4.28	-	-	-	52.18	0.39
Range/Total	-	-	-	2.20	1.96	-1.78	13.56	0.85
Jet Range (9-13)								
C-/Range	0.62	-	-	-	-0.60	-	6.51	0.44
C=/Range	-2.13	-	1.98	2.52	-	-	26.89	0.60
=C=/Range	-	-	-	3.67	-	-	27.76	0.53
(1x)Ar(=)/Range	-	-0.96	-1.40	1.67	2.47	-1.32	8.14	0.99
(2/3x)Ar(=)/Range	-	-0.38	-	0.54	0.57	-0.39	2.55	0.94
COOH/Range	-	-	-	-6.63	-3.19	2.88	28.15	0.65
Range/Total	-	-	-	-1.01	-	-	15.12	0.59
Diesel Range (14-18)								
C-/Range	1.88	-	-0.92	-	-	-0.89	4.98	0.91
C=/Range	-	-	2.91	-6.48	-4.09	2.85	23.55	0.94
=C=/Range	-3.81	-	-	-	-	2.45	24.27	0.91
(1x)Ar(=)/Range	-	-	-1.08	-	2.10	-0.90	7.52	0.90
(2/3x)Ar(=)/Range	-0.64	-	-0.77	-	1.18	-	10.09	0.85
COOH/Range	8.83	-	-	-	-	-5.13	29.59	0.88
Range/Total	2.58	-	-	-	-	-1.72	20.19	0.75
Fuel Oils (>C18)								
[19-25]/Range	-	-2.04	-2.31	-	2.09	-	50.80	0.97
[26-36]/Range	-	-	1.93	-	-1.16	-	34.20	0.68
[37-55]/Range	-	-	-	-	-	-	14.31	-
[56-74]/Range	-	-	-	-	-0.22	0.14	0.69	0.56
Range/Total	-3.71	-	1.15	-	-2.69	3.98	42.37	0.97

Table 127. Regression coefficients showing the effect of temperature and space time on the distribution of products from triglyceride cracking in tubular cracking reactors

Operating Condition(s)		T	Tau	T×Tau	Const	Coeff. Det.
Coded Variable		X7	X8	X7·X8	B2	R^2
Effect Coefficients	wt. %					
Gaseous Fuel Range (1-4)						
H$_2$/Range		-0.03	-	-	0.41	0.54
CO/Range		-	1.6	-	13.4	-
CO$_2$/Range		-1.5	-	-	30.5	0.45
C-/Range		3.0	2.5	-	23.3	0.77
C=/Range		1.2	1.5	-	11.0	0.74
COOH/Range		-2.5	-6.3	-	21.4	0.94
Range/Total		1.8	3.1	-	12.2	0.95
Naphtha Range (5-8)						
C-/Range		1.0	1.3	-	12.2	0.59
C=/Range		1.8	2.9	-	19.6	0.89
=C=/Range		-	2.4	-	16.2	0.66
(1x)Ar(=)/Range		-	0.4	-	1.8	0.42
COOH/Range		-4.0	-7.1	-	50.2	0.84
Range/Total		1.6	2.0	-	15.9	0.79
Jet Range (9-13)						
C-/Range		-	2.1	-	8.6	0.68
C=/Range		-	-	-	25.1	0.11
=C=/Range		-	-1.6	-	32.0	0.63
(1x)Ar(=)/Range		-	2.1	-	10.7	0.70
(2/3x)Ar(=)/Range		-	-	0.3	2.9	0.54
COOH/Range		-1.1	-2.5	-1.0	20.7	0.86
Range/Total		2.0	2.8	-	15.2	0.78
Diesel Range (14-18)						
C-/Range		1.1	2.7	1.1	7.2	0.89
C=/Range		1.2	1.7	-	19.4	0.63
=C=/Range		-	2.8	-	22.8	0.60
(1x)Ar(=)/Range		-	2.1	-	8.4	0.59
(2/3x)Ar(=)/Range		0.3	0.5	-0.4	9.5	0.70
COOH/Range		-4.6	-9.8	-	32.7	0.76
Range/Total		-	0.9	-	21.2	0.55
Fuel Oils (>C18)						
[19-25]/Range		4.7	4.7	4.4	50.2	0.82
[26-36]/Range		-1.9	-	-1.9	34.2	0.59
[37-55]/Range		-2.8	-3.5	-2.4	15.3	0.75
[56-74]/Range		-	-0.2	-	0.3	0.47
Range/Total		-5.9	-9.0	-	38.1	0.88

Table 128. Regression coefficients showing the effect of pressure on the distribution
of products from triglyceride cracking in tubular cracking reactors

Operating Condition Coded Variable		Pressure X9	Const B3	Coeff. Det. R^2
Effect Coefficients	wt. %			
Gaseous Fuel Range (1-4)				
H_2/Range		0.04	0.31	0.78
CO/Range		-1.3	13.8	0.70
CO_2/Range		-	28.1	-
C-/Range		0.9	24.7	0.68
C=/Range		-	12.1	-
COOH/Range		-	21.0	-
Range/Total		-	13.7	-
Naphtha Range (5-8)				
C-/Range		1.0	16.8	0.87
C=/Range		-	24.3	-
=C=/Range		-	21.4	-
(1x)Ar(=)/Range		0.7	2.2	0.95
COOH/Range		-1.2	35.3	0.83
Range/Total		1.4	22.3	0.73
Jet Range (9-13)				
C-/Range		1.1	9.6	0.88
C=/Range		-	32.3	-
=C=/Range		1.5	26.3	0.85
(1x)Ar(=)/Range		1.7	9.2	0.89
(2/3x)Ar(=)/Range		0.4	2.2	0.72
COOH/Range		-4.0	20.4	0.69
Range/Total		0.6	27.5	0.68
Diesel Range (14-18)				
C-/Range		0.8	6.3	0.69
C=/Range		-2.6	34.9	0.90
=C=/Range		-	31.0	-
(1x)Ar(=)/Range		1.5	10.7	0.73
(2/3x)Ar(=)/Range		-	9.2	-
COOH/Range		-	8.0	-
Range/Total		-1.8	24.3	0.92
Fuel Oils (>C18)				
[19-25]/Range		-4.5	68.6	0.91
[26-36]/Range		2.6	21.1	0.94
[37-55]/Range		2.1	9.1	0.91
[56-74]/Range		-	1.3	-
Range/Total		-	12.6	-

Table 129. TAG compositions and cracked product compositions from the cracking of various triglycerides in the 100 mL lab-scale tubular cracking reactor

		Soybean	VHONO	HENO	Linseed	Camelina	Corn	Cottonseed	Canola	HONO
TAG Fatty Acid Moieties	wt. %									
Palmitic (COOH 16:0)		11.4	3.2	3.5	6.0	6.0	11.4	23.9	3.6	3.7
Stearic (COOH 18:0)		4.2	2.3	1.2	0.0	2.0	1.7	2.4	1.5	2.0
Oleic (COOH 18:1)		26.1	84.1	18.5	17.0	13.0	26.6	17.4	61.6	73.3
Linoleic (COOH 18:2)		50.3	4.0	13.2	14.0	16.0	57.6	53.4	21.7	14.8
Linolenic (COOH 18:3)		7.9	2.6	7.7	60.0	39.0	1.0	0.0	9.6	2.6
Erucic (COOH 22:1)		0.0	0.0	41.2	0.0	4.0	0.0	0.0	0.2	0.0
Other		0.1	3.8	13.6	3.0	20.0	1.7	3.0	1.8	3.7
Product Composition										
Misc. Compounds	wt. %									
H_2		0.07	0.05	0.07	0.07	0.06	0.06	0.07	0.05	0.06
CO		1.56	1.11	1.46	1.58	1.43	1.46	1.57	1.18	1.48
CO_2		3.42	2.65	3.33	3.27	3.08	2.89	3.33	2.59	3.51
Group C-	wt. %									
C1-C4		3.13	1.85	2.22	3.36	2.68	2.54	3.01	2.22	2.56
C5-C8		1.61	1.79	1.26	1.50	1.89	2.10	1.93	1.97	2.34
C9-C12		0.63	0.77	0.89	0.64	0.88	0.73	0.74	0.90	0.81
C13-C18		1.53	0.60	0.65	1.25	1.25	1.31	2.63	1.03	0.89
Group C=	wt. %									
C1-C4		1.28	0.91	1.13	1.34	1.26	1.53	1.34	1.06	1.42
C5-C8		2.06	1.70	1.27	2.14	2.64	3.03	3.05	2.69	2.82
C9-C12		4.34	4.49	4.36	4.10	4.75	4.68	4.13	4.87	5.04
C13-C18		5.27	7.23	5.64	4.63	4.28	4.08	3.77	5.35	6.21
Group =C=	wt. %									
C5-C8		1.97	1.57	1.21	2.17	2.58	2.28	2.11	2.26	2.31
C9-C12		3.76	2.82	3.14	4.16	3.93	3.93	3.85	3.65	3.36
C13-C18		5.80	5.37	5.37	5.79	5.30	5.44	4.91	5.78	5.59
Group COOH	wt. %									
C1-C5		2.37	1.46	1.43	2.80	3.38	3.42	2.59	2.21	1.76
C6-C9		7.81	5.10	4.79	9.18	7.70	8.92	7.96	7.44	5.01
C10-C13		3.31	6.97	5.41	3.92	3.58	2.64	2.39	3.34	3.60
C14-C18		8.49	5.20	3.50	7.41	5.02	7.35	11.97	5.73	4.18
Group (1x)Ar / (1x)Ar=	wt. %									
C6-C8		0.19	0.11	0.12	0.36	0.31	0.20	0.21	0.23	0.19
C9-C12		1.01	0.43	0.65	1.67	1.36	1.05	1.05	0.80	0.59
C13-C18		1.93	1.01	1.23	3.05	2.16	1.81	1.85	1.74	1.41
All (2x) & (3x) Ar	wt. %									
C10-C13		0.40	0.27	0.27	0.60	0.44	0.40	0.40	0.36	0.33
C14-C18		2.13	1.61	1.61	2.79	2.18	2.08	2.20	2.00	1.71
>C18 Carbon Groups	wt. %									
C19-C25		19.63	21.75	26.24	21.17	22.24	20.30	18.76	21.63	21.42
C26-C36		14.38	18.07	17.12	11.79	12.57	13.72	12.22	14.98	15.89
C37-C55		5.52	6.55	7.04	3.51	6.45	6.31	5.57	6.82	6.98
C56-C74		0.24	0.38	0.47	0.04	0.33	0.30	0.21	0.37	0.37

Table 130. Summary of cracked product compositions from the cracking of soybean oil in the 100 mL lab-scale tubular cracking reactor at various temperatures and space times

		A-Soy	B-Soy	C-Soy	D-Soy	E-Soy	F-Soy	G-Soy	H-Soy	I-Soy
Temperature	(C)	420	430	440	420	430	440	420	430	440
Space Time	(h)	0.27	0.27	0.27	0.69	0.70	0.69	1.22	1.17	1.10
Product Composition										
Misc. Compounds	wt. %									
H_2		0.03	0.04	0.04	0.05	0.05	0.05	0.06	0.07	0.07
CO		0.96	1.05	1.27	1.51	1.53	1.87	2.05	2.30	2.47
CO_2		2.49	2.58	3.16	3.45	3.46	4.20	4.45	4.95	4.74
Group C-	wt. %									
C1-C4		1.47	1.82	2.17	2.33	2.87	4.40	2.98	3.56	4.87
C5-C8		1.13	1.39	1.62	1.80	2.60	2.51	1.77	2.34	2.53
C9-C12		0.42	0.61	0.78	1.12	1.21	1.15	1.08	1.40	1.96
C13-C18		0.90	1.05	1.21	1.88	2.01	1.83	1.91	2.31	3.21
Group C=	wt. %									
C1-C4		0.58	0.81	1.07	1.20	1.55	1.89	1.43	1.83	2.17
C5-C8		1.68	2.30	2.62	2.99	3.58	4.00	3.03	3.90	4.49
C9-C12		2.93	3.18	3.56	3.53	6.07	5.99	4.11	4.57	5.33
C13-C18		3.53	3.89	4.12	4.65	5.21	5.04	4.63	4.93	5.86
Group =C=	wt. %									
C5-C8		1.42	1.79	2.24	2.63	3.08	2.85	2.61	3.07	3.80
C9-C12		3.21	3.48	3.81	3.65	5.07	4.71	3.95	4.45	4.98
C13-C18		3.99	4.60	4.92	5.82	6.47	5.77	5.81	6.41	7.27
Group COOH	wt. %									
C1-C5		2.37	2.55	2.57	2.32	2.69	2.68	2.43	2.38	2.23
C6-C9		7.48	7.79	7.97	7.52	8.39	8.47	7.74	7.57	7.50
C10-C13		2.28	2.60	2.66	2.49	3.06	3.12	2.69	2.72	2.90
C14-C18		9.75	9.69	8.54	6.86	5.70	6.34	7.45	5.95	4.71
Group (1x)Ar / (1x)Ar=	wt. %									
C6-C8		0.15	0.18	0.26	0.30	0.35	0.29	0.26	0.36	0.53
C9-C12		0.67	0.78	0.92	1.34	1.51	1.43	1.33	1.67	2.26
C13-C18		1.14	1.43	1.68	2.38	2.66	2.05	2.18	2.62	3.28
All (2x) & (3x) Ar	wt. %									
C10-C13		0.35	0.36	0.36	0.40	0.48	0.47	0.39	0.45	0.62
C14-C18		1.56	1.90	2.02	2.01	2.14	1.92	2.10	2.19	2.28
>C18 Carbon Groups	wt. %									
C19-C25		23.18	22.81	20.41	19.81	16.69	15.88	17.69	16.02	15.69
C26-C36		18.31	16.57	15.80	15.75	10.47	10.06	13.23	11.34	6.87
C37-C55		11.37	8.37	7.82	6.00	4.80	4.71	6.38	4.47	1.29
C56-C74		0.39	0.16	0.20	0.00	0.17	0.20	0.04	0.00	0.00

Table 131. Summary of product compositions from the cracking of canola oil
in the 200 mL lab-scale tubular cracking reactor at various pressures

		J-Canola	K-Canola	L-Canola	M-Canola	N-Canola
Pressure	(MPa)	0.79	1.83	2.86	3.90	4.94
Product Composition						
Misc. Compounds	wt. %					
H_2		0.04	0.04	0.05	0.05	0.05
CO		2.01	1.87	2.01	1.84	1.67
CO_2		3.82	3.76	3.80	3.69	4.14
Group C-	wt. %					
C1-C4		3.22	3.26	3.32	3.42	3.61
C5-C8		3.08	3.74	3.85	3.92	4.13
C9-C12		1.86	2.25	2.24	2.35	2.57
C13-C18		1.75	1.91	1.89	1.82	2.11
Group C=	wt. %					
C1-C4		1.36	1.83	1.83	1.73	1.49
C5-C8		4.34	5.77	5.63	5.45	5.97
C9-C12		9.13	10.53	10.25	10.21	10.10
C13-C18		11.47	10.16	9.14	8.77	8.54
Group =C=	wt. %					
C5-C8		5.02	4.41	4.80	4.79	4.75
C9-C12		5.67	6.28	6.33	6.31	6.86
C13-C18		9.20	8.85	8.52	8.40	8.29
Group COOH	wt. %					
C1-C5		2.78	2.98	2.73	2.90	2.96
C6-C9		7.29	8.17	7.81	7.89	8.05
C10-C13		6.79	5.05	4.86	4.73	4.52
C14-C18		2.57	2.26	2.31	2.40	2.18
Group (1x)Ar / (1x)Ar=	wt. %					
C6-C8		0.28	0.45	0.52	0.57	0.65
C9-C12		1.49	1.88	2.18	2.40	2.35
C13-C18		2.60	3.10	3.17	3.17	3.22
All (2x) & (3x) Ar	wt. %					
C10-C13		0.44	0.58	0.66	0.70	0.67
C14-C18		2.40	2.09	2.21	2.26	2.19
>C18 Carbon Groups	wt. %					
C19-C25		10.28	8.40	8.37	8.58	7.73
C26-C36		2.51	2.36	2.73	2.88	2.77
C37-C55		1.03	0.92	1.12	1.23	1.40
C56-C74		0.00	0.34	0.22	0.25	0.00

Appendix Q.
Representative Chemical Composition

Table 132. Relative chemical composition (RCC) component list and properties

C#	Class	Component Name	Formula	MW	T_{boil} (C)	Density	T_{melt} (C)
57	Miscellaneous	Triolein[*]	$C_{57}H_{104}O_6$	885.4	846.9	0.915	
0	Miscellaneous	Water	H_2O	18.0	100.0	0.998	
0	Miscellaneous	Hydrogen	H_2	2.0	□	□	
0	Miscellaneous	Carbon Monoxide	CO	28.0	□	□	
0	Miscellaneous	Carbon Dioxide	CO_2	44.0	□	□	
1	Paraffins	Methane	CH_4	16.0	-162.0	□	-183.2
2	Paraffins	Ethane	C_2H_6	30.1	-89.0	□	-184.2
3	Paraffins	Propane	C_3H_8	44.1	-42.0	□	-188.2
4	Paraffins	Butane	C_4H_{10}	58.1	0.0	□	-137.2
5	Paraffins	Pentane	C_5H_{12}	72.1	36.0	0.631	-129.8
6	Paraffins	Hexane	C_6H_{14}	86.2	69.0	0.661	-95.2
7	Paraffins	Heptane	C_7H_{16}	100.2	98.0	0.686	-90.6
8	Paraffins	Octane	C_8H_{18}	114.2	126.0	0.703	-56.9
9	Paraffins	Nonane	C_9H_{20}	128.3	151.0	0.718	-53.7
10	Paraffins	Decane	$C_{10}H_{22}$	142.3	174.0	0.730	-29.9
11	Paraffins	Undecane	$C_{11}H_{24}$	156.3	196.0	0.740	-25.8
12	Paraffins	Dodecane	$C_{12}H_{26}$	170.3	216.0	0.749	-9.6
13	Paraffins	Tridecane	$C_{13}H_{28}$	184.4	235.0	0.756	-5.1
14	Paraffins	Tetradecane	$C_{14}H_{30}$	198.4	254.0	0.763	5.6
15	Paraffins	Pentadecane	$C_{15}H_{32}$	212.4	271.0	0.768	9.9
16	Paraffins	Hexadecane	$C_{16}H_{34}$	226.4	287.0	0.773	17.9
17	Paraffins	Heptadecane	$C_{17}H_{36}$	240.5	302.0	0.777	22.0
18	Paraffins	Octadecane	$C_{18}H_{38}$	254.5	316.0	0.782	27.9
19	Paraffins	Nonadecane	$C_{19}H_{40}$	268.5	330.0	0.786	30.9
20	Paraffins	Eicosane	$C_{20}H_{42}$	282.5	344.0	0.789	36.9
21	Paraffins	Uneicosane	$C_{21}H_{44}$	296.6	356.0	0.792	40.3
22	Paraffins	Docosane	$C_{22}H_{46}$	310.6	369.0	0.795	43.9
23	Paraffins	Tricosane	$C_{23}H_{48}$	324.6	380.0	0.797	46.9
24	Paraffins	Tetracosane	$C_{24}H_{50}$	338.7	391.0	0.798	50.9
25	Paraffins	Pentacosane[*]	$C_{25}H_{52}$	352.7	402.0	0.801	53.9
26	Paraffins	Hexacosane	$C_{26}H_{54}$	366.7	412.0	0.803	56.9
27	Paraffins	Heptacosane[*]	$C_{27}H_{56}$	380.7	422.0	0.804	58.9
28	Paraffins	Octacosane	$C_{28}H_{58}$	394.8	431.0	0.804	60.9
29	Paraffins	Nonacosane[*]	$C_{29}H_{60}$	408.8	440.0	0.807	63.9
30	Paraffins	Triacontane	$C_{30}H_{62}$	422.8	449.0	0.809	65.8
31	Paraffins	Untriacontane[*]	$C_{31}H_{64}$	436.8	458.0	0.811	68.4
32	Paraffins	Dotriacontane	$C_{32}H_{66}$	450.9	466.0	0.813	69.9
33	Paraffins	Tritriacontane[*]	$C_{33}H_{68}$	464.9	474.0	0.813	71.9
34	Paraffins	Tetratriacontane[*]	$C_{34}H_{70}$	478.9	481.0	0.814	72.9
35	Paraffins	Pentatriacontane[*]	$C_{35}H_{72}$	492.9	489.0	0.814	74.9
36	Paraffins	Hexatriacontane	$C_{36}H_{74}$	507.0	496.0	0.815	75.9
38	Paraffins	Octatriacontane[*]	$C_{38}H_{78}$	535.0	509.0	0.824	76.9
40	Paraffins	Tetracontane[*]	$C_{40}H_{82}$	563.1	522.0	0.826	80.9
42	Paraffins	Dotetracontane[*]	$C_{42}H_{86}$	591.1	534.0	0.827	82.9
44	Paraffins	Tetratetracontane[*]	$C_{44}H_{90}$	619.2	545.0	0.828	85.9
46	Paraffins	Hexatetracontane[*]	$C_{46}H_{94}$	647.2	556.0	0.829	87.9
48	Paraffins	Octatetracontane[*]	$C_{48}H_{98}$	675.3	566.0	0.831	87.9
50	Paraffins	Pentacontane[*]	$C_{50}H_{102}$	703.3	575.0	0.831	91.9
52	Paraffins	Dopentacontane[*]	$C_{52}H_{106}$	731.4	584.0	0.832	93.9
54	Paraffins	Tetrapentacontane[*]	$C_{54}H_{110}$	759.5	592.0	0.833	94.9
56	Paraffins	Hexapentacontane[*]	$C_{56}H_{114}$	787.5	600.0	0.834	95.9
58	Paraffins	Octapentacontane[*]	$C_{58}H_{118}$	815.6	608.0	0.835	96.9
60	Paraffins	Hexacontane[*]	$C_{60}H_{122}$	843.6	615.0	0.835	99.9
62	Paraffins	Dohexacontane[*]	$C_{62}H_{126}$	871.7	622.0	0.836	101.9
64	Paraffins	Tetrahexacontane[*]	$C_{64}H_{130}$	899.7	629.0	0.836	101.9

Table 132. cont.

C#	Class	Component Name	Formula	MW	T_boil (C)	Density	T_melt (C)
66	Paraffins	Hexahexacontane*	$C_{66}H_{134}$	927.8	635.0	0.837	103.9
68	Paraffins	Octahexacontane*	$C_{68}H_{138}$	955.8	641.0	0.837	104.9
70	Paraffins	Heptacontane*	$C_{70}H_{142}$	983.9	647.0	0.838	105.9
72	Paraffins	Doheptacontane*	$C_{72}H_{146}$	1011.9	653.0	0.838	105.9
74	Paraffins	Tetraheptacontane*	$C_{74}H_{150}$	1040.0	658.0	0.839	106.9
4	Paraffin Isomers	Isobutane	C_4H_{10}	58.1	□	□	□
5	Paraffin Isomers	2-Methylbutane	C_5H_{12}	72.1	27.8	0.658	-160.2
6	Paraffin Isomers	2-Methylpentane	C_6H_{14}	86.2	60.3	0.683	-153.2
7	Paraffin Isomers	2-Methylhexane	C_7H_{16}	100.2	90.1	0.702	-118.5
8	Paraffin Isomers	2-Methylheptane	C_8H_{18}	114.2	117.7	0.713	-110.2
9	Paraffin Isomers	2-Methyloctane	C_9H_{20}	128.3	143.3	0.732	-80.2
10	Paraffin Isomers	2-Methylnonane	$C_{10}H_{22}$	142.3	167.0	0.738	-73.2
11	Paraffin Isomers	2-Methyldecane	$C_{11}H_{24}$	156.3	182.2	0.755	-48.9
12	Paraffin Isomers	3-Methylundecane	$C_{12}H_{26}$	170.3	210.8	0.757	-55.2
13	Paraffin Isomers	2-Methyldodecane*	$C_{13}H_{28}$	184.4	229.6	0.750	-27.2
14	Paraffin Isomers	2-Methyltridecane*	$C_{14}H_{30}$	198.4	247.9	0.756	-24.2
15	Paraffin Isomers	2-Methyltetradecane*	$C_{15}H_{32}$	212.4	265.3	0.762	-9.1
16	Paraffin Isomers	2-Methylpentadecane*	$C_{16}H_{34}$	226.4	281.6	0.767	-10.8
17	Paraffin Isomers	2-Methylhexadecane*	$C_{17}H_{36}$	240.5	297.0	0.772	4.9
18	Paraffin Isomers	2-Methylheptadecane*	$C_{18}H_{38}$	254.5	312.0	0.776	4.9
19	Paraffin Isomers	2-Methyloctadecane*	$C_{19}H_{40}$	268.5	326.0	0.780	11.9
20	Paraffin Isomers	2-Methylnonadecane*	$C_{20}H_{42}$	282.5	339.0	0.783	18.9
21	Paraffin Isomers	2-Methyleicosane*	$C_{21}H_{44}$	296.6	354.3	0.794	23.6
22	Paraffin Isomers	2-Methyluneicosane*	$C_{22}H_{46}$	310.6	366.2	0.796	28.4
23	Paraffin Isomers	2-Methyldocosane*	$C_{23}H_{48}$	324.6	376.3	0.798	33.1
24	Paraffin Isomers	2-Methyltricosane*	$C_{24}H_{50}$	338.7	386.4	0.799	37.9
26	Paraffin Isomers	2-Methylpentacosane*	$C_{26}H_{54}$	366.7	405.7	0.803	-273.2
28	Paraffin Isomers	2-Methylheptacosane*	$C_{28}H_{58}$	394.8	423.2	0.804	-273.2
30	Paraffin Isomers	2-Methylnonacosane*	$C_{30}H_{62}$	422.8	439.7	0.808	-273.2
5	Cyclics	Cyclopentene	C_5H_{10}	70.1	49.3	0.750	-94.0
6	Cyclics	Methylcyclopentane	C_6H_{12}	84.2	80.7	0.777	-142.1
7	Cyclics	Ethylcyclopentane	C_7H_{14}	98.2	118.8	0.783	-138.7
8	Cyclics	Propylcyclopentane	C_8H_{16}	112.2	131.8	0.788	-118.2
9	Cyclics	Butylcyclopentane	C_9H_{18}	126.2	156.8	0.794	-108.2
10	Cyclics	Butylcyclohexane	$C_{10}H_{20}$	140.3	181.0	0.799	-74.9
11	Cyclics	Hexylcyclopentane	$C_{11}H_{22}$	154.3	203.2	0.802	-73.0
12	Cyclics	Heptylcyclopentane	$C_{12}H_{24}$	168.3	224.2	0.810	-61.2
13	Cyclics	Octylcylopentane	$C_{13}H_{26}$	182.3	243.8	0.818	-44.5
14	Cyclics	Nonylcyclopentane	$C_{14}H_{28}$	196.4	262.2	0.826	-29.0
15	Cyclics	Decylcyclopentane	$C_{15}H_{30}$	210.4	279.4	0.834	-22.4
16	Cyclics	Decylcyclohexane	$C_{16}H_{32}$	224.4	297.6	0.842	-1.8
17	Cyclics	Dodecylcyclopentane	$C_{17}H_{34}$	238.5	311.0	0.850	-4.9
18	Cyclics	Tridecylcyclopentane	$C_{18}H_{36}$	252.5	325.5	0.858	5.0
19	Cyclics	Tetradecylcyclopentane	$C_{19}H_{38}$	266.5	325.9	0.866	8.9
20	Cyclics	Pentadecylcyclopentane	$C_{20}H_{40}$	280.5	351.9	0.874	16.9
21	Cyclics	Hexadecylcyclopentane	$C_{21}H_{42}$	294.6	363.9	0.882	21.1
22	Cyclics	Heptadecylcyclopentane*	$C_{22}H_{44}$	308.6	377.0	0.891	27.0
23	Cyclics	Octadecylcyclopentane*	$C_{23}H_{46}$	322.6	389.0	0.896	30.1
24	Cyclics	Nonadecylcyclopentane*	$C_{24}H_{48}$	336.6	400.0	0.899	35.0
26	Cyclics	Uneicosylcyclopentane*	$C_{26}H_{52}$	364.7	420.0	0.915	42.1
28	Cyclics	Tricosylcyclopentane*	$C_{28}H_{56}$	392.7	439.0	0.919	49.1
30	Cyclics	Pentacosylcyclopentane*	$C_{30}H_{60}$	420.8	456.0	0.935	54.1
2	Olefins	Ethylene	C_2H_4	28.1	□	□	-169.2
3	Olefins	Propylene	C_3H_6	42.1	□	□	-185.3
4	Olefins	1-Butene	C_4H_8	56.1	□	□	-185.4
5	Olefins	1-Pentene	C_5H_{10}	70.1	30.0	0.646	-165.2
6	Olefins	1-Hexene	C_6H_{12}	84.2	63.5	0.672	-139.8
7	Olefins	1-Heptene	C_7H_{14}	98.2	93.6	0.693	-118.9
8	Olefins	1-Octene	C_8H_{16}	112.2	121.3	0.715	-102.2
9	Olefins	1-Nonene	C_9H_{18}	126.2	146.9	0.728	-81.3
10	Olefins	1-Decene	$C_{10}H_{20}$	140.3	170.6	0.741	-66.3
11	Olefins	1-Undecene	$C_{11}H_{22}$	154.3	192.7	0.750	-49.3

Table 132. cont.

C#	Class	Component Name	Formula	MW	T_{boil} (C)	Density	T_{melt} (C)
12	Olefins	1-Dodecene	$C_{12}H_{24}$	168.3	213.4	0.759	-35.2
13	Olefins	1-Tridecene	$C_{13}H_{26}$	182.3	232.8	0.765	-22.9
14	Olefins	1-Tetradecene	$C_{14}H_{28}$	196.4	251.1	0.771	-13.0
15	Olefins	1-Pentadecene	$C_{15}H_{30}$	210.4	268.5	0.776	-3.8
16	Olefins	1-Hexadecene	$C_{16}H_{32}$	224.4	284.9	0.782	5.9
17	Olefins	1-Heptadecene	$C_{17}H_{34}$	238.5	300.3	0.784	10.9
18	Olefins	1-Octadecene	$C_{18}H_{36}$	252.5	314.8	0.787	17.9
19	Olefins	1-Nonadecene	$C_{19}H_{38}$	266.5	329.0	0.791	23.4
20	Olefins	1-Eicosene	$C_{20}H_{40}$	280.5	342.4	0.795	28.6
21	Olefins	1-Uneicosene[*]	$C_{21}H_{42}$	294.6	355.0	0.796	33.3
22	Olefins	1-Docosene[*]	$C_{22}H_{44}$	308.6	367.0	0.797	37.8
23	Olefins	1-Tricosene[*]	$C_{23}H_{46}$	322.6	379.0	0.802	41.6
24	Olefins	1-Tetracosene	$C_{24}H_{48}$	336.6	380.0	0.803	45.0
26	Olefins	1-Hexacosene[*]	$C_{26}H_{52}$	364.7	407.5	0.808	51.8
28	Olefins	1-Octacosene[*]	$C_{28}H_{56}$	392.7	426.4	0.809	-273.2
30	Olefins	1-Triacontene[*]	$C_{30}H_{60}$	420.8	444.4	0.814	-273.2
6	Aromatics	Benzene	C_6H_6	78.1	80.1	0.884	5.5
7	Aromatics	Toluene	C_7H_8	92.1	110.6	0.878	-95.2
8	Aromatics	Ethylbenzene	C_8H_{10}	106.2	136.2	0.872	-94.2
9	Aromatics	Propylbenzene	C_9H_{12}	120.2	159.2	0.867	-100.2
10	Aromatics	Butylbenzene	$C_{10}H_{14}$	134.2	183.3	0.864	-88.1
11	Aromatics	Pentylbenzene	$C_{11}H_{16}$	148.2	205.5	0.864	-78.3
12	Aromatics	Hexylbenzene	$C_{12}H_{18}$	162.3	226.1	0.864	-63.5
13	Aromatics	Heptylbenzene	$C_{13}H_{20}$	176.3	246.1	0.862	-48.0
14	Aromatics	Octylbenzene	$C_{14}H_{22}$	190.3	264.4	0.862	-36.0
15	Aromatics	Nonylbenzene	$C_{15}H_{24}$	204.4	282.1	0.861	-24.0
16	Aromatics	Decylbenzene	$C_{16}H_{26}$	218.4	297.9	0.860	-14.4
17	Aromatics	Undecylbenzene	$C_{17}H_{28}$	232.4	313.3	0.860	-5.0
18	Aromatics	Dodecylbenzene[*]	$C_{18}H_{30}$	246.4	327.6	0.860	3.0
19	Aromatics	Tridecylbenzene	$C_{19}H_{32}$	260.5	341.3	0.860	10.0
20	Aromatics	Tetradecylbenzene[*]	$C_{20}H_{34}$	274.5	354.0	0.859	16.0
21	Aromatics	Pentadecylbenzene[*]	$C_{21}H_{36}$	288.5	366.0	0.851	22.0
22	Aromatics	Hexadecylbenzene[*]	$C_{22}H_{38}$	302.5	378.0	0.852	27.0
23	Aromatics	Heptadecylbenzene[*]	$C_{23}H_{40}$	316.6	389.0	0.852	32.0
24	Aromatics	Octadecylbenzene[*]	$C_{24}H_{42}$	330.6	400.0	0.852	36.0
26	Aromatics	Eicosylbenzene[*]	$C_{26}H_{46}$	358.6	420.0	0.852	40.0
28	Aromatics	Docosylbenzene[*]	$C_{28}H_{50}$	386.7	438.0	0.850	44.4
30	Aromatics	Tetracosylbenzene[*]	$C_{30}H_{54}$	414.7	454.0	0.850	51.0
2	Carboxylic Acids	Acetic Acid	$C_2H_4O_2$	60.1	117.9	1.054	16.7
3	Carboxylic Acids	Propionic Acid	$C_3H_6O_2$	74.1	141.2	1.000	-20.7
4	Carboxylic Acids	Butyric Acid	$C_4H_8O_2$	88.1	163.3	0.962	-5.2
5	Carboxylic Acids	Pentanoic Acid	$C_5H_{10}O_2$	102.1	185.5	0.943	-34.0
6	Carboxylic Acids	Hexanoic Acid	$C_6H_{12}O_2$	116.2	205.7	0.928	-3.0
7	Carboxylic Acids	Heptanoic Acid	$C_7H_{14}O_2$	130.2	223.0	0.924	-7.3
8	Carboxylic Acids	Octanoic Acid	$C_8H_{16}O_2$	144.2	239.7	0.917	16.5
9	Carboxylic Acids	Nonanoic Acid	$C_9H_{18}O_2$	158.2	255.6	0.910	12.4
10	Carboxylic Acids	Decanoic Acid	$C_{10}H_{20}O_2$	172.3	270.0	0.896	31.6
11	Carboxylic Acids	Undecanoic Acid	$C_{11}H_{22}O_2$	186.3	284.2	0.894	35.5
12	Carboxylic Acids	Dodecanoic Acid	$C_{12}H_{24}O_2$	200.3	298.7	0.893	43.8
13	Carboxylic Acids	Tridecanoic Acid	$C_{13}H_{26}O_2$	214.3	312.1	0.897	41.9
14	Carboxylic Acids	Tetradecanoic Acid	$C_{14}H_{28}O_2$	228.4	326.2	0.890	54.2
15	Carboxylic Acids	Pentadecanoic Acid	$C_{15}H_{30}O_2$	242.4	338.9	0.890	52.5
16	Carboxylic Acids	Hexadecanoic Acid	$C_{16}H_{32}O_2$	256.4	351.0	0.884	62.8
17	Carboxylic Acids	Heptadecanoic Acid	$C_{17}H_{34}O_2$	270.5	362.6	0.885	61.2
18	Carboxylic Acids	Octadecanoic Acid	$C_{18}H_{36}O_2$	284.5	375.2	0.885	69.6
19	Carboxylic Acids	Nonadecanoic Acid	$C_{19}H_{38}O_2$	298.5	386.0	0.885	68.1
20	Carboxylic Acids	Eicosanoic Acid	$C_{20}H_{40}O_2$	312.5	397.0	0.884	75.3
21	Carboxylic Acids	Uneicosanoic Acid[*]	$C_{21}H_{42}O_2$	326.6	405.8	0.880	73.8
22	Carboxylic Acids	Docosanoic Acid[*]	$C_{22}H_{44}O_2$	340.6	416.4	0.879	77.0
23	Carboxylic Acids	Tricosanoic Acid[*]	$C_{23}H_{46}O_2$	354.6	425.4	0.878	80.0
24	Carboxylic Acids	Tetracosanoic Acid[*]	$C_{24}H_{48}O_2$	368.6	434.6	0.878	83.0
26	Carboxylic Acids	Hexacosanoic Acid[*]	$C_{26}H_{52}O_2$	396.7	452.3	0.876	88.7

Table 132. cont.

C#	Class	Component Name	Formula	MW	T_{boil} (C)	Density	T_{melt} (C)
28	Carboxylic Acids	Octacosanoic Acid*	$C_{28}H_{56}O_2$	424.7	468.6	0.875	94.1
30	Carboxylic Acids	Triacontanoic Acid*	$C_{30}H_{60}O_2$	452.8	484.2	0.873	99.2
*	Residual	Asphaltenes*			□	0.9	
*	Residual	Coke*			□	0.9	

* Indicates a component whose properties were estimated using UNIFAC group contribution methods.
□ Indicates data that was not pertinent

Representative Chemical Composition Data for Use in ChemCAD Simulation as
Determined by Various Experiments to Model the NCP

Data in this appendix indicate the representative chemical composition (RCC) from cracking and coking experiments. This data is produced through combining the CTL yield from TCR cracking (Section VII.B.4.ii), CTL composition from FIMSDIST (Section VI.D.3), gas composition from GC-FID/TCD (Section VII.E.2), and coke yield (indicated as asphaltenes) from combination experiments (Section VII.C).

Table 133. Representative ChemCAD composition from data produced by
cracking various TAGs in the 100 mL lab-scale TCR

Name		AA-Soy	BB-VHONO	CC-HENO	DD-Linseed	EE-Camelina	FF-Corn	GG-Cottonseed	HH-Canola	II-HONO
Triolein	wt. %	0.000	0.000	0.000	0.000	0.000	0.000	0.000	0.000	0.000
Water		0.000	0.000	0.000	0.000	0.000	0.000	0.000	0.000	0.000
Hydrogen		0.001	0.001	0.001	0.001	0.001	0.001	0.001	0.001	0.001
Carbon Monoxide		0.017	0.013	0.016	0.017	0.016	0.016	0.018	0.013	0.016
Carbon Dioxide		0.038	0.030	0.037	0.036	0.034	0.032	0.037	0.029	0.039
Methane		0.003	0.002	0.003	0.004	0.003	0.003	0.003	0.003	0.003
Ethane		0.008	0.006	0.008	0.012	0.007	0.007	0.007	0.006	0.007
Propane		0.008	0.005	0.007	0.010	0.007	0.007	0.007	0.006	0.007
Butane		0.014	0.007	0.007	0.011	0.012	0.011	0.016	0.010	0.010
Pentane		0.006	0.005	0.002	0.005	0.004	0.007	0.006	0.003	0.004
Hexane		0.005	0.005	0.002	0.003	0.004	0.004	0.006	0.005	0.006
Heptane		0.005	0.006	0.007	0.005	0.010	0.009	0.007	0.011	0.012
Octane		0.007	0.008	0.005	0.008	0.008	0.007	0.006	0.007	0.007
Nonane		0.004	0.006	0.006	0.004	0.006	0.005	0.004	0.007	0.007
Decane		0.003	0.002	0.003	0.003	0.003	0.003	0.003	0.003	0.002
Undecane		0.002	0.001	0.002	0.002	0.002	0.002	0.003	0.002	0.001
Dodecane		0.002	0.002	0.002	0.003	0.003	0.002	0.004	0.002	0.001
Tridecane		0.004	0.002	0.002	0.003	0.003	0.004	0.006	0.004	0.003
Tetradecane		0.004	0.002	0.002	0.003	0.003	0.003	0.005	0.003	0.002
Pentadecane		0.008	0.002	0.004	0.005	0.008	0.010	0.015	0.006	0.006
Hexadecane		0.005	0.001	0.001	0.005	0.002	0.002	0.002	0.002	0.002
Heptadecane		0.003	0.001	0.001	0.003	0.003	0.002	0.004	0.002	0.001
Octadecane		0.002	0.001	0.001	0.002	0.002	0.002	0.007	0.001	0.001
Nonadecane		0.035	0.053	0.037	0.034	0.036	0.038	0.035	0.042	0.044
Eicosane		0.048	0.041	0.055	0.054	0.066	0.037	0.034	0.042	0.041
Uneicosane		0.029	0.040	0.042	0.032	0.030	0.037	0.035	0.038	0.040
Docosane		0.019	0.019	0.020	0.023	0.022	0.021	0.019	0.023	0.018

Table 133. cont.

Name	AA-Soy	BB-VHONO	CC-HENO	DD-Linseed	EE-Camelina	FF-Corn	GG-Cottonseed	HH-Canola	II-HONO
Tricosane	0.023	0.022	0.042	0.023	0.023	0.023	0.022	0.023	0.023
Tetracosane	0.017	0.016	0.025	0.018	0.019	0.020	0.019	0.020	0.021
Pentacosane	0.016	0.016	0.027	0.016	0.015	0.015	0.013	0.016	0.016
Hexacosane	0.017	0.038	0.020	0.013	0.013	0.016	0.014	0.022	0.029
Heptacosane	0.014	0.015	0.015	0.013	0.011	0.013	0.011	0.014	0.014
Octacosane	0.013	0.018	0.018	0.011	0.013	0.014	0.012	0.016	0.015
Nonacosane	0.011	0.013	0.012	0.009	0.010	0.011	0.010	0.012	0.013
Triacontane	0.015	0.016	0.024	0.011	0.012	0.013	0.011	0.012	0.013
Dotriacontane	0.028	0.028	0.031	0.023	0.023	0.025	0.024	0.026	0.026
Tetratriacontane	0.021	0.024	0.022	0.017	0.019	0.020	0.018	0.021	0.021
Hexatriacontane	0.017	0.020	0.019	0.014	0.017	0.018	0.015	0.018	0.019
Octatriacontane	0.013	0.015	0.015	0.009	0.013	0.014	0.012	0.014	0.014
Tetracontane	0.011	0.012	0.012	0.007	0.011	0.011	0.009	0.012	0.012
Dotetracontane	0.008	0.009	0.010	0.005	0.009	0.009	0.007	0.009	0.009
Tetratetracontane	0.006	0.007	0.008	0.004	0.007	0.007	0.006	0.007	0.007
Hexatetracontane	0.004	0.006	0.006	0.003	0.005	0.005	0.005	0.006	0.006
Octatetracontane	0.003	0.004	0.005	0.002	0.005	0.004	0.004	0.005	0.005
Pentacontane	0.002	0.003	0.004	0.001	0.004	0.004	0.003	0.004	0.004
Dopentacontane	0.002	0.003	0.003	0.001	0.003	0.003	0.003	0.003	0.004
Tetrapentacontane	0.001	0.002	0.003	0.001	0.003	0.002	0.002	0.003	0.003
Hexapentacontane	0.001	0.002	0.002	0.000	0.002	0.002	0.001	0.002	0.002
Octapentacontane	0.001	0.001	0.002	0.000	0.001	0.001	0.001	0.001	0.001
Hexacontane	0.001	0.001	0.001	0.000	0.001	0.001	0.000	0.001	0.001
Dohexacontane	0.000	0.000	0.001	0.000	0.000	0.000	0.000	0.000	0.000
Tetrahexacontane	0.000	0.000	0.000	0.000	0.000	0.000	0.000	0.000	0.000
Hexahexacontane	0.000	0.000	0.000	0.000	0.000	0.000	0.000	0.000	0.000
Octahexacontane	0.000	0.000	0.000	0.000	0.000	0.000	0.000	0.000	0.000
Heptacontane	0.000	0.000	0.000	0.000	0.000	0.000	0.000	0.000	0.000
Doheptacontane	0.000	0.000	0.000	0.000	0.000	0.000	0.000	0.000	0.000
Tetraheptacontane	0.000	0.000	0.000	0.000	0.000	0.000	0.000	0.000	0.000
Isobutane	0.000	0.000	0.000	0.000	0.000	0.000	0.000	0.000	0.000
2-Methylbutane	0.000	0.000	0.000	0.000	0.000	0.000	0.000	0.000	0.000
2-Methylpentane	0.000	0.000	0.000	0.000	0.000	0.000	0.000	0.000	0.000
2-Methylhexane	0.000	0.000	0.000	0.000	0.000	0.000	0.000	0.000	0.000
2-Methylheptane	0.000	0.000	0.000	0.000	0.000	0.000	0.000	0.000	0.000
2-Methyloctane	0.000	0.000	0.000	0.000	0.000	0.000	0.000	0.000	0.000
2-Methylnonane	0.000	0.000	0.000	0.000	0.000	0.000	0.000	0.000	0.000
2-Methyldecane	0.000	0.000	0.000	0.000	0.000	0.000	0.000	0.000	0.000
3-Methylundecane	0.000	0.000	0.000	0.000	0.000	0.000	0.000	0.000	0.000
2-Methyldodecane	0.000	0.000	0.000	0.000	0.000	0.000	0.000	0.000	0.000
2-Methyltridecane	0.000	0.000	0.000	0.000	0.000	0.000	0.000	0.000	0.000
2-Methyltetradecane	0.001	0.000	0.000	0.000	0.001	0.001	0.001	0.000	0.000
2-Methylpentadecane	0.000	0.000	0.000	0.000	0.000	0.000	0.000	0.000	0.000
2-Methylhexadecane	0.000	0.000	0.000	0.000	0.000	0.000	0.000	0.000	0.000
2-Methylheptadecane	0.000	0.000	0.000	0.000	0.000	0.000	0.000	0.000	0.000
2-Methyloctadecane	0.000	0.000	0.000	0.000	0.000	0.000	0.000	0.000	0.000
2-Methylnonadecane	0.000	0.000	0.000	0.000	0.000	0.000	0.000	0.000	0.000
2-Methyleicosane	0.000	0.000	0.000	0.000	0.000	0.000	0.000	0.000	0.000
2-Methyluneicosane	0.000	0.000	0.000	0.000	0.000	0.000	0.000	0.000	0.000
2-Methyldocosane	0.000	0.000	0.000	0.000	0.000	0.000	0.000	0.000	0.000
2-Methyltricosane	0.000	0.000	0.000	0.000	0.000	0.000	0.000	0.000	0.000
2-Methylpentacosane	0.000	0.000	0.000	0.000	0.000	0.000	0.000	0.000	0.000
2-Methylheptacosane	0.000	0.000	0.000	0.000	0.000	0.000	0.000	0.000	0.000
2-Methylnonacosane	0.000	0.000	0.000	0.000	0.000	0.000	0.000	0.000	0.000
Cyclopentene	0.003	0.002	0.002	0.003	0.004	0.004	0.005	0.003	0.004
Methylcyclopentane	0.003	0.003	0.002	0.004	0.004	0.004	0.004	0.004	0.004
Ethylcyclopentane	0.004	0.003	0.003	0.004	0.005	0.006	0.005	0.006	0.006
Propylcyclopentane	0.005	0.004	0.003	0.005	0.006	0.007	0.005	0.006	0.006
Butylcyclopentane	0.004	0.004	0.004	0.005	0.006	0.005	0.004	0.004	0.004
Butylcyclohexane	0.006	0.005	0.005	0.006	0.005	0.004	0.005	0.005	0.005
Hexylcyclopentane	0.008	0.008	0.008	0.007	0.008	0.008	0.008	0.009	0.009

Table 133. cont.

Name	AA-Soy	BB-VHONO	CC-HENO	DD-Linseed	EE-Camelina	FF-Corn	GG-Cottonseed	HH-Canola	II-HONO
Heptylcyclopentane	0.006	0.004	0.006	0.005	0.006	0.006	0.005	0.005	0.005
Octylcylopentane	0.005	0.004	0.003	0.004	0.003	0.003	0.003	0.004	0.004
Nonylcyclopentane	0.006	0.006	0.007	0.005	0.006	0.005	0.004	0.005	0.006
Decylcyclopentane	0.006	0.008	0.006	0.006	0.004	0.004	0.003	0.006	0.006
Decylcyclohexane	0.006	0.008	0.007	0.007	0.006	0.006	0.005	0.007	0.008
Dodecylcyclopentane	0.009	0.010	0.008	0.008	0.008	0.008	0.007	0.010	0.011
Tridecylcyclopentane	0.004	0.007	0.008	0.004	0.004	0.003	0.002	0.005	0.006
Tetradecylcyclopentane	0.000	0.000	0.000	0.000	0.000	0.000	0.000	0.000	0.000
Pentadecylcyclopentane	0.000	0.000	0.000	0.000	0.000	0.000	0.000	0.000	0.000
Hexadecylcyclopentane	0.000	0.000	0.000	0.000	0.000	0.000	0.000	0.000	0.000
Heptadecylcyclopentane	0.000	0.000	0.000	0.000	0.000	0.000	0.000	0.000	0.000
Octadecylcyclopentane	0.000	0.000	0.000	0.000	0.000	0.000	0.000	0.000	0.000
Nonadecylcyclopentane	0.000	0.000	0.000	0.000	0.000	0.000	0.000	0.000	0.000
Uneicosylcyclopentane	0.000	0.000	0.000	0.000	0.000	0.000	0.000	0.000	0.000
Tricosylcyclopentane	0.000	0.000	0.000	0.000	0.000	0.000	0.000	0.000	0.000
Pentacosylcyclopentane	0.000	0.000	0.000	0.000	0.000	0.000	0.000	0.000	0.000
Ethylene	0.002	0.002	0.002	0.002	0.002	0.002	0.002	0.002	0.002
Propylene	0.005	0.003	0.004	0.005	0.004	0.004	0.004	0.004	0.004
1-Butene	0.003	0.002	0.003	0.003	0.005	0.007	0.005	0.004	0.005
1-Pentene	0.005	0.003	0.004	0.005	0.007	0.008	0.008	0.006	0.007
1-Hexene	0.006	0.005	0.003	0.006	0.007	0.007	0.008	0.007	0.007
1-Heptene	0.007	0.006	0.005	0.007	0.009	0.010	0.009	0.010	0.010
1-Octene	0.008	0.007	0.006	0.009	0.011	0.012	0.010	0.010	0.010
1-Nonene	0.007	0.006	0.007	0.009	0.009	0.008	0.006	0.007	0.007
1-Decene	0.009	0.008	0.007	0.010	0.008	0.007	0.007	0.008	0.008
1-Undecene	0.013	0.013	0.013	0.012	0.012	0.013	0.013	0.015	0.015
1-Dodecene	0.009	0.007	0.009	0.008	0.009	0.009	0.009	0.009	0.009
1-Tridecene	0.007	0.007	0.005	0.007	0.005	0.005	0.005	0.006	0.006
1-Tetradecene	0.009	0.010	0.011	0.008	0.009	0.008	0.007	0.008	0.009
1-Pentadecene	0.010	0.013	0.009	0.009	0.006	0.006	0.005	0.009	0.010
1-Hexadecene	0.009	0.013	0.011	0.011	0.009	0.009	0.008	0.012	0.013
1-Heptadecene	0.015	0.016	0.012	0.013	0.013	0.014	0.011	0.016	0.017
1-Octadecene	0.007	0.012	0.012	0.006	0.007	0.006	0.004	0.008	0.010
1-Nonadecene	0.000	0.000	0.000	0.000	0.000	0.000	0.000	0.000	0.000
1-Eicosene	0.000	0.000	0.000	0.000	0.000	0.000	0.000	0.000	0.000
1-Uneicosene	0.000	0.000	0.000	0.000	0.000	0.000	0.000	0.000	0.000
1-Docosene	0.000	0.000	0.000	0.000	0.000	0.000	0.000	0.000	0.000
1-Tricosene	0.000	0.000	0.000	0.000	0.000	0.000	0.000	0.000	0.000
1-Tetracosene	0.000	0.000	0.000	0.000	0.000	0.000	0.000	0.000	0.000
1-Hexacosene	0.000	0.000	0.000	0.000	0.000	0.000	0.000	0.000	0.000
1-Octacosene	0.000	0.000	0.000	0.000	0.000	0.000	0.000	0.000	0.000
1-Triacontene	0.000	0.000	0.000	0.000	0.000	0.000	0.000	0.000	0.000
Benzene	0.000	0.000	0.000	0.000	0.000	0.000	0.000	0.000	0.000
Toluene	0.001	0.000	0.000	0.001	0.001	0.001	0.001	0.001	0.001
Ethylbenzene	0.001	0.001	0.001	0.002	0.001	0.001	0.001	0.001	0.001
Propylbenzene	0.001	0.001	0.001	0.001	0.002	0.001	0.001	0.001	0.001
Butylbenzene	0.003	0.001	0.002	0.005	0.004	0.003	0.003	0.002	0.002
Pentylbenzene	0.004	0.002	0.003	0.006	0.005	0.005	0.005	0.003	0.002
Hexylbenzene	0.004	0.002	0.002	0.007	0.004	0.003	0.003	0.003	0.002
Heptylbenzene	0.004	0.002	0.003	0.006	0.005	0.004	0.004	0.004	0.003
Octylbenzene	0.006	0.004	0.004	0.010	0.007	0.006	0.006	0.005	0.004
Nonylbenzene	0.006	0.004	0.004	0.010	0.007	0.006	0.006	0.006	0.005
Decylbenzene	0.007	0.005	0.005	0.010	0.007	0.006	0.007	0.006	0.005
Undecylbenzene	0.008	0.005	0.005	0.010	0.009	0.008	0.008	0.007	0.006
Dodecylbenzene	0.009	0.007	0.006	0.012	0.009	0.008	0.008	0.008	0.007
Tridecylbenzene	0.000	0.000	0.000	0.000	0.000	0.000	0.000	0.000	0.000
Tetradecylbenzene	0.000	0.000	0.000	0.000	0.000	0.000	0.000	0.000	0.000
Pentadecylbenzene	0.000	0.000	0.000	0.000	0.000	0.000	0.000	0.000	0.000
Hexadecylbenzene	0.000	0.000	0.000	0.000	0.000	0.000	0.000	0.000	0.000
Heptadecylbenzene	0.000	0.000	0.000	0.000	0.000	0.000	0.000	0.000	0.000
Octadecylbenzene	0.000	0.000	0.000	0.000	0.000	0.000	0.000	0.000	0.000

Table 133. cont.

Name	AA-Soy	BB-VHONO	CC-HENO	DD-Linseed	EE-Camelina	FF-Corn	GG-Cottonseed	HH-Canola	II-HONO
Eicosylbenzene	0.000	0.000	0.000	0.000	0.000	0.000	0.000	0.000	0.000
Docosylbenzene	0.000	0.000	0.000	0.000	0.000	0.000	0.000	0.000	0.000
Tetracosylbenzene	0.000	0.000	0.000	0.000	0.000	0.000	0.000	0.000	0.000
Acetic Acid	0.005	0.005	0.005	0.005	0.009	0.009	0.007	0.008	0.008
Propionic Acid	0.002	0.002	0.002	0.003	0.003	0.002	0.002	0.002	0.002
Butyric Acid	0.002	0.001	0.002	0.004	0.003	0.002	0.001	0.002	0.001
Pentanoic Acid	0.004	0.002	0.002	0.005	0.006	0.008	0.005	0.003	0.002
Hexanoic Acid	0.007	0.004	0.004	0.009	0.008	0.011	0.008	0.007	0.004
Heptanoic Acid	0.017	0.007	0.007	0.018	0.014	0.017	0.016	0.014	0.007
Octanoic Acid	0.012	0.010	0.011	0.017	0.014	0.014	0.014	0.012	0.011
Nonanoic Acid	0.013	0.016	0.013	0.017	0.015	0.015	0.013	0.015	0.015
Decanoic Acid	0.021	0.059	0.033	0.020	0.018	0.015	0.011	0.022	0.026
Undecanoic Acid	0.004	0.004	0.009	0.007	0.007	0.004	0.004	0.004	0.004
Dodecanoic Acid	0.003	0.002	0.005	0.005	0.004	0.003	0.003	0.003	0.002
Tridecanoic Acid	0.003	0.001	0.005	0.005	0.004	0.003	0.003	0.003	0.002
Tetradecanoic Acid	0.003	0.002	0.003	0.005	0.004	0.003	0.008	0.003	0.002
Pentadecanoic Acid	0.004	0.002	0.003	0.005	0.004	0.003	0.004	0.003	0.002
Hexadecanoic Acid	0.036	0.012	0.013	0.019	0.020	0.042	0.081	0.027	0.013
Heptadecanoic Acid	0.005	0.003	0.003	0.006	0.004	0.004	0.005	0.004	0.003
Octadecanoic Acid	0.033	0.031	0.012	0.035	0.015	0.017	0.015	0.018	0.018
Nonadecanoic Acid	0.000	0.000	0.000	0.000	0.000	0.000	0.000	0.000	0.000
Eicosanoic Acid	0.000	0.000	0.000	0.000	0.000	0.000	0.000	0.000	0.000
Uneicosanoic Acid	0.000	0.000	0.000	0.000	0.000	0.000	0.000	0.000	0.000
Docosanoic Acid	0.000	0.000	0.000	0.000	0.000	0.000	0.000	0.000	0.000
Tricosanoic Acid	0.000	0.000	0.000	0.000	0.000	0.000	0.000	0.000	0.000
Tetracosanoic Acid	0.000	0.000	0.000	0.000	0.000	0.000	0.000	0.000	0.000
Hexacosanoic Acid	0.000	0.000	0.000	0.000	0.000	0.000	0.000	0.000	0.000
Octacosanoic Acid	0.000	0.000	0.000	0.000	0.000	0.000	0.000	0.000	0.000
Triacontanoic Acid	0.000	0.000	0.000	0.000	0.000	0.000	0.000	0.000	0.000
Asphaltenes	0.051	0.051	0.051	0.051	0.051	0.051	0.051	0.051	0.051
Coke	0.000	0.000	0.000	0.000	0.000	0.000	0.000	0.000	0.000

Table 134. Representative ChemCAD composition from data produced by cracking soybean TAG in the 100 mL lab-scale TCR at various temperatures and space times

Name		A-Soy	B-Soy	C-Soy	D-Soy	E-Soy	F-Soy	G-Soy	H-Soy	I-Soy
Triolein	wt. %	0.000	0.000	0.000	0.000	0.000	0.000	0.000	0.000	0.000
Water		0.000	0.000	0.000	0.000	0.000	0.000	0.000	0.000	0.000
Hydrogen		0.000	0.000	0.000	0.001	0.001	0.001	0.001	0.001	0.001
Carbon Monoxide		0.011	0.012	0.014	0.017	0.017	0.020	0.022	0.025	0.026
Carbon Dioxide		0.030	0.030	0.036	0.039	0.038	0.045	0.049	0.053	0.051
Methane		0.001	0.002	0.002	0.003	0.003	0.005	0.003	0.004	0.006
Ethane		0.003	0.004	0.005	0.007	0.008	0.011	0.009	0.010	0.013
Propane		0.003	0.004	0.005	0.006	0.008	0.012	0.008	0.010	0.013
Butane		0.009	0.011	0.011	0.010	0.012	0.019	0.012	0.013	0.019
Pentane		0.003	0.004	0.006	0.006	0.007	0.007	0.006	0.007	0.007
Hexane		0.003	0.003	0.003	0.005	0.007	0.007	0.005	0.007	0.007
Heptane		0.004	0.006	0.007	0.008	0.011	0.009	0.007	0.010	0.012
Octane		0.005	0.006	0.007	0.007	0.008	0.009	0.008	0.009	0.009
Nonane		0.003	0.005	0.005	0.007	0.008	0.007	0.006	0.009	0.011
Decane		0.002	0.002	0.003	0.004	0.004	0.004	0.004	0.005	0.007
Undecane		0.002	0.002	0.003	0.004	0.003	0.003	0.004	0.005	0.007
Dodecane		0.002	0.002	0.003	0.004	0.004	0.004	0.004	0.005	0.007
Tridecane		0.003	0.003	0.003	0.005	0.006	0.005	0.005	0.006	0.008
Tetradecane		0.002	0.003	0.003	0.005	0.005	0.004	0.005	0.006	0.008
Pentadecane		0.006	0.006	0.007	0.010	0.012	0.012	0.011	0.013	0.016
Hexadecane		0.001	0.002	0.002	0.003	0.003	0.002	0.003	0.004	0.004
Heptadecane		0.002	0.002	0.003	0.005	0.004	0.003	0.005	0.006	0.011
Octadecane		0.001	0.001	0.002	0.002	0.002	0.002	0.002	0.003	0.004
Nonadecane		0.044	0.044	0.037	0.033	0.032	0.031	0.031	0.030	0.030
Eicosane		0.036	0.040	0.036	0.038	0.033	0.032	0.034	0.033	0.042
Uneicosane		0.054	0.046	0.041	0.031	0.026	0.026	0.030	0.024	0.020
Docosane		0.018	0.019	0.019	0.022	0.017	0.016	0.019	0.018	0.016
Tricosane		0.027	0.026	0.024	0.025	0.021	0.019	0.020	0.018	0.016
Tetracosane		0.023	0.022	0.021	0.021	0.014	0.015	0.017	0.015	0.012
Pentacosane		0.018	0.018	0.016	0.017	0.014	0.012	0.016	0.013	0.012
Hexacosane		0.020	0.020	0.017	0.018	0.012	0.011	0.014	0.014	0.010
Heptacosane		0.015	0.016	0.016	0.014	0.010	0.009	0.014	0.010	0.008
Octacosane		0.023	0.020	0.019	0.015	0.011	0.010	0.013	0.009	0.007
Nonacosane		0.011	0.011	0.011	0.010	0.008	0.008	0.010	0.008	0.005
Triacontane		0.014	0.012	0.012	0.016	0.010	0.009	0.011	0.011	0.006
Dotriacontane		0.033	0.029	0.028	0.036	0.020	0.019	0.025	0.027	0.013
Tetratriacontane		0.028	0.024	0.024	0.024	0.015	0.015	0.021	0.017	0.009
Hexatriacontane		0.030	0.024	0.023	0.017	0.013	0.013	0.017	0.012	0.007
Octatriacontane		0.028	0.021	0.018	0.013	0.010	0.010	0.012	0.009	0.005
Tetracontane		0.023	0.016	0.013	0.011	0.008	0.008	0.010	0.007	0.004
Dotetracontane		0.015	0.010	0.009	0.009	0.007	0.006	0.008	0.006	0.002
Tetratetracontane		0.011	0.008	0.008	0.007	0.005	0.005	0.006	0.004	0.001
Hexatetracontane		0.008	0.006	0.006	0.007	0.004	0.004	0.005	0.006	0.001
Octatetracontane		0.006	0.005	0.006	0.004	0.003	0.003	0.005	0.003	0.000
Pentacontane		0.007	0.006	0.006	0.003	0.003	0.003	0.005	0.005	0.000
Dopentacontane		0.005	0.004	0.004	0.003	0.002	0.002	0.004	0.002	0.000
Tetrapentacontane		0.003	0.003	0.003	0.001	0.002	0.002	0.003	0.000	0.000
Hexapentacontane		0.002	0.002	0.001	0.000	0.001	0.001	0.000	0.000	0.000
Octapentacontane		0.002	0.001	0.001	0.000	0.001	0.001	0.000	0.000	0.000
Hexacontane		0.000	0.000	0.000	0.000	0.000	0.000	0.000	0.000	0.000
Dohexacontane		0.000	0.000	0.000	0.000	0.000	0.000	0.000	0.000	0.000
Tetrahexacontane		0.000	0.000	0.000	0.000	0.000	0.000	0.000	0.000	0.000
Hexahexacontane		0.000	0.000	0.000	0.000	0.000	0.000	0.000	0.000	0.000
Octahexacontane		0.000	0.000	0.000	0.000	0.000	0.000	0.000	0.000	0.000
Heptacontane		0.000	0.000	0.000	0.000	0.000	0.000	0.000	0.000	0.000
Doheptacontane		0.000	0.000	0.000	0.000	0.000	0.000	0.000	0.000	0.000
Tetraheptacontane		0.000	0.000	0.000	0.000	0.000	0.000	0.000	0.000	0.000
Isobutane		0.000	0.000	0.000	0.000	0.000	0.000	0.000	0.000	0.000
2-Methylbutane		0.000	0.000	0.000	0.000	0.000	0.000	0.000	0.000	0.000
2-Methylpentane		0.000	0.000	0.000	0.000	0.000	0.000	0.000	0.000	0.000
2-Methylhexane		0.000	0.000	0.000	0.000	0.000	0.000	0.000	0.000	0.000

Table 134. cont.

Name	A-Soy	B-Soy	C-Soy	D-Soy	E-Soy	F-Soy	G-Soy	H-Soy	I-Soy
2-Methylheptane	0.000	0.000	0.000	0.000	0.000	0.000	0.000	0.000	0.000
2-Methyloctane	0.000	0.000	0.000	0.000	0.001	0.000	0.000	0.001	0.001
2-Methylnonane	0.000	0.000	0.000	0.000	0.000	0.000	0.000	0.000	0.000
2-Methyldecane	0.000	0.000	0.000	0.000	0.000	0.000	0.000	0.000	0.000
3-Methylundecane	0.000	0.000	0.000	0.000	0.000	0.000	0.000	0.000	0.000
2-Methyldodecane	0.000	0.000	0.000	0.000	0.000	0.000	0.000	0.000	0.001
2-Methyltridecane	0.000	0.000	0.000	0.000	0.000	0.000	0.000	0.000	0.001
2-Methyltetradecane	0.000	0.000	0.001	0.001	0.001	0.001	0.001	0.001	0.001
2-Methylpentadecane	0.000	0.000	0.000	0.000	0.000	0.000	0.000	0.000	0.000
2-Methylhexadecane	0.000	0.000	0.000	0.000	0.000	0.000	0.000	0.000	0.001
2-Methylheptadecane	0.000	0.000	0.000	0.000	0.000	0.000	0.000	0.000	0.000
2-Methyloctadecane	0.000	0.000	0.000	0.000	0.000	0.000	0.000	0.000	0.000
2-Methylnonadecane	0.000	0.000	0.000	0.000	0.000	0.000	0.000	0.000	0.000
2-Methyleicosane	0.000	0.000	0.000	0.000	0.000	0.000	0.000	0.000	0.000
2-Methyluneicosane	0.000	0.000	0.000	0.000	0.000	0.000	0.000	0.000	0.000
2-Methyldocosane	0.000	0.000	0.000	0.000	0.000	0.000	0.000	0.000	0.000
2-Methyltricosane	0.000	0.000	0.000	0.000	0.000	0.000	0.000	0.000	0.000
2-Methylpentacosane	0.000	0.000	0.000	0.000	0.000	0.000	0.000	0.000	0.000
2-Methylheptacosane	0.000	0.000	0.000	0.000	0.000	0.000	0.000	0.000	0.000
2-Methylnonacosane	0.000	0.000	0.000	0.000	0.000	0.000	0.000	0.000	0.000
Cyclopentene	0.002	0.002	0.003	0.003	0.004	0.005	0.004	0.005	0.006
Methylcyclopentane	0.002	0.003	0.004	0.004	0.006	0.006	0.004	0.006	0.007
Ethylcyclopentane	0.004	0.005	0.006	0.006	0.007	0.007	0.006	0.007	0.008
Propylcyclopentane	0.004	0.004	0.005	0.005	0.008	0.008	0.006	0.006	0.008
Butylcyclopentane	0.003	0.003	0.004	0.004	0.006	0.007	0.004	0.005	0.006
Butylcyclohexane	0.003	0.004	0.004	0.005	0.007	0.006	0.005	0.006	0.007
Hexylcyclopentane	0.007	0.007	0.008	0.006	0.010	0.009	0.007	0.008	0.008
Heptylcyclopentane	0.005	0.005	0.005	0.004	0.007	0.007	0.005	0.005	0.005
Octylcylopentane	0.003	0.003	0.003	0.004	0.004	0.004	0.004	0.005	0.005
Nonylcyclopentane	0.003	0.003	0.004	0.004	0.006	0.006	0.004	0.005	0.005
Decylcyclopentane	0.004	0.005	0.005	0.005	0.005	0.004	0.005	0.005	0.006
Decylcyclohexane	0.005	0.005	0.005	0.007	0.007	0.006	0.006	0.006	0.008
Dodecylcyclopentane	0.007	0.008	0.008	0.008	0.010	0.010	0.009	0.009	0.011
Tridecylcyclopentane	0.003	0.003	0.004	0.004	0.004	0.004	0.004	0.004	0.004
Tetradecylcyclopentane	0.000	0.000	0.000	0.000	0.000	0.000	0.000	0.000	0.000
Pentadecylcyclopentane	0.000	0.000	0.000	0.000	0.000	0.000	0.000	0.000	0.000
Hexadecylcyclopentane	0.000	0.000	0.000	0.000	0.000	0.000	0.000	0.000	0.000
Heptadecylcyclopentane	0.000	0.000	0.000	0.000	0.000	0.000	0.000	0.000	0.000
Octadecylcyclopentane	0.000	0.000	0.000	0.000	0.000	0.000	0.000	0.000	0.000
Nonadecylcyclopentane	0.000	0.000	0.000	0.000	0.000	0.000	0.000	0.000	0.000
Uneicosylcyclopentane	0.000	0.000	0.000	0.000	0.000	0.000	0.000	0.000	0.000
Tricosylcyclopentane	0.000	0.000	0.000	0.000	0.000	0.000	0.000	0.000	0.000
Pentacosylcyclopentane	0.000	0.000	0.000	0.000	0.000	0.000	0.000	0.000	0.000
Ethylene	0.001	0.002	0.002	0.002	0.002	0.002	0.002	0.002	0.003
Propylene	0.002	0.002	0.003	0.004	0.004	0.006	0.004	0.005	0.007
1-Butene	0.003	0.004	0.004	0.005	0.007	0.007	0.006	0.007	0.007
1-Pentene	0.003	0.004	0.005	0.006	0.007	0.010	0.007	0.008	0.011
1-Hexene	0.003	0.005	0.007	0.008	0.010	0.010	0.008	0.010	0.012
1-Heptene	0.007	0.009	0.010	0.011	0.012	0.012	0.011	0.013	0.014
1-Octene	0.006	0.008	0.009	0.009	0.015	0.014	0.010	0.011	0.014
1-Nonene	0.005	0.005	0.006	0.007	0.010	0.011	0.007	0.008	0.010
1-Decene	0.005	0.006	0.006	0.007	0.011	0.010	0.008	0.010	0.011
1-Undecene	0.012	0.012	0.012	0.010	0.016	0.015	0.012	0.012	0.013
1-Dodecene	0.008	0.007	0.008	0.007	0.011	0.011	0.008	0.008	0.009
1-Tridecene	0.004	0.005	0.006	0.006	0.007	0.006	0.007	0.007	0.008
1-Tetradecene	0.005	0.005	0.007	0.007	0.009	0.010	0.007	0.008	0.008
1-Pentadecene	0.007	0.008	0.008	0.009	0.009	0.007	0.008	0.008	0.009
1-Hexadecene	0.007	0.008	0.009	0.011	0.011	0.010	0.009	0.010	0.012
1-Heptadecene	0.011	0.012	0.012	0.012	0.016	0.015	0.015	0.015	0.017
1-Octadecene	0.005	0.005	0.006	0.007	0.007	0.006	0.006	0.007	0.007
1-Nonadecene	0.000	0.000	0.000	0.000	0.000	0.000	0.000	0.000	0.000
1-Eicosene	0.000	0.000	0.000	0.000	0.000	0.000	0.000	0.000	0.000

Table 134. cont.

Name	A-Soy	B-Soy	C-Soy	D-Soy	E-Soy	F-Soy	G-Soy	H-Soy	I-Soy
1-Uneicosene	0.000	0.000	0.000	0.000	0.000	0.000	0.000	0.000	0.000
1-Docosene	0.000	0.000	0.000	0.000	0.000	0.000	0.000	0.000	0.000
1-Tricosene	0.000	0.000	0.000	0.000	0.000	0.000	0.000	0.000	0.000
1-Tetracosene	0.000	0.000	0.000	0.000	0.000	0.000	0.000	0.000	0.000
1-Hexacosene	0.000	0.000	0.000	0.000	0.000	0.000	0.000	0.000	0.000
1-Octacosene	0.000	0.000	0.000	0.000	0.000	0.000	0.000	0.000	0.000
1-Triacontene	0.000	0.000	0.000	0.000	0.000	0.000	0.000	0.000	0.000
Benzene	0.000	0.000	0.000	0.000	0.000	0.000	0.000	0.000	0.000
Toluene	0.000	0.001	0.001	0.001	0.001	0.001	0.001	0.001	0.002
Ethylbenzene	0.001	0.001	0.001	0.001	0.002	0.001	0.001	0.002	0.003
Propylbenzene	0.001	0.001	0.001	0.002	0.002	0.002	0.002	0.002	0.003
Butylbenzene	0.002	0.002	0.002	0.003	0.004	0.004	0.003	0.004	0.005
Pentylbenzene	0.003	0.003	0.004	0.005	0.006	0.006	0.006	0.007	0.009
Hexylbenzene	0.002	0.003	0.003	0.005	0.005	0.004	0.004	0.006	0.008
Heptylbenzene	0.004	0.004	0.004	0.005	0.006	0.005	0.005	0.006	0.008
Octylbenzene	0.004	0.004	0.005	0.006	0.007	0.006	0.006	0.007	0.009
Nonylbenzene	0.004	0.005	0.006	0.007	0.008	0.006	0.007	0.007	0.010
Decylbenzene	0.004	0.005	0.006	0.007	0.008	0.006	0.007	0.008	0.010
Undecylbenzene	0.006	0.007	0.008	0.008	0.009	0.008	0.009	0.010	0.010
Dodecylbenzene	0.006	0.007	0.008	0.009	0.009	0.008	0.009	0.009	0.008
Tridecylbenzene	0.000	0.000	0.000	0.000	0.000	0.000	0.000	0.000	0.000
Tetradecylbenzene	0.000	0.000	0.000	0.000	0.000	0.000	0.000	0.000	0.000
Pentadecylbenzene	0.000	0.000	0.000	0.000	0.000	0.000	0.000	0.000	0.000
Hexadecylbenzene	0.000	0.000	0.000	0.000	0.000	0.000	0.000	0.000	0.000
Heptadecylbenzene	0.000	0.000	0.000	0.000	0.000	0.000	0.000	0.000	0.000
Octadecylbenzene	0.000	0.000	0.000	0.000	0.000	0.000	0.000	0.000	0.000
Eicosylbenzene	0.000	0.000	0.000	0.000	0.000	0.000	0.000	0.000	0.000
Docosylbenzene	0.000	0.000	0.000	0.000	0.000	0.000	0.000	0.000	0.000
Tetracosylbenzene	0.000	0.000	0.000	0.000	0.000	0.000	0.000	0.000	0.000
Acetic Acid	0.006	0.008	0.008	0.006	0.007	0.008	0.007	0.006	0.005
Propionic Acid	0.001	0.002	0.002	0.002	0.003	0.002	0.002	0.002	0.002
Butyric Acid	0.001	0.001	0.002	0.001	0.002	0.003	0.002	0.002	0.002
Pentanoic Acid	0.004	0.004	0.004	0.004	0.004	0.004	0.004	0.004	0.004
Hexanoic Acid	0.007	0.007	0.007	0.007	0.007	0.007	0.007	0.007	0.007
Heptanoic Acid	0.018	0.018	0.018	0.018	0.017	0.017	0.017	0.017	0.016
Octanoic Acid	0.010	0.011	0.012	0.010	0.015	0.016	0.013	0.012	0.012
Nonanoic Acid	0.010	0.012	0.013	0.011	0.015	0.016	0.012	0.013	0.013
Decanoic Acid	0.015	0.017	0.016	0.011	0.016	0.018	0.013	0.012	0.012
Undecanoic Acid	0.003	0.004	0.004	0.005	0.005	0.005	0.005	0.005	0.006
Dodecanoic Acid	0.002	0.002	0.003	0.004	0.004	0.003	0.004	0.004	0.005
Tridecanoic Acid	0.001	0.002	0.003	0.004	0.004	0.003	0.003	0.004	0.004
Tetradecanoic Acid	0.002	0.002	0.003	0.004	0.004	0.003	0.004	0.004	0.004
Pentadecanoic Acid	0.002	0.003	0.003	0.004	0.004	0.003	0.004	0.004	0.004
Hexadecanoic Acid	0.050	0.047	0.039	0.028	0.025	0.032	0.031	0.022	0.016
Heptadecanoic Acid	0.002	0.003	0.004	0.006	0.005	0.004	0.005	0.005	0.005
Octadecanoic Acid	0.037	0.037	0.032	0.023	0.016	0.017	0.027	0.021	0.015
Nonadecanoic Acid	0.000	0.000	0.000	0.000	0.000	0.000	0.000	0.000	0.000
Eicosanoic Acid	0.000	0.000	0.000	0.000	0.000	0.000	0.000	0.000	0.000
Uneicosanoic Acid	0.000	0.000	0.000	0.000	0.000	0.000	0.000	0.000	0.000
Docosanoic Acid	0.000	0.000	0.000	0.000	0.000	0.000	0.000	0.000	0.000
Tricosanoic Acid	0.000	0.000	0.000	0.000	0.000	0.000	0.000	0.000	0.000
Tetracosanoic Acid	0.000	0.000	0.000	0.000	0.000	0.000	0.000	0.000	0.000
Hexacosanoic Acid	0.000	0.000	0.000	0.000	0.000	0.000	0.000	0.000	0.000
Octacosanoic Acid	0.000	0.000	0.000	0.000	0.000	0.000	0.000	0.000	0.000
Triacontanoic Acid	0.000	0.000	0.000	0.000	0.000	0.000	0.000	0.000	0.000
Asphaltenes	0.051	0.051	0.051	0.051	0.051	0.051	0.051	0.051	0.051
Coke	0.000	0.000	0.000	0.000	0.000	0.000	0.000	0.000	0.000

Table 135. Representative ChemCAD composition from data produced by cracking canola TAG in the 200 mL lab-scale TCR at various pressures

Name		J-Canola	K-Canola	L-Canola	M-Canola	N-Canola
Triolein	wt. %	0.000	0.000	0.000	0.000	0.000
Water		0.000	0.000	0.000	0.000	0.000
Hydrogen		0.000	0.000	0.001	0.001	0.001
Carbon Monoxide		0.024	0.022	0.024	0.022	0.019
Carbon Dioxide		0.046	0.044	0.045	0.043	0.047
Methane		0.004	0.004	0.005	0.005	0.005
Ethane		0.007	0.008	0.009	0.009	0.010
Propane		0.006	0.007	0.008	0.009	0.010
Butane		0.019	0.016	0.016	0.016	0.015
Pentane		0.007	0.007	0.010	0.008	0.007
Hexane		0.008	0.009	0.010	0.009	0.011
Heptane		0.017	0.015	0.015	0.018	0.020
Octane		0.013	0.017	0.018	0.016	0.015
Nonane		0.012	0.014	0.013	0.014	0.018
Decane		0.006	0.007	0.008	0.008	0.008
Undecane		0.004	0.005	0.005	0.005	0.005
Dodecane		0.004	0.006	0.005	0.005	0.006
Tridecane		0.004	0.006	0.006	0.006	0.007
Tetradecane		0.004	0.005	0.005	0.006	0.006
Pentadecane		0.006	0.009	0.008	0.008	0.009
Hexadecane		0.005	0.005	0.004	0.003	0.004
Heptadecane		0.005	0.003	0.003	0.003	0.004
Octadecane		0.002	0.002	0.002	0.002	0.004
Nonadecane		0.030	0.025	0.025	0.025	0.022
Eicosane		0.020	0.020	0.019	0.021	0.017
Uneicosane		0.015	0.010	0.011	0.010	0.010
Docosane		0.010	0.008	0.008	0.008	0.007
Tricosane		0.009	0.007	0.007	0.007	0.006
Tetracosane		0.008	0.006	0.006	0.006	0.005
Pentacosane		0.005	0.004	0.004	0.004	0.004
Hexacosane		0.005	0.005	0.005	0.005	0.004
Heptacosane		0.003	0.003	0.002	0.003	0.003
Octacosane		0.003	0.003	0.003	0.003	0.003
Nonacosane		0.002	0.002	0.002	0.002	0.002
Triacontane		0.002	0.002	0.002	0.002	0.002
Dotriacontane		0.004	0.004	0.005	0.005	0.005
Tetratriacontane		0.003	0.003	0.004	0.004	0.004
Hexatriacontane		0.002	0.002	0.003	0.003	0.003
Octatriacontane		0.002	0.002	0.002	0.004	0.006
Tetracontane		0.001	0.002	0.002	0.002	0.002
Dotetracontane		0.001	0.001	0.002	0.002	0.002
Tetratetracontane		0.002	0.001	0.001	0.001	0.001
Hexatetracontane		0.002	0.001	0.001	0.001	0.001
Octatetracontane		0.002	0.001	0.001	0.001	0.001
Pentacontane		0.000	0.000	0.000	0.001	0.001
Dopentacontane		0.000	0.000	0.000	0.000	0.000
Tetrapentacontane		0.000	0.000	0.001	0.000	0.000
Hexapentacontane		0.000	0.002	0.000	0.001	0.000
Octapentacontane		0.000	0.002	0.001	0.001	0.000
Hexacontane		0.000	0.000	0.000	0.001	0.000
Dohexacontane		0.000	0.000	0.000	0.000	0.000
Tetrahexacontane		0.000	0.000	0.000	0.000	0.000
Hexahexacontane		0.000	0.000	0.000	0.000	0.000
Octahexacontane		0.000	0.000	0.000	0.000	0.000
Heptacontane		0.000	0.000	0.000	0.000	0.000
Doheptacontane		0.000	0.000	0.000	0.000	0.000
Tetraheptacontane		0.000	0.000	0.000	0.000	0.000
Isobutane		0.000	0.000	0.000	0.000	0.000
2-Methylbutane		0.000	0.000	0.000	0.000	0.000
2-Methylpentane		0.000	0.000	0.000	0.000	0.000
2-Methylhexane		0.000	0.000	0.000	0.000	0.000

Table 135. cont.

Name	J-Canola	K-Canola	L-Canola	M-Canola	N-Canola
2-Methylheptane	0.000	0.000	0.000	0.000	0.000
2-Methyloctane	0.001	0.001	0.001	0.001	0.001
2-Methylnonane	0.000	0.000	0.001	0.001	0.001
2-Methyldecane	0.000	0.000	0.000	0.000	0.000
3-Methylundecane	0.000	0.000	0.000	0.000	0.000
2-Methyldodecane	0.000	0.000	0.000	0.000	0.000
2-Methyltridecane	0.000	0.000	0.000	0.000	0.000
2-Methyltetradecane	0.000	0.001	0.001	0.001	0.001
2-Methylpentadecane	0.000	0.000	0.000	0.000	0.000
2-Methylhexadecane	0.000	0.000	0.000	0.000	0.000
2-Methylheptadecane	0.000	0.000	0.000	0.000	0.000
2-Methyloctadecane	0.000	0.000	0.000	0.000	0.000
2-Methylnonadecane	0.000	0.000	0.000	0.000	0.000
2-Methyleicosane	0.000	0.000	0.000	0.000	0.000
2-Methyluneicosane	0.000	0.000	0.000	0.000	0.000
2-Methyldocosane	0.000	0.000	0.000	0.000	0.000
2-Methyltricosane	0.000	0.000	0.000	0.000	0.000
2-Methylpentacosane	0.000	0.000	0.000	0.000	0.000
2-Methylheptacosane	0.000	0.000	0.000	0.000	0.000
2-Methylnonacosane	0.000	0.000	0.000	0.000	0.000
Cyclopentene	0.004	0.006	0.005	0.006	0.007
Methylcyclopentane	0.008	0.009	0.009	0.009	0.009
Ethylcyclopentane	0.010	0.012	0.012	0.010	0.012
Propylcyclopentane	0.011	0.011	0.012	0.013	0.013
Butylcyclopentane	0.009	0.011	0.012	0.011	0.011
Butylcyclohexane	0.008	0.010	0.010	0.010	0.011
Hexylcyclopentane	0.014	0.016	0.014	0.013	0.014
Heptylcyclopentane	0.010	0.011	0.011	0.011	0.011
Octylcyclopentane	0.008	0.007	0.007	0.006	0.007
Nonylcyclopentane	0.011	0.013	0.013	0.012	0.010
Decylcyclopentane	0.014	0.010	0.010	0.010	0.009
Decylcyclohexane	0.012	0.011	0.010	0.010	0.010
Dodecylcyclopentane	0.017	0.016	0.013	0.012	0.013
Tridecylcyclopentane	0.009	0.007	0.006	0.006	0.005
Tetradecylcyclopentane	0.000	0.000	0.000	0.000	0.000
Pentadecylcyclopentane	0.000	0.000	0.000	0.000	0.000
Hexadecylcyclopentane	0.000	0.000	0.000	0.000	0.000
Heptadecylcyclopentane	0.000	0.000	0.000	0.000	0.000
Octadecylcyclopentane	0.000	0.000	0.000	0.000	0.000
Nonadecylcyclopentane	0.000	0.000	0.000	0.000	0.000
Uneicosylcyclopentane	0.000	0.000	0.000	0.000	0.000
Tricosylcyclopentane	0.000	0.000	0.000	0.000	0.000
Pentacosylcyclopentane	0.000	0.000	0.000	0.000	0.000
Ethylene	0.003	0.002	0.001	0.001	0.001
Propylene	0.005	0.005	0.004	0.004	0.003
1-Butene	0.004	0.009	0.010	0.010	0.007
1-Pentene	0.008	0.010	0.009	0.011	0.012
1-Hexene	0.015	0.016	0.016	0.016	0.015
1-Heptene	0.018	0.021	0.021	0.018	0.021
1-Octene	0.020	0.020	0.021	0.023	0.022
1-Nonene	0.015	0.018	0.019	0.018	0.017
1-Decene	0.013	0.016	0.016	0.016	0.017
1-Undecene	0.023	0.026	0.023	0.021	0.022
1-Dodecene	0.016	0.017	0.018	0.018	0.018
1-Tridecene	0.013	0.012	0.011	0.010	0.011
1-Tetradecene	0.018	0.021	0.020	0.020	0.017
1-Pentadecene	0.022	0.017	0.016	0.016	0.014
1-Hexadecene	0.019	0.017	0.015	0.016	0.017
1-Heptadecene	0.028	0.025	0.022	0.020	0.020
1-Octadecene	0.014	0.011	0.010	0.010	0.009
1-Nonadecene	0.000	0.000	0.000	0.000	0.000
1-Eicosene	0.000	0.000	0.000	0.000	0.000

Table 135. cont.

Name	J-Canola	K-Canola	L-Canola	M-Canola	N-Canola
1-Uneicosene	0.000	0.000	0.000	0.000	0.000
1-Docosene	0.000	0.000	0.000	0.000	0.000
1-Tricosene	0.000	0.000	0.000	0.000	0.000
1-Tetracosene	0.000	0.000	0.000	0.000	0.000
1-Hexacosene	0.000	0.000	0.000	0.000	0.000
1-Octacosene	0.000	0.000	0.000	0.000	0.000
1-Triacontene	0.000	0.000	0.000	0.000	0.000
Benzene	0.000	0.000	0.001	0.000	0.001
Toluene	0.001	0.001	0.002	0.002	0.002
Ethylbenzene	0.001	0.002	0.002	0.003	0.003
Propylbenzene	0.001	0.002	0.002	0.003	0.003
Butylbenzene	0.004	0.005	0.006	0.006	0.006
Pentylbenzene	0.006	0.008	0.009	0.010	0.010
Hexylbenzene	0.006	0.007	0.007	0.008	0.008
Heptylbenzene	0.006	0.006	0.007	0.007	0.007
Octylbenzene	0.008	0.009	0.010	0.010	0.010
Nonylbenzene	0.008	0.010	0.010	0.010	0.010
Decylbenzene	0.008	0.009	0.009	0.010	0.010
Undecylbenzene	0.011	0.009	0.009	0.009	0.008
Dodecylbenzene	0.009	0.008	0.008	0.008	0.008
Tridecylbenzene	0.000	0.000	0.000	0.000	0.000
Tetradecylbenzene	0.000	0.000	0.000	0.000	0.000
Pentadecylbenzene	0.000	0.000	0.000	0.000	0.000
Hexadecylbenzene	0.000	0.000	0.000	0.000	0.000
Heptadecylbenzene	0.000	0.000	0.000	0.000	0.000
Octadecylbenzene	0.000	0.000	0.000	0.000	0.000
Eicosylbenzene	0.000	0.000	0.000	0.000	0.000
Docosylbenzene	0.000	0.000	0.000	0.000	0.000
Tetracosylbenzene	0.000	0.000	0.000	0.000	0.000
Acetic Acid	0.011	0.010	0.010	0.011	0.011
Propionic Acid	0.003	0.003	0.003	0.004	0.004
Butyric Acid	0.002	0.002	0.003	0.003	0.003
Pentanoic Acid	0.003	0.004	0.003	0.003	0.003
Hexanoic Acid	0.007	0.007	0.007	0.007	0.007
Heptanoic Acid	0.014	0.017	0.014	0.014	0.014
Octanoic Acid	0.012	0.013	0.015	0.016	0.016
Nonanoic Acid	0.015	0.016	0.017	0.017	0.018
Decanoic Acid	0.050	0.033	0.029	0.027	0.026
Undecanoic Acid	0.006	0.007	0.007	0.007	0.007
Dodecanoic Acid	0.004	0.004	0.005	0.005	0.005
Tridecanoic Acid	0.004	0.004	0.004	0.005	0.004
Tetradecanoic Acid	0.004	0.004	0.004	0.004	0.004
Pentadecanoic Acid	0.003	0.003	0.003	0.003	0.003
Hexadecanoic Acid	0.006	0.005	0.005	0.006	0.005
Heptadecanoic Acid	0.003	0.002	0.002	0.003	0.002
Octadecanoic Acid	0.009	0.007	0.007	0.007	0.006
Nonadecanoic Acid	0.000	0.000	0.000	0.000	0.000
Eicosanoic Acid	0.000	0.000	0.000	0.000	0.000
Uneicosanoic Acid	0.000	0.000	0.000	0.000	0.000
Docosanoic Acid	0.000	0.000	0.000	0.000	0.000
Tricosanoic Acid	0.000	0.000	0.000	0.000	0.000
Tetracosanoic Acid	0.000	0.000	0.000	0.000	0.000
Hexacosanoic Acid	0.000	0.000	0.000	0.000	0.000
Octacosanoic Acid	0.000	0.000	0.000	0.000	0.000
Triacontanoic Acid	0.000	0.000	0.000	0.000	0.000
Asphaltenes	0.051	0.051	0.051	0.051	0.051
Coke	0.000	0.000	0.000	0.000	0.000

REFERENCES

(1)   Brown, R. *Biorenewable Resources*; Iowa State Press: Iowa, 2003.

(2)   Mussatto, S. I.; Dragone, G.; Guimarães, P. M. R.; Silva, J. P. a; Carneiro, L. M.;
Roberto, I. C.; Vicente, A.; Domingues, L.; Teixeira, J. a. Technological Trends,
Global Market, and Challenges of Bio-Ethanol Production. *Biotechnology advances*,
28, 817–830.

(3)   Guragain, Y. N.; De Coninck, J.; Husson, F.; Durand, A.; Rakshit, S. K. Comparison
of Some New Pretreatment Methods for Second Generation Bioethanol Production
from Wheat Straw and Water Hyacinth. *Bioresour. Technol.* **2011**, *102*, 4416–4424.

(4)   Lennartsson, P. R.; Niklasson, C.; Taherzadeh, M. J. A Pilot Study on Lignocelluloses
to Ethanol and Fish Feed Using NMMO Pretreatment and Cultivation with
Zygomycetes in an Air-Lift Reactor. *Bioresour. Technol.* **2011**, *102*, 4425–4432.

(5)   Melamu, R.; von Blottnitz, H. 2nd Generation Biofuels a Sure Bet? A Life Cycle
Assessment of How Things Could Go Wrong. *J. Clean. Prod.* **2011**, *19*, 138–144.

(6)   Nielsen, J.; Larsson, C.; van Maris, A.; Pronk, J. Metabolic Engineering of Yeast for
Production of Fuels and Chemicals. *Curr. Opin. Biotechnol.* **2013**, *24*, 398–404.

(7)   Du, X.; Carriquiry, M. a. Flex-Fuel Vehicle Adoption and Dynamics of Ethanol
Prices: Lessons from Brazil. *Energy Policy* **2013**, *59*, 507–512.

(8)   Sharma, Y.; Singh, B.; Upadhyay, S. Advancements in Development and Characterization of Biodiesel: A Review. *Fuel* **2008**, *87*, 2355–2373.

(9)   Vasudevan, P. T.; Briggs, M. Biodiesel Production--Current State of the Art and Challenges. *J. Ind. Microbiol. Biotechnol.* **2008**, *35*, 421–430.

(10)   Demirbas, A. Progress and Recent Trends in Biodiesel Fuels. *Energy Convers. Manag.* **2009**, *50*, 14–34.

(11)   Shahidi, F. *Bailey's Industrial Oil and Fat Products*; Sixth.; John Wiley & Sons, Inc.: Hoboken, NJ, 2005.

(12)   Angelo, C. Growth of Ethanol Fuel Stalls in Brazil. *Nature* **2012**, *491*, 646–647.

(13)   Pearman, G. I. Limits to the Potential of Bio-Fuels and Bio-Sequestration of Carbon. *Energy Policy* **2013**, *59*, 523–535.

(14)   Gowik, U.; Westhoff, P. The Path from C3 to C4 Photosynthesis. *Plant Physiol.* **2011**, *155*, 56–63.

(15)   Chisti, Y. Biodiesel from Microalgae Beats Bioethanol. *Trends Biotechnol.* **2008**, *26*, 126–131.

(16)   U.S. Energy Information Administration. Energy Consumption by Sector and Source. **2014**.

(17)   Alternative Fuels Data Center. Emerging Alternative Fuels http://www.afdc.energy.gov/fuels/emerging.html.

(18)   Thegarid, N.; Fogassy, G.; Schuurman, Y.; Mirodatos, C.; Stefanidis, S.; Iliopoulou, E. F.; Kalogiannis, K.; Lappas, a. a. Second-Generation Biofuels by Co-Processing Catalytic Pyrolysis Oil in FCC Units. *Appl. Catal. B Environ.* **2014**, *145*, 161–166.

(19) Saidi, M.; Samimi, F.; Karimipourfard, D.; Nimmanwudipong, T.; Gates, B. C.; Rahimpour, M. R. Upgrading of Ligning-Derived Bio-Oils by Catalytic Hydrodeoxygenation. *Energy Environ. Sci.* **2014**, *7*, 103–129.

(20) Brooks, B. 80% CO2 Reduction Targeted by Join Audi-Joul Fuel Program. *Autom. Ind.* **2013**, *193*, It was announced in September 2012 that Audi and J.

(21) Woods, P. Algenol Biofuels's Direct to Ethanol^{TM} Technology. *AIChE Annu. Meet.* **2009**, *1*.

(22) Kubatova, A.; Stavova, J.; Seames, W.; Luo, Y.; Sadrameli, M.; Linnen, M.; Baglayeva, G.; Smoliakova, I.; Kozliak, E. Triacylglyceride Thermal Cracking: Pathways to Cyclic Hydrocarbons. *Energy & Fuels* **2012**, *26*, 672–685.

(23) Klingshirn, C. D.; DeWitt, M.; Striebich, R.; Anneken, D.; Shafer, L.; Corporan, E.; Wagner, M.; Brigalli, D. Hydroprocessed Renewable Jet Fuel Evaluation, Performance, and Emissions in a T63 Turbine Engine. *J. Eng. Gas Turbines Power* **2012**, *134*, 051506.

(24) Li, L. Cyclization; Catalytic Cracking; Anaerobic Fermentation. US7691159 B2, 2008.

(25) Eber, K. Can "drop-in" biofuels solve integration issues? http://www.nrel.gov/continuum/sustainable_transportation/biofuels.cfm.

(26) (2011) ASTM D975-11. Standard Specification for Diesel Fuel Oils, ASTM International: West Conshohocken, PA USA.

(27) (2011) ASTM D1655-11b. Standard Specification for Aviation Turbine Fuels., ASTM International: West Conshohocken, PA USA.

(28)   Stumborg, M.; Wong, A.; Hogan, E. Hydroprocessed Vegetable Oils for Diesel Fuel Improvement. *Bioresour. Technol.* **1996**, *56*, 13–18.

(29)   Kubičková, I.; Snåre, M.; Eränen, K.; Mäki-Arvela, P.; Murzin, D. Y. Hydrocarbons for Diesel Fuel via Decarboxylation of Vegetable Oils. *Catal. Today* **2005**, *106*, 197–200.

(30)   Snåre, M.; Kubičková, I.; Mäki-Arvela, P.; Chichova, D.; Eränen, K.; Murzin, D. Y. Catalytic Deoxygenation of Unsaturated Renewable Feedstocks for Production of Diesel Fuel Hydrocarbons. *Fuel* **2008**, *87*, 933–945.

(31)   Snåre, M.; Kubic□ková, I.; Mäki-Arvela, P.; Eränen, K.; Murzin, D. Y. Heterogeneous Catalytic Deoxygenation of Stearic Acid for Production of Biodiesel. *Ind. Eng. Chem. Res.* **2006**, *45*, 5708–5715.

(32)   Mohammad, M.; Kandaramath Hari, T.; Yaakob, Z.; Chandra Sharma, Y.; Sopian, K. Overview on the Production of Paraffin Based-Biofuels via Catalytic Hydrodeoxygenation. *Renew. Sustain. Energy Rev.* **2013**, *22*, 121–132.

(33)   Guzman, A.; Torres, J. E.; Prada, L. P.; Nuñez, M. L. Hydroprocessing of Crude Palm Oil at Pilot Plant Scale. *Catalysis Today*, 2010, *156*, 38–43.

(34)   Raseev, S. *Thermal and Catalytic Processes in Petroleum Refining*; Suciu, G. D., Ed.; Marcel Dekker, Inc.: New York, NY, USA, 2003.

(35)   El-Nahas, A. M.; Navarro, M. V; Simmie, J. M.; Bozzelli, J. W.; Curran, H. J.; Dooley, S.; Metcalfe, W. Enthalpies of Formation, Bond Dissociation Energies and Reaction Paths for the Decomposition of Model Biofuels: Ethyl Propanoate and Methyl Butanoate. *The journal of physical chemistry. A*, 2007, *111*, 3727–3739.

(36)   Ryymin, E.-M.; Honkela, M. L.; Viljava, T.-R.; Krause, A. O. I. Competitive

         Reactions and Mechanisms in the Simultaneous HDO of Phenol and Methyl

         Heptanoate over Sulphided NiMo/γ-Al2O3. *Appl. Catal. A Gen.* **2010**, *389*, 114–121.

(37)   Zuo, H.; Liu, Q.; Wang, T.; Ma, L.; Zhang, Q.; Zhang, Q. Hydrodeoxygenation of

         Methyl Palmitate over Supported Ni Catalysts for Diesel-like Fuel Production. *Energy*

         & Fuels **2012**, *26*, 3747–3755.

(38)   Rekoske, J.; Bozzano, A.; Mccall, M.; Nair, P. The Development of UOP Process to

         Produce Semi- and Fully- Synthetic Green Jet Fuel from Renewable Feedstocks. In

         Petrotech; 2010; pp. 1–6.

(39)   Dandik, L.; Aksoy, H. A.; Erdem-senatalar, A. Catalytic Conversion of Used Oil to

         Hydrocarbon Fuels in a Fractionating Pyrolysis Reactor. *Energy & Fuels* **1998**, *12*,

         1148–1152.

(40)   Dandik, L.; Aksoy, H. A. Effect of Catalyst on the Pyrolysis of Used Oil Carried out

         in a Fractionating Pyrolysis Reactor. *Renew. Energy* **1999**, *16*, 1007–1010.

(41)   Junming, X.; Jianchun, J.; Yanju, L.; Jie, C. Liquid Hydrocarbon Fuels Obtained by

         the Pyrolysis of Soybean Oils. *Bioresour. Technol.* **2009**, *100*, 4867–4870.

(42)   Dupain, X.; Costa, D. J.; Schaverien, C. J.; Makkee, M.; Moulijn, J. a. Cracking of a

         Rapeseed Vegetable Oil under Realistic FCC Conditions. *Appl. Catal. B Environ.*

         2007, *72*, 44–61.

(43)   Katikaneni, S. P. R.; Adjaye, J. D.; Idem, R. O.; Bakhshi, N. N. Performance Studies

         of Various Cracking Catalysts in the Conversion of Canola Oil to Fuels and Chemicals

         in a Fluidized-Bed Reactor. *J. Am. Oil Chem. Soc.* **1998**, *75*, 381–391.

605

(44) Katikaneni, S. P. R.; Adjaye, J. D.; Bakhshi, N. N. Studies on the Catalytic Conversion of Canola Oil to Hydrocarbons: Influence of Hybrid Catalysts and Steam. *Energy & Fuels* **1995**, *9*, 599–609.

(45) Li, L.; Coppola, E.; Rine, J.; Miller, J. L.; Walker, D. Catalytic Hydrothermal Conversion of Triglycerides to Non-Ester Biofuels. *Energy & Fuels* **2010**, *24*, 1305–1315.

(46) Blue Sun Energy, ARA Inc. and Chevron Lummus Global partner in successful biofuels isoconversion demonstration http://www.ara.com/Newsroom_Whatsnew/press_releases/biofuel_demo.htm.

(47) Holliday, R. L.; King, J. W.; List, G. R. Hydrolysis of Vegetable Oils in Sub- and Supercritical Water. *Ind. Eng. Chem. Res.* **1997**, *36*, 932–935.

(48) Egloff, G.; Morrell, J. C. The Cracking of Cottonseed Oil. *Ind. Eng. Chem.* **1932**, *24*, 1426–1427.

(49) Higman, E. B.; Schmeltz, I.; Higman, H. C.; Chortyk, O. T. Studies on the Thermal Degradation of Naturally Occurring Materials. II. Products from the Pyrolysis of Triglycerides at 400 Degrees. *J. Agric. Food Chem.* **1973**, *21*, 202–204.

(50) Schwab, A. W.; Dykstrab, G. J.; Selkeo, E.; Sorensonb, S. C.; Prydeo, E. H. Diesel Fuel from Thermal Decomposition of Soybean Oil. *J. Am. Oil Chem. Soc.* **1988**, *65*, 1781–1786.

(51) Idem, R. O.; Katikaneni, S. P. R.; Bakhshi, N. N. Thermal Cracking of Canola Oil: Reaction Products in the Presence and Absence of Steam. *Energy & Fuels* **1996**, *10*, 1150–1162.

(52) Adebanjo, A. O.; Dalai, A. K.; Bakhshi, N. N. Production of Diesel-Like Fuel and Other Value-Added Chemicals from Pyrolysis of Animal Fat. *Energy & Fuels*, 2005, *19*, 1735–1741.

(53) Doll, K. M.; Sharma, B. K.; Suarez, P. A. Z.; Erhan, S. Z. Comparing Biofuels Obtained from Pyrolysis, of Soybean Oil or Soapstock, with Traditional Soybean Biodiesel: Density, Kinematic Viscosity, and Surface Tensions†. *Energy & Fuels* **2008**, *22*, 2061–2066.

(54) Luo, Y.; Ahmed, I.; Kubátová, A.; Šťávová, J.; Aulich, T.; Sadrameli, S. M.; Seames, W. S. The Thermal Cracking of Soybean/canola Oils and Their Methyl Esters. *Fuel Process. Technol.* **2010**, *91*, 613–617.

(55) Wiggers, V. R.; Meier, H. F.; Wisniewski, a; Chivanga Barros, a a; Wolf Maciel, M. R. Biofuels from Continuous Fast Pyrolysis of Soybean Oil: A Pilot Plant Study. *Bioresour. Technol.* **2009**, *100*, 6570–6577.

(56) Seames, W.; Luo, Y.; Ahmed, I.; Aulich, T.; Kubátová, A.; Šť'Ávová, J.; Kozliak, E. The Thermal Cracking of Canola and Soybean Methyl Esters: Improvement of Cold Flow Properties. *Biomass and Bioenergy* **2010**, *34*, 939–946.

(57) Maher, K. D.; Bressler, D. C. Pyrolysis of Triglyceride Materials for the Production of Renewable Fuels and Chemicals. *Bioresour. Technol.* **2007**, *98*, 2351–2368.

(58) Kubátová, A.; Luo, Y.; Šťávová, J.; Sadrameli, S. M.; Aulich, T.; Kozliak, E.; Seames, W. New Path in the Thermal Cracking of Triacylglycerols (canola and Soybean Oil). *Fuel* **2011**, *90*, 2598–2608.

(59)   Linnen, M.; Seames, W.; Kubatova, A.; Menon, S.; Alisala, K.; Hash, S. Evaluation of Microbial Triglyceride Oil Purification Requirements for the CelTherm Process: An Efficient Biochemical Pathway to Renewable Fuels and Chemicals. *Bioprocess Biosyst. Eng.* **2014**, *37*, 2121–2129.

(60)   Snåre, M.; Kubičková, I.; Mäki-Arvela, P.; Eränen, K.; Wärnå, J.; Murzin, D. Y. Production of Diesel Fuel from Renewable Feeds: Kinetics of Ethyl Stearate Decarboxylation. *Chem. Eng. J.* **2007**, *134*, 29–34.

(61)   Mäki-Arvela, P.; Kubickova, I.; Snåre, M.; Eränen, K.; Murzin, D. Y. Catalytic Deoxygenation of Fatty Acids and Their Derivatives. *Energy & Fuels* **2007**, *21*, 30–41.

(62)   Sander, B. A Study of Bench Sscale, Pressurized, Continuous Flow Thermal Cracking of Crop Oil, University of North Dakota, 2014, pp. 1–174.

(63)   Sťávová, J.; Stahl, D. C.; Seames, W. S.; Kubátová, A. Method Development for the Characterization of Biofuel Intermediate Products Using Gas Chromatography with Simultaneous Mass Spectrometric and Flame Ionization Detections. *J. Chromatogr. A* **2012**, *1224*, 79–88.

(64)   (2010) ASTM D7500-10. Standard Test Method for Determination of Boiling Range Distribution of Distillates and Lubricating Base Oils—in Boiling Range from 100 to 735°C by Gas Chromatography., ASTM International: West Conshohocken, PA USA.

(65)   (2006) ASTM D1160-06. Standard Test Method for Distillation of Petroleum Products at Reduced Pressure., ASTM International: West Conshohocken, PA USA.

(66) Bosquez, N. High Purity Carbon from Crop Oil Tars, University of North Dakota, 2012.

(67) Qiao, X.; Xu, S.; Sui, D.; Zhao, L.; Hua, W.; Shang, Y. Progress in Spinning Band Distillation. *Xiandai Huagong/Modern Chem. Ind.* **2010**, *30*, 82–84.

(68) Khambete, M. Study of Decarboxylation and Alkylation of Catalytically Cracked Soybean Oil, 2010, pp. 1–141.

(69) Braegelmann, M. P.; Azure, A. D.; Stahl, D. C.; Kubatova, A.; Seames, W. S.; Tande, B. M. Extraction of Fatty Acids from Noncatalytically Cracked Triacylglycerides Using Aqueous Amins. *Sep. Sci. Technol.* **2011**, *46*, 2167–2173.

(70) Fagade, S. Catalytic Conversion of Crop Oil To Petrochemical Substitutes and Other Bio-Based Chemicals, University of North Dakota, 2014, pp. 1–50.

(71) Ahmad, S. .; Tanwar, R. .; Gupta, R. .; Khanna, a. Interaction Parameters for Multi-Component Aromatic Extraction with Sulfolane. *Fluid Phase Equilib.* **2004**, *220*, 189–198.

(72) Khatibi, N. Aromatics Extraction of Crop Oil Crackate Distillates, University of North Dakota, 2012.

(73) Pham, T. N.; Sooknoi, T.; Crossley, S. P.; Resasco, D. E. Ketonization of Carboxylic Acids: Mechanisms, Catalysts, and Implications for Biomass Conversion. *ACS Catal.* **2013**, *3*, 2456–2473.

(74) Glinski, M.; Kijenski, J.; Jakubowski, A. Ketones from Monocarboxylic Acids: Catalytic Ketonization over Oxide Systems. *Appl. Catal. A Gen.* **1995**, *128*, 209–217.

(75)   Snell, R. W.; Shanks, B. H. CeMOx-Promoted Ketonization of Biomass-Derived Carboxylic Acids in the Condensed Phase. *ACS Catal.* **2014**, *4*, 512–518.

(76)   Brown, R. L.; Stein, S. E. Boiling Point Data. In *NIST Chemistry WebBook, NIST Standard Reference Database Number 69*; Linstrom, P. J.; Mallard, W. G., Eds.; National Institute of Standards and Technology: Gaithersburg, MD, USA, 2014.

(77)   Burgess, D. R. Thermochemical Data. In *NIST Chemistry WebBook, NIST Standard Reference Database Number 69*; Linstrom, P. J.; Mallard, W. G., Eds.; National Institute of Standards and Technology: Gaithersburg, MD, USA, 2014.

(78)   Lide, D. R. *CRC Handbook of Chemistry and Physics*; 90th ed.; CRC Press: Boca Raton, FL, USA, 2009.

(79)   Yaws, C. L. *Thermophysical Properties of Chemicals and Hydrocarbons*; William Andrew: London, UK, 2008.

(80)   USDA Economic Research Service. Oil Crops Yearbook http://www.ers.usda.gov/.

(81)   U.S. Energy Information Administration. Spot Prices http://www.eia.gov/.

(82)   U.S. Energy Information Administration. Prime Supplier Sales Volumes http://www.eia.gov/.

(83)   U.S. Energy Information Administration. International Energy Statistics http://www.eia.gov/.

(84)   McMurry, J. *Organic Chemistry*; 8th Ed.; Cengage Learning: Stamford, CT, USA, 2012.

(85)   Blanksby, S. J.; Ellison, G. B. Bond Dissociation Energies of Organic Molecules. *Acc. Chem. Res.* **2003**, *36*, 255–263.

(86) Pedley, J. B. *Thermodynamics Data and Structure of Organic Molecules*; 6th ed.; CRC Press: College Station, Texas, USA, 1994.

(87) Sundaram, K. M.; Froment, G. F. Modeling of Thermal Cracking Kinetics-I. Thermal Cracking of Ethane, Propane and Their Mixtures. *Chem. Eng. Sci.* **1977**, *32*, 601–608.

(88) Blouri, B.; Hamdan, F.; Herault, D. Mild Cracking of High-Molecular-Weight Hydrocarbons. *Ind. Eng. Chem. Process Des. Dev.* **1985**, *24*, 30–37.

(89) (2000) ISO 5509. Animal and Vegetable Fats and Oils - Preparation of Methyl Esters of Fatty Acids, *Internatio*, International Organization for Standardization: Ge.

(90) Singh, B. K.; Bala, M.; Rai, P. K. Fatty Acid Composition and Seed Meal Characteristics of Brassica and Allied Genera. *Natl. Acad. Sci. Lett.* **2014**, *37*, 219–226.

(91) Moser, B. R.; Knothe, G.; Vaughn, S. F.; Isbell, T. A. Production and Evaluation of Biodiesel from Field Pennycress (Thlaspi Arvense L .) Oil. *Energy & Fuels* **2009**, *23*, 4149–4155.

(92) Abou-Shanab, R. a. I.; Hwang, J.-H.; Cho, Y.; Min, B.; Jeon, B.-H. Characterization of Microalgal Species Isolated from Fresh Water Bodies as a Potential Source for Biodiesel Production. *Appl. Energy* **2011**, *88*, 3300–3306.

(93) (2011) ASTM D86-11a. Standard Test Method for Distillation of Petroleum Products at Atmospheric Pressure., ASTM International: West Conshohocken, PA USA.

(94) (2007) ASTM D5236-03. Standard Test Method for Distillation of Heavy Hydrocarbon Mixtures (Vacuum Potstill Method)., ASTM International: West Conshohocken, PA USA.

(95) (2011) ASTM D2892-11. Standard Test Method for Distillation of Crude Petroleum (15-Theoretical Plate Column)., ASTM International: West Conshohocken, PA USA.

(96) Javes, A. R.; Liddell, C.; Thomas, W. H. Distillation Micromethods for the Analysis of Petroleum. *Anal. Chem.* **1955**, *27*, 991–996.

(97) Winters, J. C.; Dinerstein, R. A. Analytical Distillation in Miniature Columns: Equipment and Operation. *Anal. Chem.* **1955**, *27*, 546–550.

(98) Nerheim, A. G. Analytical Distillation in Miniature Columns: Design and Testing of Teflon Spinning Band. *Anal. Chem.* **1957**, *29*, 1546–1548.

(99) Nerheim, A. G.; Dinerstein, R. A. Analytical Distillation in Miniature Columns: Performance under Total and Partial Reflux. *Anal. Chem.* **1956**, *28*, 1029–1033.

(100) (2010) ASTM D1319-10. Standard Test Method for Hydrocarbon Types in Liquid Petroleum Products by Fluorescent Indicator Adsorption., ASTM International: West Conshohocken, PA USA.

(101) (2007) ASTM D1840-07. Standard Test Method for Naphthalene Hydrocarbons in Aviation Turbine Fuels by Ultraviolet Spectrophotometry., ASTM International: West Conshohocken, PA USA.

(102) (2009) ASTM D2425-04. Standard Test Method for Hydrocarbon Types in Middle Distillates by Mass Spectrometry., ASTM International: West Conshohocken, PA USA.

(103) Bruno, T. J.; Ott, L. S.; Lovestead, T. M.; Huber, M. L. The Composition-Explicit Distillation Curve Technique: Relating Chemical Analysis and Physical Properties of Complex Fluids. *J. Chromatogr. A* **2010**, *1217*, 2703–2715.

(104) Bruno, T. J.; Ott, L. S.; Lovestead, T. M.; Huber, M. L. Relating Complex Fluid Composition and Thermophysical Properties with the Advanced Distillation Curve Approach. *Chem. Eng. Technol.* **2010**, *33*, 363–376.

(105) Windom, B. C.; Bruno, T. J. Improvements in the Measurement of Distillation Curves . 5 . Reduced Pressure Advanced Distillation Curve Method. *Chem. Anal.* **2011**, *50*, 1115–1126.

(106) (2011) ASTM D6379-11. Standard Test Method for Determination of Aromatic Hydrocarbon Types in Aviation Fuels and Petroleum Distillates—High Performance Liquid Chromatography Method with Refractive Index Detection., ASTM International: West Conshohocken, PA USA.

(107) (2008) ASTM D6296-98. Standard Test Method for Total Olefins in Spark-Ignition Engine Fuels by Multidimensional Gas Chromatography., ASTM International: West Conshohocken, PA USA.

(108) (2011) ASTM D6730-11. Standard Test Method for Determination of Individual Components in Spark Ignition Engine Fuels by 100-Metre Capillary (with Precolumn) High-Resolution Gas Chromatography., ASTM International: West Conshohocken, PA USA.

(109) (2011) ASTM D6733-01. Standard Test Method for Determination of Individual Components in Spark Ignition Engine Fuels by 50-Metre Capillary High Resolution Gas Chromatography., ASTM International: West Conshohocken, PA USA.

(110) (2007) ASTM D6839-02. Standard Test Method for Hydrocarbon Types, Oxygenated Compounds and Benzene in Spark Ignition Engine Fuels by Gas Chromatography ., ASTM International: West Conshohocken, PA USA.

(111) (2008) ASTM D2887-08. Standard Test Method for Boiling Range Distribution of Petroleum Fractions by Gas Chromatography., ASTM International: West Conshohocken, PA USA.

(112) (2009) ASTM D3710-95. Standard Test Method for Boiling Range Distribution of Gasoline and Gasoline Fractions by Gas Chromatography., ASTM International: West Conshohocken, PA USA.

(113) (2007) ASTM D5307-97. Standard Test Method for Determination of Boiling Range Distribution of Crude Petroleum by Gas Chromatography., ASTM International: West Conshohocken, PA USA.

(114) Chen, J.; Mclean, N.; Hager, D. Prediction of Molecular Weight By-Boiling-Point Distribution of Middle Distillates from Gas Chromatography–Field Ionization Mass Spectrometry (GC–FIMS). *Energy & Fuels* **2011**, *25*, 719–726.

(115) Ha, H. Z.; Ring, Z.; Liu, S. Data Reconciliation Among PIONA, GC-FIMS, and SimDis Measurements for Petroleum Fractions. *Pet. Sci. Technol.* **2008**, *26*, 7–28.

(116) Lattimer, R. P.; Schulten, H.-R. Field Ionization and Field Desorption Mass Spectrometry: Past, Present, and Future. *Anal. Chem.* **1989**, *61*, 121–1215.

(117) Gomer, R.; Inghram, M. G. Applications of Field Ionization to Mass Spectrometry. *J. Am. Chem. Soc.* **1955**, *77*, 500.

(118) Yoshida, T.; Maekawa, Y.; Higuchi, T.; Kubota, E.; Itagaki, Y.; Yokoyama, S. Application of Field-Ionization and Field-Desorption Mass Spectrometry to the Analysis of Coal-Derived Oil. *Bull. Chem. Soc. Jpn.* **1981**, *54*, 1171–1175.

(119) Ogawa, T. Analytical Conditions for Field Ionization Mass Spectrometry of Diesel Fuel. *Fuel* **2005**, *84*, 2015–2025.

(120) Welthagen, W.; Mitschke, S.; Mühlberger, F.; Zimmermann, R. One-Dimensional and Comprehensive Two-Dimensional Gas Chromatography Coupled to Soft Photo Ionization Time-of-Flight Mass Spectrometry: A Two- and Three-Dimensional Separation Approach. *J. Chromatogr. A* **2007**, *1150*, 54–61.

(121) Eschner, M. S.; Welthagen, W.; Gröger, T. M.; Gonin, M.; Fuhrer, K.; Zimmermann, R. Comprehensive Multidimensional Separation Methods by Hyphenation of Single-Photon Ionization Time-of-Flight Mass Spectrometry (SPI-TOF-MS) with GC and GCxGC. *Anal. Bioanal. Chem.* **2010**, *398*, 1435–1445.

(122) Rohwedder, W. K. Field Ionization Mass Spectrometry of Long Chain Fatty Methyl Esters. *Lipids* **1971**, *6*, 906–911.

(123) Beckey, H.-D. *Field Ionization Mass Spectrometry*; Belcher, R.; Freiser, H., Eds.; 1st ed.; Pergamon Press, Inc.: Elmsford, New York USA, 1971; pp. 1–330.

(124) Levsen, K.; Weber, R.; Borchers, F.; Heimbach, H.; Beckey, H. D. Determination of Double Bonds in Alkenes by Field Ionization Mass Spectrometry. *Anal. Chem.* **1978**, *50*, 1655–1658.

(125) Rang, S. A.; Muurisepp, A.-M. A.; Liitmaa, M. M.; Eisen, O. G. Field Ionization Mass Spectrometry of Higher N-Alkenes. *Org. Mass Spectrom.* **1978**, *13*, 181–183.

(126) Hejazi, L.; Ebrahimi, D.; Hibbert, D. B.; Guilhaus, M. Compatibility of Electron Ionization and Soft Ionization Methods in Gas Chromatography / Orthogonal Time-of-Flight Mass Spectrometry. *Rapid Commun. Mass Spectrom.* **2009**, *23*, 2181–2189.

(127) Briker, Y.; Ring, Z.; Iacchelli, A.; Mclean, N.; Rahimi, P. M.; Fairbridge, C.; Tg, A.; Malhotra, R.; Coggiola, M. A.; Young, S. E. Diesel Fuel Analysis by GC-FIMS: Aromatics, N -Paraffins, and Isoparaffins. *Energy & Fuels* **2001**, *15*, 23–37.

(128) Malhotra, R.; Coggiola, M. J.; Young, S. E.; Tse, D.; Buttrill Jr., S. E. Analysis of Middle Distillate Fuels by High Resolution Field Ionization Mass Spectrometry. *ACS Div. Fuel Chem. Prepr.* **1985**, *30*, 192–199.

(129) Qian, K.; Dechert, G. J.; Edwards, K. E. Deducing Molecular Compositions of Petroleum Products Using GC-Field Ionization High Resolution Time of Flight Mass Spectrometry. *Int. J. Mass Spectrom.* **2007**, *265*, 230–236.

(130) Mitschke, S.; Welthagen, W.; Zimmermann, R. Comprehensive Gas Chromatography-Time-of-Flight Mass Spectrometry Using Soft and Selective Photoionization Techniques. *Anal. Chem.* **2006**, *78*, 6364–6375.

(131) Zimmermann, R.; Welthagen, W.; Gröger, T. Photo-Ionisation Mass Spectrometry as Detection Method for Gas Chromatography. Optical Selectivity and Multidimensional Comprehensive Separations. *J. Chromatogr. A* **2008**, *1184*, 296–308.

(132) Kleeblatt, J.; Ehlert, S.; Hölzer, J.; Sklorz, M.; Rittgen, J.; Baumgärtel, P.; Schubert, J. K.; Zimmermann, R. Investigation of the Photoionization Properties of Pharmaceutically Relevant Substances by Resonance-Enhanced Multiphoton Ionization Spectroscopy and Single-Photon Ionization Spectroscopy Using Synchrotron Radiation. *Appl. Spectrosc.* **2013**, *67*, 860–872.

(133) Milosavljević, A. R.; Nicolas, C.; Gil, J.-F.; Canon, F.; Réfrégiers, M.; Nahon, L.; Giuliani, A. VUV Synchrotron Radiation: A New Activation Technique for Tandem Mass Spectrometry. *J. Synchrotron Radiat.* **2012**, *19*, 174–178.

(134) Di Palma, T. M.; Prati, M. V; Borghese, A. Tunable Single-Photon Ionization TOF Mass Spectrometry Using Laser-Produced Plasma as the Table-Top VUV Light Source. *J. Am. Soc. Mass Spectrom.* **2009**, *20*, 2192–2198.

(135) Nir, E.; Hunziker, H. E.; de Vries, M. S. Fragment-Free Mass Spectrometric Analysis with Jet Cooling/VUV Photoionization. *Anal. Chem.* **1999**, *71*, 1674–1678.

(136) Aberth, W.; Spindt, C. A. Characteristics of a Volcano Field Ion Quadrupole Mass Spectrometer. *Int. J. mass Spectrom. ion Phys.* **1977**, *25*, 183 –198.

(137) Robertson, B., A. J. Field Ionization Mass Spectrometry. *J. Phys. E.* **1974**, *7*, 321–327.

(138) Speier, F.; Heinen, H. J.; Beckey, H. D. Measurement of the Field Strength at Field Anodes with Fragment of the N-Heptane. *Messtechnik* **1972**, *80*, 147–149.

(139) Scheppele, S. E.; Grizzle, P. L.; Greenwood, G. J.; Marriott, T. D.; Perreira, N. B. Determination of Field-Ionization Relative Sensitivities for the Analysis of Coal-Derived Liquids and Their Correlation with Low-Voltage Electron-Impact Relative Sensitivities. *Anal. Chem.* **1976**, *48*, 2105–2112.

(140) Scheppele, S. E.; HSU, C. S.; Marriott, T. D.; Benson, P. A.; Detwiler, K. N.; Perriera, N. B. Field-Ionization Relative Sensitivities for the Analysis of Saturated Hydrocarbons from Fossil-Energy-Related Materials. *Int. J. Mass Spectrom. Ion Phys.* **1978**, *28*, 335–346.

(141) Briker, Y.; Ring, Z.; Iacchelli, A.; Mclean, N.; Fairbridge, C.; Tg, A.; Malhotra, R.; Coggiola, M. A.; Young, S. E. Diesel Fuel Analysis by GC-FIMS: Normal Paraffins, Isoparaffins, and Cycloparaffins. *Energy & Fuels* **2001**, *15*, 996–1002.

(142) Malhotra, R.; Coggiola, M. J.; Young, S. E.; Spindt, C. A.; International, S. R. I.; Park, M.; Hsu, C. S.; Dechert, G. J.; Rahimi, P. M.; Briker, Y.; Drive, O. P.; Tg, A. Rapid Detailed Analysis of Transportation Fuels by GC-FIMS. *Prepr. - Am. Chem. Soc. Div. Pet. Chem.* **1998**, *43*, 1–12.

(143) Fraley, D. F.; Pedersen, L. G.; Bursey, M. M. Resistive Heating of Emitter Wires for Field Desorption and Ionization: A Theory. *Int. J. Mass Spectrom. Ion Phys.* **1982**, *43*, 99–129.

(144) Qian, L.; Yan, Z. Studies on Adsorption and Dissociation of Methane and Carbon Dioxide on Nickel Catalyst Temperature (K). *Fuel Chem. Div. Prepr.* **2002**, *47*, 598–602.

(145) Androulakis, I. P.; Weisel, M. D.; Hsu, C. S.; Qian, K.; Green, L. a.; Farrell, J. T.; Nakakita, K. An Integrated Approach for Creating Model Diesel Fuels. *Energy & Fuels* **2005**, *19*, 111–119.

(146) Qian, K.; Diehl, J.; Dechert, G.; DiSanzo, F. The Coupling of Supercritical Fluid Chromatography and Field Ionization Time-of-Flight High-Resolution Mass Spectrometry for Rapid and Quantitative Analysis of Petroleum Middle Distillates. *Eur. Mass Spectrom.* **2004**, *10*, 187–196.

(147) Schulz, C.; Chowdhury, S. K.; Blum, S. C. Field Ionization Mass Spectrometric Sensitivities of One-Ring Aromatic Hydrocarbons. *Anal. Chem.* **1993**, *65*, 1426–1430.

(148) (2006) ASTM D4607-94. Standard Test Method for Determination of Iodine Number of Activated Carbon, ASTM International: West Conshohocken, PA USA.

(149) (2008) ASTM D5134-98. Standard Test Method for Detailed Analysis of Petroleum Naphthas through N-Nonane by Capillary Gas Chromatography., ASTM International: West Conshohocken, PA USA.

(150) Zhenyi, C.; Xing, J.; Shuyuan, L.; Li, L. Thermodynamics Calculation of the Pyrolysis of Vegetable Oils. *Energy Sources* **2004**, *26*, 849–856.

(151) Šťávová, J.; Beránek, J.; Nelson, E. P.; Diep, B. a; Kubátová, A. Limits of Detection for the Determination of Mono- and Dicarboxylic Acids Using Gas and Liquid Chromatographic Methods Coupled with Mass Spectrometry. *J. Chromatogr. B* **2011**, *879*, 1429–1438.

(152) Stavova, J. Essential Analytical Parameters in the Gas Chromatographic-Mass Spectrometric Analysis of Complex Materials: Biofuels and Fungicide Treated Wood, University of North Dakota, 2011.

(153) (2009) ASTM E169-04. Standard Practices for General Techniques of Ultraviolet-Visible Quantitative Analysis, ASTM International: West Conshohocken, PA.

(154) (2011) ASTM D974-11. Standard Test Method for Acid and Base Number by Color-Indicator Titration., ASTM International: West Conshohocken, PA USA.

(155) Lawson, J.; Erjavec, J. *Modern Statistics for Engineering and Quality Improvement*; Duxbury, 2000; p. 810.

(156) Geetla, A. Application of Method Developed for the Identification and Quantitation of Polar Components in Organic Liquid Products of Selected Crop Oils and Deciphering the Mechanistic Aspects of Cracking, University of North Dakota, 2014, pp. 1–89.

(157) (2005) ASTM D5972-05. Standard Test Method for Freezing Point of Aviation Fuels (Automatic Phase Transition Method)., ASTM International: West Conshohocken, PA USA.

(158) (2005) ASTM D3828-05. Standard Test Methods for Flash Point by Small Scale Closed Cup Tester., ASTM International: West Conshohocken, PA USA.

(159) (2003) ASTM D1298-99. Standard Test Method for Density, Relative Density (Specific Gravity), or API Gravity of Crude Petroleum and Liquid Petroleum Products by Hydrometer Method., ASTM International: West Conshohocken, PA USA.

(160) (2005) ASTM D4809-00. Standard Test Method for Heat of Combustion of Liquid Hydrocarbon Fuels by Bomb Calorimeter (Precision Method)., ASTM International: West Conshohocken, PA USA.

(161) Fogler, H. S. *Elements of Chemical Reaction Engineering*; 4th ed.; Pearson Education, Inc.: Upper Saddle River, NJ 07458, 2006; pp. 1–1077.

(162) Pansing, W. F. The Catalytic Cracking of Hexadecane - Effects of Impurities, Olefins, and Steam. *J. Phys. Chem.* **1965**, *69*, 392–399.

(163) Chang, C.-C.; Wan, S.-W. China's Motor Fuels from Tung Oil. *Ind. Eng. Chem.* **1947**, *39*, 1534–1548.

(164) Nawar, W. W. Thermal Degradation of Lipids. *J. Agric. Food Chem.* **1969**, *17*, 18–21.

(165) Alencar, J. W.; Alves, P. B.; Craveiro, a. a. Pyrolysis of Tropical Vegetable Oils. *J. Agric. Food Chem.* **1983**, *31*, 1268–1270.

(166) Sen Gupta, A. K. Radikalreaktionen Bei Der Thermischen Behandlung von Ölsäure-Methylester Unter Ausschluß von Sauerstoff†. *Fette, Seifen, Anstrich* **1966**, *68*, 475–483.

(167) Turton, R.; Bailie, R. B.; Whiting, W. B.; Shaeiwitz, J. A. *Analysis, Synthesis, and Design of Chemical Processes*; Second Edi.; Pearson Education, Inc.: Upper Saddle River, NJ, USA, 2003; pp. 1–978.

(168) Agricultural Marketing Resource Center (AgMRC). Midwest Ethanol Prices http://www.agmrc.org/renewable_energy/.

(169) Stein, S. E. Mass Spectra. In *NIST Chemistry WebBook, NIST Standard Reference Database Number 69*; Linstrom, P.; Mallard, W., Eds.; National Institute of Standards and Technology: Gaithersburg, MD, USA, 2014.

(170) Coates, J. Interpretation of Infrared Spectra, A Practical Approach. In *Encyclopedia of Analytical Chemistry*; Meyers, R. A., Ed.; John Wiley & Sons, Ltd.: Chichester, UK, 2000; pp. 10815–10837.